Springer Proceedings in Mathematics & Statistics

Ricardo López-Ruiz
Danièle Fournier-Prunaret
Yoshifumi Nishio
Clara Grácio *Editors*

Nonlinear Maps and their Applications

Selected Contributions from the NOMA 2013 International Workshop

Springer

Springer Proceedings in Mathematics & Statistics

Volume 112

Springer Proceedings in Mathematics & Statistics

This book series features volumes composed of select contributions from workshops and conferences in all areas of current research in mathematics and statistics, including OR and optimization. In addition to an overall evaluation of the interest, scientific quality, and timeliness of each proposal at the hands of the publisher, individual contributions are all refereed to the high quality standards of leading journals in the field. Thus, this series provides the research community with well-edited, authoritative reports on developments in the most exciting areas of mathematical and statistical research today.

More information about this series at http://www.springer.com/series/10533

Ricardo López-Ruiz • Danièle Fournier-Prunaret
Yoshifumi Nishio • Clara Grácio
Editors

Nonlinear Maps and their Applications

Selected Contributions from the NOMA 2013 International Workshop

Springer

Editors
Ricardo López-Ruiz
Facultad de Ciencias
Universidad de Zaragoza
Zaragoza
Spain

Danièle Fournier-Prunaret
Université de Toulouse, LAAS-CNRS, INSA
Toulouse
France

Yoshifumi Nishio
Department of E. E. Eng.
Tokushima University
Tokushima
Japan

Clara Grácio
Department of Mathematics
University of Évora, CIMA-UE
Évora
Portugal

ISSN 2194-1009 ISSN 2194-1017 (electronic)
Springer Proceedings in Mathematics & Statistics
ISBN 978-3-319-12327-1 ISBN 978-3-319-12328-8 (eBook)
DOI 10.1007/978-3-319-12328-8

Mathematics Subject Classification (2010): 39-06, 37-06, 37E05, 37E30, 46T20

Library of Congress Control Number: 2015934824

Springer Cham Heidelberg New York Dordrecht London

Printed on acid-free paper

Springer is part of Springer Science + Business Media (www.springer.com)

Preface

The chapters in this volume of the Springer Proceedings in Mathematics & Statistics series, entitled Nonlinear Maps and Their Applications, come from the works presented in the Fourth International Workshop on Nonlinear Maps and Their Applications (NOMA 2013), which took place in Zaragoza, Spain, 3–4 September, 2013. The workshop was locally organized by Ricardo López-Ruiz (RLR) and hosted by the University of Zaragoza at its Faculty of Sciences.

This conference follows the sequence of Workshop on Nonlinear Maps and Their Applications which started in Toulouse 2007, and continued in Urbino 2009 and in Évora 2011.

The objective of the NOMA 2013 Conference was to provide a forum in the field of discrete dynamical systems. It was open for theoretical studies as well as for applications. The interaction and the knowledge exchange among mathematicians, physicists, engineers, and other specialists, and young researchers, from nonlinear sciences was very fruitful and gave rise to new insights in this area, in the pleasant atmosphere provided by the town of Zaragoza. It consisted of five invited lectures given by Yves Pomeau (École Normale Supérieure de Paris, France), Oreste Piro (University of Balearic Islands, Spain), Víctor Mañosa (Polytechnic University of Catalunya, Spain), Elena Blokhina (University College Dublin, Ireland), and Anirban Chakraborti (École Centrale de Paris, France) as well as over 20 contributed lectures of 15 different countries (Portugal, Japan, France, Spain, Czech Republic, Russia, Belgium, Iran, Poland, Mexico, Venezuela, Brazil, Tunisia, Germany, and Argentina).

This volume is a compilation of the selected works presented in the workshop and that have been accepted for publication. The diversified nature of the conference is reflected in the spectrum of the 17 chapters published here, where 36 researchers are contributing.

The editors, specially the local organizer (RLR), would like to thank all conference participants, committees, authors, who submitted papers for this volume, for their valuable contribution, as well as reviewers for their time and expertise to review the works presented here.

Editors: Ricardo López-Ruiz, Danièle Fournier-Prunaret, Yoshifumi Nishio, Clara Grácio.

Contents

Contributors

O Alvarez-Llamoza Departamento de Física, FACYT, Universidad de Carabobo, Valencia, Venezuela

Universidad Católica de Cuenca, Cuenca, Ecuador

Sergey M. Apenko P N Lebedev Physical Institute, Moscow, Russia

Francisco Balibrea Departamento de Matemáticas, Universidad de Murcia, Murcia, Spain

Malay Banerjee Department of Mathematics and Statistics, Indian Institute of Technology, Kanpur, India

S. S. Bel'mesova N.I.Lobachevsky State University of Nizhni Novgorod, Nizhni Novgorod, Russia

E. Blokhina School of Electrical, Electronic and Communications Engineering, University College Dublin, Dublin, Ireland

Jorge Buescu Centro de Matemática e Aplicações Fundamentais, Departamento de Matemática, Faculdade de Ciências, Universidade de Lisboa, Lisboa, Portugal

Anirban Chakraborti School of Computational and Integrative Sciences, Jawaharlal Nehru University, New Delhi, India

M. G. Cosenza Centro de Física Fundamental, Universidad de Los Andes, Mérida, Venezuela

M. Dominguez-Pumar Universitat Politécnica de Catalunya, Micro- and Nanotechnology Group, Barcelona, Spain

L. S. Efremova N. I. Lobachevsky State University of Nizhni Novgorod, Nizhni Novgorod, Russia

O. Feely School of Electrical, Electronic and Communications Engineering, University College Dublin, Dublin, Ireland

Danièle Fournier-Prunaret LAAS-CNRS, INSA, University of Toulouse, Toulouse, France

Imma Gálvez-Carrillo Departament de Matemàtica Aplicada III, Universitat Politècnica de Catalunya, Barcelona, Spain

P. Giounanlis School of Electrical, Electronic and Communications Engineering, University College Dublin, Dublin, Ireland

M. V. Gorbunkov P. N. Lebedev Physics Institute, Moscow, Russia

S. Gorreta Universitat Politécnica de Catalunya, Micro- and Nanotechnology Group, Barcelona, Spain

Sanchari Goswami S.N. Bose National Centre for Basic Sciences, Kolkata, India

Clara Grácio CIMA-UE-DMAT, School of Science and Technology, University of Évora, Évora, Portugal

Jun-ichi Inoue Graduate School of Information Science and Technology, Hokkaido University, Sapporo, Japan

José Luis López Dept. of Math. Engineering and Informatics, Public University of Navarre, Pamplona, Spain

Ricardo López-Ruiz Department of Computer Science & BIFI, University of Zaragoza, Zaragoza, Spain

Marek Lampart Department of Applied Mathematics & IT4Innovations, VŠB-Technical University of Ostrava, Ostrava, Czech Republic

Víctor Mañosa Departament de Matemàtica Aplicada III, Universitat Politècnica de Catalunya, Barcelona, Spain

Yu. Ya. Maslova P. N. Lebedev Physics Institute, Moscow, Russia

Christian Mira Quint, France

Carmen Pellicer-Lostao BIFI, University of Zaragoza, Zaragoza, Spain

V. A. Petukhov P. N. Lebedev Physics Institute, Moscow, Russia

Yves Pomeau Department of Mathematics, University of Arizona, Tucson, USA

J. Pons-Nin Universitat Politécnica de Catalunya, Micro- and Nanotechnology Group, Barcelona, Spain

J. Leonel Rocha Instituto Superior de Engenharia de Lisboa - ISEL, ADM and CEAUL, Lisboa, Portugal

M. A. Semenov P. N. Lebedev Physics Institute, Moscow, Russia

Cristina Serpa Centro de Matemática e Aplicações Fundamentais, Departamento de Matemática, Faculdade de Ciências, Universidade de Lisboa, Lisboa, Portugal

Yu. V. Shabalin P. N. Lebedev Physics Institute, Moscow, Russia

Elyas Shivanian Department of Mathematics, Imam Khomeini International University, Qazvin, Iran

Abdel-Kaddous Taha INSA, University of Toulouse, Toulouse, France

Chapter 1
Study of A Model for the Distribution of Wealth

Yves Pomeau and Ricardo López-Ruiz

Abstract An equation for the evolution of the distribution of wealth in a population of economic agents making binary transactions with a constant total amount of "money" has recently been proposed by one of us (RLR). This equation takes the form of an iterated nonlinear map of the distribution of wealth. The equilibrium distribution is known and takes a rather simple form. If this distribution is such that, at some time, the higher momenta of the distribution exist, one can find exactly their law of evolution. A seemingly simple extension of the laws of exchange also yields explicit iteration formulae for the higher momenta, but with a major difference with the original iteration because high-order momenta grow indefinitely. This provides a quantitative model where the spreading of wealth, namely the difference between the rich and the poor, tends to increase with time.

1.1 Introduction

This communication follows the Noma-13 conference in September 2013, an enjoyable and fruitful meeting where one of us (YP) had a chance to hear of the model considered below [1–3]. This model describes the evolution of the distribution of wealth in a population of individuals doing business pairwise. After each exchange there is a redistribution of money between the two individuals, without total loss or gain. A feature of this model, the "Z-model" (with Z for Zaragoza) is its simple equilibrium solution (written below). Under its law of evolution, this equilibrium solution is stable and so attracts most, if not all, initial conditions satisfying convergence conditions (finite total probability and finite total wealth) [4]. Moreover, an H-theorem is valid for this model [5]. We show below that the evolution of higher momenta (mean square value, mean cubic value, etc.) of the wealth can be computed

R. López-Ruiz (✉)
Department of Computer Science & BIFI,
University of Zaragoza, Zaragoza, Spain
e-mail: rilopez@unizar.es

Y. Pomeau
Department of Mathematics, University of Arizona, Tucson, USA
e-mail: pomeau@lps.ens.fr

R. López-Ruiz et al. (eds.), *Nonlinear Maps and their Applications,*
Springer Proceedings in Mathematics & Statistics 112, DOI 10.1007/978-3-319-12328-8_1

exactly, obviously under the condition that those momenta exist. We also consider situations where the momenta do not converge beyond a given order. An anonymous referee pointed out that something called "q-model" has equations similar to the Z-model. Those q-models aim at describing the distribution of stress in random set of solid grains in contact with neighbours in such a way that the downward push of the weight of a grain and of the grain above it is distributed more or less randomly between its neighbours underneath. In this theory, the equivalent of the time of the Z-model is played by the vertical direction and the time-iteration amounts to move down the pile to find the distribution of stress on grains. Even though the equations of this q-model look like the ones of the Z-model, their physical meaning is quite different. The interested reader may get a list of papers on the subject in the reference list of the lecture notes published in [6]. Moreover the q-model, in order to get a row-to-row equation of iteration like the one of the Z-model has to assume that the vertical force on beads on the same horizontal row are statistically independent, which is presumably needed to get at the end something like a hyperbolic system, although the Cauchy–Poisson equations for regular elasticity are elliptic.

Due to its simple mathematical structure, it makes sense to extend the Z-model by keeping the possibility of an exact solution for the momenta. This can be done with a straightforward extension maintaining the basic properties of conservation of the total probability and the total wealth. This modified Z-model looks very much like the original and reduces to it continuously as a parameter changes, but it has completely different properties. In particular, it shows an increase in the fluctuations of wealth as time goes, a rather unexpected property, absent in the original model. This makes the matter of Sect. 1.3. In this respect, the inequality of wealth as studied below makes only a small part of this big subject, but it is at least one that one can try to describe quantitatively.

Motivated by this consideration of momenta, we look in Sect. 1.4 at what happens in the Z-model when the momenta do not converge, specifically when the distribution of wealth decays algebraically for large values so that momenta do not exist, at least initially, beyond a certain power (This might be related to what is called Pareto law; Pareto [7] having predicted that the natural distribution of wealth decays algebraically for large values, a property of the mZ-model studied below). An interesting result of this analysis is that, after a certain number of iterations (namely after a finite amount of time), higher momenta converge although they diverged initially. Somehow, without venturing into the area of political science, this looks like the exact opposite of what is predicted sometimes (without relying on objective modelisation as much we can tell): fewer individuals get richer and richer although the other ones get poorer and poorer as time goes. This could have other explanations of course, like what is called the redistribution of wealth by the tax system in modern economies.

We shall explain first how to solve "exactly" the moment problem, for a probability distribution decaying fast enough at infinity and then look at what happens if, initially, this probability distribution decays algebraically for large values.

In sect. 1.5 we give the probability distribution of the wealth of the "richest man", namely the largest wealth of a given finite number of agents with a given probability distribution of the wealth with agents taken at random in the population. An explicit

expression of this probability distribution of the maximum of wealth, with its limit in the case of a large number of agents, is given.

The last section is "Summary and Conclusion".

1.2 The Z-Model

In this model, one considers a positive variable with various names, x, u, etc. for the amount of money owned by an individual. This amount changes in the course of time because of random exchanges between the individuals taking place at discrete time, in a synchronous way in the system. The fundamental quantity is $p_t(x)$, the probability that an individual taken at random in the population has an amount x at time t. At the next time step $(t+1)$, due to the binary exchanges, $p_t(x)$ has changed according to the law of iteration found in reference [1]

$$p_{t+1}(x) = \int\int_{S(x)} \mathrm{d}u\mathrm{d}v \frac{p_t(u)p_t(v)}{u+v}, \tag{1.1}$$

The domain of integration in Eq. (1.1) is defined by

$$S(x) = \{(u,v), u, v > 0, u+v > x\}.$$

This integral equation is for a function of x, positive variable. As $p(.)$ is a probability distribution, it has to be positive or 0. Moreover, it is normalised in such a way that $\int_0^\infty \mathrm{d}u\, p_t(u) = 1$, and t is a discrete index representing time. This law of evolution of the wealth is derived as follows. Suppose two individuals, each one with the same probability of wealth, say $p(u)$, put their money in the same basket. Then the probability distribution for what is in the basket (the amount w) is

$$q(w) = \int_0^\infty \mathrm{d}v\, p(v)p(w-v)H(w-v),$$

where $H(.)$ is Heaviside function, 0 for a negative argument and 1 otherwise. Suppose, we share the amount w between two individuals, by taking randomly a value in $[0,w]$ and give it to the first individual and the rest to the other. The probability distribution of what is taken by anyone of those individuals is

$$r(s) = \frac{\chi_w(s)}{w},$$

where $\chi_w(s)$ is the characteristic function of the interval $[0,w]$. By extending this simple formula to the probability distribution $q(w)$ of the values of w, as derived above, one obtains

$$r(s) = \int_0^\infty \frac{\mathrm{d}w}{w} H(w-s) \int_0^\infty \mathrm{d}v\, p(v)p(w-v)H(w-v).$$

After rearranging the integrals one finds

$$r(s) = \int_0^\infty \mathrm{d}v' \int_{s-v'>0}^\infty p(v')p(u') \frac{\mathrm{d}u'}{u'+v'},$$

which is a form of the right-hand side of Eq. (1.1).

Equation (1.1) can be integrated explicitly, at least in some sense. Let us define the moments of $p_t(x)$ as

$$m_k(t) = \int \mathrm{d}u u^k p_t(u). \tag{1.2}$$

We consider first the case where all momenta converge. In Sect. 1.4 we discuss the situation where some momenta do not exist at a given time because the integral (1.2) diverges at k large, which is well possible because the "physical" constraints on $p(u)$ is to have well-defined (not diverging) values of m_0 and m_1 only. From Eq. (1.1) one derives the following equation for the momenta of $p_{t+1}(.)$ as a function of the momenta of $p_t(.)$

$$m_k(t+1) = \frac{1}{k+1} \Sigma_{0\le l\le k} C_k^l m_{k-l}(t) m_l(t), \tag{1.3}$$

where $C_k^l = \frac{k!}{(k-l)!l!}$ are the binomial coefficients. This shows that the momenta of order k at time $(t+1)$ can be found if the momenta of smaller power at time t are known. The formula is also consistent with the fact that $m_0 = 1$ at any time and that m_1 is a conserved positive constant (called later m_1). Let us look at the equation for m_2. It reads

$$m_2(t+1) = \frac{2}{3}(m_2(t) + m_1^2), \tag{1.4}$$

As this equation is linear with respect to m_2, it can be integrated at once with the result (supposing $m_2(0)$ given)

$$m_2(t) = \left(\frac{2}{3}\right)^t m_2(0) + 2m_1^2 \left[1 - \left(\frac{2}{3}\right)^t\right] = \left(\frac{2}{3}\right)^t (m_2(0) - 2m_1^2) + 2m_1^2, \tag{1.5}$$

The higher momenta can also be computed explicitly as the functions of the initial data for the lower order momenta, the result become more cumbersome as the order increases. At third order one has

$$m_3(t+1) = \frac{1}{2}(m_3(t) + 3m_2(t)m_1), \tag{1.6}$$

let

$$S_3(t) = \frac{3}{2} m_2(t) m_1.$$

Therefore

$$m_3(t) = \left(\frac{1}{2}\right)^t \left[m_3(0) + \Sigma_{0\le\theta\le t} 2^\theta S_3(\theta - 1)\right],$$

is a solution for $m_3(t)$ as a function of m_1, $m_2(0)$ and $m_3(0)$. The sums can be done explicitly because they involve geometric series. The method of integration just explained does not work if one takes momenta with non-integer exponents because there is no finite equivalent of the binomial formula for such non-integer power.

1.3 Definition and Solution of a Generalised Z-Model

The Z-model can be generalised in the following way. In the original formulation, each of the two partners in a transaction have a random amount u and v. During the transaction they put first the whole amount $(u + v)$ in a basket and then share its content randomly. The Z-model describing this satisfies the constraint that the total probability is one and that the total money is also conserved. This model has also the property that the equilibrium solution (namely the distribution of wealth such that $p_t(u) = p_{t+1}(u)$) is known explicitly and is

$$p_{eq}(u) = \frac{1}{m_1} e^{-\frac{u}{m_1}}.$$

Further, we suggest a modified recursion relation analogous to the one given in Eq. (1.1), but such that no simple expression of the equilibrium distribution can be found, even though the mass and first momentum m_1 is conserved (we keep the same notation, $m_k(t)$ for the kth moment in the mZ-model, defined below, as in the Z-model). This model reads

$$P_{t+1}(x) = \int \int_{S_a(x)} \mathrm{d}u\mathrm{d}v \frac{P_t(u)P_t(v)}{au + (2-a)v}, \tag{1.7}$$

In this equation, a is a real parameter, between 0 and 2, and $S_a(x)$ is defined by the condition $x < au + (2 - a)v$. In this model, at the time of the transaction between the two individuals, one of the individual puts (au) in the basket (instead of u in the Z-model) and the other puts $(2 - a)v$ in the basket, instead of v. Although this model is apparently not conservative, this is not the case. If we consider the symmetrical interaction for the pair of agents (v, u), in this case the first agent will put (av) in the basket and the second one $(2-a)u$. For both trades, those of the pairs (u, v) and (v, u), the total money to share in the basket is $2(u + v)$, then the total wealth is conserved. It can be interpreted that the excess of money in one of the trades is injected to cover the lack of money in the other trade. This is just one of the functions done by the bank system. Perhaps this is not such an unrealistic model because, nowadays (and very likely before), banks and even states rent money they do not really have and do that within constraints based on multiplicative factors of their actual wealth.

Like the Z-model, the modified Z-model (or mZ-model) defined by the iteration (1.7) satisfies the constraints of conservation of m_0 and m_1 if $m_0 = 1$. From simple algebra, one finds

$$m_0(t + 1) = m_0(t)^2,$$

and

$$m_1(t + 1) = m_0(t)m_1(t).$$

Therefore, the first two momenta are constant if $m_0 = 1$ and if m_1 converge, as we assume it. Contrary to the case of the Z-model, there is no simple equilibrium solution. However, it is possible to derive many properties of this equilibrium from the equations for the moments. This is because the denominator in the iteration

formula is a linear function of u and v like in the Z-model. The recursion relation for the second moment is

$$m_2(t+1) = \frac{1}{3}\left[(4-4a+2a^2)m_2(t) + 2(2-a)am_1^2\right]. \tag{1.8}$$

As can be easily checked, this reduces to the formula valid for the Z-model, Eq. (1.4), in the case $a = 1$. However, a very interesting difference appears in this iteration law (again, an iteration derived from the iteration for the probability distribution with no other assumption than the existence of the second moment). Actually this iteration may lead to an exponentially growing second moment. This happens if the coefficient of $m_2(t)$ in Eq. (1.8) is larger than one. This happens if a is outside of the interval $[1-\frac{1}{\sqrt{2}}, 1+\frac{1}{\sqrt{2}}]$, which is compatible with the condition $0 < a < 2$. Therefore, there can be an instability of the second moment leading to an indefinite increase of the width of the distribution of wealth. Without overstating this, one can say that this makes a model of ever increasing inequality as predicted by some socioeconomical theories.

Moreover, for any a different from 1, the iteration of higher momenta become unstable. To show this, let us define $b = 1-a$. The iteration of the kth moment reads

$$m_k(t+1) = \frac{1}{k+1}\left[\left((1-b)^k + (1+b)^k\right)m_k(t) + l.o.t(t)\right]. \tag{1.9}$$

In this equation, $l.o.t(t)$ is for the lowest order terms, depending on momenta of order less than k. Let us consider the smallest k such that, for a given a, there is an exponential growth of this moment. Therefore, $l.o.t(t)$ remains bounded as a function of time and so, if there is an instability, it is dominated after a sufficient number of iterations by the exponentially growing $\left((1-b)^k + (1+b)^k\right)m_k(t)$. A little algebra shows that the coefficient of $m_k(t)$ on the right-hand side of Eq. (1.9) is larger than 1 and the moment grows exponentially if

$$\ln(1+|b|) > \frac{\ln(k+1)}{k}.$$

If $|b|$ is small, this is equivalent to the condition

$$k > \frac{\ln(1/|b|+1)}{|b|}.$$

It shows that, however $|b|$ is small but not 0, the large order momenta are unstable under the iteration. Recall that $|b|$ small is equivalent to have a mZ-model formally close to the original Z-model. This also shows that, however small (but non 0) $|b|$ is, the steady distribution, if it exists, given by the iteration law should decay with a power law at large values of its argument to make diverge momenta with a large power. It is planned to return to this mathematically interesting question in a future publication.

1.4 Diverging Moments at Time Zero

In this section, we return to the Z-model in its original form and consider the following question: What happens to the iterations if the initial momenta diverge beyond a certain power? Indeed, because the initial condition is in principle rather free, provided $m_0 = 1$ and m_1 converges, one can always imagine an initial condition with a distribution of wealth decreasing algebraically for large powers. In this case, momenta do not exist beyond a certain power. We consider below what happens in this case. In particular, we show that after a finite number of iterations, one recovers a converging moment with a power less than a value increasing as the iterations go.

We shall limit ourselves to situations where $p_0(u)$, the initial distribution of wealth, behaves at large u as a power law, like

$$p_0(u) \approx l_{\alpha_0} u^{-\alpha_0}, \tag{1.10}$$

where l_{α_0} is a positive constant and α_0 a positive exponent. To have finite probability and first momentum (finite total wealth) one must have $\alpha_0 > 2$. By putting this power law in the right-hand side of the functional iteration (1.1), one obtains that at time $t = 1$, the distribution of wealth $p_1(u)$ decays with the power law

$$p_1(u) \approx l_{\alpha_1} u^{-\alpha_1}, \tag{1.11}$$

where $\alpha_1 = 2\alpha_0 - 1$ and where

$$l_{\alpha_1} = l_{\alpha_0}^2 B(\alpha_0),$$

where

$$B(\alpha) = \int\int_{S(1)} \mathrm{d}u' \mathrm{d}v' \frac{(u'v')^{-\alpha}}{u' + v'}$$

is a numerical function of the argument α. As the iteration formula shows, α increases as the iteration goes and so as soon as it becomes big enough, momenta of a given power begin to exist, and follow later the explicit recursion formulae given in Eq. (1.3). This is correct because momenta of higher order begin to converge the later as their power increases. Therefore, the right-hand side of the recursion equation becomes all well-defined when the highest moment becomes well-defined, all momenta of a smaller power being already finite at this time.

1.5 Probability Distribution of the Wealth of the Richest Man

Looking at the economic magazines, one is struck by their insistence on various lists of rich, if not very rich people, lists ordered according to their supposed wealth. Therefore, it is of some interest to consider the question of the distribution of biggest

wealth that can be reached within the models outlined in this work. We begin with a basic question of probability: given a probability distribution $p(x)$, and a number ν of independent trials. What is the largest value reached among those trials? This interesting question can be answered quite simply as demonstrated below. Then we apply this result to the case of the Z- and mZ-model.

Consider first the following problem: given x_0 positive, let us draw a number x with probability distribution $p(x)$. What is the distribution of the maximum of x_0 and x, a maximum denoted as X? If x is less than x_0 the maximum is x_0, in the opposite case it is x. Define N(x) as

$$N(x) = \int_0^x \mathrm{d}x' p(x').$$

The probability that x is less than x_0 is $N(x_0)$. Therefore, the probability distribution of X is

$$\Pi(X, x_0) = N(X)\delta(X - x_0) + p(X)H(X - x_0). \tag{1.12}$$

The probability distribution $\Pi(X, x_0)$ is normalised in such a way that

$$\int_0^\infty \mathrm{d}X \Pi(X, x_0) = 1,$$

a consequence of the property $N(\infty) = 1$.

Suppose now that x_0 instead of being taken as a fixed number is drawn at random with a probability distribution $q(x_0)$. Therefore, the probability distribution of the maximum of x and x_0 has to be averaged over the choices of x_0. This yields

$$P(X) = \int_0^\infty \mathrm{d}x_0 q(x_0)\Pi(X, x_0) = N(X)q(X) + p(X)\int_0^X \mathrm{d}x' q(x'). \tag{1.13}$$

One can check by performing the integrals in the quadrant $x, x' > 0$ that

$$\int_0^\infty \mathrm{d}X\, P(X) = \int_0^\infty \mathrm{d}x p(x) \int_0^\infty \mathrm{d}x' q(x') = 1.$$

From Eq. (1.13) one can derive the probability distribution of the largest value drawn after ν (integer) independent trials , each one with the probability distribution $p(x)$. Let $P_\nu(x)$ be the probability distribution of the maximum of ν trials. After one trial $P_1(X) = p(X)$. From Eq. (1.13) one derives the recursion formula between $P_\nu(X)$ and $P_{\nu+1}(X)$

$$P_{\nu+1}(X) = N(X)P_\nu(X) + p(X)\int_0^X \mathrm{d}x' P_\nu(x'). \tag{1.14}$$

Now define $Q_\nu(X) = \int_0^X \mathrm{d}x' P_\nu(x')$. This allows to write Eq. (1.14) like

$$\frac{\mathrm{d}Q_{\nu+1}(X)}{\mathrm{d}X} = N(X)\frac{\mathrm{d}Q_\nu(X)}{\mathrm{d}X} + \frac{\mathrm{d}N(X)}{\mathrm{d}X}Q_\nu(X). \tag{1.15}$$

This can be obviously integrated as

$$Q_{\nu+1}(X) = N(X)Q_\nu(X) + S_\nu,$$

where S_ν is a constant of integration, independent on X. As $Q_\nu(0) = 0$ for all S_ν, $S_\nu = 0$ also for all ν. Therefore,

$$Q_\nu(X) = \left(\int_0^X \mathrm{d}x' p(x')\right)^\nu, \tag{1.16}$$

and

$$P_\nu(X) = \nu p(X)\left(\int_0^X \mathrm{d}x' p(x')\right)^{\nu-1}. \tag{1.17}$$

Suppose $p(x)$ is a smooth function decaying continuously to 0 as x tends to infinity. In this case, it is possible to get the asymptotic form of $P_\nu(X)$ at ν very large. Let us write $P_\nu(X)$ as an exponential

$$P_\nu(X) = e^{T(\nu,X)},$$

with

$$T(\nu, X) = \ln(\nu) + \ln(p(X)) + (\nu - 1)\ln\left(\int_0^X \mathrm{d}x' p(x')\right).$$

In the limit ν large, one expects that the distribution $P_\nu(X)$ has more weight at larger values of X, which is also what is found by looking numerically at the shape of $P_\nu(X)$ in this limit for various possible $p(X)$. See Figs. 1.1 and 1.2. Therefore, in this limit, $P_\nu(X)$ should become more concentrated around the value of X such that the derivative $\frac{\partial T(\nu,X)}{\partial X} = 0$. This derivative vanishes when X is the root X_ν of

$$\nu = 1 - \frac{p' \cdot N}{p^2},$$

where $p' = \frac{dp}{dX}$. When X_ν is large, then $N(X_\nu) = \int_0^{X_\nu} \mathrm{d}x' p(x') \approx 1$. At ν large, this root X_ν is unique and large. This can be seen by noticing that $-\frac{p'}{p^2} = \frac{d(1/p)}{dX}$, and by assuming that $1/p$ is a smooth function increasing monotonically to infinity as x tends to infinity. To make its first momentum m_1 convergent $p(X)$ must decay faster than x^{-2} at infinity, so that the derivative $\frac{d(1/p)}{dX}$ must grow faster than X at X large. Therefore, the function X_ν grows slower than ν as ν tends to infinity but it grows to infinity for any function $p(x)$ tending smoothly to 0 as x tends to infinity. This growth will depend on the behaviour of $p(x)$ as x tends to infinity.

The function X_ν gives the order of magnitude of the maximum wealth after ν iterations. By continuing the expansion of $T(\nu, x)$ near X_ν to the quadratic order with respect to the difference $\delta X = X - X_\nu$, one finds that

$$T(\nu, X) \approx T(\nu, X_\nu) + \frac{\delta X^2}{2}\frac{\partial^2 T(\nu, X)}{\partial X^2} + \ldots.$$

where the second derivative is computed at $X = X_\nu$.

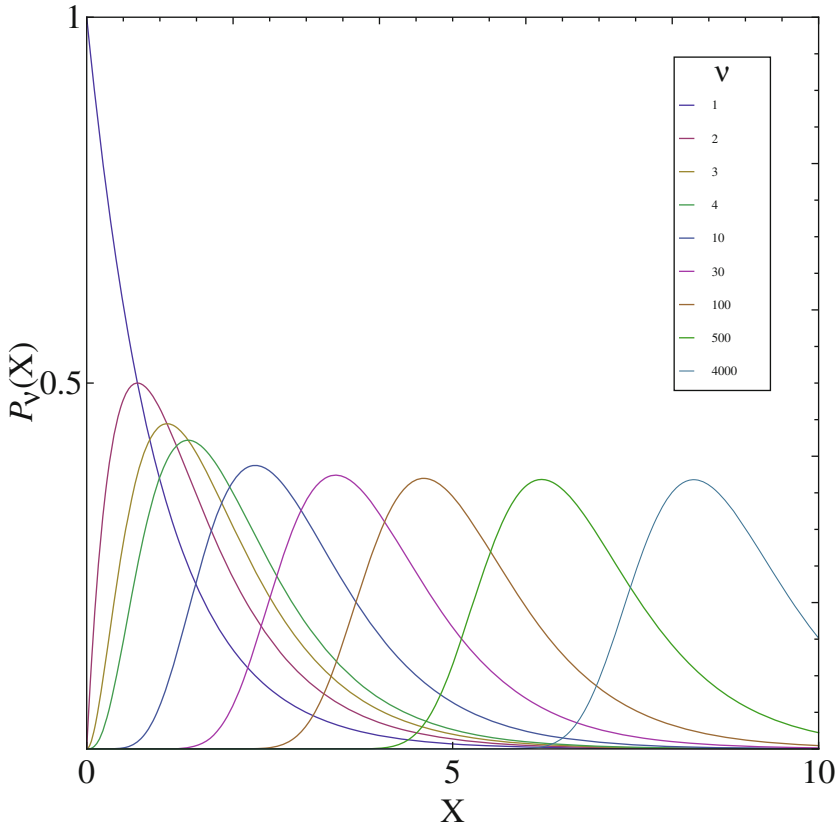

Fig. 1.1 $P_\nu(X)$ for different ν when $p(x) = e^{-x}$. Observe the monotonic increasing of X_ν with ν. For this case, when $\nu \gg 10$, observe that $P_\nu(X_\nu)$ is constant and $P_\nu(X)$ presents a soliton-like waveform

After some algebra and by taking into account that ν is large and that, in the limit X_ν large, $N(X_\nu) \approx 1$, one finds

$$\frac{\partial^2 T(\nu, X)}{\partial X^2} \approx -p(X_\nu)\frac{d^2(1/p)}{dX^2}.$$

To prove that the width of the maximum of the distribution is much less than X_ν, one can do the following approximate scaling argument. We have $\frac{p'}{p^2} \approx -\nu$. Assuming that $p' \approx \frac{p(X_\nu)}{X_\nu}$, which is certainly correct for a probability distribution $p(.)$ decaying like a power law at large arguments, one finds $\nu \sim \frac{1}{X_\nu p(X_\nu)}$. Using the same kind of scaling argument one finds that

$$\frac{\partial^2 T(\nu, X)}{\partial X^2} \sim \frac{-\nu p(X_\nu)}{X_\nu} \sim -\frac{1}{X_\nu^2}.$$

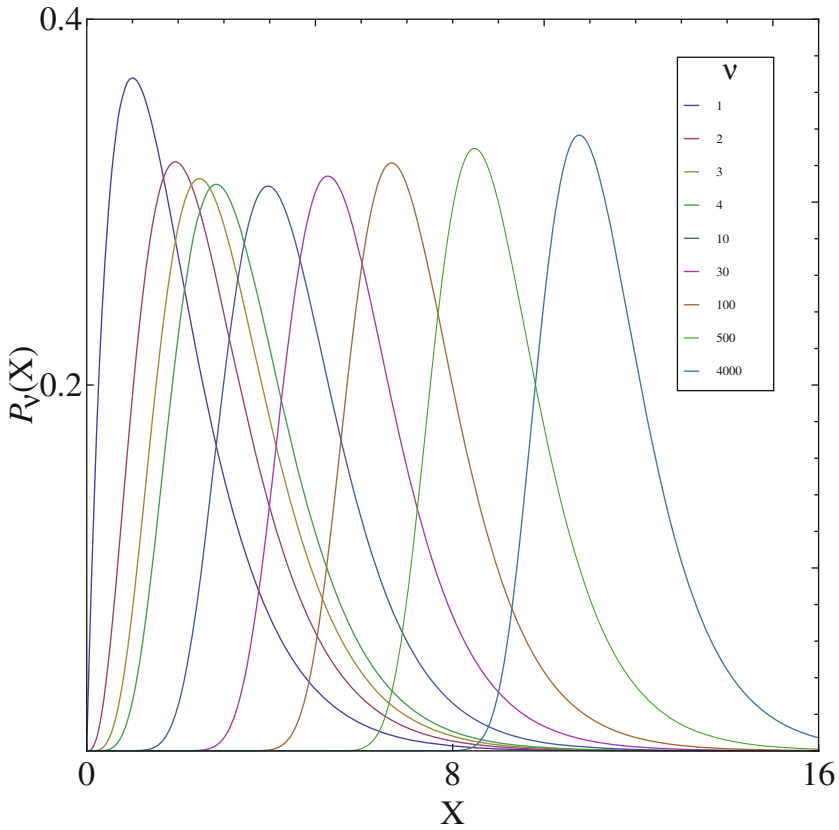

Fig. 1.2 $P_\nu(X)$ for different ν when $p(x) = xe^{-x}$. Observe the monotonic increasing of X_ν with ν. For this case, when $\nu \gg 10$, observe that $P_\nu(X_\nu)$ is not constant and $P_\nu(X)$ presents an increase of the maximal wave amplitude

This shows that, at least for distributions $p(x)$ decaying like power laws, the width of the probability distribution $P_\nu(X)$ is of order X_ν for ν very large, although its center is at X_ν. In this case, the width of the probability distribution and its center are large and of the same order of magnitude. Therefore, one may guess that it behaves like

$$P_\nu(X) \approx \frac{1}{X_\nu} \hat{P}\left(\frac{X}{X_\nu}\right).$$

where $\hat{P}$ is a positive numerical function of order one when its argument is of order one. It is normalised in such a way that $\int_0^\infty \hat{P}(z)\mathrm{d}z = 1$. From the derivation, this function depends on the way $p(x)$ behaves as x tends to infinity.

1.6 Conclusions and Perspectives

Owing to its mathematical structure, the Z-model can be solved and somehow extended to bring interesting results with, perhaps, a connection to the complicated phenomenology of real economics. Despite its strongly nonlinear character, it can be solved without assuming too many things. A remarkable feature of this model is its convergence to an exponential distribution of wealth. Of course any difference between reality and this model may have many explanations. Among others, it has been suggested, such as one of us (YP) also suggested it during the Noma-13 conference that this model lacks an important element present in economies of developed countries, the tax system, with a more or less explicit claim of redistributing the wealth. Such a tax system could be perhaps represented by adding a third partner in each binary transaction, taking its pound of flesh at the transaction and redistributing it randomly at the next step, more or less the way the VAT (added value tax) works. This chapter also introduces a modified Z-model, where at each transaction money is exchanged, which is not actually possessed by the economic agents, something occurring all the time in modern economies. Amazingly, this induces an instability in the distribution of wealth and makes grow indefinitely the higher momenta of its distribution, even though the total amount remains the same. Although this happens in a very idealised model, it could be closer to reality than the original Z-model with its rather narrow distribution of wealth.

References

1. López-Ruiz R.: Exponential wealth distribution in different discrete economic models. arXiv:1009.3550 [q-fin.GN] (2010)
2. López-Ruiz R., López J.L., Calbet X.: Exponential wealth distribution in a random market: a new approach from functional iteration theory. ESAIM Proc. **36**, 189–204 (2012)
3. López J.L., R. López-Ruiz, Calbet X.: Exponential wealth distribution in a random market: a rigorous explanation. J. Math. Anal. Appl. **386**, 195–204 (2012)
4. Katriel G.: Convergence to an exponential wealth distribution in a random market model. Appl. Anal. **93**, 1256–1263 (2014)
5. Apenko S.M.: Monotonic entropy growth for a nonlinear model of random exchanges. Phys. Rev. E **87**, 024101 (2013)
6. Bouchaud, J.P.: Granular media: some ideas from statistical physics. In: Proceedings of the 2002 Les Houches Summer School on Slow Relaxations and Nonequilibrium Dynamics in Condensed Matter, Springer (2004)
7. Pareto V.: Cours d'économie politique professé *à* l'Université de Lausanne. Vol. I (1896), Vol. II (1897)

Chapter 2
Periodic Orbits of Planar Integrable Birational Maps

Imma Gálvez-Carrillo and Víctor Mañosa

Abstract A birational planar map F possessing a rational first integral preserves a foliation of the plane given by algebraic curves which, if F is not globally periodic, is given by a foliation of curves that have generically genus 0 or 1. In the genus 1 case, the group structure of the foliation characterizes the dynamics of any birational map preserving it. We will see how to take advantage of this structure to find periodic orbits of such maps.

2.1 Introduction

A planar *rational* map $F : \mathcal{U} \to \mathcal{U}$, where $\mathcal{U} \subseteq \mathbb{K}^2$ is an open set and $\mathbb{K} \in \{\mathbb{R}, \mathbb{C}\}$, is called *birational* if it has a rational inverse F^{-1}. In this chapter, we will say that a map F is *integrable* if there exists a nonconstant function $V : \mathcal{U} \to \mathbb{K}$ such that

$$V(F(x, y)) = V(x, y),$$

which is called a *first integral* or *invariant* of F. If a map F possesses a first integral V then each orbit lies in some level set of V or, in other words, the level sets of V are invariant under F.

Planar birational maps are a classical object of study in algebraic geometry and have been the focus of intense research activity in recent years (see [24] and references therein). The integrable cases appear in many contexts, from algebraic geometry and number theory to mathematical physics. This is the case of the celebrated QRT family of maps introduced in [44, 45] (see also [26]), which contains the well-known McMillan family of maps, and some of the integrable cases studied by Gumovski and Mira [30, 40]. Many maps in this family arise as special solutions, termed discrete solitons, of differential-difference equations arising in statistical mechanics. The QRT maps all have a rational first integral.

I. Gálvez-Carrillo (✉) · V. Mañosa
Departament de Matemàtica Aplicada III, Universitat Politècnica de Catalunya, Barcelona, Spain
e-mail: m.immaculada.galvez@upc.edu

V. Mañosa
e-mail: victor.manosa@upc.edu

R. López-Ruiz et al. (eds.), *Nonlinear Maps and their Applications,*
Springer Proceedings in Mathematics & Statistics 112, DOI 10.1007/978-3-319-12328-8_2

In this chapter, we will consider only those integrable maps that have *rational first integrals*. In fact, all the examples of integrable birational maps that we know have rational first integrals, but as far as we know there is no reason for an integrable birational map to be rationally integrable. In this sense, it is interesting to recall the case given by the composition maps associated to the five-periodic Lyness recurrences. These maps are birational, and the numerical results show phase portraits compatible with the existence of first integrals, however, it has been recently proved that, generically, these maps are not rationally integrable, see [19, Theorem 19] and [14, Theorem 1 and Proposition 3].

Observe that if the first integral is a rational function,

$$V(x, y) = \frac{P(x, y)}{Q(x, y)}, \tag{2.1}$$

then the map preserves the foliation[1] of $\mathcal{U}$ is given by the algebraic curves

$$\mathcal{F} = \{P(x, y) - h\, Q(x, y) = 0, h \in \mathrm{Im}(V)\}. \tag{2.2}$$

We will assume that P and Q are coprime and, although it is not essential in this chapter, that V has *minimal* degree. Recall that the degree of a rational first integral is the greater of the degrees of P and Q. We say that the degree n of V is minimal if any other rational first integral of F has degree at least n. Given a rational first integral, one always can find a minimal rational first integral.

In this note, our objective is to show how to take advantage of the algebraic–geometric properties of the invariant foliation $\mathcal{F}$ to study the periodic orbits of the birational maps preserving it. Although the techniques explained in this chapter have been used to study several birational maps [4–7, 9, 26, 53, 54], to illustrate them we will refer only to a particular, but paradigmatic, example: the well-known Lyness family of maps.

Example 2.1 Lyness's maps are a 1-parametric family of birational maps given by

$$F_a(x, y) = \left(y, \frac{a + y}{x}\right), \tag{2.3}$$

These maps give the dynamical system associated to recurrence $x_{n+2} = (a + x_{n+1})/x_n$. There is a large recent literature concerning this family. In the appendix of this chapter the reader can also find a short account of references and the history of the Lyness recurrences and maps.

Each map F_a has the first integral

$$V(x, y) = \frac{(x + 1)(y + 1)(x + y + a)}{xy}, \tag{2.4}$$

[1] In this chapter, we say that a map F preserves a foliation of curves $\{C_h\}$ if each curve C_h is invariant under the iterates of F.

so it preserves the foliation given by

$$\mathcal{F} = \{C_h = \{(x+1)(y+1)(x+y+a) - hxy = 0\},\ h \in \mathrm{Im}(V)\}\,. \tag{2.5}$$

The chapter is structured as follows: in Sect. 2.2, we will recall the notion of genus of an algebraic curve, and we will see that if we are interested in those maps not being globally periodic, then we can consider that the curves in the foliation (2.2) have genus 0 or 1, see Corollary 2.3. In Sect. 2.3, we restrict our attention to maps having invariant curves with genus 1 (also named elliptic curves). We recall the group structure of these curves and also a result of Jogia et al. (Theorem 2.4) which relates the dynamics of a particular birational map on an invariant elliptic curve and its group operation. We will take advantage of this result to obtain a description of the periodic orbits in terms of the torsion of the curve (Eq. 2.8). In Sect. 2.4, we discuss the global dynamics of birational maps preserving a foliation given by elliptic curves C_h. First, we start by introducing and discussing the nature of the rotation number function $\theta(h)$ associated to each curve C_h. Then, we see that a typical situation occurs when there is a dense set of curves in phase space filled by p-periodic orbits of all the periods $p \geq p_0 \in \mathbb{N}$, for some integer p_0 which is sometimes computable (see Proposition 2.9 and Sect. 2.4.3).

In Sect. 2.5, as a straightforward application, we show how to address the problem of finding the curves containing periodic orbits with a prescribed period, by using the characterization of periodic orbits given by the *group law of the curve* (see Eq. (2.8)). We show the main technique by applying it to the Lyness case, as already done in [4].

In Sect. 2.6, we will see how the group structure of rational elliptic curves is strongly related to the existence of rational periodic orbits. We will recall Mazur's theorem and its dynamical implications. We also give some insight on the known results of rational periodic orbits in the Lyness case [4, 29, 54]. This section ends with a digression about why the numerical simulations of the phase portrait of birational maps preserving an elliptic foliation do not show the plethora of periodic orbits that they possess, on the contrary of what happens when general integrable diffeomorphisms are considered.

We end these notes with a comment on the genus 0 case, and with an appendix giving more information about the Lyness maps and curves.

The aim of the chapter is expository, and it is inspired in the papers of Bastien and Rogalski [4] and of Jogia et al. [33]. The reader is invited to read them, as well as their references. Another essential reference is the book of Duistermaat [26] about some algebraic–geometric aspects of QRT maps.

2.2 A First Dynamical Result: Restriction to the Genus 0 and 1 Cases

When studying the dynamics of an integrable map, a first step is to know the topology of the invariant level sets. When the level sets are algebraic curves, the natural way to study them is to consider their extension, and also the extension of the birational

maps, to the complex projective space

$$\mathbb{C}\mathbf{P}^2 = \{[x : y : z] \neq [0 : 0 : 0],\, x, y, z \in \mathbb{C}\}/\sim,$$

where $[x_1 : y_1 : z_1] \sim [x_2 : y_2 : z_2]$ if and only if $[x_1 : y_1 : z_1] = \lambda[x_2 : y_2 : z_2]$ for $\lambda \neq 0$.

In this chapter, $[x : y : 1]$ denotes an affine point, corresponding with the point $(x, y) \in \mathbb{K}^2$ (where $\mathbb{K}$ can be either $\mathbb{R}$ or $\mathbb{C}$), and $[x : y : 0]$ denotes an infinite point. The infinite points are added to real affine algebraic curves in order to capture the asymptotic directions of possible unbounded components. See Fig. 2.2 for instance.

Any real affine algebraic curve can be extended to $\mathbb{C}\mathbf{P}^2$ by the formal process of *homogenization*. For instance, any Lyness curve

$$C_h = \{(x + 1)(y + 1)(x + y + a) - hxy = 0\} \subset \mathbb{R}^2$$

where $x, y \in \mathbb{R}$ extends to $\mathbb{C}\mathbf{P}^2$ as

$$\widetilde{C_h} := \{(x + z)(y + z)(x + y + az) - hxyz = 0,\, x, y, z \in \mathbb{C}\}.$$

Notice also that any birational map in $\mathbb{R}^2$ extends formally to a polynomial map in $\mathbb{C}\mathbf{P}^2$. For instance, the Lyness map $F_a(x, y) = (y, (a + x)/y)$ extends formally to

$$\widetilde{F}_a([x : y : z]) = [xy : az^2 + yz : xz],$$

except for the points $[x : 0 : 0]$, $[0 : y : 0]$, and $[0 : -a : 1]$ (see also the alternative description given by Eq. (2.7) in Sect. 2.3), where $x, y, z \in \mathbb{C}$.

Any algebraic curve $\widetilde{C}$ in $\mathbb{C}\mathbf{P}^2$ is a Riemann surface characterized by its *genus*, [34]. On any irreducible component of a curve in $\mathbb{C}\mathbf{P}^2$, the genus g is related to the *degree* d by the *degree-genus formula*:

$$g = \frac{(d-1)(d-2)}{2} - \sum_{p \in \mathrm{Sing}(C)} \frac{m_p(m_p - 1)}{2},$$

where m_p stands for the multiplicity of any possible singular ordinary point. Recall that a singular point is called ordinary when all the tangents at the point are distinct and that, given an irreducible curve, it is always possible to find a birationaly equivalent curve with only ordinary multiple points, so that the above formula gives the genus.

In this chapter, we will say that an invariant foliation has *generic genus* g if the genus has constant value g on the irreducible components of $\{P - hQ\}$, except maybe for a finite set of values of $h \in \mathrm{Im}(V)$ for which the genus is lower. This is a common situation. The reader is addressed, for instance, to Pettigrew and Roberts [43] for a characterization of the singular curves corresponding to a biquadratic foliation that generalizes the classical elliptic QRT foliations. We will assume that in our foliations (2.2) the genus is generic.

Next, we will see that if one expects to obtain a rich dynamics of a birational map preserving a foliation $\{C_h\}$, where C_h are irreducible curves, then one has to restrict attention to those maps that preserve foliations of generic genus 0 or 1, because any

birational map F preserving a foliation of generic genus greater or equal than 2 is a globally periodic map, that is, there exists $p \in \mathbb{N}$ such that $F^p(x, y) = (x, y)$ for all (x, y) where F is defined. This fact is a consequence of the following two classical results.

Theorem 2.1 (Montgomery, [42]) *Any pointwise periodic homeomorphism in a connected metric space, locally homeomorphic to $\mathbb{R}^n$, is globally periodic.*

The next one is an adaptation to our context of the Hurwitz automorphisms theorem which states that any compact Riemann surface with genus $g > 1$ admits at most $84(g - 1)$ conformal automorphisms, that is, homeomorphisms of the surface onto itself which preserve the local structure; see [21, 22]. In our context, Hurwitz's theorem can be stated as follows, [33]:

Theorem 2.2 (Hurwitz, 1893) *The group of birational maps on a nonsingular algebraic curve of genus $g > 1$ is finite, and of order less or equal than $84(g - 1)$.*

The above result states that any birational map preserving *a particular* nonsingular curve of genus $g \geq 2$ must be periodic (on the curve) with a period bounded by $84(g - 1)$.

Corollary 2.3 ([20]) *A birational map in $\mathcal{U} \subseteq \mathbb{K}^2$ (where $\mathbb{K}$ can be either $\mathbb{R}$ or $\mathbb{C}$) preserving a foliation of nonsingular curves $\{C_h\} \subseteq \mathcal{U}$ that have generic genus $g > 1$, must be globally periodic.*

Proof If the foliation $\{C_h\}$ has generic genus $g > 1$, then there exists an open set $\mathcal{V} \subseteq \mathcal{U}$ foliated by curves of genus g. By Hurwitz's theorem on each of these curves the map must be periodic, so F is pointwise periodic on $\mathcal{V}$. Therefore, by Montgomery's theorem, F must be globally periodic on the whole $\mathcal{V}$. Since F is rational, and so the global periodicity is characterized by some formal polynomial identities, then it must be periodic on the whole $\mathbb{K}^2$ except at the points where its iterates are not well-defined. □

In summary, from a dynamic viewpoint it makes sense to restrict our attention to birational maps preserving foliations of algebraic curves with genus 0 or 1.

2.3 The Elliptic Case: Dynamics on Invariant Curves Through Its Group Structure

In this chapter, we will concentrate our attention on those birational maps that preserve a foliation of algebraic curves $\{C_h\}$ of generic genus 1. Recall that a projective algebraic curve of genus 1 is called an *elliptic curve*. Any elliptic curve has an associated group structure [34, 50, 51]. In this section, we will see that in the case that $\{C_h\}$ is generically given by elliptic curves, then the group structure of the elliptic foliation characterizes the dynamics of any birational map preserving it.

First, we recall the group structure associated with an elliptic curve $C \in \mathbb{C}\mathbf{P}^2$, the so called *chord-tangent group* law. Given two points P and Q in C, we define the addition $P + Q$ in the following way:

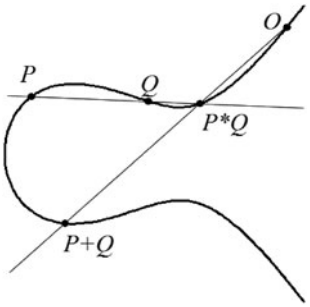

Fig. 2.1 Group law with an affine neutral element $\mathcal{O}$

1. Select a point $\mathcal{O} \in C$ to be the neutral element of the inner addition.
2. Take the chord passing through P and Q (the tangent line if $P = Q$). It will always intersect C at a unique third point denoted by $P * Q$. This is because the curves of genus 1 are birationally homeomorphic to *smooth cubic* curves, [50, Proposition 3.1].
3. The point $P + Q$ is then defined as $\mathcal{O} * (P * Q)$, see Fig. 2.1.

The curve endowed with this inner addition $(C, +, \mathcal{O})$ is an *abelian group* [51].

A brief comment on notation: typically algebraic curves are defined on $\mathbb{K}^2$, or on $\mathbb{K}P^2$, where $\mathbb{K}$ is the field of coefficients. In this chapter, this field will be mainly $\mathbb{R}$ or $\mathbb{C}$ (or $\mathbb{Q}$ in Sect. 2.6). The notation $C(\mathbb{K})$ or $C/\mathbb{K}$ denotes an elliptic curve C which has at least one point $\mathcal{O}$ with coordinates in $\mathbb{K}$. In this chapter, unless we explicitly state the contrary, we will assume that C stands for a *real* curve.

The relationship between the dynamics of a birational map preserving an elliptic curve and its group structure is given by the following adaptation of a result of Jogia et al. [33, Theorem 3], that will be referred as the *JRV theorem* from now on. In [33], the result is stated for birational maps leaving invariant an elliptic curve expressed in a certain Weierstrass normal form (see [34, 50] but especially [51, Sect. I.3]). This adaptation is immediately obtained by using the isomorphism with this normal form.

Theorem 2.4 (Jogia et al. [33]) *Let F be a birational map over a field $\mathbb{K}$, not of characteristic 2 or 3, that preserves an elliptic curve $C(\mathbb{K})$. Then, there exists a point $Q \in C(\mathbb{K})$ such that the map can be expressed in terms of the group law $+$ on $C(\mathbb{K})$ as either*

(i) $F_{|C(\mathbb{K})} : P \mapsto P + Q$, *or*
(ii) $F_{|C(\mathbb{K})} : P \mapsto i(P) + Q$, *where i is an automorphism of possible order (period) 2, 4, 3 or 6, and the map F has the same order (period) as i.*

We will give an easier dynamical interpretation of the above result, but first we will illustrate it.

Example 2.2 The Lyness curves $\widetilde{C_h} := \{(x+z)(y+z)(x+y+az) - hxyz = 0\} \subset \mathbb{C}\mathbf{P}^2$, are elliptic except for $h \in \{0, a-1, h_c^{\pm}\}$, where

$$h_c^{\pm} := \frac{2a^2 + 10a - 1 \pm (4a+1)\sqrt{4a+1}}{2a}. \tag{2.6}$$

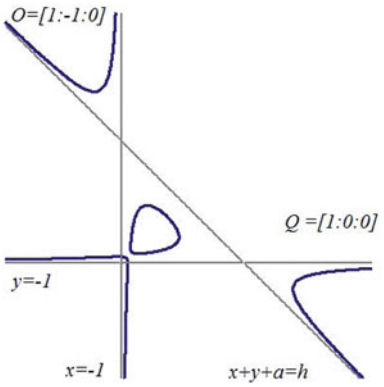

Fig. 2.2 A typical real Lyness curve $C_h = \{(x+1)(y+1)(x+y+a) - hxy = 0\}$, for $h > h_c^+$. Adding the infinite points $[1:0:0]$, $[0:1:0]$, $[1:-1:0]$, the displayed curve is isomorphic to $\mathbb{S}^1 \times \mathbb{Z}/(2)$

An interesting fact is that for all values of h the curves $\widetilde{C_h}$ contain the infinity points $[1:0:0]$, $[0:1:0]$, $[1:-1:0]$, see Fig. 2.2. An straightforward computation (or a geometrical interpretation) shows that, setting $\mathcal{O} := [1:-1:0]$, for any elliptic level h the map $\widetilde{F}_a([x:y:z]) = [xy : az^2 + yz : xz]$ can be written as:

$$\widetilde{F}_{a|\widetilde{C_h}}([x:y:z]) = [x:y:z] + [1:0:0]. \tag{2.7}$$

The nonelliptic levels correspond to curves of genus 0, and on those levels the map $\widetilde{F}_{a|\widetilde{C_h}}$ is conjugate to a Möbius transformation, see [29, Sect. 3.1].

The JRV theorem (Theorem 2.4) has the following dynamical interpretations given in Corollaries 2.5 and 2.7 below.

Corollary 2.5 *Let F be a birational map preserving a real foliation of algebraic curves $\{C_h\} \subset \mathcal{U} \in \mathbb{R}^2$ of generic genus 1. Then, on each invariant elliptic curve C_h, either F or F^2 are conjugate to a rotation.*

The above corollary is a direct consequence of Theorem 2.4 and the following result (a direct consequence of Corollary 2.3.1 in Chapter V.2 of [49]), based on the fact that every real elliptic curve (adding, if necessary, some infinite points in the real projective space) can be seen as either one or two closed simple curves, and that the inner sum can be easily represented as the usual Lie group operation of $\mathbb{S}^1$ or $\mathbb{S}^1 \times \mathbb{Z}/(2)$.

Proposition 2.6 *There is a continuous isomorphism between any nonsingular elliptic curve $(C(\mathbb{R}), +, \mathcal{O})$ and either the Lie group $\mathbb{S}^1 \times \mathbb{Z}/(2) = \{e^{it} : t \in [0, 2\pi)\} \times \{1, -1\}$ if $\Delta(C) > 0$, or $\mathbb{S}^1 = \{e^{it} : t \in [0, 2\pi)\}$ if $\Delta(C) < 0$, with the operation in $\mathbb{S}^1$ being given by $u \cdot z = uz$, where $\Delta(C)$ is the discriminant of the Weierstrass equation associated to $C(\mathbb{R})$.*

Observe that if F is a birational map preserving an elliptic curve $(C, +, \mathcal{O})$ whose dynamics corresponds to case (ii) of Theorem 2.4, then all the points in C give rise to periodic orbits. If the dynamics corresponds to case (i), then $F^n_{|C}(P) = P + n\,Q$, and we observe that P gives rise to a p-periodic orbit if and only if

$$p\,Q = \mathcal{O}. \tag{2.8}$$

In other words, in case (i) of Theorem 2.4 the curve is filled by periodic orbits of F if and only if Q is a *finite order* point of the group $(C, +, \mathcal{O})$, also called a *torsion* point (the torsion of a group G, denoted by $\mathrm{Tor}(G)$ is the set of its finite order elements). The following result characterizes the dynamics of birational maps on particular elliptic curves.

Corollary 2.7 *Let F be a birational map preserving a real elliptic curve $(C(\mathbb{R}), +, \mathcal{O})$, named C from now on, such that its dynamics is given by $F_{|C}(P) = P + Q$, where $Q \in C$. Then*

(i) If $Q \in \mathrm{Tor}(C)$, then all the orbits in C are periodic.
(ii) If $Q \notin \mathrm{Tor}(C)$, then the orbits of F fill densely the connected components of C.

2.4 Global Dynamics on Elliptic Foliations.

The JRV theorem ensures that the action of a birational map on a particular elliptic curve is linear. However, the behavior in the whole phase plane is a little bit more complex. The typical situation occurs when there is a dense set of curves filled by p-periodic orbits of all the periods $p \geq p_0 \in \mathbb{N}$, for some integer p_0. This integer p_0 is sometimes computable if the rotation set $\{\theta(h),\ h \in \mathrm{Im}(V)\}$ is known. In this section, we describe the reason for this behavior and we give an example of how to compute the set of periods of a particular map. We also will see that if a particular subinterval I in the rotation set is known, then it is possible to construct a number P such that the map F contains at least all the periods $p > P$.

2.4.1 The Rotation Number Function and Its Nature

2.4.1.1 Piecewise Continuity

From this point, we will assume that the invariant foliation of irreducible curves $\{C_h\}$ obtained from (2.2) is given by *real* curves which are generically elliptic. Also we will assume that F preserves each connected component of the invariant real elliptic curves (on the contrary, we can study F^2). Finally, we will also assume that the action of our birational maps F falls within case (i) of Theorem 2.4. Under these assumptions, Corollary 2.5 ensures that on each curve C_h the map F is conjugate to a rotation. So, we can consider a *rotation number* $\theta(h)$ associated to each level set h, or equivalently to each curve C_h.

Of course this rotation number function $\theta(h)$ can be constant. In this case, we say that the map F is *rigid*. For instance, if $a = 1$ then the Lyness map F_1 is globally five-periodic, thus $\theta(h) = 1/5$ for all $h \in \mathrm{Im}(V)$, where V is given in (2.4).

If $\theta(h)$ is not constant then it is possible to prove that this rotation number function is piecewise continuous. This is because when the irreducible components of (2.2) are generically elliptic, any birational map F (or F^2) can be thought as a family of

homeomorphisms in the circle, which is piecewise continuous in the parameter h. By using the fact that the rotation number function of a continuous family of maps of $\mathbb{S}^1$ (in the $\mathcal{C}^0$ topology) is continuous, and taking into account that, in principle, there could be levels $h \in \mathrm{Im}(V)$ corresponding to curves in the *forbidden set* of F, the piecewise continuity of $\theta(h)$ is achieved.

2.4.1.2 Piecewise Analyticity and Existence of Lie Symmetries

In fact, $\theta(h)$ is a piecewise analytic function in the domain $h \in \mathrm{Im}(V)$. This is because if the irreducible curves C_h in (2.2) are generically elliptic, then it is possible to construct an isomorphism (piecewise analytic in h) between them and a new foliation of Weierstrass curves, so that the corresponding associated map F_W defined on this foliation has the same rotation number function as F. These Weierstrass curves can be parameterized using the Weierstrass $\wp$ function (see [34, 50], and also [26, 53]). Using this parametrization, and the fact that $\wp$ satisfies a certain differential equation, it is always possible to give an integral expression of the rotation number function, from which the piecewise analyticity of it can be deduced. This approach has been introduced in [28] (and later developed in [4]) to study the rotation number function associated to a Lyness map, and has been successfully applied to study the periods of other birational maps in the successive papers of Bastien and Rogalski, and others [5–9].

An alternative proof of the piecewise analyticity of $\theta(h)$ comes from the fact that if the invariant curves C_h in (2.2) are generically elliptic, then it is possible to construct a vector field X such that the map F can be seen as the flow of this vector field at certain time $\tau(h)$. Such a vector field is called a *Lie Symmetry* of F. A Lie Symmetry of a map F in $\mathbb{R}^n$ is a *vector field* X such that F maps any orbit of the differential system

$$\dot{\boldsymbol{x}} = X(\boldsymbol{x}), \boldsymbol{x} \in \mathbb{R}^n \tag{2.9}$$

into another orbit of the system.

The existence of Lie Symmetries is an important issue in the theory of discrete integrability, see for instance [31]. From a dynamical viewpoint, this importance is clear in the case of integrable diffeomorphisms. In this case, the dynamics of the maps are in practice one-dimensional, and the existence of a Lie Symmetry whose orbits are preserved by F implies that this one-dimensional dynamics is linear on each orbit. The next results illustrate this fact.

Theorem 2.8 ([16]) *Let $F : \mathcal{U} \subseteq \mathbb{R}^n \to \mathcal{U}$ be a diffeomorphism having a Lie symmetry X, and let γ be an orbit of X, preserved by F (i.e., $F : \gamma \to \gamma$). Then the dynamics of F restricted to γ is either: (1) conjugate to a rotation with rotation number given by τ/T, where T is the period of γ and τ is defined by the equation $F(p) = \varphi(\tau, p)$, where φ denotes the flow of X; or (2) conjugate to a translation of the line; or (3) it is constant; according to whether γ is homeomorphic to $\mathbb{S}^1$, $\mathbb{R}$, or a point, respectively.*

If F is an integrable map and it possesses a Lie Symmetry X, this vector field is also integrable and shares the same first integral with F. However, in our case the curves in (2.2) would also be integral curves of any possible symmetry X. Since each connected component C_h of any curve in (2.2) is diffeomorphic to $\mathbb{S}^1$ (adding, possibly some infinite points), it is a periodic orbit of X (or a compactification of X) with period $T(h)$, see also [13]. Hence, Theorem 2.8 guarantees that

$$\theta(h) = \frac{\tau(h)}{T(h)}. \tag{2.10}$$

The regularity of the rotation number function is, then, a consequence of the regularity of the flow of X.

Again, the existence of the Lie Symmetry of a birational map preserving an elliptic foliation can be proved using the associated Weierstrass foliation associated to curve C_h, see [26, Sect. 2.6.3]. The Lie Symmetry approach was used to study the rotation number function of the Lyness map and to prove a conjecture about its monotonicity established by Zeeman [54]. This was done by Beukers and Cushman in the relevant paper [10]. This approach has been also applied to study the rotation number function and the set of periods of the extension of the Lyness map in $\mathbb{R}^3$ [15], and also to study a birational integrable map arising in the study of 2-periodic Gumovski-Mira type maps [18].

2.4.2 An Infinite Number of Periods

Taking into account the above considerations, we can prove the following result:

Proposition 2.9 *A birational map F preserving a generically real elliptic foliation $\{C_h\}$ is either rigid, or there are an infinite number of possible periods and a dense set of curves in the phase space filled with periodic orbits.*

Proof Let $\mathcal{E} = \{h$ such that the curves C_h are elliptic$\}$. From the JRV theorem on each the curve C_h with $h \in \mathcal{E}$ the map F (or F^2) is conjugate to a rotation. From the considerations in Sect. 2.4.1 (see also [26, Lemma 8.1.5]) the rotation number function $\theta(h)$ is piecewise continuous for $h \in \mathcal{E}$.

Since $\{C_h\}$ is generically elliptic, if F is not rigid, then there exists a nonempty open interval I such that $I \subseteq \{\text{Image}(\theta(h)), h \in \mathcal{E}\}$. Then, for any irreducible fraction $q/p \in I$, there exists a value of $h \in \mathcal{E}$ such that $\theta(h) = q/p$, hence an invariant real elliptic curve C_h which is full of periodic orbits of of minimal period p. □

2.4.3 Toward a Constructive Characterization of the Set of Periods

It is interesting to notice that if a rotation interval I containing some of the values of $\theta(h)$ is known, then it is always possible to compute a value P such that $q/p \in I$ for

all $p > P$, hence characterizing at least an infinite number of periods in the set of periods of F. One tool to construct a (nonoptimal) number P is the following result.

Lemma 2.1 ([15]) *Consider an open interval (c, d) with $0 \leq c < d$; denote by $p_1 = 2, p_2 = 3, p_3, \ldots, p_n, \ldots$ the set of all the prime numbers, ordered following the usual order. Also consider the following natural numbers:*

- *Let p_{m+1} be the smallest prime number satisfying that $p_{m+1} > \max(3/(d-c), 2)$*
- *Given any prime number p_n, $1 \leq n \leq m$, let s_n be the smallest natural number such that $p_n^{s_n} > 4/(d-c)$*
- *Set $P := p_1^{s_1-1} p_2^{s_2-1} \cdots p_m^{s_m-1}$.*

Then, for any $r > P$ there exists an irreducible fraction q/r such that $q/r \in (c, d)$.

In the Example 2.3, we will illustrate how to apply the above result and the known facts on the rotation number function to compute effectively some set of minimal periods appearing in a particular Lyness map F_a. Prior to stating this example we recall some basic facts. When $a > 0$ the first integral of F_a, given in (2.4), has a global minimum in $Q^+ := \{(x, y), x, y > 0\}$, located at the fixed point of F_a, given by (x_c, x_c) where $x_c = (1 + \sqrt{1+4a})/2$. This minimum corresponds to the nonelliptic level $h_c = (x_c + 1)^3/x_c$. With respect to the rotation number function, it is known that for $a > 0$

$$\theta_c = \lim_{h \to h_c^+} \theta(h) = \frac{1}{2\pi} \arccos\left(\frac{1}{1+\sqrt{1+4a}}\right),$$

see [4, 54]. Also it was conjectured in [54], and proved in [10], that when $0 < a < 1$, then $\theta(h)$ is a strictly increasing continuous function in (h_c, ∞) and strictly decreasing when $1 < a < \infty$. Moreover, in [4] it was proved (strongly using the elliptic nature of the Lyness curves) that

$$\lim_{h_c \to \infty} \theta(h) = \frac{1}{5}.$$

The case $a = 1$ corresponds to the globally five-periodic case with $\theta(h) \equiv 1/5$.

In summary, the interval

$$I^+ := (\min(\theta_c, 1/5), \max(\theta_c, 1/5))$$

gives the optimal rotation interval for the orbits in Q^+ when $a > 0$ and $a \neq 1$.

Example 2.3 When $a = 10$, the optimal rotation interval for the orbits in Q^+ is

$$I^+ := \left(\frac{1}{5}, \frac{1}{2\pi} \arccos\left(\frac{1}{1+\sqrt{41}}\right)\right).$$

Using the notation introduced in Lemma 2.1 we have $m = 27$, and $p_1 = 2$, $s_1 = 7$; $p_2 = 3$, $s_2 = 4$; $p_3 = 5$, $s_3 = 2$; $p_4 = 7$, $s_4 = 2$; $p_5 = 11$, $s_5 = 2$; $p_6 = 13$, $s_6 = 1$; $p_7 = 17$, $s_7 = 1$; ... ; $p_{27} = 103$, $s_{27} = 1$. Hence

$$P := \prod_{n=1}^{27} p_n^{s_n} = 7978311698661687899369097357894592832915294400 0,$$

and therefore there are r-periodic orbits of F_{10} for any $r > P$. Of course, using a finite algorithm one could check for any $r \leq P$ if there exist an irreducible fraction $q/r \in I^+$, obtaining in principle the forbidden denominators in I^+, but in practice the high value of P makes this observation useless.

Notice, however, that a computation (that takes 1.03 s using Maple 17 code on an Intel Core i5-3210M CPU at 2.50 GHz) gives that the numbers $S = \{2, 3, 4, 5, 6, 7, 8, 10, 11, 12, 13, 15, 16, 17, 18, 20, 21, 25, 26, 27, 28, 30, 35, 36, 38, 42, 45, 46, 48, 56, 66, 70, 72, 96, 98, 120, 126\}$ are *some* forbidden periods. It can be proved, using an alternative method that this is the *exact* set of forbidden periods, see Remark 2.2.

Another approach is the one introduced in [4] based on the following result (see also Remark 2.1 below)

Lemma 2.2 (**Bastien and Rogalski**) *Consider an open interval* (c, d) *with* $0 \leq c < d$. *Set*

$$f(x) = \frac{dx - 1}{\ln(dx - 1)} - \frac{cx}{\ln(cx)}\left(1 + \frac{3}{2\ln(cx)}\right) - 1.38402\frac{\ln(x)}{\ln(\ln(x))} - 1.$$

Then, for any $p \in \mathbb{N}$, $p \geq 17$ *such that* $f(p) > 0$ *there exists* $q \in \mathbb{N}$ *coprime with* p *such that* $c < q/p < d$.

Proof Let $\pi(x)$ be the prime-counting function, which gives the number of prime numbers which are less or equal than x. Using Theorem 1 and Corollary 1 of [47] we have that if $x \geq 17$

$$\frac{x}{\ln(x)} \leq \pi(x) \leq \frac{x}{\ln(x)}\left(1 + \frac{3}{2\ln(x)}\right). \tag{2.11}$$

So, given a number $p \in \mathbb{N}$, $p \geq 17$, we can estimate that the number of integer numbers q such that $cp < q < dp$ is at least the number of prime numbers in this interval which is, using the inequalities (2.11), at least

$$\frac{dp - 1}{\ln(dp - 1)} - \frac{cp}{\ln(cp)}\left(1 + \frac{3}{2\ln(cp)}\right). \tag{2.12}$$

Since we are interested in those values of q which are coprime with p, we should subtract from (2.12) the number of divisors of p, denoted by $\omega(p)$, which is bounded by

$$\omega(p) \leq 1.38402\frac{\ln(p)}{\ln(\ln(p))}, \text{ for} p \geq 3,$$

(see [46, Theorem 11]). So the number of integer numbers q coprime with p in (c, d) is at least

$$\frac{dp-1}{\ln(dp-1)} - \frac{cp}{\ln(cp)}\left(1+\frac{3}{2\ln(cp)}\right) - 1.38402\frac{\ln(p)}{\ln(\ln(p))}.$$

Clearly if the above number is greater than one (i.e., $f(p) > 0$), then p is a possible denominator in (c, d). □

The methodology summarized in Lemma 2.2 was introduced in [4] (see also [28, Sect. 6]), to study the set of periods for the whole family of Lyness' maps with $a \geq 0$ in Q^+ [4, Theorem 4] (see also [54, Theorem 9]). The familiar set of periods is 5, 6, 9, 11, 13, 14, 16, 17, 19 and all integers ≥ 21 except 42. Other periods appear when negative initial conditions are considered [29].

Remark 2.1 (Added in proof) Lemma 2.2 has been recently improved by Bastien and Rogalski. See [8, Proposition 23], which states that if $0 < c < d < 1/2$ then for every $p > \max\left(e^{2.55|\ln(c)|/(d-c)}, \frac{1}{c}e^{3.82/(d-c)}\right)$, there exists a prime number q with $(p, q) = 1$ such that $q/p \in (c, d)$.

Remark 2.2 With respect to the particular case studied in Example 2.3, setting $c = 1/5$ and $d = \arccos(1/(1+\sqrt{41}))/(2\pi)$, and by proving that for all $x > 6 \cdot 10^5$ the function $f(x)$ in Lemma 2.2 is positive, one would get that the set of periods of F_{10} in Q^+ contains all periods greater than $6 \cdot 10^5$. An straightforward computation (that takes 1444.23 s with the same software and CPU as in Example 2.3) gives that every integer number $r < 6 \cdot 10^5$ such that $r \notin S$ is a possible denominator in I^+. Thus, $\mathbb{N} \setminus S$ would be the complete set of periods of F_{10} in Q^+.

2.5 An Application: The Locus of Periodic Orbits

In this section, as a straightforward application of the characterization of the periodic orbits given by Eq. (2.8), we will use it to address the problem of finding the location of the curves having periodic orbits with a prescribed period. Following the aim of the notes, again we will take the Lyness maps as a paradigmatic example. This approach was used in [4] for studying Lyness' maps and, of course, can be used to study other birational maps on elliptic foliations [9].

As mentioned above, the real Lyness curves $C_h = \{(x+1)(y+1)(x+y+a) - hxy = 0\} \subset \mathbb{R}^2$ are elliptic curves except for $h \in \{0, a-1, h_c^{\pm}\}$, where $h_c^{\pm}$ are given in (2.6), and together with the infinity points $[1:0:0]$, $[0:1:0]$, $[1:-1:0]$ are isomorphic to either $\mathbb{S}^1$ or $\mathbb{S}^1 \times \mathbb{Z}/(2)$. Setting $\mathcal{O} := [1:-1:0]$, for all elliptic levels h, the dynamics on each real connected component of the Lyness' map (2.3) is

$$F_{a|C_h}([x:y:1]) = [x:y:1] + [1:0:0].$$

Hence, the characterization of the p-periodic orbits given by Eq. (2.8), implies a curve C_h will be full of periodic orbits if and only if

$$p \cdot [1:0:0] = [1:-1:0]. \tag{2.13}$$

Equation (2.13) gives a naive way for finding the locus of the periodic orbits of a prescribed period in the elliptic levels, obtaining the following result which is, in fact, the summary of well-known ones (see [3, 4] and [54] among other references).

Proposition 2.10 *Consider the real elliptic Lyness curves* $C_{h_p} = \{(x+1)(y+1)(x+y+a) - h_p\, xy = 0\}$, *then the following statements hold:*

(i) The maps F_0 *and* F_1 *are globally periodic with periods* 6 *and* 5, *respectively.*
(ii) If $a(a-1) \neq 0$ *then there are no elliptic curves* C_{h_p} *with periodic orbits of the Lyness maps* F_a *with period* $p = 1, 2, 3, 4, 5,$ *and* 6.
(iii) If $a(a-1) \neq 0$ *the elliptic curves* C_{h_p} *filled with periodic orbits of the Lyness maps* F_a *with periods* $p = 7, 8, 9, 10, 11,$ *and* 12 *are given by:*

$$\begin{aligned}
h_7 &= (a-1)/a,\\
h_8 &= -(a-1)^2/a,\\
h_9 &= (a-1)(a^2-a+1)/a,\\
h_{10} &= (a-1)/(a(a+1)),\\
h_{11} &= (a-1)\left(2a-1 \pm \sqrt{4a^3-4a^2+1}\right)/(2a^2), \text{ for } a > a_*,\\
h_{12} &= (a-1)\left(-a+3 \pm \sqrt{-3a^2+2a+1}\right)/(2a) \text{ for } a \in [-1/3, 1],
\end{aligned}$$

where $a_* \simeq -0.41964$ *is the only real root of* $4a^3 - 4a^2 + 1$.

Proof (i) Setting $Q = [1:0:0]$, using the inner addition rules of $(C_h(\mathbb{R}), +, [1:-1:0])$, and using that the infinite points $[1:0:0]$, $[0:1:0]$ and $[1:-1:0]$ are tangent to the asymptotes of C_h given by $y = -1$, $x = -1$ and $x + y + a - h = 0$ respectively, some straightforward computations[2] show that if $a = 0$ then

$$\begin{aligned}
&Q * Q = [0:-1:1] \Rightarrow 2Q := [0:-1:1] * \mathcal{O} = [-1:0:1];\\
&2Q * Q = [0:0:1] \Rightarrow 3Q := [0:0:1] * \mathcal{O} = [0:0:1];\\
&3Q * Q = [-1:0:1] = 2Q \Rightarrow 4Q := 2Q * \mathcal{O} = [0:-1:1];\\
&4Q * Q = Q \Rightarrow 5Q := Q * \mathcal{O} = [0:1:0] \text{ and finally,}\\
&5Q * Q = \mathcal{O} \Rightarrow 6Q := \mathcal{O} * \mathcal{O} = \mathcal{O}.
\end{aligned}$$

Therefore, we reobtain the well-known fact that the Lyness map F_0 is globally six-periodic.

If $a = 1$, then

$$Q * Q = [0:-1:1] \Rightarrow 2Q := [0:-1:1] * \mathcal{O} = [-1:0:1];$$

[2] Notice that the above computations can be done by using that $Q * Q$ is obtained by substituting $y = -1$ into the expression of C_h, and in general $[x_0 : y_0 : 1] * Q$ is obtained by substituting $y = y_0$ at the expression of C_h, and using also that $[x : y : z] * \mathcal{O} = [y : x : z]$ because of the symmetry of C_h with respect to $y = x$.

$$2Q * Q = 2Q \Rightarrow 3Q := 2Q * \mathcal{O} = [0 : -1 : 1];$$
$$3Q * Q = Q \Rightarrow 4Q := Q * \mathcal{O} = [0 : 1 : 0] \text{ and finally,}$$
$$4Q * Q = \mathcal{O} \Rightarrow 5Q := \mathcal{O} * \mathcal{O} = \mathcal{O},$$

so the map F_1 is globally five-periodic.

(i) and (iii) Now we assume that $a(a-1) \neq 0$ and we apply formally the addition rules obtaining that: $2Q = [-1 : 0 : 1]$; $3Q = [0 : -a : 1]$;

$$4Q = \left[-a : \frac{ah - a + 1}{a - 1} : 1\right]; \; 5Q = \left[\frac{ah - a + 1}{a - 1} : \frac{-a^2 - ah + 2a - 1}{a(a-1)} : 1\right];$$
$$6Q = \left[\frac{-a^2 - ah + 2a - 1}{a(a-1)} : \frac{a^3 - 2a^2 - ah + 2a - 1}{a(ah - a + 1)} : 1\right],$$
$$7Q = \left[\frac{a^3 - 2a^2 - ah + 2a - 1}{a(ah - a + 1)} : -\frac{(a-1)^2\left(a^2h + ah - a + 1\right)}{\left(a^2 + ah - 2a + 1\right)(ah - a + 1)} : 1\right],$$

(notice that there is a misprint in the expression of the first component of $7Q$ given in [29]). Hence, from Eq. (2.13), it is easy to see that there are no periodic orbits on the elliptic levels for $p = 1, 2, 3, 4$ and, assuming $a(a-1) \neq 0$, for $p = 5$ and 6.

Observe that $7Q$ can only be an infinite point if either $a^2 + ah - 2a + 1 = 0$ or $ah - a + 1 = 0$. The first case trivially gives that $7Q \neq \mathcal{O}$, and the second case directly gives that $7Q = [a(a-1)^3 : -a(a-1)^3 : 0] = \mathcal{O}$, thus

$$h_7 := \frac{a-1}{a}.$$

To obtain the other periods a simple way is to impose the relations $4Q = -4Q$ (period 8); $4Q = -5Q$ (period 9); $5Q = -5Q$ (period 10); $6Q = -5Q$ (period 11); and $7Q = -5Q$ (period 12). The points $-nQ$ are easily obtained from the points nQ because given a point P in a Lyness curve, it is straightforward to see that $-P$ is just the symmetric point with respect to $y = x$. So $-Q = [0 : 1 : 0]$; $-2Q = [0 : -1 : 1]$; $-3Q = [-a : 0 : 1]$;

$$-4Q = \left[\frac{ah - a + 1}{a - 1} : -a : 1\right]; \text{ and}$$
$$-5Q = \left[\frac{-a^2 - ah + 2a - 1}{a(a-1)} : \frac{ah - a + 1}{a - 1} : 1\right].$$

To obtain the elliptic curves containing nine-periodic orbits, we impose that $4Q = -5Q$, obtaining that $-a = (-a^2 - ah + 2a - 1)/(a(a-1))$. This equality yields

$$h_9 := \frac{(a-1)(a^2 - a + 1)}{a},$$

To get the elliptic levels with period 12 orbits, we impose that $7Q = -5Q$, obtaining

$$\begin{cases} \dfrac{a^3 - 2a^2 - ah + 2a - 1}{(ah - a + 1)\, a} = -\dfrac{a^2 + ah - 2a + 1}{a\,(a-1)}, \\ -\dfrac{(a-1)^2\left(a^2 h + ah - a + 1\right)}{\left(a^2 + ah - 2a + 1\right)(ah - a + 1)} = \dfrac{ah - a + 1}{a - 1}. \end{cases}$$

From these equations we obtain that h_{12} must be given by the roots of the polynomial $P(a,h) = a^2h^2 + a\,(a-1)\,(a-3)\,h + \left(a^2 - 2a + 2\right)(a-1)^2$, which gives the result. The other cases follow similarly. □

Finally, we remark that there are values of a for which the nonelliptic levels (which correspond to genus 0 curves) are filled by periodic orbits with periods 1, 2, and 3, [29, Lemma 5]. Finally, there are no Lyness maps with four-periodic orbits, although some authors consider that this period arises for the case $a = +\infty$, [54].

2.6 Rational Periodic Orbits

In this section, we will assume that F is a birational map with rational coefficients and with an invariant foliation (2.2) such that the polynomials $P(x,y) - hQ(x,y)$ are in $\mathbb{Q}[x,y]$, and $h \in \mathbb{Q}$. In this case, it makes sense to study the *rational orbits* of F. That is, orbits such that all the iterates have rational coordinates.

In the previous sections, we have seen the relationship between the dynamics of a birational map preserving an elliptic curve $C_h(\mathbb{R})$ and its group structure (Theorem 2.4 and Corollary 2.7). Under our new assumptions (F has rational coefficients) and assuming also that $\mathcal{O}$ has rational components, the rational orbits lie in the rational elliptic curves $C_h(\mathbb{Q})$ which is a subgroup of $C_h(\mathbb{R})$. In this case, the structure of each curve $C_h(\mathbb{Q})$ is characterized by the theorems of Mordell and Mazur, summarized below, and it will impose strong restrictions on the set of periods of rational orbits. Indeed, Mordell proved in 1922 that a rational elliptic curve is a finitely-generated abelian group, and in 1978 Mazur gave a description of its torsion term. The following result characterizes, therefore, the group structure of $C_h(\mathbb{Q})$.

Theorem 2.11 (Mazur, 1978) *If $\mathcal{E}$ is a nonsingular cubic, then $(\mathcal{E}(\mathbb{Q}), +)$ is a finitely-generated abelian group*

$$\mathcal{E}(\mathbb{Q}) \cong \mathbb{Z} \oplus \cdots \oplus \mathbb{Z} \oplus \mathrm{Tor}(\mathcal{E}),$$

where $\mathrm{Tor}(\mathcal{E})$ *is either the empty set; or* $\mathbb{Z}/p$ *where* p *is either* 1, 2, 3, 4, 5, 6, 7, 8, 9, 10, *or* 12*; or* $\mathbb{Z}/2 \oplus \mathbb{Z}/p$ *where* p *is* 2, 4, 6, *or* 8.

Recalling that by Corollary 2.7 on certain invariant elliptic curve $C_h(\mathbb{Q})$, there will be periodic orbits of a birational map F, if and only if the point Q of Theorem 2.4 is in $\mathrm{Tor}(C_h(\mathbb{Q}))$, we easily get that the only a priori allowed periods for rational orbits are the orders p described by the Mazur's theorem. Hence:

Corollary 2.12 *Any birational map preserving $C_h(\mathbb{Q})$ only can have, a priori, rational periodic orbits of periods* 1, 2, 3, 4, 5, 6, 7, 8, 9, 10, *or* 12.

2.6.1 Rational Periodic Orbits of the Lyness Maps

The study of the rational periodic orbits in the case of the Lyness maps and its relationship with the structure of rational points of elliptic curves can be traced back to the first papers that studied these maps from an algebraic geometric point of view [3, 4, 28, 54]. After these works it was known that for $a > 0$ and considering *positive initial conditions* only the rational periods 5 and 9 where possible. It was known that five-periodic orbits appear only when $a = 1$. However, the existence of rational nine-periodic orbits was not known, and it was left as an open problem in [4]. Their nonexistence was conjectured in [54]. Now, from [29] we know that all the Mazur periods, except 4, appear for rational orbits and $a \in \mathbb{Q}^+ \cup \{0\}$ (but the periods different from 5 and 9 are not located in $\mathbb{Q}^+ \times \mathbb{Q}^+$).

Theorem 2.13 ([29]) *For any $p \in \{1, 2, 3, 5, 6, 7, 8, 9, 10, 12\}$, there exist values of $a \in \mathbb{Q}^+ \cup \{0\}$ and rational initial conditions (x_0, x_1) giving rise to p-periodic orbits of the Lyness maps F_a. Moreover, these values of p are the only possible minimal periods for rational initial conditions and $a \in \mathbb{Q}$.*

With respect to period 9, indeed there are nine-periodic rational orbits of the Lyness maps F_a with $a \in \mathbb{Q}^+$ and initial conditions in $\mathbb{Q}^+ \times \mathbb{Q}^+$. For instance, take $a = 7$ and the initial condition $(3/2, 5/7)$. Furthermore, the next result shows that there are infinitely many positive rational values of the parameter a giving rise to nine-periodic positive rational orbits. We sketch the proof because it is constructive and because again the basic arithmetic on an elliptic curve (different from the Lyness ones) plays an essential role in the construction of the periodic orbits. See [29] for more details.

Theorem 2.14 ([29]) *There are infinitely many values $a \in \mathbb{Q}^+$ and initial conditions $x_0(a), x_1(a) \in \mathbb{Q}^+$ giving rise to nine-periodic orbits of the Lyness map F_a.*

Proof Using the characterization of the curve of nine-periodic orbits given in Proposition 2.10, it is easy to see that the proof of the result will follow if we find infinitely many points $(x, y, a) \in (\mathbb{Q}^+ \times \mathbb{Q}^+ \times \mathbb{Q}^+) \cap S_a$, where

$$\begin{aligned} S_a := \quad & \{(a; x, y) : a(x+1)(y+1)(x+y+a) \\ & -(a-1)(a^2-a+1)xy = 0,\ x > 0, y > 0, a > a_*\}, \end{aligned}$$

and $a_* \simeq 5.41147624$ is the infimum number a such that C_{h_9} has an oval in Q^+.

It can be proved that the points in S_a satisfying $x + y = 23/4$ are in an elliptic curve isomorphic to

$$\mathcal{E} := \left\{ Y^2 = X^3 - \frac{1288423179}{71639296} X + \frac{8775405707427}{303177500672} \right\}.$$

This fact is not obvious. To obtain the expression of the curve $\mathcal{E}$, some changes of variables are needed, and the extra condition $x + y = 23/4$ is imposed on the points of S_a. This condition is motivated by the fact that if $(x, y) \in S_a$ is such that $(x + y, xy) \in \mathbb{Q}^+ \times \mathbb{Q}^+$ and $\Delta := (x + y)^2 - 4xy$ is a perfect square, then

$(x, y) \in \mathbb{Q}^+ \times \mathbb{Q}^+$. The condition is found when trying to obtain a suitable expression of Δ that facilitates to find values of a for which Δ is a perfect square. The reader is referred to [29, Proof of Theorem 2] to obtain all the details.

By taking into account Proposition 2.6, it is easy to see that if we are able to find a rational point $R \in \mathcal{E}$, such that R is not in the torsion of $\mathcal{E}$, then $k\,R$ gives an infinite number of rational points in $\mathcal{E}$.

Observe that if the point $(x(R), y(R), a(R))$ corresponding to R is in the connected component of C_{h_9} in Q^+, then by recovering the values $(x(kR), y(kR), a(kR)) \in S_a$ corresponding to the points $k\,R \in \mathcal{E}$, we would get the result.

By using the software MAGMA [12], one can obtain the valid point $R = \left(\frac{18243}{8464}, \frac{81}{184}\right) \in \mathcal{E}$. □

2.6.2 A Digression on Numerics

A curious fact is that the numerical plots of the phase portrait of birational maps preserving an elliptic foliation typically contain very few periodic orbits (although sometimes it is possible to find traces of them). Bastien and Rogalski noticed this even when working with symbolic algebra software, [5]:

> If we wish to study possible periods with a computer, it is easier to work with rational numbers. So, we suppose that a is rational, and that the point (u_1, u_0) is rational. With the use of a computer and a program of calculation with fractions, is it possible to see periodic points? Only in few cases!

This is especially significant if one takes into account that Corollary 2.9 states that if a birational map preserving an elliptic foliation is not rigid, then the phase space is densely filled by invariant curves full of periodic orbits of an infinite number of periods. It is commonly thought that Mazur's theorem (in fact Corollary 2.12) is the real reason for the lack of periodic orbits in the numerical simulations, but there is not a rigorous proof of this fact.

A priori one could think, however, that the lack of periodic orbits in the numerical simulations should be a consequence of other factors, like the fact that the rotation number is a piecewise analytic function. But this is not the case as Example 2.4 shows.

Indeed, the piecewise analyticity of the rotation function indicates how far we are from the general situation in the context of diffeomorphisms. For orientable diffeomorphisms of the circle, the persistence of the rotation number is known to hold, [2, Theorem A] and [41] (see also [1]). However, there are diffeomorphisms with analytic rotation number for which it is easy to encounter periodic orbits when doing numerical simulations. This is the case, for instance, of proper Poncelet maps [17], such as the one shown in the next example.

Example 2.4 We consider the planar Poncelet map F associated to the ellipse $\gamma = \{x^2 + xy + y^2 - 1/5 = 0\}$, and the family of circles $\Gamma(h) = \{x^2 + y^2 - h = 0\}$, for $h > 2/5$ (observe that each curve $\Gamma(h)$ surrounds γ). The map F is the

diffeomorphism defined in $\mathcal{U} = \{(x, y) \in \mathbb{R}^2,\ x^2 + y^2 > 2/5\}$ in the following way: given any $p \in \Gamma(h)$ there are exactly two points q_1, q_2 in γ such that the lines $p\,q_1$, $p\,q_2$ are tangent to γ. On each curve $\Gamma(h)$ we define $F : \Gamma(h) \to \Gamma(h)$, associated to the pair as

$$F(p) = \overline{pq_1} \cap \Gamma(h),$$

where $p \in \Gamma(h)$, $\overline{pq_1} \cap \Gamma(h)$ is the first point in the set $\{\overline{pq_1} \cap \Gamma(h), \overline{pq_2} \cap \Gamma(h)\}$ that we find when, starting from p, we follow $\Gamma(h)$ counterclockwise (see Fig. 2.3c).

It can be shown that the map has an expression of the form

$$F(x, y) = \left(\frac{-N_1 N_2 - 4N_3\sqrt{\Delta}}{M}, \frac{-N_1 N_3 + 4N_2\sqrt{\Delta}}{M} \right),$$

where N_i, M, and Δ are large polynomials whose expression can be found in [17]. Observe that F is not a birational map. Additionally, the map F has the first integral $V(x, y) = x^2 + y^2$ defined in $\mathcal{U}$, and on each curve $\Gamma(h) = \{V = h\}$ the map is conjugate to a rotation with certain rotation number $\theta(h)$. This rotation function is analytic in the interval $(2/5, \infty)$ because F has the Lie Symmetry given by

$$X(x, y) = \sqrt{(x^2 + y^2)(x^2 + xy + y^2 - 1/5)} \left(-y\frac{\partial}{\partial x} + x\frac{\partial}{\partial y} \right),$$

so by Theorem 2.8 the rotation number can be obtained using Eq. (2.10). See [17] for proofs of all the above facts.

Now we show how some evidence of periodic orbits appears when considering a numerical experiment. This particular one is obtained after 5000 iterates by F from each initial condition in the set $\mathcal{I} = \{(x_j, 0) = (0.7 + (j - 1)/10, 0),\ j = 1, \ldots, 10\}$. As can be seen in Fig. 2.3a, there is a numerical evidence that the initial condition $(x_5, 0)$ is near to a 57-periodic orbit. After some approximations we locate the circle full of 57-periodic orbits close to the curve $x^2 + y^2 \simeq 1.2100099$ (for instance, by choosing $p_0 := (1.1000045, 0)$ and setting $p_n = F^n(p_0)$); we have that after 350 periods $|p_0 - p_{19950}| \simeq 0.003$. These iterates are depicted in Fig. 2.3b. In Fig. 2.3c, the construction of the 57-periodic orbit via the Poncelet process is shown.

2.7 Some Words on the Genus 0 Case

With respect to the global dynamics of birational maps preserving a genus 0 invariant foliation (2.2) no general results are known, although one should expect to have also a large number of curves with periodic orbits of arbitrary period, curves filled with dense solutions, as well as curves with one or two attractive and/or repulsive points. An example of what is expected to be found is given in the first example of [5]. We are now working on this problem together with M. Llorens.

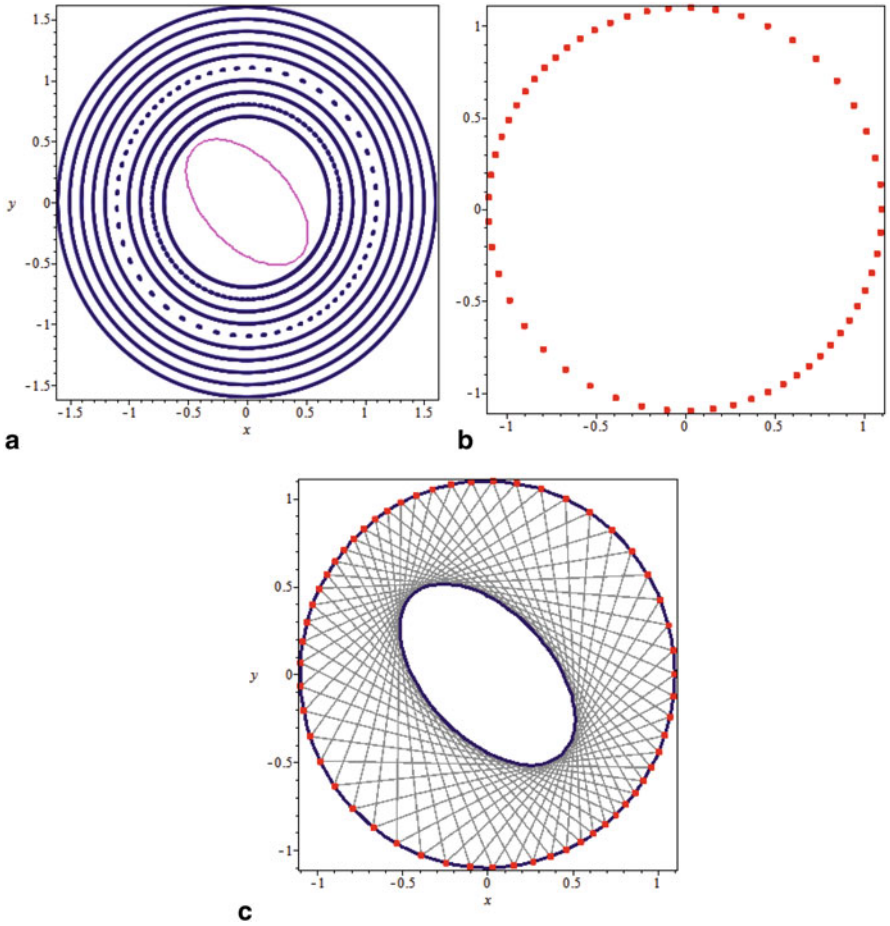

Fig. 2.3 (**a**) 5000 iterates of F with the grid of initial conditions $\mathcal{I}$. (**b**) 19, 950 iterates with initial condition $(1.1000045, 0)$. (**c**) The Poncelet's construction of the 57-periodic orbit

Acknowledgement The first author is partially supported by the FEDER-Ministry of Economy and Competitiveness of the Spanish Government through grants MTM2010-15831, MTM2010-20692, and MTM2012-38122-C03-01, and by grants 2009-SGR-1092 and 2014-SGR-634 from AGAUR, Generalitat de Catalunya. The second author is partially supported by the Ministry of Economy and Competitiveness of the Spanish Government through grant DPI2011-25822 and grants 2009-SGR-1228 and 2014-SGR-859 from AGAUR, Generalitat de Catalunya. The second author acknowledges Danièle Fournier-Prunaret and Ricardo López Ruiz for the opportunity to deliver a talk in the NOMA'13 conference. He also wants to acknowledge G. Bastien, A. Cima, A. Gasull, M. Rogalski, and X. Xarles for all that he has learned from them.

Appendix. The Lyness Map and Curves: A Bit More than an Academic Example.

The study of the Lyness map (2.3) has a long history. It started with the study of the five-cycle corresponding to the particular case $a = 1$ in the Lyness equation. According to Linero [36],

> It is precisely under this aspect that Lyness cycle appeared: in fact, Gauss obtained it when working in the spherical geometry of the *pentagrama mirificum*, a spherical pentagram formed by five successively orthogonal great-circle arcs. To see its construction and the relation with the 5-cycle, the reader can consult [23]. According to this paper, "This 5-cycle seems to have been transmitted in the form of mathematical gossip for a long time." The 5-cycle receives the name of Lyness cycle because R.C. Lyness accounted for it in a series of papers dealing with the existence of cycles (see [37–39] and also [32]). Surprisingly, the interest of Lyness was associated neither to dynamical systems nor difference equations, he found the equation while investigating a problem related to the number theory: to obtain three integer numbers such that the sum or the difference of any different pair of them is a square. The first time that the equation is referred to as the "Lyness equation" occurred in 1961, in [48].

The study of the Lyness map has attracted the attention of the dynamical systems community in the last years. Its dynamics is completely understood after the independent work done by Bastien and Rogalski [4] and Zeeman [54], and the work of Beukers and Cushman [10]. See also [3, 26, 28, 29].

The five-periodic Lyness map F_1 also plays a structural role when studying the group of symplectic birational transformations of the plane (i.e., birational transformations of $\mathbb{C}^2$ which preserve the differential form $\omega = dx \wedge dy/(xy)$), since this group is generated by compositions of the Lyness map F_1, a scaling, and a map of the form $(x, y) \to (x^a y^b, x^c y^d)$ where a, b, c, and d are such that the matrix

$$\begin{pmatrix} a & b \\ c & d \end{pmatrix} \in SL(2, \mathbb{Z}).$$

This result has been recently proved by Blanc in [11], and it was conjectured by Usnich in [52].

From the algebraic view point, it is also interesting to note that the Lyness curves are a universal normal form for most elliptic curves with a relatively easy form for the addition formula $n \cdot P$. Recall that the addition formula is useful for instance in Elliptic Curve Cryptography [35] and is generally complicated.

Theorem 2.15 (Lyness' Curves Normal Form, [29]) *The family of elliptic curves* $C_{a,h} = \{(x+1)(y+1)(x+y+a) - hxy = 0\}$ *over any field* $\mathbb{K}$ *(not of characteristic* 2 *or* 3*) together with the points* $\mathcal{O} = [1 : -1 : 0]$ *and* $Q = [1 : 0 : 0]$*, is the universal family of elliptic curves with a point of order* n*,* $n \geq 5$ *(including* $n = \infty$*).*

The above result states that for any elliptic curve $\mathcal{E}(\mathbb{K})$ with a point R of order $n \geq 5$, there exists some unique values $a_{(\mathcal{E},R)}, h_{(\mathcal{E},R)} \in \mathbb{K}$ and a unique isomorphism between $\mathcal{E}$ and $C_{a_{(\mathcal{E},R)},h_{(\mathcal{E},R)}}$ sending the neutral element of $\mathcal{E}$ to $\mathcal{O} = [1 : -1 : 0]$ and R to $Q = [1 : 0 : 0]$.

This also implies that the known results on elliptic curves with a point of order greater than 4 also holds in Lyness curves. In particular, we find the curves with high rank and prescribed torsion given in Dujella's site [27].

To prove the above result it is only needed to observe that any elliptic curve having a point R that is not a 2 or a 3 torsion point can be brought to the *Tate normal form*

$$Y^2Z + (1-c)XYZ - bYZ^2 = X^3 - bX^2Z.$$

where R is sent to $(0,0)$. But on the other hand the change of variables

$$X = bz, \quad Y = bc(y+z), \quad Z = c(x+y) + (c+1)z$$

and the relations

$$h = -\frac{b}{c^2}, \quad a = \frac{c^2+c-b}{c^2},$$

show that the curves $C_{a,h} = \{(x+z)(y+z)(x+y+az) - hxyz = 0\}$ and the Tate normal form are equivalent. Finally, observe that the case $c = 0$ corresponds to a curve with a 4-torsion point so, as seen in Sect. 2.5, it does not correspond to an elliptic Lyness curve.

References

1. Alsedà, Ll., Llibre, J., Misiurewicz, M.: Combinatorial Dynamics and Entropy in Dimension One. Word Scientific, Singapore (1993)
2. Bamon, R., Malta, I., Pacífico, M.J.: Changing rotation intervals of endomorphisms. Invent. Math. **83**, 257–264 (1986)
3. Barbeau, E., Gelbord, B., Tanny, S.: Periodicities of solutions of the generalized Lyness recursion. J. Differ. Equ. Appl. **1**, 291–306 (1995)
4. Bastien, G., Rogalski, M.: Global behavior of the solutions of Lyness' difference equation $u_{n+2}u_n = u_{n+1} + a$. J. Differ. Equ. Appl. **10**, 977–1003 (2004)
5. Bastien, G., Rogalski, M.: On some algebraic difference equations $u_{n+2}u_n = \psi(u_{n+1})$ in $\mathbb{R}^+$, related to families of conics or cubics: generalization of the Lyness' sequences. J. Math. Anal. Appl. **300**, 303–333 (2004)
6. Bastien, G., Rogalski, M.: On the algebraic difference equation $u_{n+2}u_n = \psi(u_{n+1})$ in $\mathbb{R}_*^+$ related to a family of elliptic quartics in the plane. Adv. Differ. Equ. **3**, 227–261 (2005)
7. Bastien, G., Rogalski, M.: On algebraic difference equations $u_{n+2}+u_n = \psi(u_{n+1})$ in **R** related to a family of elliptic quartics in the plane. J. Math. Anal. Appl. **326**, 822–844 (2007)
8. Bastien, G., Rogalski, M.: Periods of the solutions of a difference equation in $\mathbb{R}_*^+$ associated to a special QRT-map. Dyn. Contin. Discret. Impuls. Syst. **20**, 727–745 (2013)
9. Bastien, G., Mañosa, V., Rogalski, M.: On periodic solutions of 2-periodic Lyness difference equations. Int. J. Bifurc. Chaos **23**, 1350071 (18 pages) (2013)
10. Beukers, F., Cushman, R.: Zeeman's monotonicity conjecture. J. Differ. Equ. **143**, 191–200 (1998)
11. Blanc, J.: Symplectic birational transformations of the plane. Osaka J. Math. **50**, 573–590 (2013)
12. Bosma, W., Cannon, J.J., Fieker, C., Steel, A. (eds.): Handbook of Magma functions, Edition 2.16. http://magma.maths.usyd.edu.au/magma/handbook/ (2010). Accessed 9 Dec 2014

13. Cima, A., Mañosas, F.: Real dynamics of integrable birational maps. Qual. Theory Dyn. Syst. **10**, 247–275 (2011)
14. Cima, A., Zafar, S.: Integrability and algebraic entropy of k-periodic non-autonomous Lyness recurrences. J. Math. Anal. Appl. **413**, 20–34 (2014)
15. Cima, A., Gasull, A., Mañosa, V.: Dynamics of the third order Lyness difference equation. J. Differ. Equ. Appl. **13**, 855–884 (2007)
16. Cima, A., Gasull, A., Mañosa, V.: Studying discrete dynamical systems through differential equations. J. Differ. Equ. **244**, 630–648 (2008)
17. Cima, A., Gasull, A., Mañosa, V.: On Poncelet's maps. Comput. Math. Appl. **60**, 1457–1464 (2010)
18. Cima, A., Gasull, A., Mañosa, V.: Non-autonomous 2-periodic Gumovski-Mira difference equations. Int. J. Bifurc. Chaos **22**, 1250264 (14 pages) (2012)
19. Cima, A., Gasull, A., Mañosa, V.: Integrability and non-integrability of periodic non-autonomous Lyness recurrences. Dyn. Syst. **28**, 518–538 (2013)
20. Cima, A., Gasull, A., Mañosa, V., Mañosas, F.: Different approaches to the global periodicity problem. Preprint
21. Conder, M.: Hurwitz groups with given centre. Bull. Lond. Math. Soc. **34**, 725–728 (2002)
22. Conder, M.: An update on Hurwitz groups. Groups Complex. Cryptol. **2**, 35–49 (2010)
23. Coxeter, H.S.M.: Frieze patterns. Acta Arith. **XVIII**, 297–310 (1971)
24. Déserti, J.: Some properties of the Cremona group. Ens. Mat. **21**, 1–188 (2012)
25. Devaney, R.: An Introduction to Chaotic Dynamical Systems. Westview, Boulder (2003)
26. Duistermaat, J.J.: Discrete Integrable Systems: QRT Maps and Elliptic Surfaces. Springer, New York (2010)
27. Dujella, A.: Web page site "Infinite families of elliptic curves with high rank and prescribed torsion", University of Zagreb. http://web.math.pmf.unizg.hr/∼duje/tors/generic.html. Accessed 9 Dec 2014
28. Esch, J., Rogers, T.D.: The screensaver map: dynamics on elliptic curves arising from polygonal folding. Discret. Comput. Geom. **25**, 477–502 (2001)
29. Gasull, A., Mañosa, V., Xarles, X.: Rational periodic sequences for the Lyness equation. Discret. Contin. Dyn. Syst. A **32**, 587–604 (2012)
30. Gumovski, I., Mira, Ch.: Recurrences and Discrete Dynamic Systems. Lecture Notes in Mathematics, vol. 809. Springer, Berlin (1980)
31. Haggar, F., Byrnes, G.B., Quispel, G.R.W., Capel, H.W.: k–integrals and k–Lie symmetries in discrete dynamical systems. Physica A **233**, 379–394 (1996)
32. Howard Joint, W.: Note 1767. Cycles. Math. Gaz. **28**, 196–197 (1944)
33. Jogia, D., Roberts, J. A. G., Vivaldi, F.: An algebraic geometric approach to integrable maps of the plane. J. Phys. A Math. Gen. **39**, 1133–1149 (2006)
34. Kirwan, F.: Complex Algebraic Curves. Cambridge University Press, Cambridge (1992)
35. Koblitz, N.: A Course in Number Theory and Cryptography. Springer, New York (1994)
36. Linero, A.: Some results on periodicity of difference equations. In: Liz, E., Mañosa, V. (eds.) Proceedings of the International Workshop Future Directions in Difference Equations. Universidade de Vigo, Vigo (2011)
37. Lyness, R.C.: Note 1581. Cycles. Math. Gaz. **26**, 62 (1942)
38. Lyness, R.C.: Note 1847. Cycles. Math. Gaz. **29**, 231–233 (1945)
39. Lyness, R.C.: Note 2952. Cycles. Math. Gaz. **45**, 207–209 (1961)
40. McMillan, E.M.: A problem in the stability of periodic systems. In: Britton, E., Odabasi, H. (eds.) Topics in Modern Physics. A Tribute to E. U. Condon. Colorado University Press, Boulder (1971)
41. Misiurewicz, M.: Persistent rotation intervals for old maps. In: Krzyżewski K. (ed.) Dynamical systems and ergodic theory, vol. 23, pp. 119–124. Banach Center Publications, Warsaw (1989)
42. Montgomery, D.: Pointwise periodic homeomorphisms. Am. J. Math. **59**, 118–120 (1937)

43. Pettigrew, J., Roberts, J.A.G.: Characterizing singular curves in parametrized families of biquadratics. J. Physics A Math. Theor. **41**, 115203 (28 pages) (2008)
44. Quispel, G.R.W., Roberts, J.A.G., Thompson, C.J.: Integrable mappings and soliton equations. Phys. Lett. A **126**, 419–421 (1988)
45. Quispel, G.R.W., Roberts, J.A.G., Thompson, C.J.: Integrable mappings and soliton equations II. Physica D **34**, 183–192 (1989)
46. Robin, G.: Estimation de la fonction de Tchebychef θ sur le k-ième nombre premier et grandes valeurs de la fonction $\omega(n)$ nombre de diviseurs premiers de n. Acta Arith. **XLII**, 367–389 (1983)
47. Rosser, J.B., Schoenfeld, L.: Approximate formulas for some functions of prime numbers. Ill. J. Math. **6**, 64–94 (1962)
48. Sawyer, W.W.: Note 2951. Lyness' periodic sequence. Math. Gaz. **45**, 207 (1961)
49. Silverman, J.: Advanced Topics in the Arithmetic of Elliptic Curves. Springer, New York (1994)
50. Silverman, J.: The Arithmetic of Elliptic Curves. Springer, New York (2009)
51. Silverman, J., Tate, J.: Rational Points on Elliptic Curves. Springer, New York (1992)
52. Usnich A.: Symplectic automorphisms of $\mathbb{C}\mathbf{P}^2$ and the Thomson group T, arXiv:math/0611604v3 [math.AG]
53. Viallet, C.M., Grammaticos, B., Ramani, A.: On the integrability of correspondences associated to integral curves. Physics Lett. A **322**, 186–193 (2004)
54. Zeeman, E.C.: Geometric unfolding of a difference equation. Preprint Hertford College, Oxford. Unpublished (1996)

Chapter 3
Discrete-Time Modelling of Sigma-Delta Inspired Systems for MEMS

E. Blokhina, P. Giounanlis, M. Dominguez-Pumar, S. Gorreta, J. Pons-Nin and O. Feely

Abstract This chapter discusses a variety of system structures for microelectromechanical systems (MEMS) that employ a feedback loop inspired by sigma-delta modulation. Sigma-delta modulators are classic electronic circuits that implement data conversion. The feedback loop typical for sigma-delta modulation can be applied to actuate a MEMS device or control its state. The dynamics of such systems are described by a set of discrete-time equations (map). We show how these maps can be derived for different examples of MEMS and highlight the dynamics that are universal for all examples.

3.1 Introduction

Sigma-delta (also denoted as $\Sigma\Delta$) modulators are a class of data converters that have been in use for several decades [1]. Their main advantages are simplicity and robustness to component mismatch. The combination of the principles of oversampling, noise shaping and decimation allows this type of circuit to reach higher resolutions than in the case of other data converters, without the use of high-precision components. They can also be embedded in the control loop of sensors or actuators. In this

E. Blokhina (✉) · P. Giounanlis · O. Feely
School of Electrical, Electronic and Communications Engineering, University College Dublin, Dublin, Ireland
e-mail: elena.blokhina@ucd.ie

P. Giounanlis
e-mail: panagiotis.giounanlis@ucdconnect.ie

O. Feely
e-mail: orla.feely@ucd.ie

M. D.-Pumar · S. Gorreta · J. P.-Nin
Micro- and Nanotechnology Group, Universitat Politécnica de Catalunya, Barcelona, Spain
e-mail: manuel.dominguez@upc.edu

S. Gorreta
e-mail: sergi.gorreta@upc.edu

J. P.-Nin
e-mail: joan.pons@upc.edu

R. López-Ruiz et al. (eds.), *Nonlinear Maps and their Applications,*
Springer Proceedings in Mathematics & Statistics 112, DOI 10.1007/978-3-319-12328-8_3

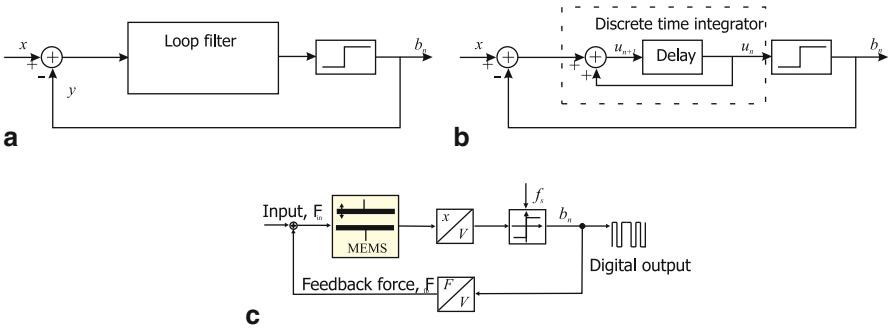

Fig. 3.1 **a** Block diagram of a generic sigma-delta modulator consisting of a filter and a quantizer (a comaprator). **b** Block diagram of a simplest first-order sigma-delta modulator. **c** Block diagram of a MEMS sigma-delta architecture

way, two different goals are achieved: first, the closed-loop control of a given variable, and second, an implicit analogue-to-digital conversion of a given magnitude.

Sigma-delta modulators convert a time-sampled analogue input signal to a stream of bits (see the generic scheme of a $\Sigma\Delta$ modulator in Fig. 3.1a). The quantised output stream must subsequently be filtered in order to achieve a good representation of the input signal. Therefore, it is necessary that the quantisation noise lie predominantly outside the signal band for the successful operation of such a modulator [2]. Sigma-delta modulators implement noise shaping by minimising an error between the input signal x and the feedback loop signal y. The difference between the two signals is passed to the loop filter. If the difference falls in the signal band, it passes to the output without attenuation. On the contrary, a difference that is out of the signal band attenuated by the filter. The signal from the filter is passed to the quantiser, which generates the next output value y. This output values is used in the next comparison step. The result of this strategy is a close match of input signal and quantised output in the pass-band of the filter and shaping of the quantisation noise outside the signal band.

There are a large number of different circuit topologies of sigma-delta modulators that include various loop filters or multiple feedback loop [2]. Continuous-time sigma-delta modulators that have analogue (continuous-time) elements in the feedback loop are also possible. However, the simplest topology is a first-order sigma-delta modulator shown in Fig. 3.1b, where the role of the loop filter is taken by a discrete integrator. Remarkably, the evolution of this feedback system is described by a simple discrete-time equation

$$u_{n+1} = u_n + x - \mathrm{sgn}(u_n) \tag{3.1}$$

that is classified as a piecewise-smooth discontinuous map. Piecewise-smooth maps model many physical systems, including switching circuits and systems with oscillatory behavior [3–6]. In 3.1, x is the magnitude to convert, u_n is the value that the integrator takes at the time $t = nT_s$ and $\mathrm{sgn}(x)$ is the signum function. It is assumed that the input x is constant or that its bandwidth is well below the sampling frequency.

It can be shown that the average value of the output bitstream b_n is x. To obtain the digital conversion of x, this bitstream is fed into a low-pass filter and decimated. We note here that in the analysis of $\Sigma\Delta$ modulators, the input x is often considered as constant. Since standard converters operate at a rate many times greater than the highest frequency of input signal, the input to the converter can be indeed considered as 'quasi'-constant. A remarkable property of sigma-delta modulators is that the output bits subsequently averaged retrieve a good approximation to the input. With ideal integrators and constant input, the output of the system when averaged over a 'long enough' time period equals exactly the input.

The field of the applications of $\Sigma\Delta$ modulators has significantly expanded during recent decades. Closed loop architectures employing the elements of sigma-delta modulations have been introduced to the area of microelectromechanical systems. In such an architecture, a microelectromechanical system serving as a physical sensing element replaces the loop filter from Fig. 3.1a. Alternatively, we can say that a $\Sigma\Delta$-like structure serves as a feedback loop for the sensor. These topologies have been proposed, designed and implemented as an essential part of inertial sensors [7–11], gyroscopes [12], resonant sensors [13–15], air flow sensors [16–19] and capacitive MEMS [20, 21]. In all these applications, physical sensing elements are embedded in the control loop of sensors or actuators to keep constant, for example, the temperature of a component, or the position of an actuator. Among many advantages of this architecture, closed loop sensors which incorporate analogue-to-digital conversion within the loop produce a digital signal in the output.

Figure 3.1c represents the generalised idea of the systems that we will study in this chapter. It describes the basic principle of operation of a MEMS system that employs the feedback loop similar to those of sigma-delta modulators. Please note here that a MEMS is mechanical system, and as a result of applied forces, the input F_{in} and/or the feedback F_{fb}, it changes its position x and velocity v. A conversion to the electrical domain is required for x and v and it is carried out by a sensing mechanism/circuit [22]. The sensing of x and v and representing them as an electrical signal before feeding them to the comparator is shown by the corresponding block ($x \rightarrow V$). The reverse conversion of the resulting actuation voltage to the mechanical domain in the form of a force is carried out by the actuation mechanism or transducer and is shown as the corresponding block after the comparator ($V \rightarrow x$). In this chapter, we will consider a range of MEMS devices serving different aims and representing different MEMS applications. Their 1D topologies are shown in Fig. 3.2, and the mechanical components can deflect as shown in the figure if an actuation voltage and/or other mechanical force is applied. The detailed description of each topology will be given in later sections.

For these feedback topologies, it has been shown that periodic sequences (cycles) appear at the output of the comparator, and this is an intrinsic property of the system observed in all types of the system—conventional sigma-delta modulators and sigma-delta MEMS [13, 23–28]. In digital accelerometers, these cycles may be utilised for self-calibration purposes in the system without input, since the MEMS parameters may be extracted from their characteristics [26]. In resonant gravimetric sensors, the frequency of oscillations of the mechanical structure can be extracted from this cycle at the output [29].

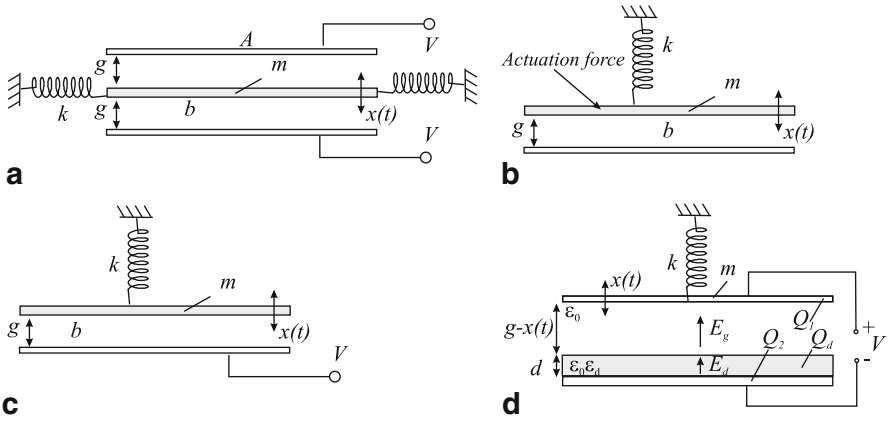

Fig. 3.2 Simple 1D models of MEMS mechanical structures from this study. **a** $\Sigma\Delta$ accelerometer has a movable mass suspended between two electrodes. Voltage is applied to either top or bottom electrode depending on the position of the movable mass. **b** Pulsed digital oscillator uses a MEMS resonators that can be modelled as a mass-spring-damper system. The actuation force is applied to the resonator depending its position and causes its displacement up or down. **c** Electrostatic pulsed digital oscillator is similar to the conventional pulsed digital oscillator. The actuation force is created by applying a voltage to a fixed bottom electrode while the movable mass is made conducting. **d** Capacitive MEMS varactor/switch is a suspended electrode that can move and therefore change the capacitance of the device if a voltage applied to it or to the fixed electrode. Every devices is characterised by its mass m, spring constant k and damping coefficient b

Our aim is to derive models in the form of a map (discrete-time system) in order to study this architecture as a *dynamical system*. We highlight here that due to the use of a 1-bit quantizer (a comparator) in the feedback loop, the resulting maps have the form of *piecewise discontinuous maps*. This approach explains the behaviour of the system from the standpoint of nonlinear dynamics and allows us not only to qualitatively explain the appearance of periodic cycles of the map but also to study the behaviour of the system over a wide range of control parameters. In particular, we introduce the plane spanned by parameters of the system where we define regions of admissibility of cycles. We outline similarities which arise between conventional $\Sigma\Delta$ [24] modulation and MEMS $\Sigma\Delta$ topologies.

We refer a reader who is interested in microtechnology and in practical aspects of MEMS to the books and articles cited in this chapter. This chapter discusses the statements of the problem that lead to piecewise-smooth discontinuous discrete-time systems and the most interesting results.

3.2 $\Sigma\Delta$ Inertial MEMS Sensors

With the advance of microelectromechanical systems technologies, force-balanced electromechanical modulation incorporating micromechanical transducers has been employed in a number of inertial and force sensing applications, including

accelerometers [6–11], gyroscopes [12] and pressure sensors [13]. Closed-loop feedback for such applications makes the sensor characteristics insensitive to mechanical properties of micromachined structures, which are often nonlinear and subject to significant variations, thereby improving the sensor scale factor accuracy.

A typical MEMS sigma-delta based accelerometer is shown in Fig. 3.1b, and many MEMS sensor systems are based on variations of this architecture. The MEMS responds to an external force (acceleration) F_{in} by acquiring a displacement. The displacement is measured and, depending whether it is below or above the rest position, an appropriate force is applied to compensate this displacement. Therefore, the micromechanical structure oscillates around its rest position. A remarkable property of this system is that the displacement of the structure and the input can be calculated simply by processing the sequence of bits b_n at the output of the comparator. In this section, we describe a MEMS accelerometer topology with the first order sigma-delta feedback loop (Fig. 3.1b), since it is an essential part of various inertial sensors, for example, digital accelerometers [7–9, 23, 25, 30, 31].

3.2.1 Statement of the Problem

The block diagram in Fig. 3.1b shows a MEMS embedded into a feedback loop. The MEMS represents a movable conducting plate/mass suspended between two electrodes. A simple 1D model of the MEMS mechanical structure is shown in Fig. 3.2a. When a voltage is applied to one of the electrodes, there is an attracting electrostatic force between the movable plate and this electrode. If a voltage is applied to the 'bottom' electrode the plate will move down, while if a voltage is applied to the 'top' electrode the plate will move up. The feedback loop processes the current position of the MEMS at every sampling time nT_s, and if this position is below zero (the decision bit from the comparator is $b_n = -1$), the voltage is applied to the top electrode (we symbolically denote this event as the application of $+V$) to compensate this position displacement, and vice versa if this position is above zero (the decision bit from the comparator is $b_n = +1$), the voltage is applied to the bottom electrode ($-V$). Thus, the system oscillates around its rest position. A typical waveform of the feedback voltage/force is shown in Fig. 3.3a where during the time interval from nT_s to $(n + 1)T_s$ a constant voltage depending on the position of movable mass is applied to it.

The displacement of the mechanical structure (in this case, a micromechanical resonator) from Fig. 3.1b as a function of time $\xi(t)$ is described by the well-known mass-spring-damper equation

$$m\ddot{\xi}(t) + b\dot{\xi}(t) + k\xi(t) = F_{in}(t) + F_{fb}(t) \tag{3.2}$$

where m is the mass of the plate, b is the damping factor and k is the effective spring constant. The net force $F(t)$ consists of the feedback $F_{fb}(t)$ and the input $F_{in}(t)$. Here, we assume that the feedback actuation takes place through electrostatic force,

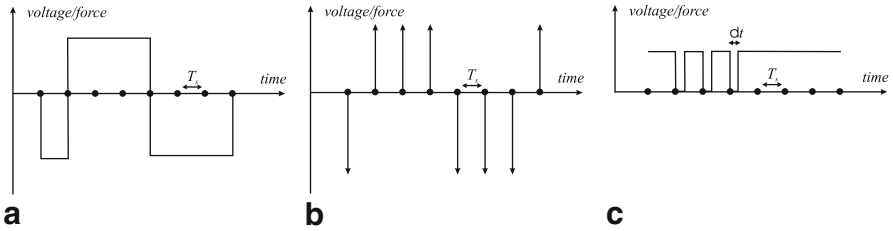

Fig. 3.3 In all examples from this chapter, the actuation force/voltage depends on the state of the MEMS mechanical structure in a similar way. However, the actuation force waveform will be specific for each example. **a** Voltage waveform for the actuation of a $\Sigma\Delta$ accelerometer. The 'polarity' of the applied voltage is defined by the sampled position of the mechanical structure at a sampling time $(n-D)T_s$, and a constant voltage is turn on for the entire interval $nT_s < t < (n+1)T_s$. The similar actuation waveform is used for capacitive MEMS to control dielectric charging. **b** Force waveform of the pulsed digital oscillator (PDO) consists of a train of very short (delta) pulses whose polarity is defined by the sampled position of the MEMS resonator. **c** Voltage waveform of the electrostatic pulsed digital oscillator. The oscillator is constantly biased. When a 'negative' pulse must be applied to the resonator, the bias voltage is turned off for time interval dt and then turned on for the rest of the sampling interval time ('anti-pulse'). When a 'positive' pulse must be applied to the resonator, the bias voltage does not change

which is the case for many systems. For Eq. (3.2), $F_{fb}(t)$ is written in the following form:

$$F_{fb}(t) = \begin{cases} -\varepsilon_0 A V_0^2/\left(2[g+\xi(t)]^2\right) & \text{for } nT_s < t < (n+1)T_s \text{ if } \xi((n-D)T_s) > 0 \\ +\varepsilon_0 A V_0^2/\left(2[g-\xi(t)]^2\right) & \text{for } nT_s < t < (n+1)T_s \text{ if } \xi((n-D)T_s) < 0 \end{cases} \tag{3.3}$$

where ε_0 is the permittivity in vacuum, A is the electrode area, V_0 is the control voltage and D is a delay in the feedback loop ($D \geq 1$). As shown in [32, 33], the number of delays is an effective control parameter that affects the dynamics of this system, and therefore we give here a generalised model accounting for an arbitrary number of delays D.

The nature of the electrostatic force is nonlinear, though it is usual to linearise it by dropping off the small displacement $\xi(t)$ compared to the equilibrium gap g. As an alternative, expanding the nonlinear part of the electrostatic force, one can use the following representation for linearised $F_{fb,lin}(t)$:

$$F_{fb,lin}(t) \approx -\text{sgn}(\xi((n-D)T_s)F_0\,\Pi(t) + 2F_0\xi(t)/g \tag{3.4}$$

which substituted in (3.2), produces a shift in the natural frequency $\omega = \sqrt{k/m}$. Thus, the new frequency now is $\omega_0 = 2\pi f_0 = \omega\sqrt{1-2F_0/g\omega^2}$ where $F_0 = \varepsilon_0 A V_0^2/2g^2$. The linearised feedback force, therefore, can be simply written as $F_{fb,lin}(t) = -\text{sgn}(\xi(t_{n-D}))F_0\Pi(t)$. The symbol $\Pi(t)$ denotes a square pulse of unit magnitude and length T_s.

Let us introduce the following variables: time $\tau = \omega_0 t$, displacement $x = m\omega_0^2\xi/F_0$, dissipation $\beta = b/(2m\omega_0)$ and normalised input $a = F_{in}/F_0$. We will

consider in this chapter that a is a constant. Indeed, since the natural and sampling frequencies are high, we may assume a time-varying input to be constant over relatively large sampling events.

Thus, we obtain the following normalised equation instead of (3.2):

$$x'' + 2\beta x' + x = a - \mathrm{sgn}(x_{n-D})\Pi(t) \tag{3.5}$$

where now x' represents the derivative with respect to dimensionless time τ. In the right-hand side of equation, the term x_{n-D}, the position at the time instance $(n-D)T_s$, is present, reflecting the presence of multiple delays in the feedback loop.

The solution of a mass spring damper equation with the left part as in (3.5) and, in the most general case, with some $F(t)$ in the right part consists of two terms, namely, the decaying free oscillations $x_1(t)$ and the forced ones $x_2(t)$. While the expression for $x_1(\tau)$ is well-known, we note that for arbitrary $F(t)$ the forced oscillations may be found as follows:

$$x_2(\tau) = \int_0^\tau \frac{F(t)e^{-\beta(\tau-t)}}{\sqrt{1-\beta^2}} \sin\left(\sqrt{1-\beta^2}(\tau - t)\right)dt \tag{3.6}$$

where the integral can be easily solved in the interval $[0, \tau]$ for certain functions $F(t)$, for instance, if it is a constant F_0. Thus, solving (3.6) for $F(t) = F_0$ and introducing the new variable $y = -(\beta x/\sqrt{1-\beta^2}) - v/\sqrt{1-\beta^2}$ (where $v = \dot{x}$ is the velocity), one obtains

$$\begin{aligned}
x_1(\tau) &= e^{-\beta\tau}\left(x_0 \cos\left(\sqrt{1-\beta^2}\tau\right) - y_0 \sin\left(\sqrt{1-\beta^2}\tau\right)\right)\\
y_1(\tau) &= e^{-\beta\tau}\left(y_0 \cos\left(\sqrt{1-\beta^2}\tau\right) + x_0 \sin\left(\sqrt{1-\beta^2}\tau\right)\right)\\
x_2(\tau) &= F_0\left(1 - e^{-\beta\tau}\cos\left(\sqrt{1-\beta^2}\tau\right) - \frac{\beta e^{-\beta\tau}}{\sqrt{1-\beta^2}}\sin\left(\sqrt{1-\beta^2}\tau\right)\right) = F_0\,\zeta(\beta,\tau)\\
y_2(\tau) &= F_0\left(\frac{-\beta}{\sqrt{1-\beta^2}} + \frac{\beta e^{-\beta\tau}}{\sqrt{1-\beta^2}}\cos\left(\sqrt{1-\beta^2}\tau\right) - e^{-\beta\tau}\sin\left(\sqrt{1-\beta^2}\tau\right)\right) = F_0\,\eta(\beta,\tau)
\end{aligned} \tag{3.7}$$

where ζ and η are defined as the expressions in the brackets in the latter two equations. Knowing the solutions, it is easy now to obtain an iterative map from (3.7) by simply assuming that $x_n = x(n\tau_s)$ and $y_n = y(n\tau_s)$ where $\tau_s = \omega_0 T_s$ and $\tau_n = n\tau_s$.

Introducing the feedback force in the form

$$F_n = a - \mathrm{sgn}(x_{n-D}) \tag{3.8}$$

(F_n will be constant during one sampling event), we write the sampled system as the following equations [34]:

$$\begin{pmatrix} x_{n+1} \\ y_{n+1} \end{pmatrix} = \alpha\mathbf{R}(2\pi\, f\sqrt{1-\beta^2}) \begin{pmatrix} x_n \\ y_n \end{pmatrix} + F_n \begin{pmatrix} \zeta(\beta, f) \\ \eta(\beta, f) \end{pmatrix} \tag{3.9}$$

where we introduce the parameters $\alpha = \exp(-\beta\tau_s) = \exp(-2\pi\beta f)$ (or, returning to the original variables, $\alpha = \exp[-bT_s/(2m)]$) and the normalised frequency $f = \tau_s/(2\pi)$ ($f = f_0/f_s$). We also used the notation $\mathbf{R}(\alpha)$ in (3.9) to denote the rotation matrix

$$\mathbf{R}(\alpha) = \begin{pmatrix} \cos\alpha & -\sin\alpha \\ \sin\alpha & \cos\alpha \end{pmatrix} \tag{3.10}$$

The terms ζ and η in (3.9) caused by the presence of $F(t)$ in the right part of equation (3.5) are functions of the parameters α, f and τ_s and not of x_n and y_n.

The system (3.9) is a piecewise-smooth discontinuous mapping

$$\mathbb{R}^2 \times \mathbf{B}^D \longrightarrow \mathbb{R}^2 \times \mathbf{B}^D \tag{3.11}$$

where $\mathbb{R}$ is the set of real numbers and $\mathbf{B}$ is a two-element set such that $\mathbf{B} = \{-1, 1\}$. Map (3.9) belongs to the class of contracting mappings considered in [35]. It is important to note that it has been formally shown there that the output of contracting mapping is always a *stable cycle*, and therefore map (3.9) displays only stable cycles.

We can define the binary output sequence $b_n \in \mathbf{B}$ as

$$b_n = \mathrm{sgn}(x_n) \tag{3.12}$$

and, according to the notes made in the introduction, this sequence represents the digital output of the system.

Strictly speaking, (3.9) is written for the *underdamped* case when $\beta < 1$. For the *overdamped* case, $\beta > 1$, the expression in the root $\sqrt{1-\beta^2}$ becomes negative and f itself complex. The map (3.9) can still be written in this form if, considering that the expression $2\pi f$ is now complex, we recall that $\cos(ix) = \cosh(x)$ and $\sin(ix) = i\sinh(x)$ in the rotation matrix. Since the root $\sqrt{1-\beta^2}$ was also used in the definition of y, the second variable must be transformed $y^* \to -iy$. (After these changes, all variables and parameters in (3.9) will be still real).

The form of the map (3.9) resembles the map proposed for the pulsed digital oscillator (PDO) topology [14]. Due to the difference in driving of the PDO and the studied system, the iterative map for the PDO may be seen as a particular case of the map (3.9) with $\zeta = 0$ and $\eta = \text{const}$ studied in detail in references [14, 28, 32]. The PDO dynamics is very different from that of first-order sigma-delta, although it shares some common features such as, for example, after a nonlinear bitstream conversion (edge detection), noise shaping [29].

3.2.2 Periodic Solutions

Independently from the study [35], it is well-known that the conventional $\Sigma\Delta$ architecture displays periodic sequences (cycles) in the output [24]. A microresonator

embedded into this type of structure displays periodic behaviour as well [26]. In this section, we study periodic sequences $\{(x_n, y_n)\}$ that are produced by the map (3.9).

For a given N-periodic sequence of signs b_n such that $x_n = x_{n+N}$, the following sequence determines the N-cycle of map (3.9)

$$\begin{pmatrix} x_n \\ y_n \end{pmatrix} = \left(\mathbf{I} - \alpha^N \mathbf{R}(N2\pi f\sqrt{1-\beta^2})\right)^{-1} \sum_{j=1}^{N} \alpha^{N-j} \mathbf{R}((N-j)2\pi f\sqrt{1-\beta^2}) \times$$

$$\times\ (a - \mathrm{sgn}(x_{n-D+j-1})) \begin{pmatrix} \zeta \\ \eta \end{pmatrix} \tag{3.13}$$

A cycle given by (3.13) will be asymptotically stable. Indeed, let us consider the evolution of a small disturbance of some point x_n, y_n that belongs to the N-cycle. Let also this disturbance lies in the δ-neighbourhood of this point such that $\delta = \min|x_n| > 0$ for all N. In this case, evolution after k iterations of $\tilde{x}_n = x_n + \delta x$ and $\tilde{y_n} = y_n + \delta y$ is defined as

$$\begin{pmatrix} \tilde{x}_{n+k} \\ \tilde{y}_{n+k} \end{pmatrix} = \begin{pmatrix} x_{n+k} \\ y_{n+k} \end{pmatrix} + \alpha^k \mathbf{R}(2\pi k f\sqrt{1-\beta^2}) \begin{pmatrix} \delta x \\ \delta y \end{pmatrix} \tag{3.14}$$

As is seen from this formula, the disturbed trajectory approaches the initial one since $\alpha < 1$.

To validate the existence and find the area of admissibility of a particular cycle over a range of control parameters of (3.9), we can apply the following strategy:

- According to [35], the output of this map is always a cycle.
- Assume the sequence b_n (3.12) for the sign of the position. For instance, studies [24, 27, 29] describe the approaches to determine sequences b_n.
- Fix the parameters of the map (namely β, f and a) and calculate $\{(x_n, y_n)\}$ using Eq. (3.13).
- Check if the condition (3.12) is fulfilled. It is worth noting that although the sequence (3.12) is used to generate the cycle (3.13), the resulting cycle may have a signature sequence that differs from the desired sequence. In this case we say that at this parameters, the cycle is not admissible.

Varying β and f over wider regions with implementation of the above strategy allows one to obtain the parameter plane (β, f) with regions of cycles admissibility—so called tongues.

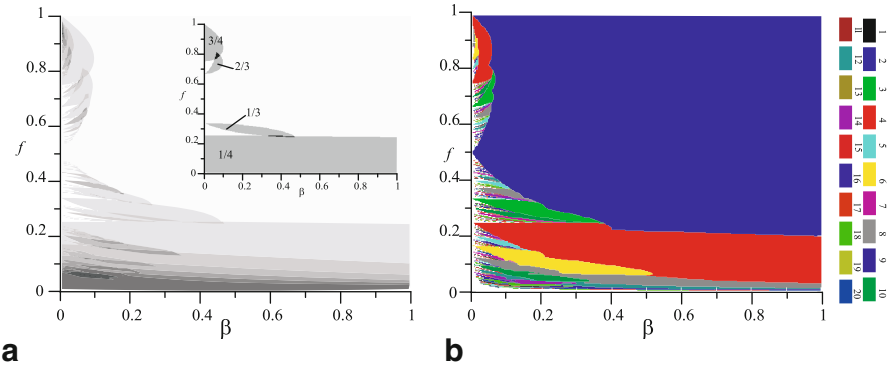

Fig. 3.4 $\Sigma\Delta$ MEMS accelerometer described by map (3.9), underdamped case. **a** Regions of admissibility (with overlapping) for N-cycles with $1 \leq N \leq 20$ in the parameter plane calculated from (3.13). The insert of the figure shows the form of the tongues that correspond to odd (by the example of the 3-cycle) and even (by the example of 4-cycle) cycles. **b** Parameter plane with tongues that correspond to different cycles obtained from numerical simulations of the map (3.9) with the zero initial conditions

3.2.3 Results

3.2.3.1 System with No Input

First, we consider the system with no input, i.e. $a = 0$. The reasons of this study are: (a) for certain types of inertial sensors, resonant accelerometers, a proof mass changes the strain of an attached resonator, hence changing its resonant frequency. The scheme may also be used as a part of a self-sustained oscillations system [11]. The parameter of interest in this case is the change of the frequency, and in terms of the model (3.9) we have only two parameters that entirely control the dynamics of the system—β and f; (b) the topology with no input displays periodic sequences (cycles) at the comparator output which may be used for self-testing purposes.

For a linear underdamped resonator, the output waveform in this case will be a sinusoid, and, therefore, one can obtain the sequence b_n for the expression (3.13) as the sign of a sampled sinusoid

$$b_n = \mathrm{sgn}(\cos(2\pi k M/N + \varphi_0)) \tag{3.15}$$

where φ_0 is an arbitrary phase and $1 \leq k \leq N$. The ratio M/N defines the rotation number of a cycle, i.e. the number of loops around the origin a trajectory makes in one iteration. The expression (3.15) is valid not only for the case of high-Q resonators but also for cycles in the overdamped case (with no input for the both cases). The most general discussion on admissible sequences is given in [27]. The sequence b_n in the case of a linear over damped resonator can be found using the algorithm described in [24].

The parameter plane (β, f) for tongues with rotation numbers $M/N, 0 < N < 15$ is shown in Fig. 3.4 (for the underdamped case) and Fig. 3.5 (for the overdamped

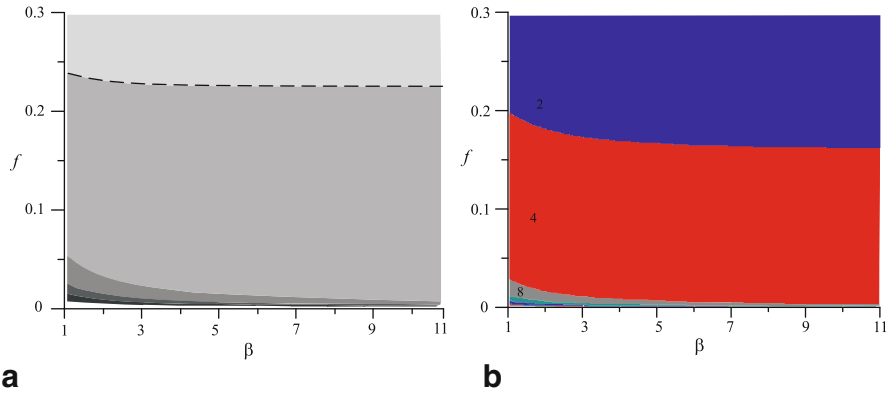

Fig. 3.5 $\Sigma\Delta$ MEMS accelerometer described by map (3.9), overdamped case. **a** Regions of admissibility (with overlapping) for the 2, 4, 8, 12, 16 and 24-cycles. **b** Parameter plane with tongues that correspond to different cycles obtained from numerical simulations of the map (3.9) with the zero initial conditions

case). The grey areas show possible values of parameters at which a specific cycle can be observed in the system. As is seen from the figure, the tongues overlap (shown by darker gray shades): at the same β and f there coexist several cycles and which one of them will eventually be displayed by the system depends only on initial conditions. For example, the planes of parameters calculated for the zero initial conditions are shown in Fig. 3.4b and 3.5b. For the areas of tongues overlapping, one can plot basins of attraction, i.e. the areas on the plane spanned by the initial conditions x_0 and y_0 (Fig. 3.6c). In general, the picture that one observes for the underdamped case is very similar to the PDO dynamics [28, 32] in the sense that tongues and overlapping areas are very typical for the system.

As far as the tongues defined by (3.13) are concerned, firstly we note that the 2-cycle (the area shown in blue) can formally exist everywhere in the plane (it is shown by the lightest grey shade in Figs. 3.4a and 3.5a). In practice, for certain parameters it would be almost impossible to obtain it since the initial conditions demanded for it may be unrealsitic. We also note that only even cycles exist for the overdamped resonator.

Secondly, we draw the attention to the different forms of tongues that correspond to odd and even N for the underdamped case (see the insert in Fig. 3.4a where the tongues with $N = 3$ and $N = 4$ are shown). Though the odd tongues have conventional form, the even tongues are rather unusual and 'cut off' large areas in the plane. To prove it, we obtained an explicit form for the 3- and 4-cycles directly from (3.13) (which we do not give here due to its complex form).

The points x_n as functions of the parameter f at a fixed β for the 3- and 4-cycles are shown in Fig 3.6a and b, respectively. Since $\mathrm{sgn}(x_n)$ must be the same as the sequence b_n which generated the cycle, we highlight the interval of the f axis over which these cycles are admissible and this area is precisely the cross section of the tongues from the plane 3.4a.

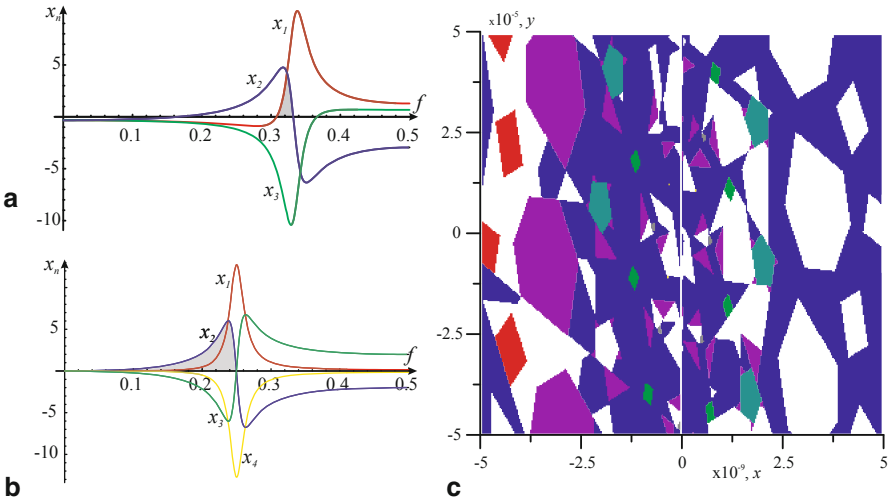

Fig. 3.6 $\Sigma\Delta$ MEMS accelerometer described by map (3.9). **a** Points x_n of the 3-cycle of map (3.9) as a function of the normalised frequency f. **b** Points x_n of the 4-cycle as a function of the normalised frequency f. The 3-cycle is admissible if $x_1 > 0$, $x_2 > 0$ and $x_3 < 0$. The interval of f where this condition is fulfilled is highlighted by *grey*. This interval is larger at larger β and tends to zero at smaller β. The 4-cycle is admissible if $x_1, x_2 > 0$ while $x_3, x_4 < 0$. This is the case for any $f < 0.25$ and does not depend on β. This explains why the odd cycles have the regions of admissibility in the form of tongues originating from a specific point at the axis f ($\beta = 0$) while all even tongues cut off large areas in the (β, f) plane. **c** Example of the basins of attraction of different cycles: at the same values of parameters various output is possible depending on initial conditions

3.2.3.2 System with Input

In this section, we briefly discuss results for the topology of a $\Sigma\Delta$ MEMS accelerometer which is used with an input (map (3.9) with $a \neq 0$). Here, we present results only for the overdamped case, though the topology may be used also with high-Q resonators [9]. We also restrict ourselves to the case when the sampling frequency is much higher than the natural frequency of the resonator and the input a is constant.

As noted before, the system output represents a cycle with a frequency that depends on the input and on the parameters of the device. Since this topology is based on the same ideas as a $\Sigma\Delta$ modulator, the input is obtained as an average of the output cycle. First, we note that the average output x_{out} that is the average on the bit sequence b_n as a function of the input a is close to a linear dependance, but a magnified part of the plot reveals that it consists of a number of steps (Fig. 3.7). We recall that the same situation is observed in a conventional $\Sigma\Delta$ modulator [24] and in the PDO [14, 28]. Such steps appear due to frequency locking and indicate that particular cycles exist in a finite interval of a control parameter.

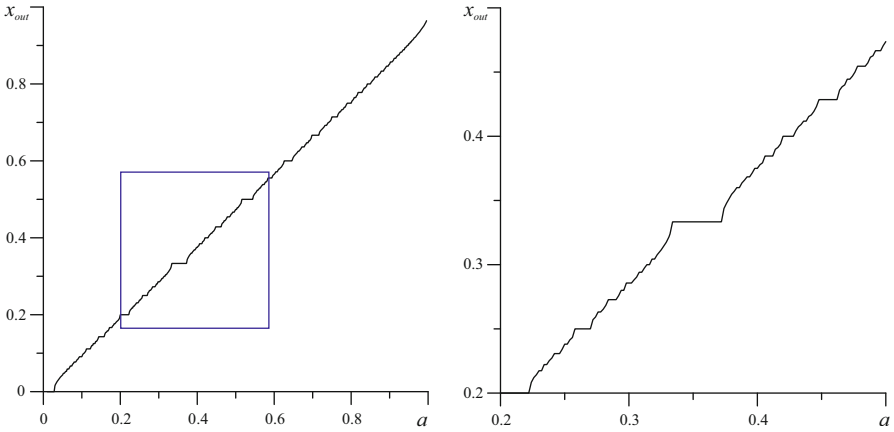

Fig. 3.7 $\Sigma\Delta$ MEMS accelerometer described by map (3.9). Average output of a $\Sigma\Delta$ accelerometer as a function of the input a and the magnified part of the plot. The plot displays a set of plateaus and resembles devil's staircase. The magnified plot also consists of a set of plateaus

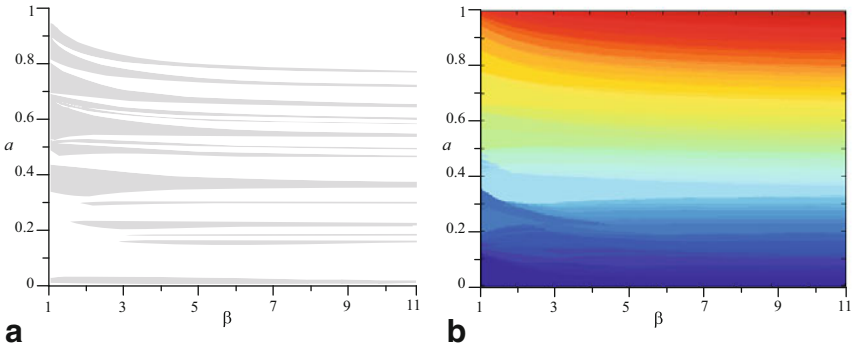

Fig. 3.8 $\Sigma\Delta$ MEMS accelerometer described by map (3.9). **a** Tongues that correspond to the widest steps of the plot (3.7) in the (a, β) plane. **b** The average output for different normalised inputs a and dissipations β presented by different colours: from 0 (*blue*) to 1 (*red*)

The output of the system can be presented in the plane of parameters (β, a), see Fig. 3.8a (similar to Fig. 3.4 and 3.5). To plot this plane, we choose those sequences b_n for the formula 3.13 that correspond to the widest steps in Fig. 3.7. Now, the steps in $x_{out}(a)$ can be considered as cross sections of areas in which cycles are admissible. As is seen from the plane (3.8), the width of steps depends on the dissipation β: the higher the dissipation, the smaller the width (and, consequently, the higher the resolution of the system). Figure 3.8(b) shows the average output coded by different colours: from 0 (blue) to 1 (red).

3.3 MEMS PDO

In this section, we describe how a map that is very similar to the one derived above appears as a model of another MEMS-based application. This application is called as a PDO. It belongs to the class of resonant sensors [36] in which an oscillating mechanical structure (put in resonance) responds to an external stimulus such as an environment change in pressure, concentration of a specific compound, viscosity, etc. These sensors typically detect shifts in the frequency or amplitude of the oscillation of a MEMS device as a result of this external influence.

The PDO is a micromechanical structure that is embedded into a sigma-delta type feedback loop with appropriate control circuitry. As a result of the feedback force applied to the microresonator, it maintains self-sustained oscillations [13–15]. Such structures can be used in resonant mass sensors. It detects the change in the environment by changing its oscillation characteristics (mainly the frequency of oscillations). These sigma-delta feedback not only allows to sustain self-oscillations but also to monitor changes in the resonant frequency of the resonator simply by processing the binary sequence b_n generated at their output. In references [33, 37] it was demonstrated how these circuits allow the actuation of multiple vibrational modes of the mechanical structure and, therefore, increasing the sensitivity of the measurements [38, 39].

3.3.1 Statement of the Problem

Similar to the previously discussed system, the PDO can be described through the diagram shown in Fig. 3.1b. In this case, we assume that there is no external input to the resonator (i.e. $F_{in} = 0$) and the system is self-oscillating. The MEMS mechanical structure in the feedback loop is schematically shown in Fig. 3.2b. The position of the MEMS resonator is evaluated at each sampling time T_s, and very short pulses of force are applied to the resonator. A typical actuation waveform is presented in Fig. 3.3b. In the case of a sigma-delta accelerometer whose actuation waveform is shown in Fig. 3.3a, the feedback force is continuously applied to the microstructure during the entire time interval T_s. In the case of the PDO, only a short pulse of a very small duration is applied. This pulse can be modelled as a Dirac delta pulse.

Let us briefly discuss a dynamical model of such system. The derivation of the governing equation is similar to those described in the previous section (Sect. 3.2). Detailed study of the model has been carried out in [13, 28, 33]. The position $x(t)$ of the MEMS resonator is described by the second-order differential equation

$$m\ddot{x}(t) + b\dot{x}(t) + kx(t) = F_{fb}(t) \tag{3.16}$$

where m is the mass of the movable plate, b is the damping factor, k is the spring factor, $F_{fb}(t)$ is the force that acts on the resonator. According to the actuation principle, the position of the MEMS resonator is evaluated discretely every sampling time instant

nT_s and depending on its value, the corresponding feedback force is applied:

$$F_{fb}(t) = \begin{cases} -F_0\,\delta(t - nT_s) & \text{if} \quad x((n-D-1)T_s) > 0 \\ +F_0\,\delta(t - nT_s) & \text{if} \quad x((n-D-1)T_s)) < 0 \end{cases} \tag{3.17}$$

where D is the number of delays in the feedback loop ($D \geq 0$). The feedback force F_{fb} represents a train of delta-pulses with a constant amplitude F_0 depending on the sign of the resonator position. For simplicity, we will use the notation $t_n = nT_s$ and $x_n = x(nT_s)$, we also use Dirac delta function $\delta(t)$ to denote a short pulse.

General solutions of inhomogeneous differential equations consist of a superpositions of decaying eigen oscillations of the free resonator and the forces oscillations. The form of the decaying oscillations is known from Sect. 3.2, and we give it here in matrix form using the rotation matrix $\mathbf{R}$

$$\begin{pmatrix} x(t) \\ y(t) \end{pmatrix} = \exp(-\omega_0 \beta\, t)\mathbf{R}(\omega_0\sqrt{1-\beta^2}\, t) \begin{pmatrix} x(t_0) \\ y(t_0) \end{pmatrix} \tag{3.18}$$

where $\beta = b/(2m\omega_0)$ and $\omega_0 = \sqrt{k/m}$. In this equation, we also introduced a new variable y that is a linear combination of the displacement x and the velocity v: $y(t) = -\beta x/\sqrt{1-\beta^2} - v/(\omega_0\sqrt{1-\beta^2})$.

The only result of the application of a delta-pulse is a change in the velocity of the MEMS resonator:

$$y(t_n+) - y(t_n-) = \frac{F_0}{\omega_0^2\sqrt{1-\beta^2}}\mathrm{sgn}(x_{n-D-1})\,. \tag{3.19}$$

Collecting these two solutions, we can write discrete-time equations to describe the evolution of the PDO. Assuming that $x_n = x(nT_s)$ and $y_n = y(nT_s+)$, we write the equation in discrete-time matrix form

$$\begin{pmatrix} x_{n+1} \\ y_{n+1} \end{pmatrix} = \alpha\mathbf{R}(2\pi f) \begin{pmatrix} x_n \\ y_n \end{pmatrix} + b_{n-D} \begin{pmatrix} 0 \\ \zeta \end{pmatrix} \tag{3.20}$$

and

$$b_n = \mathrm{sgn}(x_n) \tag{3.21}$$

In Eq. (3.20), we have introduced the following parameters: contraction coefficient $\alpha = \exp(-2\pi f/\sqrt{1-\beta^2})$, normalised sampling frequency $f = T_s\omega_0\sqrt{1-\beta^2}/2\pi$ and normalised amplitude of the pulses $\zeta = F_0/(\omega_0 m\sqrt{1-\beta^2})$. Similarly to (3.9), the system (3.20) is a piecewise-smooth discontinuous mapping of the form

$$\mathbb{R}^2 \times \mathbf{B}^{D+1} \longrightarrow \mathbb{R}^2 \times \mathbf{B}^{D+1} \tag{3.22}$$

where $\mathbb{R}$ is the set of real numbers and $\mathbf{B}$ is a two-element set such that $\mathbf{B} = \{-1, 1\}$.

3.3.2 Periodic Solutions

In [28], it was shown that periodic solutions of the mapping (3.20) are stable cycles. More generally, the system (3.20) represents a piecewise contractive map and, according to [35], always displays periodic stable sequences or cycles.

The procedure to investigate limit cycles is described in detail in the previous Sect. 3.2. By assuming a specific sequence $b_n = \mathrm{sgn}(x_n)$, we can obtain the explicit form of the N-cycles as

$$\begin{pmatrix} x_n \\ y_n \end{pmatrix} = \left(\mathbf{I} - \alpha^N \mathbf{R}(2\pi N f)\right)^{-1} \sum_{j=1}^{N} \alpha^{N-j} \mathbf{R}((N-j)2\pi f)\mathrm{sgn}(x_{n-D+j-1})) \begin{pmatrix} 0 \\ \zeta \end{pmatrix} \tag{3.23}$$

The stability analysis can be done in the same way as it was carried out in Sect. 3.2 and every cycle produced by (3.23) is stable.

To validate the existence of a particular cycle, we can apply the following strategy:

- Assume the sequence b_n (3.21) for the sign of the position.
- Fix the parameters of map (3.20) (namely β, f and a) and calculate $\{(x_n, y_n)\}$ using Eq. (3.13).
- Check if the condition (3.21) is fulfilled. It is worth noting that although the sequence (3.21) is used to generate the cycle (3.13), the resulting cycle may have a signature sequence that differs from the desired sequence. In this case we say that at this parameters, the cycle is not admissible.

Varying β and f over wider regions with implementation of the above strategy allows one to obtain the parameter plane (β, f) with regions of cycles admissibility—so called tongues.

3.3.3 Results

To analyse the output sequences of map (3.20), we note that the MEMS waveform in this case will be a sinusoid, and, therefore, one can obtain the sequence of signs b_n as the sign of a sampled sinusoid

$$b_n = \mathrm{sgn}(\cos(2\pi k M/N + \varphi_0)) \tag{3.24}$$

where φ_0 is an arbitrary phase and $1 \leq k \leq N$. The ratio M/N defines the rotation number of a cycle, i.e. the number of loops around the origin a trajectory makes in one iteration.

The 'parameter' of interest in the case of the PDO is its oscillation frequency and it can be calculated using two approaches. Since the PDO is a digital oscillator, the oscillation frequency can be directly calculated from the output bitstream [14, 29].

We will use the route suggested in [29] to generate the auxiliary sequence and obtain the digital frequency of oscillations f_D. The q_n sequence is defined as follows:

$$q_n = \begin{cases} 1, & \text{if } b_n \neq b_{n+1}\,, \\ 0, & \text{if } b_n = b_{n+1}\,. \end{cases} \tag{3.25}$$

The digital frequency of oscillations can now be written as

$$f_D = \frac{1}{2} \cdot \frac{\sum_{n=1}^{N} q_n}{N} \tag{3.26}$$

On the other hand, one can calculate the rotation number of the map. If α_n is the angle made by the point (x_n, y_n) and the origin of the x, y plane, the rotation number is defined as [40]

$$\rho = \lim_{n\to\infty} \frac{\alpha_n}{2\pi n} \tag{3.27}$$

Both, the digital frequency and the rotation number, are equivalent, and one can ensure that they give the same result. Therefore, the resulting oscillation frequency, in the oversampling regime ($f_{osc}/f_s < 1/2$), is

$$f_{osc} = f_s f_D = f_s \rho \tag{3.28}$$

where $f_s = 1/T_s$ is the sampling frequency.

The rotation number (related to the resulting oscillation frequency) as a function of the normalised frequency f (related to the sampling and natural frequency) is presented in Fig. 3.9a. In the ideal case, this should be a straight line displaying that any small change in the sampling or natural frequency will result in a change of the oscillation frequency detected by the electronics. However, this plot resembles a devil's staircase and consists of discrete steps. The oscillations are frequency-locked in this case with one frequency being a rational number times the other frequency. Practically this means that the system (MEMS sensor) has a limited resolution: if the frequency is locked, the system is not responding to a small change in the environment and this change cannot be detected from the bitstream sequence b_n. This phenomenon is only important when using resonators with low-quality factors, i.e. with high losses. From the figure, one can see a magnified part of the plot shown in Fig. 3.9b that also resembles a devil's straicase. The size of steps is defined by the dissipation parameter β: the smaller the β, the more straight and smooth the plot is.

The parameter plane (β, f) for tongues with rotation numbers $M/N, 0 < N < 16$ is shown in Fig. 3.10. Plot 3.10a shows the domains of existence of specific cycles. These domains can overlap (shown by a darker shade of gray): at the same β and f there coexist several cycles and which one of them will eventually be displayed by the system depends only on initial conditions. The planes of parameters calculated for zero initial conditions are shown in Fig. 3.10b.

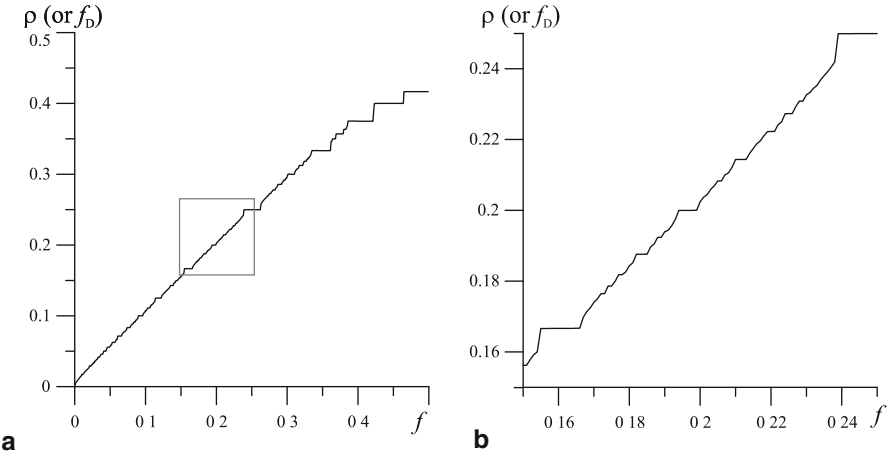

Fig. 3.9 Pulsed digital oscillator described by map (3.20). Rotation number ρ (or digital frequency f_D, both related to the resulting oscillation frequency f_{osc}) as a function of the normalised frequency f (related to the sampling frequency and/or the natural frequency. $\beta = 0.05$

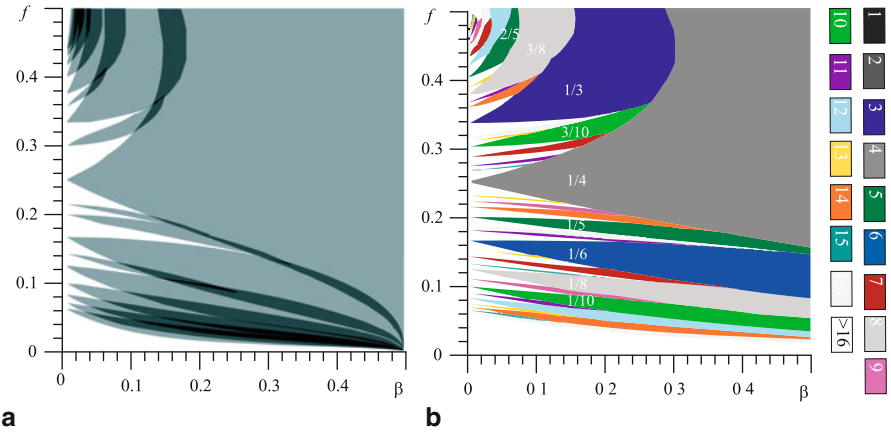

Fig. 3.10 Pulsed digital oscillator described by map (3.20). **a** Regions of admissibility (with overlapping) for N-cycles with $1 \leq N \leq 15$ in the parameter plane calculated from (3.23). **b** Parameter plane with tongues that correspond to different cycles obtained from numerical simulations of the map (3.20) with zero initial conditions

3.4 Modification of the PDO: Electrostatic MEMS Oscillator

PDOs described in Sect. 3.3 are implemented using thermoelectric actuation that allows one to emulate 'positive' and 'negative' pulses. Modern MEMS devices are often implemented using electrostatic actuation. As it was described in Sect. 3.2, the main difficulty of electrostatic actuation is that the generated force is always

attractive and it is not possible to emulate a negative pulse. Therefore, a modification of the actuation technique from Sect. 3.3 is required and we describe it in this section. The corresponding oscillator is called the electrostatic PDO or e-PDO [41].

The e-PDO has the same application as the conventional PDO. Namely, it is used as a resonant sensor that detect small shifts of the resonant frequency of a mechanical structure as a result of changes in the variable to be measured. We give here the map for this system as it has quite a complex form compared to the two studied cases, but displays very similar features to the conventional PDO map.

3.4.1 Statement of the Problem

A schematic structure of the e-PDO can be described using the block diagram from Fig. 3.1b with no external input force ($F_{in} = 0$). A simplified 1D mechanical structure of the e-PDO is shown in Fig. 3.2c. The displacement of the microresonator ξ is described by the following equation:

$$m\ddot{\xi}(t) + b\dot{\xi}(t) + k\xi(t) = F_{fb}(\xi, t) \tag{3.29}$$

where m is its mass, b is the damping factor and k is the effective spring constant. The force acting on the resonator will consist only of the feedback force F_{fb}. The e-PDO is actuated electrostatically and therefore F_{fb} is an electrostatic force. The electrostatic force is always attractive, and it is not possible to create a repulsive pulse required for sigma-delta feeedback. To overcome the similar issue, inertial sensor/accelerometers described in Sect. 3.2 employ two electrodes that located at the two opposite sides of a movable mass. However, this is not always possible because of size or design limitations. In the case of the e-PDO, we use the following actuation scheme:

$$V_{fb}(t) = \begin{cases} V_0(1 - \Pi(t)) & \text{for} \quad nT_s < t < (n+1)T_s \quad \text{if} \quad \xi((n-D)T_s) > \xi_{av} \\ V_0 & \text{for} \quad nT_s < t < (n+1)T_s \quad \text{if} \quad \xi((n-D)T_s) < \xi_{av} \end{cases} \tag{3.30}$$

where $\Pi(t)$ denotes a square-shaped pulse

$$\Pi(t) = \begin{cases} 0 & \text{for} \quad t > dt, \\ 1 & \text{for} \quad 0 < t < dt \end{cases} \tag{3.31}$$

In the above formula, ξ_{av} is the current average position of the resonator, V_0 is a constant voltage applied, D is the number of delays ($D \geq 1$) and dt is a short interval of time ($dt < T_s$). We can summarise this actuation scheme as follows. If the position of the resonator at a given sampling time is below the time averaged position ($\xi < \xi_{av}$), a constant bias voltage is held $V_{fb} = V_0$ (no pulse applied). If the position of the resonator at a given sampling time is above the time averaged position

($\xi > \xi_{av}$), an 'anti'-pulse is applied: the constant biasing voltage V_0 is turned off for a very short time dt and then turn on again. A typical actuation waveform of the e-PDO is presented in Fig. 3.3c.

The system is described by the following equation:

$$\ddot{\xi}(t) + (b/m)\dot{\xi}(t) + \omega_0^2 \xi(t) = \frac{\varepsilon_0 A V_0^2}{2mg^2(1-\xi(t)/g)^2}\left(1 - \sum_n b_n \Pi(t - nT_s)\right) \tag{3.32}$$

where the natural frequency $\omega_0 = \sqrt{k/m}$, ε_0 is the vacuum permittivity, A is the area of the actuating electrode and g is the rest gap between the movable mass and the electrode. The sequence of the position sign b_n defines the application of an anti-pulse:

$$b_n = \frac{1}{2}\left[1 + \mathrm{sgn}(\xi((n-D)T_s) - \xi_{av})\right] \tag{3.33}$$

Since most of the time a constant voltage is applied and it turned off only for short time instances dt, the resonator will oscillate around an equilibrium position ξ_0. We introduce a small dimensionless deflection x from the electrostatic equilibrium position such that $\xi = g(x_0 + x)$ and dimensionless time $\tau = \omega_0 t$. A linearised equation describing the deflection x will have form

$$x'' + 2\beta x' + x = \frac{2\psi_0 x}{(1-x_0)^3}\left(1 - \sum_n b_n \Pi(\tau - n\tau_s)\right) - \frac{\psi_0}{(1-x_0)^2}\sum_n b_n \Pi(\tau - n\tau_s) \tag{3.34}$$

where $\beta = b/(2m\omega_0)$ is the normalised dissipation coefficient and $\psi_0 = \varepsilon_0 A V_0^2/(2m\omega_0^2 g^3)$ is the normalised force amplitude and the prime sign denotes the derivative with respect to dimensionless time τ. The electrostatic equilibrium x_0 is the solution of the equation

$$x_0 - \frac{\psi_0}{(1-x_0)^2} = 0 \tag{3.35}$$

and it is worth mentioning that $x_0 \approx x_{av}$ and with good accuracy we can assume that $x_{av} = x_0$. To obtain a map, one has to solve differential Eq. (3.34). Let us consider two cases.

No anti-pulse is applied. This case corresponds to $b_n = 0$, and the system is constantly biased. Equation (3.34) can be written into a simpler form

$$0 \le \tau < \tau_s: \qquad x'' + 2\beta x' + x(1 - 2\psi_0/(1-x_0)^3) = 0 \tag{3.36}$$

where $\tau_s = \omega_0 T_s$. Denoting $\omega_1 = \sqrt{1-\beta^2}$ and $\omega_2 = \sqrt{1-\beta^2-2\psi_0/(1-y_0)^3}$, we can write the solution of (3.36) in the form:

$$\begin{pmatrix} x(\tau_s) \\ y(\tau_s) \end{pmatrix} = e^{-\beta\tau_s}\mathbf{R}(\omega_2\tau_s)\begin{pmatrix} x(\tau_0) \\ y(\tau_0) \end{pmatrix} \tag{3.37}$$

where $\mathbf{R}$ is the rotation matrix. In the above equation, we used the variable $y = -\beta x/\omega_2 - x'/w_2$.

Anti-pulse is applied. This corresponds to the case $b_n = 1$. Equation (3.34) can be split into two equations

$$\begin{aligned} 0 \le \tau < d\tau: &\qquad x'' + 2\beta x' + x = -\frac{\psi_0}{(1-x_0)^2} \\ d\tau \le \tau < \tau_s: &\qquad x'' + 2\beta x' + x(1 - 2\psi_0/(1-x_0)^3) = 0 \end{aligned} \tag{3.38}$$

The solution of (3.38) is

$$\begin{aligned} \begin{pmatrix} x(\tau_s) \\ y(\tau_s) \end{pmatrix} = e^{-\beta\tau_s}\mathbf{R}(\omega_2(\tau_s - d\tau))\mathbf{A}\mathbf{R}(\omega_1 d\tau)\begin{pmatrix} x(\tau_0) \\ (\omega_2/\omega_1)y(\tau_0) \end{pmatrix} \\ + e^{-\beta\tau_2}\mathbf{R}(\omega_2(\tau_s - d\tau))F_0\begin{pmatrix} \zeta \\ (\omega_1/\omega_2)\eta \end{pmatrix} \end{aligned} \tag{3.39}$$

where $F_0 = -\psi_0/((1-y_0)^2)$ and $\mathbf{A} = \begin{pmatrix} 1 & 0 \\ 0 & (\omega_1/\omega_2)^b \end{pmatrix}$. The coefficients ζ and η are the same as described in Sect. 3.2 and using the notation introduced in this section, they can be presented in the following form:

$$\begin{aligned} \zeta &= 1 - e^{-\beta\tau_1}\cos(\omega_1 d\tau) - \frac{\beta\, e^{-\beta d\tau}}{\sqrt{1-\beta^2}}\sin(\omega_1 d\tau), \\ \eta &= -\frac{\beta}{\sqrt{1-\beta^2}} + \frac{\beta\, e^{-\beta d\tau}}{\sqrt{1-\beta^2}}\cos(\omega_1 d\tau) - e^{-\beta\tau_1}\sin(\omega_1 d\tau) \end{aligned} \tag{3.40}$$

An iterative system of equations can be obtained from (3.37) and (3.39) by assuming that $x_n = x(nT_s)$ and $y_n = y(nT_s)$. In its compact form, the resulting map can be written as

$$\begin{aligned} \begin{pmatrix} x_{n+1} \\ y_{n+1} \end{pmatrix} = \alpha\mathbf{R}(\omega_2(\tau_s - d\tau))\mathbf{A}\mathbf{R}(\omega_2(\omega_1/\omega_2)^{b_n} d\tau)\begin{pmatrix} x_n \\ (\omega_2/\omega_1)^{b_n} y_n \end{pmatrix} \\ + \alpha_\tau\mathbf{R}(\omega_2(\tau_s - d\tau))F_0 b_n\begin{pmatrix} \zeta \\ (\omega_1/\omega_2)^{b_n}\eta \end{pmatrix} \end{aligned} \tag{3.41}$$

where the sequence of signs b_n is defined as follows

$$b_n = \frac{1}{2}\left[1 + \mathrm{sgn}(x((n-D)T_s))\right] \tag{3.42}$$

In these equations, $\alpha = \exp(-\beta\tau_s)$ and $\alpha_\tau = \exp(-\beta(\tau_s - d\tau))$. This is a piecewise-smooth discontinuous map

$$\mathbb{R}^2 \times \mathbf{B}^D \longrightarrow \mathbb{R}^2 \times \mathbf{B}^D \tag{3.43}$$

where $\mathbb{R}$ is the set of real numbers and $\mathbf{B}$ is a two-element set such that $\mathbf{B} = \{0, 1\}$. Note that the this map transforms into to the conventional PDO map if $\omega_1 = \omega_2$ and $d\tau \ll \tau_s$ [41].

3.4.2 Results

Here we briefly discuss some of the results. Since the standard application for an e-PDO is as part of a resonant sensor and it is important to extract the change in the oscillation frequency in this system, the important parameter is the digital frequency of oscillations f_D or the rotation number ρ (recall that the actual frequency of oscillation is $f_{osc} = f_D f_s = \rho f_s$. The digital frequency can be calculated using the approach discussed in Sect. 3.3 and formula (3.26). The digital frequency of oscillation as a function of the normalised frequency $f = T_s\omega_0\sqrt{1-\beta^2}/2\pi$ is shown in Fig. 3.11a. This figure shows the same fractalised characteristic already seen in sigma-delta accelerometers and PDOs. The smaller the dissipation parameter β, the more straight is the plot. We also note that the system displays multistability, and a large number of stable cycles are admissible in the output at the same parameters. To demonstrate this, we present the basins of attractions corresponding to different cycles (Fig. 3.11b). Depending on the initial conditions (x_0, y_0), the system converges to different periodic solutions.

3.5 Control of Dielectric Charge for Capacitive MEMS

So far we have considered examples that are related to the actuation and control of movable mechanical components of MEMS. In this section, we discuss a very different example that is related to MEMS reliability and does not directly involve the control of MEMS mechanics.

The electrostatic mechanism of actuation already mentioned in this study is very common in MEMS. However, in some types of MEMS that utilise dielectric materials, it leads to the accumulation of charge in these dielectrics. It is known to be a major reliability problem for these devices and especially a problem for radio frequency (RF) MEMS [42]. As is reported in recent reviews [43, 44], the accumulation of charge by dielectrics is very common and all typical dielectric materials are

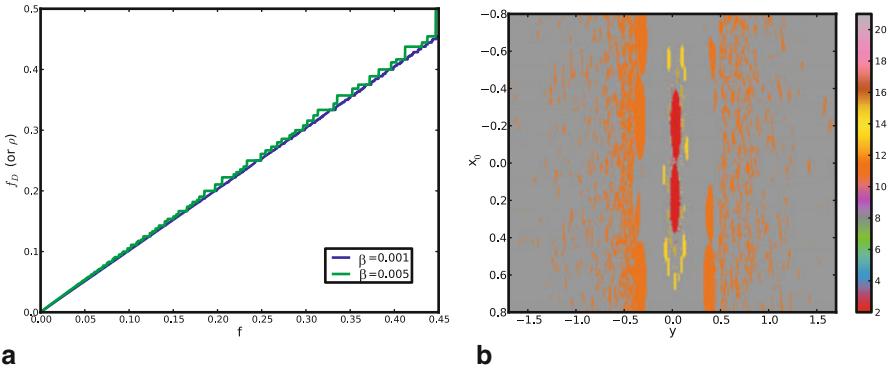

Fig. 3.11 Electrostatic pulsed digital oscillator described by map (3.41). **a** Digital frequency of oscillation (related to the actual oscillation frequency of the e-PDO) as a function of a normalised frequency f (rested to the sampling frequency and the natural frequency). The plot consists of a number of plateaus that are more visible when β is larger. **b** Example of the basins of attraction of different cycles in the plane of initial conditions (x_0, y_0)

prone to it. In recent years, an alternative approach that consists of bipolar [45] and smart actuation techniques [20, 46] is suggested to address the problem of dielectric charging.

In references [20], a smart actuation method based on a feedback control was proposed for the actuation of capacitive MEMS with dielectrics. The aim of the actuation and control method is to ensure that the charge accumulated in the dielectric is not increasing and stays fixed at a desired level by applying a bipolar actuation voltage. We have investigated this method for a simple 1D model suitable for MEMS positioners and varactors which operate below pull-in of the MEMS structure. (*Pull-in* is a phenomenon when the movable suspended electrode collapses onto the fixed electrode, since the electrostatic force can no longer be compensated by the restoring mechanical force). In addition, we experimentally demonstrated that the method can be applied to switches which operate beyond pull-in. The proposed closed-loop feedback technique is based on the measurement of the MEMS capacitance at fixed time instances nT_s. The total capacitance of the device is a function of the position $x(t)$ which is directly linked to the accumulated total charge in the dielectric Q_d. Thus, the value of the total capacitance for a given voltage can be treated as an 'indicator' of the value of the total accumulated dielectric charge.

3.5.1 Statement of the Problem

A simple 1D model of a variable capacitor is shown in Fig. 3.2d. The deflection of the top electrode y is described by a mass-spring-damper ordinary differential equation

$$m\ddot{x}(t) + b\dot{x}(t) + kx(t) = F_{\text{el}}(V, x) \tag{3.44}$$

where m is the mass of the movable electrode, b is the damping factor and k is the spring coefficient. The value of the damping coefficient is large as the top electrode is moving in air, so the first two terms can be neglected. Thus, the system will reach the steady state relatively fast. Then, the position $x(t)$, for a given value of voltage, is obtained analytically by solving the equation which expresses the balance of forces

$$ky = F_{el}(V, x) \tag{3.45}$$

where

$$F_{\text{el}} = \frac{\varepsilon_0 A}{2} \frac{(V - V_{\text{shift}})^2}{(g - x + \frac{d}{\varepsilon_d})^2}. \tag{3.46}$$

Here, V is the applied voltage, ε_0 is the vacuum permittivity, ε_d is the relative permittivity of the dielectric, g is the gap distance between the upper electrode and the dielectric, d is the thickness of the dielectric layer, A is the area of the device and $V_{\text{shift}} = Q_d/C_d$ is the voltage shift due to the accumulated charge Q_d into the dielectric. The capacitance C_d associated with the dielectric layer is given by $C_d = \varepsilon_0 \varepsilon_d A/d$. From (3.45), it follows that there is a critical value of F_{el} that exceeds the restoring spring force ky. In this case, the equilibrium position of the device cannot be maintained any longer. This results in the instantaneous collision of the top electrode onto the dielectric layer and the bottom electrode. Such an event (the collapse of the movable electrode) is called the pull-in event and the corresponding voltage is known as the pull-in voltage V_{PI}.

To make the above equations self-consistent, we must supply the equations that define the evolution of the dielectric charge with the applied voltage and time. The electrostatic force in (3.46) depends on the voltage shift

$$V_{\text{shift}}(t) = Q_d(t)/C_d, \quad V_{\text{eff}}(t) = V - V_{\text{shift}}(t) \tag{3.47}$$

that is a function of the charge accumulated in the dielectric. The device 'sees' that effective voltage which deviates from the applied voltage V. The evolution of the dielectric charge Q_d is related to the actuation voltage and time. In principle, positive and negative charge can be accumulated into the dielectric. There are various proposed models which describe that evolution taking into account charge injection, dipole orientation, charge trapping along with others or combination of those [42]. The exact mechanism depends also on the device characteristics. Here, we will use a semi-empirical multi-exponential charging model where positive and negative charging components are included [20]. The time evolution of each component is

$$Q^p(t) = \begin{cases} Q^p_{max} \sum_i \zeta_i^p e^{-t/t^p_{Di}} & V > 0 \\ Q^p_{max}(1 - \sum_i \zeta_i^p e^{-t/t^p_{Ci}}) & V < 0 \end{cases}$$

$$Q^n(t) = \begin{cases} Q^n_{max}(1 - \sum_i \zeta_i^n e^{-t/t^n_{Ci}}) & V > 0 \\ Q^n_{max} \sum_i \zeta_i^n e^{-t/t^n_{Di}} & V < 0 \end{cases} \tag{3.48}$$

where Q^p_{max} and Q^n_{max} are the maximum values of positive and negative charges, respectively, t_{Ci} and t_{Di} the charging and discharging time constants and ζ_i coefficients which express the weight of each exponential to the total charge (thus $\sum_i \zeta_i = 1$ for each component). The coefficients ζ_i and the characteristic times τ_i are can be determined from experiment data and are different, in general, between the positive and negative components. Now, the evolution of the total charge will be

$$Q_d(t) = Q^p(t) + Q^n(t) \tag{3.49}$$

The control method from [20] monitors the parasitic charge in the dielectric by comparing the capacitance C_n of the device in each sampling time nT_s with a threshold value C_{th}, where

$$C_n = \frac{C_{g,0}}{1 - \frac{x_n}{g} + \frac{C_{g,0}}{C_d}} \tag{3.50}$$

its discretised expression with $C_{g,0} = A\varepsilon_0/g$ the capacitance of the gap and x_n the discretised position of the up electrode in sampling time nT_s. As long as the value of C_n is less than C_{th} a positive actuation voltage V^+ is applied. When the value of C_n exceeds the threshold value the polarity in the next time instant will be inversed and negative voltage V^- will be applied. Summarising, the control method follows the scheme:

$$V_n = \begin{cases} V^+ & \text{if} \quad C_n < C_{th} \\ V^- & \text{if} \quad C_n > C_{th} \end{cases} \tag{3.51}$$

with V_n the applied voltage at the nth sampling time. The capacitance threshold value C_{th} biuniquely corresponds to a charge target value Q_{th} that the control method aims to fix into the dielectric. The voltage actuation waveform will be somewhat similar to the waveform shown in Fig. 3.3a.

By defining the quantities $\alpha_C = e^{-T_s/\tau_C}$ and $\alpha_D = e^{-T_s/\tau_D}$ the discretised equations for charge evolution Eq. 3.48 for the case $i = 1$ will have form

$$Q_{n+1} = \alpha_D \left(\frac{\alpha_C}{\alpha_D}\right)^{b_n} Q_n + Q_{max}(1 - \alpha_C)b_n = \Phi(Q_n, b_n) \tag{3.52}$$

where we introduced the decision bit sequence b_n as

$$b_n = \frac{1}{2}(1 + \text{sgn}(C_{th} - C_n)). \tag{3.53}$$

The complete model that describes the evolution of charge can be expressed as

$$Q_{n+1} = \sum_i \Phi_i(Q_n^{(i)}, b_n) = \Theta(Q_n, b_n) \tag{3.54}$$

The general form of the map which expresses the evolution of the charge dynamics under the operation of this control algorithm can be written for the state vector (Q, b)

$$\begin{pmatrix} Q_{n+1} \\ b_{n+1} \end{pmatrix} = \begin{pmatrix} \Theta(Q_n, b_n) \\ \frac{1}{2}\left[1 + \mathrm{sgn}\left(C_{th} - \frac{C_{g,0}}{1+\gamma-x(Q_n,b_n)/g}\right)\right] \end{pmatrix} \tag{3.55}$$

and this is a piecewise-smooth mapping of the form

$$\mathbb{R} \times \mathbf{B} \to \mathbb{R} \times \mathbf{B} \tag{3.56}$$

where $\mathbb{R}$ is the set of real numbers and $\mathbf{B} = \{0, 1\}$.

3.5.2 Periodic Solutions

According to [35], the output of the map (3.55) are stable periodic sequences, or cycles. By considering for simplicity $i = 1$ in (3.48) and introducing the parameters $\nu = \alpha_C/\alpha_D$, $\mu = Q_{max}(1 - \alpha_C)$ and the sum

$$S_p^q = \sum_{j=p}^{q} b_{n+j} \tag{3.57}$$

for $p \leq q$, the kth iteration of the map is

$$Q_{n+k} = \alpha_D^k \nu^{S_0^{k-1}} Q_n - \mu \sum_{j=1}^{k-1} \alpha_D^{k-j} \nu^{S_j^{k-1}} b_{n+j-1} - \mu b_{n+k-1} \tag{3.58}$$

Since the sequence $\{b_n\}$ is periodic [35], $Q_n = Q_{n+N}$. Using N instead of k and $S^N = S_0^{N-1}$ as the sum of all b_n in the sequence, we write that

$$Q_n = \frac{-\mu}{1 - \alpha_D^N \nu^{S^N}} \left(b_{n+N-1} + \sum_{j=1}^{N-1} \alpha_D^{N-j} \nu^{S_j^{N-1}} b_{n+j-1} \right) \tag{3.59}$$

and this equation defines the cycles of charge displayed by map (3.55) if the sequence b_n for $1 \geq n \leq N$ is given. The stability analysis of a cycle can be done using the approach discussed in Sect. 3.2 and one can ensure that this cycle is asymptotically stable.

3.5.3 Results

An important property of this control method is that subsequent discharging events are not possible, i.e. the bitstream sequence cannot contain two subsequent zeros. At the moment the polarity of the applied voltage changes (when the total capacitance

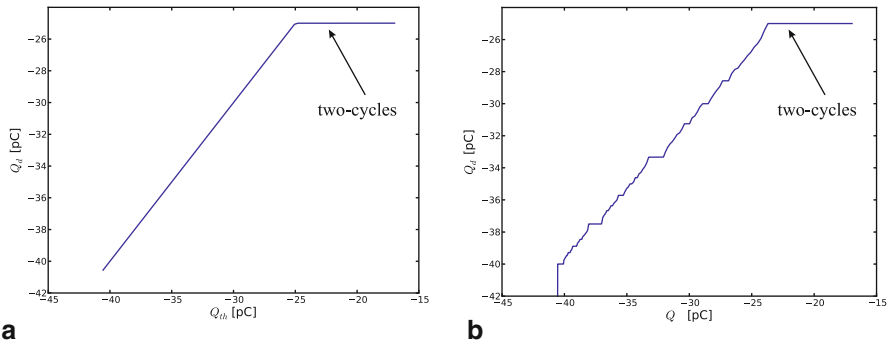

Fig. 3.12 Control of dielectric charge for capacitive MEMS described by map (3.55). Charge Q_d fixed by the control method in the dielectric as a function of a desired charge amount Q_{th}. **a** corresponds to a short sampling time ($T_s = 0.01$ s) while **b** corresponds to a larger sampling time ($T_s = 5$ s). The large plateau seen in both figures corresponds to the 2-cycle. The parameters of the device used in this simulation are taken from [20]

exceed the C_{th} value) the total capacitance drops below the C_{th} value. Thus, the next event will be a charging event (of the opposite polarity). This means that the minimum amount of charge the control algorithm is able to fix in the device is restricted to one charging and one discharging events defining the *two-cycle*

$$\begin{aligned} \hat{Q}_1 &= -\frac{\alpha_D \mu}{(1-\beta)}, \qquad (b_1 = 1) \\ \hat{Q}_2 &= -\frac{\mu}{(1-\beta)}, \qquad (b_2 = 0) \end{aligned} \tag{3.60}$$

where we denoted $\beta = \alpha_C \alpha_D$.

Therefore, the minimum amount of charge in the dielectric is defined by this two-cycle. If the target charge Q_{th} set for the algorithm is less than the charge defined by the two-cycle, the control algorithm will not be able to fix the desired dielectric charge. Instead, the charge corresponding to the two-cycle will be fixed. Thus, depending on the system parameters, the control method will yield either the sequence of charge Q_n given by (3.59) with $N > 2$ whose average value is equal to the desired amount of charge Q_{th} or a two-cycle (3.60) whose average value will be, in the most general case, larger than the desired amount. Therefore, we say that the control algorithm operates successfully if the output bit sequence b_n corresponds to a cycle with $N > 2$.

For the illustration of the control method, the parameters given in [20] are used in this study. The parameter of interest in such a system is the time-averaged charge in the dielectric controlled by the algorithm. In order to show the performance of the control method, in Fig. 3.12 we plot the average dielectric charge as a function of the target charge $Q_d(Q_{th})$. In the ideal case, this must be a straight line: a small change in Q_{th} must result in the small change of Q_d that algorithm fixes in the dielectric. This plot is shown in Fig. 3.12. Figure 3.12a corresponds to a very short sampling

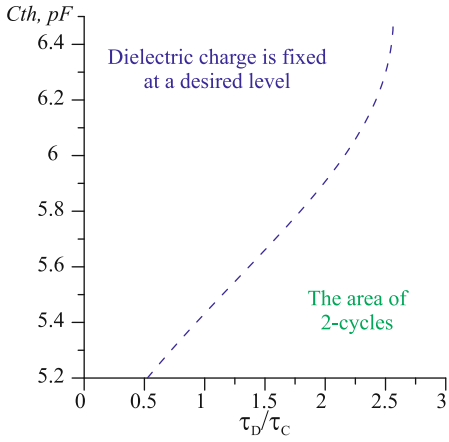

Fig. 3.13 Control of dielectric charge for capacitive MEMS described by map (3.55). Simulated capacitance and dielectric charge transients applying the charge control method

time T_s while Fig. 3.12b corresponds to a very long sampling time. For a relatively large T_s, the plot is not a straight line, but resembles rather a devils staircase plot. The devils staircase has already appeared in other examples from this study. Practically, the presence of devils staircase in this system means that the algorithm will have a finite resolution/accuracy of fixing the dielectric charge when T_s is large. There is a large plateau seen in both figures for smaller Q_{th}. This large plateau corresponds to a two-cycle. In this case, some charge is fixed in the dielectric, but it does not correspond to a desired level.

To obtain a broader understanding of the system dynamics, we can consider a plane of parameters spanned by the target capacitance C_{th} (related to the desired charge Q_{th}) and the ratio of the discharging and charging times τ_D/τ_C that strongly affect the behaviour of the system. We can define the area where the algorithm is able to fix Q_{th} (successful operation of the algorithm) and where the algorithm is not able to fix Q_{th} (the output of the algorithm is a two-cycle). The two boundary is given by the following equation:

$$-\frac{\alpha_D \mu}{(1-\beta)} = Q_{th} \tag{3.61}$$

Figure 3.13 shows such a plane with the above boundary plotted. Practically, this means that for realistic devices one should select the algorithm parameters above the dashed line shown in the figure.

3.6 Conclusions

We have considered a number of examples describing a MEMS, actuated or controlled, by a feedback inspired by sigma-delta modulation. In the introduction, we described the principles of sigma-delta conversion and showed how they can be applied to actuated or controlled MEMS. We discussed three examples: an inertial

sensor, a self-sustained oscillator and a charge control actuation method. In all cases, we have shown how a piecewise-smooth discontinuous map arises as a model of these systems. Although belonging to different class of devices, all the examples display a number of similar features, for instance, a devil's staircase as the representation of frequency or charge locking. For all these models, the output is a stable sequence (cycle) and frequency/charge locking corresponds to a specific cycle of the map that persists or dominates in a large area of control parameters. A very similar phenomenon was found in conventional leaky sigma-delta modulators and it reflects the finite resolution in representing the input signal. In a self-sustained oscillator, the persistence of limit cycles give rise to frequency locking, i.e. the inability of the oscillator to change its frequency for certain values of control parameters. Finally, in the problem of charge control in capacitive MEMS, we observe charge locking. Charge locking is very similar to frequency locking and it displays the finite resolution of charge control in MEMS. The persistence of limit cycles and frequency and charge locking are parasitic phenomena. Since we present the study of the system dynamics over wide range of parameters, we can estimate the values of parameters in order to avoid these undesirable effects. The models we present in this chapter that describe realistic systems and behaviour were experimentally validated in a number of cited studies. We refer a reader who is interested in further investigation of MEMS, and in particular of sigma-delta inspired MEMS to the literature cited in this chapter.

Acknowledgement This work was supported by Science Foundation Ireland.

References

1. Norsworthy, S., Schreier, R., Temes, G.: Delta-Sigma Data Converters: Theory, Design, and Simulation, vol. 309. IEEE press, New York, 1996
2. Janssen, E., van Roermund, A., Look-Ahead Based Sigma-Delta Modulation in Analog Circuits and Signal Processing. Springer, New York, 2011
3. Avrutin, V., Schanz, M., Banerjee, S.: Multi-parametric bifurcations in a piecewiselinear discontinuous map. Nonlinearity **19**, 2006
4. Simpson, D.J.W., Meiss, J.D.: Neimarksacker bifurcations in planar, piecewise-smooth, contimaps. J. Appl. Dyn. Syst. **7**, 2008
5. Feely, O.: Nonlinear dynamics of discrete-time circuits: a survey. Int. J. Circuit Theory Appl. **35**(5/6), 515–531 (2007)
6. Feely, O.: Discontinuous piecewise-linear discrete-time dynamics—maps with gaps in electronic systems. Int. J. Comput. Math. Electrical Electronic Eng. **30**, 1296–1306 (2011)
7. Boser, B.E., Howe, R.T.: Surface micromachined accelerometers. IEEE Trans. Syst. Sci. Cybernetics **31**, 366 (1996)
8. Kraft, M., Lewis, C.P., Hesketh, T.: Closed loop silicon accelerometers. IEE Proc. Circuits Devices Syst. **145**, 325 (1998)
9. Wu, J., Carley, L.R.: Electromechanical $\Delta\,\Sigma$ modulation with high-Q micromechanical accelerometers and pulse density modulated force feedback. IEEE Trans. Circuits Syst. I **53**, 274 (2006)
10. Soen, J., Voda, A., Condemine, C.: Controller design for a closed-loop micromachined accelerometer. Control Eng. Pract. **15**, 57 (2007)

11. Comi, C., Corigliano, A., Langfelder, G., et al.: A resonant microaccelerometer with high sensitivity operating in an oscillating circuit. J. Microelectromech. Syst. **10**, 1140 (2010)
12. Raman, J., Cretu, E., Rombouts, P., Weyten, L.: A closed-loop digitally controlled MEMS gyroscope with unconstrained sigma-delta force-feedback. IEEE Sensors J. **9**, 297 (2009)
13. Domínguez, M., Pons-Nin, J., Ricart, J., Bermejo, A., Figueras Costa, E.: A novel $\Sigma - \Delta$ pulsed digital oscillator (PDO) for MEMS. IEEE Sensors J. **5**, 1379–1388 (2005)
14. Domínguez, M., Pons-Nin, J., Ricart, J., Bermejo, A., Figueras Costa, E., Morata, M.: Analysis of the $\Sigma - \Delta$ pulsed digital oscillator for MEMS. IEEE Trans. Circuits Syst. I **52**, 2286 (2005)
15. Ricart, J., Pons, J., Domínguez, M., Rodríguez, A., Figueras, E., Gutiérrez, M.C.H.J., Sayago, I.: Application of pulsed digital oscillators to volatile organic compounds sensing. Sens. Actuators B **134**, 773–779 (2008)
16. Makinwa, K., Huijsing, J.: A wind-sensor with integrated interface electronics. In: Circuits and Systems, 2001. ISCAS 2001. The 2001 IEEE International Symposium on, vol. 1. IEEE, pp. 356–359 (2001)
17. Makinwa, K., Huijsing, J.: A smart wind sensor using thermal sigma-delta modulation techniques. Sens. Actuators A Phys. **97**, 15–20 (2002)
18. Domínguez, M., Masana, F., Jiménez, V., Bermejo, S., Amirola, J., Ballester, J., Fueyo, N., Castañer, L.: Low-cost thermal Σ-Δ air flow sensor. Sens. J. IEEE **2**(5), 453–462 (2002)
19. Dominguez, M., Jiménez, V., Ricart, J., Kowalski, L., Torres, J., Navarro, S., Romeral, J., Castañer, L.: A hot film anemometer for the martian atmosphere. Planet. Space Sci. **56**(8), 1169–1179 (2008)
20. Blokhina, E., Gorreta, S., Lopez, D., Molinero, D., Feely, O., Pons-Nin, J., Dominguez-Pumar, M.: Dielectric charge control in electrostatic MEMS positioners/varactors. Microelectromech. Syst. J. **21**(3), 559–573 (2012)
21. Gorreta, S., Pons-Nin, J., Blokhina, E., Feely, O., Dominguez-Pumar, M.: Delta-sigma control of dielectric charge for contactless capacitive MEMS. IEEE/ASME J. MEMS (2014) (in press)
22. Senturia, S.D.: Microsystem Design. Springer, New York, (2004)
23. Fedder, G.K.L: Simulation of microelectromechanical systems. Ph.D. dissertation, U. C. Berkeley (1994)
24. Feely, O., Chua, L.: The effect of integrator leak in Σ–Δ modulation. IEEE Trans. Circuits Syst. **38**, 1293 (1991)
25. Kraft, M.: Closed loop accelerometer employing oversampling conversion. Ph.D. dissertation, Coventry University (1997)
26. Colinet, E., Juillard, J., Nicu, L., Bergaud, C.: Digital self-calibration method for MEMS sensors. IEEE Trans. Instrum. Meas. **54**, 1438 (2005)
27. Juillar6d, J., Colinet, E.: Using Tsypkin's approach for the study of a class of mixed-signal nonlinear systems. IEEE Trans. Circuits Syst. I **53**, 2746 (2006)
28. Teplinsky, A., Feely, O.: Limit cycles in a MEMS oscillator. IEEE Trans. Circuits Syst. II **55**, 882 (2008)
29. Domínguez, M., Pons-Nin, J., Ricart, J.: General dynamics of pulsed digital oscillators. IEEE Trans. Circuits Syst. I **55**, 2038–2050 (2008)
30. Kraft, M., Redmen-White, W., Mokhtari, M.E.. Closed loop micromachined sensors with higher order $\Sigma\,\Delta$–modulators. In: Proceeding of the 4th Conference on Modeling and Simulation of Microsystems, Hilton Head Island, p. 104 (2001)
31. Dong, Y., Kraft, M., Redman-White, W.: Force feedback linearization for higher-order electromechanical sigmadelta modulators. J. Micromech. Microeng. **16**, 54 (2006)
32. Blokhina, E., Feely, O., Dominguez, M.: Dynamics of the MEMS pulsed digital oscillator with multiple delays in the feedback loop. In: Proceeding of IEEE ISCAS 2009, Taipei, Taiwan, p. 1903, 24–27 May 2009
33. Blokhina, E., Pons, J., Ricart, J., Feely, O., Pumar, M.: Control of MEMS vibration modes with pulsed digital oscillators: part itheory. Circuits Syst. I Regu. Pap. IEEE Trans. **57**(8), 1865–1878 (2010)
34. Pladys, M., Blokhina, E.: MEMS with Σ-Δ type of feedback loop control as an iterative map. In Circuits and Systems (ISCAS), 2011 IEEE International Symposium on. IEEE, pp. 977–980 (2011)

35. Bruin, H., Deane, J.H.B.: Piecewise contractions are asymptotivally periodic. Proc. Am. Math. Soc. **137**, 1389–1395 (2008)
36. Beeby, S., Ensell, G., Kraft, M., White, N.: MEMS Mechanical Sensors. London, Artech House Inc (2004)
37. Domínguez Pumar, M., Ricart, J., Pons Nin, J., Blokhina, E., Gorreta, S., Hernando, J., Manzaneque, T., Sanchez Rojas, J., Feely, O.: Control of MEMS vibration modes with pulsed digital oscillators. part ii: simulation and experimental results. Circuits Syst. I Regu. Pap. IEEE Trans. **57**(8), 1879–1890 (2010)
38. Wu, T., Chang, W., Hsu, J.: Effect of tip length and normal and lateral contact stifness on the flexural vibration responses of atomic force microscope cantilevers. Microelectron. Eng. **71**, 15–20 (2004)
39. Chang, W., Lee, H., Chen, T.Y.: Study of the sensitivity of the first four flexural modes of an AFM cantilever with a sidewall probe. Ultramicroscopy **108**, 619–624 (2008)
40. Hilborn, R.: Chaos and Nonlinear Dynamics: An Introduction for Scientists and Engineers. Oxford University Press, USA (2000)
41. Gorreta, S., Fernández, D., Blokhina, E., Pons-Nin, J., Jiménez, V., O'Connell, D., Feely, O., Madrenas, J., Dominguez, M.: Pulsed digital oscillators for electrostatic MEMS. IEEE Trans. Circuit. Syst. I. **59**, 2835–2845 (2012)
42. Lucuszyn, E.S.: Advanced RF MEMS. Cambridge, Cambridge University Press (2010)
43. van Spengen, W.M.: Capacitive RF MEMS switch dielectric charging and reliability: a critical review with recommendations. J. Micromech. Microeng. **22**(7), 074001 (2012)
44. de Groot, W., Webster, J., Felnhofer, D., Gusev, E.: Review of device and reliability physics of dielectrics in electrostatically driven MEMS devices. Device Mater. Reliab. IEEE Trans. **9**(2), 190–202 (2009)
45. Peng, Z., Yuan, X., Hwang, J.C., Forehand, D.I., Goldsmith, C.L.: Superposition model for dielectric charging of RF MEMS capacitive switches under bipolar control-voltage waveforms. Microw. Theory Tech. IEEE Trans. **55**(12), 2911–2918 (2007)
46. Ikehashi, T., Miyazaki, T., Yamazaki, H., Suzuki, A., Ogawa, E., Miyano, S., Saito, T., Ohguro, T., Miyagi, T., Sugizaki, Y., Otsuka, N., Shibata, H., Toyoshima, Y.: An RF MEMS variable capacitor with intelligent bipolar actuation. In: Solid-State Circuits Conference, 2008. ISSCC 2008. Digest of Technical Papers. IEEE International (2008)

Chapter 4
Kinetic Exchange Models in Economics and Sociology

Sanchari Goswami and Anirban Chakraborti

Abstract In this chapter, we briefly review the different aspects and applications of kinetic exchange models in economics and sociology. Our main aim is to show in what manner the kinetic exchange models for closed economic systems were inspired by the kinetic theory of gas molecules. The simple yet powerful framework of kinetic theory, first proposed in 1738, led to the successful development of statistical physics of gases towards the end of the nineteenth century. This framework was successfully adapted to modelling of wealth distributions in the early 2000s. In later times, it was applied to other areas like firm dynamics and opinion formation in the society, as well. We have tried to present the flavour of the several models proposed and their applications, intentionally leaving out the intricate mathematical and technical details.

4.1 Introduction

The aim of statistical physics is to study the physical properties of macroscopic systems consisting of a large number of particles. In such large systems, the number of particles is of the order of Avogadro number. Thus, it is extremely difficult to have a complete microscopic description of such a system, both experimentally and by the way of solving equations of motion. In spite of the complexity of such systems, they exhibit some macroscopic observable quantities, which represent averages over microscopic properties [1–3].

A society can be described as a group of people sharing the same geographical or social territory and involved with each other by means of sharing different aspects of life.

A. Chakraborti (✉)
School of Computational and Integrative Sciences,
Jawaharlal Nehru University, New Delhi 110067, India
e-mail: anirban@mail.jnu.ac.in

S. Goswami
S.N. Bose National Centre for Basic Sciences,
JD Block, Sector III, Salt Lake City, Kolkata 700098, India
e-mail: sanchari.goswami@bose.res.in

R. López-Ruiz et al. (eds.), *Nonlinear Maps and their Applications,*
Springer Proceedings in Mathematics & Statistics 112, DOI 10.1007/978-3-319-12328-8_4

In sociology, a branch of social sciences, one studies the human social behaviour in a society. Economics is another branch of the social sciences which analyses the production, distribution, and consumption of goods and services. Since the society is usually formed with a very large number of people, the study of an individual is extremely difficult. However in various cases, one can observe and characterize some average behaviour of the people, e.g. in case of a voting a large number of people selects a particular opinion. Similar to many physical phenomena, quite well-understood by physicists, it has been found that a study of crime, a social phenomenon, displays a first-order transition between states of high- and low-crime rates as a function of severity of the criminal justice system. Also, a model of marriage, another social phenomenon, shows critical behaviour such that the relation among marriage rates, economic incentives, and social pressures show a surface similar to a P-V-T surface of a fluid. Also, the dynamical nature of interaction of any economic sector which is composed of a large number of cooperatively interacting agents, has many features in common with the interacting systems of statistical physics. These naïvely suggest that study of society as viewed by the economists and sociologists, can also be done using the tools of statistical mechanics developed by the physicists. The application of statistical mechanics to the fields of economics and sociology have resulted in the interdisciplinary fields namely "econophysics" [4] and "sociophysics" [5]. According to P. Ball [6],

> At face value, there might seem to be little room left for statistical physics to make a realistic contribution. But if there is one message that emerges clearly from this discipline, it is that sometimes the details do not matter. That, in a nutshell, is what is meant by universality. It does not matter that the Ising model is a ridiculously crude description of a real fluid; they both have the same behaviour at the critical point because in that circumstance only the broad-brush features of the system, such as the dimensionality and range of particle interactions, determine the behaviour.

The kinetic exchange model is one of the simplest models in statistical mechanics, which derives the average macroscopic behaviours from the microscopic properties of particles. The kinetic exchange model is in general based on the exchange of energy among particles due to elastic collisions occurring among them. Bernoulli, in 1738, gave a complete description of the movement and activities of gas molecules in *Hydrodynamica* which is well known as "Kinetic theory of gases". This attempt was later developed and formalized by several other pioneers of "Statistical Thermodynamics", such as Clausius, Maxwell, Boltzmann, Planck, and Gibbs. In this chapter, we will present some existing models in several fields of, not only natural sciences but also social sciences, such as economics and sociology [7].

4.2 Kinetic Exchange Models in Economics

An economy can be studied in various ways. For example, one can study the economy in the light of individual's wealth as well as production of goods or wealth by firms in that economy. The economy consists of a large number of firms populated by

workers. By firms we mean production units, each and every one of which is capable of producing any kind of goods and services.

The famous Italian economist Vilfredo Pareto, in 1897, observed that the income distribution in Europe follow a power-law tail [8]. The tail-end distribution of income is given as,

$$p(m) \sim m^{-(1+\nu)}, \tag{4.1}$$

where ν is called the Pareto exponent. The value of the exponent as measured by Pareto for different kingdoms and countries varied between 1.1 to 1.7 [8]. Pareto also observed that roughly 80% of the total wealth is limited to the hands of only 20% people of the society; this signifies that there is a small finite number of extremely rich people in a society.

Several surveys were done to verify Pareto law. Japanese, Australian, and Italian personal income distribution have been shown to have a log-normal distribution for the lower income range and a power-law tail at higher income portion [9–11]. In India, studies revealed that the income of rich people follow power-law distribution [12]. Similar thing is observed for the income and wealth distribution in the modern USA and UK [13, 14], and other countries. All these studies show the evidence of the power law tail but the Pareto exponent is found to vary between 1 and 3 [4, 9–22].

In any society or country, one finds that the total wealth remains fairly constant on a longer time scale than its movement from individual to individual. This is because the dynamics of the latter occurs at shorter time scales (e.g., daily or weekly). This in turn results in very robust type of wealth distributions. Empirical data for society show a small variation in the value of the power-law exponent at the "tail" of the distribution, while it equals to unity for firms.

The interesting question is then, why is such "universal" behaviour as the widespread Pareto law, observed in the case of wealth distribution in the society. To this aim, a number of models have been proposed to reproduce these observed features, specifically to obtain a power-law tail as was observed in empirical data. Many of these models have been inspired by the kinetic theory of gas-like exchanges. Notably, in 1960, the mathematician and economist Mandelbrot, wrote:

> There is a great temptation to consider the exchanges of money which occur in economic interaction as analogous to the exchanges of energy which occur in physical shocks between molecules. In the loosest possible terms, both kinds of interactions should lead to similar states of equilibrium. That is, one should be able to explain the law of income distribution by a model similar to that used in statistical thermodynamics: many authors have done so explicitly, and all the others of whom we know have done so implicitly.

4.2.1 Ideal Gas-Like Kinetic Wealth Exchange Models (KWEM)

A trading process may be realized in a manner similar to the gas molecules exchanging energy in the kinetic theory of gases, where now a pair of traders exchange wealth, respecting local conservation in any trading [23–30]. These models have a

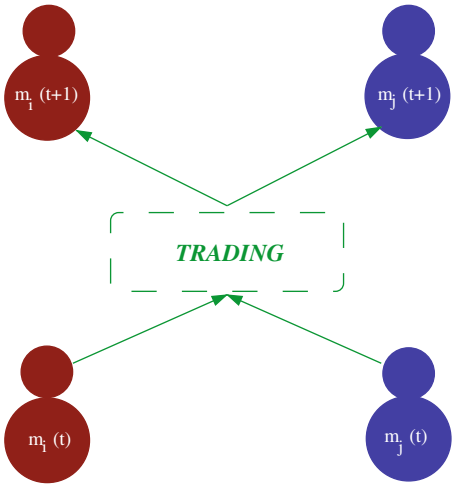

Fig. 4.1 A typical example of two agents i and j taking part in a trading process. Agent i and j have wealth $m_i(t)$ and $m_j(t)$ at time t. After a trading their wealth become $m_i(t+1)$ and $m_j(t+1)$ respectively

microcanonical description and nobody ends up with negative wealth (i.e. debt is not allowed). Thus, for two agents i and j with wealth $m_i(t)$ and $m_j(t)$ at time t, the general trading is given by:

$$m_i(t+1) = m_i(t) + \Delta m;\ m_j(t+1) = m_j(t) - \Delta m; \tag{4.2}$$

time t changes by one unit after each trading. A typical wealth exchange process is shown in Fig. 4.1.

4.2.1.1 Model with No Saving

In a simple conservative model proposed by Drăgulescu and Yakovenko (DY model) [25], N agents exchange wealth randomly keeping the total wealth M constant. The simplest model considers a random fraction of total wealth to be shared:

$$\Delta m = \varepsilon_{ij}(m_i(t) + m_j(t)) - m_i(t), \tag{4.3}$$

where ε_{ij} is a random fraction ($0 \leq \varepsilon_{ij} \leq 1$). The steady-state ($t \to \infty$) wealth follows a Boltzmann–Gibbs distribution: $P(m) = (1/T)\exp(-m/T)$; $T = M/N$, a result which is robust and independent of the topology of the (undirected) exchange space [27, 28].

The Boltzmann–Gibbs distribution, a fundamental law of equilibrium statistical mechanics, states that the probability $P(\varepsilon)$ of finding a physical system or subsystem in a state with the energy ε is given by the exponential function

$$P(\varepsilon) = ce^{\varepsilon/T}.$$

Here, the conserved quantity is the total energy.

If $m_1 > m_2$ and the agents share some random fraction of wealth $2m_2$ and not of the total $(m_1 + m_2)$, which indicates trading at the level of lower economic class in the trade, then all the wealth in the market drifts to one agent drastically [31, 32]. In [33], different approaches to obtain the exponential Boltzmann–Gibbs distribution have been addressed and a new operator in the framework of functional iteration theory has been proposed. It shows the exponential distribution to be ubiquitous in the framework of many multi-agent systems, not only economic ones but more diverse ones which have some economic inspiration included.

4.2.1.2 Model with Uniform Saving

An additional concept of *saving propensity* was considered first by Chakraborti and Chakrabarti [26] (CC model hereafter). Here, the agents save a fixed fraction λ of their wealth when interacting with another agent. Thus, two agents with initial wealth $m_i(t)$ and $m_j(t)$ at time t interact such that they end up with wealth $m_i(t+1)$ and $m_j(t+1)$ given by

$$\begin{aligned} m_i(t+1) &= \lambda m_i(t) + \varepsilon_{ij}\left[(1-\lambda)(m_i(t)+m_j(t))\right], \\ m_j(t+1) &= \lambda m_j(t) + (1-\varepsilon_{ij})\left[(1-\lambda)(m_i(t)+m_j(t))\right]; \end{aligned} \tag{4.4}$$

ε_{ij} being a random fraction between 0 and 1, modelling the stochastic nature of the trading. It is easy to see that the $\lambda = 0$ case is equivalent to the DY model—the market is noninteracting in this case, and the most probable wealth per agent is 0 here. The market is again noninteracting for $\lambda = 1$ when the most probable wealth per agent is M/N. We have a so-called "interacting" market when λ has any nonvanishing value between 0 and 1. The steady state distribution $P(m)$ is exponentially decaying on both sides. It is interesting to note that, the most probable value for such λ's is something in between 0 and M/N so that the fraction of deprived people decrease with saving fraction λ and most people end up with some finite fraction of the average wealth in the market. This is a "self-organizing" feature of the market. This results in completely different types of wealth distribution curves, very well approximated by Gamma distributions [34–36] given by,

$$P(m) = Cm^{\alpha} \exp(-m/T), \tag{4.5}$$

where $T = \frac{1}{\alpha+1}$ and $C = \frac{(\alpha+1)^{\alpha+1}}{\Gamma(\alpha+1)}$. The exponent α is related to the saving propensity λ by the relation :

$$\alpha = \frac{3\lambda}{1-\lambda}. \tag{4.6}$$

The $\lambda = 0$ limit can be verified from the above results. This fits well to empirical data for low and middle wealth regime [9–14, 19–22]. The model features are somewhat similar to Angle's work [37, 38]. Obviously, the CC model did not lead to the expected behaviour according to Pareto law.

In [39–41], the equivalence between kinetic wealth-exchange models and mechanical models of particles was shown and the universality of the underlying dynamics was studied both through a variational approach based on the minimization of the Boltzmann entropy and a microscopic analysis of the collision dynamics of molecules in a gas. In case of systems with a homogeneous quadratic Hamiltonian and N (effective) degrees of freedom, the canonical equilibrium distribution is a gamma distribution of order $N/2$. For the CC model, the effective dimension $N = 2(1+\alpha) = 2\frac{1+2\lambda}{1-\lambda}$ and therefore, the corresponding distribution has the special property that it becomes a Dirac-δ or fair distribution when $\lambda \to 1$ or $N(\lambda) \to \infty$.

4.2.1.3 Model with Distributed Savings

In a later model proposed by Chatterjee et al. [42, 43] (CCM model hereafter) it was assumed that the saving propensity has a distribution and this immediately led to a wealth distribution curve with a Pareto-like tail having $\nu = 1$. Here,

$$\begin{aligned} m_i(t+1) &= \lambda_i m_i(t) + \varepsilon_{ij}\left[(1-\lambda_i)m_i(t) + (1-\lambda_j)m_j(t)\right], \\ m_j(t+1) &= \lambda_j m_j(t) + (1-\varepsilon_{ij})\left[(1-\lambda_i)m_i(t) + (1-\lambda_j)m_j(t)\right]; \end{aligned} \tag{4.7}$$

which are different from the CC model equations as λ's are now agent dependent. The steady state wealth distribution gave rise to a power law tail with exponent 2. Various studies on the CCM model have been made soon after [44–55].

Manna et al. [56] used a preferential selection rule using a pair of continuously tunable parameters upon traders with distributed saving propensities and was able to mimic the trend of enhanced rates of trading of the rich. The wealth distribution was found to follow Pareto law. It might be mentioned that in a similar context of preferential selection rules in wealth exchange processes, Iglesias et al. [57, 58] had considered much earlier a model for the economy, where the poorest in the society at any stage takes the initiative to go for a trade (random wealth exchange) with anyone else. Interestingly, in the steady state, one obtained a self-organized poverty line, below which none could be found and above which, a standard exponential decay of the distribution (Gibbs) was obtained.

4.2.1.4 Extended CCM Model

In the extended CCM model [59, 60], a trade takes place between two agents in such a way that the investments of both agents are the same. For two agents i and j having wealth m_i and m_j respectively, the "effective" saving propensities are $\lambda_i = \frac{m_i}{m_i+m_j}$ and $\lambda_j = \frac{m_j}{m_i+m_j}$ respectively, which are functions of time. It is observed that in steady state, the wealth condenses to a single agent, a feature very similar to the results obtained by Chakraborti [31]. By introducing taxation in the system not only condensation can be avoided but at the same time the model tends towards reality. The tax is applied for the agents who have wealth greater than the average wealth

and this tax is collected periodically after a constant time interval. The total collected tax is then redistributed over all the agents. It is found that the distribution of wealth again has a power law tail with exponent 1.5.

4.2.2 Model with Phase Transition

In [61], the authors introduced the concept of "poverty line", i.e. a threshold θ, in the CCM model. A trade between two agents occurs as it is in the CCM model but with the restriction that at least one of the two agents should possess wealth less than θ. However, if all agents accumulate wealth greater than θ, then in such a situation the dynamics stops. To continue the dynamics a perturbation is applied such that a particle having energy above θ is selected randomly and its energy fully transferred to any other particle. The maximum limit of the threshold value θ below which the dynamics is stopped within some finite time, is the critical value of the threshold θ_c. The order parameter O is defined as the average total number of agents having wealth less than θ, i.e. $O = \int_0^\theta P(m)dm$, where $P(m)$ is the wealth distribution. After a certain "relaxation time" τ, the system attains a steady state and several quantities are measured. If the order parameter O is plotted against θ, it is observed that after the point $\theta = \theta_c = 0.6075$ the order parameter increases. The model thus has a "phase transition" near θ_c below which the number of particles in the steady state goes to zero. Near the critical point, the order parameter obeys a scaling form as $O \sim (\theta - \theta_c)^\beta$, where $\beta = 0.97$ is the order parameter exponent. Time variation of the order parameter has the scaling form $O(t) \sim t^\delta$ with exponent $\delta = 0.93$. Also a clear time scale divergence behaviour is observed with scaling form $\tau \sim |\theta - \theta_c|^{-z}$.

4.2.3 Nature of Transactions in Gas-Like Models with Distributed Savings

The agent dynamics for models with saving propensity can be studied with emphasis on the nature of transactions, i.e. whether it is a gain or a loss [62]. In order to study the dynamics of the transactions (i.e. gain or loss), a walk was conceived for the agents in an abstract one dimensional gain-loss space (GLS) where the agents conventionally take a step towards right if a gain is made and left otherwise. Here the amount of gain or loss was not considered, i.e. whatever be the amount of gain or loss, the step length is only 1. If it is a gain, the corresponding walker moves one step to the right and if it is a loss, walker moves one step to the left. For better understanding this is shown in Fig. 4.2. It can be observed that in the CCM model, the amount of wealth gained or lost by a tagged agent in a single interaction follows a distribution which is not symmetric in general, well after equilibrium has been reached. The distribution depends strongly on the saving propensity of the agent. For example, an agent with larger λ suffers more losses of less denomination compared to an agent

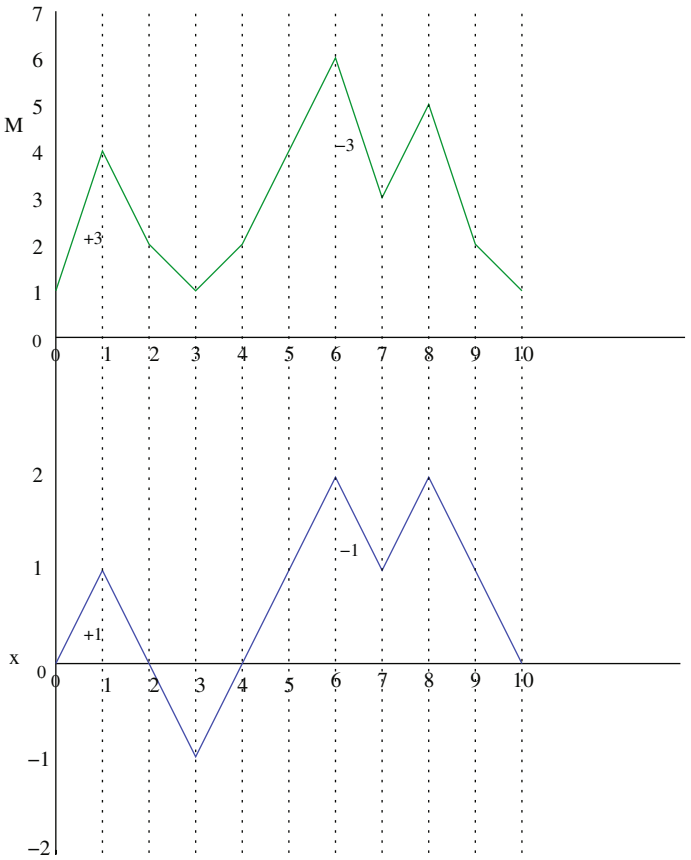

Fig. 4.2 Above : Plot of wealth M of an agent in different steps. *Below* : Plot of the distance travelled x in the gain–loss space by the corresponding walker. Note that, whatever be the amount of gain or loss, the step length of the walker is only 1

with smaller λ, although, in this case, the total wealth of the two agents has reached equilibrium, i.e. each agent's wealth fluctuates around a λ dependent value.

For such a walk, it can be found that $\langle x \rangle$, the distance travelled, scales linearly with time t suggesting a ballistic nature of the walk for the CCM walk. Moreover, the slope of the $\langle x \rangle$ versus t curves is dependent on λ; it is positive for small λ and continuously goes to negative values for larger values of λ. The slope becomes zero at a value of $\lambda^* \simeq 0.469$. In general for the CCM walk $\langle x^2 \rangle$ scales with t^2 . For the CC model on the other hand, $\langle x^2 \rangle$ scaled with t as in a random walk while $\langle x \rangle \approx 0$. The above results naïvely suggests that the walk in the GLS is like a biased random walk (BRW; except perhaps at λ^*) for the CCM model while it is like a random walk (RW) for the CC model.

4.2.4 Antipersistence Effect in CC/CCM Walk

In [63], the exact nature of the walk associated with CC and CCM model was explored and it was shown through the effective bias p associated with the walks, distribution of walk lengths at a stretch, etc. that CCM is not a simple BRW and CC is not a simple RW.

For BRW, the probability of direction reversal is simply $2p(1-p)$ which has a maximum value of $1/2$ for $p = 1/2$. But for CCM, the direction reversal probability f is greater than $1/2$ for all $\lambda < 1$ and $f \to 1/2$ for $\lambda \to 1$. Through further analysis of time correlation and other relevant quantities it was shown that direction reversal is preferred in these cases [63]. In the equivalent picture of the walk in the abstract space for gains and losses, it is similar to the fact that here individuals has a tendency to make a gain immediately after a loss and vice versa. This so called antipersistence effect is in fact compatible with human psychology where one can afford to incur a loss after a gain and will try to have a gain after suffering a loss.

It was also shown in [63] that the "antipersistence effect" is maximum for no saving and decreases with saving. This is perhaps in tune with the human feeling of security associated with the saving factor. In the CCM model, the saving propensity is randomly distributed and the antipersistence effect occurs with a simultaneous bias that too depends on λ.

4.2.5 Firm Dynamics

Size of a firm is measured by the strength of its workers. A firm grows when worker leaves another firm and joins it. The rate at which a firm gains or loses workers is called the "turnover rate" in economics literature. Thus, there is a redistribution of workers and the corresponding dynamics can be studied. In the models of firm dynamics, one assumes the following facts :

1. Any formal unemployment is avoided in the model. Thus, one does not have to keep track of the mass of workers who are moving in and out of the employed workers' pool.
2. The workers are treated as a continuous variable.
3. The definition that size of a firm is just the mass of workers working in the firm, is adopted.

In firm dynamics models, we may make an analogy with the previous subsections that firms are agents and the number of workers in the firm is its wealth. Assuming no migration, birth and death of workers, the economy thus remains conserved. As the "turnover rate" dictates both the inflow and outflow of workers, we need another parameter to describe only the outflow. That parameter may be termed as "retention rate", which describes the fraction of workers who decide to stay back in their firm. This is identical to saving propensity in wealth exchange models, discussed earlier.

4.2.5.1 Model with Constant Retention Rate

In this model [64, 65], the economy was considered to have N firms and any firm could absorb any number of workers. Initially, all firms have one unit of workers. The retention rate is denoted by λ. For this model, the retention rate of all firms are taken to be identical, as was in [26], which in reality is not true. The size of the ith firm was w_i $(i \leq N)$. At each time, it was considered that $(1-\lambda)$ fraction of the workforce of n firms (not $N!$), wanted to leave voluntarily or the firms wanted them to leave. The dynamics for the ith firm can be given as follows :

$$w_i(t+1) = \lambda w_i(t) + \varepsilon_{i(t+1)}(1-\lambda)\sum_{j}^{n} w_j(t), \tag{4.8}$$

where $\varepsilon_{i(t+1)}$ are random variables which describes the fraction of workers actually moved to the ith firm at time $t+1$ among those who wanted to move. Note that, we use t within the first bracket when referring to the endogenous variables[1] like the size of the firm $w_i(t)$ and the same in subscript when referring to the exogenous random variables[2] $\varepsilon_{i(t)}$.

Restrictions on ε

1. $\sum_j^n \varepsilon_j(t) = 1$ for all t as the economy should be conserved.
2. Expectation $E(\varepsilon_i) = 1/n$ for all i indicating that distributions of all ε_i's are identical.
3. If $n = 2$, $\varepsilon_i \sim [0, 1]$ so that at the lower limit of n, CC/CCM can be got back.

An exact solution was given in [64, 65] where it was assumed that all firms interact at every step. The steady-state distribution of the firms was shown to be

$$f(w) = \lim_{\bar{k}\to\infty} \sum_{i=1}^{\bar{k}} \phi_i \exp(-\phi_i w) \prod_{i=1, j\neq i}^{\bar{k}} \left(\frac{\phi_j}{\phi_j - \phi_i}\right), \tag{4.9}$$

where $\phi_i = \frac{1}{\lambda^i(1-\lambda)}$.

4.2.5.2 Model with Distributed Retention Rate

Here instead of a fixed retention rate, we consider distributed λ, i.e. Eq. 4.8 can now be written as

$$w_i(t+1) = \lambda_i w_i(t) + \varepsilon_{i(t+1)} \sum_{j}^{n} (1-\lambda_j) w_j(t). \tag{4.10}$$

[1] A classification of a variable generated by a statistical model that is explained by the relationships between functions within the model.
[2] A variable whose value is determined outside the model in which it is used.

The distribution of firm sizes can be shown to be a powerlaw, by calculations similar to the one followed in [45].

4.2.5.3 Model with Time-Varying Retention Rate

In this model, the retention rate λ was taken to be a function of the evolving variable, the work-force w [64, 65]. Thus Eq. 4.8 can be modified in the following way,

$$w_i(t+1) = \lambda(w_i(t))w_i(t) + \varepsilon_{i(t+1)}(1 - \lambda(w_i(t)))\sum_j^n w_j(t). \tag{4.11}$$

Following [64, 65] the functional form of λ can be assumed as,

$$\lambda(w) = c_1(1 - \exp(-c_2 w)); \qquad c_1,\ c_2 \text{ are constants}, \tag{4.12}$$

which signifies a more realistic scenario that retention rate increases as current work-force increases. This model leads to prominent bimodality in the size distribution of firms [64, 65]. This has been empirically found in the developing economies.

4.3 Kinetic Exchange Models in Sociology

Social systems offer some of the richest complex dynamical systems, which can be studied using the standard tools of statistical physics. The study of Sociophysics became popular in the last part of twentieth century [41, 66–68].

Auguste Comte used the term "social physics" in his 1842 work. He defined social physics as the study of the laws of society or the science of civilization. In particular, Comte (1856) stated that,

> Now that the human mind has grasped celestial and terrestrial physics, mechanical and chemical, organic physics, both vegetable and animal, there remains one science, to fill up the series of sciences or observation—social physics. This is what men have now most need of...

Emergence of consensus is an important issue in sociophysics problems. Here, people interact to select an option among different options of a subject which may be vote, language, culture, opinion, etc. This then leads to a state of consensus. In opinion formation, consensus is an "ordered Phase", where most of the people have a particular opinion. Several models can be proposed to mimic the dynamics of opinion spreading. In the models of opinion dynamics, opinions are usually modelled as discrete or continuous variables and are subject to either spontaneous changes or changes due to binary interactions, global feedback, and external factors (see [66] for a general review).

However, in this chapter, only kinetic exchange models of opinion dynamics, analogous to the ones in economics is discussed. These models are named after Lallouache, Chakrabarti, Chakraborti, and Chakrabarti and are called LCCC model hereafter. The opinions of individuals are assumed to be continuous variables in $[-1, 1]$ and change due to binary interactions. The tuning parameter in these models is "conviction" λ, which is similar to the "saving propensity" as in KWEM. It determines the extent to which one remains biased to its own opinion, while interacting with the other. Unlike KWEM, there is no stepwise opinion conservation.

4.3.1 LCCC Model

In this model [69, 70], opinion can be shared only in the two-body interaction mode. At any time t a person i is assigned with an opinion value $o_i(t) \in [-1, 1]$. For two persons i and j, the interaction can be described in the following way :

$$\begin{aligned} o_i(t+1) &= \lambda[o_i(t) + \varepsilon o_j(t)], \\ o_j(t+1) &= \lambda[o_j(t) + \varepsilon' o_i(t)], \end{aligned} \tag{4.13}$$

where ε and ε' are uncorrelated random numbers between 0 and 1.

This type of interactions lead to a polarity or consensus formation depending upon the value of λ. The steady state average opinion after a long time t would be given by $O = \sum_i |o_i|/N$. This represents the "ordering" in the system. The system starts from a random disordered state ($O \sim 0$) and after a certain relaxation time $t = \tau$ moves to the "para" or "absorbing" state where all individual agents have zero opinion for $\lambda \leq 2/3$ or continuously changes to a "symmetry broken" or "active" state where all individuals have opinion of same sign for $\lambda \geq 2/3$. The variance of O shows a cusp near $\lambda = 2/3$. The growth behaviour of the fraction of agents p having extreme opinions $o_i = \pm 1$ was found to be similar to O [71]. The relaxation time behaviour of the system shows a critical divergence of τ, $\tau \sim |\lambda - \lambda_c|^{-z}$ for both O and p at $\lambda = \lambda_c = 2/3$. Values of z for O and p are 1.0 ± 0.1 and 0.7 ± 0.1, respectively.

Notably, this model with interactions has a behaviour very similar to the simple iterative map,

$$y(t+1) = \lambda(1 + \varepsilon_t)y(t), \tag{4.14}$$

with $y \leq 1$, where it was assumed that if $y(t) \geq 1$, $y(t)$ will be set equal to 1. $\varepsilon_t \in [0, 1]$ is a stochastic variable. In a mean-field approach Eq. 4.14 reduces to

$$y(t+1) = \lambda(1 + \langle\varepsilon_t\rangle)y(t), \tag{4.15}$$

where $\langle\varepsilon_t\rangle = 1/2$. For $\lambda \leq 2/3$ $y(t)$ converges to 0. An analytical derivation for the critical point was also given where it was found that $\lambda_c = \exp\{-(2\ln 2 - 1)\} \approx 0.6796$.

4.3.1.1 Generalized LCCC Model

In the generalized LCCC model [72], another parameter μ is introduced which is called the "influence" parameter. It is a measure of the influencing power or the ability of an individual to impose its opinion on some other individual. Thus the interactions are described as follows,

$$\begin{aligned} o_i(t+1) &= \lambda_i o_i(t) + \varepsilon \mu_j o_j(t), \\ o_j(t+1) &= \lambda_j o_j(t) + \varepsilon' \mu_i o_i(t). \end{aligned} \tag{4.16}$$

Note that here conviction and influence parameters of individual agents are different which lead to inhomogeneity in the society. In a simpler version, we may consider a homogeneous society so that all λ's of different people are same. Also μ's for different people are same.

In this generalized version, the average opinion shows spontaneous symmetry breaking in the $\lambda - \mu$ plane. In the steady state the condition for nonzero solution of O is

$$(1-\lambda)^2 = \langle \varepsilon \varepsilon' \rangle \mu^2, \tag{4.17}$$

which gives that "active" and "absorbing" phases, separated by a phase boundary given by $\lambda = 1 - \mu/2$.

4.3.1.2 Other Variants of the LCCC Model

Biswas et al. [71] studied some variants of the models discussed above. In one version, it was considered that when an individual i meets another individual j, she retains her own opinion proportional to her conviction parameter and picks up a random fraction of j's opinion. Thus the interaction in equation form would now be,

$$\begin{aligned} o_i(t+1) &= \lambda o_i(t) + \varepsilon o_j(t), \\ o_j(t+1) &= \lambda o_j(t) + \varepsilon' o_i(t). \end{aligned} \tag{4.18}$$

For $\lambda < \lambda_c$, for all agents $o_i = 0$ giving $O = 0$. For $\lambda > \lambda_c$, $O > 0$ and $O \to 1$ as $\lambda \to 1$. Numerical value of $\lambda_c = 1/2$. Mean field estimate gives for the stable value of O

$$O(1 - \lambda - \langle \varepsilon \rangle) = 0. \tag{4.19}$$

Thus $\lambda_c = 1/2$.

Another variant of the LCCC model was studied [71] with a slight modification to the original model that here a person in addition to being influenced by the interacting person's opinion, was influenced by the average opinion of the community. Thus, the interaction equations read,

$$o_i(t+1) = \lambda[o_i(t) + \varepsilon o_j(t)] + \varepsilon' O(t),$$

$$o_j(t+1) = \lambda[o_j(t) + \eta o_i(t)] + \eta' O(t). \tag{4.20}$$

The symmetric phase occurs for $\lambda \leq 1/3$ and symmetry-broken phase is obtained for $\lambda > 1/3$.

By a mean-field approach as O reached a steady state value,

$$O = \lambda(1 + \langle \varepsilon \rangle)O + \langle \varepsilon' \rangle O, \tag{4.21}$$

we have $\lambda_c = 1/3$. In all these models, the critical exponents associated with the physics of phase transitions were all estimated.

4.3.1.3 Discrete LCCC Model

In the discrete version of LCCC model one considers that opinions can take only discrete values, i.e. o_i can take only three values $[o_i \in \{-1, 0, +1\}]$. This particular version of the LCCC model was exactly solved [73], which also showed an "active-absorbing phase transition" as was seen in the continuous version [69, 70]. Apart from the two-agent or binary interaction, the three-agent interaction were also taken into account. While the phase diagram of the two-agent interaction led to a continuous transition line, the three-agent interaction showed a discontinuous transition [73].

4.3.1.4 Disorder Induced Phase Transition in Kinetic Exchange Models of Opinion Formation

In this model of continuous opinion dynamics, both positive and negative mutual interactions were studied [74]. The interaction equations are as follows :

$$\begin{aligned} o_i(t+1) &= o_i(t) + \mu_{ij} o_j(t), \\ o_j(t+1) &= o_j(t) + \mu_{ij} o_i(t), \end{aligned} \tag{4.22}$$

where μ_{ij} are randomly chosen to be either $+1$ or -1. Negative interactions are included here with probability p, the role of which is like a disordering field, similar to temperature in thermally driven phase transitions. Beyond a particular value $p = p_c$ a phase transition from an ordered phase to a disordered phase occurs. Results from exact calculation of a discrete version also shows the phase transition at p_c.

4.3.1.5 LCCC Model with Bounded Confidence

In this restricted LCCC model [75], two agents interact according to Eq. 4.13 only when $|o_i - o_j| \leq 2\delta$, where the parameter $\delta \in [0, 1]$ represents the "confidence" level. There are two extreme limits corresponding to this model:

1. $\delta = 1$ which brings it back to the original model (LCCC model).

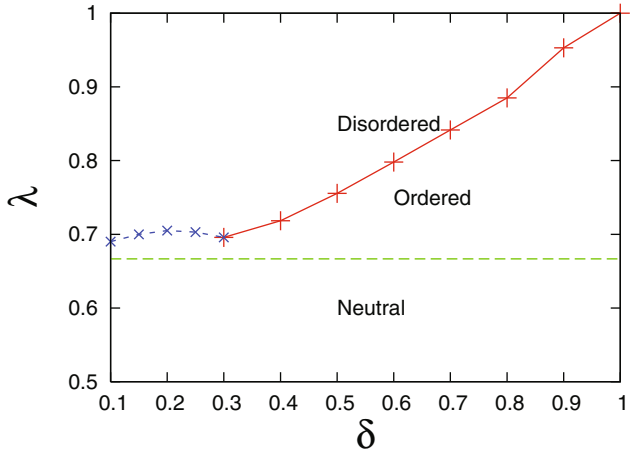

Fig. 4.3 Phase diagram on the $\delta - \lambda$ plane. Plot shows the existence of the neutral region for $\lambda \leq \lambda_{c1} \simeq 2/3$, the ordered region and the disordered region. The ordered and disordered regions are separated by a first order boundary for $\delta \geq 0.3$. For $\delta < 0.3$, the phase boundary has been obtained approximately only from the behaviour of the order parameter. Taken from [75]

2. $\delta = 0$ which is the case when two agents interact only when their opinions are exactly same.

Three different states were defined to identify the status of the system.

- Neutral State : When $o_i = 0$ for all i, the state is called neutral state.
- Disordered State : $o_i = 0$ for all i, but $O \sim 0$, the state is called disordered state.
- Ordered State : when $O = 0$ corresponding state is called an ordered state.

The three states are located in the $\delta - \lambda$ plane. The ordered and disordered regions in the plane are separated by a first order boundary (continuous line in red) for $\delta \geq 0.3$ (obtained using a finite size scaling analysis). For $\delta < 0.3$, the phase boundary (broken line in blue) has been obtained approximately only from the behaviour of the order parameter (Fig. 4.3).

4.3.1.6 Percolation in LCCC Model

The opinion spreading among people in a society may be compared to the percolation problem in physics. The agents are assumed to be placed on the sites of a square lattice and follow the LCCC dynamics [76]. A geometrical cluster consisting of the adjacent sites having opinion value more than or equal to a predefined threshold value Ω. At steady state, the percolation order parameter is measured. At a particular value of $\lambda = \lambda_c^p$, the system undergoes a percolation transition. As Ω decreases, λ_c^p also and approaches λ_c as $\Omega \to 0$. The critical exponents are independent of Ω as well as λ and μ. The critical exponents are significantly different from those obtained for

static and dynamic Ising system and standard percolation. The exponents suggest that this LCCC model has a separate universality class from the viewpoint of percolation transition.

4.3.1.7 Damage Spreading in Model of Opinion Dynamics

The damage spreading phenomena was studied in the opinion dynamics model proposed in [74] in two ways,

- Traditional method (TM) : In this method, two systems of N individuals are simulated using the same initial random opinions either discrete or continuous, except for one randomly chosen individual. The two systems are then allowed to evolve using same random numbers.
- Nature versus nurture method (NVN) : In this (NVN) method, the initial systems are identical but different random numbers are used for the time evolution.

In both cases, a damage spreading transition occurs at p_d where $p_d \approx 0.18$ for TM and $p_d = 0$ for NVN [77]. Here it is found that $p_d < p_c$, the order–disorder transition point. The result signifies that for TM, for $p_d < p < p_c$, even when consensus is reached, if we make very small changes even in a single agent, there is always a finite probability that the system leads to a different consensus state. In NVN, $p_d = 0$ signifies that if the same agent goes through a different sequence of interactions, the result will be different for any p with finite probability. However, the dynamics of the damage shows a nonmonotonicity making it difficult to comment on the exact nature of damage or to estimate the exponents related to it.

4.4 Summary and Discussions

We briefly described here, the kinetic exchange models for economics and sociology and some applications derived from these models. Taking inspiration from kinetic theory of gas molecules, a purely statistical system, these kind of models give an idea of how completely different systems might lead to similar or emergent collective behaviour, as they have some similar connections in the microscopic units. However, due to such "micro-oriented" framework one overlooks the system-wide effects which can be very important for a real economy and society. However, one should bear in mind that whatever we discussed here in this chapter, is to a large extent idealistic. A real economy is much more complex than any or all of these models. In case of a real economy, minute changes in the characteristics of the agents or firms, or simply the addition or deletion of a link of the socioeconomic network, can alter the emergent behaviour to a great extent. Models originating from simple multiagent models such as the ones described here, should be extended to incorporate such features and emergent behaviours, which might help one to understand many real-life

economic phenomena or even the financial crisis, such as the one observed during $2007 - 2008$.

It should also be borne in mind that besides being models of idealized economy or society, these simple models have a very nice mathematical or statistical appeal. Mathematicians, physicists, and economists, have tried to play around with these models (or their variants) and studied the associated nonlinear dynamics, steady-state behaviours, and related questions. Apenko [78] used a different approach and proved the monotonic entropy growth for a nonlinear discrete-time model of a random market, based on binary collisions, which may be also viewed as a particular case of the Ulam's redistribution of energy problem. In that study, a single step of the nonlinear evolution was treated as a combination of two steps, first one is related to an auxiliary linear two-particle process and second one is a kind of a coarse-graining. It was shown that on both steps the entropy increases. Therefore he concluded that the entropy is indeed monotonically increasing for the original nonlinear problem. A similar entropy approach was followed in [79], where they considered different versions of a continuous economic model, which takes into account some idealistic characteristics of the markets and agents randomly exchange in pairs, and their functional mappings. They showed that the system had a fixed point which can be reached asymptotically following a trajectory of monotonically increasing entropy which takes its maximum value on the equilibrium. In this manner, the existence of an H-theorem could be computationally checked.

Acknowledgement The authors would like to thank all their collaborators and students, whose works have been presented here.

References

1. Mandl, F.: Statistical Physics, 2nd edn. Wiley, New York (2002)
2. ter Haar, D.: Elements of Statistical Mechanics. Butterworth-Heinemann, Oxford (1995)
3. Sethna, J.P.: Statistical Mechanics. Oxford University Press, Oxford (2006)
4. Sinha, S., Chatterjee, A., Chakraborti, A., Chakrabarti, B.K.: Econophysics: An Introduction. Wiley-VCH, Berlin (2010)
5. Sen, P., Chakrabarti, B.K.: Sociophysics : An Introduction. Oxford University Press, Oxford (2013)
6. Ball, P.: Physica. A **314**, 1 (2002)
7. Chakrabarti, B.K., Chakraborti, A., Chakravarty, S.R., Chatterjee, A.: Econophysics of Income and Wealth Distributions. Cambridge University Press, Cambridge (2013)
8. Pareto, V.: Cours d'economie Politique. F. Rouge, Lausanne (1897)
9. Souma, W.: Growth and fluctuations of personal income. Fractals. **9**, 463 (2001)
10. Di Matteo, T., Aste, T., Hyde, S.T.: In: Mallamace, F., Stanley, H.E. (eds.) The Physics of Complex Systems (New Advances and Perspectives), p. 435. IOS Press, Amsterdam (2004)
11. Clementi, F., Gallegati, M.: Power law tails in the Italian personal income distribution. Physica. A **350**, 427 (2005)
12. Sinha, S.: Evidence for power-law tail of the wealth distribution in India. Physica. A **359**, 555 (2006)
13. Silva, A.C., Yakovenko, V.M.: Temporal evolution of the "thermal" and "superthermal" income classes in the USA during 1983–2001. Europhys. Letts. **69**, 304 (2005)

14. Drăgulescu, A.A., Yakovenko, V.M.: Statistical mechanics of money, income, and wealth: a short survey. Physica. A **299**, 213 (2001)
15. Mandelbrot, B.B.: Fractional Brownian motions, fractional noises and applications. Int. Econ. Rev. **1**, 79 (1960)
16. Chatterjee, A., Yarlagadda, S., Chakrabarti, B.K. (eds.): Econophysics of Wealth Distributions. Springer, Milan (2005)
17. Chakrabarti, B.K., Chakraborti, A., Chatterjee, A. (eds.): Econophysics and Sociophysics. Wiley-VCH, Berlin (2006)
18. Yakovenko, V.M. , Barkley Rosser, J. Jr. Colloquium: statistical mechanics of money, wealth, and income. Rev. Mod. Phys. **81**, 1703 (2009)
19. Drăgulescu, A.A., Yakovenko, V.M.: Evidence for the exponential distribution of income in the USA. Eur. Phys. J. B **20**, 585 (2001)
20. Levy, M., Solomon, S.: New evidence for the power-law distribution of wealth. Physica. A **242**, 90 (1997)
21. Aoyama, H., Souma, W., Fujiwara, Y.: Growth and fluctuations of personal and company's income. Physica. A **324**, 352 (2003)
22. Ding, N., Wang, Y.: Power-law tail in the Chinese wealth distribution. Chinese Phys. Letts. **24**, 2434 (2007)
23. Chakrabarti, B.K., Marjit, S., Econophysics research in India in the last two decades. Ind. J. Phys. B **69**, 681 (1995)
24. Ispolatov, S., Krapivsky, P.L., Redner, S.: Wealth distributions in asset exchange models. Eur. Phys. J. B **2**, 267 (1998)
25. Drăgulescu, A.A., Yakovenko, V.M.: Statistical mechanics of money. Eur. Phys. J. B **17**, 723 (2000)
26. Chakraborti, A., Chakrabarti, B.K.: Statistical mechanics of money: how saving propensity affects its distribution. Eur. Phys. J. B **17**, 167 (2000)
27. Chatterjee, A., Chakrabarti, B.K.: Kinetic exchange models for income and wealth distributions. Eur. Phys. J. B **60**, 135 (2007)
28. Chatterjee, A., Sinha, S., Chakrabarti, B.K.: Economic inequality: is it natural? Curr. Sci. **92**, 1383 (2007)
29. Chakrabarti, A.S., Chakrabarti, B.K.: Statistical theories of income and wealth distribution. Economics E-journal **4** (2010) (http://www.economics-ejournal.org/economics/journalarticles/2010–4)
30. Chatterjee, A.: In: Naldi, G., et al. (eds.) Mathematical Modeling of Collective Behavior in Socio-Economic and Life Sciences, p. 31. Birkhaüser, Boston (2010)
31. Chakraborti, A.: Distributions of money in model markets of economy. Int. J. Mod. Phys. C **13**, 1315 (2002)
32. Hayes, B.: Follow the money. Am. Sci. **90**, 400 (2002)
33. López-Ruiz, R., López, J.L., Calbet, X.: Complex systems with trivial dynamics. ESAIM Proc. **36**, 189 (2012)
34. Patriarca, M., Chakraborti, A., Kaski, K.: Statistical model with a standard Gamma distribution. Phys. Rev. E **70**, 016104 (2004)
35. Repetowicz, P., Hutzler, S., Richmond, P.: Dynamics of money and income distributions. Physica. A **356**, 641 (2005)
36. Lallouache, M., Jedidi, A., Chakraborti, A.: Wealth distribution: to be or not to be a Gamma. Sci. Cult. **76**, 478 (2010)
37. Angle, J.: The surplus theory of social stratification and the size distribution of personal wealth. Soc. Forc. **65**, 293 (1986)
38. Angle, J.: The inequality process as a wealth maximizing process. Physica. A **367**, 388 (2006)
39. Chakraborti, A., Patriarca, M.: Gamma-distribution and wealth inequality. Pramana J. Phys. **71**, 233 (2008)
40. Chakraborti, A., Patriarca, M.: Variational principle for the pareto power law. Phys. Rev. Lett. **103**, 228701 (2009)

41. Patriarca, M., Chakraborti, A.: Kinetic exchange models: from molecular physics to social science. Am. J. Phys. **81**, 618 (2013)
42. Chatterjee, A., Chakrabarti, B.K., Manna, S.S.: Pareto law in a kinetic model of market with random saving propensity. Physica. A **335**, 155 (2004)
43. Chatterjee, A., Chakrabarti, B.K., Manna, S.S.: Money in gas-like markets: Gibbs and Pareto Laws. Phys. Scr. T **106**, 36 (2003)
44. Chatterjee, A., Chakrabarti, B.K., Stinchcombe, R.B.: Master equation for a kinetic model of a trading market and its analytic solution. Phys. Rev. E **72**, 026126 (2005)
45. Mohanty, P.K.: Generic features of the wealth distribution in ideal-gas-like markets. Phys. Rev. E **74**, 011117 (2006)
46. Kar Gupta, A.: In: Chakrabarti, B.K., Chakraborti, A., Chatterjee, A. (eds.) Econophysics and Sociophysics, p. 161. Wiley-VCH, Berlin (2006)
47. Chatterjee, A., Chakrabarti, B.K.: Ideal-gas-like market models with savings: quenched and annealed cases. Physica. A **382**, 36 (2007)
48. Düring, B., Toscani, G.: Hydrodynamics from kinetic models of conservative economies. Physica. A **384**, 493 (2007)
49. Düring, B., Matthes, D., Toscani, G.: Kinetic equations modelling wealth redistribution: a comparison of approaches. Phys. Rev. E **78**, 056103 (2008)
50. Matthes, D., Toscani, G.: On steady distributions of kinetic models of conservative economies. J. Stat. Phys. **130**, 1087 (2008)
51. Matthes, D., Toscani, G.: On steady distributions of kinetic models of conservative economies. Kinet. Relat. Models **1**, 1 (2008)
52. Comincioli, V., Della Croce, L., Toscani, G.: A Boltzmann-like equation for choice formation. Kinet. Relat. Model. **2**, 135 (2009)
53. Chatterjee, A.: Kinetic models for wealth exchange on directed networks. Eur. Phys. J. B **67**, 593 (2009)
54. Chakrabarti, A.S., Chakrabarti, B.K.: Microeconomics of the ideal gas like market models. Physica. A **388**, 4151 (2009)
55. Chakrabarti, A.S., Chakrabarti, B.K.: Inequality reversal: effects of the savings propensity and correlated returns. Physica. A **389**, 3572 (2010)
56. Chakraborty, A., Manna, S.S.: Weighted trade network in a model of preferential bipartite transactions. Phys. Rev. E **81**, 016111 (2010)
57. Iglesias, J.R.: How Simple Regulations can Greatly Reduce Inequality Science and Culture (Kolkata) **76**, 437 (2010)
58. Pianegonda, S., Iglesias, J.R., Abramson, G., Vega, J.L.: Wealth redistribution with conservative exchanges Physica. A **322**, 667 (2003)
59. Ghosh, A. (unpublished); Ghosh, A., Chakrabarti, A.S., Chandra, A.K., Chakraborti, A.: In: Abergel, F., Aoyama, H., Chakrabarti, B.K., Chakraborti, A., Ghosh, A. (eds.) Econophysics of Agent-Based Models, pp 99–129. Springer, Milan (2014)
60. Independent studies (unpublished) made by S. Sinha and also A. Chatterjee in 2005–2006, had similar observations; private communications
61. Ghosh, A., Basu, U., Chakraborti, A., Chakrabarti, B.K.: Threshold-induced phase transition in kinetic exchange models. Phys. Rev. E **83**, 061130 (2011)
62. Chatterjee, A., Sen, P.: Agent dynamics in kinetic models of wealth exchange. Phys. Rev. E **82**, 056117 (2010)
63. Goswami, S., Sen, P., Das, A.: Quantum persistence: a random-walk scenario. Phys. Rev. E **81**, 021121 (2010)
64. Chakrabarti, A.S.: Bimodality in the firm size distributions: a kinetic exchange model approach. Eur. Phys. J. B **86**, 255 (2013)
65. Chakrabarti, A.S.: Effects of the turnover rate on the size distribution of firms: An application of the kinetic exchange models Physica. A **391**, 6039 (2012)
66. Castellano, C., Fortunato, S., Loreto, V.: Statistical physics of social dynamics. Rev. Mod. Phys. **81**, 591 (2009)

67. Galam, S.: Sociophysics: A Physicist's Modeling of Psycho-Political Phenomena (Understanding Complex Systems). Springer, Heidelberg (2012)
68. Stauffer, D.: A biased review of sociophysics. J. Stat. Phys. **151**, 9 (2013)
69. Lallouache, M., Chakraborti, A., Chakrabarti, B.K.: Kinetic exchange models for social opinion formation. Sci. Cult.**76**, 485 (2010)
70. Lallouache, M., Chakrabarti, A.S., Chakraborti, A., Chakrabarti, B.K.: Opinion formation in the kinetic exchange models: spontaneous symmetry breaking transition. Phys. Rev. E **82**, 056112 (2010)
71. Biswas, S., Chandra, A.K., Chatterjee, A., Chakrabarti, B.K.: Phase transitions and non-equilibrium relaxation in kinetic models of opinion formation. J. Phys. Conf. Ser. **297**, 012004 (2011)
72. Sen, P.: Phase transitions in a two-parameter model of opinion dynamics with random kinetic exchanges. Phys. Rev. E **83**, 016108 (2011)
73. Biswas, S.: Mean-field solutions of kinetic-exchange opinion models. Phys. Rev. E **84**, 056106 (2011)
74. Biswas, S., Chatterjee, A., Sen, P.: Disorder induced phase transition in kinetic models of opinion dynamics. Physica A **391**, 3257 (2012)
75. Sen, P.: Nonconservative kinetic exchange model of opinion dynamics with randomness and bounded confidence. Phys. Rev. E **84**, 016115 (2012)
76. Chandra, A.K.: Percolation in a kinetic opinion exchange model. Phys. Rev. E **85**, 021149 (2012)
77. Khaleque, A., Sen, P.: Damage spreading transition in an opinion dynamics model. Available at arXiv: 1312.7718v1 (2013)
78. Apenko, S.: Monotonic entropy growth for a nonlinear model of random exchanges. Phys. Rev. E **87**, 024101 (2013)
79. López-Ruiz, R., Shivanian, E., López, J.L.: Random Market Models with an H-Theorem. Available at arXiv:1307.2169 (2013)

Chapter 5
Nonlinear Maps: From the Toulouse Colloqium (1973) to NOMA'13

Christian Mira

Abstract From the 1962s, a group of researchers located in Toulouse (France) devoted a large part of its activity to the qualitative methods of nonlinear dynamics, in this framework specially to nonlinear maps. In 1973, the group organized the first international conference dedicated to nonlinear maps and their applications. The purpose of this chapter is to present the original contribution of this research group during about 40 years. Taking into account their particular interest, results on the fractal bifurcations structure called *box-within-the-box* (1975) are here given in a more developed form.

5.1 Introduction

From the 1962s, at times when the results on the nonlinear maps dynamics were virtually unknown outside the Soviet Union, a group of researchers located in Toulouse (France) devoted a large part of its activity to the qualitative methods of this topic. In 1973, the Toulouse group organized the first international conference dedicated to nonlinear maps and their applications [1, 2]. The group founded its work on results of the French school of iteration theory, and those of teams of the former USSR, which occupied the first rank in the nonlinear field, their contribution remaining unfamiliar in Western countries until the 1980s. These USSR teams developed the Birkhoff and Poincaré [3, 4] results, so giving rise to the *qualitative theory of dynamical systems*, which developed at the same time as the analytical methods of nonlinear differential equations.

With papers firstly published in French, some of the Toulouse group results were rediscovered afterward, and are now known differently. This situation led Prof. Ralf Abraham to ask the writing of Chap. 8 (*I. Gumowski and a Toulouse research group in the "prehistoric" times of chaotic dynamics*) of the book [5] dealing with the *early days of chaos theory*.

C. Mira (✉)
19 rue d'Occitanie, Fonsegrives, 31130 Quint, France
e-mail: christian.mira@sfr.fr

R. López-Ruiz et al. (eds.), *Nonlinear Maps and their Applications,*
Springer Proceedings in Mathematics & Statistics 112, DOI 10.1007/978-3-319-12328-8_5

The purpose of this chapter is to present the original contribution of the Toulouse group. Taking into account their importance, results on the fractal bifurcations structure called *box-within-the-box* (1975) are given in a more developed form with respect to the other topics of this text.

5.2 The International Colloquium *Points Mappings and Applications* (Toulouse 1973)

Exactly 40 years prior to the NOMAD'13 workshop *Nonlinear maps, and their applications* (Zaragoza, Spain, Sept. 3–4, 2013), in Sept. 1973 an international colloquium held on the same topic, equivalently entitled *Points Mappings and Applications* (French title *Transformations Ponctuelles et leurs Applications*) [1], in the framework of the *Laboratoire d'Automatique et d'Analyse des Systèmes* (LAAS) of Toulouse. According to the mathematical field, and authors, *map, point mapping, recurrence relationship, iteration*, correspond to the same discrete model, so the title of each of the two conferences is the same. Eleven papers were devoted to *stochastic* behaviors (i.e., *chaotic*, at that time the name did not exist), in the midst of the 33 ones presented.

Prof. Lagasse, director of the LAAS, was the colloquium's chairman. Igor Gumowski led the scientific committee. As a vice-chairman, I devoted the introductory presentation of the colloquium to a short history of nonlinear dynamics (cf. [2], pp. 19–27). It is in this framework that I announced an exhibition of *stochastic* (i.e., *chaotic*) images, quoting the Birkhoff's papers dealing with the laws of aesthetic (vol. 3 of [3], pp. 320–364), and a Poincaré's text extracted from a *Notice sur Halphen* (*Journal de l'Ecole Polytechnique*, 60, 137–161, 1890), also cf. [4]. In this text Poincaré deals with the aesthetic emotion which can be communicated by mathematics in the following terms:

> Le savant digne de ce nom, le géomètre surtout, éprouve en face de son œuvre la même impression que l'artiste; sa jouissance est aussi grande et de même nature. Si je n'écrivais pour un public amoureux de la Science, je n'oserais pas m'exprimer ainsi; je redouterais l'incrédulité des profanes. Mais ici, je puis dire toute ma pensée. Si nous travaillons, c'est moins pour obtenir ces résultats positifs auxquels le vulgaire nous croit uniquement attachés, que pour ressentir cette émotion esthétique et la communiquer à ceux qui sont capables de l'éprouver.

I took the liberty of saying that exhibited images had begun to manifest such an emotion in a form opened not only to specialists as Poincaré said, but also to a general public (cf. [2], p. 27), this due to the new possibilities offered by numerical simulations. A part of these images can be shown in Chap. 8 (*I. Gumowski and a Toulouse research group in the "prehistoric" times of chaotic dynamics*) of [5].

As far as I know, the Toulouse colloquium was the first to deal specifically with nonlinear maps and their applications. It also gave the opportunity to present a series of original results obtained by the LAAS group, which devoted its activity in the nonlinear dynamics field, this at a time when this research type was relatively uncommon in Western countries. Under the professor Targonski's leadership, then

this colloquium has given rise to a series of regular meetings with a modified title *European Conferences on Iteration Theory* (the last one was held in Ponta Delgada, São Miguel Island, Azores, Sept. 2012). It also appears that another originality of the colloquium was the exhibition of chaotic images, generated by solutions of nonlinear maps. The same exhibition, entitled *Morphogénèse et Mathématiques*, was organized by Marcel Barthes, Director of the *Alliance Française Rio de Janeiro-Centre* in the *Centre Culturel de la Maison de France*, from May 8 to 30, 1975.

5.3 Researches on Nonlinear Maps and Applications in Toulouse (1958–1973)

The organization of the colloquium *Points Mappings and Applications* was possible from the experience of a research group, which dedicated its work to the study of nonlinear maps and their applications. Indeed the first researches in the nonlinear dynamics field were beginning in Toulouse from the 1958s, and for nonlinear maps from 1962. This period was characterized by a close collaboration with Gumowski (*Université Laval* Québec) who stayed 2 years in Toulouse as a visiting professor. At that time, via his excellent knowledge of the Russian language, and other Slavic languages, he was the Western scientist having the largest and the most profound information, and understanding on the results of the schools on nonlinear dynamics (*qualitative and analytical methods*) in the former Soviet Union [6–8]. So I had access from 1958 to exceptionally wide information, rather unknown in Western countries at that time. This unawareness occurred in spite of a text due to J.P. La Salle and S. Lefschetz (J. of Math. Anal. and Appl., 2, pp. 467–499, 1961), who wrote in 1961:

> In USSR the study of differential equations has profound roots, and in this subject the USSR occupies incontestably the first place. One may also say that Soviet specialists, far from working in vacuum, are in intimate contact with applied mathematicians and front rank engineers. This has brought great benefits to the USSR and it is safe to say that USSR has no desire to relinquish these advantages.

It is essentially on the basis of such an information, joined to the Poincaré's results, and those of the French school of iteration theory (Grévy, Koenigs, Leau, Lémeray, Hadamard, Lattès, Julia, Fatou, Montel) that researches in Toulouse were led. This French school was the most active one in this field from the nineteenth century end to around 1930. The Toulouse group operated under different names depending upon the administrative place of its activity: *Groupe Théorie et Simulation* in *Laboratoire de Génie Electrique* of ENSEEHT, and afterward with the same name in *Laboratoire d'Automatique et Applications Spatiales* (CNRS) Toulouse, *Groupe Systèmes Dynamiques Non Linéaires* in "Faculté des Sciences of Université Paul Sabatier of Toulouse", *Groupe d'Études des Systèmes Non Linéaires et Applications*" in *Laboratoire d'Études des Systèmes Informatiques et Automatiques* of "Institut National des Sciences Appliquées de Toulouse". For simplicity sake we shall always speak in this text of the *Toulouse Group*, the responsibility and the theses orientation of which I had until 1997.

My first meeting with Gumowski in 1958 was followed by a long and friendly collaboration, source of fruitful results based on the qualitative methods [6], which achieved their highest level of evolution in the framework of the *Andronov' School* (in Gorki, now Nijnynovgorod) [8], and the analytical methods [6] related to nonlinear dynamical systems. For ODE, analytical methods (*Poincaré's small parameter method*, and *asymptotic methods* developed by Krylov, Bogoliubov, Mitropolski in Kiev) quickly attain limits (case of complex dynamics, especially chaotic dynamics), which restrict their use to some limited local behaviors. In the case of discrete dynamics (models in the form of maps, recurrence relationships), the limits are more quickly attained. It is the reason why the basic tools, at the origin of the Toulouse group results, have been essentially those of the qualitative methods. Published in French until 1980, a part of essential results were rediscovered afterward, as this will appear below. The pioneering role of this group is presented in Chap. 8 (*I. Gumowski and a Toulouse research group in the "prehistoric" times of chaotic dynamics*) of the book [5], and in the paper *Writing the History of Dynamical Systems and Chaos: Longue Durée and Revolution, Disciplines and Cultures* (cf. [9] § 1.2, 1.3, 1.8, 3.3, and 4.1) devoted to the history of dynamical systems (authors D. Aubin and A. Dahan Dalmedico).

5.4 Original Results Obtained by the Toulouse Group

5.4.1 Two-Dimensional Noninvertible Maps—Basin Boundaries (1963–1975)

In 1963, the results on nonlinear maps were in an underdeveloped state with respect to those related to ordinary differential equations. The first basic references of the Toulouse group were those of the French school of iteration theory, more precisely those of Grévy, Koenigs, Leau, Lémeray, Hadamard, Lattès [10], for the local behavior in a neighborhood of a stationary state (fixed point, or cycle, or other type), and those of Julia and Fatou for a global behavior (basin boundary of a stable stationary state).

The Julia and Fatou's papers are related to one-dimensional maps $z' = f(z)$ with a complex variable z [11, 12], i.e., to the restricted class of two-dimensional noninvertible maps with real variables defined by two functions satisfying the Cauchy–Riemann conditions. In spite of this limitation, Julia and Fatou results offered a starting point for studies of basin boundaries generated by more general two-dimensional noninvertible maps with real variables. In 1963, I consulted Julia about the existence of eventual results on basin boundaries, when they are generated by two-dimensional real maps not satisfying the particular Cauchy–Riemann conditions. He said that such an extension did not exist, adding that cases which do not satisfy the Cauchy–Riemann conditions might present high difficulties associated with a lot of possible different qualitative situations. Such difficulties emerged gradually and laboriously long afterward in the Toulouse group researches, from

studies of well chosen examples showing a lot of new properties. These obstacles were progressively overcome. An idea of the richness of possibilities, mentioned by Julia, is given in Chap. 5 of the book (1996) [13].

The beginning of studies on basin boundaries, generated by two-dimensional real noninvertible maps, consisted in collecting many very simple generic examples illustrating different qualitative situations generated by either quadratic or cubic maps, and also by continuous piecewise linear maps. A first basic tool was obtained with the generalization of the notion of *critical point* generated by one-dimensional noninvertible maps: the *critical curve* for two-dimensional noninvertible maps, the *critical set* for higher dimensions. It seems that this extension, defined as locus of points having two merging rank-one preimages (inverses), was firstly introduced by the Toulouse Group (1964) [14]. Such a set separates regions, the points of which have a different number of preimages (cf. Chap. 3 of the more recent book [13] for more details). Such a non classical singularity plays a fundamental role in the structure of attractors and basins, ditto for their bifurcations. It is the case of *contact bifurcations*, resulting from the meeting of two singularities of different nature: an invariant manifold of a saddle fixed point with the critical set. This situation generally gives rise to global bifurcations, which may be related to *homoclinic* and *heteroclinic* bifurcations (cf. p. 605, index of the book [13], for sections dealing with these topics).

A second tool was given by the determination of the stable (resp. unstable) manifold of a saddle fixed point, or cycle, from the series expansions defined by Lattès [15]. This permits to obtain a "germ," the iterates (resp. inverse iterates) of which lead to get the unstable (resp. stable) manifold of a saddle. The references of the books [16] (1980), and [13] (1996), give the list of publications made at that time about the properties of some basin boundaries.

Following this way, step-by-step, after understanding of many "generic" examples of two-dimensional real maps not satisfying the Cauchy–Riemann conditions, quickly three basic types of basins, with possible properties of self-similarity; appeared: *simply connected basin*, *nonconnected basin*, *multiply connected basin*. From 1964 to 1999 many results were obtained for noninvertible maps of the plane, on the basis of the first ones obtained in the years 1965– 1972. New properties were identified. They are related to the following global bifurcations:

- *Simply connected basin* $\longleftrightarrow$ *nonconnected basin without basin self-similarity* (at that time the word *fractal* had not been introduced [17], also cf. [13], pp. 243–244, [18, 19]). An application to a sampled data control system, the non linearity being piecewise linear, made up of five segments, is given in [17].
- *Simply connected basin* $\longleftrightarrow$ *nonconnected basin with basin self-similarity* (1969) [20] (also [13], pp. 243–247). This is the first example of bifurcation leading to a fractal basin generated by a noninvertible plane map.
- *Simply connected basin* $\longleftrightarrow$ *multiply-connected basin* (1973; cf. [21], § 2.1), with or without self-similarity properties.

Another type of nonclassical global bifurcation occurs by crossing through the situation of a whole singular curve made up of fixed points, or period-k cycle points, described in [22] (1966), [19] (1969). More details about this global bifurcation

(which seems remained quasi unknown even now) are given in pp. 399–406, 437–442 of the more recent book [13] (1996).

Chapter 5 of the book [13] collects the results on basin structures, identified since 1969. So, with many references, this document gives a larger view about basin bifurcations, and related "mechanisms" of basin fractalization. Moreover, the article *Noninvertible maps* (2007), published on the Website *Scholarpedia* (Mira C., 2 (9): 2328) gives a general presentation of the matter, associated with references and with illustrative examples of basin evolutions described in its *First Subpage*.

5.4.2 *Two-Dimensional Conservative, and Almost Conservative, Maps (1970–1976)*

From 1966 to 1976, Gumowski occupied a position of Senior Physicist in the *European Organization for Nuclear Research* in Geneva. In this framework he had particularly to study the problem of *stochastic* instability in accelerators and storage rings. Such instabilities appear to increase with the amount of nonlinearity. Here *stochastic*, adjective also used in the Geneva research center, has been called *chaotic* from 1975. The new Gumowski's position led to a collaboration with the Toulouse group on a new topic: *two-dimensional conservative* (or *Hamiltonian*) *maps*, and *almost conservative maps* [23–28]. Considering the results obtained in the framework of this collaboration, it must be noted that the Gumowski's part was the most important.

The nonlinear terms, considered in such studies, were either quadratic, or cubic, or exponential, or trigonometric, and also of unbounded, bounded type, symmetrical and asymmetrical [29]. The corresponding results are the object of Chaps. 3 (conservative maps) and 4 (almost conservative maps) of the book [30], and Chap. 5 of the book [16]. An abbreviated presentation of the results is given in Chap. 8 of [5]. As far as I know these results, with the considered particular nonlinear characteristics, were new at the time of their publications. Their application was made to two models of the longitudinal motion of particles in an accelerator.

5.4.3 *Chaotic Attractors of Two-Dimensional Noninvertible Maps (1968–1975)*

The first publication of the Toulouse group, on what has been called afterward *chaotic attractor*, or *strange attractor*, was made in the *Proceedings of the International Pulse Symposium* (Budapest 1968) [18], with an attractor generated by a piecewise linear two-dimensional noninvertible map. This example was also presented in a paper of the journal *Automatica* (1969) [19], and with more details, indicating the role of *critical curves* and bifurcations, in the Proceedings of the colloquium *Point Mapping and Applications* (Toulouse, Sept. 10–14, 1973) [21], which gave other

examples of attractors. The piecewise linear map gives rise to a period two area, without stable cycle, denoted *attractive limit set* in [18], *stochastic area* in [21] (*zones stochastiques attractives* in this text published in French). The use of such terms illustrates the level of uncertainty about new complex dynamical behaviors called *chaotic* afterward. More details are given in pp. 205–212, 463–467 of the 1996 book [13]. The Toulouse group also used the expression *Pulkin's phenomenon* associated with such behaviors. This designation was inspired from a Russian paper published in 1950 [31], showing that in an one-dimensional noninvertible map infinitely many unstable cycles and increasing classes of their limit points may lead to bounded complex iterated sequences.

More details on the different types of attractors generated by noninvertible maps are given with references in Chap. 4 (1996 book [13], pp. 185–337).

Another type of attractors, called *stochastic* in the framework of the colloquium *Point Mapping and Applications* [1], is the one generated by maps resulting from a perturbation of conservatives cases. Such attractors, with "conservative images," were the object of the exhibition of aesthetical images. Some of them can be seen in § 9 of Chap. 8 of the book [5].

5.4.4 Normal Forms and Resonant Bifurcations (1969–1974)

Consider a two-dimensional nonlinear map. When a fixed point (or a cycle) has the modulus of one of its two multipliers (or eigen values) equal to unity, this situation leads to a *critical case in the Ljapunov' sense* (notion extended from the ODE case). This means that it is impossible to define the fixed point nature (node, saddle, and focus) and its stability, from the linear approximation related to this point. In a neighborhood of the point, however small it may be, the phase portrait depends on nonlinear terms. The more interesting cases are those related to multipliers (eigen values) $S_{1,2} = e^{\pm j\varphi}$. From a parameter variation, the bifurcation by crossing through such a critical case may give rise to an invariant closed curve, very often wrongly called *Hopf bifurcation*. This appellation is even more surprising as historically it does not relate maps but ODE with the birth of a limit cycle described by Poincaré , and incorrectly attributed to Hopf (1942). This illustrates the confusion of quotations in Western countries until the 1980s. In the case of maps, since 1967 the Toulouse group has always called *Neïmark's bifurcation*, this qualitative change leading in the simplest situation to the birth of a closed invariant curve. Indeed the first contribution is due to Neïmark, in the particular case giving rise to only one invariant closed curve (1959) [32], φ being not commensurable with 2π. Moreover, the crossing through critical situations with angles $\varphi = 2\pi/3$, $\varphi = 2\pi/4$, was also considered by this author. Since, some 20 years this bifurcation is also known as *Neïmark-Saker bifurcation*, but the Saker's result (1964) is subsequent to the basic one due to Neïmark.

The Neïmark's results [32–35] furnished the basic first information for the Toulouse group studies. A generalization of these results, in a neighborhood of a fixed point, leads to normal forms by using a variant of the *Cigala's method*. This

method was described in [36] at the beginning of the twentieth century, in order to solve the particular problem of stability in two-dimensional conservative diffeomorphisms. Extended to dissipative two-dimensional maps having a sufficiently high degree of smoothness [37–43], the reduction to a normal form consists in identifying and isolating the *dominating terms* of the nonlinear parts. This objective is achieved by means of a sequence of nonlinear transformations of almost-identity type, which successively remove the non dominating terms.

The critical case $S_{1,2} = e^{\pm j\varphi}$ leads to two essentially different situations. The most complex one, called *exceptional critical case*, occurs when the angle φ is commensurable with 2π, $\varphi = 2k\pi/q$ (k and q being integers). After a certain number of applications of Cigala's transformations, it leads to a problem of denominators which cancel, and small denominators near this angle value. Then at this level the normal form is obtained, because it is impossible to continue the process of successive transformations. The exceptional cases lead to new singular points of different types described in [37–39] (1969, 1970). Among them those defined locally by $2q$ asymptotes (*complex saddle*) are associated with *resonant cases*. The second situation, called *nonexceptional case*, is related to the angle φ, either incommensurable with 2π or if it is commensurable with 2π it does not lead to a problem of small denominators. Such results were directly applied to resonant Hamiltonian bifurcations generated by area-preserving maps (cf. the book [30], $\varphi = 2\pi/3$ pp. 134–136, $\varphi = 2\pi/4$ pp. 137–140). The case of a four-dimensional map, leading to two multipliers with angles φ_1 and φ_2, was dealt in [43]. It gives rise to eight basic situations of exceptional cases (also cf. [16] pp. 205–211).

In nonexceptional cases the Cigala's method permitted to extend the Neïmark's results to bifurcations by crossing through the situation of a complex focus of multiplicity m, $m > 1$, when $S_{1,2} = e^{\pm j\varphi}$. This bifurcation may give rise to s, $0 \leq s \leq m$, invariant closed curves. In exceptional cases the method permitted to extend the Neïmark's results for $\varphi = 2k\pi/q$ with $q \neq 3$ and $q \neq 4$. Such studies of exceptional and nonexceptional cases were followed by their equivalent related to a four-dimensional map, a fixed point having two pairs of complex multipliers.

The maps family defined by a plane conservative linear part with a fixed point of *center* type ($S_{1,2} = e^{\pm j\varphi}$), the nonlinear terms having a small parameter α as coefficient, generates very interesting properties associated with resonant phenomena. This family was studied by the Toulouse group with results presented in the framework of the colloquium *Points mapping and Applications* [45] (1973), and also in an extended form pp. 260–270 of [16] (in French), and in pp. 251–279 of [44] (in English).

Other results about critical cases were obtained in Toulouse when the two multipliers $S_{1,2}$ of a fixed point are simultaneously equal, either to $+1$ or -1 in two situations: (a) the linear approximation matrix is reducible to a diagonal form, (b) it is not reducible to a diagonal form. The case (c) with $S_1 = +1$, $S_2 = -1$, was also considered. Then, it was possible to identify the bifurcations by crossing through such critical values (cf. pp. 181–222 of [16] (in French, 1980), and in pp. 207–279 of the book [44] (in English)).

These results on normal forms have been quoted in p. 184 of the Holmes and Williams paper [46].

5.5 Box-Within-a-Box Bifurcations Structure of Dim 1 Noninvertible Maps

From 1967, I had a regular correspondence with Sharkovskij. Shortly, after the publication of his famous paper *Coexistence of cycles of a continuous mapping of the line into itself* (in Russian) [47] (1964), given the cycles ordering related to their period k, this author sent me this text, with other papers in Russian and Ukrainian. At that time his outstanding theorem, which includes as a particular case the T.Y. Li and A.J. York result *Period three implies chaos* [48] (1975), was not known in Western countries. Considering the particular case of a smooth unimodal map, the Sharkovskij's paper [47] was at the origin of a thought about a possible refining of his general ordering of cycles. Indeed, the number of cycles having the same period k, generated by a smooth unimodal map, increases quickly with k. These cycles having the same period differ from each other in different permutations of their points by k successive iterations. So each period k-cycle can be identified by a symbolism $(k; j)$, j being an index related to this permutation. In 1963, Myrberg [49] made this characterization for the quadratic map, and called *spectrum* the parameter interval of bifurcations by period doubling with its limit value when the period tends toward infinity. In the Myrberg' sense a *spectrum* is the infinite sequence of bifurcations by period doubling related to a basic cycle $(k; j)$ created from a fold bifurcation (multiplier, or eigen value, $S = +1$). Now this interval is known as *Feigenbaum cascade*, result published (1978) 15 years after the Myrberg one. Theses considerations led to the identification of the *box-within-the-box bifurcation structure* (*structure boîtes-emboîtées* in French).

First identified with a well-defined symbolism (cf. below) in Toulouse, and published from 1975, this bifurcation structure is common in nonlinear maps dynamics. It has been qualified under different names, generally without a real understanding, in particular from numerical simulations in a lot of papers. With respect to other sections of this text, this is why more details are given lower down.

5.5.1 Toward the Identification of the Fractal Bifurcations Organization

The bases of the results obtained in Toulouse were:

- The Pulkin's paper [31], published in 1950: This publication deals with one-dimensional maps generating infinitely many unstable cycles, giving rise to what he named *completely invariant sets*. Such sets are related to the existence of limit sets of different *classes*. So infinitely many limit points of the unstable cycles set, when their period tends toward infinity, lead to *class 1 limit sets*. The limit sets of *class 1* generate limit points of *class 2*, and so on until limit points of *class* ∞. Increasing rank classes of limit points leads to what was called 25 years afterward *fractal structure*.

- The Myrberg [49] and Sharkovskji [47] results: From 1972, step-by-step, they gave the reference points, which permitted to identify the global fractal bifurcation organization generated by smooth maps defined by a function with only one extremum. This organization was called *box-within-the-box bifurcation structure* (*structure boîtes-emboîtées* in French) [50, 51] by the Toulouse group, and *embedded boxes* by Guckheimer when he quoted these results [52].

From the Pulkin's results, the Sharkovskij's cycles ordering compared with the Myrberg's one was the germinal point to study the global bifurcations organization generated by a unimodal map. Indeed the Sharkovskij's ordering is general in the sense that it concerns general forms of continuous of one-dimensional maps with any extremums, but cannot discern between the cycles having the same period k, the number of which drastically increases with the period growth (cf. [44] p. 96). For example, in the case of unimodal maps (i.e., with only one extremum) the number of cycles of period $k = 30$ is $N_k = 35,790,267$, and the number of bifurcation values generating them is $N_\lambda(k) = 17,895,679$. Considering these basic results as a starting point, to go further in the study of unimodal maps, the adopted guide line was to introduce the set of *critical points* of rank $r = 1, 2, 3, ...$, (i.e., the increasing sequence of images of the map extremum). Such a set is made up of *nonclassical* singularities introduced by the map noninvertibility. This leads to identify *nonclassical bifurcations* corresponding to the merging of two singular points of different nature: a critical point and an unstable cycle. Then the fractal organization of bifurcations is known from an identification of these nonclassical bifurcations. This permitted a new classification of the *Myrberg' spectra*, through the fractal *box-within-the-box bifurcation structure* (or *embedded boxes*). As indicated above, at that time the word *fractal* did not exist, the Toulouse group used *like a Von Koch curve*, or the descriptive sentence *the whole is similar to the parts even if they are infinitesimal*, "image" of self similarity properties. This sentence was due to the French mathematician Paul Levy (1928), who after 1938 was the author of the *Levy's curve*, its Hausdorff dimension being equal to 2, and the topological dimension equivalent to 1.9340, values determined after Levy. In this chapter, as at the time of the description of the *box-within-the-box bifurcation structure*, on purpose it is not useful to introduce the notions of *topological dimension*, and *fractal Hausdorff dimension*, for preserving the first introduction of the term *fractal* (by Mandelbrot who was one of the Levy' students at the *Ecole Polytechnique* Paris) in its relation to objects whose structure is invariant by scale change.

All these fundamental results have been passed over in most of papers dealing with this subject, which has a very large vogue since 1978. The most part of these results have been very often attributed to authors who rediscovered them after using another forms of quadratic map, such as the *logistic map*, or maps of the unit interval. So the publication [53] (1976) describes the situation called *cycle en valeur moyenne* near one of the two boundaries of each box, which was rediscovered in 1980 under the name *intermittency phenomenon*. The other box boundary, called in [53] *segment stochastique cyclique en valeur moyenne*, was rediscovered in 1982 under the name *chaotic attractor in crisis*, or *boundary crisis*. All the results of this section were

published in French before 1976, but with more details they are presented in English in Chaps. 3 and 4 of the book [44]. An abbreviated description is given in the more recent paper [54].

In a first step, the bifurcation structure was identified via the quadratic map,

$$T: \qquad x' = x^2 - \lambda. \tag{5.1}$$

Here x is a real variable, λ a real parameter. Such a map, called *Myrberg's map*, is defined by a parabola with an ordinate minimum C_{-1} ($x = 0$), its rank-one image $C = T(C_{-1})$ being the *rank-one critical point* of T. The inverse map T^{-1} is defined by $x = \pm\sqrt{x' + \lambda}$. The map T is characterized by the following properties.

(a) All the bifurcations values of (5.1) occur into the parameter interval $\Omega_1 = [\lambda_{(1)_0}, \lambda_1^*]$, called *overall box*, $\lambda_{(1)_0} = -1/4$, $\lambda_1^* = 2$. For each λ-value, $-1/4 < \lambda < 2$, the map generates a unique attractor (a stable fixed point, or a stable period k cycle, or a chaotic attractor). The value $\lambda_{(1)_0} = -1/4$ corresponds to a *fold bifurcation* giving rise to two fixed points q_i, $i = 1, 2$, with multiplier $S = 2x(q_i)$: q_1 always unstable ($S > 1$), and q_2 ($S < 1$, attracting when $-1 \leq S < 1$). No real fixed point exists for $\lambda < \lambda_{(1)_0} = -1/4$. The value $\lambda = \lambda_1^* = 2$ is a basic nonclassical bifurcation resulting from the merging of the unstable fixed point q_1 with the rank-two critical point $C_1 = T(C) = T^2(C_{-1})$. It is characterized by the relations $x(C_1) = x(q_1) = 2$, $x(C) = x(q_1^{-1}) = -2$, $T^{-1}(q_1) = q_1 \cup q_1^{-1}$. When $0 < \lambda < \lambda_1^*$ the invariant segment $[q_1^{-1}, q_1]$ is the closure of the basin of the absorbing segment $\overline{CC_1}$, which contains the unique attractor. When $\lambda = \lambda_1^*$ the segment $\overline{CC_1}$ is chaotic and merges with $[q_1^{-1}, q_1]$, all the possible cycles have been created, they belong to $\overline{CC_1}$. Then $\overline{CC_1}$ is *invariant but not absorbing*. An initial condition x_0 on this segment gives a bounded orbit, belonging to the interval $[q_1^{-1}, q_1]$, orbit very sensitive to very small changes of x_0. The repelling cycles and their increasing rank preimages constitute a real set (E), the derived set (set of limit points) (E') of which is perfect. The preimages of (E) are everywhere dense on (E').

For $\lambda > 3/4$, the fixed point q_2 is always repelling with $S(q_2) < -1$ and a period $k = 2$ cycle, made up of two points q_{2i}, $i = 1, 2$, having the multiplier $S(q_{2i}) = 4 - 4\lambda$, emerges from q_2 . The value $\lambda = \lambda_{b1} = 3/4$ corresponds to a *flip bifurcation*. New increasing values of λ generates a sequence of flip bifurcations for $\lambda = \lambda_{bm}$ related to period 2^i cycles, $i = 1, 2, ..., m$, with an accumulation value $\lim_{m\to\infty} \lambda_{bm} = \lambda_{1s} \simeq 1.401155189$ given by Myrberg. For $\lambda < \lambda_{1s}$ the number of repelling cycles is finite. They have the period 2^m and have been created after crossing through each λ_{bm} value. For $\lambda > \lambda_{1s}$ infinitely many repelling period 2^i cycles ($i = 0, 1, 2, ...$) exist, and they constitute a fractal set. Myrberg calls *spectrum* the parameter interval $\omega_1 \equiv [\lambda_{(1)_0}; \lambda_{1s}]$, here related to the sequence (cascade) of bifurcations by period doubling from the fixed point q_2 ($i = 0$).

(b) The number N_k of all possible cycles having the same period k, and the number $N_\lambda(k)$ of bifurcation values giving rise to these cycles, increase very rapidly with k (book [44], pp. 93–94). Cycles with the same period k differ from one

another by the cyclic transfer (permutation) of one of their points by k successive iterations by T. Then a period k-cycle is identified by the symbolism $(k; j)$, j being an index characterizing this cyclic transfer. Considering a $(k; j)$ cycle, it can be generated from two basic bifurcations: either a fold one, or a flip one. A fold bifurcation generates two *basic cycles* from $\lambda = \lambda^j_{(k)_0}$, one with a multiplier (or eigen value) $S > 1$, the other with $S < 1$. With increasing values of λ, from the cycle $(k; j)_{S<1}$ a flip bifurcations cascade occurs for $(k2^i; j_i)_{S<1}$ cycles with accumulation at a value λ^j_{ks} when $i \to \infty$, $2 > \lambda^j_{ks} > \lambda_{1s}$. Myrberg calls *spectrum* the parameter interval $\omega^j_k = [\lambda^j_{(k)_0}; \lambda^j_{ks}]$, $k = 1, 3, 4, ...$, made up of parameter intervals leading to attracting cycles of period $k2^i$, $i = 0, 1, 2, ...$ The cycle symbolisms $(k; j)$ and $(k2^i; j_i)$ correspond to what is called a *nonembedded representation* [44].

When $\lambda > \lambda^*_1 = 2$, $[q_1^{-1}, q_1] \subset \overline{CC_1}$, the only attractor is the point at infinity, and no bifurcation takes place. The set (E) (without the point at infinity) constitutes the nonwandering set $(E) \in [q^1_{-1}; q_1]$. All the possible cycles have been created by the map T (5.1). They are real and repelling. (E) is *completely disjointed*, and is a *Cantor set*. The situation equivalent to the λ^*_1 one (but now with an attractor inside $\overline{CC_1}$) is met for a $(k; j)$ cycle with multiplier $S > 1$ (thus generated from a fold bifurcation), for a parameter value denoted by λ^{*j}_k. In this case, λ^{*j}_k is the least λ-value such that the critical points $C_k = T^k(C)$, C_{k+1}, ..., C_{2k-1} merge into the k points of the $(k; j)$ cycle with $S > 1$. By consideration of T^k the value λ^{*j}_k reproduces qualitatively the situation of T when $\lambda = \lambda^*_1$. Differently from $\lambda = \lambda^*_1$, for λ^{*j}_k the map T generates k attracting segments constituting a *period-k chaotic segment* which is now *absorbing*.

5.5.2 Description of the Structure

The fractal *box-within-a-box* structure, here defined for the map T (5.1), concerns all types of smooth unimodal maps with correctly chosen parameter variation. This structure is of "Russian dolls" type. It considers the parameter interval $\Omega_1 = [\lambda_{(1)_0}, \lambda^*_1]$ (*overall box*) inside which all the possible bifurcations occur. Out of Ω_1 no bifurcation happens. Ω_1 is generated from the two basic period $k = 1$ cycles, i.e., the fixed points q_1 and q_2. Taking into account the Myrberg' spectrum ω_1 related to the fixed point q_2 ($S < 1$), the box Ω_1 is defined by:

$$\Omega_1 = [\lambda_{(1)_0}, \lambda^*_1] = \omega_1 \cup \Delta_1, \quad \Delta_1 =]\lambda_{1s}, \lambda^*_1].$$

Note that the symbolism "2^i" excludes even period cycles born from a fold bifurcation, or a flip bifurcation related to a *basic cycle* appearing out of ω_1 ($2^2 \neq 4$, $2^3 \neq 8$, ..., with such a symbolism). So cycles different from $(2^i; j_i)$ can appear only for $\lambda \in \Delta_1$. For $\lambda < \lambda_{(1)_0} = -1/4$ the map has neither fixed point (except the point at infinity) nor cycles, every orbit is divergent. For $\lambda > \lambda^*_1 = 2$ all the possible period k cycles have been created. They are repelling, and the map has the properties indicated above.

Two period-k ($k = 3, 4, ...$) basic cycles $(k; j)$, one with $S > 1$, the other with $S < 1$, generate a parameter interval, provisionally denoted $\widehat{\Omega}_k$, having the same behavior as Ω_1, $\widehat{\Omega}_k \subset \Delta_1$. If $\widehat{\Omega}_k$ is not contained into another interval $\widehat{\Omega}_{k'}$, k being a multiple of k', $\widehat{\Omega}_k$ is called *rank-one box*, or *box*$(k; j)$ (*embedded representation*). Then, it is denoted Ω_k^j with:

$$\Omega_k^j = [\lambda_{(k)_0}^j, \lambda_k^{*j}], \Delta_k^j =]\lambda_{ks}^j, \lambda_k^{*j}], \Omega_k^j = \omega_k^j \cup \Delta_k^j \subset \Delta_1.$$

Here ω_k^j is the *spectrum* $(k; j)$. Then for T^k the box Ω_k^j reproduces in the same form (self similarity property) all the bifurcations contained in the box Ω_1 for a set of cycles having periods multiple of k. Denote $\Omega_{k_1}^{j_1}$ one of such boxes. Inside $\Omega_{k_1}^{j_1}$ it is possible to define *rank-two* boxes $\Omega_{k_1.k_2}^{j_1,j_2} = [\lambda_{(k_1.k_2)_0}^{j_1,j_2}, \lambda_{k_1.k_2}^{*j_1,j_2}] \subset \Delta_{k_1}^{j_1}$, related to two $(k_1.k_2; j_1, j_2)$ basic cycles, which for $(T^{k_1})^{k_2}$ undergoes in the same order all the bifurcations of the box $\Omega_{k_1}^{j_1}$, and so those of Ω_1:

$$\Omega_{k_1.k_2}^{j_1,j_2} = [\lambda_{(k_1.k_2)_0}^{j_1,j_2}, \lambda_{k_1.k_2}^{*j_1,j_2}] = \omega_{k_1.k_2}^{j_1,j_2} \cup \Delta_{k_1.k_2}^{j_1,j_2} \subset \Delta_{k_1}^{j_1}, \Delta_{k_1.k_2}^{j_1,j_2} =]\lambda_{(k_1.k_2)_s}^{j_1.j_2}, \lambda_{k_1.k_2}^{*j_1,j_2}].$$

More generally it is possible to define *rank-a boxes*, embedded into a rank-$(a-1)$ box

$$\Omega_{k_1....k_a}^{j_1...,j_a} = [\lambda_{(k_1....k_a)_0}^{j_1...,j_a}, \lambda_{k_1....k_a}^{*j_1...,j_a}] = \omega_{k_1....k_a}^{j_1...,j_a} \cup \Delta_{k_1....k_a}^{j_1...,j_a} \subset \Delta_{k_1....k_{a-1}}^{j_1...,j_{a-1}}.$$

So $\Omega_{k_1....k_a}^{j_1...,j_a} \subset \Omega_{k_1....k_{a-1}}^{j_1...,j_{a-1}}$, $a = 1, 2, ...$ The boundary parameter λ^* of each of these boxes ($a = 1, 2, ...$) is defined from the merging of well defined critical points with a repelling basic cycle having the multiplier $S > 1$. They are called *boxes of first kind*. The representation of these boxes is given by Fig. 5.1a, with the enlargement of Fig. 5.1b, c representing the embedding of boxes called *of second kind* (cf. next page) [13, 54].

Other type of parameter λ^* can be also defined from a repelling cycle with $S < -1$, born from a flip bifurcation. Then when $\lambda = \lambda_{k2^i}^{*j}$, $i = 1, 2, ..., k = 1, 3, 4, ..., k2^{i-1}$ critical points of well defined rank merge into a period $k2^{i-1}$ cycle with $S < -1$ (born from a flip bifurcation). We call *box of second kind*, a box denoted $\Omega_{k2^i}^j$ which has $\lambda_{k2^i}^{*j}$ as one of the two boundary points (cf. Fig. 5.1c for $k = 1$). The second boundary point is the flip bifurcation $\lambda = \lambda_{bk2^{i-1}}^{j_i}$, parameter generating the attracting cycle $(k; 2^i)$. When $i \to \infty$, the two boundaries tend toward λ_{ks}^j, with $\lambda_{k2^i}^{*j} > \lambda_{ks}^j$. The first and largest box of second kind is $\Omega_{2^1} \equiv [\lambda_{b1}, \lambda_{2^1}^*]$, $\lambda_{2^1}^*$ $(k = 1)$ corresponding to $C_2 \equiv q_2$. Figure 5.1 represents the whole *box-within-a-box* (or *embedded boxes*) bifurcations structure. It is fractal because the boxes are self similar, i.e., the organization of the set Ω_1 is similar to that of its parts (the above defined boxes), even if these parts are infinitesimal.

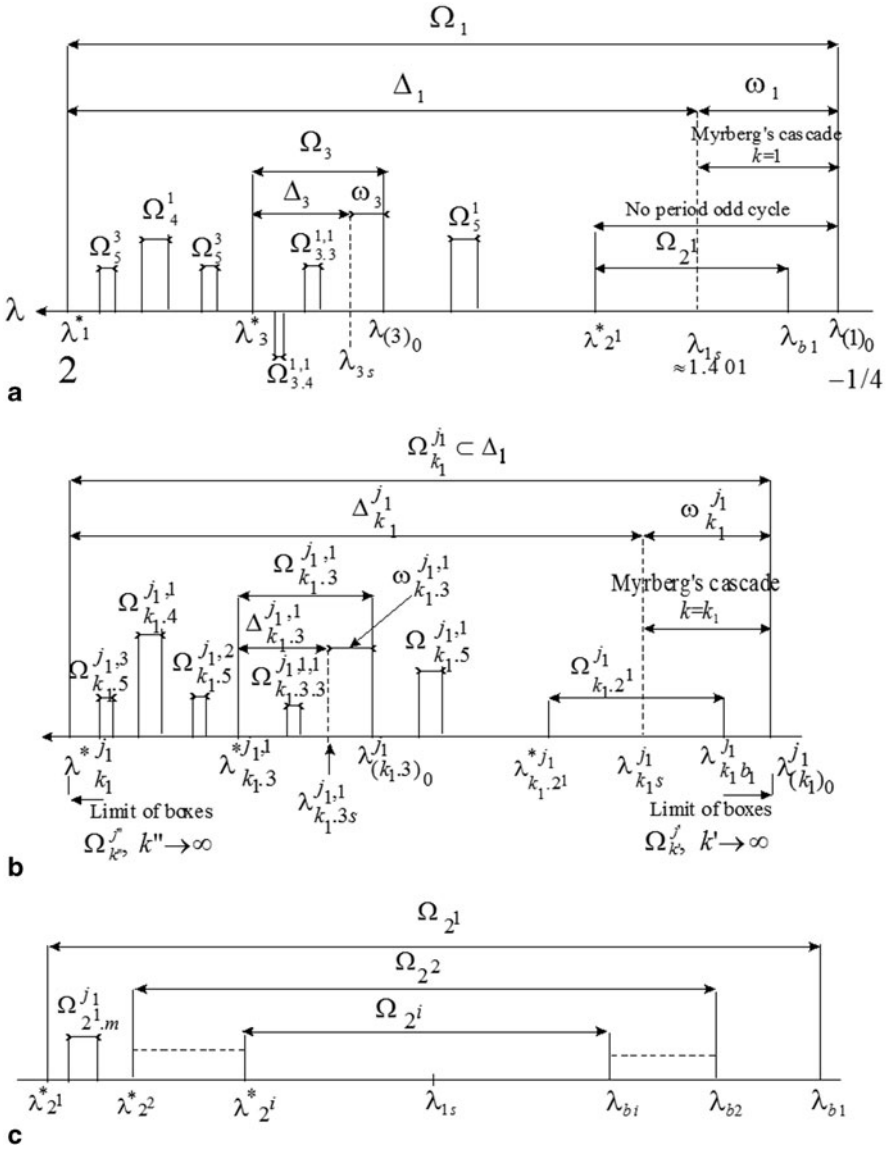

Fig. 5.1 *Box-within-a-box* (or *embedded boxes*) bifurcations structure

5.5.3 Properties

The box boundaries satisfy the following properties: out of Ω_k^j , $\lambda < \lambda_{(k)_0}^j$, the value $\lambda_{(k)_0}^j$ *is a limit point of boxes* $\Omega_{k'}^{j'}$ *for* $k' \to \infty$, with $\lambda > \lambda_k^{*j}$ the value λ_k^{*j} *is a limit point of boxes* $\Omega_{k''}^{j''}$ *when* $k'' \to \infty$. Considering the map T (5.1) and increasing values of the parameter λ, the multiplier S of a cycle $(k; j)_{S>1}$ increases and the multiplier S of a cycle $(k; j)_{S<-1}$ decreases. So these cycles become more and more repelling and they cannot disappear via a bifurcation. The following properties results:

(a) *Let* $[k, j]$ *(nonembedded representation),* $k = 1, 3, 4, ...$, *be the given basic cycle of the box* Ω_k^j *with* $S < 1$. *For* $\lambda \geq \lambda_{ks}^j$, Ω_k^j *has generated a Cantor set* $Cs[k, j]$ *made up of all the repelling* $(k2^i, j_i)$*-cycles,* $i = 0, 1, 2, ...$, *with multiplier* $S < -1$, *born from the flip bifurcations of* ω_k^j.

(b) *Let* $(k_1; j_1)$ *(embedded representation) be the basic cycle (*$S < 1$*) of the rank-one box* $\Omega_{k_1}^{j_1}$. *For* $\lambda \geq \lambda_{k_1}^{*j_1}$, *the box* $\Omega_{k_1}^{j_1}$ *has generated the Cantor set* $Cs[k_1, j_1]$, *and infinitely many Cantor sets,* $Cs[k_1k_2; j_1, j_2]$, ..., $Cs[k_1k_2...k_a; j_1, j_2, ...j_a]$, ..., $a = 1, 2, ..., \infty$, *from the infinitely many boxes (with fractal organization) embedded into* $\Omega_{k_1}^{j_1}$.

(c) *For* $\lambda \geq \lambda_{k_1}^{*j_1}$, *the map* T (thus not only $\Omega_{k_1}^{j_1}$) *has generated infinitely many Cantor sets related to the infinitely many boxes created for* $\lambda \leq \lambda_{k_1}^{*j_1}$. *For* $\lambda < \lambda_{(k_1)s}^{j_1}$ *the map has generated infinitely many Cantor sets related to the infinitely many boxes created for* $\lambda \leq \lambda_{(k_1)_0}^{j_1}$.

(d) *For* $\lambda \geq \lambda_1^*$, *T has generated all the possible Cantor sets, related to all the basic cycles of T, from the infinitely many boxes embedded into the over all box* Ω_1.

The two boundaries of a given box are accumulation points (said of 1st type) of infinitely many external boxes related to cycles with $k \to \infty$. Another type of boxes accumulation point for $\lambda = \widetilde{\lambda}$ (said of 2nd type) has different properties (cf. [44], pp. 156–161), particularly it gives rise to nonclassical *invariant measure* situations (cf. [44], pp. 166–174). Such singular accumulation points, λ_k^{*j}, $\lambda_{k2^i}^*$, $\widetilde{\lambda}$, and their embedded forms, are now known as *Misiurewicz points* (Publ. Math. I.H.E.S. 53, 17–51, 1981). Nevertheless, these parameter values were identified before (from 1975) in different terms by the Toulouse group.

Denote Λ_λ^*, the fractal set resulting from the union of all the above Cantor sets, and cycles with $S > 1, k \geq 3$, including their limit points, generated for $\lambda \geq \lambda_{1s}$. This set satisfies the property $\Lambda_\lambda^* \subseteq \overline{CC_1}$, and its structure is well defined from the knowledge of fractal structure. When $\lambda_{1s} < \lambda < \lambda_1^*$, the set Λ_λ^* constitutes the *nucleus of a strange repeller SR*, made up of Λ_λ^* and its increasing rank preimages. From the initial point $x_0 \in \overline{CC_1} \backslash \Lambda_\lambda^*$, n iterations, $n < N$ (N depending on x_0) give rise to a *chaotic transient*, followed by a regular convergence toward the attractor of T. When $\lambda > \lambda_1^*$ and $x_0 \in]q_1^{-1}, q_1[\backslash \Lambda_\lambda^*$, the set Λ_λ^* generates for $n < N$ a chaotic transient occurring in the interval $]q_1^{-1}, q_1[$, and for $n > N$ the orbit diverges tending toward infinity. On the x-axis, the repelling cycles, and their limits for the period $k \to \infty$, have a fractal organization when $\lambda \geq \lambda_{1s}$. For each point of the parameter λ-axis,

$\lambda \geq \lambda_{1s}$, the fractal structure of the map singularities is completely identified from the box-within-a-box bifurcation structure. Consider $\lambda \in \omega_k^j$, with λ sufficiently near $\lambda_{(k)0}^j$ for giving an attracting cycle $(k; j)$. For the map T^k this cycle gives k attracting fixed points P_i, $i = 1, ..., k$, each of them with an *immediate basin* $D_0(P_i)$, and a *total nonconnected basin* $D(P_i) = \cup_{n>0} T^{-n} D_0(P_i)$. The basins $D(P_i)$ are fractal, and have SR as a common limit set.

The above properties (a)–(d) bring out the limit points of different classes mentioned by Pulkin in 1950 [31].

Variants of the fractal box-within-the-box bifurcation structure was extended to one-dimensional maps defined by smooth functions with two extrema (cf. [16], pp. 401–418), and can be identified for smooth functions having more than two extrema.

5.6 Foliated Bifurcation Structures

This topic was the object of many studies (1980–1999) in the Toulouse group. They were based on the fact that the set of bifurcation curves in a parameter plane must be considered as giving only a coarse information about the map dynamics. Indeed this set only represents the "skeleton" of a larger information permitting to follow the dynamical evolution in presence of parameter variations. This evolution can be identified by considering the parameter plane as made up of sheets, each sheet being associated with a well defined stable, or unstable, cycle (with its period k and an index j characterizing the permutation of its k points after k iterations). Then the parameter plane is said *foliated*, and can be associated with a three-dimensional representation of the sheets. Covering areas of several sheets, associated with stable cycles (or more complex attractors), gives rise to the *multistability phenomenon*. Information from a set of bifurcation curves alone, and that from the foliated parameter plane can be compared with that obtained from an X-ray image and that of Magnetic Resonance Imaging.

These sheets present folds along *fold curves* (one the multiplier is $S = +1$), have junctions with branching along *pitchfork curves* (one the multiplier is $S = +1$), and *flip curves* (one the multiplier is $S = -1$). Such curves correspond to *codimension-1 bifurcations*. The simplest singularities on these curves are of *codimension-2 type*. Two among them have a particular importance: the *cusp point* of a fold curve, called the *fold codimension-2 point*; and the tangential point of a flip curve and a fold one having a double period, called the *flip codimension-2 point* (for more details, and a three-dimensional representation of the sheets cf. [55–63], and the book [44], pp. 349–395). These singular points correspond to complex communications between the sheets. Then the association of fold and flip curves in the neighborhood of a fold cusp leads to the definition of three types of fundamental communications between sheets: *crossroad area*, *saddle area* , and *spring area*. So a three-dimensional representation of the foliation appears particularly interesting for a complete characterization of the sheets organization. In particular, it is possible to define the path

followed by a stable cycle to continuously pass from a sheet to another one (*crossroad area*), or after having turned unstable, recovering its stability to attain another sheet (*spring area*).

A third parameter variation may lead to foliation bifurcations such as:

- *Crossroad area* $\longleftrightarrow$ *saddle area*; *spring area* $\longleftrightarrow$ *crossroad area* [55],
- *Crossroad area* $\longleftrightarrow$ *dissymmetrical spring area* $\longleftrightarrow$ *symmetrical spring area* [58],
- *Double crossroad area* $\longleftrightarrow$ *double spring area* [58].

Other types of foliation bifurcations are possible [57, 59, 61–63]. Moreover, the Myrberg' spectrum may give rise to other dynamical behaviors such as: cascade of *spring areas* by period doubling, *crossroad area* communication between two *spring areas* with period doubling of this structure (cf. the book [44], pp. 361–373). Algorithms for identifying communication areas, with generalization to n - dimensional maps have been the object of several papers [64–67].

Using a Poincaré section, various types of ordinary differential equations were studied from the point of view of the foliated parameter plane, and its communication areas, this via a three-dimensional representation of the foliation. Out of the Toulouse group, such studies have been very rare. Generally, the parameter plane, related to maps, or ODE, is analyzed from a numerical scanning which permits to identify regions corresponding to the existence of stable cycles, or other complex attractors. This method is coarse and the results interpretation is a cause of frequent errors due to a lack of precision, and difficulties to follow the same cycle during the plane scanning (jump from a sheet to another one). Nevertheless, a numerical scanning of the parameter plane permits to detect the existence of *crossroad area* structures. It is the case of structures called *shrimps* in [68] which are images of *crossroad areas*.

5.7 Imbedding of a Dim $(p-1)$ Noninvertible Map into a Dim p Invertible One

The simplest situation is the case of a one-dimensional noninvertible map embedded into a two-dimensional invertible map ($p = 2$). It was considered in [69] (1978) and pp. 291–296 of the book [44]. It is about two-dimensional ($p = 2$) invertible maps T_b (Jacobian $J = -b$) (written here in the recurrence form):

$$\begin{aligned} x_{n+1} &= f(x_n, a) + y_n \\ y_{n+1} &= bx_n\,, \qquad\qquad n = 0, 1, ... \end{aligned} \tag{5.2}$$

When $b = 0$, from the initial condition (x_0, y_0), $y_0 \neq 0$, T_b turns into the one-dimensional ($r = 1$) noninvertible map T_0:

$$x_{n+1} = f(x_n, a), \qquad n = 1, 2, ..., \tag{5.3}$$

with the initial condition x_1 for $n = 1$. If f is a quadratic function (5.2) is of Henon's map type.

The case of the Hénon's map ($f(x_n, a) \equiv 1 - ax^2$) was widely studied in the Toulouse group, which has been the first to give the organization of the bifurcation curves in the parameter plane (a, b) with its foliation [70, 71], and pp. 326–397 of the book [44]. The bifurcations organization for $b = 0$ is nonfoliated, fractal of *box-within-a- box* type, so well known. The $(k; j)$ cycles of the plane axis $b = 0$, associated with the multipliers $S = +1$ (resp. $S = -1$) were the germ for determining *fold* (resp. *flip*) bifurcation curves of the parameter plane (a, b). For $b \neq 0$, such curves intersect, which shows that the parameter plane is foliated. In the years 1984–1985, Hiroshi Kawakami stayed for 6 months in the Toulouse group. During his stay, he considered the ordered list of $(k; j)$ cycles having the same period k, associated with a binary word made up of k bits (0,1), equivalent of the Myrberg rotation sequence made up of $(k - 2)$ signs $+$ and $-$, characterizing the index j. From a rotational shift on the inverse of the binary word (cf. [72] and the book [44], pp. 130–131, 341–349), he introduced the notions of *adjoint cycles* having a link with another period k cycle, and *self-adjoint cycles* without no link without another period k cycle. From these additional characteristics, in a complete list period k cycles (cf. [44], pp. 342–343), it was possible to introduce the notions of *connections chains* and *communications cells* (cf. [44], pp. 375–395). Associated with a *contracted representation of the parameter plane*, they permit to forecast the existence of different types of communication between the sheets of the foliated parameter plane *(a;b)* (cf. [44], pp. 373–395).

The case $p = 3$ is shortly formulated in pp. 565–567 of the book [13], and in a more developed form in [73].

The particular illustrative imbedding considered in the paper [72] is defined by the invertible map T_b:

$$\begin{aligned} x' &= f(x, y, \alpha), \\ y' &= g(x, y, \lambda) + z, \\ z' &= b(x + y). \end{aligned} \tag{5.4}$$

The following assumptions are made for the functions $f(x, y, \alpha)$ and $g(x, y, \lambda)$:

(i) The map T_0 is noninvertible.
(ii) The Jacobian of T_b does not change its sign for $b \neq 0$.

The condition (ii) ensures that the map T_b is invertible, whether the map is smooth or nonsmooth. When the parameter of embedding is $b = 0$, the invertible map T_b turns into a two-dimensional noninvertible map T_0 :

$$x' = f(x, y, \alpha), \qquad y' = g(x, y, \lambda). \tag{5.5}$$

From the Valiron's results [74], the book [13] considers (pp. 8–13) the formulation of the general embedding problem of a $(p - k)$-dimensional noninvertible map into a p-dimensional invertible one, $p = 3, 4, ..., k = 2, 3, ...$

5.8 Maps with Vanishing Denominators

From 1996, this research field was developed with the collaboration of Laura Gardini and Gian-Italo Bischi (University of Urbino). Let T be a two-dimensional invertible, or noninvertible map, denoted $(x\prime, y\prime) = T(x, y) = [F(x, y), G(x, y)]$, where at least one of the components F or G has a denominator that vanishes in a one-dimensional subset of the phase plane. Here (*x'*,*y'*) denotes the image of the point (*x*,*y*). Consequently, T is not defined in the whole plane and there can arise singular sets called *focal points* (cf. [75], first introduction of this term) and *prefocal sets*. These singularities give rise to nonclassical topological structures of attractors and their basins, and to bifurcations that do not occur in continuous maps. At a *focal point*, one of the components has the form 0/0. Roughly speaking, a *prefocal curve* is a set of points for which there exists at least one inverse, that maps (or *focalizes*) the whole set into a single point, the *focal point*. Note that these singularities also play an important role for smooth maps (e.g., polynomial maps) without cancelling denominator, but for which the inverse of the map has a denominator that vanishes on a subset of phase space.

The article *Maps with vanishing denominators* (2007), published on the Website *Scholarpedia* (Gardini L., Bischi G.I., Mira C., 2 (9): 3277) gives a general presentation of the matter, associated with references and five illustrative examples in the *First Subpage*.

5.9 Applications

Conducted in an engineering department, the Toulouse group researches on nonlinear maps were originally motivated by models of discrete-time control systems (nonlinear *sampled data control*), in which a continuous plant is controlled via a digital device. The results obtained by the group are presented in pp. 339–393 of the book [76], which gives the associated references. The text below provides a brief description of some contributions.

The simplest case is that of a periodic sampler, which may give rise to typical nonlinear behaviors. So, in presence of two attractors (fixed point and period two cycles) the phenomenon of nonconnected basin for one of them, multiply connected basin for the other one, was identified. Moreover, the sampler playing the role of a parametric periodic excitation, a variation of the sampling period may lead to parametric resonances due to *exceptional critical cases* generated by the map model (resonant bifurcations).

It is worth noting that the contribution of Alain Giraud played a fundamental role in the Toulouse group history, for engineering applications, as well as for dynamical behaviors of maps. In particular, he developed a theory of what was called at that time *Systèmes à Commutations* (cf. Chap. 4 of the 1969 thesis [77], and [76], § 8.4), which has appeared to belong to what has been called afterward *Hybrid Systems*.

The general form of the model is the following:

$$F_i[X_{n+1}, X_n, t_{n+1}] = 0, \qquad g_k(X_n, t) = 0, \qquad X(t_n) = X_n, \tag{5.6}$$

where X is the state vector, the indices i and k correspond to different possible forms of F and g, t_{n+1} is the smallest root of the relation $g(X_n, t) = 0$, larger than t_n (switching time, generally related to the determination having a physical sense). The simplest case is that of sampled data systems with width modulation, or with frequency modulation, or control systems with variable structure, which lead to the explicit form:

$$X_{n+1} = F(X_n, t_{n+1}), \qquad g(X_n, t) = 0, \qquad X(t_n) = X_n. \tag{5.7}$$

In the Toulouse group, applications using variable structure control were made for two one-link manipulators, speed and position control of an asynchronous motor, adaptive control using only input and output measurements with two sliding surfaces.

The *Systèmes à Commutations* theory was elaborated for preparing a study of rectifiers "*alternating current*→ *direct current*, using thyristors with voltage feedback, or current feedback, the load being made up of a resistance and an inductance (1967–1971). A discrete model in the form of a recurrence relationship was constructed, the discrete states of this systems being determined at two consecutive switching times of the thyristors. The analytical form of this model is very complex and bulky, but can be programmed in a computer without any difficulty. It is of implicit and parametric type, including several relations (Chap. 5 of [77], and [76], § 8.5). For a voltage feedback, X is a one-dimensional vector. For a current feedback, X is a two-dimensional vector. In such a problem a stable fixed point corresponds to the user specifications about what is called *residual ripple* of the rectifier output, the mean value of which is associated with the system input. More details are given in the Giraud's thesis [77], a shorter version with figures being accessible in Chap. 8 of the book [5].

It is important to note that p. 190 of the Giraud's thesis [77] says that the expression *cycle stable d'ordre élevé* (very high period cycle) is used for convenience sake in order to qualify a steady state without any periodicity (obtained in the framework of this study), called *pseudo-périodique* by this researcher. Such a denomination gives another example of the fluctuations in the vocabulary choice of the group, revealing its perplexity in presence of phenomena identified as *chaotic* afterward (in 1975). At a time of very bad performances of computers, Giraud defined exactly the basin of the specified *residual ripple*, in presence of another attractor (a period 3 chaotic one), and bifurcation curves in the parameter plane (K gain of the control amplifier, τ time constant of the load). Before the Toulouse group studies (1967–1971), the manufacturers of rectifiers thought that subharmonic behaviors (which increase the *residual ripple* amplitude), and other complex behaviors in such systems, were essentially due to asymmetries of the phases of the secondary winding of the transformer, and to "antenna effects." The Toulouse group results have shown that, even with a perfect phases symmetry, the thyristors nonlinearities generate nonwanted behaviors (subharmonics and chaos). Moreover, a correct choice of the

gain K for a given τ can lead to the global stability of a correct residual oscillation specified by the users.

Other applications giving rise to complex dynamics have been made for systems of satellite attitude controlled by a frequency modulator of second kind, and in a satellite with inertia being a periodic function of time (1969–1975).

5.10 Conclusion

At a time when the results on the nonlinear maps dynamics were virtually unknown outside the former Soviet Union, from the year 1962 the Toulouse group based its researches not only on the results of the French school of iteration theory but also on the works of the Gorki teams (called *Andronov school*) and those of the Kiev school, which occupied the first rank in the nonlinear field, as noted in 1961 by P. La Salle and S. Lefschetz (cf. Sect. 3). Such results, published in Russian, remained rather unknown in Western countries until the 1980s. It was the same for the original Myrberg contribution on one-dimensional noninvertible maps, firstly quoted in the Toulouse group papers from 1975, but now attributed to authors who long afterward rediscovered his results published in *Annales Academiae Scientarum Fennicae* (1958–1963). It is the case of Metropolis N., Stein M.L., Stein P.R. (characterization of a cycle by a binary code *L, R*), and Feigenbaum (cascades of bifurcations by period doubling with their limit points), that the popular notions of *invariant coordinate* and that of *kneading invariant* are variants of the Myrberg's ordering law of cycles. In contemporary quotations, Cigala (1905) and Pulkin (1950) have also been remained unknown, in spite of the importance of their results.

With papers firstly published in French, some of the Toulouse group results were rediscovered, and are now known differently. In particular, it is the case of *compound windows* (about the fractal *box-within-the-box bifurcation structure*), *Misiurewicz points* (singular accumulation points of infinitely many boxes), *intermittency phenomenon* (called in 1976 *cycle en valeur moyenne* near one of the two boundaries of each box), *chaotic attractor in crisis,* or *boundary crisis* (called in 1976 *segment stochastique cyclique en valeur moyenne*). It is this situation, related to many papers written in French, which led Prof. Ralf Abraham to ask the writing of Chap. 8 (*I. Gumowski and a Toulouse research group in the "prehistoric" times of chaotic dynamics*) of the book [5] dealing with the *early days of chaos theory*.

Due to the extent of the topic to be exposed, this article only gives an overview of the work of the *Toulouse group* over a period of 40 years.

Acknowledgments Referees remarks improved the paper writing.

References

1. Colloque International du CNRS n° 229: Transformations Ponctuelles et Applications (Toulouse Sept. 1973). Proceedings: Editions du CNRS Paris (1976)
2. Mira, C.: Exposé d'Introduction. Colloque International du CNRS n° 229 Transformations Ponctuelles et Applications (Toulouse Sept. 1973), pp. 19–27. Proceedings: Editions du CNRS Paris, (1976)
3. Birkhoff, G.D.: Collected Mathematical Papers. Dover Publications, New York (1968)
4. Poincaré, H.: Oeuvres, Tome II. Gauthier-Villars, Paris (1916)
5. Abraham, R., Ueda Y. (eds): The chaos avant-garde. Memories of the early days of chaos theory. World Scientific Series on Nonlinear Science, Series A 39 (2000)
6. Mira, C.: Some historical aspects of nonlinear dynamics. Possible trends for the future. Int. J. Bif. Chaos **7**(9–10), 2145–2174 (1997)
7. Mira, C.: Chua's circuit and the qualitative theory of dynamical systems. Int. J. Bif. Chaos **7**(9–10), 1911–1916 (1997)
8. Boïko, E. S.: The Academician A. A. Andronov' school (in Russian) ed. Nauka, Moscow (1983)
9. Aubin, D., Dahan Dalmedico, A.: Writing the history of dynamical systems and chaos: Longue Durée and revolution, disciplines and cultures. Hist. Math. **29**, 273–339 (2002)
10. Montel, P.: Leçons sur les récurrences et leurs applications. Gauthier-Villars, Paris (1957)
11. Julia, G.: Mémoire sur l'itération des fonctions rationnelles. J. Math. Pures Appl. **4**(1), 7ème série, 47–245 (1918)
12. Fatou, P.: Mémoire sur les équations fonctionnelles. Bull. Soc. Math. France, **47**, 161–271 (1919) (**48**, 33–94; 208–314 (1920))
13. Mira, C., Gardini, L., Barugola, A., Cathala, J.C.: Chaotic Dynamics in two-dimensional noninvertible maps. World Scientific, Series A on Nonlinear Sciences, 20 (1996)
14. Mira, C.: Détermination pratique du domaine de stabilité d'un point d'équilibre d'une récurrence non linéaire du deuxième ordre Ã variables réelles. Comptes Rendus Acad. Sci. Paris, Série A, 261, groupe 2, 5314–5317 (1964)
15. Lattes, S.: Sur les équations fonctionnelles qui définissent une courbe ou une surface invariante par une transformation. Ann. di Mat. **3**(13), 1–137 (1906)
16. Gumowski I., Mira, C.: Dynamique chaotique. Transition ordre-désordre. Ed. Cépadués Toulouse (1980)
17. Mira, C., Roubellat, F.: Cas où le domaine de stabilité d'un ensemble limite attractif d'une récurrence du deuxième ordre n'est pas simplement connexe. Comptes Rendus Acad. Sci. Paris, Série A, 268, 1657–1660, (1969)
18. Mira, C.: Étude de la frontière de stabilité d'un point double stable d'une récurrence non linéaire autonome du deuxième ordre. Proceedings of International Pulse Symposium, Budapest, D43-7/II, 1–28 (1968)
19. Gumowski, I., Mira, C.: Sensitivity problems related to certain bifurcations in nonlinear recurrences relations. Automatica **5**, 303–317 (1969)
20. Roubellat, F.: Contribution Ã l'étude des solutions des ré currences non linéaires et applications aux systèmes à données échantillonnées. Thèse de Doctorat ès-sciences Physiques n° 364, Faculté des Sciences de l'Université de Toulouse, (1969)
21. Bernussou J., Hsu, L., Mira, C.: Quelques exemples de solutions stochastiques bornées dans les récurrences autonomes du second ordre. Collected preprints of Colloque International du CNRS n° 229 Transformations Ponctuelles et Applications, Toulouse Sept. 1973. Proceedings. Editions du CNRS Paris, pp. 195–226 (1976)
22. Mira, C.: Sur quelques propriétés de la frontière du domaine de stabilité d'un point double stable d'une récurrence du deuxième ordre, Ã variables réelles, et sur un cas de bifurcation de cette frontière. Comptes Rendus Acad. Sci. Paris. Série A, 262, 951–954 (1966)
23. Gumowski, I., Mira, C.: Boundaries of stochasticity domains in Hamiltonian systems. Proc. 8th Conf. on High-Energy Accelerators. CERN Gen ève, pp. 374–376 (1971)

24. Gumowski, I., Mira, C.: Sur la distribution des cycles d'une récurrence, ou transformation ponctuelle, conservative du deuxième ordre. Comptes Rendus Acad. Sci. Paris, Série A, 274, 1271–1274 (1972)
25. Gumowski, I., Mira, C.: Sur la structure des lignes invariantes d'une r écurrence, ou transformation ponctuelle, conservative du deuxième ordre. Comptes Rendus Acad. Sci. Paris. Série A, 275, 869–872 (1972)
26. Gumowski I., Mira, C.: Stochastic solutions in a conservative dynamic system. Proc. of 6th Int. Conf. on Nonlinear Oscillations (ICNO) Poznan 1972. PWN-Warzawa, pp. 417–438 (1973)
27. Gumowski I.: Solution structure of a conservative second order recurrence with an unbounded nonlinearity. Colloque International CNRS (n° 229) Transformations Ponctuelles et leurs Applications. Toulouse, 10–14 Sept. 1973. Proceedings: Editions du CNRS, Paris, pp. 79–92 (1976)
28. Gumowski I., Trickett, J.K.: Some properties of a conservative second order recurrence with a bounded nonlinearity. Colloque International CNRS (n° 229) Transformations Ponctuelles et leurs Applications. Toulouse, 10-14 Sept. 1973. Proceedings:Editions du CNRS, Paris, pp. 144–153 (1976)
29. Gumowski I.: Some properties of large amplitude solutions of conservative dynamic systems. Part 1: Quadratic and cubic non-linearities. Part 2 Bounded nonlinearities. Rapport CERN/SI/Int. BR/72-1, Genève (1972)
30. Gumowski I., Mira, C.: Recurrences and discrete dynamic systems - An introduction. 250 pages. Lecture notes in mathematics n° 809, Springer, Berlin (1980)
31. Pulkin C.P.: Oscillating iterated sequences (in Russian). Dokl. Akad. Nauk SSSR,**76**(6), 1129–1132 (1950)
32. Neïmark, Yu.I.: Method of maps in the nonlinear oscillations theory. In Russian. Int. Conf. on Nonlinear Oscillations (ICNO). Kiev, 1961. Proceedings Ukr. Acad. Nauk., 2, pp. 285–298 (1963)
33. Neïmark, Yu.I.: Stability of a fixed point of a map for a critical case. Russ. Radiofisika, **3**(2), 342–343 (1960)
34. Neïmark, Yu.I.: Method of Maps in the Nonlinear Oscillations Theory (In Russian. Ed). Nauka, Moscow (1972)
35. Barsuk, L.O., Belosludstiev, N.M., Neïmark, Yu.I., Salganskaja, N.M.: Stability of a fixed point in a critical case. Bifurcations (in Russian). Radiofisika, **11**(11), 1632–1641 (1968)
36. Cigala, A.R.: Sopra un criterio di instabilita. Annali di matematica Ser. **3**(11), 67–75 (1905)
37. Mira, C.: Etude d'un premier cas d'exception pour une récurrence, ou transformation ponctuelle, du deuxième ordre. Comptes Rendus Acad. Sci. Paris. Série A, 269, 1006–1009 (1969)
38. Mira, C.: Etude d'un second cas d'exception pour une récurrence, ou transformation ponctuelle, du deuxième ordre. Comptes Rendus Acad. Sci. Paris. Série A, 270, 332–335 (1970)
39. Mira, C.: Sur les cas d'exception d'une récurrence, ou transformation ponctuelle, du deuxième ordre. Comptes Rendus Acad. Sc. Paris. Série A, 270, 466–469 (1970)
40. Babary, J.P., Mira, C.: Sur un cas critique pour une récurrence autonome du deuxième ordre. Comptes Rendus Acad. Sci. Paris. Série A, 268, 129–132 (1969)
41. Mira, C.: Traversée d'un cas critique pour une récurrence autonome du deuxième ordre, sous l'effet d'une variation de paramè tre. Comptes Rendus Acad. Sci. Paris. Série A, 268, 621–624 (1969)
42. Gumowski I., Mira, C.: Bifurcation pour une récurrence du deuxième ordre par traversée d'un cas critique avec deux multiplicateurs complexes conjugués. Comptes Rendus Acad. Sci. Paris. Série A, 278, 1591–1594 (1974)
43. Mira, C.: Cas critique d'une récurrence, ou transformation ponctuelle, du quatrième ordre avec multiplicateurs complexes. Comptes Rendus Acad. Sci. Paris. Série A, 272, 1727–1730 (1971)
44. Mira, C.: Chaotic Dynamics. From the One-Dimensional Endomorphism to the Two-Dimensional Diffeomorphism. World Scientific, Singapore (1987)

45. Mira, C.: Sur les courbes invariantes fermées des récurrences non linéaires voisines d'une récurrence linéaire conservative du deuxième ordre. Collected Preprints of Colloque International du CNRS n° 229 Transformations Ponctuelles et Applications, Toulouse Sept. 1973. Proceedings, Editions du CNRS Paris, pp. 177–194 (1976)
46. Holmes Ph., Williams F.: Knotted periodic orbits in suspensions of Smale's horseshoe: torus knots and bifurcation sequences. Arch. Ration. Mech. Anal. **90**(2), 115–194 (1985)
47. Sharkovskij, A.N.: Coexistence of cycles of a continuous map of a line into itself (in Russian). Ukr. Math. J. **16**(1), 61–71 (1964)
48. Li, T.Y., York, A.J.: Period three implies chaos. Am. Math. Mon. 82, 985–992 (1975)
49. Myrberg P. J.: Iteration von Quadratwurzeloperationen III. Ann. Acad. Sci. Fenn. Ser. A, **336**, 1–10 (1963)
50. Gumowski I., Mira, C.: Accumulation de bifurcations dans une récurrence. Comptes Rendus Acad. Sci. Paris, Série A, 281, 45–48 (1975)
51. Mira, C.: Accumulation de bifurcations et structures boîtes emboîtées dans les récurrences et transformations ponctuelles. VII th Int. Conf. on Nonlinear Oscillations (ICNO) Berlin, Sept. 1975. Proceedings in Akademic Verlag, Berlin (1977)
52. Guckenheimer J.: The bifurcation of quadratic functions. N. Y. Acad. Sci. **75**(1), 343–347 (1980)
53. Mira, C.: Sur la double interprétation, déterministe et statistique, de certaines bifurcations complexes. Comptes Rendus Acad. Sci. Paris Série A, 283, 911–914 (1976)
54. Mira, C., Gardini, L.: From the box-within-a-box bifurcation organization to the Julia set. Part I: revisited properties of the sets generated by a quadratic complex map with a real parameter. Int. J. Bif. Chaos **19**(1), 281–327 (2009)
55. Mira, C., Carcassès J.P.: On the crossroad area—saddle area and spring area-crossroad area transitions. Int. J. Bif. Chaos **1**(3), 641–655 (1991)
56. Cathala, J.C., Mira, C., Kawakami H.: Singular points with two multipliers $S1 = -1$, $S2 = 1$ in the bifurcation curves of maps. Int. J. Bif. Chaos **2**(4), 1001–1004 (1992)
57. Mira, C., Djellit, I.: Bifurcation structure in a model of a frequency modulated CO2 laser. Int. J. Bif. Chaos **3**(1), 97–111 (1993)
58. Allam R., Mira, C.: Crossroad area—dissymmetrical spring area–symmetrical spring area, and double crossroad area–double spring area transitions. Int. J. Bif. Chaos **3**(2), 429–435 (1993)
59. Mira, C., Kawakami, H., Allam R.: The dovetail bifurcation structure and its qualitative changes. Int. J. Bif. Chaos **3**(4), 903–919 (1993)
60. Mira, C., Qriouet, M.: On a crossroad area—spring area transition occurring in a Duffing–Rayleigh equation with a periodic excitation. Int. J. Bif. Chaos **3**(4), 1029–1037 (1993)
61. Qriouet M., Mira, C.: Fractional harmonic synchronization in the Duffing–Rayleigh differential equation. Int. J. Bif. Chaos **4**(2), 411–426 (1994)
62. Mira, C., Touzani-Qriouet, M., Kawakami, H.: Bifurcation structures generated by the nonautonomous Duffing equation. Int. J. Bif. Chaos **9**(7), 1363–1379, (1999)
63. Touzani-Qriouet, M., Mira, C., Kawakami, H.: Reducible fractional harmonics generated by the nonautonomous Duffing–Rayleigh equation. Pockets of reducible harmonics and Arnold's tongues. Int. J. Bif. Chaos **10**(6), 1345–1366 (2000)
64. Carcasses, J.P.: Determination of different configurations of fold and flip bifurcation curves of a one or two-dimensional map. Int. J. Bif. Chaos **3**(4), 869–902 (1993)
65. Carcasses, J.P.: Singularities of the parameter plane of a n-Dimensional map. Determination of different configurations of fold and flip bifurcation curves. Int. J. Bif. Chaos **5**(2), 419–447 (1995)
66. Carcasses, J.P., Kawakami, H.: Appearance and disappearance of a dovetail structure in the parameter plane of a n-dimensional map. Int. J. Bif. Chaos **9**(4), 769–783 (1999)
67. Carcasses, J.P., Kawakami, H.: Existence of a cusp point on a fold bifurcation curve and stability of the associated fixed point. Case of a n-dimensional map. Int. J. Bif. Chaos **9**(5), 875–894 (1999)

68. Gallas, J.A.C.: Dissecting shrimps, results for some one-dimensional physical systems. Phys. A **202**, 196–223 (1994)
69. Mira, C.: Sur quelques problèmes de dynamique complexe (Colloque Mod èles Mathématiques en Biologie, 22–24 Nov. 1978). Lect. Notes Bio-Math. **41**, 169–205 (1981)
70. El Hamouly, H., Mira, C.: Lien entre les propriétés d'un endomorphisme et celles d'un difféomorphisme. Comptes Rendus Acad. Sci. Paris, Série 1 293, 1591–1594 (1982)
71. El Hamouly, H., Mira, C.: Singularités dues au feuilletage du plan des bifurcations d'un difféomorphisme bi-dimensionnel. Comptes Rendus Acad. Sci. Paris, Série 1 294, 387–390 (1982)
72. Kawakami H.: Algorithme définissant les suites de rotation de la récurrence de Myrberg. Notion de cycle adjoint. Comptes Rendus Acad. Sci. Paris, Série 1 301, 643–648 (1985)
73. Mira, C., Gracio C.: On the embedding of a (p-1)-dimensional noninvertible map into a p-dimensional invertible map (p=2, 3). Int. J. Bif. Chaos **13**(7), 1787–1810 (2003)
74. Valiron, G.: Théorie des fonctions. Masson, Paris (1948)
75. Mira, C.: Singularités non classiques d'une récurrence et d'une équation différentielle. Comptes Rendus Acad. Sci. Paris, Série 1, 292, 146–151 (1981)
76. Mira, C.: Systèmes asservis non linéaires; aspects continus et discrets. Hermes (Traité des nouvelles technologies; série Automatique), Paris (1990)
77. Giraud, A.: Application des récurrences à l'étude de certains systèmes de commande. Thèse d'Ingénieur-Docteur, Facult é des Sciences de l'Université de Toulouse (1969)

Chapter 6
Lebesgue Measure of Recurrent Scrambled Sets

Marek Lampart

Abstract It was proved by M. Babilonová-Štefánková (Int J Bifurc Chaos 13(7):1695–1700, 2003) that each bitransitive continuous map f of the interval is conjugated to a map g which is distributionally chaotic with a distributionally scrambled set D. The goal of this chapter is to improve this result, by showing that D is formed by points that are recurrent but not almost periodic. Moreover, as a main result it will be proved that any bitransitive map $f \in C(I, I)$ is topologically conjugate to a map $g \in C(I, I)$ which satisfies the following conditions: (i) g is extremally Li–Yorke chaotic with Li–Yorke scrambled set S with full Lebesgue measure and $S \subset R(g)\backslash \mathrm{A}(g)$, (ii) g is ω chaotic and every ω scrambled set Ω has zero Lebesgue measure and $\Omega \subset R(g)\backslash \mathrm{A}(g)$, (iii) g is distributionally chaotic with a distributionally scrambled set D with full Lebesgue measure and $D \subset R(g)\backslash \mathrm{A}(g)$.

6.1 Introduction

Within the last 40 years numerous papers and books have been devoted to the research of discrete dynamical systems. The main aim of the theory of discrete dynamical systems is focused the understanding of what the trajectories of all points from the state space look like. Mostly the periodic structures and asymptotic properties of the orbit were studied. Many authors were fascinated by those motions which are not only periodic but also are not quasiperiodic. These movings were assumed to be *unpredictable* or *sensitive to initial conditions*, later named as *chaotic*.

The first and crucial development in the field of dynamical systems was made by H. Poincaré in 1890 [25] by *recurrence*, that is a point returns to itself arbitrarily close under the actions (iterations), or equivalently the point belongs to its omega limit set. Hence, a dynamical system preserves volume, all trajectories return arbitrarily close to their initial position and they do this an infinite number of times. More precisely, H. Poincaré discovered: *If a flow preserves volume and has only bounded orbits then for each open set there are orbits that intersect the set infinitely often*.

M. Lampart (✉)
Department of Applied Mathematics & IT4Innovations,
VŠB—Technical University of Ostrava, 17. listopadu 15/2172, 70833 Ostrava, Czech Republic
e-mail: marek.lampart@vsb.cz

R. López-Ruiz et al. (eds.), *Nonlinear Maps and their Applications,*
Springer Proceedings in Mathematics & Statistics 112, DOI 10.1007/978-3-319-12328-8_6

As a consequence of the orbit observation situations where the trajectory is dense in the state space appear. Such a property is called *transitivity* and could be defined equivalently for action F (under some assumptions of the state space): for any two nonempty open sets U, V, that are subsets of the state space, there is $n \in \mathbb{N}$ such that $F^n(U) \cap V \neq \emptyset$. The notion of transitivity was introduced by G. D. Birkhoff in 1920 for flows [5].

Consequently, a transitive dynamical system has points which eventually move under iteration from one arbitrarily small open set to any other. Such a dynamical system cannot be decomposed into two disjointed sets with nonempty interiors which do not interact under the transformation. So, the notion of transitivity is still too rough for the observation of a local dynamics and moreover it is not possible to quantify (and compare) the complexity of systems. The *topological entropy* (defined by R. L. Adler, A. G. Konheim, and M. H. McAndrew in 1965 [1]) measures the complexity of the dynamical system. Later on the notion of topological entropy was equivalently formulated for compact metric spaces by R. Bowen in 1971 [9].

The periodic structure for continuous maps on the interval was also investigated and the crucial and well-known result on periodic structure was proved by A. N. Sharkovskiĭ [27] in 1965 where *chaos* is due to infinitely many repulsive cycles of increasing period, and their limit sets of increasing "classes" in the sense of C. P. Pulkin [26] form 1950.

There appeared many notions of chaos, starting with the famous paper by T. Y. Li and J. Yorke [19] in 1975. Later on, several notions of chaos motivated by diverse aspects were introduced (for more see, e.g., [6, 11] and references therein). Many natural questions arose. Which notion of chaos is the best one, or stronger than others (see, e.g., [14] and references therein)? Or, if the map is chaotic in some sense, how big is the scrambled set (in the sense of Lebesgue measure or Baire category, see, e.g., [6])? Motivated by these questions, the goal in this chapter is to study scrambled sets of Li–Yorke chaos, ω chaos, and distributional chaos for continuous maps on the interval. For this purpose, the following conventions are recalled.

Let (X, d) be a compact metric space with metric d and $C(X, X)$ the set of all continuous maps $f : X \to X$. Let $f \in C(X, X)$, $x \in X$ and n be a positive integer. The nth iteration of x under f is denoted by f^n, the set of all fixed points of f by $\mathrm{Fix}(f)$, the set of periodic points of f by $Per(f)$. The sequence $\{f^n(x)\}_{n=0}^{\infty}$ is the trajectory of x, and the set $\omega_f(x)$ of all limit points of the trajectory is the *ω-limit set* of x. An ω-limit set is *maximal* if it is not properly contained in any other ω-limit set. A point $x \in X$ is said to be *recurrent* for f if $x \in \omega_f(x)$, this means that for each neighborhood U of the point x there is positive n such that $f^n(x) \in U$. A point $x \in X$ is called an *almost periodic* point of f provided that for any neighborhood U of $x \in X$, there exists $N \in \mathbb{N}$ such that $\{f^{n+i}(x) : \ i = 0, 1, 2, \ldots, N\} \cap U \neq \emptyset$ for all $n \in \mathbb{N}$. $R(f)$ denotes the set of all recurrent points of $f \in C(X, X)$ and $\mathrm{A}(f)$ the set of all almost periodic points of $f \in C(X, X)$ (for more about recurrence see, e.g., [12] or [29]). A map $f \in C(X, X)$ is *conjugate* to $g \in C(X, X)$ if there is a bijective map $h \in C(X, X)$ such that $h \circ f = g \circ h$. Let $[0, 1]$ be the closed unite interval I.

It is worthy of noticing that results of this chapter, and references, stand for a "macroscopic" point of view, that correspond to what can be either called as *stable*

chaos (*strange attractors* or *invariant bounded sets*), or *chaotic transients* in other disciplines, see, e.g., [21] and [22].

In this chapter notions of Li and Yorke chaos, ω chaos, and distributional chaos are researched. These notions of chaos were introduced by T. Y. Li and J. Yorke [19], S. Li [18], and B. Schweizer and J. Smítal [28] in 1975, 1993, and 1994, respectively, which are defined as follows.

The map $f \in C(X, X)$ is *Li and Yorke chaotic* (briefly, *LYC*) if there is an uncountable set $S \subset X$ such that for any two different points x, y is

$$\limsup_{n\to\infty} d(f^n(x), f^n(y)) > 0$$

and

$$\liminf_{n\to\infty} d(f^n(x), f^n(y)) = 0.$$

This set is called an *LY-scrambled set*. Moreover, $f \in C(X, X)$ is *extremally LYC* if $\limsup_{n\to\infty} d(f^n(x), f^n(y)) = \operatorname{diam}(X)$.

The map $f \in C(X, X)$ is *ω-chaotic* (briefly, ωC) if there is an uncountable set $\Omega \subset X$ such that for any two different points x, y holds:

1. $\omega_f(x) \backslash \omega_f(y)$ is uncountable,
2. $\omega_f(x) \cap \omega_f(y) \neq \emptyset$ and
3. $\omega_f(x) \backslash Per(f) \neq \emptyset$.

The set Ω is called *ω-scrambled*. Remember that the third condition from the definition of ωC is not needed if $X = I$ (see, e.g., [18] and for more about ωC see [17]).

For $f \in C(X, X)$, $x, y \in X$, $t \in \mathbb{R}$ and a positive integer n, let

$$\xi(x, y, n, t) = \sharp\{i;\ 0 \leq i < n \text{ and } |f^i(x) - f^i(y)| < t\}.$$

Put

$$F^*_{xy}(t) = \limsup_{n\to\infty} \frac{1}{n} \sharp\xi(x, y, n, t),$$

and

$$F_{xy}(t) = \liminf_{n\to\infty} \frac{1}{n} \sharp\xi(x, y, n, t).$$

Then both F^*_{xy} and F_{xy} are nondecreasing maps, with $0 \leq F_{xy} \leq F^*_{xy} \leq 1$, $F^*_{xy}(t) = 0$ for $t < 0$, and $F_{xy}(t) = 1$ for $t > 1$. F^*_{xy} and F_{xy} are referred to the *upper* and *lower distribution map* of x and y, respectively. The map f is *distributionally chaotic* (briefly, *dC*) if there is a set $S \subset X$ containing at least two points such that, for any $x \neq y$ in S, $F_{xy} < F^*_{xy}$ (by this it is meant that $F_{xy}(t) < F^*_{xy}(t)$ for all t in an interval), this set is called a *d-scrambled set* for the map f. There were stronger forms of distributional chaos introduced in [4] (for progress paper comparing *dC* and *LYC* see [30] and references therein).

A pair of points (x, y), $x, y \in I$, is called *isotectic* if for every positive integer n the ω-limit set $\omega_{f^n}(x)$ and $\omega_{f^n}(y)$ are subsets of the same maximal ω-limit set of f^n.

The *spectrum* of $f \in C(I,I)$, denoted by $\Sigma(f)$, is the set of minimal elements of the set $\{F_{xy};\ (x,y) \text{ is isotectic}\}$. By [10], $\Sigma(f)$ is always a finite nonempty set, and if f is bitransitive then $\Sigma(f)$ is singleton.

In the following section the result by M. Babilonová-Štefánková from [3] will be improved and the analogous results by M. Babilonová from [2] and M. Lampart from [15] will be summarized. The main result of the paper was announced (without proof) by M. Lampart in [16]. Here complete proofs will be given.

As main result it will be proved that any bitransitive map $f \in C(I,I)$ is topologically conjugate to a map $g \in C(I,I)$ which satisfies the following conditions:

i. g is extremally LYC with LY-scrambled set S with full Lebesgue measure and $S \subset R(g)\backslash \mathrm{A}(g)$,
ii. g is ωC and every ω-scrambled set Ω has zero Lebesgue measure and $\Omega \subset R(g)\backslash \mathrm{A}(g)$,
iii. g is dC with d-scrambled set D with full Lebesgue measure and $D \subset R(g)\backslash \mathrm{A}(g)$.

6.2 Properties of Bitransitive Maps

A map $f \in C(I,I)$ is *(topologically) transitive* if for any open intervals $U, V \subset I$ there is a positive integer n such that $f^n(U) \cap V \neq \emptyset$; f is *bitransitive* if f^2 is transitive.

Proposition 6.1 ([7] or [10]). *Let $f \in C(I,I)$ be a bitransitive map, and $J, K \subset (0,1)$ compact intervals. Then $f^n(J) \supset K$, for any sufficiently large n.*

Let $f \in C(I,I)$, $A, B \subset I$. It is said that *$f-$approximates A* if, for any $\varepsilon > 0$ and $\mu \in (0,1)$, there is a $K > 0$ such that, for any $x \in A$ and any integer $m > K$ there is a $y \in B$ with $\sharp\{i, 0 \leq i \leq m \text{ and } |f^i(x) - f^i(y)| < \varepsilon\} > \mu m$.

Proposition 6.2 ([3]). *Let $f \in C(I,I)$ be bitransitive. Then $Per(f)\backslash\{0,1\}$ f-approximates $Per(f)$.*

Proposition 6.3 ([3]). *Let $f \in C(I,I)$ and $A \subset Per(f)$. Then there is a countable set $B \subset A$ which $f-$approximates A.*

Proposition 6.4 ([28]). *If $f \in C(I,I)$ is bitransitive then $\Sigma(f) = F$, i.e., the spectrum of f is a singleton.*

Proposition 6.5 ([3]). *Let $f \in C(I,I)$ and $\Sigma(f) = F$. If $A \subset I$ $f-$approximates I then F is the pointwise infimum of $\{F_{xy};\ x, y \in A\}$.*

Formulas (6.2), (6.3), and (6.4) from the following Lemma 6.1 correspond with those in Lemma 3.1 from [3]. Conclusion *i.* from Theorem 6.1 equates with the property of Theorem 3.2 from [3]. These formulas are recalled for completeness since they are needed as well for the proof of new parts of Lemma 6.1 and Theorem 6.1 as entire proof of the main statement, Theorem 6.2.

For simplicity the following special notation will be used. If a sequence α is a subsequence of β, it is denoted $\alpha \prec \beta$; sequences may be finite or infinite. So it can be written, e.g., $\{a_n\}_{n=1}^{\infty} \prec \{b_n\}_{n=1}^{\infty}$.

Throughout this section, $\{A_n\}_{n=1}^{\infty}$ is a fixed sequence of blocks of positive integers determined by a division of the sequence $\{n\}_{n=1}^{\infty}$ such that

$$\lim_{n\to\infty} \sum_{i=1}^{n-1} \frac{|A_i|}{|A_n|} = 0, \tag{6.1}$$

where $|A_k|$ denotes the number of elements of A_k. Let us denote by m_k the first element of A_k.

Lemma 6.1 *Let $f \in C(I, I)$ be bitransitive, $\{A_n\}_{n=1}^{\infty}$ a sequence satisfying (6.1), $X \subset (0, 1)$ a nonempty countable set, and $\{p_n\}_{n=1}^{\infty}$ a sequence in X containing any member of X infinitely many times, and let $\{r_n\}_{n=1}^{\infty}$ be a sequence of all rational numbers in I.*

Then, for any compact interval $J \subset (0, 1)$ and any sequence $\alpha = \{a_n\}_{n=1}^{\infty} \prec \{n\}_{n=1}^{\infty}$ there is a nonempty nowhere dense perfect set $P \subset J$, and a sequence $\beta = \{b_n\}_{n=1}^{\infty} \prec \alpha$ with the following properties:

$$\{(b_n, p_n)\}_{n=1}^{\infty} \prec \{(a_n, p_n)\}_{n=1}^{\infty}, \tag{6.2}$$

$$f^k(P) \subset B\left(f^{k-m_{b_n}}(p_n), \frac{1}{n}\right), \ \text{for } k \in A_{b_n}, \tag{6.3}$$

where $B(x, r)$ stands for $[x - r, x + r]$,

$$F_{xy} \leq \inf\{F_{pq};\ p, q \in X\}, \text{ for each } x, y \in P, x \neq y, \tag{6.4}$$

and

$$\omega_f(x) = I, \text{ for any } x \in P. \tag{6.5}$$

Proof Let $\{p_n\}_{n=1}^{\infty}$ be a sequence in X such that the sequence $\{(p_n, q_n)\}_{n=1}^{\infty}$ contains every pair of points of X infinitely many times. Let the set P be in the form $P = \bigcap_{n=1}^{\infty} P_n$ where, for any n, P_n is the union of pairwise disjoint compact intervals $U_s, s \in \{0, 1\}^n$, and $P_{n+1} \subset P_n$. The intervals U_s are defined inductively by n.

Stage 1: Let U_0, U_1 be disjoined closed subintervals of J. Put $P_1 = U_0 \cup U_1$, and let $k(1, 0) < k(1, 1)$ be positive integers such that $(k(1, 0), p_1, q_1)$ is a member of a sequence $\{(a_n, p_n, q_n)\}_{n=1}^{\infty}$.

Stage $n + 1$: Sets $P_1, \ldots, P_n$ and positive integers $k(1, 0) < k(1, 1) < k(2, 0) < k(2, 1) < k(2, 2) < \cdots < k(n, 0) < k(n, 1) < \cdots k(n, n)$ are available from stage n such that, for any $s = s_1, \ldots, s_v \in \{0, 1\}^v$, $1 \leq v \leq n$, $1 \leq j \leq v + 1$,

$$\{(k(j, 0), p_j, q_j)\}_{j=1}^{\infty} \prec \{(a_i, p_i, q_i)\}_{i=1}^{\infty}, \tag{6.6}$$

for any $s = s_1, \ldots, s_v \in \{0, 1\}^v$, $1 \leq v \leq n, 0 \leq j \leq v$,

$$|U_s| \leq \frac{1}{v}, \tag{6.7}$$

$$f^k(U_s) \subset B\left(f^{k-m_{k(v,j)}}(p_v), \frac{1}{v}\right) \text{ for } k \in A_{k(v,j)}, \text{ if } j = 0 \text{ or } s_j = 0, \tag{6.8}$$

$$f^k(U_s) \subset B\left(f^{k-m_{k(v,j)}}(q_v), \frac{1}{v}\right) \text{ for } k \in A_{k(v,j)}, \text{ if } s_j = 1, \tag{6.9}$$

$$f^{k(v,0)}(U_s) \subset B\left(r_v, \frac{1}{v}\right). \tag{6.10}$$

By Proposition 6.1 there is an integer $k(n+1,0) > k(n,n)$ such that, for any

$$s \in \{0,1\}^n, r_{n+1} \in f^{k(n+1,0)}(U_s).$$

Hence, for any $s \in \{0,1\}^n$ there is a compact interval $V_s \subset U_s$ such that

$$f^{k(n+1,0)}(V_s) \subset B\left(r_{n+1}, \frac{1}{n+1}\right). \tag{6.11}$$

Again by Proposition 6.1 there is an integer $k(n+1,1) > k(n+1,0)$ such that

$$\{(k(j,0), p_j, q_j)\}_{j=1}^{\infty} \prec \{(a_i, p_i, q_i)\}_{i=1}^{\infty}, \tag{6.12}$$

and, for any $s \in \{0,1\}^n$, $p_{n+1} \in f^{m_{k(n+1,0)}}(U_s)$. Hence, for any $s \in \{0,1\}^n$, there is a compact interval $V_s^1 \subset V_s$ such that

$$f^k(V_s^1) \subset B\left(f^{k-m_{k(n+1,0)}}(p_{n+1}), \frac{1}{n+1}\right) \text{ for } k \in A_{k(n+1,0)}. \tag{6.13}$$

Also for any $s \in \{0,1\}^n, r_{n+1} \in f^{t(n+1,0)}(U_s)$. Therefore, for any $s \in \{0,1\}^n$, there is a compact interval $V_s \subset U_s$ such that

$$f^{t(n+1,0)}(V_s) \subset \left(r_{n+1}, \frac{1}{n+1}\right). \tag{6.14}$$

Next, there is an integer $k(n+1,2) > k(n+1,1)$ such that, for any $s \in \{0,1\}^n$, $\{p_{n+1}, q_{n+1}\} \subset f^{m_{k(n+1,1)}}(V_s^1)$. Thus, for any $s = s_1, s_2, \ldots, s_n \in \{0,1\}^n$ there is a compact interval $V_s^2 \subset V_s^1$ such that $z \in f^{m_{k(n+1,1)}}(V_s^2)$, where $z = p_{n+1}$ if $s_1 = 0$ and $z = q_{n+1}$ otherwise, and such that $|f^k(V_s^2)| \leq 1/(n+1)$ where $k \in A_{k(n+1,1)}$. By applying this process n times, integers $k(n+1,2) < k(n+1,3) < \cdots < k(n+1,n+1)$ and compact intervals $V_s^2 \supset V_s^3 \supset \cdots \supset V_s^{n+1}$ are obtained such that, for any $s = s_1 s_2 \cdots s_n \in \{0,1\}^n$ and any $2 \leq j \leq n+1$,

$$f^k(V_s^j) \subset B\left(f^{k-m_{k(n+1,j)}}(p_{n+1}), \frac{1}{n+1}\right) \text{ for } k \in A_{k(n+1,j)} \text{ if } s_j = 0, \tag{6.15}$$

and

$$f^k(V_s^j) \subset B\left(f^{k-m_{k(n+1,j)}}(q_{n+1}), \frac{1}{n+1}\right) \text{ for } k \in A_{k(n+1,j)} \text{ if } s_j = 1. \tag{6.16}$$

Finally, let $k(n+1,n+2) > k(n+1,n+1)$ be such that, for any $s \in \{0,1\}^n$, $f^{m_{k(n+1,n+2)}}(V_s^{n+1}) \supset \{p_{n+1}, q_{n+1}\}$. Then there are disjoint compact intervals $U_{s0}, U_{s1} \subset V_s^{n+1}$ such that

$$|U_{s0}|, |U_{s1}| \leq \frac{1}{n+1}, \tag{6.17}$$

$$f^k(U_{s0}) \subset B\left(f^{k-m_{k(n+1,n+2)}}(p_{n+1}), \frac{1}{n+1}\right) \text{ for } k \in A_{k(n+1,n+2)}, \tag{6.18}$$

and

$$f^k(U_{s1}) \subset B\left(f^{k-m_{k(n+1,n+2)}}(q_{n+1}), \frac{1}{n+1}\right) \text{ for } k \in A_{k(n+1,n+2)}. \tag{6.19}$$

Thus sets U_s are defined for any $s \in \{0,1\}^{n+1}$. They satisfy the formulas (6.6), (6.7), (6.8), and (6.9), for $n := n+1$, by (6.12), by (6.17), by (6.13), (6.15), (6.18), or by (6.16), (6.19), respectively. This completes the induction.

For any n put $b(n) = k(n,1)$. Then (6.6) implies (6.2). Let $P = \bigcap_{n=1}^{\infty} \bigcup_{s\in\{0,1\}^n} U_s$. Then P is a nowhere dense perfect set; this follows by (6.7). By (6.8), P satisfies (6.3). It remains to prove (6.4) and (6.5).

Let x and y be distinct points in P. Then for any positive integer K there are $s, s' \in \{0,1\}^K$ such that $x \in U_s$, $y \in U_{s'}$. Take $K > 1/(2|x-y|)$. Thus, by (6.7), $U_s \cup U_{s'} = \emptyset$ and hence $s \neq s'$. Consequently, $s_r \neq s'_r$ for some r. Without loss of generality it can be assumed that $s_r = 0$ and $s'_r = 1$.

Now, to prove (6.4) it suffices to show that, for any positive integer N, $F_{xy} \leq F_{p_N q_N}$. Let $n > \max\{N, K\}$ be such that $(p_n, q_n) = (p_N, q_N)$. By (6.8) and (6.9) it follows that, for $k \in A_{k(n,r)}$, $|f^k(x) - f^{k-m_{k(n,r)}}(p_N)| \leq 1/n$, and $|f^k(y) - f^{k-m_{k(n,r)}}(q_N)| \leq 1/n$. Hence, $\{k \in A_{k(n,r)}; |f^k(x) - f^k(y)| < t\} \subset \{k \in A_{k(n,r)}; |f^{k-m_{k(n,r)}}(p_N) - f^{k-m_{k(n,r)}}(q_N)| < t + 2/n\}$, and consequently, by (6.1), since n can be taken arbitrarily large,

$$F_{xy}(t) \leq F_{p_N q_n}(t+\delta),$$

for any $\delta > 0$ and $t \in \mathbb{R}$. Thus, if t is a point of continuity of $F_{p_N q_N}$, then $F_{xy}(t) < F_{p_N q_N}(t)$ which proves (6.4).

Finally, it remains to prove (6.5). Since $(\{r_n\}_{n=1}^{\infty})' = I$ the condition (6.10) is fulfilled, consequently the property (6.5) is satisfied.

6.3 Main Results

Denote the upper and lower distributional map of x and y for a map g by G_{xy} and G^*_{xy}, respectively.

Theorem 6.1 *Any bitransitive map $f \in C(I,I)$ is topologically conjugate to a map $g \in C(I,I)$ which is dC almost everywhere. More precisely, there is a set H with $\lambda(H) = 1$ such that:*

i. for any distinct x and y in H, $G_{xy} = G$ where G is the unique member of $\Sigma(g)$, and $G^*_{xy} \equiv 1$,
ii. $H \subset R(g) \backslash \mathrm{A}(g)$.

Proof By Proposition 6.4, f has a one-point spectrum, $\Sigma(f) = \{F\}$, and by Propositions 6.2, 6.3, and 6.5 there is a countable set $X \subset Per(f)\backslash\{0,1\}$ such that $F = \inf\{F_{pq};\ p,q \in X\}$ (note that the relation of f-approximability is transitive). Let $\{p_n, q_n\}_{n=1}^{\infty}$ be a sequence in X^2 containing any pair of points o X infinitely many times, and $\{A_n\}_{n=1}^{\infty}$ blocks satisfying (6.1).

Firstly, to prove the first condition of Theorem 6.1, it suffices to define an increasing sequence $S_1 \subset S_2 \subset \cdots \subset (0,1)$ of perfect sets, and a decreasing sequence $\{n\}_{n=1}^{\infty} = \alpha_0 \succ \alpha_1 \succ \alpha_2 \succ \cdots$ of sequences of positive integers with the following properties:

$$f^k(S_m) \subset B\left(f^{k-m_{a_n}}(p_n), \frac{1}{n}\right) \text{ for } k \in A_{a_n}, \tag{6.20}$$

where $\{a_n\}_{n=1}^{\infty}$ is the sequence of α_m,

$$F_{xy} \leq \inf\{F_{uv};\ u,v \in X\} \text{ for } x \neq y \text{ in } S_m, \tag{6.21}$$

$$S = \bigcup_{m=1}^{\infty} S_m \text{ is dense and hence } c\text{-dense in I.} \tag{6.22}$$

Indeed, by [13], any c-dense set F_σ is homeomorphic to a set of full Lebesgue measure. So let ϕ be a homeomorphism of I such that $\lambda(\phi(S)) = 1$. Put $g = \phi \circ f \circ \phi^{-1}$ and $H = \phi(S)$. It is easy to see that $\phi(X) = Y \subset Per(g)\backslash\{0,1\}$ g-approximates I. Hence, by (6.21) and Proposition 6.5, for any m and any $x, y \in H_m = \phi(S_m)$, $G_{xy} = \inf\{G_{pq};\ p,q \in Y\} = G$, where G is the unique distribution function in the spectrum of g. On the other hand, by (6.20),

$$g^k(H_m) \subset B\left(g^{k-m_{a_n}}(\phi(p_n)), \nu_\phi\left(\frac{1}{n}\right)\right) \text{ for } k \in A_{a_n}, \tag{6.23}$$

where ν_ϕ is defined by $\nu_\phi(d) = \sup_{|x-y|\leq d}|\phi(x) - \phi(y)|$. This gives $G^*_{xy} \equiv 1$ for any $x, y \in H_m$ and hence for any $x, y \in H$.

Thus, it remains to define S_m and α_m for any m. Apply Lemma 6.1 to $J = [1/3, 2/3]$, and $\alpha = \alpha_0$ to get P and $\beta = \alpha_1$, and put $S_1 = P$.

Now assume by induction that S_m and α_m satisfy (6.20) and (6.21). Let V be the component interval of $I \setminus S_m$ of the maximal length and let $J \subset \{0, 1\}$ be a compact interval containing the center of V. Apply Lemma 6.1 to J, $\alpha = \alpha_m$ and to the sequence $\{q_n\}_{n=1}^{\infty}$ instead of $\{p_n\}_{n=1}^{\infty}$ to get a set P, and a sequence $\beta = \{b_n\}_{n=1}^{\infty}$, and put $S_{m+1} = S_m \cup P$. By (6.2) and (6.20) it derives

$$f^k(S_m) \subset B\left(f^{k-m_{b_n}}(p_n), \frac{1}{n}\right) \text{ for } k \in A_{b_n}, \tag{6.24}$$

and by (6.2) and (6.3)

$$f^k(P) \subset B\left(f^{k-m_{b_n}}(q_n), \frac{1}{n}\right) \text{ for } k \in A_{b_n}. \tag{6.25}$$

Hence, for $x \in S_m$ and $y \in P$, $F_{xy} \leq \inf\{F_{uv};\, u, v \in X\}$ and $F^*_{xy} \equiv 1$ (see the final part of the proof of the Lemma 6.1). Thus, (6.21) is true for $m := m + 1$. Finally, let $\{d_n\}_{n=1}^{\infty} \prec \beta$ be such that $p_{d_n} = q_{d_n}$ for any n, and let $\alpha_{m+1} = \{d_n\}_{n=1}^{\infty}$. This implies (6.20) for $m := m + 1$. Finally, condition (6.22) follows as a consequence of properties described above.

Finally, the main result, the following theorem, can be proved by using the main results of [2], [15], and Theorem 6.1.

Theorem 6.2 *Any bitransitive map $f \in C(I, I)$ is topologically conjugate to a map $g \in C(I, I)$ which satisfies the following conditions:*

i. g is extremally LYC with LY-scrambled set S with full Lebesgue measure and $S \subset R(g)\setminus \mathrm{A}(g)$,
ii. g is ωC and every ω-scrambled set Ω has zero Lebesgue measure and $\Omega \subset R(g)\setminus \mathrm{A}(g)$,
iii. g is dC with d-scrambled set D with full Lebesgue measure and $D \subset R(g)\setminus \mathrm{A}(g)$.

As a consequence of Theorem 6.1 and a result by A. M. Blokh [8], that any continuous map of the interval with positive entropy has an iteration which is semiconjugate to a bitransitive map, the next corollary follows.

Corollary 6.1 *Let $f \in C(I, I)$ be a map with positive topological entropy. Then, for some $k \geq 1$, f^k is semiconjugate to a map $g \in C(I, I)$ which satisfies the following conditions:*

i. g is extremally LYC with LY-scrambled set S with full Lebesgue measure and $S \subset R(g)\setminus \mathrm{A}(g)$,
ii. g is ωC and every ω-scrambled set Ω has zero Lebesgue measure and $\Omega \subset R(g)\setminus \mathrm{A}(g)$,
iii. g is dC with d-scrambled set D with full Lebesgue measure and $D \subset R(g)\setminus \mathrm{A}(g)$.

Remark 6.1 It is worthy to note that it is possible to construct scrambled sets using residual relations and Mycielski's theorem [23], that is the scrambled set consists of

pairs which are proximal but not asymptotic. Additionally, in a transitive nonminimal system the set of points (or pairs in a weakly mixing system) which are recurrent but not almost periodic is residual (points with dense orbit are residual). Now, applying this to our set adds that additional property to the scrambled set (all points will be recurrent but not almost periodic). Unfortunately, it is not possible to get the properties of ω - limit sets, hence ω chaos directly, which makes our construction essential (for further reading compare with [20] and [24]).

Acknowledgments This work was supported by the European Regional Development Fund in the IT4Innovations Centre of Excellence Project (CZ.1.05/1.1.00/02.0070). The work was also supported by the Grant Agency of the Czech Republic, Grant No. P201/10/0887.

The author is grateful to Piotr Oprocha for helpful discussions on Mycielski's theorem and its relation to the topic, to Referees for their relevant comments that made this chapter more readable for researchers coming from different disciplines.

References

1. Adler, R.L., Konheim, A.G., McAndrew, M.H.: Topological entropy. Trans. Am. Math. Soc. **114**, 309–319 (1965)
2. Babilonová, M.: The bitransitive continuous maps of the interval are conjugate to maps extremely chaotic a.e. Acta Math. Univ. Comen. LXIX. **2**, 229–232 (2000)
3. Babilonová-Štefánková, M.: Extreme chaos and transitivity. Int. J. Bifurc. Chaos **7**, 1695–1700 (2003)
4. Balibrea, F., Smítal, J., Štefánková, M.: The three versions of distributional chaos. Chaos Solitons Fractals **23**, 1581–1583 (2005)
5. Birkhoff, G.D.: Recent advances in dynamics. Science **51**(1307), 51–55 (1920)
6. Blanchard, F., Huang, W., Snoha, L.: Topological size of scrambled sets. Colloq. Math. **110**(2), 293–361 (2008)
7. Block, L., Coppel, W.A.: Dynamics in One Dimension. Lecture Notes in Mathematics, vol. 1513, Springer, Berlin (1992).
8. Blokh, A.M.: The "spectral" decomposition for one-dimensional maps. Dyn. Rep. **4**, 1–59 (1995)
9. Bowen, R.: Entropy for group endomorphisms and homogeneous spaces. Trans. Am. Math. Soc. **153**, 401–414 (1971)
10. Bruckner, A.M., Hu, T.: On scrambled sets for chaotic functions. Trans. Am. Math. Soc. **301**, 289–297 (1987)
11. Forti, G.L.: Various notions of chaos for discrete dynamical systems. Aequ. Math. **70**, 1–13 (2005)
12. Furstenberg, H.: Recurrence in ergodic theory and combinational number theory. Princeton University Press, Princeton (1981)
13. Gorman, W.J.: The homeomorphic transformation of c-sets into d-sets. Proc. Am. Math. Soc. **17**, 825–830 (1966)
14. Guirao, J.L.G., Lampart, M.: Relations between distributional, Li–Yorke and ω chaos. Chaos Solitons Fractals **28**, 788–792 (2006)
15. Lampart, M.: Scrambled sets for transitive maps. Real Anal. Exch. **27**(2), 801–808 (2001/2002)
16. Lampart, M.: Chaos, transitivity and recurrence. Grazer Math. Ber. **350**, 169–174 (2006)
17. Lampart, M., Oprocha, P.: On omega chaos and specification property. Topol. Appl. **156**(18), 2979–2985 (2009)
18. Li, S.: ω-chaos and topological entropy. Trans. Am. Math. Soc. **339**, 243–249 (1993)

19. Li, T.Y., Yorke, J.: Period three implies chaos. Am. Math. Mon. **82**, 985–992 (1975)
20. Li, J., Oprocha, P.: On n-scrambled tuples and distributional chaos in a sequence. J. Differ. Equ. Appl. **19**(6), 927–941 (2013)
21. Mira, C.: Noninvertible maps. Scholarpedia **2**(9), 2328 (2007)
22. Mira, C.: Noninvertible maps/first subpage. Scholarpedia **2**(9), 2328 (2007)
23. Mycielski, J.: Independent sets in topological algebras. Fund. Math. **55**, 137–147 (1964)
24. Oprocha, P.: Coherent lists and chaotic sets. Disc. Cont. Dyn. Syst. **31**(3), 797–825 (2011)
25. Poincaré H. Sur le problème des trois corps et les équations de la dynamique. Mittag-Leffler, Paris 1890
26. Pulkin, C.P.: Oscillating Iterated Sequences. Dokl. Akad. Nauk USSR. **73**(6), 1129–1132 (1950)
27. Sharkovskiĭ, A.N.: Coexistence of cycles of a continuous map of the line into itself. Ukrain. Mat. Zh. **16**, 61–71 (1964); trans. J. Tolosa, Proceedings of Thiry Years after Sharkovskiĭs Theorem: New Perspectives (Murcia, Spain 1994), Int. J. Bifurc. Chaos Appl. Sci. Eng. **5** 1263–1273 (1995)
28. Schweizer, B., Smítal, J.: Measures of chaos and a spectral decomposition of dynamical systems on the interval. Trans. Am. Math. Soc. **344**, 737–754 (1994)
29. Walters, L.: An Introduction to Ergodic Theory. Springer, New York (1982)
30. Wanga, H., Leia, F., Wang, L.: DC3 and Li–Yorke chaos. Applied Mathematics Letters, **31**, 29–39 (2014)

Chapter 7
On the Concept of Integrability for Discrete Dynamical Systems. Investigation of Wandering Points of Some Trace Map

S. S. Bel'mesova and L. S. Efremova

Abstract We extend the concept of integrability suggested by R.I. Grigorchuk for a polynomial discrete dynamical system to an arbitrary discrete dynamical system in the plane. This extension makes it possible to reduce an integrable dynamical system to a dynamical system of the skew products class.

We formulate and prove the criterion for integrability. As the first step of the investigation of the nonwandering set of the trace map $F(x, y) = (xy, (x-2)^2)$, which arises in quasicrystal physics, we describe some geometric constructions. We prove that all points of constructed set are wandering.

7.1 Introduction

Traditionally, the problem of integrability for dynamical systems is of great interest. In [1], Birkhoff has written: "If we try to formulate the exact definition of integrability, we see that many definitions are possible, and every of them is of specific theoretical interest." Therefore, there is a vast bibliography on integrability problem for dynamical systems. We mention here only three papers [2–4], where different concepts of integrability for different classes of discrete dynamical systems are suggested. In this chapter, we extend the concept of integrability given for a polynomial discrete dynamical system in [4] to an arbitrary discrete dynamical system defined in the plane.

The problem of reducibility of integrable discrete dynamical systems to discrete dynamical systems of the skew products class has been formulated by R.I. Grigorchuk in 2002.

Definition 7.1 We say that a map $G : \Pi \to \Pi$, where $\Pi \subseteq \mathbf{R^2}$ is a domain in the plane $\mathbf{R^2}$, is *an integrable map* if there exists a map $\psi : J \to J$, where $J \subseteq \mathbf{R^1}$ is an

S. S. Bel'mesova (✉) · L. S. Efremova
N. I. Lobachevsky State University of Nizhni Novgorod, Gagarin avenue, 23,
Nizhni Novgorod, Russia
e-mail: belmesovass@mail.ru

L. S. Efremova
e-mail: lefunn@gmail.com

R. López-Ruiz et al. (eds.), *Nonlinear Maps and their Applications,*
Springer Proceedings in Mathematics & Statistics 112, DOI 10.1007/978-3-319-12328-8_7

interval in the real line $\mathbf{R^1}$, such that ψ is semiconjugate with G under a continuous surjection $\widetilde{H} : \Pi \to J$, i.e., the equality

$$\widetilde{H} \circ G = \psi \circ \widetilde{H} \tag{7.1}$$

is valid.

Definition 7.1 for integrability of a discrete dynamical system generalizes analogous definition from paper [4], where polynomial, but not arbitrary, maps G and ψ are considered. Note also that in Definition 7.1 maps G and ψ can be discontinuous.

In this chapter, we formulate and prove integrability criterion for a continuous map $G : \Pi \to \Pi$ defined in a convex domain $\Pi \subseteq \mathbf{R^2}$.

Theorem 7.1 *Let $G : \Pi \to \Pi$ be a continuous map of a compact convex domain $\Pi \subseteq \mathbf{R^2}$ such that the section of Π (if it is not empty) by every line $y = const$ is a nondegenerate interval;*
$\psi : J \to J$ be a continuous map of an interval $J \subseteq \mathbf{R^1}$.

Then G is integrable in the sense of Definition 7.1 with a continuous surjection $\widetilde{H} : \Pi \to J$ such that $\widetilde{H}$ is injective with respect to x

iff G is reducible under some homeomorphism to a skew product defined on a compact rectangle in the plane.

Theorem 7.1 gives one of the main technical tools for description of the nonwandering set of the quadratic map

$$F(x, y) = (xy, (x - 2)^2). \tag{7.2}$$

In [5–14], a scheme is used that makes it possible to reduce investigation of discrete Schrödinger equation to investigation of special, so-called trace maps. It is shown in [7] that study of passing and reflecting coefficients of the plane wave with a given impulse in the field of a crystal lattice with knots formed Thue–Morse chain, can be reduced to investigation of the trace map conjugate with map (7.2). Map (7.2) is included into the family

$$F_\mu(x, y) = (xy, (x - \mu)^2), \text{where } \mu \in [0, 2].$$

Different aspects of dynamics of maps from the above one-parameter family for $\mu \in [0, 2)$ are investigated in [15–19].

Call attention also on papers [20–23], where some aspects of dynamics of Lotka–Volterra map are investigated.

The problem of investigation of map (7.2) was tackled by A.N. Sharkovsky who posted some questions about this map in 1993. The questions formulated by A.N. Sharkovsky are given below (see [24]).

1. Does map (7.2) possess unbounded ω-limit sets?
2. Is hypotenuse of the invariant triangle $\Delta = \{(x; y) \in \boldsymbol{R}^2 : x, y \geq 0, x + y \leq 4\}$ an attractor of F (in Milnor sense)?
3. Is the triangle Δ an attractor of F (in Milnor sense)?

4. Is restriction of map (7.2) on Δ topologically transitive?
5. Are periodic points of F everywhere dense in Δ?

In studying properties of a dynamical system, its set of nonwandering points (the nonwandering set) plays an important role (see e.g., [25]).

Definition 7.2 Let $\Phi : X \to X$ be a continuous map of a metric phase space. A point $x \in X$ is a *nonwandering point* of the map Φ if for every neighborhood $U(x)$ of x there exists a natural number m such that $U(x) \bigcap \Phi^m(U(x)) \neq \emptyset$. The set $\Omega(\Phi)$ of all nonwandering points of Φ is the *nonwandering set*.

Let us note that the nonwandering set is not empty for a dynamical system with a compact phase space. If the phase space of a dynamical system is not compact then any of its point can be wandering. It's not the case for map (7.2).

We formulate here the complete result concerning the nonwandering set $\Omega(F)$ of map (7.2). For this goal, we distinguish the following sets on the plane xOy:

1. The closed triangle $\Delta = \{(x; y) \in \boldsymbol{R}^2 : x, y \geq 0, x + y \leq 4\}$
2. The unbounded set $G_\Delta = \{(x; y) \in \boldsymbol{R}^2 : x, y \geq 0, x + y \geq 4\}$
3. The unbounded set $G_\Delta^\circ = \{(x; y) \in \boldsymbol{R}^2 : x, y \geq 0, x + y > 4\}$
4. The unbounded set $D_{+\infty} = \{(x; y) \in \boldsymbol{R}^2 : x \geq 3, y \geq 1\}$
5. The unbounded set $\widetilde{G} = G_\Delta^\circ \cap (\bigcup_{i=0}^{+\infty} F^{-i}(D_{+\infty})$, where $F^{-i}(\cdot)$ is ith complete preimage of a set
6. The unbounded set $G' = G_\Delta \backslash \widetilde{G}$

Theorem 7.2 *The nonwandering set $\Omega(F)$ of map (7.2) is the union of the triangle Δ and perfect nowhere dense in G_Δ set G' satisfying*

(2.1) *the set G' is the union of unbounded curves such that $G' \cap G_\Delta^\circ$ is F-completely invariant local lamination*[1] *of codimension 1 in the set G_Δ°, in addition, the set of algebraic curves is everywhere dense in G';*

(2.2) *the map $F_{|\Delta}$ is topologically mixing, and its periodic points are everywhere dense in Δ.*

Let us note that claim (2.2) of Theorem 7.2 gives a positive answer on 4th and 5th problems by A.N. Sharkovsky. Point out, for the comparison, that in [22], transitivity (but not topological mixing) in analogous invariant triangle for Lotka–Volterra map is proved.

In contrast to the announced result (Theorem 7.2), papers [28] and [29] contain examples of the polynomial maps that have bounded nonwandering sets.

We divide the proof of Theorem 7.2 in some steps. First, geometric step of the proof of Theorem 7.2 is fulfilled in this chapter. Reducing of map (7.2) to the skew product on the unbounded rectangle $[0, 4] \times [0, +\infty)$, analytic description of the nonwandering set of map (7.2) based on the concept of weakly nonwandering points with respect to the family of fibers maps (see [32]) is left to a future paper.

[1] One can find the definition of a lamination in the book [26] and the definition of a local lamination in the book [27]

In Sect.7.2 of this chapter, we prove the criterion of integrability for a discrete dynamical system (Theorem 7.1).

In Sects. 7.3 and 7.4, we prove the following geometric result.

Theorem 7.3 *The set $\widetilde{G}$ is open everywhere dense in G_Δ and consists of F-wandering points. The perfect nowhere dense in G_Δ set G' is the union of unbounded curves such that $G' \cap G_\Delta^\circ$ is F-completely invariant local lamination of codimension 1 in the set G_Δ°, in addition, the set of algebraic curves is everywhere dense in G'.*

Our concluding remarks (see Sect. 7.5) are devoted to saddle periodic points of map (7.2) considered in this chapter.

7.2 Proof of the Integrability Criterion

We begin this part of the work from formulation of the existence theorem for a nonlocal C^1-smooth implicit function [30].

Theorem 7.4 *Let a function $\Phi : (a,b) \times (c',d') \to \mathbf{R^1}$ defined on a rectangle*

$$(a,b) \times (c',d') \subset \mathbf{R^2}$$

be such that

1. *$\Phi \in C^1((a,b) \times (c',d'); \mathbf{R^1})$ (as usually, $C^1((a,b) \times (c',d'); \mathbf{R^1})$ means the space of C^1-smooth maps of a rectangle $(a,b) \times (c',d')$ into the real line $\mathbf{R^1}$);*
2. *in every point $(x;y) \in (a,b) \times (c',d')$ satisfying $\Phi(x;y) = 0$ the inequality*

$$\frac{\partial}{\partial x}\Phi(x;y) \neq 0 \text{ (the inequality } \frac{\partial}{\partial y}\Phi(x;y) \neq 0)$$

is valid; in addition,

$$pr_1(\{(x;y) : \Phi(x;y) = 0\}) = (a,b),$$

$$pr_2(\{(x;y) : \Phi(x;y) = 0\}) = (c,d), (c,d) \subseteq (c',d'),$$

where pr_1, pr_2 are natural projections of the plane $\mathbf{R^2}$ on the x-coordinate and the y-coordinate axes, respectively.

Then there exists a function $x = x(y)$, $x(y) \in C^1((c,d),(a,b))$ (a function $y = y(x)$, $y(x) \in C^1((a,b),(c,d))$) satisfying $\Phi(x(y);y) \equiv 0$ for every $y \in (c,d)$ (respectively $\Phi(x;y(x)) \equiv 0$ for every $x \in (a,b)$).

One can find example of the application of Theorem 7.4 for bounded intervals (a,b) and (c,d) in [31]. In paper [17], Theorem 7.4 is used for the case of unbounded interval (a,b) or (c,d). In this chapter, we use above Theorem 7.4 in the case when one of the intervals, (a,b), or $(c,\ d)$ is unbounded too.

We get over the proof of Theorem 7.1.

Proof 1. Let a continuous map $G : \Pi \to \Pi$ be integrable, and a domain $\Pi \subset \mathbf{R^2}$ satisfy conditions of Theorem 7.1. Then by Definition 7.1, Theorem 7.4 and properties of $\widetilde{H}$ (see formulation of Theorem 7.1) the following claims are valid:

(i) The set $\Pi \bigcap (J \times \{y\})$ is a nondegenerate interval for every point $y \in pr_2(\Pi)$.
(ii) The complete preimage $\widetilde{H}^{-1}(x)$ of every point $x \in J$ has the unique common point with every horizontal fiber $\Pi \bigcap (J \times \{y\})$.
(iii) The equality $\widetilde{H}^{-1}(x') \bigcap \widetilde{H}^{-1}(x'') = \emptyset$ holds for every different points $x', x'' \in J$.
(iv) The equality $\Pi = \bigcup\limits_{x' \in J} \widetilde{H}^{-1}(x')$ is valid.

Hence, the set $\widetilde{H}^{-1}(x')$ for every $x' \in J$ is the graph (denoted by $\gamma_{x'}$) of some continuous function $x = \gamma_{x'}(y)$, and $\widetilde{H}^{-1}(x')$ is the connected set. Thus, by properties $(ii) - (iv)$ the one-parameter family $\{\gamma_{x'}\}_{x' \in J}$ of graphs of the above functions defines the foliation in domain Π. By equality (7.1), the foliation $\{\gamma_{x'}\}_{x' \in J}$ is invariant: the inclusion $G(\gamma_{x'}) \subseteq \gamma_{\psi(x')}$ holds for every $x' \in J$.

2. The map $\theta : \Pi_{xOy} \to \Pi'_{uO'v}$, where θ is defined by formulas

$$\begin{cases} u = \widetilde{H}(x, y) \\ v = y, \end{cases} \tag{7.3}$$

is the continuous bijective map of the domain Π_{xOy} on the domain $\Pi'_{uO'v}$. Let us prove that $\theta : \Pi_{xOy} \to \Pi'_{uO'v}$ is homeomorphism.

Indeed, since Π_{xOy} is the compact set, and θ is the continuous map then $\Pi'_{uO'v}$ is the compact set; in addition, θ is surjection. All these properties imply the following property of the map θ: a set $A \subset \Pi'_{uO'v}$ is closed iff the set $\theta^{-1}(A)$ is closed. Hence, θ is mutually continuous map (see [33]). If θ is mutually continuous and bijective map then θ is a homeomorphism [33].

By formula (7.3), the set $\theta(\gamma_{x'})$ is an interval of the straight line $u = x'$ for every $x' \in J$. By this property and above property (i), domain $\Pi'_{uO'v}$ is the rectangle in the plane.

Denoted by G', the map corresponding to G in the plane of variables u and v. Then $G' : \Pi'_{uO'v} \to \Pi'_{uO'v}$; G' is topologically conjugate with G under θ, i.e.,

$$G' = \theta \circ G \circ \theta^{-1}.$$

The first and second coordinate functions of the map G' are denoted by g'_1 and g'_2, respectively. Let us show that g'_1 does not depend on the variable v.

In fact, G' maps every vertical interval $\Pi'_{uO'v} \bigcap \{(x'; v) : v \in \mathbf{R^1}\}$ into the vertical interval $\Pi'_{uO'v} \bigcap \{(\psi(x'); v) : v \in \mathbf{R^1}\}$. Let us show that the partial derivative $\frac{\partial}{\partial v} g'_1(u, v)$ exists in every point $(u; v) \in \Pi'_{uO'v}$ and equals 0.

Let $(x'; v')$ and $(x'; v)$ be the arbitrary points of the vertical interval $\Pi'_{uO'v} \bigcap \{(x'; v) : v \in \mathbf{R^1}\}$. Then, we have

$$\frac{\partial}{\partial v} g'_1(u, v) = \lim_{v \to v'} \frac{g'_1(x'; v) - g'_1(x', v')}{v - v'} = \lim_{v \to v'} \frac{\psi(x') - \psi(x')}{v - v'} = 0. \tag{7.4}$$

Since Π'_{uO_v} is the convex connected set then by equality (7.4), coordinate function g'_1 of the map G' does not depend[2] on the variable v. Thus, G' is the skew product in the plane.[3]

3. Since every continuous skew product on a rectangle $\Pi = J_x \times J_y$ ($J_x, J_y \subset \mathbf{R^1}$ are intervals) is semiconjugate under the first natural projection $pr_1 : \Pi \to J_x$ with its quotient map (such that Definition 7.1 is fulfilled) then every skew product is an integrable map. Theorem 7.1 is proved. □

7.3 Geometric Constructions in G_Δ

Geometric constructions of this part of the work can be considered as the special analog of Denjoy construction (see [34–36]).

1. In this part of § 3, we give the preliminary information that will be used.

The first and second coordinate functions of nth iteration of F are denoted by $f_n(x, y)$ and $g_n(x, y)$, respectively. Then $F^n(x, y) = (f_n(x, y), g_n(x, y))$ for every $n \geq 1$.

By formula (7.2), the following recurrent relations hold:

$$f_n(x, y) = f_{n-1}(x, y)g_{n-1}(x, y); g_n(x, y) = (f_{n-1}(x, y) - 2)^2. \tag{7.5}$$

Using formula (7.5), we obtain

$$f_n(x, y) = f_1(x, y) \prod_{i=0}^{n-2} (f_i(x, y) - 2)^2, n \geq 2; \tag{7.6}$$

$$g_n(x, y) = (f_1(x, y) \prod_{i=0}^{n-3} (f_i(x, y) - 2)^2 - 2)^2, n \geq 3. \tag{7.7}$$

$$\frac{\partial f_n(x, y)}{\partial x} = g_{n-1}(x, y)\frac{\partial f_{n-1}(x, y)}{\partial x} + f_{n-1}(x, y)\frac{\partial g_{n-1}(x, y)}{\partial x}; \tag{7.8}$$

$$\frac{\partial g_n(x, y)}{\partial x} = 2(f_{n-1}(x, y) - 2)\frac{\partial f_{n-1}(x, y)}{\partial x}. \tag{7.9}$$

The presentation of the partial derivative $\frac{\partial f_n(x,y)}{\partial y}$ $\left(\frac{\partial g_n(x,y)}{\partial y}\right)$ can be obtained from the right side of equality (7.8) (of equality (7.9)) with using of corresponding partial derivatives with respect to y.

---

[2] Assumption on the convexity of domain Π'_{uO_v} cannot be omitted.

[3] Direct products are considered as elements of the set of skew products dynamical systems.

Let $J(F^n(x,y)) = \frac{\partial F^n(x,y)}{\partial(x;y)}$ and $det\, J(F^n(x;y))$ be Jacobian matrix and Jacobian of the map F^n, $n \geq 1$, respectively.

Let us formulate the main properties of the map F (see e.g., [15, 17]) will be used for our geometric constructions.

Proposition 7.1 *Map (7.2) possesses the properties:*

1. *The equality $det\, J(F^n(x;y)) = 0$ holds iff coordinates of a point (x,y) satisfy one of the equations $f_i(x,y) = 2$ for some $0 \leq i \leq n-1$, $x = 0$ or $y = 0$ for $n \geq 2$; in particular, the set of critical points (critical set) of the map F consists of two straight lines $x = 0$ and $x = 2$.*
2. *The map F has three fixed points: the flat singular saddle point $A_1(0;4)$ and two sources $A_2(3;1)$ and $A_3(1;1)$.*
3. *The following inclusions hold for every open quadrant K_i $(i = 1,2,3,4)$ of the plane xOy: $F(\overline{K}_3) \subset K_1$, $F(\overline{K}_4) \subset K_2$ and $F(\overline{K}_2) \subset K_2$, $F(\overline{K}_1) \subset K_1$, where $\overline{(\cdot)}$ means the closure of a set.*
4. *For every point $(x;y)$ of the unbounded invariant set $D_{+\infty}$ (see §1) the equalities hold: $\lim\limits_{n\to+\infty} f_n(x,y) = +\infty$, $\lim\limits_{n\to+\infty} g_n(x,y) = +\infty$; in addition, restriction $F|_{D_{+\infty}}$ is diffeomorphism of $D_{+\infty}$ on $F(D_{+\infty}) \subset D_{+\infty}$.*
5. *The set $D_{+\infty}$ contains the graph of the C^1-smooth strictly increasing function $y = \Gamma^{(1)}(x)$ defined on the interval $[3,+\infty)$ and such that $\Gamma^{(1)}([3,\infty)) = [1,+\infty)$; moreover, the graph $\Gamma^{(1)}$ of this function is a F-invariant curve [19].*
6. *Triangle Δ (see §1) is completely invariant (i.e., the equality $F(\Delta) = \Delta$ is valid) such that its legs $k_x = \{(x;0) : 0 \leq x \leq 4\}$ and $k_y = \{(0;y) : 0 \leq y \leq 4\}$ satisfy the equalities $F(k_x) = k_y$, $F(k_y) = (0;4)$, in addition, the restriction $F_{|h}$ on its hypotenuse h is defined by the equality $F_{|h}(x,y) = (x(4-x)); (2-y)^2)$ such that $F(h) = h$.*
7. *Hypotenuse h contains:*
   everywhere dense set of periodic points (the set of their (least) periods coincides with the set $\mathbf{N}$ of natural numbers), in particular, the unique F-periodic orbit with the (least) period 2 belongs to h; for every natural number $l \geq 1$ the subset of periodic points set with (least) periods $ln, n \geq 1$, is everywhere dense in the periodic points set (and, consequently, in h);
   the residual set of points with everywhere dense trajectories,
   everywhere dense set of $F_{|h}$-homoclinic points[4]; in addition, between every two homoclinic points to the fixed point $A_1(0;4)$ there exists, at least, one homoclinic point to the fixed point $A_2(3;1)$, and, vice versa, between every two homoclinic points to the fixed point $A_2(3;1)$ there exists at least, one homoclinic point to the fixed point $A_1(0;4)$;
   moreover, $F|_h$ possesses the property of complete extension: for every interval $J \subset h$ there is a natural number n_0 such that $F|_h^{n_0}(I) = h$.

[4] One can find definition of homoclinic points for a map of an interval in [37].

2. Our next step is to prove that the set $\widetilde{G} = G^{\circ}_{\Delta} \cap (\bigcup\limits_{i=0}^{+\infty} F^{-i}(D_{+\infty})$ (see § 1) is open and is the union of interior points of pairwise disjoint maximal wedge-shaped domains[5] with vertexes in the fixed point $A_2(3;1)$ and in homoclinic points of the restriction $F|_h$ to the fixed point $A_2(3;1)$ such that the interior of every maximal wedge-shaped domain is a connected component of the set $\widetilde{G}$.

Since $F|_{D_\infty}$ is the diffeomorphism (see claim 4 of Proposition 7.1) then we use the boundary ∂D_∞ of the set D_∞ in our geometric constructions, where

$$\partial D_\infty = \{(x;y) : x = 3, y \geq 1\} \bigcup \{(x;y) : x \geq 3, y = 1\}.$$

Let us note that

$$F(\{(x;y) : x = 3, y \geq 1\}) = \{(x;y) : y = 1, x \geq 3\}.$$

Therefore, the following equality is valid for every $n \geq 1$:

$$\partial F^{-n}(D_\infty) = F^{-n}(\{(x;y) : x = 3, y \geq 1\}) \cup F^{-(n-1)}(\{(x;y) : x = 3, y \geq 1\}).$$

Thus, preimages of the ray $\{(x;y) : x = 3, y \geq 1\}$ play the most important role in our geometric constructions.

We begin from the construction of the first connected component of the set $\widetilde{G}$ with the vertex in the fixed point $A_2(3;1)$. For this goal, we consider the existence problem for implicit functions defined by the equations

$$f_n(x,y) = 3, \tag{7.10}$$

with the initial conditions

$$f_n(3,1) = 3, n \geq 1. \tag{7.11}$$

We use mathematical induction principle. In fact, C^1-smooth strictly decreasing brunches of graphs of functions $y = 3/x$ for $x \geq 3$ and $y = 3/x(x-2)^2$ for $2 < x \leq 3$ give solutions of problem (7.10) with initial condition (7.11) for $n = 1$ and $n = 2$ respectively; moreover, the inequalities

$$\frac{\partial f_1(x,y)}{\partial x} > 0, \frac{\partial f_1(x,y)}{\partial y} > 0$$

are valid for every point $(x;y)$, $x \geq 3$, which lies on the graph of the function $y = 3/x$, and the inequalities

$$\frac{\partial f_2(x,y)}{\partial x} > 0, \frac{\partial f_2(x,y)}{\partial y} > 0$$

are fulfilled for every point $(x;y)$, $2 \leq x \leq 3$, which lies on the graph of the function $y = 3/x(x-2)^2$.

[5] Explanation of the term "maximal wedge-shaped domain" will be given below (after Corollaries 20 and 21).

Suppose that after $n-1$ ($n \geq 4$) steps, we constructed C^1-smooth strictly decreasing nonlocal brunches of implicit functions $y = \eta_{i,3}^{A_2}(x)$, $1 \leq i \leq n-1$, such that each one of them is the solution of the problem $f_i(x,y) = 3$ with the initial condition $f_i(3,1) = 3$ ($1 \leq i \leq n-1$).

If $i = 2m$, then $y = \eta_{i,3}^{A_2}(x)$ is defined on the interval $(2,3]$, and the set of its values equals $[1,+\infty)$; in addition, the inequalities

$$\frac{\partial f_i(x,y)}{\partial x} > 0, \frac{\partial f_i(x,y)}{\partial y} > 0$$

are fulfilled for every point $(x;y)$, which belongs to the graph $\eta_{i,3}^{A_2}$ of the function $y = \eta_{i,3}^{A_2}(x)$.

If $i = 2m-1$, then the function $y = \eta_{i,3}^{A_2}(x)$ is defined on the interval $[3,+\infty)$ and takes values on the interval $(0,1]$; in addition, the inequalities

$$\frac{\partial f_i(x,y)}{\partial x} > 0, \frac{\partial f_i(x,y)}{\partial y} > 0$$

are fulfilled in every point $(x;y)$, which belongs to the graph $\eta_{i,3}^{A_2}$ of the function $y = \eta_{i,3}^{A_2}(x)$. Hence, the inclusion

$$\eta_{i,3}^{A_2} \subset \{(x;y) \in G_\Delta : x > 2\} \tag{7.12}$$

holds for every $1 \leq i \leq n-1$.

Let us describe nth step. If the fixed point $A_2(3;1)$ is a source then the following inequalities hold

$$\frac{\partial f_n(x,y)}{\partial x}|_{A_2(3;1)} > 0, \frac{\partial f_n(x,y)}{\partial y}|_{A_2(3;1)} > 0.$$

Thus, there are $\varepsilon > 0$ (let ε be less than 1) and the strictly decreasing implicit function $y = y_{loc,n}^{A_2}(x)$ ($n \geq 1$), which is the solution of problem (7.10)–(7.11) on the interval $[3, 3+\varepsilon]$ for odd numbers and on the interval $[3-\varepsilon, 3]$ for even numbers. The local function $y = y_{loc,n}^{A_2}(x)$ admits extension on the interval $[3,+\infty)$ for odd numbers n and on the interval $(2,3]$ for even numbers n.

In fact, let us use formulas (7.8) and (7.9) and inclusion (7.12). Then we obtain that the inequalities

$$\frac{\partial f_n(x,y)}{\partial x} > 0, \frac{\partial f_n(x,y)}{\partial y} > 0$$

hold for every point $(x;y)$, $x > 2$, satisfying (7.10). Then by Theorem 7.4, there exist C^1-smooth strictly decreasing nonlocal implicit functions $y = \eta_{n,3}^{A_2}(x)$ satisfying equation (7.10) with initial condition (7.11); moreover, every function $y = \eta_{n,3}^{A_2}(x)$ is defined on the interval $(2,3]$ for even n and on the interval $[3,+\infty)$ for odd n.

Thus, the following result is obtained.

Theorem 7.5 *Let F be quadratic map (7.2). Then*

1. *There are C^1-smooth strictly decreasing functions $y = \eta^{A_2}_{n,3}(x)$ $(n \geq 1)$ defined on the interval $(2, 3]$ for even n (on the interval $[3, +\infty)$ for odd n) with the values on the interval $[1, +\infty)$ for even n (on the interval $(0, 1]$ for odd n); moreover, these functions satisfy the initial condition $\eta^{A_2}_{n,3}(3) = 1$.*
2. *The graph of every function $y = \eta^{A_2}_{2m}(x)$ $(m \geq 1)$ has the vertical asymptote, which coincides with the critical line $x = 2$, in addition, $\eta^{A_2}_{2m+2,3} \prec \eta^{A_2}_{2m,3}$ on the interval $(2, 3)$.*
3. *The graph of every function $y = \eta^{A_2}_{2m-1}(x)$ $(m \geq 1)$ has the horizontal asymptote, which coincides with the straight line $y = 0$, in addition, $\eta^{A_2}_{2n+1,3} \prec \eta^{A_2}_{2n-1,3}$ on the interval $(3, +\infty)$*[6].

Claims 2 and 3 of Theorem 7.5 follows immediately from formulas (7.6)–(7.7). Let $[a, 3] \subset (2, 3]$ and $[3, b] \subset [3, +\infty)$ be arbitrary closed intervals.

Theorem 7.6 *Sequences of restrictions*

$$\{\eta^{A_2}_{2m,3}|_{[a,3]}(x)\}_{m\geq 1} \quad \text{and} \quad \{\eta^{A_2}_{2m-1,3}|_{[3,b]}(x)\}_{m\geq 1}$$

converge on the closed intervals $[a, 3]$ and $[3, b]$ in C^1-norm to C^1-smooth strictly decreasing functions $y = \eta^{A_2}_l|_{[a,3]}(x)$ and $y = \eta^{A_2}_r|_{[3,b]}(x)$ respectively.

C^1-smooth functions $y = \eta^{A_2}_l(x)$ with the graph $\eta^{A_2}_l$ and $y = \eta^{A_2}_r(x)$ with the graph $\eta^{A_2}_r$ are defined on the intervals $(2, 3]$ and $[3, +\infty)$ respectively and the following equalities hold:

$$F(\eta^{A_2}_l) = \eta^{A_2}_r, F(\eta^{A_2}_r) = \eta^{A_2}_l$$

such that

$$F^2(\eta^{A_2}_l) = \eta^{A_2}_l, F^2(\eta^{A_2}_r) = \eta^{A_2}_r.$$

Proof For determination, we give the proof for the sequence $\{\eta^{A_2}_{2m-1,3}|_{[3,b]}(x)\}_{m\geq 1}$.

1. Using claim 3 of Theorem 7.5 and Weierstrass Theorem (on convergence of a monotone bounded number sequence) we obtain that pointwise convergence to the function $y = \eta^{A_2}_r(x)$ is realized for the functional sequence $\{\eta^{A_2}_{2m-1,3}(x)\}_{m\geq 1}$ on the unbounded interval $[3, +\infty)$. It implies the equality $F^2(\eta^{A_2}_r) = \eta^{A_2}_r$.

2. Let us prove that C^1-smooth functions $y = \eta^{A_2}_{2m-1,3}(x)$ are convex on the interval $[3, +\infty)$ for every $m \geq 1$. We use mathematical induction principle.
For $n = 1$, the function $\eta^{A_2}_{1,3}(x) = 3/x$ is strictly convex on the interval $[3, +\infty)$. Suppose, that functions $y = \eta^{A_2}_{2n-1,3}(x)$ are strictly convex on the interval $[3, +\infty)$

[6] We say that $\eta^{A_2}_{2m+2,3}$ *precedes* $\eta^{A_2}_{2m,3}$ $(\eta^{A_2}_{2m+2,3} \prec \eta^{A_2}_{2m,3})$ *on the interval* $(2, 3]$ $(\eta^{A_2}_{2m+1,3}$ *precedes* $\eta^{A_2}_{2m-1,3}$ $(\eta^{A_2}_{2m+1,3} \prec \eta^{A_2}_{2m-1,3})$ *on the interval* $[3, +\infty)$) if the inequality $x_{2m+2,3} < x_{2m,3}$ is correct for every $y \in (1, +\infty)$ (the inequality $x_{2m+1,3} < x_{2m-1,3}$ is correct for every $y \in (0, 1)$), where values $x_{2m+2,3}$ and $x_{2m,3}$ (values $x_{2m+1,3}$ and $x_{2m-1,3}$) are defined uniquely by the equalities $y = \eta^{A_2}_{2m+2,3}(x_{2m+2,3}) = \eta^{A_2}_{2m,3}(x_{2m,3})$ (by the equalities $y = \eta^{A_2}_{2m+1,3}(x_{2m+1,3}) = \eta^{A_2}_{2m-1,3}(x_{2m-1,3})$).

for all $1 \leq n \leq m-1$. Prove that the function $y = \eta^{A_2}_{2m-1,3}(x)$ is strictly convex on the interval $[3, +\infty)$. For this goal, we use the geometric criterion of convexity based on the arrangement of the graph of a differentiable function with respect to tangents in points of the graph. A differentiable function is strictly convex on an interval iff every point of the graph of this function, with the exception of the point of contact, lies above the tangent in this point [38].

Let $M = (\overline{x}; \overline{y})$ be an arbitrary point of the graph $\eta^{A_2}_{2m-3,3}$, and $\tau_{(\overline{x};\overline{y})}(\eta^{A_2}_{2m-3,3})$ be the tangent to $\eta^{A_2}_{2m-3,3}$ in the point M. By inductive hypothesis, $\tau_{(\overline{x};\overline{y})}(\eta^{A_2}_{2m-3,3})$ lies below the graph $\eta^{A_2}_{2m-3,3}$ everywhere, with the exception of the point M. Then the derivative $(\eta^{A_2}_{2m-3,3})'_x(x)$ strictly increases from $(\eta^{A_2}_{2m-3,3})'(3)$ up to 0. Therefore, the tangent $\tau_{(\overline{x};\overline{y})}(\eta^{A_2}_{2m-3,3})$ intersects the graph $\eta^{A_2}_{2m-1,3}$ in some point $M' = (\overline{x}'; \overline{y}')$ such that the closed interval $[M, M']$ of the tangent $\tau_{(\overline{x};\overline{y})}(\eta^{A_2}_{2m-3,3})$ belongs to the unbounded domain between graphs $\eta^{A_2}_{2m-1,3}$ and $\eta^{A_2}_{2m-3,3}$ (see Theorem 7.5).

Differential DF^{-2} maps the tangent $\tau_{(\overline{x};\overline{y})}(\eta^{A_2}_{2m-3,3})$ on the tangent $\tau_{F^{-2}(\overline{x};\overline{y})}(\eta^{A_2}_{2m-1,3})$ for the graph $\eta^{A_2}_{2m-1,3}$ in the point $F^{-2}(\overline{x}; \overline{y})$.

The map F^{-2} transforms the closed interval $[M, M']$ of the tangent $\tau_{(\overline{x};\overline{y})}(\eta^{A_2}_{2m-3,3})$ such that $F^{-2}([M, M'])$ is a closed arc of some curve, which lies in the unbounded domain between graphs $\eta^{A_2}_{2m-1,3}$ and $\eta^{A_2}_{2m+1,3}$. By definition of differential, this arc is tangent $\tau_{F^{-2}(\overline{x};\overline{y})}(\eta^{A_2}_{2m-1,3})$ in the point $F^{-2}(\overline{x}; \overline{y})$. Therefore, there exists a neighborhood $U(F^{-2}(\overline{x}; \overline{y}))$ of the point $F^{-2}(\overline{x}; \overline{y})$ such that the interval

$$\tau_{F^{-2}(\overline{x};\overline{y})}(\eta^{A_2}_{2m-1,3}) \bigcap U(F^{-2}(\overline{x}; \overline{y}))$$

lies below the graph $\eta^{A_2}_{2m-1,3} \bigcap U(F^{-2}(\overline{x}; \overline{y}))$ everywhere, with the exception of the contact point $F^{-2}(\overline{x}; \overline{y})$.

Since the tangent $\tau_{(\overline{x};\overline{y})}(\eta^{A_2}_{2m-3,3})$ for the graph $\eta^{A_2}_{2m-3,3}$ in the point $M(\overline{x}; \overline{y})$ has the unique common point with $\eta^{A_2}_{2m-3,3}$ then the tangent $\tau_{F^{-2}(\overline{x};\overline{y})}(\eta^{A_2}_{2m-1,3})$ for the graph $\eta^{A_2}_{2m-1,3}$ in the point $F^{-2}(\overline{x}; \overline{y})$ has the unique common point with $\eta^{A_2}_{2m-1,3}$ (it's the point $F^{-2}(\overline{x}; \overline{y})$). Therefore, by the above, the tangent $\tau_{F^{-2}(\overline{x};\overline{y})}(\eta^{A_2}_{2m-1,3})$ for the graph $\eta^{A_2}_{2m-1,3}$ in the point $F^{-2}(\overline{x}; \overline{y})$ lies below the graph $\eta^{A_2}_{2m-1,3}$ everywhere, with the exception of the point $F^{-2}(\overline{x}; \overline{y})$). Since $M(\overline{x}; \overline{y})$ is an arbitrary point of the graph $\eta^{A_2}_{2m-3,3}$, and the equality

$$\eta^{A_2}_{2m-1,3} = (F_{|\eta^{A_2}_{2m-1,3}})^{-2}(\eta^{A_2}_{2m-3,3})$$

holds, then the function $y = \eta^{A_2}_{2m-1,3}(x)$ is strictly convex. Thus, C^1-smooth functions $y = \eta^{A_2}_{2m-1,3}(x)$ are strictly convex for every $m \geq 1$.

3. Let us note that the number sequence $\{(\eta^{A_2}_{2m-1,3})'(3)\}_{m\geq 1}$ decreases and is bounded, moreover, the inequality

$$-1 < (\eta^{A_2}_{2m-1,3})'(3) \leq -\frac{1}{3}$$

holds for every $m \geq 1$. Let us show that the sequence $\{(\eta^{A_2}_{2m-1,3})'(x)\}_{m\geq 1}$ decreases with respect to m for every $x \in (3, +\infty)$.

In fact, by above item 2, the derivative $(\eta^{A_2}_{2m-1,3})'(x)$ strictly increases with respect to x from $(\eta^{A_2}_{2m-1,3})'(3)$ up to 0. Therefore, the inclusion

$$E((\eta^{A_2}_{2m-1,3})') \subset E((\eta^{A_2}_{2m+1,3})')$$

holds, where $E(\cdot)$ is the set of values of a function $(\cdot)$. Then there exists a point $x_m \in (3, +\infty)$ satisfying

$$(\eta^{A_2}_{2m+1,3})'(x_m) = (\eta^{A_2}_{2m-1,3})'(3). \tag{7.13}$$

It implies the inequality

$$(\eta^{A_2}_{2m+1,3})'(x) < (\eta^{A_2}_{2m-1,3})'(3),$$

which is valid for every $x \in (3, x_m)$. On the other hand, by strict convexity of the function $y = \eta^{A_2}_{2m-1,3}(x)$, we have the inequality

$$(\eta^{A_2}_{2m-1,3})'(x) > (\eta^{A_2}_{2m-1,3})'(3).$$

Consequently, the inequality

$$(\eta^{A_2}_{2m+1,3})'(x) < (\eta^{A_2}_{2m-1,3})'(x)$$

holds for every $x \in (3, x_m)$.

If $x = x_m$ then by equality (7.13) and by strict convexity of the function $y = \eta^{A_2}_{2m-1,3}(x)$ the inequality

$$(\eta^{A_2}_{2m+1,3})'(x_m) < (\eta^{A_2}_{2m-1,3})'(x_m) \tag{7.14}$$

is fulfilled.

Let $x > x_m$. Then by previous inequality (7.14) and by strict convexity of the function $y = \eta^{A_2}_{2m-1,3}(x)$, the equality

$$(\eta^{A_2}_{2m+1,3})'(x) = (\eta^{A_2}_{2m-1,3})'(x')$$

is fulfilled for some $x' < x_m$. Using strict increase with respect to x of the derivative $(\eta^{A_2}_{2m-1,3})'(x)$ of the strict convex function $y = \eta^{A_2}_{2m-1,3}(x)$, we obtain from here the inequality

$$(\eta^{A_2}_{2m+1,3})'(x) < (\eta^{A_2}_{2m-1,3})'(x).$$

Thus, it is proved that the sequence $\{(\eta^{A_2}_{2m-1,3})'(x)\}_{m\geq 1}$ decreases with respect to m for every $x \in [3, +\infty)$.

4. Hence, by above item 3, the sequence of derivatives $y = (\eta_{2m-1,3}^{A_2})'(x)$ $(m \geq 1)$ converges pointwisely on the unbounded interval $[3, +\infty)$ to some nonincreasing function $y = \kappa(x)$. Let us prove that

$$\kappa(x) = (\eta_r^{A_2})'(x)$$

for every $x \in [3, +\infty)$.

Let $\overline{x}$ be an arbitrary point of the interval $[3, +\infty)$. Use arcs of tangent curves (denote these arcs by κ_m) for graphs of functions $y = \eta_{2m-1,3}^{A_2}(x)$ $(m \geq 2)$ in the points $(\overline{x}, \overline{y}_m) \in \eta_{2m-1,3}^{A_2}$ (see item 2 of this proof). Since arcs κ_m lie between the graphs $\eta_{2m+1,3}^{A_2}$ and $\eta_{2m-1,3}^{A_2}$ then by item 3 there exists a right-side neighborhood of the point $\overline{x} \in [3, +\infty)$, where every function $y = \kappa_m(x)$ is defined (the arc κ_m is the graph of this function for $m \geq 2$). Thus, there exists the finite limit

$$\lim_{m \to +\infty} \kappa_m(\overline{x}) = \kappa_*(\overline{x}).$$

The angle between the graph $\eta_{2m-1,3}^{A_2}$ and the arc κ_m in the point $(\overline{x}, \overline{y}_m)$is denoted by α_m. By item 2, the equality $\alpha_m = 0$ holds for every $m \geq 2$. Therefore, the angle between κ_* and $\eta_r^{A_2}$ in the point $(\overline{x}, \eta_r^{A_2}(\overline{x}))$ equals 0 too. Using definition of the angle between two differentiable curves and the equality

$$(\kappa_m)'(\overline{x}) = (\eta_{2m-1,3}^{A_2})'(\overline{x}) (m \geq 2),$$

we obtain

$$(\kappa_*)'(\overline{x}) = \kappa(\overline{x}) = (\eta_r^{A_2})'(\overline{x}).$$

Hence, it is proved that

$$\kappa(x) = (\eta_r^{A_2})'(x) \text{ for every } x \in [3, +\infty). \tag{7.15}$$

5. Monotone function $y = \kappa(x)$ either is continuous, or admits discontinuity points of first kind. On the other hand, $y = \kappa(x)$ as the derivative of the function $y = \eta_r^{A_2}(x)$ (see equality (7.15)) either is continuous, or admits discontinuity points of second kind. It means that the derivative $(\eta_r^{A_2})'(x)$ is continuous.

6. Thus, by Dini Theorem [38], the sequence of restrictions $\{\eta_{2m-1,3}^{A_2}|_{[3,b]}(x)\}_{m \geq 1}$ uniformly converges in C^1-norm on the closed interval $[3, b]$ to C^1-smooth strictly decreasing function $y = \eta_r^{A_2}|_{[3,b]}(x)$.

7. Analogous considerations for the functional sequence $\{\eta_{2m,3}^{A_2}(x)\}_{m \geq 1}$ show that the sequence of restrictions $\{\eta_{2m,3}^{A_2}|_{[a,3]}(x)\}_{m \geq 1}$ converges on every closed intervals $[a, 3] \subset (2, 3]$ in C^1-norm to C^1-smooth strictly decreasing function $y = \eta_l^{A_2}|_{[a,3]}(x)$; in addition, C^1-smooth function $y = \eta_l^{A_2}(x)$ with the graph $\eta_l^{A_2}$ is defined on the intervals $(2, 3]$, and the following equalities hold:

$$F(\eta_l^{A_2}) = \eta_r^{A_2}, F(\eta_r^{A_2}) = \eta_l^{A_2} \text{ such that } F^2(\eta_l^{A_2}) = \eta_l^{A_2}.$$

Theorem 7.6 is proved. □

Let us formulate important Corollaries of Theorem 7.6.

Eigenvalues $\lambda_1(A_2)$, $\lambda_2(A_2)$ of differential DF in the fixed point A_2 take values $\lambda_1(A_2) = 3$, $\lambda_2(A_2) = -2$. Eigenvector $q_{\lambda_2(A_2)} = (\frac{-1}{\sqrt{2}}; \frac{1}{\sqrt{2}})$ corresponds to the least eigenvalue $\lambda_2(A_2)$ and lies on the hypotenuse h of the triangle Δ.

Using Theorem 7.6 and the limit equality $\lim\limits_{n \mapsto +\infty} |(\frac{\lambda_2}{\lambda_1})^n| = 0$, we obtain

Corollary 7.1 *Union of graphs $\eta_l^{A_2} \cup \eta_r^{A_2}$ of two strictly decreasing functions such that $y = \eta_l^{A_2}(x)$ is defined on the interval $(2, 3]$ and takes values on the interval $[1, +\infty)$, $y = \eta_r^{A_2}(x)$ is defined on the interval $[3, +\infty)$ and takes values on the interval $(0, 1]$, is C^1-smooth F-invariant curve, which is tangent hypotenuse h of triangle Δ in the point $A_2(3; 1)$.*

The graph $\eta_l^{A_2}$ has the vertical asymptote $x = 2$, and the graph $\eta_r^{A_2}$ has the horizontal asymptote $y = 0$.

Since the graphs $\eta_l^{A_2}$ and $\eta_r^{A_2}$ are C^1-smooth curves then these curves are measurable on the closed intervals $[a, 3]$ and $[3, b]$ respectively. Therefore, the following claim is valid.

Corollary 7.2 *The graphs $\eta_l^{A_2}$ and $\eta_r^{A_2}$ admit parametrization with the use of natural parameter s with the origin in the fixed point A_2 such that $\eta_l^{A_2}$ is represented in the form $x = {\eta_1}^{l,A_2}(s)$, $y = {\eta_2}^{l,A_2}(s)$; and $\eta_r^{A_2}$ is represented in the form $x = {\eta_1}^{r,A_2}(s)$, $y = {\eta_2}^{r,A_2}(s)$, where $x = {\eta_1}^{p,A_2}(s)$, $y = {\eta_2}^{p,A_2}(s)$ $(p = l, r)$ are C^1-smooth functions on the interval $[0, +\infty)$.*

Corollary 7.3 *Let $M_0 \in h$ be F-periodic point with the (least) period $m \geq 1$. Let $\{M_n\}_{n\geq 1} \subset h$ be a monotone sequence of points convergent to M_0 on hypotenuse h (in particular, the equality $M_n = M_0$ $(n \geq 1)$ can be valid). Let $\gamma_{M_n} \subset G_\Delta$ be a continuous curve beginning from the point M_n for every $n \geq 1$ such that curves of the set $\{\gamma_{M_n}\}_{n\geq 1}$ are pairwise disjoint in $intG_\Delta$. Let the equality $F^m(\gamma_{M_n}) = \gamma_{M_{n-1}}$ (or $F^m(\gamma_{M_{n-1}}) = \gamma_{M_n}$) be valid. Then the pointwise limit of the sequence of curves $\{\gamma_{M_n}\}_{n\geq 1}$ is F^m-invariant set, which contains the initial point M_0.*

Denote by $H_0^{max}(A_2)$ the closed unbounded domain, which contains the set $D_{+\infty}$ and has the boundary $\partial H_0^{max}(A_2)$ satisfying the equality

$$\partial H_0^{max}(A_2) = \eta_l^{A_2} \cup \eta_r^{A_2}. \tag{7.16}$$

Definition 7.3 Domain $H_0^{max}(A_2)$ is called *the maximal wedge-shaped domain with the vertex in the fixed point A_2.*

Let us consider connected components of kth $(k \geq 1)$ complete preimage (with respect to F) of the maximal wedge-shaped domain $H_0^{max}(A_2)$ and construct maximal wedge-shaped domains with vertexes in $F|_h$-homoclinic points for the fixed point $A_2(3; 1)$. For this goal, we introduce the concept of the order of a homoclinic point.

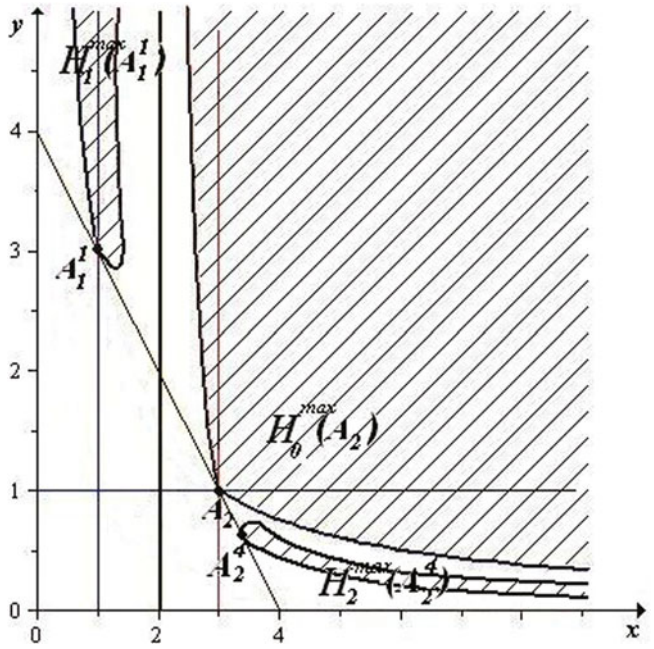

Fig. 7.1 Maximal *wedge-shaped* domains $H_0^{max}(A_2)$, $H_1^{max}(A_1^1)$ è $H_2^{max}(A_2^4)$ with the vertexes in the fixed point A_2 and in the homoclinic points A_1^1 and A_2^4, respectively

Definition 7.4 Let $(x; y)$ be a $F|_h$-homoclinic point for a fixed point $(x^*; y^*)$. The least natural number n such that $F^n(x, y) = (x^*; y^*)$ is called *the order* of a homoclinic point $(x; y)$.

As it follows from Definition 7.4, the equality $F^k(x, y) = (x^*;\ y^*)$ holds for every $k \geq n$. By claim 6 of Proposition 7.1, the complete preimage of kth order ($k \geq 1$) of the fixed point $A_2(3; 1)$ with respect to the restriction $F|_h$ consists of $(2^k - 1)$ $F_{|h}$-homoclinic points for the fixed point $A_2(3; 1)$ and the fixed point $A_2(3; 1)$. Denote by $\{A_k^i(x_{A_k^i}; y_{A_k^i})\}_{1 \leq i \leq 2^k - 1}$ the set of $F_{|h}$-homoclinic points of an order $k \geq 1$ for the fixed point $A_2(3; 1)$.

Definition 7.5 The unbounded domain $H_k^{max}(A_k^i)$ is said to be the *maximal wedge-shaped domain with the vertex in a homoclinic point* A_k^i of order $k \geq 1$, $i \in \{1, 2, \ldots, 2^k - 1\}$, if $H_k^{max}(A_k^i)$ is a connected component of kth complete preimage of $H_0^{max}(A_2)$ contained $F_{|h}$-homoclinic point A_k^i.

By claim 4 of Proposition 7.1, Definitions 7.3 and 7.5 the following statement holds.

Corollary 7.4 *Every point*

$$(x; y) \in (int\, H_0^{max}(A_2)) \bigcup \bigcup_{k=1}^{+\infty} \bigcup_{i=1}^{2^k=1} (int\, H_k^{max}(A_k^i))$$

possesses the property:

$$\lim_{n\to+\infty} f_n(x;y) = \lim_{n\to+\infty} g_n(x;y) = +\infty.$$

Using claim 4 of Proposition 7.1 and Definitions 7.3 and 7.5, we obtain that the map $(F|_{H_k^{max}(A_k^i)})^k$ is C^1-diffeomorphism of the set $H_k^{max}(A_k^i)$ on the set $H_0^{max}(A_2)$. Therefore, $(F|_{H_k^{max}(A_k^i)})^{-k}$ maps the interior $int\, H_0^{max}(A_2)$ of the set $H_0^{max}(A_2)$ on the interior $int\, H_k^{max}(A_k^i)$ of the set $H_k^{max}(A_2)$ and the boundary $\partial H_0^{max}(A_2)$ of the set $H_0^{max}(A_2)$ on the boundary $\partial H_k^{max}(A_k^i)$ of the set $H_k^{max}(A_2)$.

Lemma 7.1 *$(F|_{H_1^{max}(A_1^1)})^{-1}(\eta_l^{A_2})$ and $(F|_{H_1^{max}(A_1^1)})^{-1}(\eta_r^{A_2})$ are C^1-smooth curves given by formulas*

$$x = {\eta_1}^{p,A_1^1}(s),\ y = {\eta_2}^{p,A_1^1}(s),\ s \in [0,+\infty)\ (p = l,r)$$

with the use of natural parameter s; moreover, these curves intersect each other in the unique point A_1^1 such that one of them has asymptote $x = 0$, and the other has asymptote $x = 2$.

Proof In fact, using formula (7.5), we obtain the system

$$\begin{cases} {\eta_1}^{p,A_1^1}(s){\eta_2}^{p,A_1^1}(s) = {\eta_1}^{p,A_2}(s), \\ ({\eta_1}^{p,A_1^1}(s) - 2)^2 = {\eta_2}^{p,A_2}(s), \end{cases}$$

where $s \in [0,+\infty)$, $p = l,r$. Using this system, we find the unique solution

$${\eta_1}^{p,A_1^1}(s) = 2 - \sqrt{{\eta_2}^{p,A_2}(s)},\ {\eta_2}^{p,A_1^1}(s) = \frac{{\eta_1}^{p,A_2}(s)}{2 - \sqrt{{\eta_1}^{p,A_2}(s)}},$$

corresponding to the boundary of the domain $H_1^{max}(A_1^1)$ with the vertex in the homoclinic point $A_1^1(1;3)$.

As it follows from the last formulas, every function $x = {\eta_1}^{p,A_1^1}(s)$ and $y = {\eta_2}^{p,A_1^1}(s)$, $s \in [0, +\infty)$ $(p = l, r)$ is a C^1-smooth function of variable s. With the use of Corollary 7.1, we obtain from here that one of the constructed curves has asymptote $x = 0$, and the other has asymptote $x = 2$. Lemma 7.1 is proved. □

Corollary 7.5 *$(F|_{H_0^{max}(A_2)})^{-k}(\eta_l^{A_2})$ and $(F|_{H_0^{max}(A_2)})^{-k}(\eta_r^{A_2})$ $(k \geq 1)$ are C^1-smooth curves, which form the boundary of the domain $H_k^{max}(A_k^i)$; in addition, these curves are defined by the parametric equations*

$$x = {\eta_1}^{p,A_k^i}(s),\ y = {\eta_2}^{p,A_k^i}(s);\ s \in [0,+\infty)(p = l,r).$$

Let us study the mutual disposition of curves forming the boundary of every domain $H_k^{max}(A_k^i)$, $k \geq 1$, $1 \leq i \leq 2^k - 1$.

Let $D\Phi$ be differential of an arbitrary smooth map $\Phi : \mathbf{R^2} \to \mathbf{R^2}$. Then

$$D\Phi : T_{(x;y)} \to T_{\Phi(x,y)},$$

where $T_{(\cdot)}$ is the tangent space for $\mathbf{R^2}$ in a point $(\cdot) \in \mathbf{R^2}$. Therefore, Corollary 7.1 and invariance of hypotenuse h imply the following statement.

Corollary 7.6 *Every curve* $(F|_{H_k^{max}(A_k^i)})^{-k}(\eta_l^{A_2})$ *and* $(F|_{H_k^{max}(A_k^i)})^{-k}(\eta_r^{A_2})$ $(k \geq 1)$ *is tangent hypotenuse* h.

Let us use the invariant curve $\Gamma^{(1)} \subset D_{+\infty} \subset H_0^{\max}$ (see claim 5 of Proposition 7.1), which is tangent to the eigenvector (of the differential DF in the fixed point A_2) $(3/\sqrt{13}; 2/\sqrt{13}) \subset D_{+\infty}$. Then the inclusion

$$(F_{|H_k^{max}(A_k^i)})^{-k}(\Gamma^{(1)}) \subset H_k^{max}(A_k^i)$$

holds for every $k \geq 1$, $i \in \{1, \ldots, 2^k - 1\}$; in addition, there exists an interval of the tangent for the curve $(F_{|H_k^{max}(A_k^i)})^{-k}(\Gamma^{(1)})$, which contains the point A_k^i and lies in the unbounded domain $H_k^{max}(A_k^i)$.

This property with Theorem 7.6 and Corollary 7.1 proves the following claim.

Corollary 7.7 *There exists a neighborhood* $U(A_k^i)$ *of every point* A_k^i $(k \geq 1,\ i \in \{1, \ldots, 2^k - 1\})$ *such that for every point* $(x; y) \in U(A_k^i)$, $(x; y) \neq A_k^i$, *which lies either on the curve* $(F|_{H_k^{max}(A_k^i)})^{-k}(\eta_l^{A_2})$ *or on the curve* $(F|_{H_k^{max}(A_k^i)})^{-k}(\eta_r^{A_2})$, *the inequality* $x < x_{A_k^i}$ *holds, and on the other curve the inequality* $x > x_{A_k^i}$ *holds, where* $x_{A_k^i}$ *is the abscissa of the point* A_k^i.

We denote by $l_l^{-k}(A_k^i)$ and by $l_r^{-k}(A_k^i)$ first and second curve respectively indicated in Corollary 7.7. Thus, we have

$$\partial H_k^{max}(A_k^i) = l_l^{-k}(A_k^i) \cup l_r^{-k}(A_k^i). \tag{7.17}$$

Denote by $l_l^0(A_2)$ and by $l_r^0(A_2)$ graphs of the functions $y = \eta_l^{A_2}(x)$ and $y = \eta_r^{A_2}(x)$ respectively. Hence, equality (7.16) can be written in the form

$$\partial H_0^{max} = l_l^0(A_2) \cup l_r^0(A_2). \tag{7.18}$$

By Corollary 7.1 and Lemma 7.1, the maximal wedge-shaped domains H_0^{max} and H_1^{max} lie from different sides of the critical line $x = 2$ such that

$$H_1^{max}(A_1^1) \cap H_0^{max}(A_2) = \emptyset.$$

Then by Definition 7.5, the following statement is correct.

Corollary 7.8 *The maximal wedge-shaped domains*

$$\{H_0^{max}(A_2), H_k^{max}(A_k^i)\}_{k\geq 1, i\in\{1,\ldots,2^k-1\}}$$

are pairwise disjoint, and the equalities hold:

$$F(H_1^{max}(A_1^1)) = H_0^{max}(A_2), F(H_k^{max}(A_k^i)) = H_{k-1}^{max}(A_{k-1}^j)$$

for some j, $1 \leq j \leq 2^{k-1} - 1$.

Since the restrictions $F|_{H_k^{max}}(A_k^i)$ and $F|_{H_0^{max}}(A_2)$ are diffeomorphisms then we immediately obtain the claim.

Corollary 7.9 *The curves $l_l^{-k}(A_k^i)$ and $l_r^{-k}(A_k^i)$ ($k \geq 1$, $i \in \{1, 2, \cdots, 2^k - 1\}$) are pairwise disjoint in $intG_\Delta$, and the following equality*

$$F^k(l_l^{-k}(A_k^i) \cup l_r^{-k}(A_k^i)) = l_l^0(A_2) \cup l_r^0(A_2)$$

holds.

Results of this part of the chapter prove the following statement.

Lemma 7.2 *The set $\widetilde{G}$ is open, and the equality*

$$\widetilde{G} = (int H_0^{max}(A_2)) \bigcup \bigcup_{k=1}^{+\infty} \bigcup_{i=1}^{2^k-1} (int H_k^{max}(A_k^i))$$

holds.

7.4 Geometric Assistance of the Proof of Theorem 7.3

1. We begin this section from the construction of parts of preimages of the critical line $x = 0$ ($x = 2$), which belongs to G_Δ. Let us consider the problem

$$f_m(x, y) = 2 \tag{7.19}$$

with initial conditions

$$f_m(x_{B_m^j}, y_{B_m^j}) = 2, \tag{7.20}$$

where $\{B_m^j(x_{B_m^j}; y_{B_m^j})\}_{m \geq 1, j \in \{1, \ldots 2^m - 1\}}$ is the set of $F|_h$ – homoclinic points of order m for the saddle $A_1(0; 4)$, $B_m^j \neq (4; 0)$.

Lemma 7.3 *There exist C^1-smooth unbounded algebraic curves $\varphi^{B_m^j}$ defined by parametric equations*

$$x = \varphi_1^{B_m^j}(s), y = \varphi_2^{B_m^j}(s), s \in [0, +\infty),$$

moreover, each of these curves is the solution of equation (7.19) ($m \geq 3$) with initial conditions (7.20).

Proof Both coordinates of every homoclinic point B_m^j ($m \geq 1$, $j \in \{1, \ldots 2^m - 1\}$) are the simple roots of the equation $f_m(x, 4-x) = 2$ and $f_m(4-y, y) = 2$ respectively (see item 6 of Proposition 7.1). Therefore, the following inequalities are valid:

$$\frac{\partial f_m(x_{B_m^j}, y_{B_m^j})}{\partial x} \neq 0, \frac{\partial f_m(x_{B_m^j}, y_{B_m^j})}{\partial y} \neq 0.$$

Then conditions of the local existence theorem for C^1-smooth implicit function are fulfilled in every homoclinic point B_m^j. By claim 1 of Proposition 7.1 the inequality

$DF^m(x, y) \neq 0$ holds on the connected components of algebraic curves defined by the equation $f_m(x, y) = 2$. Therefore, the inequality

$$\left(\frac{\partial f_m(x, y)}{\partial x}\right)^2 + \left(\frac{\partial f_m(x, y)}{\partial y}\right)^2 \neq 0$$

is valid for these points $(x; y)$. The algebraic equations

$$\frac{\partial f_m(x, y)}{\partial x} = 0 \tag{7.21}$$

and

$$\frac{\partial f_m(x, y)}{\partial y} = 0 \tag{7.22}$$

have a finite set of solutions.

Let us use the version of the local existence theorem for C^1-smooth implicit function from [39], which admits vanishing of one partial derivative $\frac{\partial f_m(x,y)}{\partial x}$ or $\frac{\partial f_m(x,y)}{\partial y}$ on a finite set of points. Then we obtain that in some neighborhood of every root of the equations (7.21) or (7.22), there exists a local implicit function of the variable x (if $\frac{\partial f_m(x,y)}{\partial y} \neq 0$) or the variable y (if $\frac{\partial f_m(x,y)}{\partial x} \neq 0$). Thus, the finite union of graphs of C^1-smooth implicit functions of either the variable x or the variable y is C^1-smooth unbounded algebraic curve, which is the solution of equation (7.19) with initial condition (7.20).

Every constructed C^1-smooth curve admits parametrization with the use of natural parameter $s \in [0, +\infty)$ such that

$$x = \varphi_1^{B_m^j}(s), y = \varphi_2^{B_m^j}(s).$$

Lemma 7.3 is proved. □

Unbounded C^1-smooth algebraic curves constructed in Lemma 7.3 are connected components of intersection of the stable manifold of the saddle $A_1(0; 4)$ with G_Δ.

Corollary 7.10 *For every $m \geq 1$ and $j \in \{1, \ldots, 2^m - 1\}$, there are natural numbers $m_1 \geq 1$ and $j_1 \in \{1, \ldots, 2^{m_1} - 1\}$ such that $\varphi^{B_{m_1}^{j_1}} = F_2(\varphi^{B_m^j})$.*

Corollary 7.11 *Any curves $\varphi^{B_{m_1}^{j(m_1)}}$ and $\varphi^{B_{m_2}^{j(m_2)}}$ ($j(m_1) \neq j(m_2)$ for $m_1 = m_2$) starting from different points of the set $\{(F|_h)^{-j}(A_1)\}_{j\geq 0}$ do not intersect each other in the set G_Δ.*

Using Theorem 7.6, Lemma 7.3, and claim 7 of Proposition 7.1 we obtain the statement.

Corollary 7.12 *Any curves starting from different points of the set*

$$\{(F|_h)^{-j}(A_1)\}_{j\geq 0} \cup \{(F|_h)^{-k}(A_2)\}_{k\geq 0}$$

do not intersect each other in G_{Δ_2}.

Between every two curves starting from points of the set $\{(F|_h)^{-j}(A_1)\}_{j\geq 0}$ *there exists at least one maximal wedge-shaped domain with the vertex in a point of the set* $\{(F|_h)^{-k}(A_2)\}_{k\geq 0}$*;*

and between two curves starting from different points of the set $\{(F|_h)^{-k}(A_2)\}_{k\geq 0}$ *there exists at least one curve starting from a point of the set* $\{(F|_h)^{-j}(A_1)\}_{j\geq 0}$.

Using Lemma 7.3 and formulas (7.6) and (7.7), we obtain

Corollary 7.13 *Every curve* $\varphi^{B_m^j}$ $(m \geq 1)$ *has asymptote* $x = 0$ *or* $x = 2$ *if* $x_{B_m^j} \in (0, 2)$*; asymptote* $x = 2$ *if* $x_{B_m^j} \in (2, 3)$*; and asymptote* $y = 0$ *if* $x_{B_m^j} \in (3, 4)$.

2. Let us obtain the complement information concerning a mutual disposition of curves constructed above. First, we consider the part of the critical line C_0, which lies in domain G_Δ. Since $A_1(0; 4)$ is a source of the restriction $F|_h$ then by claim 7 of Proposition 7.1 there is a sequence of homoclinic points B_m^j $(m \geq 1,$ $1 \leq j \leq 2^m - 1)$ for the fixed point A_1 satisfying

$$F(B_m^{j(m)}) = B_{m-1}^{j(m-1)}, (m \geq 2);\ \text{moreover,}\ \lim_{m\to+\infty} B_m^{j(m)} = A_1. \tag{7.23}$$

By Lemma 7.3, there are unbounded C^1-smooth curves $\varphi^{B_m^j}$ given by parametric equations $x = \varphi_1^{B_m^j}(s)$, $y = \varphi_2^{B_m^j}(s)$, $s \in [0, +\infty)$, which are nonlocal solutions of equation (7.19) with initial condition (7.20).

Take an arbitrary $s_* \in (0, +\infty)$. Consider the space $2^{\Gamma_{s_*}}$ of all closed C^1-smooth arcs parametrized by natural parameter $s \in [0, s_*]$, which lie in the set G_Δ, start from points of hypotenuse h. Endow the space $2^{\Gamma_{s_*}}$ with Hausdorff metric $dist$ (see [33]). Remind that

$$dist(\gamma_{1|[0,s_*]}, \gamma_{2|[0,s_*]}) =$$
$$= \max\{\sup_{(x;y)\in\gamma_{1|[0,s_*]}} \rho((x; y), \gamma_{2|[0,s_*]}), \sup_{(x;y)\in\gamma_{2|[0,s_*]}} \rho((x;\ y),\ \gamma_{1|[0,\,s_*]})\}$$

for any closed arcs $\gamma_{1|[0,s_*]}, \gamma_{2|[0,\,s_*]} \subset G_\Delta$, where

$$\rho((x_1; y_1), (x_2; y_2)) = \max\{|x_1 - x_2|, |y_1 - y_2|\}.$$

The closed arc of the C^1-smooth curve $\varphi^{B_m^j}$ corresponding to the closed interval $[0, s_*]$ is denoted by $\varphi^{B_m^j, s_*}$. Then $x = \varphi_1^{B_m^j, s_*}$, $y = \varphi_2^{B_m^j, s_*}$.

Let us show that a sequence of arcs $\{\varphi^{B_m^j, s_*}\}_{m\geq 1}$ starting from homoclinic points B_m^j and satisfying the second equality (7.23) converges to the segment of ordinate axes

$$x(s) = 0, y(s) = s, s \in [0, s_*],^7$$

with respect to Hausdorff metric in the space $2^{\Gamma_{s_*}}$.

---

[7] The equality $(x'(s))^2 + (y'(s))^2 = 1$ holds for an arc of a curve parametrized by natural parameter $s \in [0, s_*]$. Therefore, the segment of y-axes starting from the point A_1 and corresponding to the parameter value s_* is defined parametrically in the form $x(s) = 0$, $y(s) = s$, $s \in [0, s_*]$. Analogously, the closed interval of x-axes starting from the point $(4; 0)$ and corresponding to the parameter value s_* is given parametrically in the form $x(s) = s$, $y(s) = 0$, $s \in [0, s_*]$.

Denote by $\varphi_{0,s}$ the segment $x(s) = 0, y(s) = s, s \in [0, s_*]$.

Lemma 7.4 *The equality*

$$\lim_{m \to +\infty} dist(\varphi_1^{B_m^j, s_*}, \varphi_{0,s}) = 0$$

holds.

Proof In fact, $A_1(0; 4)$ is the saddle of the map F such that one of its eigenvectors corresponding to $\lambda_1(A_1) = 0$ belongs to y-axes, and the other (corresponding to $\lambda_2(A_1) = 4$) belongs to hypotenuse h. Therefore, there is a relative δ - neighborhood U_δ in the set G_Δ of the segment $x(s) = 0, y(s) = s, s \in [0, s_*]$, defined by the equality

$$U_\delta = G_\Delta \cap ((0, \delta] \times [4 - \delta, 4 + \delta])$$

such that the restriction $(F|_{U_\delta})^{-1} : F(U_\delta) \mapsto U_\delta$ is the diffeomorphism contracting along the hypotenuse not less than in 3 times and expanding along y-axis not less than in 10 times. The set $\overline{U}_\delta \cap F^{-1}(\overline{U}_\delta)$ is the proper subset of $\overline{U}_\delta$, which contains the segment $[0, \delta^*] \times \{4 + \delta\}$ for some $0 < \delta^* \leq \frac{\delta}{3}$. Thus, the following inclusions

$$\overline{U}_\delta \supset \overline{U}_\delta \cap (F|_{U_\delta})^{-1}(\overline{U}_\delta) \supset \ldots \supset \overline{U}_\delta \cap (F|_{U_\delta})^{-n}(\overline{U}_\delta) \supset \ldots \tag{7.24}$$

hold for every $n \geq 1$. Then by [33] there is the topological limit

$$Lim_{n \to +\infty} \overline{U}_\delta \cap (F|_{U_\delta})^{-n}(\overline{U}_\delta) = \{0\} \times [4, 4 + \delta].$$

Using second equality (7.23) we find a natural number m_0 such that for every $m \geq m_0$ the following properties hold:

$$B_m^{j(m)} \in U_\delta \text{ and } \varphi^{B_m^j, s_*} \cap U_\delta \neq \emptyset.$$

Then using equalities (7.23) we indicate $m_1 \geq m_0$ such that the inequality

$$\varphi^{B_m^j, s_*} \cap ([4, 4 + \delta] \times \{4 + \delta\}) \neq \emptyset$$

holds for every $m \geq m_1$. Using Lemma 7.3 and [33], we receive that there exists the topological limit $Lim_{m \to +\infty} \varphi^{B_m^j, s_*} = \{0\} \times [4, 4 + \delta]$. It implies the equality (see [33])

$$\lim_{m \to +\infty} dist(\varphi_1^{B_m^j, s_*}, \varphi_{0,s}) = 0.$$

Lemma 7.4 is proved. □

Using uniform continuity of F on compact sets, Lemma 7.4, and Corollary 7.10 we obtain the following statement.

Corollary 7.14 *Let* $\{B_m^j\}_{m\geq 1}$ *be a sequence convergent to the point* $(4;0)$. *Then the equality*

$$\lim_{m\to+\infty} dist(\varphi_2^{B_m^j,s_*}, \varphi_{s,0}) = 0$$

holds.

Take an arbitrary homoclinic point $B_{m^*}^{j^*}$ ($m^* \geq 1$, $j^* \in \{1,\ldots,2^{m^*}-1\}$) for the fixed point A_1. Then by claim 7 of Proposition 7.1, there is a sequence of homoclinic points $\{B_m^j\}_{m\geq 1}$ ($j = j(m)$, $j \in \{1,\ldots,2^m-1\}$) satisfying the equality $\lim\limits_{m\to+\infty} B_m^j = B_{m^*}^{j^*}$.

Using Lemma 7.4, we obtain the following claim.

Corollary 7.15 *The equality*

$$\lim_{m\to+\infty} dist(\varphi^{B_m^j,s_*}, \varphi^{B_{m^*}^{j^*},s_*}) = 0$$

holds for every sequence of homoclinic points $\{B_m^j\}_{m\geq 1}$ *convergent to the homoclinic point* $B_{m^*}^{j^*}$.

Lemma 7.4, Corollaries 7.14, 7.15, and [33] imply the statement.

Corollary 7.16 *In conditions of Lemma 7.4, Corollary 7.14 or Corollary 7.15 there exists the topological limit* $\mathop{Lim}\limits_{m\to+\infty} \varphi^{B_m^j,s_*}$. *Moreover, in conditions of Lemma 7.4 the equality* $\mathop{Lim}\limits_{m\to+\infty} \varphi^{B_m^j,s_*} = \varphi_{0,s}$ *is valid; in conditions of Corollaries 7.14 and 7.15 the equalities* $\mathop{Lim}\limits_{m\to+\infty} \varphi^{B_m^j,s_*} = \varphi_{s,0}$ *and* $\mathop{Lim}\limits_{m\to+\infty} \varphi^{B_m^j,s_*} = \varphi^{B_{m^*}^{j^*},s_*}$ *hold respectively.*

Corollary 7.17 *The set of the curves*

$$\{\{\varphi^{B_m^j,s_*}\}_{m\geq 1, j\in\{1,\ldots,2^m-1\}}, \varphi_{0,s}, \varphi_{s,0}, \}_{s\in[0,s_*]}$$

is dense in itself with respect to Hausdorff metric $dist$ *in the space* $2^{\Gamma_{s_*}}$ *for every* $s_* \in [0,+\infty)$.

We denote the closed arcs of the curves $l_l^0(A_2)$, $l_r^0(A_2)$, $l_l^{-k}(A_k^i)$, $l_r^{-k}(A_k^i)$ by $l_l^{0,s_*}(A_2)$, $l_r^{0,s_*}(A_2)$, $l_l^{-k,s_*}(A_k^i)$, $l_r^{-k,s_*}(A_k^i)$ respectively, corresponding to the natural parameter $s \in [0,s_*]$.

Using Corollaries 7.12 and 7.17, we obtain the following claim.

Corollary 7.18 *The set of the curves*

$$\{\{\varphi^{B_m^j,s_*}\}_{m\geq 1, j\in\{1,\ldots,2^m-1\}}, \varphi_{0,s}, \varphi_{s,0}, \}_{s\in[0,s_*]}$$

is contained in the closure (with respect to Hausdorff metric $dist$ *in the space* $2^{\Gamma_{s_*}}$*) of the set of the curves*

$$\{l_l^{0,s_*}(A_2), l_r^{0,s_*}(A_2), l_l^{-k,s_*}(A_k^i), l_r^{-k,s_*}(A_k^i)\}_{k\geq 1, 1\leq i\leq 2^k-1, s\in[0,s^*]}.$$

3. In this part of the chapter, we prove the inverse inclusion (with respect to the inclusion indicated in Corollary 7.18), i.e., we prove that the set of the curves

$$\{l_l^{0,s_*}(A_2), l_r^{0,s_*}(A_2), l_l^{-k,s_*}(A_k^i), l_r^{-k,s_*}(A_k^i)\}_{k\geq 1, 1\leq i\leq 2^k-1, s\in[0,s^*]}$$

is contained in the closure of the set of the curves

$$\{\{\varphi^{B_m^j,s_*}\}_{m\geq 1, j\in\{1,..,2^m-1\}}, \varphi_{0,s}, \varphi_{s,0}, \}_{s\in[0,s_*]}.$$

In fact, since $A_2(3;\,1)$ is a source of F then by claims 6 and 7 of Proposition 7.1 for every $k \geq 1$ there exists $i'(k) \in \{1, \ldots, 2^{2k}-1\}$ such that the sequence of homoclinic points $\{A_{2k}^{i'}\}_{k\geq 1}$ for the fixed point possesses the properties:

(i) The sequence $\{x_{A_{2k}^{i'}}\}_{k\geq 1}$ decreases

(ii) $F^2(A_{2k}^{i'(k)}) = A_{2(k-1)}^{i'(k-1)}$, $k \geq 1$

(iii) $\lim\limits_{k\to+\infty} A_{2k}^{i'(k)} = A_2$

Consider the sequence of the unbounded arcs $\{\eta_{2k,3}^{A_{2k}^{i'}}\}_{k\geq 1}$ such that each one of them is the C^1-smooth extension (through the triangle Δ) into the set G_Δ of the graph $\eta_{2k,3}^{A_2}$ (of the corresponding C^1-smooth function $y = \eta_{2k,3}^{A_2}(x)$) starting from the fixed point A_2 and belonging to the strip $\{(x; y) : 2 < x \leq 3, x + y \geq 4\}$. We have for $k = 1$:

$$\eta_{2,3}^{A_2}(x) = \frac{3}{x(x-2)^2} \text{and} (\eta_{2,3}^{A_2})''(x) = \frac{12x(3x^2-4x+2)}{x^4(x-2)^4}.$$

Hence, the curve $\eta_{2,3}^{A_2^3}$ (for $k = 1$ the equality $i' = 3$ holds) is the graph of the C^1-smooth strictly decreasing convex function $y = \eta_{2,3}^{A_2^3}(x)$ with the initial condition $\eta_{2,3}^{A_2^3}(x_{A_2^3}) = y_{A_2^3}$.

Using mathematical induction principal and repeating arguments of the proof of Theorems 7.5 and 7.6 we make sure of the correctness of the claim.

Lemma 7.5 *There is a natural number $k_0 \geq 1$ such that for every $k \geq k_0$ the unbounded arcs $\eta_{2k,3}^{A_{2k}^{i'}} \subset G_\Delta$ starting from homoclinic points $A_{2k}^{i'}$ are the graphs of the C^1-smooth decreasing convex functions $y = \eta_{2k,3}^{A_{2k}^{i'}}(x)$.*

Using the method described in the proof of Theorem 7.6; we obtain the following statement.

Lemma 7.6 *The sequence of restrictions $\{\eta_{2k,3}^{A_{2k}^{i'}}|_{[3,b]}\}_{k\geq 1}$ on an arbitrary closed interval $[3, b]$ converges in C^1-norm to the C^1-smooth decreasing convex function $y = l_r^{*,A_2}|_{[3,b]}(x)$.*

Corollary 7.19 *There exists the C^1-smooth strictly decreasing convex function $y = l_r^{*,A_2}(x)$ (with the graph l_r^{*,A_2}), which is extension of the function $y = l_r^{*,A_2}|_{[3,b]}(x)$ on the interval $[3, +\infty)$; in addition, the function $y = l_r^{*,A_2}(x)$ has the horizontal*

asymptote $y = 0$, and the graphs of the functions $y = l_r^{*,A_2}(x)$ and $y = \eta_r^{A_2}$ intersect each other in the fixed point A_2. Moreover, l_r^{*,A_2} is F^2-invariant curve.

Prove the following statement.

Lemma 7.7 *The equality $l_r^{*,A_2} = l_r^0(A_2)$ holds.*

Proof Suppose the contrary. Let the inequality $l_r^{*,A_2} \neq l_r^0(A_2)$ hold. It means that the inequality $l_r^{*,A_2}(x) < \eta_r^{A_2}(x)$ is valid for every $x > 3$. If not, then the map F^2 has the fixed point in $intG_\Delta$. It contradicts claims 2 and 7 of Proposition 7.1.

Let a number c satisfy the inequality $c > 3$. Denote by V_c the domain bounded by the arcs of the curves l_r^{*,A_2}, $l_r^0(A_2)$ for $x \in [3, c]$ and by the nondegenerate vertical closed interval $\{c\} \times [l_r^{*,A_2}(c), \eta_r^{A_2}(c)]$. By Lemma 7.6, Corollaries 7.12 and 7.19 the restriction $F^2|_{V_c}$ is the diffeomorphism.

By the definition of the curve $l_r^0(A_2)$ the inequality $\eta_r^{A_2}(c) < 1$ holds for every $c > 3$. Then we have:

$$3 < 2 + \sqrt{\frac{1}{\eta_r^{A_2}(c)}}.$$

Hence, we can choose a number c satisfying the inequality

$$3 < c < 2 + \sqrt{\frac{1}{\eta_r^{A_2}(c)}} \tag{7.25}$$

such that the inequality

$$||D(F^2|_{V_c})^{-1}|| < \frac{1}{2} \tag{7.26}$$

holds for the maximal row norm of the differential of the map $(F^2|_{V_c})^{-1}$. Correctness of (7.26) follows immediately from the equality $||DF^2(A_2)|| = 10$. By inequality (7.26) the following inclusion is valid:

$$(F^2|_{V_c})^{-1}(V_c) \subset V_c$$

and, in particular,

$$(F^2|_{V_c})^{-1}(\{c\} \times [l_r^{*,A_2}(c), \eta_r^{A_2}(c)]) \subset V_c.$$

Since $F^2|_{V_c}$ is the diffeomorphism, then the arc

$$(F^2|_{V_c})^{-1}(\{c\} \times [l_r^{*,A_2}(c), \eta_r^{A_2}(c)]) \tag{7.27}$$

has the unique common point both with the curve l_r^{*,A_2} and with the curve $\eta_r^{A_2}$; moreover, these points are different.

At the same time, (7.27) is the arc of the graph of function $y = \frac{c}{x(x-2)^2}$ for $x > 3$. Let us note that $y(3) = \frac{c}{3}$, where $y(3) > 1$; and $y(c) = \frac{1}{(c-2)^2}$. Since c satisfies the inequality (7.25), and the function $y = \frac{c}{x(x-2)^2}$ strictly decreases for $x > 3$, then the

arc (7.27) does not intersect with the closed domain V_c. Thus, our assumption is not valid, and the equality $l_r^{*,A_2} = l_r^0(A_2)$ is fulfilled. Lemma 7.7 is proved. □

Take an arbitrary homoclinic point $A_{k^*}^{i^*(k^*)}$ for the fixed point A_2. By Lemma 7.7 and Corollary 7.12, the following statement holds.

Corollary 7.20 *Let a sequence of homoclinic points* $\{A_k^i\}_{k\geq 1}$ *or* $\{B_m^j\}_{m\geq 1}$ *converges to the homoclinic point* $A_{k^*}^{i^*(k^*)}$ *from the right (from the left). Then, the sequences of arcs* $\{l_r^{-k,s_*}(A_k^i)\}$ *and* $\{l_l^{-k,s_*}(A_k^i)\}$ *or* $\{\varphi^{B_m^j,s_*}\}$ *satisfy the equalities:*

$$\lim_{k\to+\infty} dist(l_r^{-k,s_*}(A_k^i), l_r^{-k^*,s_*}(A_{k^*}^{i^*})) = \lim_{k\to+\infty} dist(l_l^{-k,s_*}(A_k^i), l_r^{-k^*,s_*}(A_{k^*}^{i^*})) = 0,$$

or

$$\lim_{k\to+\infty} dist(\varphi^{B_m^j,s_*}, l_r^{-k^*,s_*}(A_{k^*}^{i^*})) = 0$$

$$\Big(\lim_{k\to+\infty} dist(l_r^{-k,s_*}(A_k^i), l_l^{-k^*,s_*}(A_{k^*}^{i^*})) = \lim_{k\to+\infty} dist(l_l^{-k,s_*}(A_k^i), l_l^{-k^*,s_*}(A_{k^*}^{i^*})) = 0.$$

or

$$\lim_{k\to+\infty} dist(\varphi^{B_m^j,s_*}, l_l^{-k^*,s_*}(A_{k^*}^{i^*})) = 0\Big).$$

Corollary 7.21 *Let a sequence of homoclinic points* $\{A_k^i\}_{k\geq 1}$ *or* $\{B_m^j\}_{m\geq 1}$ *converges to the homoclinic point* $A_{k^*}^{i^*(k^*)}$ *from the right (from the left). Then, the sequences of arcs* $\{l_r^{-k,s_*}(A_k^i)\}$ *and* $\{l_l^{-k,s_*}(A_k^i)\}$ *or* $\{\varphi^{B_m^j,s_*}\}$ *satisfy the equations:*

$$\underset{k\to+\infty}{Lim}\, l_r^{-k,s_*}(A_k^i) = \underset{k\to+\infty}{Lim}\, l_l^{-k,s_*}(A_k^i) = l_r^{-k^*,s_*}(A_{k^*}^{i^*})$$

$$or \underset{k\to+\infty}{Lim}\, \varphi^{B_m^j,s_*} = l_r^{-k^*,s_*}(A_{k^*}^{i^*})$$

$$\Big(\underset{k\to+\infty}{Lim}\, l_l^{-k,s_*}(A_k^i) = \underset{k\to+\infty}{Lim}\, l_r^{-k,s_*}(A_k^i) = l_l^{-k^*,s_*}(A_{k^*}^{i^*})$$

$$or \underset{k\to+\infty}{Lim}\, \varphi^{B_m^j,s_*} = l_l^{-k^*,s_*}(A_{k^*}^{i^*})\Big).$$

Results of Corollaries 7.20 and 7.21 make it possible to explain the term "maximal wedge-shaped domain." First, every maximal wedge-shaped domain is a connected component of the set $\widetilde{G}$. Second, in every neighborhood of an arbitrary maximal wedge-shaped domain (in G_Δ), there are the points, which belong to the stable manifold of the saddle A_1; at the same time by claim 4 of Proposition 7.1 and Definitions 7.3, 7.5 every point from the interior of a maximal wedge-shaped domain tends to $+\infty$ by coordinates.

Corollary 7.22 *The set of arcs*

$$\{l_l^{0,s_*}(A_2), l_r^{0,s_*}(A_2), l_l^{-k,s_*}(A_k^i),\ l_r^{-k,s_*}(A_k^i)\}$$

is dense in itself in the space $2^{\Gamma_{s_*}}$ *and is contained in the closure (with respect to Hausdorff metric* $dist$ *in the space* $2^{\Gamma_{s_*}}$*) of the set*

$$\{\{\varphi^{B_m^j,s_*}\}_{m\geq 1, j\in\{1,\dots,2^m-1\}}, \varphi_{0,s},\ \varphi_{s,0},\}_{s\in[0,s_*]}.$$

By Corollaries 7.18 and 7.22, the closure of the set

$$\{l_l^{0,s_*}(A_2), l_r^{0,s_*}(A_2), l_l^{-k,s_*}(A_k^i),\ l_r^{-k,s_*}(A_k^i)\}$$

coincides with the closure of the set

$$\{\{\varphi^{B_m^j,s_*}\}_{m\geq 1, j\in\{1,\dots,2^m-1\}}, \varphi_{0,s},\ \varphi_{s,0},\}_{s\in[0,s_*]}$$

(with respect to Hausdorff metric $dist$ in the space $2^{\Gamma_{s_*}}$).

Corollary 7.23 *The closure of the set of points of the curves*

$$\{l_l^0(A_2), l_r^0(A_2), l_l^{-k}(A_k^i), l_r^{-k}(A_k^i)\}_{k\geq 1, i\in\{1,\dots,2^k-1\}}$$

(of the curves $\{\{\varphi^{B_m^j}\}_{m\geq 1,\ j\in\{1,\dots,2^m-1\}},\ \varphi_{0,s},\ \varphi_{s,0}\}$*) is perfect nowhere dense subset of* G_Δ.

The curves

$$\{l_l^0(A_2), l_r^0(A_2), l_l^{-k}(A_k^i), l_r^{-k}(A_k^i)\}$$

and the rays $\{x = 0, y \geq 4\}$, $\{y = 0, x \geq 4\}$ are said to be *one-sided curves*.

4. Let us prove that the space $2^{\Gamma_{s_*}}$ with Hausdorff metric $dist$ is the complete metric space, i.e., we should prove, using Corollary 7.22, that the topological limit of a convergent sequence of continuous arcs from the set

$$\{l_l^{0,s_*}(A_2), l_r^{0,s_*}(A_2), l_l^{-k,s_*}(A_k^i), l_r^{-k,s_*}(A_k^i)\}$$

is a continuous parametrized curve.

Lemma 7.8 *The space* $2^{\Gamma_{s_*}}$ *with Hausdorff metric* $dist$ *is the complete metric space.*

Proof 1. Let a sequence of the closed arcs $\{l_r^{-k,s_*}(A_k^i)\}_{k\geq 1}$ be fundamental in the space $2^{\Gamma_{s_*}}$ and such that the sequence of the initial points $\{A_k^i\}_{k\geq 1}$ of these arcs converges to a point $(x^*; y^*) \in h\backslash\{A_2, A_1, \{A_k^i\}_{k\geq 1}, \{B_m^j\}_{m\geq 1}\}$. Then, first, there is the topological limit of this sequence, which is a compact subset of the set G_Δ; and, second, for any $\varepsilon > 0$ there exists a natural number $k_0 \geq 1$ such that for any natural numbers $k, q \geq k_0$ the inequality

$$dist\ (l_r^{-k,s_*}(A_k^{i(k)}), l_r^{-q,s_*}(A_q^{i(q)})) < \varepsilon \tag{7.28}$$

holds.

Let c be an arbitrary number satisfying the inequality $c > 4$, and such that the straight line $x+y=c$ intersects every arc of the set $\{l_r^{-k,s_*}(A_k^i)\}_{k\geq 1}$. By Corollary 7.12 and formula (7.6), the straight line $x+y=c$ has the unique common point with every arc $l_r^{-k,s_*}(A_k^i)$ $(k \geq 1)$. Denote this point of intersection by $C(l_r^{-k,s_*}(A_k^i))$. By the inequality (7.28), the sequence of points $\{C(l_r^{-k,s_*}(A_k^i))\}_{k\geq 1}$ is fundamental. Hence, this sequence converges on the straight line $x+y=c$ to the unique point $C^*(c)$.

2. Closed arcs $l_r^{-k,s_*}(A_k^i)$ $(k \geq 1)$ are subcontinua of the compact subset of the set G_Δ such that their low topological limit $\underset{k\to+\infty}{Li}\, l_r^{-k,s_*}(A_k^i)$ coincides with their topological limit and, hence, the low topological limit of the sequence of these arcs is not empty. Then, using [33] we obtain from here that their upper topological limit $\underset{k\to+\infty}{Ls}\, l_r^{-k,s_*}(A_k^i)$, which coincides with the topological limit of the sequence of these arcs, is the continuum, i.e., a compact connected Hausdorff space [33].

By item 1 of this proof the above continuum L has the unique common point $C^*(c)$ with every straight line $x+y=c$. It means that with the use of straight lines $x+y=c$, we obtain homeomorphic correspondence between L and an arbitrary arc $l_r^{-k,s_*}(A_k^i)$. Thus, L is the one-dimensional continuum, i.e., the topological limit L of the sequence of arcs $\{l_r^{-k,s_*}(A_k^i)\}_{k\geq 1}$ is the continuous curve (see [33]). It implies that L is the continuous image of an interval.

3. The result of previous item 2 makes it possible to apply fundamental Hahn–Mazurkiewizc–Sierpinski theorem (see [33]). By this theorem, L is the locally connected curve. Hence, for every $\varepsilon' > 0$, there exists a distribution of L onto a finite number of arcs with lengths $< \varepsilon'$. Thus, L is the measurable arc. It means that L admits parametrization with the use of natural parameter.

Completeness of the space $2^{\Gamma_{s_*}}$ is established. Lemma 7.8 is proved. □

Let $c > 4$ be an arbitrary number. Using Corollary 7.22, Lemma 7.8, and criterion for a perfect bounded set on the straight line [40], we obtain the following statement.

Corollary 7.24 *The set of the intersection points of the straight line $x+y=c$ with the closure of the set of points of the curves $l_l^0(A_2), l_r^0(A_2), l_l^{-k}(A_k^i), l_r^{-k}(A_k^i)$ $(k \geq 1)$ is perfect nowhere dense subset of the segment of the straight line $x+y=c$ between the points $(0; c)$ and $(c; 0)$ of continuum cardinality.*

Intervals of intersection of interiors of maximal wedge-shaped domains with the straight line $x+y=c$ are the complement intervals for the above perfect nowhere dense set; moreover, the points of intersection of the straight line $x+y=c$ with the curves $l_l^0(A_2), l_r^0(A_2), l_l^{-k}(A_k^i), l_r^{-k}(A_k^i)$ $(k \geq 1)$ are the boundary points of complement intervals (i.e., one-sided points of the perfect nowhere dense set).

The following important result is the direct corollary of the above Lemma 7.8, Theorem 7.6, Definitions 7.3, 7.5, and Corollaries 7.22, 7.24.

Theorem 7.7 *The closure of the set of points belonging to the curves of the family $\{l_l^0(A_2), l_r^0(A_2), l_l^{-k}(A_k^i), l_r^{-k}(A_k^i)\}$ is F-completely invariant, consists of curves, which are elements of the set of the continuum cardinality and start from every point of the hypotenuse h.*

Moreover, a unique double-sided curve starts from every point of the set $h\backslash\{A_1, (4; 0), A_2, A_k^i\}_{k\geq 1}$*; the unique one-sided curve (the part of the axes* Oy *in* G_Δ*) starts from the point* A_1*, the unique one-sided curve (the part of the axes* Ox *in* G_Δ*) starts from the point* $(4; 0)$*, a pair of one-sided curves starts from every point of the set* $\{A_2, A_k^i\}_{k\geq 1}$ *such that these curves form the boundary of the maximal wedge-shaped domain with the vertex in this point.*

Every two curves of the closure of the set of points belonging to the curves of the family $\{l_l^0(A_2), l_r^0(A_2), l_l^{-k}(A_k^i), l_r^{-k}(A_k^i)\}$ *do not intersect each other in the set* G_Δ°.

Corollary 7.25 *The set* $\widetilde{G}$ *is open and everywhere dense in* G_Δ.

Corollary 7.26 *The perfect nowhere dense in* G_Δ *set* $G' = G_\Delta\backslash\widetilde{G}$ *is the union of unbounded curves such that* $G' \cap G_\Delta^\circ$ *is* F*-completely invariant local lamination of codimension 1 in the set* G_Δ°*; in addition, the set of algebraic curves is everywhere dense in* G'.

Lemma 7.9 *The set* $\widetilde{G}$ *consists of* F*-wandering points.*

Proof By Corollary 7.4 and Lemma 7.2, the limit equalities

$$\lim_{n\to} f_n(x, y) = +\infty, \lim_{n\to} g_n(x, y) = +\infty. \tag{7.29}$$

are valid for every point $(x; y) \in \widetilde{G}$.

Since the fixed point A_2 is the source of F, then an arbitrary neighborhood $U(A_2)$ possesses the property:

$$H_0^{max}(A_2)\cap U(A_2) \subset F(H_0^{max}(A_2)\cap U(A_2)) \subset \ldots \subset F^n(H_0^{max}(A_2)\cap U(A_2)) \subset \ldots,$$

moreover, by equalities (7.29), the sets $\{F^n(H_0^{max}(A_2) \cap U(A_2))\}_{n\geq 0}$ form the exhaustion of $H_0^{max}(A_2)$, i.e.,

$$H_0^{max}(A_2) = \bigcup_{n=0}^{+\infty} F^n(H_0^{max}(A_2) \cap U(A_2)). \tag{7.30}$$

Let $(x^0; y^0)$ be an arbitrary point of $int\, H_0^{max}(A_2)$. Separate the points A_2 and $(x^0;\ y^0)$ by neighborhoods $U(A_2)$ and $U((x^0;\ y^0)) \subset int\, H_0^{max}(A_2)$ such that

$$\overline{U}(A_2) \bigcap \overline{U}((x^0; y^0)) = \emptyset. \tag{7.31}$$

By the equality (7.30), there exists a natural number $n_0 \geq 1$ such that

$$U((x^0; y^0)) \subset F^{n_0}(H_0^{max}(A_2) \cap U(A_2)).$$

By this inclusion and the equality (7.31), the equality

$$U((x^0; y^0)) \bigcap (F|_{H_0^{max}(A_2)})^{-n}(U((x^0; y^0))) = \emptyset \tag{7.32}$$

is valid for every $n \geq n_0$. The equality (7.32) means that the point $(x^0; y^0)$ is a wandering point of F. Hence, $int\, H_0^{max}(A_2)$ consists of F-wandering points. Using

Definition 7.5, we obtain from here that $int H_k^{max}(A_k^{i(k)})$ consists of F-wandering points for every $k \geq 1$. Then, using Lemma 7.2 we obtain from the above that the set $\widetilde{G}$ consists of F-wandering points. Lemma 7.9 is proved. □

Thus, Theorem 7.7, Lemma 7.9, and Corollaries 7.25, 7.26 prove the main Theorem 7.3 of this chapter. □

7.5 Concluding Remarks: Saddle Periodic Points of the Map F

We prove here the existence of saddle F-periodic points different from $A_1(0;4)$ on the hypotenuse h of the invariant triangle Δ.

Proposition 7.2 *There exists the set $C^* \subset h$ possessing the properties*

1. *C^* is homeomorphic to Cantor discontinuum*
2. *There are natural numbers $m^*, n^* \geq 1$ such that $C^* = F^{m^*+n^*}(C^*)$*
3. *Saddle F-periodic points, homoclinic points for saddle F-periodic points, and recurrent nonperiodic points are everywhere dense in C^*.*

Proof 1. The equality $det\, J(F(x,y)) = 2x(2-x)$ is valid for Jacobian of the map F. The inequality $|2x^2 - 4x| \leq 1$ is fulfilled on the closed intervals $[0, \frac{2-\sqrt{2}}{2}]$ and $[\frac{2+\sqrt{2}}{2}, \frac{2+\sqrt{6}}{2}]$. In addition, the equality $|det\, J(F(x,y))| = 1$ is correct for $x = \frac{2\pm\sqrt{2}}{2}$, $x = \frac{2+\sqrt{6}}{2}$. Denote by $I_1^{''}$, $I_1^{''} \subset h$, the closed interval corresponding $[0, \frac{2-\sqrt{2}}{2}]$ and by $I_2^{''}$, $I_2^{''} \subset h$, the closed interval corresponding $[\frac{2+\sqrt{2}}{2}, \frac{2+\sqrt{6}}{2}]$.

By claim 7 of Proposition 7.1 for every segment $I_1^{''}$ and $I_2^{''}$, there are natural numbers $n^*(I_1^{''})$ and $n^*(I_2^{''})$ such that

$$(F|_h)^{n^*(I_1^{''})}(I_1^{''}) = (F|_h)^{n^*(I_2^{''})}(I_2^{''}) = h.$$

Set $n^* = \mathrm{LCM}(n^*(I_1^{''}), n^*(I_2^{''}))$ (where $\mathrm{LCM}(\cdot)$ is the least common multiple of numbers). Then, there exist subintervals $I_1^{'} \subset I_1^{''}$, $I_2^{'} \subset I_2^{''}$ such that

$$(F|_h)^{n^*}(I_1^{'}) = (F|_h)^{n^*}(I_2^{'}) = [A_1; E^*], \tag{7.33}$$

where $E^* = (\frac{2+\sqrt{6}}{2}; 3 - \frac{\sqrt{6}}{2})$ is the right boundary point of the segment $I_2^{'}$, saddle F-fixed point $A_1(0;4)$ is the left boundary point of the segment $I_1^{'}$. Let us note that $I_1^{'} \cap I_2^{'} = \emptyset$. Since the point $A_1(0;4)$ is the source of the restriction $F|_h$ (see claims 6 and 7 of Proposition 7.1), there are the segment $I^* \subset I_1^{'}$ ($A_1(0;4)$ is the left boundary point of I^*) and the natural number m^* so large that $(F|_h)^{m^*}(I^*) = I_1^{'}$, and

$$|det\, J((F|_{I^*})^{m^*+n^*})| \leq 1. \tag{7.34}$$

By formula (7.33) the equality $(F|_h)^{m^*+n^*}(I^*) = [A_1, E^*]$ holds. Hence, there are disjoint segments $I_1, I_2 \subset I^*$ (A_1 is the left boundary point of I_1) such that

$$(F|_h)^{m^*+n^*}(I_1) = (F|_h)^{m^*+n^*}(I_2) = I^*.$$

In addition, by formula (7.34) the inequality $|det J((F|_{I_{i_1}})^{m^*+n^*})| \leq 1$ is valid for $i_1 \in \{1, 2\}$. Using mathematical induction principle, we construct pairwise disjoint segments $I_{i_1 \dots i_{q-1} i_q} \subset I_{i_1 \dots i_{q-1}}$ ($q \geq 2$, $i_1, \dots, 2$}) satisfying the equality $(F|_h)^{n^*+m^*}(I_{i_1 \dots i_q}) = I_{i_1 \dots i_{q-1}}$. Then, the equality

$$\lim_{q \mapsto +\infty} l(I_{i_1 \dots i_q}) = 0 \tag{7.35}$$

follows immediately from claim 7 of Proposition 7.1 (here $l(\cdot)$ is the length of a segment). By equality (7.35) the set $C^* = \bigcap_{q=1}^{+\infty} \bigcup_{i_1, \dots, i_q \in \{1,2\}} I_{i_1 \dots i_q}$ is homeomorphic to Cantor discontinuum and

$$|det J(F|_{C^*})^{m^*+n^*}| \leq 1. \tag{7.36}$$

By the properties of closed intervals $I_{i_1 \dots i_q}$ and definition of the set C^*, the equality $F^{m^*+n^*}(C^*) = C^*$ is valid.

2. Saddle periodic points are everywhere dense in C^* (see claim 6 of Proposition 7.1 and inequality (7.36)). By claim 7 of Proposition 7.1, $F_{|C^*}$-homoclinic points for saddle periodic points of C^* are everywhere dense in C^*. The horseshoe C^* has continuum cardinality, and recurrent nonperiodic points are everywhere dense in C^*. Proposition 7.2 is proved. □

Let us set $C = \bigcup_{i=0}^{m^*+n^*-1} F^i(C^*)$.

Corollary 7.27 *The sets $C^s = \bigcup_{i=0}^{+\infty} F^{-i}(C)$ and $C^u = h \backslash C^s$ are everywhere dense in h; in addition, sources of F, $F_{|h}$-homoclinic points for sources of F and $F_{|h}$-transitive points are everywhere dense in the set C^u.*

Corollary 7.27 and Theorem 7.3 imply the following unusual property of the fibers of the local lamination in the set G°_Δ.

Proposition 7.3 *Fibers over the points of the set C^s just as over the points of the set C^u are everywhere dense in the set of all fibers of the local lamination in the set G°_Δ.*

Let us note that Proposition 7.3 generalizes the claims of Corollaries 7.18 and 7.22.

Acknowledgments We address our deep acknowledgment to the Seminar "Ergodic Theory and Dynamical Systems" under the supervision of Academician D. V. Anosov and Professor A. M. Stepin where this research was presented. We thank Professor E. A. Sataev for helpful discussion of geometry of boundaries of maximal wedge-shaped domains. We are thankful to the referees for their useful remarks and comments, which promoted improving of the paper writing.

This investigation is supported in the part by Education and Science Ministry of Russia (grant No 14-10).

References

1. Birkhoff, G.: Dynamical Systems. OGIZ State Publishing House of Engineering and Theoretical Literature, moscow-leningrad (1941) [in Russian]
2. Suris, Yu.B.: On the integrable maps of the type of the standard map. Func. Anal. Appl. **23**(1), 84–85 (1989) [in Russian]
3. Veselov, A.P.: Integrable maps. Russ. Math. Surv. **46**(1), 1–51 (1991)
4. Grigorchuk, R.I., Žuk, A.: The Lamplighter group as a group generated by a 2-state automata, and its spectrum. Geom. Dedic. **87**, 209–244 (2001)
5. Avishai, Y., Berend, D.: Transmission through a one-dimensional Fibonacci sequence of δ-function potentials. Phys. Rev. B **41**(9), 5492–5499 (1990)
6. Avishai, Y., Berend, D.: Transmission through a Fibonacci chain. Phys. Rev. B **43**(9), 6873–6879 (1991)
7. Avishai, Y., Berend, D.: Transmission through a Thue–Morse chain. Phys. Rev. B **45**, 2717–2724 (1992)
8. Avishai, Y., Berend, D., Tkachenko, V.: Trace maps. Int. J. Mod. Phys. B **11**(30), 3525–3542 (1997)
9. Bellisard, J.: Spectral properties of Schrödinger's operator with a Thue-Morse potential. Number Theory and Phisics(Les Houches, 1989), Springer Proceedings in Physics, Springer, no 47, 140–150 (1990)
10. Bellisard, J., Bovier, A., Ghez, J.-M.: Gap labelling theorems for one-dimensional discrete Schrödinger operators. Rev. Math. Phys. **4**, 1–37 (1992)
11. Baake, M., Grimm, U., Joseph, D.: Trace maps, invariants, and some of their applications. Int. J. Mod. Phys. **B 7**, 1527–1550 (1993)
12. Baake, M., Roberts, J.: The dynamics of trace maps in hamiltonian mechanics (Torun, 1993) NATO Adv. Sci. Inst. Ser. B Phys., Plenum, N.Y., vol. 331, 275–285 (1994)
13. Damanik, D., Gorodetski, A.: Hyperbolicity of the trace map for the weakly coupled Fibonacci hamiltonian. Nonlinearity **22**, 123–143 (2009)
14. Damanik, D., Gorodetski, A.: The spectrum of the weakly coupled Fibbonacci hamiltonian. Electron. Res. Announc. Math. Sci. **16**, 23–29 (2009)
15. Belmesova, S.S., Efremova, L.S.: On unbounded trajectories of a certain quadratic mapping of the plane. J. Math. Sci. (N.Y.) **157**(3), 433–441 (2009).
16. Belmesova, S.S., Efremova, L.S.: On quadratic maps of the one-parameter family, closed to the unperturbed map. Proc. MIPT **2**(2), 46–57 (2010) [in Russian]
17. Belmesova, S.S., Efremova, L.S.: On invariant sets of some quadratic maps of the plane. Vestn. NNGU **2**(2), 152–158 (2012) [in Russian]
18. Belmesova, S.S., Efremova, L.S.: A one-parameter family of quadratic maps of a plane including Morse–Smale endomorphisms. Russ. Math. **57**(8), 70–74 (2013)
19. Belmesova, S.S., Efremova, L.S., Fournier-Prunaret, D.: Invariant curves of quadratic maps of the plane from the one-parameter family containing the trace map. ESAIM: Proceedings and surveys. **76**, 98–110 (2014)
20. Świrszcz, G.: On a certain map of a triangle. Fundam. Math. **155**, 45–57 (1998)
21. Balibrea, F., Guirao, J.G., Lampart, M., Llibre, J.: Dynamics of a Lotka–Volterra map. Fundam. Math. **191**, 265–279 (2006)
22. Guirao, J.G., Lampart, M.: Transitivity of Lotka–Volterra map. Discret. Contin Dyn. Syst. Ser. B **9**(1), 75–82 (2008)
23. Maličky, P.: Interior periodic points of a Lotka—Volterra map. J. Differ. Equ. Appl. **18**(4), 553–567 (2012)
24. Sharkovskii, A.N.: Problem list. "International Conference on & Low Dimensional Dynamics" (Oberwolfach, Germany, April 25–May 1 1993), Tagungsbericht, 17, (1993)
25. Katok, A., Hasselblatt, B.: Introduction to the Modern Theory of Dynamical Systems, Encyclopedia of Mathematics and its Applications, vol. 54. Cambridge University Press, Cambridge (1995)

26. Thurston, W.P.: Three Dimensional Geometry and Topology, vol. 1. Princeton University Press, Princeton (1997) (Princeton Mathematical Series; vol. 35)
27. Anosov, D.V., Zhuzhoma, Y.V.: Nonlocal asymptotic behavior of curves and leaves of laminations on universal coverings. Proc. Steklov Inst. Math. **249**, 1–221, (2005)
28. Friedland, S., Milnor, J.: Dynamical properties of plane polynomial automorphisms. Ergod. Theory Dyn. Syst. **9**, 67–99, (1989)
29. Li, M.-C., Malkin, M.: Bounded nonwandering sets for polynomial mappings. J. Dyn. Control Syst. **10**(3), 377–389, (2004)
30. Sukhinin, M.F.: Selected Chapters of Nonlinear Analysis. People Friendship University Press, Moscow, (1992) [in Russian]
31. Efremova, L.S.: Differential properties and attracting sets of a simplest skew product of interval maps. Sb. Math. **201**(6), 873–907 (2010)
32. Efremova, L.S.: Remarks on the Nonwandering Set of Skew Products with a Closed Set of Periodic Points of the Quotient Map. Nonlinear Maps and their Applications. Springer Proceedings in Mathematics and Statistics, Springer New York, vol. 57, 39-58 (2014).
33. Kuratowski, K.: Topology. Academic Press, New York (1966)
34. Denjoy, A.: Sur les courbes definies par les equations differentielles a la surface du tore. J. Math. Pures Appl. **11**(9), 333–375 (1932)
35. Denjoy, A.: Les trajectories a la surface du tore. C.R. Acad. Sci. **223**, 5–8 (1946)
36. Denjoy, A.: Theorie des fonctions sur les characteristiques a la surface du tore. C.R. Acad. Sci. **194**, 830–833 (1932)
37. Block, L.: Homoclinic points of mapping of the interval. Proc. Am. Math. Soc. **72**(3), 576 – 580 (1978)
38. Zorich, V.A.: Mathematical Analysis, vol. 1, Universitext, Springer-Verlag, Berlin, (2004)
39. Erugin, N.P.: Implicit Functions. Leningrad University Press, Leningrad (1956) [in Russian]
40. Natanson, I.P.: Theory of Functions of a Real Variable. Ungar Publication, New York (1955)

Chapter 8
Discrete Maps and the Problem of Round Trip Time Scale Nonlinear Dynamics in Solid-State Lasers

M. V. Gorbunkov, Yu. Ya. Maslova, V. A. Petukhov, M. A. Semenov and Yu. V. Shabalin

Abstract We show numerically and analytically that the control based on the combination of optoelectronic negative and positive feedback loops allows one to obtain new time scale nonlinear dynamics regimes in solid-state lasers. The combination of feedbacks enables the realization of nonlinear dynamics of the logistic map. In lasers with external harmonic modulation of losses the combination of positive and negative feedback loops makes it possible to obtain period doubling bifurcation at the time scale in the range of few up to hundreds laser-cavity round trip times.

8.1 Introduction

Lasers, including class B, are a well-known object of nonlinear dynamics in optical range [2, 6, 8, 13, 17]. Our investigation is based on the analysis of various discrete maps and examination of laser generation regimes with ordered radiation fine time structure (the time structure at a time scale of less than a cavity round trip time). The approach gives ability to take a fresh look at the problem of nonlinear dynamics in solid-state lasers. The main idea of this work is to show how the control based on the combination of two feedback loops gives a solution to the problem of laser-cavity round trip time scale nonlinear dynamics. In this work, we assume that feedback is sensitive enough to minimize saturation of active medium. Section 8.2 focuses on the realization of nonlinear dynamics of the logistic map by using the memory-erasing method. In Sect 8.3 we analyze the dynamics of systems with external harmonic loss modulation and two feedback control.

M. V. Gorbunkov (✉) · Yu. Ya. Maslova · V. A. Petukhov · M. A. Semenov · Yu. V. Shabalin
P. N. Lebedev Physics Institute, Leninskii prospect 53, 119991 Moscow, Russia
e-mail: gorbunk@sci.lebedev.ru

Yu. Ya. Maslova
e-mail: jmaslova@mail.ru

R. López-Ruiz et al. (eds.), *Nonlinear Maps and their Applications,*
Springer Proceedings in Mathematics & Statistics 112, DOI 10.1007/978-3-319-12328-8_8

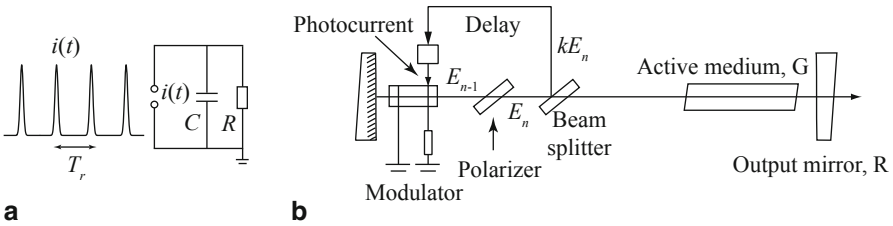

Fig. 8.1 *RC* circuit (**a**) and the simplified scheme of the laser with the optoelectronic modulator (**b**). k is a fraction of radiation which is reflected to the feedback system, E_n is non-normalized pulse energy at the kth pass. The number of pass is incremented when the light pulse passes through the polarizer and thus loses some energy

8.2 Nonlinear Dynamics in the Memory-Erasing Regime

Systems with controlled chaotic dynamics find increasing applications in science and engineering. New methods of cryptography and wideband communication require fast, simple, and reliable chaotic generators to be developed [4, 16, 20]. In optical region, such a generator could be realized in a solid-state laser controlled by feedback. Chaotic dynamics of the logistic map seems to be attractive for this reason. The dynamics closest to that one may be expected in a mode-locked laser when a single laser pulse circulates in a laser cavity. In such a case, if a negative feedback is fast and memoryless, the energy of a pulse x normalized to the feedback sensitivity is defined by the recurrence equation, also known as the logistic map [3, 7]:

$$x_{n+1} = r x_n (1 - x_n), \tag{8.1}$$

where x_{n+1} is the pulse energy at the $(n + 1)$th pass, x_n is the pulse energy at the nth pass, r is the overall gain normalized to the threshold value, and the term in parentheses represents the one-pass delayed feedback loop action. We say that feedback is fast if the intrinsic delay of the feedback is short enough to control pulse energy on the next pass.

Ultrashort-pulse lasers and methods of mode locking have been and remain a subject of investigation in a field of laser physics [15]. It was shown in [18] that a laser can be self mode-locked by the inertial (opposite to memoryless) negative feedback which acts with a certain delay. An example of a laser controlled by a negative feedback loop based on an intracavity optoelectronic modulator is schematically presented in Fig. 8.1. The optoelectronic modulator based on Pockels cell is controlled by the photocurrent generated by the light deflected to the feedback loop with a splitter. In the simplest case, electric circuit is formed by the modulator capacity C and the resistor R. The characteristic time of the control circuit is $\tau = RC$. The importance of the feedback delay for the self-mode-locking regime is illustrated in Fig. 8.2. Suppose that a single and short enough laser pulse has been formed and circulates in a laser cavity, and the cavity round trip time is T_r. The sequence of ultrashort pulses would generate photocurrent pulses with period T_r (we assume here

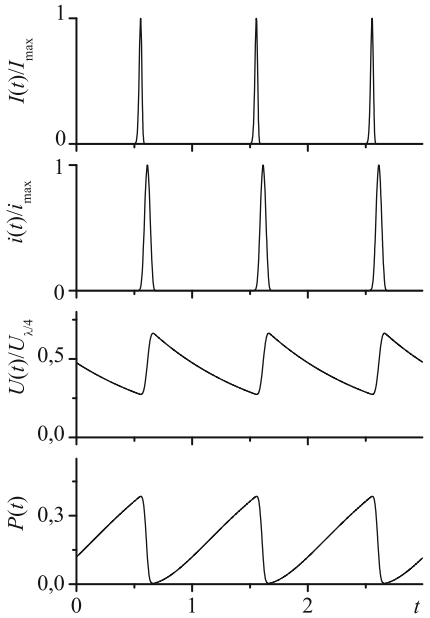

Fig. 8.2 Temporal variations of laser intensity $I(t)$, photocurrent $i(t)$, modulator control voltage $U(t)$, and modulator transmission $P(t)$. Time is normalized to T_r

that the duration of a laser pulse τ_l and the response time of the photocell τ_{ph} are connected by the relation $\tau_l < \tau_{ph} \ll T_r$). In its turn, the sequence of photocurrent pulses, when fed to the RC circuit input, forms on the capacity C sawtooth voltage with a short front (determined by the photocurrent pulse duration) and a long tail (determined by the RC circuit time constant τ).

The sawtooth voltage has maximum and minimum values U_{max} and U_{min}, that are related by the feedback memory

$$U_{min} = U_{max} e^{-T_r/RC}. \tag{8.2}$$

The Pockels cell transmission is

$$P = \cos^2\left(\frac{\pi}{2} \cdot \frac{U + U_0}{U_{\lambda/4}}\right), \tag{8.3}$$

where U_0 is the initial static bias voltage, U is the voltage generated by the optical signal, $U_{\lambda/4}$ is the voltage needed to turn off the cell (see Fig. 8.1). If the control is designed on the principle of negative feedback, then with the increase of the laser intensity the control voltage increases and the modulator transmission decreases. To realize the regime of self-mode-locking, it is necessary that photocurrent pulses have a delay that corresponds to the laser pulse's passage through the modulator at the moment of maximum transmission. The regime of self-mode-locking occurs in a number of regions of optical signal delay time. The first region corresponds to

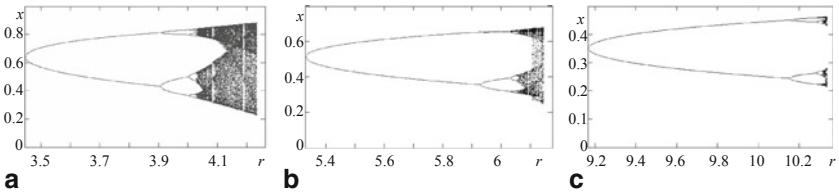

Fig. 8.3 Parts of bifurcation diagrams of system with memory (8.4) that correspond to the nonlinear dynamics: **a** $\tau = 0.43T_r$, **b** $\tau = T_r$, **c** $\tau = 2T_r$

the minimal delay of the control action. In this case, the control pulse turns off the Pockels cell, and the laser pulse passes through it at the moment of nearly maximum transmission. The transmission of the cell in the moment of the pulse passage is determined by the pulse energy and by the energy of pulses on the previous round trips taking into account the discharge of the capacity C. This case corresponds to the recurrence relation [9]:

$$x_{n+1} = rx_n\left(1 - \sum_{m=0}^{\infty} x_{n-m}\gamma^m\right), \tag{8.4}$$

where $\gamma = e^{-T_r/\tau}$. A good example of such a system with minimal delay is the optoelectronically controlled solid-state laser in which the intracavity Pockels cell is controlled by the photocurrent generated by high voltage subnanosecond semiconductor structures [21]. In the case of mode-locking, $(1–2)T_r$ is the optimal value of the discharge time τ for the generation of self-sustained single on the axial interval pulses with minimal duration [9, 22].

Bifurcation diagrams of map presented in Fig. 8.3 show the dynamics of system with memory (8.4). Even at $\gamma = 0.1$ ($\tau = 0.43T_r$) the periodic window (superstable cycle) with period of $3T_r$, which occurs in map (8.1) at $r > 1+\sqrt{8} \approx 3.83$, vanishes. As γ is further increased, the dynamics of the system becomes less rich. Bifurcation diagrams shown in Fig. 8.3b and c correspond to the values of $\tau = T_r$ and $\tau = 2T_r$.

Nonlinear dynamics of the logistic map can be obtained in the system controlled by a combination of two feedback loops: the negative feedback and the positive feedback delayed by ΔT with respect to the negative one. The relative feedback sensitivity α is adjusted to compensate the residual control effect (after the relative delay time) of the negative feedback. Such a control design results in the memory erasing. A discrete map that corresponds to the combination of the negative and the positive feedback, where the delay of negative one is minimum, and $\Delta T = T_r$, is

$$x_{n+1} = rx_n\left(1 - \sum_{m=0}^{\infty} x_{n-m}\gamma^m + \alpha\sum_{m=0}^{\infty} x_{n-m-1}\gamma^m\right) \tag{8.5}$$

If $\alpha = \gamma$ the sums almost cancel out and map (8.5) is reduced exactly to map (8.1). Nevertheless, the temporal variation of modulator transmission remains similar to the behaviour transmission in Fig. 8.2, which allows one to lock modes (i.e., to generate ultrashort laser pulses) by means of optoelectronic feedback itself. Therefore,

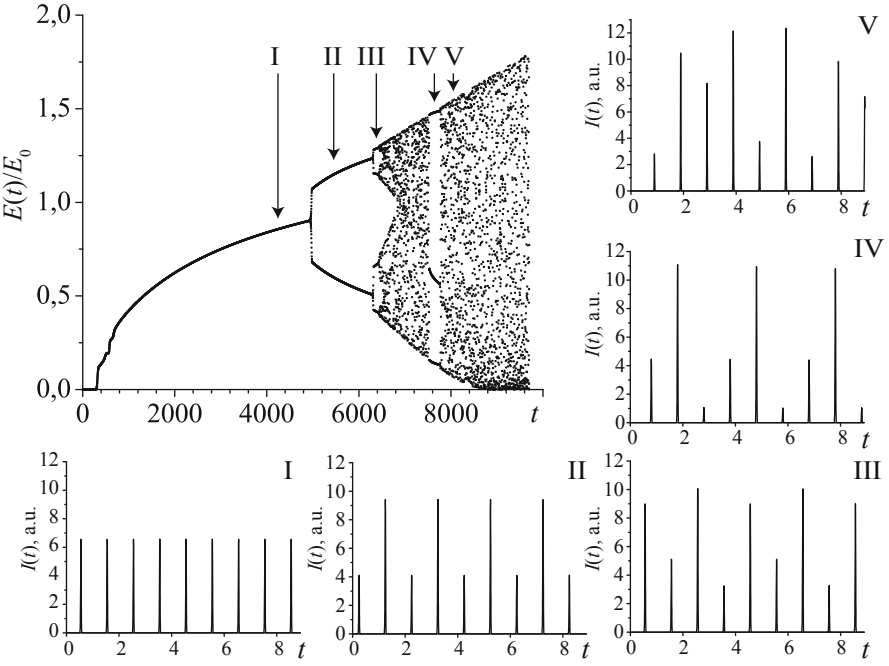

Fig. 8.4 Results of high-resolution numerical simulation of the laser system with "memory erasing" in self-mode-locking regime. Main plot: energy of short laser pulses E versus time t (in units of T_r). The gain r is linearly changed from 1 to 5.5 with the cavity round trip number; the total number of cavity round trips is $n = 10,000$. Insets I–V: laser output intensity $I(t)$ at different gain levels, see text

the modification of control system up to the combination of negative and positive feedback allows to enrich the laser dynamics.

The regimes of memory erasing were reproduced in numerical simulation when the laser output radiation fine time structure evolution was taken into account (Fig. 8.4). We followed the approach described in [9, 22]. It allows us to trace the development of radiation fine time structure with resolution much less than T_r taking into account finite amplification linewidth of active medium and spontaneous emission noise. The model is based on successive (round trip by round trip) calculation of the laser intensity, the photocurrent, the voltage on capacitor C, and the Pockels cell losses. The following parameters were used in the simulation: cavity round trip time $T_r = 10$ ns, passive losses $R = 50\%$, active medium linewidth 120 GHz (corresponds to Nd:YAG), shift voltage of negative feedback $U_0 = 0.3U_{\lambda/4}$, photocurrent response time for both feedback loops $\tau_{\text{ph}} = 500$ ps. Relative sensitivity of positive feedback in the memory-erasing regime was set according to the formula

$$\alpha = e^{-\Delta T/\tau}, \tag{8.6}$$

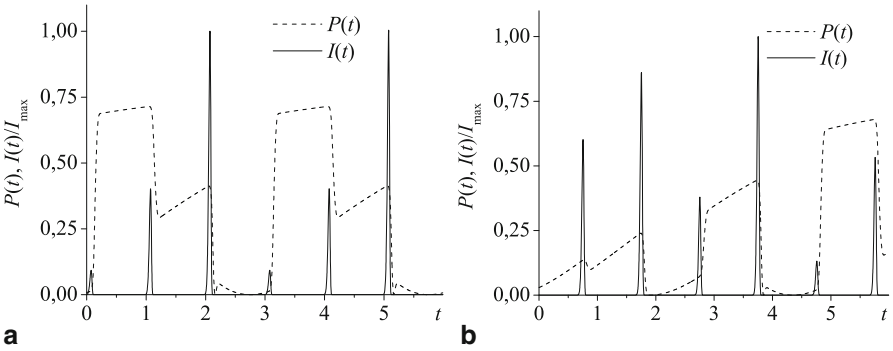

Fig. 8.5 Results of high-resolution numerical simulation: radiation fine time structure of the laser system with memory erasing in self-mode-locking regime. Temporal variation of laser intensity $I(t)$ and modulator transmission $P(t)$: **a** in the period $3T_r$ window; **b** in the intermittency region (at lower gain level). Time is normalized to T_r

where ΔT is the relative feedback delay, and $\tau = RC$ is the control circuit time constant. Spontaneous emission noise was placed in the laser cavity and being subsequently transformed. The process of a single short laser pulse development takes several hundreds of laser-cavity round trip times. The numerical simulation showed that in a solid-state laser, it is possible to organize the dynamics of the logistic map at the time scale of a round trip time. For example, the well-defined period doubling is observed which is followed by the chaotic dynamics, then the period $3T_r$ is formed after the intermittency regime, etc. Insets I–V in Fig. 8.4 demonstrate the radiation fine time structure in the typical regimes: I is a fixed point, II is the period doubling, III is the period quadrupling, IV is the dynamics in period $3T_r$ window, and V is deterministic chaos. The dynamics chaotization does not affect the mode locking regime when the gain is increased to $r = 4.5$. The modulator transmission in the regimes of period $3T_r$ and intermittency is shown in Fig. 8.5. In spite of local dramatic step-wise variation of the transmission, every jump occurs on the time scale of a cavity round trip and it should be noted that a single laser pulse exists in a laser cavity.

The locking of modes and a possibly short delay of negative feedback is important for the realization of the dynamics of the logistic map. If the positive feedback delay remains slightly larger than T_r while negative feedback is increased up to the value slightly less than T_r (this corresponds to the smoothing of laser radiation instead of short pulse generation), memory-erasing results in generation of a square envelope shown in Fig. 8.6b. Starting from weak harmonic modulation at $r = 3.63$, the envelope becomes square rapidly with the increase of gain (Fig. 8.6a). Period doubling cascade is not observed. The development of chaotic dynamics starts with high-frequency modulation (see Fig. 8.6c, d, and e).

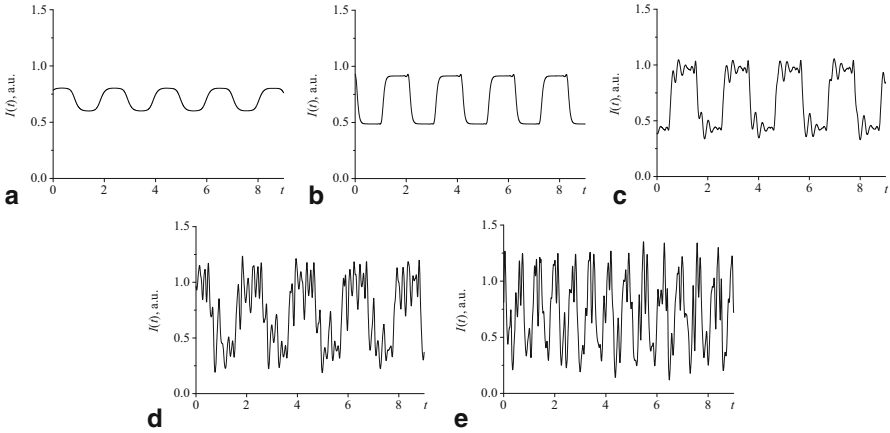

Fig. 8.6 Results of high-resolution numerical simulation: fine time structure of the output intensity of the laser system with memory erasing in "square wave" regime: **a** $r = 3.69$, **b** $r = 4$, **c** $r = 4.3$, **d** $r = 4.58$, **e** $r = 4.7$

8.3 Period Doubling in a Laser with Harmonic Loss Modulation Under Feedback Control

Nonlinear dynamics of class B lasers have been discussed since 1980's [1]. It was shown that the observation of period doubling bifurcation is realized under the condition of external loss modulation in the range close to relaxation oscillation frequency [23]:

$$\Omega_0 = \sqrt{\frac{\eta - 1}{T_1 t_c} - \left(\frac{\eta}{2T_1}\right)^2} \approx \sqrt{\frac{\eta - 1}{T_1 t_c}}, \tag{8.7}$$

where η is the ratio of unsaturated to saturated gain, t_c is the photon lifetime in the laser cavity, T_1 is the lifetime of the upper laser level. For example, the period doubling has been observed at 60 kHz [14] (corresponds to $2.5 \cdot 10^3$ of cavity round trip time T_r).

The regime of period doubling at frequencies substantially higher than Ω_0 can be observed if the laser control is based on the combination of feedbacks. In contrast to the previous section, we consider the case when positive feedback acts earlier than the negative one and the map that corresponds to the combination of feedback loops can be written as

$$x_{n+1} = r x_n \left(1 + \beta \sum_{m=i}^{\infty} x_{n-m} \gamma^{m-i} - \sum_{m=i+1}^{\infty} x_{n-m} \gamma^{m-i-1}\right), \tag{8.8}$$

where $i = 0, 1, 2 \ldots$ is the delay of positive feedback normalized by T_r, $\beta > 0$ is the relative sensitivity of positive feedback, γ is the damping coefficient. It has

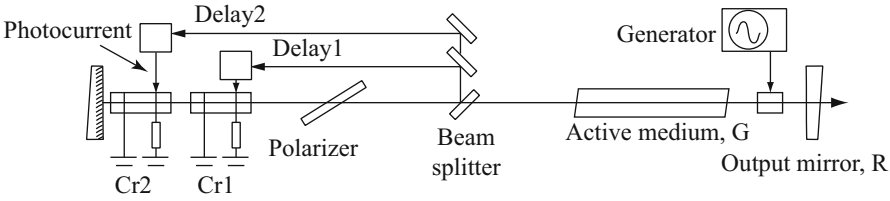

Fig. 8.7 A simplified scheme of the laser controlled by two feedback loops based on optoelectronic modulator (crystals Cr1 and Cr2). *R* accounts for passive losses, *G* is one-pass active medium gain coefficient

been shown [12] that the regular nonlinear dynamics in such self-mode-locked lasers looks like microtrains of pulses, and the period of microtrains increases dramatically when the relative sensitivity β tends to 1. The simplicity of map (8.8) allows us to determine easily typical periods of laser dynamics under the control based on the combination of feedbacks. In the case of noninertial feedback ($\gamma = 0$), the period of nonlinear dynamics (just after Neimark–Saker bifurcation when r is increased, over the boundary of stability region) can be approximated by [10]:

$$T = \frac{2\pi}{\sqrt{1-\beta}} - \frac{\pi\sqrt{1-\beta}}{12} + o(\sqrt{1-\beta}) \tag{8.9}$$

If feedback loops are inertial ($\gamma > 0$), period increases with γ. When $\beta \to 0$, period equals several tens of cavity round trip times (and depends on γ). Thus, by varying the relative sensitivity of feedback loops one can obtain intrinsic periods in the range of few up to hundreds laser cavity round trip times.

In the case of one memoryless feedback ($\gamma = 0$) which is delayed by k cavity round trip times:

$$x_{n+1} = r x_n (1 - x_{n-k}), \quad k = 1, 2, 3 \ldots \tag{8.10}$$

we have obtained an exact analytic formula for period T:

$$T = 4k + 2, \quad k = 1, 2, 3 \ldots \tag{8.11}$$

The period of harmonic modulation $6T_r$ ($k = 1$) could be reached in the case of $\beta = 0$ and $\gamma = 0$:

$$x_{n+1} = r x_n \, (1 - x_{n-1}) \tag{8.12}$$

To accomplish this experimentally in a real laser system, one needs to use the memory-erasing regime discussed in the previous section, but with delays increased by a cavity round trip time compared to logistic map case. Numeric calculation of dynamics of map (8.8) with $\gamma = 0$ and harmonic loss modulation has been performed using the following formula:

$$x_{n+1} = r\left(1 + \delta \sin\left(2\pi \frac{n}{N}\right)\right) x_n \, (1 + \beta x_n - x_{n-1}), \tag{8.13}$$

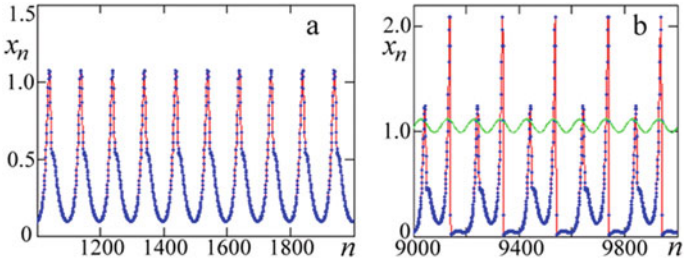

Fig. 8.8 Dynamics of map (8.13) at $\beta = 0.9$, $N = 100$, $\delta = 0.06$: **a** regular pulsation with period 100 at $r = 1.0385$; **b** period doubling at further r increase to 1.0485, the harmonic modulation of gain is shown for period doubling demonstration

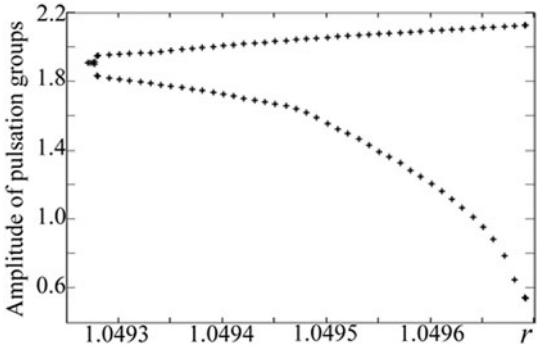

Fig. 8.9 Bifurcation diagram of map (8.13) at $\beta = 0.9$, $N = 100$, $\delta = 0.06$. The amplitudes of two pulsation groups are plotted versus gain r

where N is the modulation period and δ is the modulation depth. In such a system, nonlinear dynamics starts from sharpening of harmonic pulsation maxima, at larger values of gain r we observe an equidistant sequence of pulses with typical shape: on the body of pulsations there appear short peaks shifted to the rising front (Fig. 8.8a). A period doubling bifurcation results in generation of two groups of pulses of different form and amplitude (Fig. 8.8b). Increase of gain results in noticeable suppression of pulses of lower amplitude (Fig. 8.9).

The numeric calculation of the system dynamics at higher frequencies has showed that the period doubling bifurcation can be observed down to $N = 4$ (Fig. 8.10). The period introduced by the combination of feedback loops in such case has to be decreased to $6T_r$ (using $\beta = 0$). The calculations of the dynamics of simple maps prove that the period doubling is caused by the presence of two periods in the system: a period which is determined by the control scenario, and the external period of loss modulation. In this way the period which is introduced by the feedback control substitutes for the relaxation oscillation period.

Experimentally, the regime of period doubling at frequencies higher than Ω_0 was obtained in a self-mode-locked Nd:YAG laser controlled by the combination of

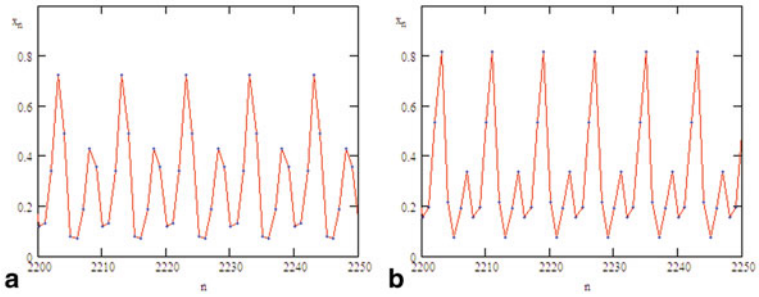

Fig. 8.10 Dynamics of map (8.13) at $\beta = 0$, $\delta = 0.7$: **a** $N = 5$, $r = 1.74$, **b** $N = 4$, $r = 1.9$

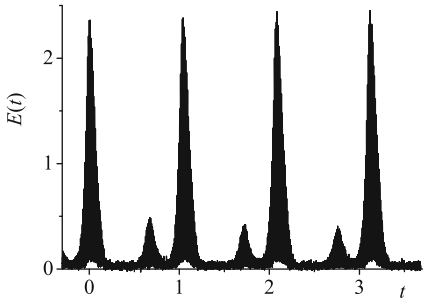

Fig. 8.11 Oscilloscope trace of period doubling bifurcation for the frequency corresponding to the 19th mode of shear vibration of DKDP crystal ($T = 0.52$ μs, $2T = 1.04$ μs, t is in microseconds)

positive and negative feedback loops and harmonic loss modulation [11]. Harmonic modulation was caused by shear acoustic vibration of the DKDP crystal of the intracavity modulator [5, 19], and the modulation frequency corresponded to one of vibration mode (in the range approximately from $50T_r$ to $800T_r$). Electrooptic modulator based on a DKDP crystal (cross section 8×8 mm^2) allowed us to obtain a set of periods corresponding to the first ten shear modes of the crystal by adjusting the beam position in the intracavity DKDP crystal aperture. Pulsation periods down to 0.52 μs were observed (cavity round trip time was equal 10 ns). The calculation results show a very good match to the experimental observations in the microtrain shape and period doubling scenario (Fig. 8.11).

The conclusion of this section is: if feedback is sensitive enough to minimize saturation of active medium, it would be possible to observe the period doubling bifurcation not only in the relaxation oscillation frequency range, but also at frequencies close to the reciprocal of the period introduced by the combination of feedback in the range of several cavity round trip times.

8.4 Conclusions

It has been shown that the combination of two inertial feedback loops is able to open up a round trip time scale for nonlinear dynamics in solid-state lasers.

Application of negative and delayed positive optoelectronic feedback makes it possible to observe the nonlinear dynamics of logistic map in a solid-state laser on the time scale of one cavity round trip time. To accomplish this, it is necessary to use memory-erasing technique. The detailed numeric simulation showed that laser parameters are realistic for experimental realization on the basis of the optoelectronically controlled solid-state laser in self-mode-locking regime.

In the regime of smoothing of laser radiation fine time structure, memory-erasing technique leads to dynamics in the form of a square wave with period of two cavity round trip times. However, further development of nonlinear dynamics differs from that of the logistic map.

The combination of a positive and a delayed negative feedback loops allows one to shift the range of period doubling bifurcation in a solid-state laser with harmonic loss modulation up to much higher frequencies than ever before (relaxation oscillation frequency), namely from several up to several hundreds laser cavity round trip times. The frequency is determined by the relative sensitivity of feedback loops. Periods $4T_r$ can be realized in the regime of memory erasing with delays increased by a round trip time compared to the logistic map case.

Acknowledgments The authors thank A.V. Vinogradov, L.E. Semenova, L.S. Efremova, and E. Blokhina for fruitful discussions. This work was supported by the Program PSD RAS Fundamental photonics problems and new materials physics, and by the Young Scientists Support Program of the Educational-Scientific Center of P. N. Lebedev Physics Institute and the RAS Presidium Program "Support of Young Scientists."

References

1. Arecchi, F.T., Meucci, R., Puccioni, G., Tredicce, J.: Experimental evidence of subharmonic bifurcations, multistability, and turbulence in a Q-switched gas laser. Phys. Rev. Lett. **49**, 1217–1220 (1982)
2. Arecchi, F., Gadomski, W., Meucchi, R.: Generation of chaotic dynamics by feedback on a laser. Phys. Rev. A **34**, 1617–1620 (1986)
3. Bayanov, I.M., Gordienko, V.M., Zvereva, M.G., Magnitskii, S.A., Tarasevich, A.P.: Highly stable picosecond YAG:Nd^{3+} laser with a negative feedback. Sov. J. Quantum Electron. **19**, 994–996 (1989) doi:10.1070/QE1989v019n08ABEH008662
4. Colet, P., Roy, R.: Digital communication with synchronized chaotic lasers. Opt. Lett. **19**, 2056–2058 (1994)
5. Ekstein, H.: Free vibrations of anisotropic bodies. Phys. Rev. **66(5/6)**, 108–118 (1944)
6. Erneux, T., Glorieux, P.: Laser dynamics. Cambridge University Press, Cambridge (2010)
7. Feigenbaum, M.J.: Universal behavior in nonlinear systems. Los Alamos Sci. **1**, 4–27 (1980)
8. Gibbs, H.M., Hopf, F.A., Kaplan, D.L., Shoemaker, R.L.: Observation of chaos in optical bistability. Phys. Rev. Lett. **46**, 474–477, (1981)

9. Gorbunkov, M.V., Shabalin, Yu.V.: Two-loop feedback controlled laser: new possibilities for ultrashort pulses generation and high-level stabilization. Proc. SPIE **4751**, 463 (2002)
10. Gorbunkov, M.V., Maslova, Yu.Ya., Petukhov, V.A., Semenov, M.A., Shabalin, Yu.V., Vinogradov, A.V.: Submicrosecond regular and chaotic nonlinear dynamics in a pulsed picosecond Nd:YAG laser with millisecond pumping. Appl. Optics **48**(12), 2267–2274 (2009)
11. Gorbunkov, M.V., Maslova, Yu.Ya., Shabalin, Yu.V.: Generation of a regular sequence of short-pulse microtrains with a discretely varied repetition period. Bull. Lebedev Phys. Inst. **36**(9), 29–39 (2009)
12. Gorbunkov, M.V., Maslova, Yu.Ya., Vinogradov, A.V.: Optical unit of laser-electron X-ray generator designed for medical applications. Nucl. Instr. Methods A **608**, S32–S35 (2009)
13. Grigorieva, E., Haken, H., Kaschenko, S.: Theory of quasiperiodicity in model of lasers with delayed optoelectronic feedback. Optics Commun. **165**, 279–292 (1999)
14. Khandokhin, P.A., Khanin, Ya.I.: Chaotic dynamics of a YAG:Nd laser with a ring resonator. Sov. J. Quantum Electron. **18**, 1248–1251 (1988)
15. Kryukov, P.G.: Ultrashort-pulse lasers. Quantum Electron. **31**(2), 95–119 (2001)
16. Larger, L., Goedgebuer, J.-P.: Encryption using chaotic dynamics for optical telecommunications. C. R. Physique **5**, 609–611 (2004)
17. Loiko, N.A., Samson, A.M.: Nonlinear dynamics of laser systems with a delay. Quantum Electron. **24**(8), 657–672 (1994)
18. Makukha, V.K., Smirnov, V.S., Semibalamut, V.M.: Generation of ultrashort pulses in a negative-feedback laser. Sov. J. Quantum Electron. **7**, 573–575 (1977) doi:10.1070/QE1977v007n05ABEH012561
19. Stephany, J.F.: Piezo-optic resonances in crystals of the dihydrogen phosphate type. JOSA **55**(2), 136–141 (1965)
20. Suneel, M.: Electronic circuit realization of the logistic map. Sādhanā **31**, 69–78 (2006)
21. Vorchik, D.B., Gorbunkov, M.V.: Optoelectronic control of solid state lasers using new high voltage silicon elements. In Proc. CLEO/Europe'96, Hamburg, Germany, p. 282 (1996)
22. Vorchik, D.B., Gorbunkov, M.V.: Self mode locking in Nd glass laser by fast negative feedback with solid state optoelectronic system. Bull. Lebedev Phys. Inst. **12**, 70–76 (1997)
23. Yariv, A.: Quantum Electronics (2nd Russian edition) (1980)

Chapter 9
The Importance of the Strategy in Backward Orbits

Carmen Pellicer-Lostao and Ricardo López-Ruiz

Abstract This work considers reversed evolution in dynamical systems. In particular, asymptotic behavior of chaotic systems, when their orbits evolve backward in time. Reversed dynamics reveals important aspects of the trajectories, such as a new necessary parameter. This is the strategy through which one orbit reaches an original state in the past. As a result, it is found that backward orbits exhibit sensitivity to the strategy. This gives additional evidence about the unpredictability of the past.

9.1 Introduction

Traditionally, the study of dynamical systems has been mostly concerned about forward evolution, considering long term behavior of the orbits in the future. As a consequence of these studies, chaos theory developed since the 1960s gave to an end with the ideas about the possibility of predicting the future [8] in chaotic systems. These ideas became the base of the well-known "butterfly effect," which is the property of nonlinear systems to have sensibility to initial conditions [9, 14]. Since then, dynamical systems have been widely used to model many kind of phenomena showing complex evolution and unpredictability in the distant future [7, 10, 13, 15].

Conversely, backward evolution of dynamical systems [2, 3, 5] can also be of interest to model complex phenomena [4, 6, 11, 12]. Such as for example, to be able to predict the origin of the evolution of a complex system given a known present state. This work travels into the past states of the dynamical systems and analyzes the asymptotic behavior of backward orbits. In particular, it will try to unravel some amazing properties of predictability of earliest states of a system when coming from a given state in the present.

C. Pellicer-Lostao (✉)
BIFI, University of Zaragoza, Zaragoza, Spain
e-mail: carmen.pellicer@bifi.es

R. López-Ruiz
Deptartment of Computer Science & BIFI,
University of Zaragoza, Zaragoza, Spain
e-mail: rilopez@unizar.es

R. López-Ruiz et al. (eds.), *Nonlinear Maps and their Applications,*
Springer Proceedings in Mathematics & Statistics 112, DOI 10.1007/978-3-319-12328-8_9

9.2 Backward Trajectories

An N dimensional iterative dynamical system is given by a function $F : U \subseteq R^N \rightarrow U$ that maps a state into a future state. Time is considered to be a discrete variable and they are formulated as follows:

$$X_{t+1} = F(X_t) \tag{9.1}$$

where $t = 0, 1, \ldots, n$ represents the temporal variable, $X_0, X_1, \ldots, X_n$ are the states of the system in different instants of time, and U is the region of the N-dimensional space R^N where the system evolves, also referred as the phase space.

The consecutive iterates of the system from an initial point X_0 is called the *forward orbit* of X_0 under F. It is customary to express the sequence of iterates that represent the forward orbit as $\{F^i(X_0)\}_{i=0}^{\infty}$, which is fully expanded in the following equation.

$$\{F^0(X_0) = X_0, F^1(X_0) = F(X_0), \ldots, F^{n+1}(X_0) = F(F^n(X_0)), \ldots\} \tag{9.2}$$

If the function F is invertible, we can also talk about the *backward orbit* of X_0 under F, described as $\{F^{-i}(X_0)\}_{i=0}^{\infty}$. Pairing the time variable with the space variable gives us the full view of the evolution of the dynamical system:

$$\{\ldots, (t_{-n}, F^{-n}(X_0)), .., (t_{-1}, F^{-1}(X_0)), (t_0, X_0), (t_1, F(X_0)), .., (t_n, F^n(X_0)), \ldots\} \tag{9.3}$$

Considering chaotic systems, chaos requires F to be a nonlinear function. Consequently, the inverse map F^{-1} is typically a multivalued function. This means that there are multiple ways to map a unique future state into the past. Then, it will always be necessary to define a strategy to map a state into a previous one.

To see that, observe for example Fig. 9.1. In this figure, a one-dimensional iterative dynamical system, the tent map, and its inverse functions are depicted. In Fig. 9.1 (right), it can be seen that two different prior states X_{-1} are obtained, when iterating backward from an initial state X_0.

To produce a reversed orbit or backward orbit, it is necessary to select iteratively one of these two values as we to follow our trip into the past. The selection of a different path at any step means that it is necessary to choose a different *strategy of backward evolution*. This is going to produce a different backward orbit and presumably a different original state. Then, we can conclude that *backward evolution is deterministic* only when the strategy is fully known. Also, a future state is not necessarily linked to any fixed past state. This is so, in the sense that for a given present state there are different options, that turn up to be possible prior states.

The above discussion is related in some way to iterated function system (IFS) [1] formed by the collection of its inverse functions.

In fact, IFS provides a convenient framework to study this collection of functions. However, we have to take into account that IFS perspective is quite different from reverse dynamics. Actually, this is basically a geometric perspective, considering these functions compressors of the phase space and global constructors of fractals.

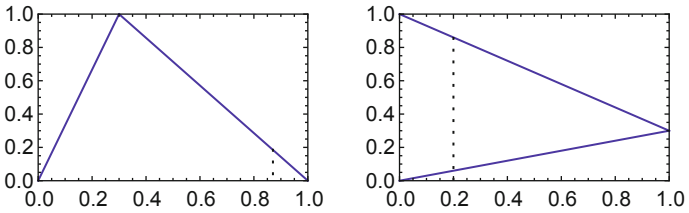

Fig. 9.1 (*Left*) Tent map and its inverse functions. (*Right*) Illustration of bivalued past sttes in the inverse tent map

In this work, it is our interest to explore these systems from a temporal perspective. Considering the temporal dimension, backward trajectories expose a new evidence of nondeterminism worth to be explored. As a consequence, our objective is to find out the relevance of the backward strategy and to seek for its significance in reversed evolution. To study this, the mechanism of calculating the backward orbits is expressed formally in the following section.

9.3 A New Parameter in Backward Dynamics

Let's say, F is an noninvertible chaotic map, whose inverse map is a multivalued function F^{-1}. Let us suppose that the values of the inverse map at a point X_{-t} are a total of b possible $X_{-(t+1)}$ points, denoted as:

$$\{F^{-1}(X_{-t})\}^{\{b\}} \tag{9.4}$$

To take a step backward in the evolution of the system, it is necessary to choose one of these b values. Let us say that this decision may be called a *backward selection* and let us represent it as s. In a backward iteration of n steps, it is necessary to make n of such selections. Then, a series of selections can be called as a *strategy* of length n and it will be denoted as S^n . Consequently, the strategy can be expressed as a vector that stores the decisions taken at every step:

$$S^n = \{s_i\}_{i=1}^{i=n} = \{s_1, s_2, .., s_n\} \tag{9.5}$$

Here s_i describes the backward selection at instant $-i$.

Now, let us discuss how to code the values of a backward selection, s_i. Following Eq. 9.4, the set of possible pasts of X_{-t} at instant $-i$ can expressed as:

$$\{F^{-i}(X_{-t})\}^{\{b\}} = \{X_{-t-i}\}^{\{b\}} \tag{9.6}$$

To make a backward selection at instant $-i$ is nothing but to pick one state out of this set. Let us say that state k is chosen, being $k = 0, 1, .., b-1$, and this state is denoted as $X_{-t-i}^{(k)}$. Then the backward selection at instant $-i$ is coded as $s_i = k$.

Observe that with b possible values and n back steps, there will be a total of b^n possible back strategies S^n. Then let us express any of these possible backward strategies as S_r^n, where the value of r is coded as follows:

$$r = s_1 * b^{n-1} + ... + s_n = \sum_{i=1}^{i=n} s_i * b^{n-i} \tag{9.7}$$

From the discussion above, let us conclude that the calculus of a backward trajectory of length n from a present point $X_0 = P$ according to the strategy S_r^n can be obtained by applying the following iterative procedure:

$$X_{-i}^{(k)} = \{F^{-i}(X_0)\}^{(k)}, \; when \, k = s_i \tag{9.8}$$

Here, $k = 0, 1, ..., b-1$ and the iteration step is denoted by $i = 0, 1, ..., n$. This means that to calculate a backward trajectory from P, given a specific strategy S_r^n, we need to set the initial point in the present $X_0 = P$, then calculate n-times the composite inverse map F^{-n} choosing at each iteration $-i$ one state out of all the possible b past states. The selection $X_{-i}^{(k)}$ is given by the value of $s_i = k$, the strategy of backward evolution at step $-i$.

The strategy for traveling into the past appears here as a new parameter in the evolution of the dynamic system. This parameter rules the strategy through which one orbit reaches an original state in the past. Now, the point of interest is to consider the predictability of the past states in terms of this strategy. To do that, a practical example is considered in the following section. This illustrates the relevance of the backward strategy in the dynamics of the system.

9.4 The Tent Map Moving Backward

A particular chaotic map is considered in order to illustrate the previous discussions and measuring them in full detail. Simple examples make relevant concepts more obvious. Then, for simplicity we take the skew tent map, whose F and F^{-1} are given by the following equations:

$$x_{n+1} = \begin{cases} x_n/\alpha, & 0 \le x_n \le \alpha, \\ (x_n - 1)/(\alpha - 1), & \alpha \le x_n \le 1, \end{cases} \tag{9.9}$$

$$x_{n-1} = \begin{cases} \alpha x_n, & 0 \le x_n \le 1, \\ (\alpha - 1)x_n + 1, & 0 \le x_n \le 1, \end{cases} \tag{9.10}$$

This map has a parameter of evolution α, where $\alpha \in [0, 1]$.

The tent map and its inverse functions for the case of $\alpha = 0.3$ are depicted in Fig. 9.1, right and left, respectively. The figures illustrate how a forward iteration

calculates the value of $X_0 = 0.2$ from a previous state $X_{-1} = 0.86$. Continuing this route of evolution the map advances into the future. Conversely, backward iteration in the right panel of Fig. 9.1 shows how a future state $X_0 = 0.2$ produces two possible previous states $X_{-1} = 0.86$ and $X_{-1} = 0.06$.

In Eqs. (9.9 and 9.10), it can be seen that two functions $F^{-1}[0,1] \rightarrow [0,1]$ are defined for the tent map in the range $X_t \in [0,1]$. Then, the inverse map $F^{-1}(X_t)$ is a bivalued function and there are $b = 2$, two possible values of X_{t-1} upon which we can make a single backward selection s_{-1}. These values are labeled $X_{t-1}^{(0)}$ and $X_{t-1}^{(1)}$.

Here the code of this selection means the following: when $k = 0$ the point in the upper line of F^{-1} is chosen, and when $k = 1$ the lower line. Note that in this map when $X_t = 1$, it occurs that $X_{t-1}^{(0)} = X_{t-1}^{(1)} = \alpha$. Then, for a given subset $V \subset U$ and $X_t \in V$, it is possible that a different number of inverse options [12] are found and so, different values of b will exist for different V depending on the number of precedents.

In a general form, it is possible to go n steps backward following a given S^n strategy. In this case S^n is going to be a binary array of length n. The values s_i of the strategy array S^n, are going to be either 0 or 1, depending on the selection of the $X_{-i}^{(0)}$ or $X_{-i}^{(1)}$, respectively.

Additionally, chaotic maps are dependent on the parameters of evolution. Then, backward dynamics is dependent on these parameters. As we can see in Eq. (9.10), the inverse functions obtained for the tent map are dependent on α parameter . In the following sections this dependence along with the strategy is illustrated.

9.4.1 Measuring Parameters of Backward Evolution

In this section, we will consider how we represent a given strategy and the details of how this strategy rules the path to a given initial state in the past. To do that, consider the case of moving from $X_0 = 0.2$, $n = 5$ steps into the past. Then, one will find $b^n = 2^5 = 32$ different possible backward strategies, and so 32 different X_{-5} past values giving rise to $X_0 = 0.2$ in the future.

Let's choose a strategy to travel into the past, such as for example $S_{11}^5 = \{0,1,0,1,1\}$, where $r = 11$ is calculated according to Eq. (9.7). This particular S_{11}^5 means that we move backward, choosing in the first step the upper branch of F^{-1} in Fig. 9.1 (right), lower branch in the second step, upper in the third, and so on. Table 9.1 and Fig. 9.2 show the details of this particular example.

Table 9.1 shows the details of the particular backward selections taken at every step with strategy S_{11}^5. The resulting backward orbit is called O_b and its values are $O_b = \{0.2, 0.86, 0.258, 0.8194, 0.24582, 0.073746\}$. As we can see in this table, this strategy lead the tent map to an initial state $X_{-5} = 0.073746$. This table reveals the detail of every backward selection. At every step $-i$, two new possible values $\{F^{-i}(X_0)\}^{\{2\}} = \{X_{-i}^{(0)}, X_{-i}^{(1)}\}$ are calculated.

The past state remains uncertain unless the strategy of backward selection is defined. Then, it is the value of s_i, the one that fixes the next step into the past, $X_{-i}^{(s_i)}$.

Table 9.1 List of values for calculating backward trajectory O_b

i	0	1	2	3	4	5
$X_{-i}^{(0)}$	*0.2*	*0.86*	0.398	*0.8194*	0.42624	0.827926
$X_{-i}^{(1)}$	–	0.06	*0.258*	0.0774	*0.2458*	*0.073746*
s_i	–	0	1	0	1	1

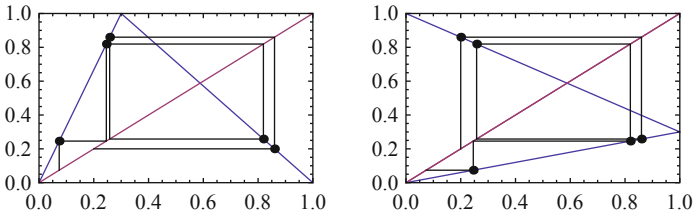

Fig. 9.2 (*Left*) Forward orbit O_f and (*right*) backward orbit O_b to arrive $X_n = 0.2$ in five steps from $X_{n-5} = 0.073746$

The value of $X_{-i}^{(s_i)}$ is printed in italics in the table, to remark the selection taken at each step. Then, this value $X_{-i}^{(s_i)}$ produces two new possible past values $\{F^{-1}(X_{-i}^{(s_i)})\}^{\{2\}}$ in the next step and then, backward iteration continues selecting one value of $\{X_{-i}\}^{\{2\}}$ according to s_i until $i = n$ is reached.

Figure 9.2 shows the graphics considered in this example, the forward orbit O_f and the backward orbit O_b. The points of this orbits are $O_f = \{0.073746, 0.24582, 0.8194, 0.258, 0.86, 0.2\}$ and $O_b = \{0.2, 0.86, 0.258, 0.8194, 0.24582, 0.073746\}$. In Fig. 9.2 (left), the forward orbit O_f is obtained from its reversed associate O_b Fig. 9.2 (right). Moving into the future from an initial state $X_{-5} = 0.073746$ is a complete deterministic process. The tent map evolves inevitably from $X_{-5} = 0.073746$ to the future state $X_0 = 0.2$, following the determined orbit O_f.

In contrast, it is interesting to remark that moving in reverse is a nondeterministic process unless the strategy is fixed. Here Fig. 9.2 (right) shows in detail the points of O_b. O_b is one of the $2^5 = 32$ possible backward orbits considered in this example. This particular trajectory O_b is obtained moving from $X_0 = 0.2$ to $X_{-5} = 0.073746$ according to a specific selected strategy, $S_{11} = \{0, 1, 0, 1, 1\}$.

9.4.2 Deterministic Backward Evolution with a Strategy

It is observed that every strategy carries us to a particular different past state, while traveling through different branches of the inverse tent map. From this, it is logical to think that if other branches are visited in the travel to the past, the initial state to which the system returns is going to be different than $X_{-5} = 0.073746$. To see this, let us move from $X_0 = 0.2$, $n = 5$ steps into the past and compute all different backward origins X_{-5} given by the $b^n = 2^5 = 32$ different possible backward

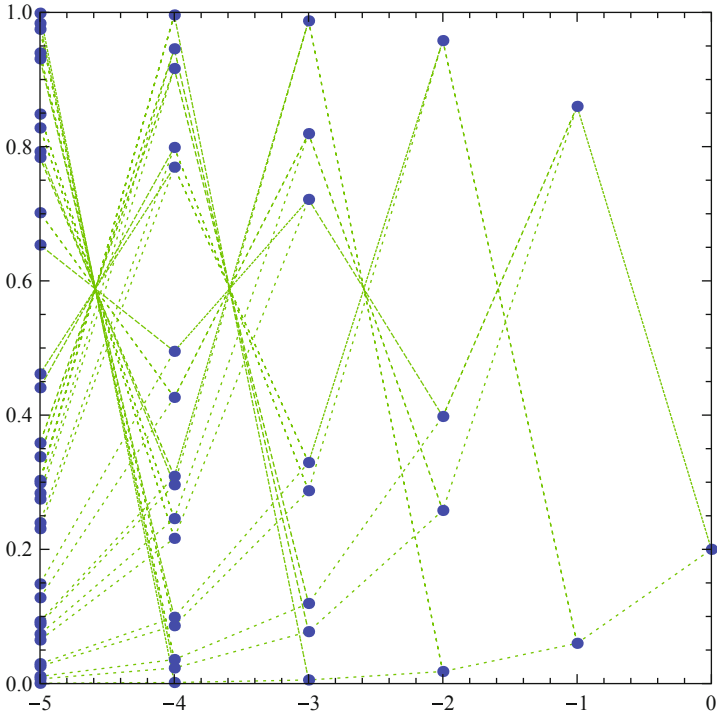

Fig. 9.3 Points of all possible 32 backward orbits that start from $X_0 = 0.2$, move $n = 5$ steps into the past. A total of $2^{15} = 32$ different initial past states are found for X_{-5}

strategies S_r^n. Figure 9.3 shows the backward computation of all possible values of X_{-1}, X_{-2}, X_{-3}, and X_{-4} obtained at every step, up to reaching an earliest state X_{-5}. The x-axis presents the backward steps and the y-axis the different values of X in the interval $[0, 1]$ obtained at every step. The dotted lines link the states obtained for every different possible strategy.

In Fig. 9.3, it can be observed that moving $n = 5$ steps backward from an initial state $X_0 = 0.2$ is a nondeterministic process. In fact, there are as may as $b^n = 2^5 = 32$ strategies that lead the system to 32 different initial past states. It can be seen that every strategy takes the system to a completely different X_{-5} point in the past. The interested reader can easily recognize in this figure the particular backward orbit O_b illustrated in Table 9.1 and Fig. 9.2 (right).

As a result, it can be said that *reversed dynamics is sensitive to the backward strategy*. That situation is similar to the sensitivity to initial conditions observed in forward dynamics. Note that a small change in the trajectory, modifying just one s_i will lead the system to a completely different original state. Also note that as we travel deeper into the past, many more possible origins may appear and the origin of the system will be more difficult to predict, if the strategy is not recalled precisely. This can be explicitly seen in Fig. 9.4 (left) where we take the evolution of $n = 10$

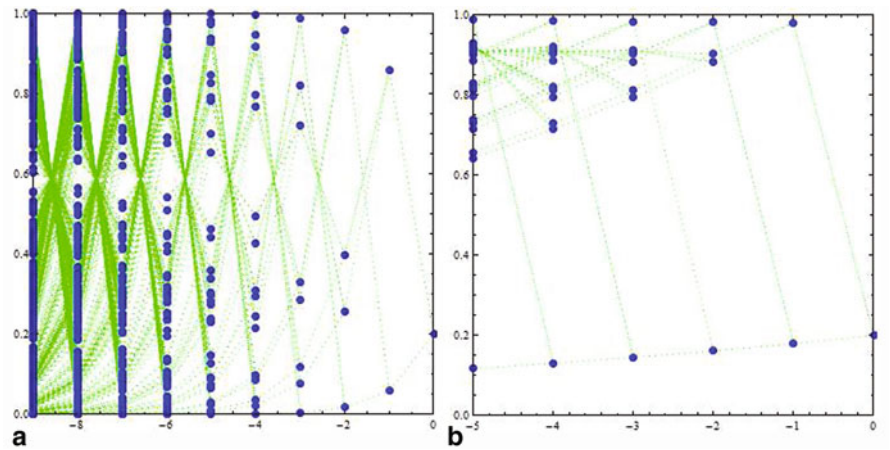

Fig. 9.4 (*Left*) Points of all possible 2^{10} backward orbits, that start from $X_0 = 0.2$ with $\alpha = 0.3$, move $n = 10$ steps into the past, and arrive to 1024 different initial past states, X_{-10}. (*Right*) Points of all possible 2^5 backward orbits, that start from $X_0 = 0.2$ with $\alpha = 0.9$, move $n = 10$ steps into the past, and arrive to 32 different initial past states, X_{-5}

steps into the past instead of $n = 5$ as in Fig. 9.3. In Fig. 9.4 (left) there are 2^{10} possible backward orbits and the same number of possible past points X_{-10}. A small change in the strategy takes us to a very different past state.

Therefore, similarly to the "Butterfly effect" observed in forward dynamics, the sensitivity to the strategy tells us something important about the uncertainty of the past. It is impossible to predict the origin of a system unless the strategy is precisely known. It also can be said that, accurate data of a strategy may be unfeasible when the origin is remote and exceeds the physical capabilities of knowledge. This gives some evidence for the unpredictability of the past.

To illustrate dependence of backward dynamics to the other parameters of evolution, Fig. 9.4 (right) displays the 2^5 possible backward orbits that can be obtained moving $n = 5$ steps backward from an initial state $X_0 = 0.2$ when $\alpha = 0.9$. This figure can be compared with Fig. 9.3 where $\alpha = 0.3$ and compare the difference obtained in the orbits when the parameter $\alpha = 0.9$.

9.4.3 Sensitivity of Backward Evolution with the Strategy

Finally, let us measure the sensitivity of past trajectories to the backward strategy. To do that, let us take the same case as before, traveling backward n steps into the past form $X_0 = 0.2$ with F^{-1} of Eqs. (9.9 and 9.10) and $\alpha = 0.3$. The initial state X_{-n} is calculated for any of the 2^n possible strategies, that takes the inverse tent map from $X_0 = 0.2$ to X_{-n}. As it was shown before, for every different strategy S_r^n a different origin point X_{-n} is produced. It can also be seen that as n grows and the

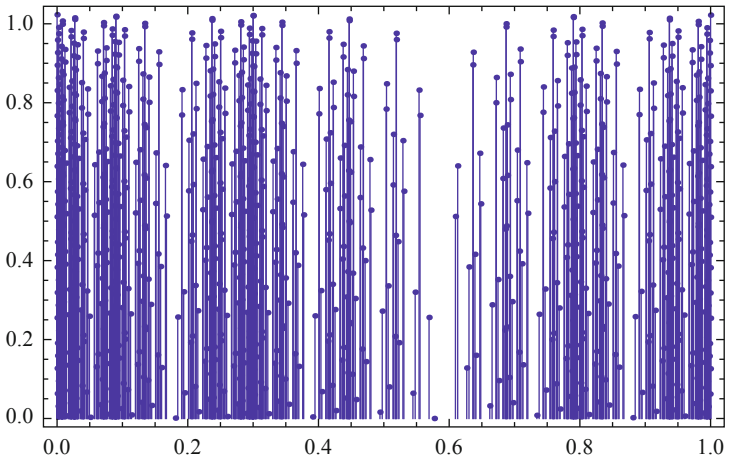

Fig. 9.5 Representations of $2^{10} = 1024$ possible past points obtained for a trip of $n = 10$ steps into the past from $X_0 = 0.2$ with $\alpha = 0.3$

system travels deeper into the past, the values of X_{-n} spread in a fractal way over the interval of the phase space $U = [0, 1]$.

To illustrate these facts, the pairs $(X_{-n}, r/2^n)$ are plotted in Fig. 9.5. Here r is the number of the strategy S_r^n that leads to the state X_{-n} in the past. This number is normalized to one, taking $r/2^n$, in order to get a representation independent of n, the number of steps into the past. In Fig. 9.5, a total of $n = 10$ is considered and so, a total of $2^{10} = 1024$ different strategies are depicted. The y-axis represent the normalized value $r/2^n$ of the number of the strategy and the x-axis the past state X_{-n} reached with strategy number r. This figure can be a more useful representation than Fig. 9.3 in order to show all the possible X_{-n} states in a travel to a remoter past state.

As it is observed in this figure, the unpredictability of the original state can be appreciated graphically. This is due to the sensitivity to the backward strategy. In particular, three important facts are observed. The first one is that the values of X_{-n} spread in a fractal way over the phase space, the interval $U = [0, 1]$, in accordance with IFS framework [1]. The second is that when n grows and the system travels deeper into the past, many more possible values of X_{-n} arise. And the third one is that strategies differing just a single bit give very different initial states, that again spread in a fractal way over the phase space.

This means that traveling into an initial state in the past requires recalling every decision in the strategy. If a single bit of the strategy is forgotten the system arrives to a different past origin. This can be explicitly seen in Fig. 9.6 (left) where we take the evolution of $n = 18$ steps into the past instead of $n = 10$ as in Fig. 9.5. In Fig. 9.6 (left) there are 2^{18} possible backward orbits and the same number of possible past points X_{-18}. A small change in the number of the strategy take us to a very different past state.

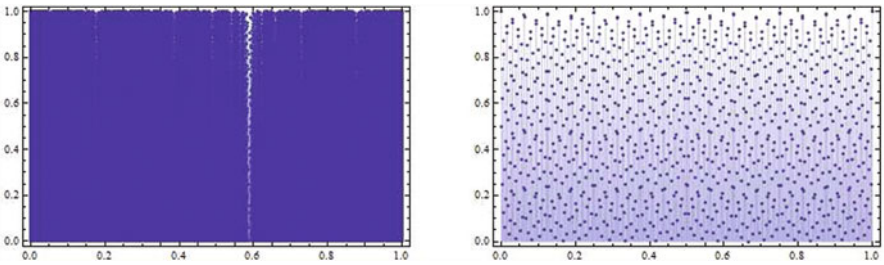

Fig. 9.6 (*Left*) Representations of $2^{18} = 262144$ possible past points obtained for a trip of $n = 18$ steps into the past from $X_0 = 0.2$ with $\alpha = 0.3$. (*Right*) Representations of $2^{10} = 1024$ possible past points obtained for a trip of $n = 10$ steps into the past from $X_0 = 0.2$ with $\alpha = 0.5$

These results give a new perspective for modeling the origins of complex systems. They offer a complementary point of view to the "butterfly effect" observed in forward dynamics. The study of reversed dynamics reveals that it is impossible to discover the remote origin of complex phenomena. This is so, because this calculus exceeds the capabilities of knowledge, when the origin is in the distant past. Put it in another words, for chaotic systems not only the far future, but also the remote past is unpredictable.

At this point let us remark that the unpredictability of future phenomena has had great significance for applied sciences. The theory of complex systems has given new perspectives to sciences where chaotic behaviors have been observed like meteorology [9], economy [7], or others. In those sciences the discovery of the future has been granted as limited. One striking example can be the present economic and financial crisis, not predicted by anyone. Hence, the future is taken as uncertain and it is gradually enlightened at every forward step. Conversely, the acknowledgment of the unpredictability of the past exposes a new perspective to applied sciences, that model the origin of complex phenomena. These sciences must consider the irony of this uncertainty and be aware that the discovery of past must be granted as limited. The past must be taken as uncertain, and it will only be gradually enlightened at every backward step we make.

To illustrate dependence of backward dynamics to the other parameters of evolution, Fig. 9.6 (right) displays the 2^{10} possible backward orbits that can be obtained moving $n = 10$ steps backward from an initial state $X_0 = 0.2$ when $\alpha = 0.5$. This figure can be compared with Fig. 9.5 where $\alpha = 0.3$ and compare the difference of the fractal depicted in x-axis when the parameter $\alpha = 0.5$.

9.5 Conclusions

Reversed dynamics shows amazing mathematical aspects of the structure of the trajectories. Precisely, it can be said that it is possible to construct backward orbits and travel with reversed dynamics to the initial state of a nonlinear system. This is

done through a new parameter of dynamical evolution, the so called *the backward strategy*. Backward dynamics demonstrates high sensitivity to this strategy. Hence, to calculate the earliest state of the system requires to recall precisely every step in the past history of the system. If a single bit of the strategy is forgotten or misunderstood, the system arrives to a completely different original state. In this sense and from an asymptotic perspective, it can be concluded that the past is, in fact, unpredictable.

This can sound as a tautology but it could have some consequence in the studies of complex phenomena. In noninvertible dynamical systems, not only the far future can be chaotic and unpredictable, but the remote past is also uncertain. Applied sciences that model the origin of the evolution of complex systems must be aware of that, just that the discovery of the past must be taken as limited.

In summary, this work portrays the relevance of the strategy in backward orbits. Backward dynamics turns out to be sensitive to the strategy and that makes it eligible as a new parameter of the evolution of dynamical systems. Considering that so, the strategy takes us to the evidence of the unpredictability of the past.

References

1. Barnsley, M.F., Demko, S.: Iterated function systems and the global construction of fractals. Proc. R. Soc. Lond. **A399**, 243–275 (1985).
2. Bennett, R.: On Inverse Limit Sequences, Master's thesis, University of Tennessee (1962).
3. Davis, J.F.: Confluent mappings on [0, 1] and inverse limits. Topol. Proc. **15**, 1–9 (1990).
4. Gardini, L., Hommes, C., Tramontanac, F., de Vilderd, R.: Forward and backward dynamics in implicitly defined overlapping generations models. J. Econ. Behav. Organ. **71**, 110–129 (2009).
5. Ingram, W.T.: Invariant sets and inverse limits. Topol. Appl. **126**, 393–408 (2002).
6. Kennedy, J., Stockman, D. R., Yorke, J.A.: Inverse limits and an implicitly defined difference equation from economics. Topol. Appl. **154**, 2533–2552 (2007).
7. Kyrtsou, C., Vorlow, C.: Complex dynamics in macroeconomics: a novel approach. In: Diebolt, C., Kyrtsou, C. (eds.) New Trends In Macroeconomics, pp. 223–245, Springer-Verlag, Berlin (2005).
8. Laplace, P.S.: Traité de Mécanique Céleste. Oeuvres complètes, Vol. 5, Gauthier-Villars, Paris (1825).
9. Lorenz, E.N.: Deterministic non-periodic flow. J. Atmos. Sci. **20**, 130–141 (1963).
10. May, R.M., McLean, A.R.: Theoretical Ecology: Principles and Applications. Blackwell, Oxford (2007).
11. Medio, A., Raines, B.E.: Inverse limit spaces arising from problems in economics. Topol. Appl. **153**, 3437–3449 (2006).
12. Mira, C., Gardini L., Barugola, A., Cathala, J.-C.: Chaotic Dynamics in Two-Dimensional Noninvertible Maps. Series A, 20. World Scientific Publishing, Singapore (1996).
13. Pellicer-Lostao, C., López-Ruiz, R.: A chaotic gas-like model for trading markets. J. Comput. Sci. **1**, 24–32 (2010).
14. Poincaré, H.: Les méthodes Nouvelles de la Mécanique Céleste, 3 volumes. Gauthiers-Villars, Paris (1892).
15. Bergé, P., Pomeau, Y., Vidal, C.: L'Ordre dans le Chaos. Hermann, Paris (1984).

Chapter 10
Minimal Cantor Type Sets on Discrete Dynamical Systems

Francisco Balibrea

Abstract Cantor sets on topological spaces can be obtained as minimal sets with respect to discrete dynamical systems (d.d.s.), (X, f) where X is a compact metric space and f could be an homeomorphism or a non-invertible continuous map. In general, given a Cantor type set or simply a Cantor set in a compact metric space, it is difficult to obtain a d.d.s. having it as minimal. Examples of Cantor sets that are minimal or non-minimal can be obtained using the ternary Cantor set on the real interval and constructing appropriate continuous maps. In the case of the minimality of such Cantor sets, every point of them are uniformly recurrent points for f. Other examples of minimal Cantor sets like the shift space Σ^2 or subsets of it are given for homeomorphisms. The whole Smale horseshoe is non-minimal for an adequate homeomorphism or one of its subsets is minimal for it.

10.1 Introduction and Some Definitions

In what follows in Sects. 10.1, 10.2, and 10.3, we will concentrate mainly in discrete dynamical systems (d.d.s.) of the form (I, f), where $I = [0, 1]$ and $f : I \to I$ is continuous. The main aim is to study the behavior of the orbits of all points in I by f. The orbit generate by the point $x \in I$, denoted by $Orb_f(x) = (f^n)_{n=0}^{\infty}$, where $f^n = f(f^{n-1})$ and f^0 is the identity in I.

A point $x \in I$ is *periodic of minimal period p* if p is the minimum positive integer for which is $f^p(x) = x$, when $p = 1$ we say the point is *fixed*. The point x is *eventually periodic*, if there exists a positive integer m for which $f^m(x)$ is periodic. The knowledge of the periodic points allow us to state a criterium for chaotic behavior. We will say that the d.d.s. (I, f) is *chaotic* if it has a periodic point of a period not a power of two which is equivalent to have positive *topological entropy* (see [2]). We will say that a point $x \in I$ is *approximately periodic* if for every $\epsilon > 0$ there exists a periodic point y and a positive integer N such that

$$| f^n(x) - f^n(y) | < \epsilon \ \textit{for all} \quad n > N$$

F. Balibrea (✉)
Departamento de Matemáticas, Universidad de Murcia, Campus de Espinardo,
30100 Murcia, Spain
e-mail: balibrea@um.es

R. López-Ruiz et al. (eds.), *Nonlinear Maps and their Applications,*
Springer Proceedings in Mathematics & Statistics 112, DOI 10.1007/978-3-319-12328-8_10

We say a point $x \in I$ is *asymptotically periodic* for (I, f) if $lim_{n\to\infty} f^{nm}(x)$ exists for some $m \in N$. The system (I, f) is *uniformly non-chaotic* if every point $x \in I$ is approximate periodic. The same system is *strongly non-chaotic* if every $x \in I$ is asymptotically periodic. Thus, if a system is strongly non-chaotic, then it is uniformly non-chaotic. It can be proved also that if a d.d.s. is uniformly non-chaotic, then it is non-chaotic (see [3]).

A point $x \in I$ is *uniformly recurrent* if for every open set U containing x, there exists a positive integer $N = N(U)$ such that if $f^m(x) \in U$ with $m \geq 0$, then $f^{m+k}(x) \in U$ for some k holding $0 < k \leq N$. It is clear that a strongly recurrent point is one recurrent with bounded return times. A simple sufficient condition for a point x to be uniformly recurrent is to be *regularly recurrent*, that is, for each open set U containing x there exists a positive integer $N = N(U)$ such that $f^{kN}(x) \in U$ for all $k > 0$.

10.2 Construction and Properties of the Ternary Cantor Set

We start recalling (see [12]) the well-known construction of the ternary Cantor set on the unit interval $I = [0, 1]$ of the real line. First, we remove the open interval of length $1/3$ from the center of I and we denote the remaining open set by I_1, $I_1 = [0, \frac{1}{3}] \bigcup [\frac{2}{3}, 1]$. We continue with the process of removing from the center of each new created subinterval the open interval whose length is one third of the length subinterval to define inductively the kth set I_k; I_k is a union of 2^k subintervals of length 3^{-k} and $(I_k)_k$ is a monotone decreasing sequence of compact sets. The limit of such sequence is

$$C = \bigcap_{k=1}^{\infty} I_k$$

is a compact set called the *ternary Cantor or Cantor set*, which will be denoted by C. We think of this set as a porous set. More precisely, the connected component at each point of C is the singleton set of the point itself. We say that C is a *totally disconnected set*. C is also *perfect* which means that it is closed and contains no isolated point. As a consequence, there exists a ball center at each point of C with arbitrary small radius such that its circumference does not intersect C. Therefore, it follows that the *topological dimension* of C is zero (see [12]).

The ternary Cantor set is of measure zero since it is covered by interval of length $\frac{2}{3^n}$ which is arbitrarily small for large enough n. Although C has no length, it contains many points of I. Obviously 0 and 1 belongs to it. Similarly, both endpoints of any deleted middle third also belong to it. After all, they will never end up in the middle third of a remaining subinterval at any stage of the construction.
Surprisingly, the end points compose only a nonsignificative portion of the points of C. For example the number $1/4$, although never is an endpoint of any subinterval in the construction, belongs to C. To see it, it is useful to prove the following result,

Theorem 10.1 *The ternary Cantor set consists of all points in I that can be represented in base* 3 *using only the digits* 0 *and* 2.

Proof (see [1]) Express the numbers between 0 and 1 in base-3 representation. For any point from I, this representation is unique except for points with a finite base-3 representation. By a finite base-3 representation we mean that the ternary digit a_n is non-zero and $0 = a_{n+1} = a_{n+2} = \ldots$. In this case a point $r \in [0, 1]$ is represented by exactly two base-3 expansions:

$$r = .a_1a_2...a_n = .a_1a_2...(a_n - 1)222...$$

The subinterval $(\frac{1}{3}, \frac{2}{3})$ consists of the points whose base-3 representation satisfy $a_1 = 1$. The number $1/3$ can be expressed in two ways, as $.1 = 0\overline{2}$ in base 3. As a consequence, the set $I_1 = [0, \frac{1}{3}] \bigcup [\frac{2}{3}, 1]$ consists of all numbers in I that can be represented in base 3 with $a_1 = 0$ or 2. Similarly, the set

$$I_2 = [0, \frac{1}{9}] \bigcup [\frac{2}{9}, \frac{1}{3}] \bigcup [\frac{2}{3}, \frac{7}{9}] \bigcup [\frac{8}{9}, 1]$$

from the second step of the Cantor set construction is the set that consists of all points having representations with a_1 and a_2 being either 0 or 2. We can ask what the analogous property is for I_n and then ask what property a number must have if it is simultaneously in all the I_n, that is, if it belongs to C.

For example, the base-3 point $r = .\overline{02}$ belongs to C. To see it, note that

$$r = 0 \times 3^{-1} + 2 \times 3^{-2} + 0 \times 3^{-3} + 2 \times 3^{-4} + \cdots = \frac{2}{9} \frac{1}{1 - \frac{1}{9}} = \frac{1}{4}$$

As mentioned above, some points have two base-3 representations, for example, $\frac{1}{3}$ can be expressed as either $.1\bar{0}$ or .1 in ternary expansion. However, each point in C has exactly one representation including no $1's$. Using now the binary representation of points in C, and the Cantor selection method, it is possible to prove that C is an uncountable set (see for example [1]).

C has the following curious property (see [12]): *for an arbitrary real number* $x \in [-1, 1]$, *there exist numbers* $y, z \in C$ *such that* $x = y - z$. We indicate this property by $[-1, 1] \subset C - C$. Since C has zero Lebesgue measure, we compare it with the known property due to Steinhaus: *If the Lebesgue measure of A is positive, then A - A contains some neighborhood of the origin*.

The set L of Liouville numbers is even thinner than C but satisfies the above property. In [7], Erdös proved that $L - L = R$. Before proving such property, it was known that the Hausdorff dimension of L was zero (see [8]). To this respect, assume that while L is a set of *second category* in the sense of Baire, C is of the *first category*.

10.3 An Interval Map for Which the Ternary Cantor Set is Minimal

In [3], Block and Coppel give an example of an interval map having interesting dynamical properties concerning chaoticity and which is an elaborate variant of another previously constructed by Delahaye in [4].

Example (see [3])

Let $f \in C(I)$ defined by

$$f(0) = \frac{2}{3}, f(1) = 0,$$

$$f\left(1 - \frac{2}{3^k}\right) = \frac{1}{3^{k-1}}, f\left(1 - \frac{1}{3^k}\right) = \frac{2}{3^{k+1}} (k \geq 1)$$

and in the rest of the interval we connect the points. The result is a piecewise linear map.

More precisely, the map is

$$f(x) = x + \frac{2}{3} \quad for \quad 0 \leq x \leq \frac{1}{3}$$

$$f(x) = \frac{16}{9} - \frac{7x}{3} \quad for \quad \frac{1}{3} \leq x \leq \frac{2}{3}$$

$$f(x) = \frac{f(3x-2)}{3} \quad for \quad \frac{2}{3} \leq x \leq 1.$$

From definition, we have that for any $0 \leq x \leq 1$

$$f^2\left(\frac{x}{3}\right) = \frac{f(x)}{3} (1)$$

and for iteration is

$$f^{2n}\left(\frac{x}{3}\right) = \frac{f^n(x)}{3} \quad for\, any \quad n \geq 1.$$

It is immediate that the map has a unique fixed point $x_0 = 8/15$ and also that for any $x \neq x_0$ is $f^p(x) \in (0, \frac{1}{3})$ for some $p = p(x) \geq 0$. If $x \neq x_0$, it is immediate that $f^m(x) \in (0, \frac{1}{3})$ for some positive integer $m = m(x) \geq 0$. It means that any periodic orbit with period greater than one, has a point in $(0, \frac{1}{3})$.

Since f maps the interval $[0, \frac{1}{3}] = I$ onto $[\frac{2}{3}, 1] = J$ and vice versa, it follows that the orbit of x must be of even period. To see it, since $f(I) = J$ and $f(J) = I$, then $f^2(I) = I$, that is f^2 has in I a fixed point which is a periodic point of f of even period (see for example, [3]). In addition, using (1), $\frac{x}{3}$ is periodic if and only if x is periodic. Then, if x has period n, $\frac{x}{3}$ has period $2n$.

Let y be a point of period $n = 2^d q$, where $q > 1$ is odd and let $d \geq 1$. By what was said previously, assume $y \in (0, \frac{1}{3})$. Then $x = 3y$ has period $n/2$. Repeating

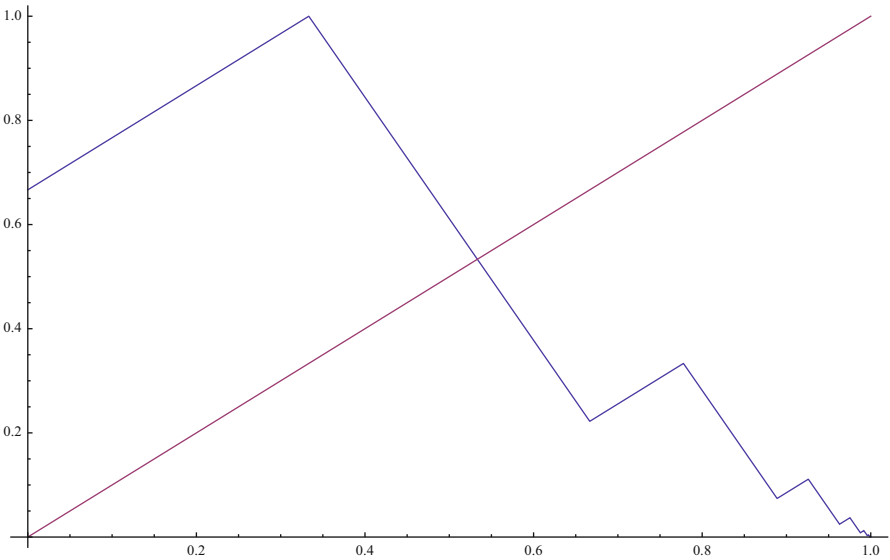

Fig. 10.1 Minimal piecewise linear map

the argument, we obtain a point of odd period q, which is a contradiction. Then the topological entropy of f is zero and then the map is non-chaotic. Similarly, we find that if there exists a unique periodic orbit of period n, then there exists a unique orbit of period $2n$. Therefore, f has a unique orbit of period 2^d for every $d \geq 0$.

Let $I_0^1 = [0, \frac{1}{3}]$, $I_1^1 = [\frac{2}{3}, 1]$ and suppose we have defined 2^j pairwise disjoint closed intervals $I^j = [\alpha_i^j, \alpha_i^j + \frac{1}{3^j}]$ (with $0 \leq i \leq 2^j$) of length $\frac{1}{3^j}$. Then we introduce 2^{j+1} pairwise disjoint closed intervals I_i^{j+1} by setting

$$I_i^{j+1} = \left[\alpha_i^j, \alpha_i^j + \frac{1}{3^{j+1}}\right], I_{i+2^j}^{j+1} = \left[\alpha_i^j + \frac{2}{3^{j+1}}, \alpha_i^j + \frac{1}{3^j}\right]$$

for $0 \leq i \leq 2^j$. In this way it is possible to define by induction, the intervals $I_i^j (0 \leq i \leq 2^j)$ for every positive integer j. The left points α_i^j of I_i^j are rational numbers of the form

$$\frac{b_1}{3} + \frac{b_2}{3^2} + \ldots + \frac{b_j}{3^j}$$

with $b_j = 0$ *or* 2. From the definition of f it is easy to see that the 2^j intervals I_i^j are permuted cyclically by f. Therefore, the orbit of period $2^j (j > 0)$ is contained in $\bigcup_i I_i^j$.

For any $x_0 \in I$, with $x_0 \neq \overline{x}$, it is possible to choose $m_0 \geq 0$ such that $x_1 = f^{m_0}(x_0) \in I_0^1$. If x_1 is not periodic, then neither is $3x_1$ and as a consequence we can choose $m_1 \geq 0$ such that $f^{m_1}(3x_1)/3 \in I_0^1$. Then we construct $x_2 = f^{m_0+2m_1}(x_0) = f^{2m_1}(x_1) = f^{m_1}\frac{(3x_1)}{3} \in I_0^2$. Following with this procedure, we see that, for any $x \in I$,

is either x eventually periodic or, for every positive integer j, $f^n(x) \in \bigcup_i I_i^j$, for all large n. It follows that x is approximately periodic, and therefore, f is a uniformly non-chaotic map.

Besides the previous geometric introduction of the ternary Cantor set C_0, it can also be described [3] as the set of all points in I whose ternary expansion contain only 0's and 2's (including points like 1 whose expansion can be expressed by $0.2222\ldots$). From the above constructions, it is immediate to see that $I_{a_1}^1 \supset I_{a_2}^2 \supset \ldots$ is a nested sequence of intervals of type I_i^j, then $\bigcap I_{a_j}^j = y$ where y belongs to C_0. Moreover, each point of C_0 can be obtained in this way. This means that the closure of the orbit of 0 by f is C_0 and in fact this is the case for all $x \in I$ not being eventually periodic. Thus, C_0 is a *minimal set* of f and

$$R(f) = P(f) \bigcup C_0$$

In addition, since each point of C_0 is regularly recurrent, it follows (see [3]) that $f|C_0$ is topologically conjugate to the *adding machine transformation* ([3]) τ. Such transformation acts in the following way. If $x \in C_0$ has the ternary expansion $x = \sum_{i=0}^{\infty} \frac{2b_i}{3^{i+1}}$, then $f(x)$ has the ternary expansion $f(x) = \sum_{i=0}^{\infty} \frac{2c_i}{3^{i+1}}$ determined by the rule $\gamma = \beta + 1$, where $\beta = (b_0, b_1, \ldots)$ and $\gamma = (c_0, c_1, \ldots)$.

In the next result we state that any Cantor set on I can be obtained as minimal of a map g.

Theorem 10.2 *Let $C \subset I$ be a Cantor set. Then there exists a continuous interval map g such that C is minimal with respect to it.*

Proof Let consider the interval map f constructed in the previous paragraphs and C_0 the ternary Cantor set. Using the result in topology saying that all Cantor sets are homeomorphic (see for example [10]), there exists an homeomorphism $h : C \to C_0$. Since the complement in I of C is a union of countably many open sets, C results minimal with respect to the map g defined when $g(x) = h^{-1} \circ f \circ h(x)$ when $x \in C_0$ and linearly on any component of the complement of C.

The result cannot be extended to general metric spaces, since in such setting, a *Cantor set* is a subset without isolated points and totally disconnected but we do not know the structure of the complement of the Cantor set and as consequence it is not possible to define a map in such general setting. But recently in maps from the unit square $Q = [0, 1]^2$ into itself called *triangular*, that is, continuous maps $F(x, y) = (f(x), g(x, y))$ with f and g continuous, the above map has been used to close some open problems in a so called *Sharkovsky's program for triangular maps* (see [5] and [6]).

10.4 A Minimal Cantor Set in the Full Shift Σ^2 and in the Smale Horseshoe

The full shift on two symbols Σ^2 is the Cantor space composed of all bi-sequences of the form $(\ldots s_{-n} \ldots s_{-1} \cdot s_0 s_1 s_2 \ldots s_n \ldots)$, where $s_i \in 0, 1$ for $i \in Z$. It is well-known that in the thirties, Marston Morse showed that there exists an element in such space that is uniformly recurrent under the shift map σ, where

$$\sigma(\ldots s_{-n}\ldots s_{-1}s_0 \cdot s_1 s_2 \ldots s_n \ldots) = (\ldots s_{-n}\ldots s_{-1} \cdot s_0 s_1 s_2 \ldots s_n \ldots)$$

Such bi-sequence is called the *Morse sequence*. If (X, h) is a d.d.s. where X is a metric space and $h : X \to X$ a homeomorphism, then it is well-known (see for example [3]) that if $M \subseteq X$ is a minimal set, then every $x \in X$ is uniformly recurrent, and conversely, if $x \in X$ is uniformly recurrent, then the closure of its orbit, $Orb_h(x)$ is a minimal set of X. Such results are also valid when $f : X \to X$ is a continuous map and we use forward orbits. Since the Morse sequence is not periodic we have that its orbit contains infinite distinct elements.

Since the closure of the Morse sequence, M is closed in Σ^2, then M is a Cantor set and additionally it is minimal.

In [11] is given a detailed account of the construction of a two-dimensional d.d.s. which contains an invariant set called the Smale horseshoe denoted by Λ. In this previous sections it is proved that there exists a homeomorphism $\Phi : \Lambda \to \Sigma^2$. Since Cantor sets are kept by homeomorphisms, then $\Phi^{-1}(M)$ the inverse image by such homeomorphism of the closure of Morse sequence, is also an example of a minimal Cantor set.

In fact the d.d.s. $\left(\Sigma^2, \sigma\right)$ contains copies of all possible orbits of all d.d.s.. This fact is proved in [9] by the result

Theorem 10.3 *Let $Orb_f(x)$ be the orbit by a homeomorphism h on a metric space X. Then there is a conjugation $j : Orb_f(x) \to 0, 1^Z$ such that $\sigma j = jh$.*

10.5 Non-Minimal Cantor Sets

To have non-minimal Cantor sets in d.d.s. is a usual situation since it is sufficient to have a periodic orbit included in the Cantor set to be non-minimal. In such cases, it is unusual to have a Cantor set as a unique invariant set. This is the situation that arises in the following example. Let the d.d.s. (R, f) and,

$$f(x) = 3x \quad if \quad 0 \leq x \leq \frac{1}{2}$$

and

$$f(x) = 3(1 - x) \quad if \quad \frac{1}{2} \leq x \leq 1$$

the orbit of any point x_0 from the open interval $(\frac{1}{3}, \frac{2}{3})$ holds $lim_{n\to\infty} f^n(x_0)_{n=0}^{\infty} = -\infty$. But all open subintervals of I that are pre-images of it hold the same property. The rest of I is composed of points belonging to the ternary Cantor set included 0 which is a fixed point of f. Outside I all points hold the former asymptotic property. The unique invariant set is precisely the ternary Cantor set C.

Similarly, for the Smale horseshoe, the set $\Phi(\Lambda) = \Sigma^2$ is a Cantor set but non-minimal, since it contains infiniteperiodic orbits (for a detailed account of such details, see [11]).

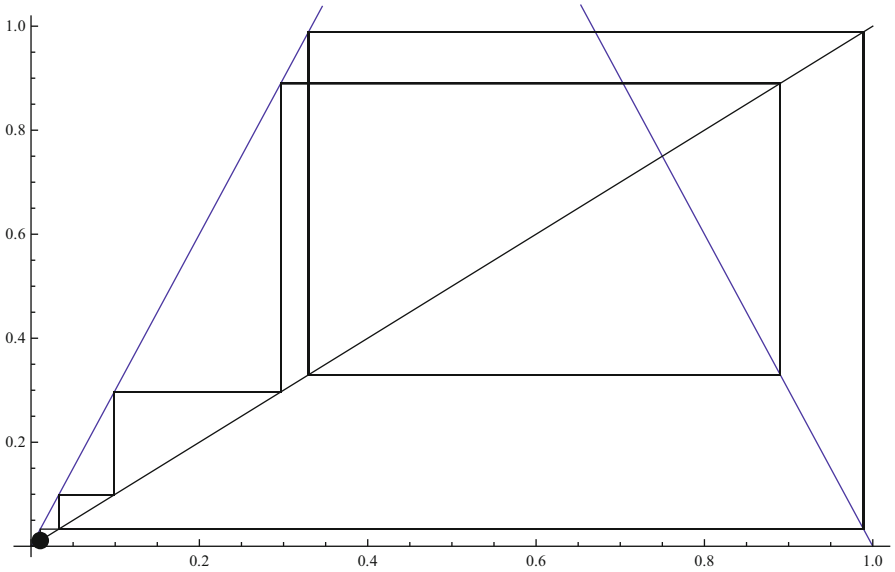

Fig. 10.2 Non-minimal piecewise linear map and the orbit of a point starting close to zero

Acknowledgment I thank both referees, for their careful reading of the text which has made possible to improve the chapter too much. This research has been partially supported by Grant MT2011-23221 from *Ministerio de Ciencia y Tecnología* (Spain) and by Grant 08667/PI/08 from *Fundación Séneca de la Región de Murcia* (Spain).

References

1. Alligood K, Sauer, T., Yorke, J.: CHAOS. An Introduction to Dynamical Systems. Textbooks in Mathematical Sciences, 3rd edn. Springer, New York (2000)
2. Alsedà L., Llibre J., Misiurewicz M.: Combinatorial Dynamics and Entropy in Dimension One. World Scientific, Singapore, (1993)
3. Block, L., Coppel, W.: Dynamics on One Dimension, Lecture Notes in Mathematics, vol. 1513. Springer, Berlin (1992)
4. Delahaye, J.: Fonctions admettant des cycles d'ordre n'importe quelle puissance de 2 et aucun autre cycle. C. R. Acad. Sci. Paris Ser. A-B **125**, 323–325 (1980)
5. Downarowicz, T.: Minimal subsystems of triangular maps of type 2^∞. Conclusion of the Sharkovsky classification program. Chaos, Solitons Fractals **49**, 61–71 (2013)
6. Downarowicz, T., Stefánkova, M.: Embedding Toeplitz systems in triangular maps. The last but one problem of the Sharkovsky classification program. Chaos, Solitons Fractals **45**, 1566–1572 (2012)
7. Erdös, P.: Representations of real numbers as sums and products of Liouville numbers. Michigan Math. J. **9**, 59–60 (1962)
8. Falconer, K.: Fractal Geometry. Mathematical Foundations and Applications. Wiley, Hoboken (1990)
9. Fokkink, R.: A note on the shift on the Cantor set. Proc. Am. Math. Soc. **112**(4), 1153–1155 (1991)

10. Munkres, J.: Topology, 2nd edn. Prentice Hall, New Jersey (2000)
11. Wiggins, S.: Introduction to Applied Nonlinear Dynamical Systems and Chaos, Texts in Applied Mathematics, vol 2. Springer, New York (1990)
12. Yamaguchi, M., Hata, M., Kigami, J.: Mathematics of Fractals. American Mathematical Society, Providence (1997)

Chapter 11
Piecewise Expanding Maps and Conjugacy Equations

Cristina Serpa and Jorge Buescu

Abstract Topological invariants of interval maps are preserved by conjugacy. We investigate some features of the conjugacy equations associated to piecewise expanding maps. For special cases, it is possible to construct explicitly a conjugacy function in terms of the a-base expansion of numbers through a solution of the corresponding functional equations.

One possible interest of conjugacy equations is to simplify the study of a family of maps by considering the simplest possible cases while preserving topological properties. In our case these will be the piecewise linear and expanding interval maps.

The conjugacy equation $h \circ g = f \circ h$ (where h is the unknown function) is the subject of much research in the field of functional equations. The main results already obtained for this kind of equation are those for invertible functions f, g (see [9]), where f is a scalar or a linear operator on the range of h (see the Schröder equation in [9, 10]). Other cases of interest arise when f, g are continuous functions with real domain and real range, strictly increasing and fixed-point free (see [11]), or f strictly decreasing continuous and g continuous (maybe nonmonotonic; see [14]). Usual references of one-dimensional dynamics [2, 12, 13] treat the case where f is continuous. In our case f is piecewise continuous.

We focus our attention on particular cases of the equation $h \circ g = f \circ h$, which correspond to a conjugacy equation involving the piecewise linear case. From the functional point of view we refer to results of de Rham [5] and their generalization by Girgensohn [8]. Since this last generalization provides an explicit solution in terms of the a-base expansion of numbers it is possible to construct explicitly a solution of our equation.

Definition 11.1 (see [3]) A map $f : I \to I$ is a *horseshoe map* if it has more than one lap and each lap is mapped onto the whole of I.

C. Serpa (✉) · J. Buescu
Centro de Matemática e Aplicações Fundamentais, Departamento de Matemática, Faculdade de Ciências, Universidade de Lisboa, 1749-016, Lisboa, Portugal
e-mail: mcserpa@fc.ul.pt

J. Buescu
e-mail: jsbuescu@fc.ul.pt

R. López-Ruiz et al. (eds.), *Nonlinear Maps and their Applications,*
Springer Proceedings in Mathematics & Statistics 112, DOI 10.1007/978-3-319-12328-8_11

The next Lemma is a generalization of a result of Ciepliński and Zdun [4] to noncontinuous functions (only piecewise continuity is required).

Lemma 11.1 *Let $a \geq 2$, be an integer, $g : [\alpha_1, \beta_1] \to [\alpha_1, \beta_1]$, $G : [\alpha_2, \beta_2] \to [\alpha_2, \beta_2]$ be piecewise continuous functions, respectively, with laps $I_i = \left[x_i, x_{i+1}\right]$, $J_i = \left[y_i, y_{i+1}\right]$, $i \in \{0, 1, \ldots, a-1\}$. Consider the conjugacy equation*

$$h\left(g\left(x\right)\right) = G\left(h\left(x\right)\right), \; x \in [\alpha_1, \beta_1], \tag{11.1}$$

where $h : [\alpha_1, \beta_1] \to [\alpha_2, \beta_2]$ is the unknown function.

Suppose g, G are horseshoe maps, and φ is a monotone and surjective solution of (11.1). If φ is increasing, then $\varphi\left(x_i\right) = y_i$, and $\varphi\left[I_i\right] = J_i$ for $i \in \{0, 1, \ldots, a-1\}$. If φ is decreasing, then $\varphi\left(x_i\right) = y_{a-i}$, and $\varphi\left[I_i\right] = J_{a-i-1}$ for $i \in \{0, 1, \ldots, a-1\}$.

Proof Since g is a horseshoe map and φ is a monotone and surjective solution of Eq. (11.1), we have for each $i \in \{0, 1, \ldots, a-1\}$,

$$\begin{aligned} \varphi\left(g\left(x_i\right)\right) = G\left(\varphi\left(x_i\right)\right) &\Rightarrow G\left(\varphi\left(x_i\right)\right) \in \left\{\varphi\left(\alpha_1\right), \varphi\left(\beta_1\right)\right\} \\ &\Rightarrow G\left(\varphi\left(x_i\right)\right) \in \{\alpha_2, \beta_2\} \\ &\Rightarrow \varphi\left(x_i\right) \in \{y_0, y_1, \ldots, y_a\}. \end{aligned}$$

Suppose for each $i \in \{0, 1, \ldots, a-1\}$, $\varphi\left(x_i\right) = \varphi\left(x_{i+1}\right)$. Since φ is monotone, $\varphi\left[I_i\right]$ is a single point, as is $G\left[\varphi\left[I_i\right]\right]$. Again by Eq. (11.1) and surjectivity of φ we obtain $G\left[\varphi\left[I_i\right]\right] = \varphi\left[g\left[I_i\right]\right] = \varphi\left[\alpha_1, \beta_1\right] = [\alpha_2, \beta_2]$. Then $\varphi\left(x_i\right) \neq \varphi\left(x_{i+1}\right)$, $i \in \{0, 1, \ldots, a-1\}$.

If φ is increasing, then $\varphi\left(x_0\right) < \varphi\left(x_1\right) < \cdots < \varphi\left(x_a\right)$, implying $\varphi\left(x_i\right) = y_i$, because $\varphi\left(x_i\right) \in \left\{y_0, y_1, \ldots, y_p\right\}$. Then $\varphi\left[I_i\right] = J_i$, $i \in \{0, 1, \ldots, a-1\}$. If φ is decreasing, then $\varphi\left(x_0\right) > \varphi\left(x_1\right) > \cdots > \varphi\left(x_a\right)$, implying $\varphi\left(x_i\right) = y_{a-i}$, because $\varphi\left(x_i\right) \in \{y_0, y_1, \ldots, y_a\}$. Then $\varphi\left[I_i\right] = J_{a-i-1}$, $i \in \{0, 1, \ldots, a-1\}$.

We will restrict attention to the family $\mathcal{M}$ of piecewise monotone and expanding interval maps $f : [0, 1] \to [0, 1]$ where there exists a partition $0 = a_0 < a_1 < \cdots < a_r = 1$, with $r \geq 2$, of $[0, 1]$ such that $f_{|[a_{i-1}, a_i]}$, for $i = 1, 2, \ldots, r$, is a monotone piecewise continuous function for which there exists $\lambda > 1$ such that $\left|f'\left(x\right)\right| \geq \lambda$, for almost every $x \in [0, 1]$.

Note that the expansivity condition does not necessarily require that the function be differentiable. The definition of $\mathcal{M}$ may be weakened to the following expansivity condition.

Definition 11.2 A continuous map $f : X \to X$ on a metric space (X, d) is expanding if there exist constants $\varepsilon > 0$ and $\lambda > 1$ such that, for all $x, y \in X$,

$$d\left(x, y\right) < \varepsilon \Rightarrow d\left(f\left(x\right), f\left(y\right)\right) \geq \lambda d\left(x, y\right),$$

λ is called the expansion factor of f.

Let $f \in \mathcal{M}$ with partition $0 = \alpha_0 < \alpha_1 < \cdots < \alpha_a = 1$ of $[0, 1]$ such that $f_{|[\alpha_{i-1}, \alpha_i]}$, for $i = 1, 2, \ldots, a$, is an increasing, continuous and expanding function satisfying $f\left(\alpha_{i-1}, \alpha_i\right) = (0, 1)$, for every $i = 1, 2, \ldots, a$. We will see, in the

piecewise linear case, that f is topologically conjugate to the map,

$$g_a(x) = \begin{cases} ax \pmod 1, & \text{if } x \in [0,1) \\ 1, & \text{if } x = 1, \end{cases}$$

i.e, there exists a homeomorphism h such that

$$h \circ g_a = f \circ h. \tag{11.2}$$

Let $a \geq 2$. Define $\mu_0, \mu_1, \ldots, \mu_{a-1} \in (0,1)$ by $\mu_i = \alpha_{i+1} - \alpha_i$ for $i \in \{0, 1, \ldots, a-1\}$. Clearly $\sum_{j=0}^{a-1} \mu_j = 1$.

In the linear case, is given by

$$f(x) = \begin{cases} \frac{1}{\mu_i} x - \frac{\alpha_i}{\mu_i} & , \text{if } x \in [\alpha_{i-1}, \alpha_i), \ i \in \{0, 1, \ldots, a-1\} \\ 1 & , \text{if } x = 1, \end{cases}$$

it is possible to construct an explicit solution using the following results.

Theorem 11.1 *Any monotone increasing and surjective solution of the conjugation equation $h \circ g_a = f \circ h$ satisfies the functional equation*

$$h(x) = \mu_i h(ax - i) + \alpha_i, \text{for each } i \in \{0, 1, \ldots, a-1\}, \ x \in \left[\frac{i}{a}, \frac{i+1}{a}\right]. \tag{11.3}$$

Proof Let M be an increasing and surjective solution of Eq. (11.3). Then

$$M(ax - i) = \frac{1}{\mu_i} M(x) - \frac{\alpha_i}{\mu_i}, i \in \{0, 1, \ldots, a-1\}, \ x \in \left[\frac{i}{a}, \frac{i+1}{a}\right].$$

By direct computation,

$$M \circ g_a(x) = \begin{cases} M(ax - i) & , \text{if } x \in \left[\frac{i}{a}, \frac{i+1}{a}\right), \ i \in \{0, 1, \ldots, a-1\} \\ 1 & , \text{if } x = 1. \end{cases}$$

$$= \begin{cases} \frac{1}{\mu_i} M(x) - \frac{\alpha_i}{\mu_i} & , \text{if } x \in \left[\frac{i}{a}, \frac{i+1}{a}\right), \ i \in \{0, 1, \ldots, a-1\} \\ 1 & , \text{if } x = 1, \end{cases}$$

and

$$f \circ M(x) = \begin{cases} \frac{1}{\mu_i} M(x) - \frac{\alpha_i}{\mu_i} & , \text{if } M(x) \in [\alpha_{i-1}, \alpha_i), \ i \in \{0, 1, \ldots, a-1\} \\ 1 & , \text{if } M(x) = 1. \end{cases}$$

By Lemma 11.1, if M is monotone increasing and surjective, then for each $i \in \{0, 1, \ldots, a-1\}$ $M(x) \in \left[\alpha_{i-1}, \alpha_i\right)$ is equivalent to $x \in [i/a, (i+1)/a)$. □

Remark 11.1 An analogous result holds for decreasing and surjective solutions as a consequence of Lemma 11.1.

Example For $a = 3$, Eq. (11.3) is

$$h(x) = \begin{cases} \mu_0 h(3x) & , \text{if } x \in \left[0, \frac{1}{3}\right] \\ \mu_1 h(3x-1) + \alpha_1 & , \text{if } x \in \left[\frac{1}{3}, \frac{2}{3}\right] \\ \mu_2 h(3x-2) + \alpha_2 & , \text{if } x \in \left[\frac{2}{3}, 1\right]. \end{cases}$$

Lemma 11.2 *Let $a \geq 2$ be an integer. Consider the system of functional equations*

$$h\left(\frac{k+t}{a}\right) = F_k h(t), \tag{11.4}$$

where $k \in \{0, 1, 2, \ldots, a-1\}$, F_k are contractions mappings and $h : [0,1] \to [0,1]$ is the unknown function.

Then the system of functional equations (11.4) is equivalent to the functional equation

$$h(t) = F_k h(at - k), t \in \left[\frac{k}{a}, \frac{k+1}{a}\right], k \in \{0, 1, 2, \ldots, a-1\}.$$

Theorem 11.2 *(Girgensohn [9]) Let $a \geq 2$ be an integer. Let $s_k : [0,1] \to \mathbb{R}$ be continuous, $|r_k| < 1$ for $0 \leq k \leq a-1$ and assume*

$$\frac{r_{k-1}}{1 - r_{a-1}} s_{a-1}(1) + s_{k-1}(1) = \frac{r_k}{1 - r_0} s_0(0) + s_k(0), \ 1 \leq k \leq a-1. \tag{11.5}$$

Then there exists exactly one bounded function $f : [0,1] \to \mathbb{R}$ which satisfies the system

$$f\left(\frac{x+k}{a}\right) = r_k f(x) + s_k(x), \ x \in [0,1], \ 0 \leq k \leq a-1. \tag{11.6}$$

The function f is continuous and given in terms of the a-base expansion of x by

$$f\left(\sum_{n=1}^{\infty} \frac{\xi_n}{a^n}\right) = \sum_{n=1}^{\infty} \left(\prod_{k=1}^{n-1} r_{\xi_k}\right) s_{\xi_n}\left(\sum_{k=1}^{\infty} \frac{\xi_{k+n}}{a^k}\right). \tag{11.7}$$

We now return to the study of the general Eq. (11.2).

Lemma 11.3 *Any monotone increasing and surjective solution of the conjugation equation $h \circ g_a = f \circ h$ satisfies the functional equation*

$$h(x) = \mu_i h(ax - i) + \alpha_i, i \in \{0, 1, \ldots, a-1\}, \; x \in \left[\frac{i}{a}, \frac{i+1}{a}\right],$$

i.e.,

$$h\left(\frac{x+i}{a}\right) = \mu_i h(x) + \alpha_i, i \in \{0, 1, \ldots, a-1\}, \; x \in \left[\frac{i}{a}, \frac{i+1}{a}\right].$$

The condition

$$\frac{r_{k-1}}{1 - r_{a-1}} s_{a-1}(1) + s_{k-1}(1) = \frac{r_k}{1 - r_0} s_0(0) + s_k(0), \; 1 \le k \le a-1$$

in this case assumes the form

$$\frac{\mu_{i-1}}{1 - \mu_{a-1}} \alpha_{a-1} + \alpha_{i-1} = \frac{\mu_i}{1 - \mu_0} 0 + \alpha_i, \; 1 \le i \le a-1,$$

which is equivalent to

$$\mu_{i-1} = \alpha_i - \alpha_{i-1}, \; 1 \le i \le a-1,$$

coinciding with the original hypothesis.

Applying Theorem 11.2, we obtain the following explicit solution in terms of the a-base expansion of numbers.

Theorem 11.3 *Let $a \ge 2$, $0 = \alpha_0 < \alpha_1 < \cdots < \alpha_a = 1$, and $\mu_0, \mu_1, \ldots, \mu_{a-1} \in (0,1)$, such that $\mu_i = \alpha_{i+1} - \alpha_i$, for $i \in \{0, 1, \ldots, a-1\}$.*

Given f and g_a defined above, there exists exactly one increasing homeomorphism $h : [0,1] \to [0,1]$ such that $h \circ g_a = f \circ h$, defined by

$$h\left(\sum_{n=1}^{\infty} \frac{\xi_n}{a^n}\right) = \sum_{n=1}^{\infty} \left(\prod_{i=1}^{n-1} \mu_{\xi_i}\right) \alpha_{\xi_n}. \tag{11.8}$$

Proof By Lemma 11.3 and Theorem 11.2, there exists exactly one-bounded monotone increasing and surjective $h : [0,1] \to [0,1]$, such that $h \circ g_a = f \circ h$ which is defined by formula (11.8). Lemma 1 in [18] by Zdun shows that function h is a homeomorphism. □

Remark 11.2 An analogous result may be proved for the case of a decreasing homeomorphism.

We next provide two examples of application of the explicit formula (11.8) to problems of Number Theory and Probability Theory.

11.1 Applications: Variable Base Expansions and Bold Play

11.1.1 Q-Representation of Real Numbers

The usual a-base representation of a number is given by

$$x = \sum_{n=1}^{\infty} \frac{\xi_n}{a^n}. \tag{11.9}$$

Turbin and Prats'ovytyi [15, 16] introduced a more general representation, where the length of the intervals defining the expansion is not uniform.

Let $a \geq 2$ be a fixed positive integer, and $q_0, q_1, \ldots, q_{p-1} \in (0,1)$, such that $\sum_{j=0}^{p-1} q_j = 1$. Let $r_0 = 0$, $r_j = \sum_{k=0}^{j} q_{k-1}$, for $j \in \{1, 2, \ldots, a\}$, $A = \{0, 1, 2, \ldots, a-1\}$, and $Q = \left\{q_0, q_1, \ldots, q_{p-1}\right\}$.

Theorem 11.4 *(Turbin and Prats'ovytyi) For any number $x \in [0,1]$, there exists a sequence of numbers $v = (v_n) \in A$ such that*

$$x = \sum_{n=1}^{\infty} \left(\prod_{k=1}^{n-1} q_{v_k} \right) r_{v_n}. \tag{11.10}$$

Remark 11.3 Obviously, for any real number x there exists an expansion

$$x = [x] + \sum_{n=1}^{\infty} \left(\prod_{k=1}^{n-1} q_{v_k(x)} \right) r_{v_n(x)}. \tag{11.11}$$

Definition 11.3 Given $x \in \mathbb{R}$, the representation by series (11.10) or (11.11) is called a-symbol Q-representation or a-symbol Q-expansion of x. For $x \in [0,1]$ we use the notation given by

$$\triangle_v^Q = \triangle_{v_1 v_2 \cdots v_n \cdots}^Q := \sum_{n=1}^{\infty} \left(\prod_{k=1}^{n-1} q_{v_k} \right) r_{v_n}. \tag{11.12}$$

Remark 11.4 An algorithm to find an a-symbol Q-representation of a number $x \in [0,1]$ is:

0. Let $n = 1$ and $x_1 = x$.
1. Find $v_n \in \{0, 1, \ldots, p-1\}$, such that $r_{v_n} \leq x_n < r_{v_n+1}$. If $x = r_{v_n}$, do $v_N = 0$, for $N > n$, and the process is finished. Else do step 2.
2. Find the difference $x_n - r_{v_n}$ and divide by q_{v_n}:

$$x_{n+1} = \frac{x_n - r_{v_n}}{q_{v_n}}.$$

3. Do step 1 for $n + 1$.

The sequence $\nu = (\nu_n) \in A$ determines the a-symbol Q-representation of x. We now show that representations (11.9) and (11.12) are related by a homeomorphism which is a solution of an equation of the form (11.2).

Theorem 11.5 *There is a homeomorphism φ such that the image of each $x \in [0,1]$ by φ is the a-symbol Q-expansion of x, where the sequence of numbers $(\nu_n) \in A$ of the image obtained is the same as the a-base representation of x, i.e., $\nu_n = \xi_n$, $\forall n \in \mathbb{N}$. Moreover, φ is the unique bounded solution of the system of equations*

$$\varphi\left(\frac{x+k}{a}\right) = q_k \varphi(x) + r_k,\ x \in [0,1],\ 0 \le k \le a-1. \tag{11.13}$$

Proof By definition of q_k and r_k, condition (11.5) is satisfied. Applying Theorem 11.2 there exists a unique bounded solution of (11.13) given, in terms of the a-base representation, by

$$\varphi\left(\sum_{n=1}^{\infty} \frac{\xi_n}{a^n}\right) = \sum_{n=1}^{\infty} \left(\prod_{k=1}^{n-1} q_{\xi_k}\right) r_{\xi_n}. \tag{11.14}$$

□

This result may be viewed as a special case of Lemma 1 in [18] by Zdun which shows that the function φ is a homeomorphism. Girgensohn's result (Theorem 11.2) is more general, since in its statement the r_k are allowed to be continuous functions of x, $r_k : [0,1] \to \mathbb{R}$, instead of constants.

Remark 11.5 The function φ in (11.14) may be given in the equivalent forms

$$\varphi\left(\sum_{n=1}^{\infty} \frac{\xi_n}{a^n}\right) = \triangle_{\xi}^{Q}, \tag{11.15}$$

$$\varphi^{-1}\left(\triangle_{\xi}^{Q}\right) = \sum_{n=1}^{\infty} \frac{\xi_n}{a^n}. \tag{11.16}$$

In a similar fashion, the function that transforms a-symbol Q-expansions in other a-symbol Q-expansions was given by Prats'ovytyi and Kalashnikov [17]. If we denote by $\triangle_{\nu}^{Q[q,r]} = \triangle_{\nu_1\nu_2\cdots\nu_n\cdots}^{Q[q,r]}$ the a-symbol Q-expansion in terms of q_j, r_j, and ν, defined above, the system of functional equations

$$\psi\left(\triangle_{k\nu_1\nu_2\cdots\nu_n\cdots}^{Q[q,r]}\right) = t_k \psi\left(\triangle_{\nu_1\nu_2\cdots\nu_n\cdots}^{Q[q,r]}\right) + s_k,\ k \in \{0,1,\ldots,a-1\}$$

has a unique bounded solution ψ defined by

$$\psi\left(\triangle_{\nu}^{Q[q,r]}\right) = \triangle_{\nu}^{Q[t,s]}. \tag{11.17}$$

We note that our results imply immediately construction (11.17). In fact, let $a \geq 2$ be an integer, and let $(a, Q[q,r])$ and $(a, Q[t,s])$ be bases of a-symbol Q-representations. Remark 11.5 implies that the diagram

$$\begin{array}{ccc} \sum_{n=1}^{\infty} \frac{\xi_n}{a^n} & \xrightarrow{\mathrm{id}_{[0,1]}} & \sum_{n=1}^{\infty} \frac{\xi_n}{a^n} \\ \varphi_{q,r} \downarrow & & \downarrow \varphi_{t,s} \\ \triangle_{\xi}^{Q[q,r]} & \xrightarrow{\psi} & \triangle_{\xi}^{Q[t,s]} \end{array}$$

is commutative, where the indices of φ correspond to the parameters of the system (11.13) for which φ is solution.

Thus the required homeomorphism ψ in (11.17) is given by

$$\psi = \varphi_{t,s} \circ \varphi_{q,r}^{-1}. \tag{11.18}$$

Thus Theorem 11.2 allows us to construct an alternative, equivalent representation of the homeomorphism ψ.

11.1.2 Bold Play Gambling

Our second example, bold play gambling, originates in casino games (see [1] for a detailed description). Consider a gambler playing roulette, staking the amount of money s at each turn of the wheel. The probability of winning s is p and the probability of losing s is $q = 1 - p$.

Suppose the initial capital is C and the gambler's goal is G. The gambler will play until his fortune has reached G or has dwindled to nothing. The game strategy called *bold play* is the following: in each turn of the wheel the gambler either stakes his entire fortune, if this fortune does not exceed half the goal, or bets the difference between the goal and his current fortune. For a normalized problem, consider $G = 1$, and the domain will be the interval $[0, 1]$.

Formalizing the problem, denote the gambler's current fortune by x, so that $0 \leq x \leq 1$. If $0 \leq x \leq 1/2$, he bets x (all the money); a win gives him a new fortune of $2x$, and a loss ruins him (lose everything). If $1/2 \leq x \leq 1$, he bets $1 - x$, just enough to carry him to his goal of 1; a win gives him a new fortune of 1 (a success), and a loss leaves him with $2x - 1$.

Proposition 11.1 *Let $p + q = 1$, $p > 0$, $q > 0$. The probability of success under bold play $f(x)$ for an initial fortune x is the unique solution of the system of equations*

$$\begin{cases} f(x) = pf(2x) & , \text{if } 0 \leq x \leq \frac{1}{2} \\ f(x) = p + qf(2x-1) & , \text{if } \frac{1}{2} \leq x \leq 1, \end{cases} \tag{11.19}$$

constrained to $f(0) = 0$, $f(1) = 1$.

Remark 11.6 If $p = q = 1/2$, it is immediate that the identity is a solution of (11.19). From Proposition 11.1 this solution is unique.

Proof (see [1]) For the case $p = q = 1/2$, a classical result in probability applies (see e.g. [7]). For $x = 0$, $f(x) = 0$, and equation $f(x) = pf(2x)$ is satisfied. For $x = 1$, $f(x) = 1$, and equation $f(x) = p + qf(2x - 1)$ is verified. For $0 < x \leq 1/2$, under bold play the gambler stakes the amount x. In case of success in the first turn, with probability p, his new fortune is $2x$. Since each turn has independent outcomes, the probability of success in the second turn $f(2x)$ multiplied by p equals the initial probability of success $f(x)$, proving the first equation of (11.19).

For $1/2 \leq x < 1$, the first stake is $1 - x$. In case of success in the first turn, with probability p, his new fortune is 1. In case of loss, with probability q, his new fortune is $2x - 1$. The probability of success after a loss is $f(2x - 1)$. Since each turn has independent outcomes, the probability of success given by $p + qf(2x - 1)$ equals the initial probability of success $f(x)$, proving the second equation of (11.19). Uniqueness of the solution now follows from Theorem 11.3 given initial conditions.

The probability of success of a strategy of bold play gamble satisfies a system of equations of type (11.3). Applying Theorem 11.3 we have the following explicitly defined function of probability of success, in terms of binary representation of real numbers.

Corollary 11.1 *The probability of success under bold play for an initial fortune*

$$x = \sum_{n=1}^{\infty} \frac{\xi_n}{2^n}$$

is

$$f\left(\sum_{n=1}^{\infty} \frac{\xi_n}{2^n}\right) = \sum_{n=1}^{\infty} \left(\prod_{i=1}^{n-1} \mu_{\xi_i}\right) \alpha_{\xi_n},$$

where $\alpha_0 = 0$, $\alpha_1 = p$, $\mu_0 = p$, *and* $\mu_1 = q$.

Dubins and Savage [6] showed that in case where the game is unfair for the player ($p < q$), the bold play strategy is optimal, although it is not the only optimal strategy.

Acknowledgements The first author acknowledges support by Fundação para a Ciência e Tecnologia, grant SFRH/BD/77623/2011. The second author acknowledges partial support by Fundação para a Ciência e Tecnologia, PEst-OE/MAT/UI0209/2013. The authors are also indebted to the anonymous referees for their sharp suggestions.

References

1. Billingsley, P.: The singular function of bold play. Am. Sci. **71**, 4 (1983)
2. Block, L. S., Coppel, W. A.: Dynamics in One Dimension, Lecture Notes in Mathematics, 1513, Springer-Verlag, Berlin, Heidelberg (1992)

3. Blokh, A., Coven, E., Misiurewicz, M., Nitecki, Z.: Roots of continuous piecewise monotone maps of an interval. Acta Math. Univ. Comenian. LX **1**, 3–10 (1991)
4. Ciepliński, K., Zdun, M.: On uniqueness of conjugacy of continuous and piecewise monotone functions. Fixed Point Theory A **2009**, 230414 (2009)
5. de Rham, G.: Sur quelques courbes définies par des équations fonctionnelles. Rend. Sem. Math. Torino **16**, 101–113 (1956)
6. Dubins, L. E., Savage, L. J.: Optimal gambling systems. PNAS **46**, 1597–1598 (1960)
7. Feller, W.: An Introduction to Probability Theory and Its Applications , I, 3rd edn., John Wiley & Sons, Inc., New York (1968)
8. Girgensohn, R.: Functional equations and nowhere differentiable functions. Aequationes Math. **48**, 243–256 (1993)
9. Kuczma, M.: Functional Equations in a Single Variable. PWN Warszawa (1968)
10. Kuczma, M., Choczewski, B., Ger, R.: Iterative Functional Equations. Encyclopedia Math. Appl., Cambridge University Press, New York, Melbourne (1990)
11. Laitochová, J.: On conjugacy equations for iterative functional equations. Int. J. Pure Appl. Math. **26**(3), 421–430 (2006)
12. May, R. M.: Simple mathematical models with very complicated dynamics. Nature **261**, 459–467 (1976)
13. Melo, W., van Strien, S.: One-Dimensional Dynamics. Springer-Verlag, Berlin, Heidelberg (1993)
14. Shi, Y.-G.: Non-monotonic solutions and continuously differentiable solutions of conjugacy equations. Appl. Math. Comput. **215**, 2399–2404 (2009)
15. Turbin, A. F., Prats'ovytyi, M. V.: Fractal Sets, Functions and Distributions. Naukova Dumka, arXiv:math/0308007v2 (1992)
16. Prats'ovytyi, M. V.: Fractal approach to investigations of singular probability distributions, Kiyv, Drahomanov National Pedagogical Univ. (1998)
17. Prats'ovytyi, M. V., Kalashnikov, A. V.: Self-affine singular and monotone functions related to the Q-representation of real numbers. Ukr. Math. J. **65**, 448–462 (2013)
18. Zdun, M.: On conjugacy of some systems of functions. Aequationes Math. **61**, 239–254 (2001)

Chapter 12
In Search of H-theorem for Ulam's Redistribution of Energy Problem

Sergey M. Apenko

Abstract We discuss the possibility of deriving an H-theorem for the nonlinear discrete time evolution known as Ulam's redistribution of energy problem. In this model particles are paired at random and then their total energy is redistributed between them according to some probability law. It appears useful to represent the evolution as a combination of two processes. The first is a linear transformation of two-particle distribution function due to redistribution while the second one is a kind of "reduction" which corresponds to new random pairing. Then information theory approach leads to a general inequality for the Ulam's problem, which may be viewed as a kind of Clausius inequality. However, only for a special set of redistribution laws, given by symmetric beta distributions, this inequality results in the H-theorem. The H-functional in this case differs from the usual entropy by an additional term that vanishes only for the uniform redistribution law.

12.1 Introduction

Ulam's redistribution of energy problem was introduced in a paper by Blackwell and Mauldin [1] and was formulated as follows: "Consider a vast number of particles and let us redistribute the energy of these particles ... First, pair the particles at random. Second, for each pair, redistribute the total energy of the pair between these particles according to some given fixed probability law of redistribution ... ." This means that if initial energies of two particles were x and y, then after the redistribution

$$x' = \epsilon(x + y), \qquad y' = (1 - \epsilon)(x + y), \tag{12.1}$$

where $0 < \epsilon < 1$ is a random number with a distribution $D(\epsilon)$. Since particles are indistinguishable we assume that $D(\epsilon) = D(1-\epsilon)$ so that the mean value of ϵ is just $1/2$. Ulam had suggested that after many iterations of this process the energy distribution $p(x)$ $(x > 0)$ should finally converge to some fixed equilibrium distribution $p_0(x)$, which depends only on a given redistribution law, and this conjecture was proved in [1, 2]. For absolutely random redistribution, when $D(\epsilon) = 1$, it was shown

S. M. Apenko (✉)
P N Lebedev Physical Institute, Moscow 119991, Russia
e-mail: apenko@lpi.ru

R. López-Ruiz et al. (eds.), *Nonlinear Maps and their Applications,*
Springer Proceedings in Mathematics & Statistics 112, DOI 10.1007/978-3-319-12328-8_12

that in equilibrium $p_0(x) = \lambda \exp(-\lambda x)$ [1], where $1/\lambda = \langle x \rangle$ is determined by the mean energy $\langle x \rangle$, which is conserved in this process. Later it was realized, however, that this problem was actually just a particular case of a more general one, related to "smoothing transformations," discussed in details earlier in [3, 4], where almost all necessary theorems had been already proved and exact equilibrium solutions for some other redistribution laws were found.

All these papers remained practically unknown to physicists for several decades, while similar models were independently introduced in an economic context as random market models, which assume that transactions occur by binary "collisions" between agents, who, e.g., exchange money in the same way as particles in a gas exchange their energy (see e.g., [5–7] and references therein). It is interesting that one toy model of money redistribution, introduced among several others by Drăgulescu and Yakovenko [8] was exactly the same as (12.1) with uniform redistribution law $D(\epsilon) = 1$.

Our study of Ulam's redistribution problem is based on the approach initiated by López-Ruiz and his colleagues [9, 10], who have proposed a discrete time nonlinear evolution equation for the process (12.1) with uniform redistribution law in terms of a distribution function $p(x)$. An obvious generalization of their equation for general $D(\epsilon)$, which will be studied below, is

$$p'(x) = \int_0^\infty \int_0^\infty du dv \, \frac{\theta(u+v-x)}{u+v} D\left(\frac{x}{u+v}\right) p(u) p(v). \tag{12.2}$$

This nonlinear mapping shows how the probability distribution function transforms on each step of iterations when $p(x) \to p'(x)$. For uniform redistribution law $D = 1$ and only the factor $1/(u+v)$ remains, which is just the normalized probability distribution for x that can have any value from zero to $u+v$. In this case Eq. (12.2) coincides with the one used in [9, 10].

Since this evolution is based on pairwise interactions, just as in a gas of particles, described by the Boltzmann equation, one might expect some kind of H-theorem to be valid here. And indeed, for the uniform redistribution law the Boltzmann entropy

$$S(p) = -\int dx \; p(x) \ln p(x)$$

increases on each time step [9, 11], i.e., $S(p') \geq S(p)$. However for an arbitrary $D(\epsilon)$ one cannot expect that the entropy $S(p)$ always grows. Thus a question arises—What is the proper H-function (if it exists) that is monotone during the relaxation for an arbitrary redistribution law?

Here we will follow the approach of [11] which makes use of the two-particle distribution function. However, this will lead to an H-theorem only for a special case of symmetric beta redistribution law. We will be able to obtain H-functional which is equal to the Boltzmann entropy plus some additional term. For the general case, however, only some more general inequality, similar to Clausius inequality in ordinary thermodynamics, is available. This suggests a point of view that the system of particles with redistribution of energy according to (12.1) is, in fact, an open system in contact with a reservoir of the special type with a "heat" flow to this reservoir due to redistribution of energy.

12.2 Two-Stage Representation of the Redistribution Process

Our search for the H-theorem is based on the approach of [11] which transforms initial nonlinear problem into a linear one, supplemented by a subsequent projection operation, by introducing a two-particle distribution function $f(x, y)$. After a "collision" and redistribution of energy $f(x, y) \to f'(x, y)$ and it appears possible to write down a simple equation describing this evolution.

12.2.1 Two-Particle Distribution Function

There exist a regular way to obtain an equation for the two-particle probability distribution function $f(x, y)$ from the original equation for $p(x)$. We start from the integral representation for the theta-function in (12.2)

$$\theta(u + v - x) = \int_0^\infty dy\, \delta(x + y - u - v). \tag{12.3}$$

Since the delta-function here obviously represents the conservation law during the collision, it is quite natural to view y as energy of the second particle after the collision. Now we substitute this expression into Eq. (12.2) and after changing the order of integration we may write

$$p'(x) = \int_0^\infty dy\, f'(x, y), \tag{12.4}$$

where $f'(x, y)$ is given by

$$f'(x, y) = D\left(\frac{x}{x + y}\right) \int_0^\infty \int_0^\infty du dv\, \frac{\delta(x + y - u - v)}{u + v} f(u, v), \tag{12.5}$$

with $f(u, v) = p(u)p(v)$. Now we make a change of variables in the integral $u, v \to E, \xi$ where $E = u + v$ and $\xi = u/(u + v)$. The Jacobian of this transformation is just $u + v$ so it exactly cancels the denominator in the integrand. Integration over E is trivial because of the delta-function, so finally we arrive at

$$f'(x, y) = D\left(\frac{x}{x + y}\right) \int_0^1 d\xi\, f(\xi(x + y), (1 - \xi)(x + y)), \tag{12.6}$$

For $D = 1$ this equation was obtained in [11]. This is a linear transformation and it conserves positivity of $f(x, y)$, its norm and the mean "energy" $\langle x + y \rangle$.

Physically it is rather obvious that $f(x, y)$ is a two-point distribution function that gives the probability that one particle has the energy x while the other has y. It should be noted, however, that Eq. (12.6) alone does not describe correctly the true evolution of the two-particle probability distribution in Ulam's problem. It takes into account only collisions within fixed pairs of particles while the true evolution includes also new random pairings of particles on each step, not accounted for in (12.6).

The transformation of the original nonlinear equation made above suggests a new physical representation of the problem. In terms of of the two-particle function $f(x, y)$ the evolution may be represented as consisting of two steps.

1. On the first step, when we pair particles at random, we have $f(x, y) = p(x)p(y)$ and then, as a result of energy redistribution,

$$f(x, y) = p(x)p(y) \to f'(x, y), \tag{12.7}$$

   where the new probability distribution is given by (12.6).
2. Next we perform a new random pairing, destroying all correlations induced by previous interactions. Therefore, this second step may be describes as a "reduction"

$$f'(x, y) \to p'(x)p'(y), \tag{12.8}$$

   where $p'(x)$ is a marginal distribution given by (12.4). One can easily verify, that combination of these two steps is completely equivalent to the original nonlinear equation, i.e., the final $p'(x)$ is indeed given by (12.2).

This approach is actually an opposite one to the normal derivation of the Boltzmann-type equation from the general equation for many-particle distribution function. For wealth exchange problems such a derivation was performed in [12] for the continuous time evolution. Obviously our reduction condition (12.8) is similar to "molecular chaos" assumption used when Boltzmann equation is obtained. But here we already have this nonlinear equation for $p(x)$ as a starting point and simply restore the corresponding exact two-stage evolution of the two-particle function.

12.2.2 Inequality for Two-Particle Relative Entropy

The advantage of Eq. (12.6) is that this is a linear evolution equation similar to what we have for a stationary Markov chain for which the monotone functional can be easily constructed. Normally, it is the relative entropy with respect to a stationary state $f_0(x, y)$ that monotonically decreases during relaxation for such equations.

The regular way to prove such monotonicity theorems is to start from the relative entropy, or Kullback–Leibler (KL) distance $D(\mu||\nu) = \sum \mu \ln \mu/\nu$ between two probability distributions μ and ν. It is well-known from information theory that $D(\mu||\nu)$ cannot increase under "coarse-graining" of these distributions, when some variables are integrated out. This immediately follows from the chain rule for relative entropy [13]. Consider now the distribution

$$\mu(\xi, x, y) = D\left(\frac{x}{x+y}\right) f(\xi(x+y), (1-\xi)(x+y)), \tag{12.9}$$

defined on the space $\xi \in [0, 1]$, $x, y \in [0, \infty)$ and define $\nu(\xi, x, y)$ in the same way through the stationary solution $f_0(x, y)$ of (12.6), i.e., with $f(x, y) \to f_0(x, y)$ in

(12.9). Both $\mu(\xi, x, y)$ and $\nu(\xi, x, y)$ are obviously positive and normalized to unity (this follows from $\int d\epsilon\, D(\epsilon) = 1$).

It is easy to see that Eq. (12.6) actually has many stationary solutions. In fact, any probability distribution of the form

$$f_0(x, y) = D\left(\frac{x}{x+y}\right) F(x+y) \tag{12.10}$$

with arbitrary $F(x + y)$, is such a stationary solution.

Next, define the coarse-graining procedure $\mu \to \tilde{\mu}$ as averaging over the ξ variable, i.e.,

$$\tilde{\mu}(x, y) = \int_0^1 d\xi\, \mu(\xi, x, y) = f'(x, y), \tag{12.11}$$

according to Eq. (12.6), and, obviously, $\tilde{\nu}(x, y) = f_0(x, y)$.

The above statement about the monotonic behavior of KL distance can be written as

$$\int_0^1 d\xi \int_0^\infty dx dy\, \mu(\xi, x, y) \ln \frac{\mu(\xi, x, y)}{\nu(\xi, x, y)} \geq \\ \geq \int_0^\infty dx dy\, \tilde{\mu}(x, y) \ln \frac{\tilde{\mu}(x, y)}{\tilde{\nu}(x, y)} \tag{12.12}$$

In the integral on the left-hand side we now make a change of variables

$$u = \xi(x + y), \quad v = (1 - \xi)(x + y), \quad z = x - y \tag{12.13}$$

with the obvious property $x + y = u + v$. Then the integration measure and ranges of integration transform as follows

$$\int_0^1 d\xi \int_0^\infty dx dy \ldots = \frac{1}{2} \int_0^\infty du dv \int_{-(u+v)}^{(u+v)} dz \frac{1}{u+v} \ldots \tag{12.14}$$

According to (12.9) the ratio μ/ν does not depend on z, so integration over z reduces simply to

$$\int_{-(u+v)}^{(u+v)} dz\, D\left(\frac{u+v+z}{2(u+v)}\right) = 2(u+v) \int_0^1 d\epsilon D(\epsilon), \tag{12.15}$$

and gives $2(u + v)$ which exactly cancels the Jacobian in (12.14).

Then, using also exact expressions for $\tilde{\mu}$ and $\tilde{\nu}$, we can finally rewrite Eq. (12.12) as expected monotonicity of relative entropy

$$\int_0^\infty du dv\, f(u, v) \ln \frac{f(u, v)}{f_0(u, v)} \geq \\ \geq \int_0^\infty dx dy\, f'(x, y) \ln \frac{f'(x, y)}{f_0(x, y)}. \tag{12.16}$$

12.2.3 Redistribution as Interaction with Reservoir: Clausius Inequality

Next, we can recall that initial distribution is factorized, $f(x,y) = p(x)p(y)$, and hence for the entropy $S(f) = -\int dxdy\, f \ln f$ we have

$$S(f) = 2S(p). \tag{12.17}$$

And for the distribution $f'(x,y)$ we have a simple information theory inequality, which follows from the positivity of the mutual information of x and y variables after the collision [13]

$$I = \int\int dxdy\, f'(x,y) \ln \frac{f'(x,y)}{p'(x)p'(y)} \geq 0. \tag{12.18}$$

This mutual information obviously can be written as

$$I = 2S(p') - S(f'), \tag{12.19}$$

where $S(p') = -\int dx p'(x) \ln p'(x)$. Hence from $I \geq 0$ it follows

$$2S(p') \geq S(f'). \tag{12.20}$$

Combining this inequality with (12.16), substituting Eq. (12.10) for the stationary solution, and noticing that terms with F cancels from both sides of (12.16), because the total energy $x + y$ is not changed in a collision, we finally arrive at an inequality

$$\begin{aligned} S(p') + \frac{1}{2}\int_0^\infty dxdy\, f'(x,y) \ln\left[D\left(\frac{x}{x+y}\right)\right] \geq \\ \geq S(p) + \frac{1}{2}\int_0^\infty dxdy\, p(x)p(y) \ln\left[D\left(\frac{x}{x+y}\right)\right]. \end{aligned} \tag{12.21}$$

Only in the case when $D = 1$ there are no additional terms in this inequality and we have entropy growth $S(p') \geq S(p)$. Unfortunately $f'(x,y)$ cannot be expressed in terms of p', therefore for arbitrary D we cannot derive any H-theorem from Eq. (12.21). But we will see now that actually this inequality may be interpreted as a Clausius inequality for an irreversible process, accompanied by some "heat" flow.

For this purpose we first introduce new variables: the total energy of a given pair E and a fraction of this total energy that one of the particles has

$$E = x + y, \qquad \xi = \frac{x}{x+y}. \tag{12.22}$$

In terms of these variables the redistribution process (12.1) looks very simple $E \to E' = E$ and $\xi \to \xi' = \epsilon$. The two-particle probability distribution as a function of these new variables is

$$\phi(E,\xi) = Ef(\xi E, (1-\xi)E), \tag{12.23}$$

where the additional factor appears because of the normalization condition (it cancels the Jacobian of the transformation from ξ, E to x, y). Then we can rewrite the linear Eq. (12.6) in terms of $\phi(\xi, E)$ in a very simple form

$$\phi'(\xi, E) = D(\xi) \int_0^1 d\xi' \phi(\xi', E). \tag{12.24}$$

This means that after the energy exchange all information about the original distribution of ξ is completely destroyed and the distribution in question is simply substituted by $D(\xi)$. But this is just the same thing that happens when we put a system in a contact with a thermal reservoir, with $D(\xi)$ playing the role of the Gibbs distribution. We can even introduce the new "pseudoenergy" $\mathcal{E}(\xi)$ according to

$$D(\xi) = \frac{1}{Z} \exp(-\mathcal{E}(\xi)/T), \qquad Z = \int_0^1 d\xi \exp(-\mathcal{E}(\xi)/T) \tag{12.25}$$

In general, introducing an independent "temperature" T does not make much sense, but in the next section we will see that sometimes this may be quite reasonable. Now, if we change variables in additional integrals in Eq. (12.21) we can rewrite them in terms of $\mathcal{E}(\xi)$ and marginal distributions $\phi(\xi) = \int dE \phi(\xi, E)$ and $\phi'(\xi) = D(\xi)$ before and after the collision.

Then our main inequality (12.21) may be rewritten in the form of a Clausius inequality for Boltzmann entropy on each time step

$$S(p') - S(p) \geq \frac{Q}{T}, \tag{12.26}$$

where the "heat" transferred during the relaxation $\phi(\xi) \to D(\xi)$ is given by the change in mean pseudoenergy per particle

$$Q = \frac{1}{2} \int_0^1 d\xi \mathcal{E}(\xi)[D(\xi) - \phi(\xi)]. \tag{12.27}$$

This inequality suggests the following interpretation of the evolution. We should probably assume that particles are essentially noninteracting and the usual Boltzmann expression for entropy is valid, but consider the system as an open one, which on every time step is brought in contact with a thermal reservoir in a very specific way. Namely, we pair particles at random and then the distribution of ξ, defined for these pairs, irreversibly relax to equilibrium with the reservoir while the amount of "heat" Q is transmitted to the system.

It is interesting that in general we do not expect, that in a stationary state $\phi(\xi) = D(\xi)$. This means that Q may be nonzero even in equilibrium and then $Q \leq 0$, as follows from (12.26) for $p(x) = p'(x) = p_0(x)$, i.e., there is a constant heat flow to the reservoir. But this implies in its turn that in the two-stage representation we have a nonequilibrium steady state instead of a true equilibrium. The evolution of the two-particle function in such a steady state looks like a kind of a cyclic process, consisting of an instantaneous "thermalization" $\phi(\xi) \to D(\xi)$ followed by a subsequent new random pairing that drives pairs out of this equilibrium.

12.3 H-Theorem for Beta Redistribution Laws

There exist, however, special cases, when $Q = 0$ in a stationary state. This happens when we take the redistribution law in the form of symmetric beta distribution

$$D(\epsilon) = C\epsilon^a(1-\epsilon)^a, \tag{12.28}$$

where C is a normalization constant and $a > -1$ is a parameter that determines the shape of the distribution. When $a \to \infty$ this distribution tends to a delta-function located at $\epsilon = 1/2$ (the total energy of a pair is divided in half), while for negative a the distribution $D(\epsilon)$ diverge at $\epsilon = 0$ and $\epsilon = 1$ indicating that after the redistribution one particle normally gets much more energy than the other.

For these redistribution laws, equilibrium solutions are already known

$$p_0(x) \sim x^a \exp(-\lambda x). \tag{12.29}$$

These solutions were obtained by Bassetti and Toscani [14] (see also [3]) for their pure gambling model which is in fact a continuous time version of Ulam's redistribution problem. For $a \to \infty$ with fixed mean energy this distribution tends to a delta-function and then in equilibrium all particles have the same energy, as was noticed already in [1], i.e., the system finally is in a fully "ordered" state.

The important thing is that for beta redistribution laws (12.28) the equilibrium two-particle distribution function, which was factorized, $f_0(x, y) = p_0(x)p_0(y)$, before the collision, was factorized also in variables ξ and E. Indeed, in this case $\phi_0(\xi, E)$, given by (12.23), is simply a product of $D(\xi)$ and a function that depends only on E. This factorization in its turn implies that the two-particle distribution is not changed during the collision and remains factorized after the redistribution, so that $f_0(x, y) = p_0(x)p_0(y)$ is a stationary solution of the linear evolution equation (12.6).

But for a factorized $f_0(x, y)$ it immediately follows from (12.16) that also the single-particle relative entropy

$$K = \int_0^\infty dx\, p(x) \ln \frac{p(x)}{p_0(x)} \tag{12.30}$$

is monotonic during the relaxation. Such a monotonicity is a rather nontrivial result for a nonlinear evolution, because contrary to a Markov process with linear master equation no general theorem exists in this case. Similar monotonicity was found recently also for a Boltzmann equation with nonconservative interactions[15].

It is also easy to obtain an H-theorem for beta redistribution law from the Clausius-like inequality (12.21). For D from (12.28) we can take

$$\mathcal{E}(\xi) = \ln(\xi(1-\xi)), \qquad T = 1/a, \tag{12.31}$$

so the inverse "temperature" may be taken as just a. This seems quite natural, since then $a \to \infty$ corresponds to zero temperature with fully-ordered steady state, while in case of uniform redistribution we have $a = 0$ with maximum disorder in equilibrium. For factorized D, the logarithm in Eq. (12.21) is a sum of functions that

depend either only on x, or y, or on $x+y$. Terms with $x+y$ cancel because the total energy of a pair is conserved and we finally obtain the H-theorem $H(p') \geq H(p)$ from Eq. (12.21) with

$$H(p) = S(p) + a \int_0^\infty dx\ p(x) \ln x. \tag{12.32}$$

Thus only for the uniform redistribution law, when $a = 0$ it is the entropy $S(p)$ that always grows. This H-functional is maximized by the equilibrium distribution $p_0(x)$ from (12.29) under the constraint that the mean energy is conserved.

There are many ways to understand the result (12.32). First note that H-functional (12.32) has a very general form, the same as discussed by Attard [16]. Entropy usually has such a form when x represents some macrostate for which a lot of microstates are possible, so that this macrostate has a nonzero entropy.

Next, the H-functional from (12.32) may be rewritten as

$$H(p) = -\int_0^\infty dx\ p(x) \ln \frac{p(x)}{x^a}. \tag{12.33}$$

This suggests that probably the additional term in H may be related to the "graining" with which the space of x is actually resolved [17]. Indeed, in their paper Maynar and Trizac argued that because of the measure problem the entropy for a continuous variable should generally be of the form $-\int dx\ p(x) \ln [\Lambda(x) p(x)]$ and clearly (12.33) is exactly the same with $\Lambda(x) = x^{-a}$. It should be noted, however, that this result was derived in [17] from the Jacobian of the transformation $x, y \to x', y'$ while in our case the Jacobian of (12.1) is exactly zero (the transformation does not have the inverse) so that the method of Maynar and Trizac can not be directly applied here.

Surely other interpretations of H are also possible, probably because nonlinear equation (12.2) for a one-point distribution function does not uniquely determines the underlying stochastic process. Different physical realizations of the process determine then what interpretation is more adequate. However, here we prefer to think that the system of particles in question is actually an open one, subjected to the action of some external agents, that actually redistribute the energy, so that H is likely related to the total entropy of the whole system, including these additional agents.

12.4 Conclusion

We have tried to obtain an H-theorem for Ulam's redistribution of energy problem, but it appeared possible only for special redistribution laws, given by symmetric beta distributions. H-functional differs from the Boltzmann entropy by an additional term, which may be interpreted in different ways. Also the relative entropy in these cases decreases monotonically just as for an ordinary stationary Markov chain (compare with [15]). Unfortunately, in a general case only some Clausius-type inequality is available from which no proper H-theorem follows.

Interpretations of the H-functional obtained depend on how we view the redistribution process. Certainly it is tempting to call this functional "entropy" in agreement with [16, 17]. One can also recall that for a system of hard spheres described by the nonlinear Enskog equation, the true entropy functional also differs from the simple Boltzmann entropy [18, 19]. Indeed, it is generally accepted that Boltzmann expression for the entropy is actually valid only for dilute gases.

However, in the present case it seems that quite a different interpretation is possible. Probably here there is no need to change the usual expression for the entropy of a gas, but one should simply consider the system of particles as an open one. In the redistribution problem there is one important element that is hidden in the original formulation, where it is assumed that particles somehow perform this redistribution by themselves. But actually we need some additional agent, or a device that performs this control function, because general redistribution laws are not quite "natural". This agent is, of course, similar to Maxwell's demon, as was already noticed in [5]. In this situation the Clausius-type inequality (12.26) seems more adequate for the description of the irreversibility in this problem.

Thus finally we believe that the two-stage evolution in terms of the two-particle distribution function is probably the most instructive way to view the redistribution of energy process. This approach suggests that the regulating device is actually a special type of a thermal reservoir and for a general redistribution law the final state of evolution is not a true equilibrium, but rather a non-equilibrium steady state, with constant production of 'heat' in each irreversible act of redistribution. Certainly this makes the search for a possible general H-theorem much more difficult.

Acknowledgements I am very grateful to J. Gaite for pointing out Ref. [1], to R. López-Ruiz for kind hospitality in Zaragoza during NOMA'13, to A. Puglisi and E. Trizac for stimulating correspondence, and to A. Chakraborty for many interesting discussions. The work was supported in part by RFBR Grants No. 12-02-00520, 13-02-00457.

References

1. Blackwell, D., Mauldin, R.D.: Ulam's redistribution of energy problem: collision transformations. Lett. Math. Phys. **10**, 149–153 (1985)
2. Pietruska-Pałuba, K.: On Ulam's redistribution of energy problem. Lett. Math. Phys. **14**, 247–252 (1987)
3. Holley, R., Liggett T.M.: Generalized potlatch and smoothing processes. Z. Warscheinlichkeitstheorie Verw Geb. **55**, 165–195 (1981)
4. Durrett, R, Liggett T.M.: Fixed points of the smoothing transformation. Z. Warscheinlichkeitstheorie Verw Geb. **64** 275–301 (1983)
5. Yakovenko, V.M., Barkley R.J. Jr.: Statistical mechanics of money, wealth, and income. Rev. Mod. Phys. **81**, 1703–1725 (2009)
6. Patriarca, M., Heinsalu E., Chakraborti, A.: Basic kinetic wealth-exchange models: common features and open problems. Eur. Phys. J. B **73**, 145–153 (2010)
7. Chakraborti, A., Toke, I.M., Patriarca, M., Abergel, F.: Econophysics review: II. Agent-based models. Quant. Financ., **11**, 1013–1041 (2011)

8. Drăgulescu, A.A., Yakovenko, V.M.: Statistical mechanics of money. Eur. Phys. J. B **17**, 723–729 (2000)
9. López-Ruiz, R., López, J.-L., Calbet, X.: Exponential wealth distribution : a new approach from functional iteration theory. ESAIM Proc. **36**, 189–196 (2012)
10. López, J.-L., López-Ruiz, R., Calbet, X.: Exponential wealth distribution in a random market. A rigorous explanation. J. Math. Anal. Appl. **386**, 195 (2012)
11. Apenko, S.M.: Monotonic entropy growth for a nonlinear model of random exchanges. Phys. Rev. E **87**, 024101 (2013)
12. Lallouache, M., Jedidi, A., Chakraborti, A.: Wealth distribution: to be or not to be a Gamma? Sci. Cult. (Kolkata, India) **76**, 478 (2010)
13. Cover, T.M., Thomas, J.A.: Elements of Information Theory, 2nd ed., Wiley, Hoboken (2006)
14. Bassetti, F., Toscani, G.: Explicit equilibria in a kinetic model of gambling. Phys. Rev. E **81**, 066115 (2010)
15. Marconi, U.M.B., Puglisi, A., Vulpiani, A.: About an H-theorem for systems with non-conservative interactions. J. Stat. Mech. **8**, 2 (P08003) (2013)
16. Attard, P.: Is the information entropy the same as the statistical mechanical entropy? arXiv:1209.5500
17. Maynar, P., Trizac, E.: Entropy of continuous mixtures and the measure problem. Phys. Rev. Lett. **106**, 160603 (2011)
18. Resibois, P.: H-theorem for the (modified) nonlinear Enskog equation. J. Stat. Phys. **19**, 593–609 (1978)
19. Garrido, P., Goldstein, S., Lebowitz, J.L.: Boltzmann entropy for dense fluids not in local equilibrium. Phys. Rev. Lett. **92**, 050602 (2003)

Chapter 13
Random Market Models with an H-Theorem

R. López-Ruiz, E. Shivanian and J. L. López

Abstract In this chapter, some economic models given by functional mappings are addressed. These are models for random markets where agents trade by pairs and exchange their money in a random and conservative way. They display the exponential wealth distribution as asymptotic equilibrium, independently of the effectiveness of the transactions and of the limitation of the total wealth. The entropy increases with time in these models and the existence of an H-theorem is computationally checked. Also, it is shown that any small perturbation of the models equations make them to lose the exponential distribution as an equilibrium solution.

13.1 Introduction

In the past years, it has been reported [1, 2] that in Western societies, around 95 % of the population, the middle and lower economic classes of society arrange their incomes in an exponential wealth distribution. The incomes of the rest of the population, around 5 % of individuals, fit a power law distribution [3].

The kind of models considering the randomness associated to markets are the gas-like models [4]. These random models interpret economic exchanges of money between agents similarly to collisions in a gas where particles share their energy [5].

In this chapter, we consider a continuous version of a homogeneous gas-like model [6, 7], which we generalize to a situation where the agents present a control parameter to decide the degree of interaction with the rest of economic agents [8] and also to another new situation where there is an upper limit of the total richness.

R. López-Ruiz (✉)
Department of Computer Science & BIFI, University of Zaragoza, Zaragoza, Spain
e-mail: rilopez@unizar.es

E. Shivanian
Department of Mathematics, Imam Khomeini International University, Qazvin, Iran
e-mail: shivanian@ikiu.ac.ir

J. L. López
Department of Math. Engineering and Informatics, Public University of Navarre, Pamplona, Spain
e-mail: jl.lopez@unavarra.es

R. López-Ruiz et al. (eds.), *Nonlinear Maps and their Applications,*
Springer Proceedings in Mathematics & Statistics 112, DOI 10.1007/978-3-319-12328-8_13

The appearance of the exponential (Gibbs) distribution as a fixed point for all these three cases is mathematically explained [7]. Also, the increase in the entropy when these systems evolve toward the asymptotic equilibrium is checked. This is associated with the existence of an H-theorem for all these economic models [9, 10]. Despite their apparent simplicity, these models based on functional mappings can help to enlighten the reasons of the ubiquity of the exponential distribution in many natural phenomena but in particular in the random markets.

13.2 The Continuous Gas-Like Model

We consider an ensemble of economic agents trading with money by pairs in a random manner. The discrete version of this model is as follows [5]. For each interacting pair (m_i, m_j) of the ensemble of N economic agents the trading rules can be written as

$$\begin{aligned} m_i' &= \varepsilon\ (m_i + m_j), \\ m_j' &= (1-\varepsilon)(m_i + m_j), \\ i, j &= 1 \ldots N, \end{aligned} \tag{13.1}$$

where ε is a random number in the interval $(0, 1)$. The agents (i, j) are randomly chosen. Their initial money (m_i, m_j), at time t, is transformed after the interaction in (m_i', m_j') at time $t+1$. The asymptotic distribution $p_f(m)$, obtained by numerical simulations, is the exponential (Boltzmann–Gibbs) distribution,

$$p_f(m) = \beta \exp(-\beta\, m), \quad \text{with} \quad \beta = 1/ <m>_{gas},$$

where $p_f(m)\mathrm{d}m$ denotes the *probability density function* (PDF), i.e., the probability of finding an agent with money (or energy in a gas system) between m and $m + \mathrm{d}m$. Evidently, this PDF is normalized, $||p_f|| = \int_0^\infty p_f(m)\mathrm{d}m = 1$. The mean value of the wealth, $<m>_{gas}$, can be easily calculated directly from the gas by $<m>_{gas} = \sum_i m_i/N$.

The continuous version of this model [6] considers the evolution of an initial wealth distribution $p_0(m)$ at each time step n under the action of an operator T. Thus, the system evolves from time n to time $n+1$ to asymptotically reach the equilibrium distribution $p_f(m)$, i.e.,

$$\lim_{n\to\infty} T^n\,(p_0(m)) \to\ p_f(m).$$

In this particular case, $p_f(m)$ is the exponential distribution with the same average value, $< p_f >$, than the initial one, $< p_0 >$, due to the local and total richness conservation.

The derivation of the operator T is as follows [6]. Suppose that p_n is the wealth distribution in the ensemble at time n. The probability to have a quantity of money x at time $n+1$ will be the sum of the probabilities of all those pairs of agents (u, v)

able to produce the quantity x after their interaction, that is, all the pairs verifying $u + v > x$. Thus, the probability that two of these agents with money (u, v) interact between them is $p_n(u) * p_n(v)$. Their exchange is totally random and then they can give rise, with equal probability, to any value x comprised in the interval $(0, u + v)$. Therefore, the probability to obtain a particular x (with $x < u+v$) for the interacting pair (u, v) will be $p_n(u) * p_n(v)/(u+v)$. Then, T has the form of a nonlinear integral operator,

$$p_{n+1}(x) = Tp_n(x) = \int\int_{u+v>x} \frac{p_n(u)p_n(v)}{u+v}\,\mathrm{d}u\mathrm{d}v\,.$$

If we suppose T acting in the PDFs space, it has been proved [7] that T conserves the mean wealth of the system, $< Tp >=< p >$. It also conserves the norm $(||\cdot||)$, i.e., T maintains the total number of agents of the system, $||Tp|| = ||p|| = 1$, that by extension implies the conservation of the total richness of the system. We have also shown that the exponential distribution $p_f(x)$ with the right average value is the only steady state of T, i.e., $Tp_f = p_f$. Computations also seem to suggest that other high-period orbits do not exist. In consequence, it can be argued that the convergence relation toward the limit point above explained is true. We sketch some of these properties.

First, in order to set up the adequate mathematical framework, we provide the following definitions.

Definition 13.1 We introduce the space L_1^+ of positive functions (wealth distributions) in the interval $[0, \infty)$,

$$L_1^+[0,\infty) = \{y : [0,\infty) \to R^+ \cup \{0\}, \quad ||y|| < \infty\},$$

with norm

$$||y|| = \int_0^\infty y(x)dx.$$

Definition 13.2 We define the mean richness $< x >_y$ associated to a wealth distribution $y \in L_1^+[0,\infty)$ as the mean value of x for the distribution y. Then,

$$<x>_y = ||xy(x)|| = \int_0^\infty xy(x)dx.$$

Definition 13.3 For $x \geq 0$ and $y \in L_1^+[0,\infty)$ the action of operator T on y is defined by

$$T(y(x)) = \int\int_{S(x)} dudv\frac{y(u)y(v)}{u+v},$$

with $S(x)$ the region of the plane representing the pairs of agents (u, v) which can generate a richness x after their trading, i.e.,

$$S(x) = \{(u, v), \quad u, v > 0, \quad u + v > x\}.$$

Now, we remind the following results recently presented in Ref. [7, 8].

Theorem 13.1 *For any $y \in L_1^+[0,\infty)$ we have that $||Ty|| = ||y||^2$. In particular, consider the subset of PDFs in $L_1^+[0,\infty)$, i.e., the unit sphere $B = \{y \in L_1^+[0,\infty), ||y|| = 1\}$. Observe that if $y \in B$ then $Ty \in B$. (It means that the number of agents in the economic system is conserved in time).*

Theorem 13.2 *The mean value $<x>_y$ of a PDF y is conserved, that is $<x>_{Ty}=<x>_y$ for any $y \in B$. (It means that the mean wealth, and by extension the total richness, of the economic system are preserved in time).*

Theorem 13.3 *Apart from $y = 0$, the one-parameter family of functions $y_\alpha(x) = \alpha e^{-\alpha x}$, $\alpha > 0$, are the unique fixed points of T in the space $L_1^+[0,\infty)$.*

Proposition 13.1 *For some members $y, w \in B$, $||Ty - Tw|| \geq ||y - w||$, hence T is not a contraction.*

Example 13.1 Take $y(x) = \frac{1}{(1+x)^2}$ and $w(x) = e^{-x}$ which belong to B. By using Mathematica, it is seen that $||y - w|| = 0.407264$ and $||Ty - Tw|| = 0.505669$.

If we consider the restriction of T for the subset B_{x_0} of distributions with the same mean wealth x_0, i.e., $B_{x_0} = \{y \in B | <x>_y = x_0\}$, then by using the Laplace transform of the operator T, it has been proved [11] that T is a contraction in B_{x_0}, hence the truth of the following relation:

$$\lim_{n\to\infty} T^n y(x) = \begin{cases} \delta e^{-\delta x} & with \quad \delta = 1/x_0\,, \\ \qquad\quad or & \\ 0^+ & when \quad <x>_y = +\infty\,. \end{cases}$$

Let us observe that the above pointwise limit of $T^n y$ when $n \to \infty$ can be outside of B in the case that $<x>_y = +\infty$. See the next example.

Example 13.2 Take $y(x) = \frac{1}{(1+x)^2}$ which belongs to B, with $< x >_y = +\infty$. Evidently, $T^n y \in B$ for all n. But it can be seen that $\lim_{n\to\infty} T^n y(x) = 0^+ \notin B$.

Example 13.3 Assume now the rectangular distribution: $y(x) = \frac{1}{2}$ if $2 < x < 4$, and $y(x) = 0$ otherwise. So, $y \in B$ and $\delta = \frac{1}{3}$, then the steady state in this case is $\mu(x) = \frac{1}{3}e^{-\frac{1}{3}x}$. We find numerically that $||y-\mu|| > ||Ty-\mu|| > ||T^2y-\mu|| > ||T^3y-\mu||$, and so on. This is shown in Fig. 13.1. Then we can guess that $\lim_{n\to\infty} ||T^n y-\mu|| = 0$.

If we consider the entropy of $y(x)$ given by $H = -\int y(x) \log y(x) dx$, then it is found that H increases in a monotonic way when T is successively applied to an initial state $y_0(x)$. If we define $H_n = H(T^n y_0(x))$, then the following H-theorem [10] yields:

$$\lim_{n\to\infty} H_n = H(\delta e^{-\delta x}) \quad \text{with} \quad \delta = 1/ <x>_{y_0}\,,$$

$$H_n \leq H_{n+1} \quad \forall n\,.$$

Summarizing, the system has a fixed point, $\delta e^{-\delta x}$, which is asymptotically reached depending on the initial average value $<x>_{y_0}$ and following a trajectory of increasing entropy. This behavior is essentially maintained in the extension of this model for other similar random markets (see the next sections).

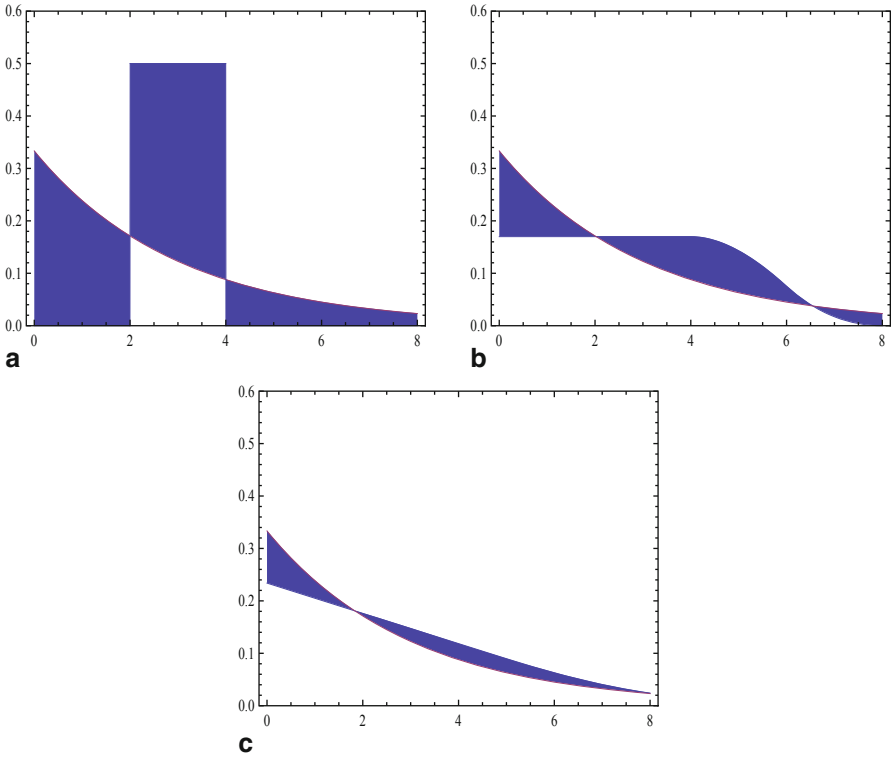

Fig. 13.1 Plot of $y(x) = \frac{1}{2}$ if $2 < x < 4$, and $y(x) = 0$ otherwise, T-iterates of y and $\mu(x) = \frac{1}{3}e^{-\frac{1}{3}x}$. (a) $||y - \mu||$, (b) $||Ty - \mu||$, (c) $||T^2y - \mu||$

13.3 The Continuous Gas-Like Model with Homogeneous Effectiveness

Let us think now that many of the economical transactions planned in markets are not successful and they are finally frustrated. It means that markets are not totally effective. We can reflect this fact in our model in a qualitative way by defining a parameter $\lambda \in [0, 1]$, which indicates the *degree of effectiveness* of the random market. When $\lambda = 1$, the market will have total effectiveness and all the operations will be performed under the action of the random rules (13.1). The evolution of the system in this case is given by the operator T. When $\lambda = 0$, all the operations become frustrated, there is no exchange of money between the agents and then the market stays frozen in its original state. The operator representing this type of dynamics is just the identity operator. Therefore, we can establish a *generalized continuous economic model* whose evolution in the PDFs space is determined by the operator T_λ, which depends on the parameter λ as follows:

Definition 13.4 $T_\lambda y(x) = (1-\lambda)y(x) + \lambda T y(x)$, with $\lambda \in [0,1]$.

Observe that the parameter $(1-\lambda)$ can also be interpreted as a kind of *saving propensity* of the agents, in such a way that for $\lambda = 1$ they do not save anything and they game all their resources, and for $\lambda = 0$ they save the totality of their money and then all the transactions are frustrated and the market stays in a frozen state.

We present some properties of the operator T_λ, which shows a dynamical behavior essentially similar to the behavior of T. Concretely, the exponential distribution is also the asymptotic wealth distribution reached by the system governed by T_λ, independently of the effectiveness λ of the random market.

Let us observe that $T_\lambda = I$ for $\lambda = 0$ and $T_\lambda = T$ for $\lambda = 1$, where I is the identity operator.

Proposition 13.2 *T_λ conserves the norm, i.e., for each $y \in B$, we have $T_\lambda y \in B$.*

Proposition 13.3 *T_λ conserves the average value of $y \in B$, i.e., $<x>_y = <x>_{T_\lambda y}$, where $<x>_y$ represents the mean value expressed in Definition 13.2.*

Theorem 13.4 *For any $\lambda \in (0,1)$, the operators T and T_λ have the same fixed points.*

Corollary 13.1 *The function $y(x) = 0$ and the family of exponential distributions $y_\delta(x) = \delta e^{-\delta x}$, $\delta > 0$, are the only fixed points of T_λ in $L_1^+[0,\infty)$, with $\lambda \in (0,1]$.*

Theorem 13.5 *Suppose that for a given $\lambda \in (0,1)$ we have $\lim_{n\to\infty} ||T_\lambda^n y(x) - \mu(x)|| = 0$, with $\mu(x)$ a continuous function, then $\mu(x)$ should be the fixed point of the operator T_λ for the initial condition $y(x) \in B$. In other words, $\mu(x) = \delta e^{-\delta x}$ with $\delta = \frac{1}{<x>_y}$.*

Example 13.4 Take the Gamma distribution $y(x) = xe^{-x}$, so that $y \in B$ and $\delta = \frac{1}{2}$, then in this case $\mu(x) = \frac{1}{2}e^{-\frac{1}{2}x}$. For $\lambda = 0.5$, we find numerically that $||y - \mu|| = 0.368226$, $||T_\lambda y - \mu|| = 0.273011$, $||T_\lambda^2 y - \mu|| = 0.206554$, $||T_\lambda^3 y - \mu|| = 0.158701$, and so on. This is shown in Fig. 13.2. Then we can guess that $\lim_{n\to\infty} ||T_\lambda^n y - \mu|| = 0$.

Also, the increasing of entropy in the system evolution can be checked. Then, similarly to the first model, this model has a fixed point, $\delta e^{-\delta x}$, which is asymptotically reached depending on the initial average value $<x>_{y_0}$ and following a trajectory of increasing entropy. The difference with the first model remains in the transient toward equilibrium, that evidently is a longer time for a lower effectiveness λ of the random market.

13.4 The Continuous Gas-Like Model with Limitation of the Richness

Here, we study the effect of a limitation in the maximum richness that an agent can have. We establish this upper limit to be Λ for x: $x \in [0,\Lambda]$. Now, the mean wealth of the system is:

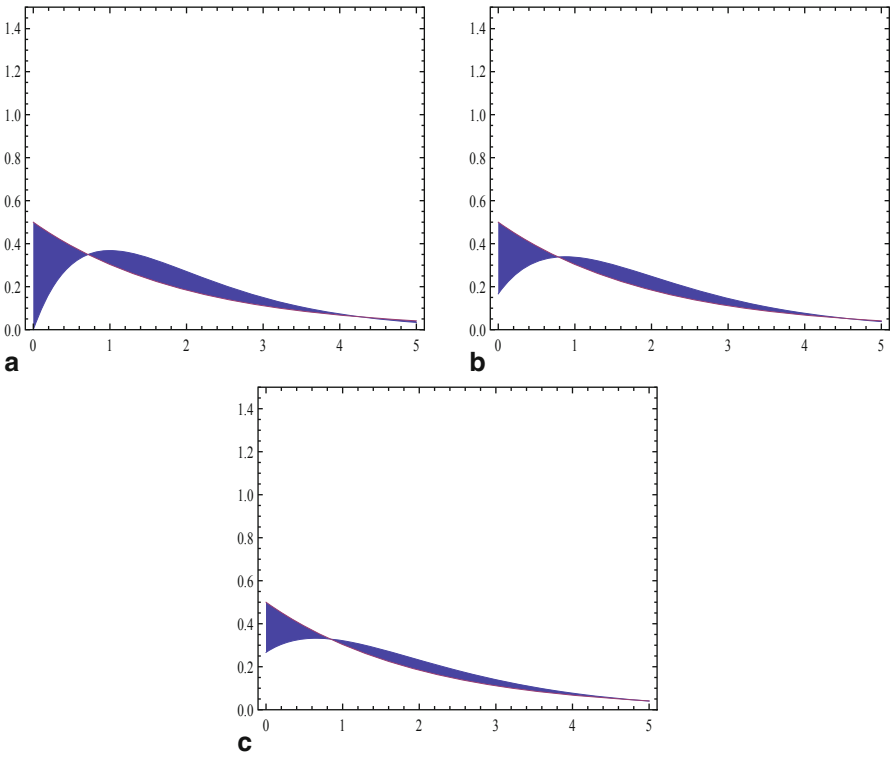

Fig. 13.2 Plot of $y(x) = xe^{-x}$, T_λ-iterates of y for $\lambda = 0.5$ and $\mu(x) = \frac{1}{2}e^{-\frac{1}{2}x}$. **(a)** $||y - \mu||$, **(b)** $||T_\lambda y - \mu||$, **(c)** $||T_\lambda^2 y - \mu||$

$$<x>_y = \int_0^\Lambda xy(x)dx.$$

Evidently, $<x>_y < \Lambda$.

The existence of the cutoff Λ in the economic system not only means that agents can not have more money than Λ if not the creation of some kind of control on the system that do not let the agents to perform trades that surpass the limit Λ. In the case of interaction by pairs, it implies that only the pairs verifying $u + v < \Lambda$ are allowed to trade and then they can exchange their money according to rules (13.1). In the rest of interactions surpassing the upper limit, that is $u + v > \Lambda$, the agents are not allowed to trade and then they conserve their original money. Hence, the generalization of the operator T for this system is the following:

$$[T_\Lambda y](x) = \int\int_{x \le u+v \le \Lambda} \frac{y(u)y(v)}{u+v} dudv + y(x) \int_{\Lambda - x}^{\Lambda} y(v)dv,$$

where the first term integrates the allowed trades according to rules (13.1) and the second term gives account of the total probability of encounters with forbidden trades that an agent of richness x can have with other agents of the ensemble.

Observe that $\lim_{\Lambda\to\infty} T_\Lambda = T$. Also:

$$[T_\Lambda y](x) = \int_0^x du \int_{x-u}^{\Lambda-u} dv \frac{y(u)y(v)}{u+v} +$$

$$+ \int_x^\Lambda du \int_0^{\Lambda-u} dv \frac{y(u)y(v)}{u+v} + y(x) \int_{\Lambda-x}^\Lambda y(v)dv.$$

Theorem 13.6 *For any $y \in L_1^+[0,\infty)$ and $\Lambda > 0$ we have that $||T_\Lambda y|| = ||y||^2$. In particular, if $||y|| = 1$ then $||T_\Lambda y|| = 1$.*

Proof Take $y \in L_1^+[0,\infty)$. Then

$$||T_\Lambda y|| = \int_0^\Lambda [T_\Lambda y](x)dx =$$

$$\int_0^\Lambda du \int_0^{\Lambda-u} dv \int_0^{u+v} dx \frac{y(u)y(v)}{u+v} + \int_0^\Lambda y(x)dx \int_{\Lambda-x}^\Lambda y(v)dv =$$

$$\int_0^\Lambda y(u)du \int_0^{\Lambda-u} y(v)dv + \int_0^\Lambda y(u)du \int_{\Lambda-u}^\Lambda y(v)dv = ||y||^2.$$

□

Theorem 13.7 *The mean richness is conserved by T_Λ, that is $<x>_{T_\Lambda y}=<x>_y$ for any $y \in B$.*

Proof

$$<x>_{T_\Lambda y} = \int_0^\Lambda xy(x)dx =$$

$$\int_0^\Lambda du \int_0^{\Lambda-u} dv \int_0^{u+v} xdx \frac{y(u)y(v)}{u+v} + \int_0^\Lambda xy(x)dx \int_{\Lambda-x}^\Lambda y(v)dv$$

$$= \frac{1}{2}\int_0^\Lambda du \int_0^{\Lambda-u} dv(u+v)y(u)y(v) + \int_0^\Lambda xy(x)dx \int_{\Lambda-x}^\Lambda y(v)dv$$

$$= \frac{1}{2}\int_0^\Lambda uy(u)du \int_0^{\Lambda-u} y(v)dv + \frac{2}{2}\int_0^\Lambda uy(u)du \int_{\Lambda-u}^\Lambda y(v)dv$$

$$+ \frac{1}{2}\int_0^\Lambda y(u)du \int_0^{\Lambda-u} vy(v)dv$$

$$= \frac{1}{2}\int_0^\Lambda uy(u)du \int_0^\Lambda y(v)dv + \frac{1}{2}\int_0^\Lambda y(v)dv \int_{\Lambda-v}^\Lambda uy(u)du$$

$$+ \frac{1}{2}\int_0^\Lambda y(u)du \int_0^{\Lambda-u} vy(v)dv$$

$$= \frac{1}{2}\int_0^\Lambda uy(u)du \int_0^\Lambda y(v)dv + \frac{1}{2}\int_0^\Lambda y(v)dv \int_0^\Lambda uy(u)du$$
$$= \frac{1}{2} <x>_y + \frac{1}{2} <x>_y = <x>_y .$$

□

Theorem 13.8 *The function*

$$y_{a,\Lambda}(x) = \frac{ae^{-ax}}{1 - e^{-a\Lambda}}$$

has $||y_{a,\Lambda}|| = 1$ *and is a fixed point of the operator* T_Λ *for any* $a > 0$. *The mean richness for this function is*

$$<x>_{y_{a,\Lambda}} = \frac{1}{a} + \frac{\Lambda}{1 - e^{a\Lambda}}.$$

Proof It is just a straightforward computation. □

Proposition 13.4 *For the fixed point* $y_{a,\Lambda}(x)$, *we have* $2 <x>_{y_{a,\Lambda}} < \Lambda$.

Hence, if we define $m = <x>_{y_{a,\Lambda}}$, we can consider *the middle class*, CM, as all those agents having richness between $m/2$ and $2m$, that is,

$$CM(a, \Lambda) = \int_{m/2}^{2m} y_{a,\Lambda}(x)dx = \frac{e^{-am/2} - e^{-2am}}{1 - e^{-a\Lambda}}.$$

The richness accumulated by the middle class is

$$< xCM > (a, \Lambda) = \int_{m/2}^{2m} xy_{a,\Lambda}(x)dx$$

$$= m\frac{(2 + am)e^{-am/2} - 2(1 + 2am)e^{-2am}}{2am[1 - e^{-a\Lambda}]},$$

where

$$am = 1 + \frac{a\Lambda}{1 - e^{a\Lambda}}, \quad x = a\Lambda.$$

When we plot $CM(x)$ or $< xCM > (x)$ for fixed m, we see that it is always a decreasing function of $x = a\Lambda$. Therefore, the smaller the richness limit Λ is, the larger the middle class is.

The same tendency can be observed if we calculate the mean wealth per individual of the middle class:

$$\frac{< xCM > (a, \Lambda)}{< CM > (a, \Lambda)} = \frac{m}{am} + \frac{m[e^{-am/2} - 4e^{-2am}]}{2[e^{-am/2} - e^{-2am}]},$$

which is also a decreasing function of $x = a\Lambda$, for fixed m.

The proportion of the total richness accumulated by the middle class is

$$\frac{< xCM > (a, \Lambda)}{m} = \frac{(2 + am)e^{-am/2} - 2(1 + 2am)e^{-2am}}{2am[1 - e^{-a\Lambda}]},$$

that is again a decreasing function of $x = a\Lambda$.

Summarizing, an upper limit in the richness allowed in a random market provokes an enlargement of the middle class and also an enrichment of such a middle class.

13.5 Slightly Perturbed Gas-Like Models

Here, we put in evidence that the asymptotic equilibrium distributions for these models are not stable under slight perturbations. It means that even a small modification that conserves the mean value and the total wealth of the system provokes the loss of the exponential distribution as a fixed point of the perturbed model equations. This fact also has its consequences on the behavior of the entropy of the system, concretely the H-theorem is not already verified, unless new forms for the H functional are introduced.

As an example, define the modified operator

$$(T_K y)(x) = \int \int_{u+v \geq x} K(u, v, x) \frac{y(u)y(v)}{u + v} du dv,$$

with the kernel

$$K(u, v, x) = \sum_{n=0}^{N} (n + 1)a_n \left(\frac{x}{u + v} \right)^n,$$

where eventually N may be infinity. It is straightforward to check that

$$||T_{Ky}|| = ||y||^2 \sum_{n=0}^{N} a_n$$

and

$$<x>_{T_K y} = 2 <x>_y \sum_{n=0}^{N} \frac{n + 1}{n + 2} a_n.$$

Therefore, the operator verifies $T_K : B \to B$ and conserves the wealth when

$$\sum_{n=0}^{N} a_n = 1,$$

$$\sum_{n=0}^{N} \frac{n + 1}{n + 2} a_n = \frac{1}{2}.$$

For $N = 1$ the unique solution of this system is $a_0 = 1$ and $a_1 = 0$, that is, the well-known operator studied elsewhere. For $N = 2$ we have an infinity of solutions parametrized with $\varepsilon \in R$: $a_0 = 1 - \varepsilon/3$, $a_1 = \varepsilon$ and $a_2 = -2\varepsilon/3$. That is,

$$K(u, v, x) = 1 - \frac{\varepsilon}{3} + \frac{2\varepsilon x}{u + v} - \frac{2\varepsilon x^2}{(u + v)^2}.$$

If we take the exponential distribution $y(x) = ae^{-ax}$ and $N = 2$ we find that

$$(T_K y)(x) = \left(1 - \frac{\varepsilon}{3}\right) ae^{-ax} - 2\varepsilon x a^2 Ei(-ax) - 2\varepsilon x^2 a^2 \left[\frac{e^{-ax}}{x} + aEi(-ax)\right],$$

where $Ei(x)$ is the exponential integral,

$$Ei(-ax) = -\int_x^\infty \frac{e^{-at}}{t} dt.$$

It means that $y(x) = ae^{-ax}$ is not the fixed point of the perturbed operator T_K and a new asymptotic equilibrium emerges for this ε-slightly modified system.

13.6 Conclusions

Different versions of a continuous economic model [6] that takes into account idealistic characteristics of the markets have been considered. In these models, the agents interact by pairs and exchange their money in a random way. The asymptotic steady state of these models is the exponential wealth distribution. The system decays to this final distribution with a monotonic increasing of the entropy taking its maximum value just on the equilibrium. These are specific H-theorems that can be computationally checked, independently on the effectiveness of the markets or the limitation of the richness in the economic system. Also, it has been argued that slight modifications of these models provoke the loss of the exponential distribution as an asymptotic equilibrium and its correspondent consequences for the establishment of an H-theorem for the new perturbed models.

References

1. Dragulescu A., Yakovenko V.M.: Exponential and power-law proba-bility distributions of wealth and income in the United Kingdom and the United States. Physica A **299**, 213–221 (2001)
2. Chakrabarti B.K., Chatterjee A., Chakraborti A., Sinha S.: Econophysics: An Introduction. Willey-VCH Verlag GmbH, Germany (2010)
3. Levy M., Solomon S.: New evidence for the power-law distribution of wealth. Physica A **242**, 90–94 (1997)

4. Yakovenko V.M.: Econophysics, Statistical mechanics approach to. In: Meyers, R.A. (ed.) Encyclopedia of Complexity and System Science. Springer, Germany (2009)
5. Dragulescu A., Yakovenko V.M.: Statistical mechanics of money. Eur. Phys. J. B **17**, 723–729 (2000)
6. Lopez-Ruiz R., Lopez J.L., Calbet X.: Exponential wealth distribution: a new approach from functional iteration theory. ESAIM: Proc. (of ECIT-2010 Conference) **36**, 183–190 (2012)
7. Lopez J.L., Lopez-Ruiz R., Calbet X.: Exponential wealth distribution in a random market. A rigorous explanation. J. Math. Anal. Appl. **386**, 195–204 (2012)
8. Lopez-Ruiz R., Shivanian E., Abbasbandy S., Lopez J.L.: A generalized continuous model for random markets. Math. Aeterna **3**, 317–328 (2013)
9. Shivanian E., Lopez-Ruiz R.: A new model for ideal gases. Decay to the Maxwellian distribution. Physica A **391**, 2600–2607 (2012)
10. Apenko S.M.: Monotonic entropy growth for a nonlinear model of random exchanges. Phys. Rev. E **87**(4), 024101 (2013)
11. Gutriel K.: Convergence to the exponential wealth distribution in a discrete-time random market model. Appl. Anal. **93**, 1256–1263 (2014)

Chapter 14
Synchronization and Phase Ordering in Globally Coupled Chaotic Maps

O. Alvarez-Llamoza and M. G. Cosenza

Abstract We investigate the processes of synchronization and phase ordering in a system of globally coupled maps possessing bistable, chaotic local dynamics. The stability boundaries of the synchronized states are determined on the space of parameters of the system. The collective properties of the system are characterized by means of the persistence probability of equivalent spin variables that define two phases, and by a magnetization-like order parameter that measures the phase-ordering behavior. As a consequence of the global interaction, the persistence probability saturates for all values of the coupling parameter, in contrast to the transition observed in the temporal behavior of the persistence in coupled maps on regular lattices. A discontinuous transition from a nonordered state to a collective phase-ordered state takes place at a critical value of the coupling. On an interval of the coupling parameter, we find three distinct realizations of the phase-ordered state, which can be discerned by the corresponding values of the saturation persistence. Thus, this statistical quantity can provide information about the transient behaviors that lead to the different phase configurations in the system. The appearance of disordered and phase-ordered states in the globally coupled system can be understood by calculating histograms and the time evolution of local map variables associated to the these collective states.

14.1 Introduction

Globally coupled systems have been a research topic receiving a large amount of attention because of their applicability to a variety of contexts. The dynamical elements in such systems are subject to a common interaction field. Global interactions arise in the description of many physical, biological, chemical, and social systems,

O. A.-Llamoza (✉)
Departamento de Física, FACYT, Universidad de Carabobo, Valencia, Venezuela
e-mail: llamoza@gmail.com

Universidad Católica de Cuenca, Cuenca, Ecuador

M. G. Cosenza
Centro de Física Fundamental, Universidad de Los Andes, Mérida, Venezuela
e-mail: mcosenza@ula.ve

R. López-Ruiz et al. (eds.), *Nonlinear Maps and their Applications,*
Springer Proceedings in Mathematics & Statistics 112, DOI 10.1007/978-3-319-12328-8_14

such as Josephson junction arrays [1], multimode lasers [2], coupled oscillators [3, 4], charge density waves [5], parallel electric circuits, neural dynamics, ecological systems, evolution models [6], economic exchange [7], social networks [8], mass media models [9], cross-cultural interactions [10], etc. Global interactions also play a relevant role in models of many systems driven by long-range interactions, able to generate strong correlations between highly interconnected elements. Systems with global interactions can exhibit a variety of phenomena, such as chaos synchronization, nontrivial collective behavior, dynamical clustering, chaotic itineracy [6, 11], quorum sensing [12], etc. These behaviors have been experimentally investigated in arrays of globally coupled oscillators in several systems [13–17].

In addition to these phenomena, the description of generic effects associated to the presence of global coupling in dynamical processes in complex systems is still an open problem. In this respect, globally coupled maps [18] constitute paradigmatic models for the study of dynamical systems with global interactions. Spatial concepts lose meaning and only temporal properties become relevant in globally coupled maps. These characteristics should introduce new features in many processes that have been investigated in spatially extended systems with short range interactions.

In particular, there has been much interest in the study of the phase-ordering properties of systems of coupled bistable maps and their relationship with Ising models in statistical physics [19–28]. These works have mainly assumed the phase competition dynamics taking place on networks with local interactions.

In this chapter we investigate the collective behavior of a system of globally coupled bistable chaotic maps, including the occurrence of synchronized states and the phenomenon of phase competition. This model provides a scenario to compare the roles that local and global interactions play on the occurrence of phase growth and phase transitions on spatiotemporal systems. In Sect. (14.2) we present the model of globally coupled maps and describe local dynamics that exhibits bistable, chaotic behavior. In Sect. (14.3) we determine analytically the stability condition for synchronized states on the space of parameters of the system. The phase-ordering properties associated to the collective dynamics of the system are studied in Sect. (14.4) by employing appropriate statistical quantities. Section (14.5) contains the conclusions of this work.

14.2 Globally Coupled Bistable Chaotic Maps

We consider a globally coupled map system defined by

$$x_{t+1}^i = (1-\varepsilon) f(x_t^i) + \frac{\varepsilon}{N} \sum_{j=1}^{N} f(x_t^j), \tag{14.1}$$

where x_t^i describes the state variable of element i ($i = 1, 2, \ldots, N$), at discrete time t, the parameter ε measures the coupling strength between the elements, and $f(x)$ is a map that expresses the local dynamics. The term expressing the global coupling

between the maps corresponds to the mean field of the system. In this chapter, we employ a system size $N = 10^5$.

The local dynamics is given by a piecewise linear, odd map

$$f(x) = \begin{cases} -2\mu/3 - \mu x, & \text{if } x \in [-1, -1/3], \\ \mu x, & \text{if } x \in [-1/3, 1/3], \\ 2\mu/3 - \mu x, & \text{if } x \in [1/3, 1], \end{cases} \tag{14.2}$$

where the local parameter $\mu \in [-3, 3]$ and $x \in [-1, 1]$. For $\mu = 3$, $f(x)$ becomes the chaotic map introduced by Miller and Huse [19]. For $\mu \in [-1, 1]$, the map possesses the stable fixed point $f(x^*) = x^* = 0$. When the parameter $\mu \in (1, 2)$, the local map is chaotic and bistable: There are two symmetric chaotic band attractors, corresponding to the invariant intervals $I^{\pm} = [\pm\mu(2-\mu)/3, \pm\mu/3]$, and separated by a finite gap about the origin. This map has been shown to exhibit phase-ordering properties on locally coupled map lattices [21, 22].

14.3 Synchronized States

The coupled map system Eq. (14.1) can be expressed in vector form as

$$\mathbf{x}_{t+1} = (1-\varepsilon)\mathbf{f}(x_t) + \frac{\varepsilon}{N}\mathbf{M}\mathbf{f}(x_t) = \left[(1-\varepsilon)\mathbf{I} + \frac{\varepsilon}{N}\mathbf{M}\right]\mathbf{f}(x_t), \tag{14.3}$$

where $\mathbf{x}_t$ and $\mathbf{f}(x_t)$ are N-dimensional vectors with components $[\mathbf{x}_t]_i = x_t^i$ and $[\mathbf{f}(x_t)]_i = f(x_t^i)$, respectively, $\mathbf{I}$ is the $N \times N$ identity matrix, and $\mathbf{M}$ is an $N \times N$ matrix expressing the coupling between the elements. For the global coupling, Eq. (14.1), all the components of $\mathbf{M}$ are equal to 1.

A synchronized state occurs when $x_t^i = x_t^j, \forall\, i, j$. From the linear stability analysis of synchronized states in coupled map lattices, it can be shown that these states are stable if the following condition is satisfied [18, 29],

$$\left|\left(1 - \varepsilon + \frac{\varepsilon}{N} m_k\right) e^{\lambda}\right| < 1, \tag{14.4}$$

where $\{m_k : k = 1, 2, \ldots, N\}$ is the set of eigenvalues of the coupling matrix $\mathbf{M}$ and λ is the Lyapunov exponent of the local map, Eq. (14.2). In the globally coupled case, the eigenvalues are $m_k = 0, k = 1, \ldots, (N-1)$, which has $(N-1)$-fold degeneracy, and $m_N = N$. Because of these eigenvalues, the synchronization condition, Eq. (14.4), is independent of the size of the system N.

The set of eigenvectors of the matrix $\mathbf{M}$ constitutes a complete orthogonal basis in terms of which any state $\mathbf{x}_t$ of the system Eq. (14.3) can be represented as a linear combination. The eigenvector corresponding to $m_N = N$ is homogeneous and it expresses the coherent or synchronized state at any time. Thus, perturbations of the state $\mathbf{x}_t$ along this eigenvector do not destroy the coherence, and the stability condition

associated with $m_N = N$ is irrelevant for the synchronized state. The other $(N-1)$ eigenvectors associated with $m_k = 0$ are not homogeneous, and perturbations along their directions affect the synchronized state. Thus, the stability condition Eq. (14.4) with $m_k = 0$ defines a region on the space of parameters (μ, ε) where all the stable synchronized states can be found.

Two types of synchronized states fulfilling condition Eq. (14.4) can be observed in the system:

1. Synchronized stationary states, for which $x_t^i = x^*$, $\forall\, i$. This corresponds to the range of parameter $\mu \in [-1, 1]$, where the local map possesses the stable fixed point $f(x^*) = x^* = 0$. The boundaries of the region of parameters where this state is stable are given by Eq. (14.4) with $\mu_k = 0$ and $e^{\lambda} = f'(x^*)$,

$$(1-\varepsilon)\,|f'(x^*)| = \pm 1. \tag{14.5}$$

2. Synchronized chaotic states, for which $x_t^i = f(x_t)$, $\forall\, i$. This occurs in the regions $\mu \in [-3, -1] \cup [1, 3]$, where the local map is chaotic. The region of stability of these states is bounded by the curves

$$(1-\varepsilon)\, e^{\lambda} = \pm 1, \tag{14.6}$$

Since $f'(x^*) = \mu$ and $\lambda = \ln|\mu|$ for the map Eq. (14.2), both boundaries (14.5) and (14.6) can be expressed on the space of parameters (μ, ε) by the curves

$$(1-\varepsilon)\,|\mu| = \pm 1, \tag{14.7}$$

with μ in the appropriate range for each state. The straight lines $\mu = -1$ and $\mu = 1$ separate the synchronized stationary states from the synchronized chaotic states on the plane (μ, ε).

The occurrence of synchronization can also be numerically characterized by the asymptotic time-average $\langle\sigma\rangle$ (after discarding a number of transients) of the instantaneous standard deviations σ_t of the distribution of state variables x_t^i, defined as

$$\sigma_t = \left[\frac{1}{N}\sum_{i=1}^{N}\left(x_t^i - \bar{x}_t\right)^2\right]^{1/2}, \tag{14.8}$$

where

$$\bar{x}_t = \frac{1}{N}\sum_{i=1}^{N} x_t^i\,. \tag{14.9}$$

Then, a synchronization state corresponds to a value $\langle\sigma\rangle = 0$. In practice, we use the numerical criterion $\langle\sigma\rangle < 10^{-7}$ as a synchronization condition.

For some values of parameters, the iterates of the state variables x_t^i in the system Eq. (14.1) leave the interval $[-1, 1]$ and, eventually, escape to infinity. The iterates of x_t^i stay in the interval $[-1, 1]$ if the product $(1-\varepsilon)\mu$ lies in the range $[-3, 3]$, that

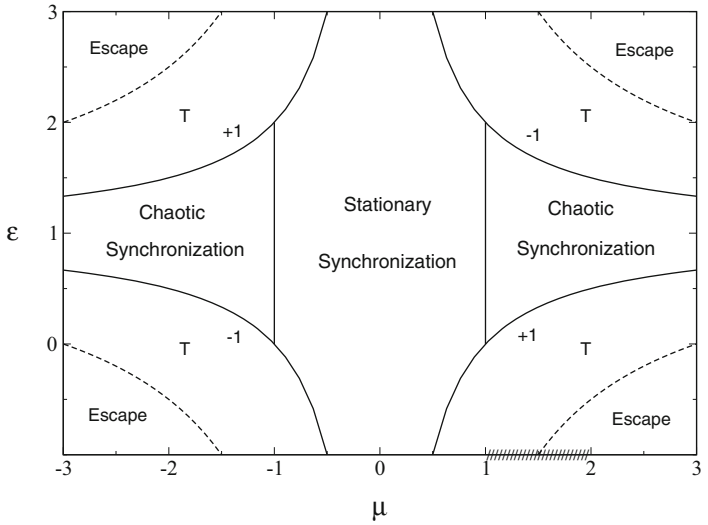

Fig. 14.1 Regions of stable synchronized states for the system Eq. (14.1) on the space of parameters (μ, ε). The labels indicate where the synchronized stationary states and the synchronized chaotic states occur. The synchronization boundaries correspond to *continuous lines*. The labels ± 1 on each curve identify the corresponding sign in Eq. (14.7). The *dashed lines* indicate the escape boundaries Eq. (14.10) beyond which the iterates of the state variables of the system Eq. (14.1) leave the interval $[-1, 1]$. The interval $\mu \in [1, 2]$ for bistability is marked on the μ axis. T identifies the regions where collective turbulent states exist

is, if $|(1 - \varepsilon)\mu| < 3$. Thus, the boundaries for escape from the interval $[-1, 1]$ are described by the curves

$$(1 - \varepsilon)\, \mu = \pm 3. \tag{14.10}$$

Figure (14.1) shows the stability boundaries of the synchronized states and the escape boundaries for the globally coupled system Eq. (14.1) on the space of parameters (μ, ε).

14.4 Collective Phases

For $\mu \in (1, 2)$, the local map displays bistability in the form of two chaotic band attractors: corresponding to the interval I^+ for the positive values of the iterates, and the interval I^- for the negatives values. Then the states of the elements in the system Eq. (14.1) can be associated to two well-defined symmetric phases that can be characterized by spin variables associated to the sign of the state at time t, defined as $s_t^i = +1$ if $x_t^i > 0$, and $s_t^i = -1$ if $x_t^i < 0$.

To study the collective behavior of the globally coupled map system Eq. (14.1) in the bistable chaotic range, we fix the value of the local parameter $\mu = 1.9$

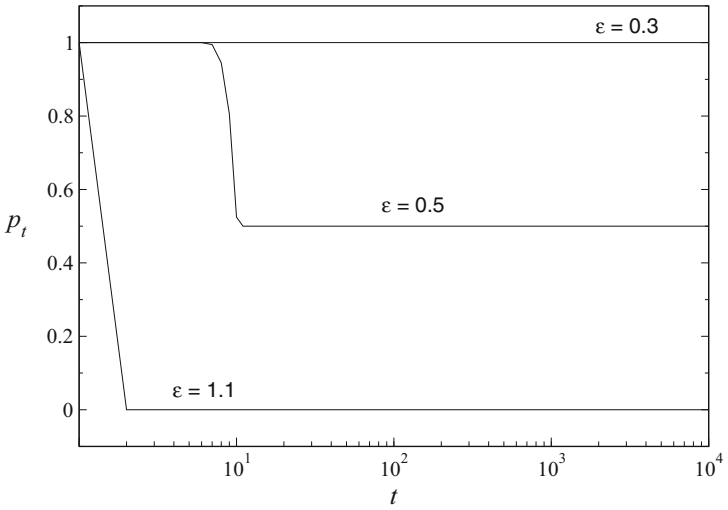

Fig. 14.2 Persistence probability as a function of time for the system Eq. (14.1) with fixed $\mu = 1.9$ and size $N = 10^5$, for different values of the coupling parameter ε, as indicated on each curve

and choose an even number N as system size. Then we set the initial conditions symmetrically as follows: one half of the maps are randomly chosen and assigned random values uniformly distributed on the positive attractor while the other half are similarly assigned values on the negative attractor.

The dynamical properties of the phase-ordering process can be described by using the persistence probability p_t, defined as the fraction of maps that have not changed spin variable (sign) up to time t [30]. Figure (14.2) shows p_t as a function of time for the globally coupled map system Eq. (14.1), for several values of the coupling parameter ε. The persistence probability saturates in a few iterations for all positive values of the coupling ε. This means that the phases associated to the spin variables freeze in the globally coupled system. In contrast, in regular lattices the persistence saturates for small couplings, while it decays algebraically in time for coupling strengths greater than some critical value, corresponding to the growth of one phase at the expense of the other [21].

Figure (14.2) reveals that the saturation value of the persistence probability, denoted by p_∞, depends on the value of the coupling parameter. Figure (14.3a) shows the quantity p_∞ as a function of ε. We find that p_∞ displays different constant values in different intervals of the coupling parameter and exhibits discontinuous transitions at critical values $\varepsilon_1 = 0.43$ and $\varepsilon_2 = 1$. For $\varepsilon < \varepsilon_1$, we have $p_\infty = 1$, indicating that for small enough coupling, every map remains in its initial chaotic attractor, I^- or I^+. In the intermediate range of coupling parameters $\varepsilon_1 < \varepsilon < 1$, the saturation value of the persistence changes to $p_\infty = 0.5$, indicating that one-half of the total number of maps have switched attractor. Finally, for $\varepsilon > 1$, we obtain $p_\infty = 0$; this means that all the maps have changed their initial attractors at some time during the evolution of the system. The value of ε_1 depends on the value of the local map parameter μ, but $\varepsilon_2 = 1$, independently of μ.

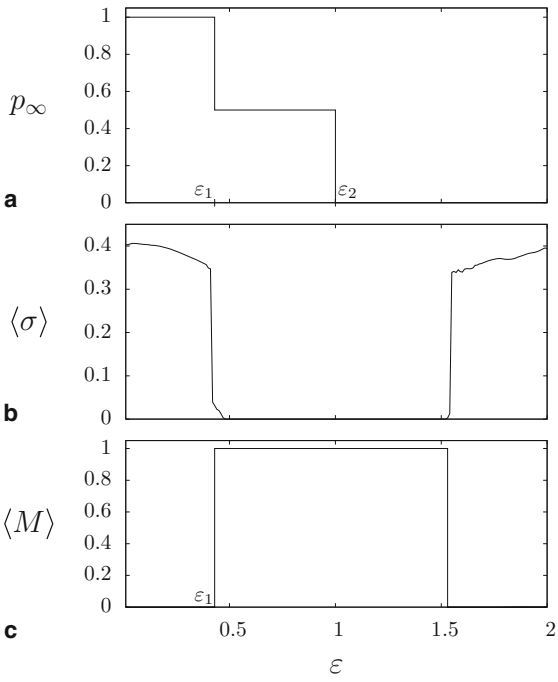

Fig. 14.3 Statistical quantities as functions of the coupling parameter ε for system Eq. (14.1) with fixed $\mu = 1.9$ and size $N = 10^5$. **a** p_∞, **b** $\langle\sigma\rangle$, **c** $\langle M\rangle$. The critical values ε_1 and ε_2 are marked on the ε axis

Figure (14.3b) shows the synchronization measure $\langle\sigma\rangle$, given by Eq. (14.8), as a function of ε. For the value $\mu = 1.9$, the chaotic synchronization range of the coupling, obtained from Eq. (14.7), is $\varepsilon \in [0.473, 1.526]$. For this interval of the coupling, we get $\langle\sigma\rangle = 0$ as expected.

To characterize the statistical properties of the phase-ordering process in the globally coupled map system Eq. (14.1), we define the instantaneous "magnetization" of the system M_t, as

$$M_t = \frac{1}{N}\sum_{i=1}^{N} s_t^i. \tag{14.11}$$

Then, we employ, as an order parameter, the absolute value of the asymptotic time-average (after discarding a number of transients) of the values M_t, denoted by $\langle M\rangle$.

Figure (14.3c) shows the order parameter $\langle M\rangle$ as a function of the coupling ε. The critical value of the coupling ε_1 marks a discontinuous transition from a collective state characterized by $\langle M\rangle = 0$, where the maps remain symmetrically distributed about the two attracting intervals I^+ and I^-, to an ordered state characterized by $\langle M\rangle = 1$, where all the maps settle on one of the attractors, either I^+ or I^-. Note that the critical value ε_1 is smaller than the lower synchronization boundary at $\varepsilon = 0.473$. This means that the phase-ordering transition occurs before full synchronization is achieved. When the value of the coupling strength reaches the upper synchronization

boundary, there is another discontinuous transition to the turbulent, disordered state, for which $\langle M \rangle = 0$.

The quantities p_∞ and $\langle \sigma \rangle$ in Fig. (14.3) allow to distinguish three different situations in the range of the parameter ε where the collective phase-ordered state with $\langle M \rangle = 1$ occurs: (i) a desynchronized ordered state, where $\langle M \rangle = 1$, $\langle \sigma \rangle > 0$, and $p_\infty = 0.5$; (ii) a synchronized ordered state, where $\langle M \rangle = 1$, $\langle \sigma \rangle = 0$, and $p_\infty = 0.5$; and (iii) a synchronized ordered state, characterized by $\langle M \rangle = 1$, $\langle \sigma \rangle = 0$, and $p_\infty = 0$.

In order to elucidate the nature of these three realizations of the phase-ordered state, as well as the transitions exhibited by the statistical quantities p_∞ and $\langle M \rangle$, we plot in Fig. (14.4) the instantaneous probability distributions (normalized histograms) of the states x_t^i of the system Eq. (14.1) with fixed $\mu = 1.9$, denoted by $\rho(x)$, for different values of the coupling parameter ε.

Figure (14.4a) corresponds to $\varepsilon = 0.2 < \varepsilon_1$. The probability distribution $\rho(x)$ at $t = 2000$ shows two separated peaks that maintain the initial symmetrical distribution of the maps on the two chaotic band attractors. The mean field coupling term is negligible in this situation Fig. (14.5a) shows the time evolution of the state variables x_t^i of two maps in the system Eq. (14.1) for $\varepsilon = 0.2$: one having positive initial spin variable and another with negative initial spin variable. Each trajectory remains in its attractor. Since no map has left its initial attractor, no spin variable has changed sign, and thus $p_\infty = 1$. Then, two symmetric subsets associated to the spin variables coexist in the globally coupled system for these parameters values, yielding $\langle M \rangle = 0$ as a result.

For couplings $\varepsilon_1 < \varepsilon < 0.473$ in Fig. (14.4b), the probability distribution $\rho(x)$ at time $t = 2000$ displays one single peak. This indicates that the $N/2$ maps that initially belonged to one attractor have switched to the other attractor; the direction of the change depends on the initial conditions, in this case from I^- to I^+. All the maps form a cluster that moves chaotically and stays in the interval I^+. Then, the saturation value of the persistence probability is $p_\infty = 0.5$ in this range of the coupling strength. Figure (14.5b) illustrates this process through the time evolution of the orbits of two maps that have been initially assigned opposite spin variables. Note that the two chaotic orbits do not synchronize on the interval I^+. This situation corresponds to the presence of a single ordered phase of spin variables in the system, and therefore the magnetization becomes $\langle M \rangle = 1$. The discontinuous change in the statistical quantities occurring at the critical value ε_1 in Fig. (14.3) describes a first order phase transition in the collective behavior of the system, from a non-ordered state, characterized by the values $\langle \sigma \rangle > 0$, $p_\infty = 1$, $\langle M \rangle = 0$, to a desynchronized phase-ordered state, characterized by $\langle \sigma \rangle > 0$, $p_\infty = 0.5$, $\langle M \rangle = 1$, and denoted as situation (i) above.

For coupling values $0.473 < \varepsilon < 1$, the probability $\rho(x)$ at $t = 2000$ displays a single vertical line on one of the attracting intervals, as shown in Fig. (14.4c). This indicates that the $N/2$ maps initially assigned to one of the attractors have switched to the other attractor, resulting in the synchronization of the N maps on a single chaotic orbit that stays on that attractor. The corresponding time evolution of two maps with initial opposite spin variables is shown in Fig. (14.5c). Thus,

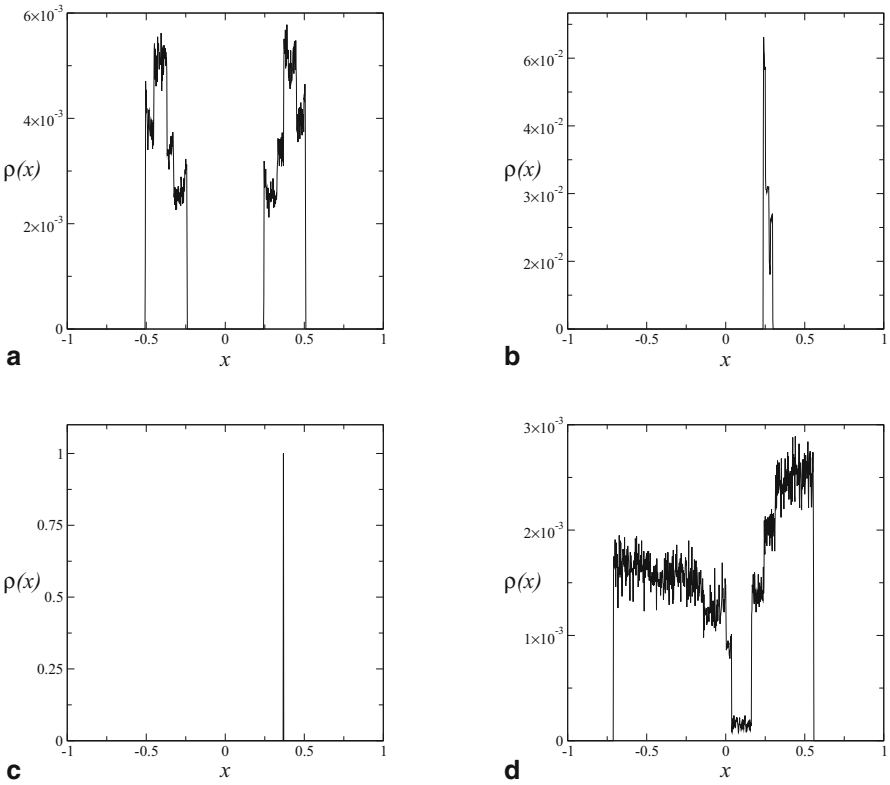

Fig. 14.4 Instantaneous probability distributions $\rho(x)$ of states at time $t = 2000$ on the interval $[-1, 1]$ for the system Eq. (14.1) with $N = 10^5$ and fixed $\mu = 1.9$, for different values of the coupling ε. The interval $[-1, 1]$ on the x axis was divided into 1000 subintervals, and the value of ρ for a given subinterval corresponds to the number of points x_t^i falling into that subinterval, divided by N. **a** $\varepsilon = 0.2$ (nonordered phase, $p_\infty = 1$, $\langle M \rangle = 0$), **b** $\varepsilon = 0.45$ (desynchronized ordered phase, $\langle \sigma \rangle > 0$, $p_\infty = 0.5$, $\langle M \rangle = 1$), **c** $\varepsilon = 0.55$ (synchronized ordered phase, $\langle \sigma \rangle = 0$, $p_\infty = 0.5$, $\langle M \rangle = 1$), **d** $\varepsilon = 2.4$ (turbulent)

the system displays a synchronized, phase-ordered state characterized by $\langle \sigma \rangle = 0$, $p_\infty = 0.5$, and $\langle M \rangle = 1$ in this parameter range. This constitutes realization (ii) of the phase-ordered state.

If the coupling is increased to values $1 < \varepsilon < 1.526$, we observe realization (iii) of the ordered state. In this case, the factor $(1 - \varepsilon)$ in Eq. (14.1) becomes negative allowing the maps to reverse the signs of their initial spin variables at early times during the evolution of the system. This transient behavior of the spin variables is reflected in the quantity $p_\infty = 0$; the parameter $\varepsilon_2 = 1$ marks the discontinuity in the value of the saturation value of the persistence. Since the synchronized state is stable for this range of coupling parameters, the maps eventually become synchronized on one of the attracting intervals, yielding $\langle \sigma \rangle = 0$. In addition, we obtain $\langle M \rangle = 1$. Figure (14.5d) portrays the time evolution of the orbits of two maps with different

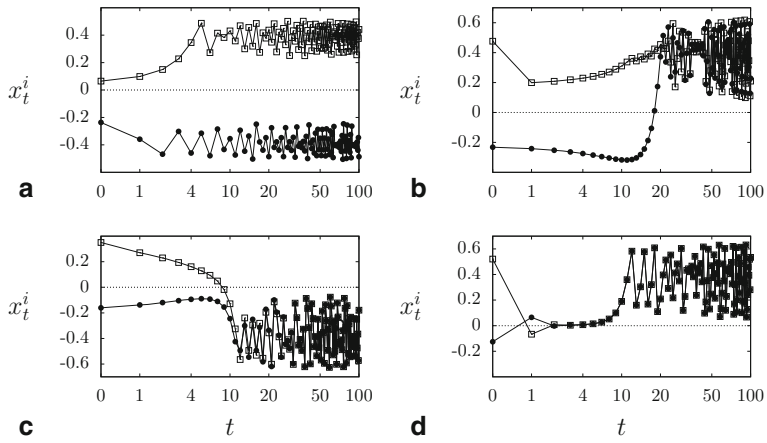

Fig. 14.5 Temporal evolution of the state variables x_t^i of a map with positive initial spin variable (*empty squares*) and a map with negative initial spin variable (*black circles*) in the globally coupled system Eq. (14.1) with $N = 10^5$ and fixed $\mu = 1.9$, for different values of the coupling ε. For $t > 0$, time is displayed in a logarithmic scale. **a** $\varepsilon = 0.2$; nonordered state, with $\langle\sigma\rangle > 0$, $p_\infty = 1$, $\langle M\rangle = 0$. **b** $\varepsilon = 0.45$; desynchronized, ordered state, with $\langle\sigma\rangle > 0$, $p_\infty = 0.5$, $\langle M\rangle = 1$. **c** $\varepsilon = 0.55$; synchronized, ordered state, with $\langle\sigma\rangle = 0$, $p_\infty = 0.5$, $\langle M\rangle = 1$. **d** $\varepsilon = 1.1$; synchronized, ordered state, with $\langle\sigma\rangle = 0$, $p_\infty = 0$, $\langle M\rangle = 1$

initial spin variables in this situation. Then, we have again a synchronized, phase-ordered state, distinguished by the value $p_\infty = 0$, in contrast to realization (ii) where $p_\infty = 0.5$. Thus, the saturation value of the persistence probability can provide information about the transient processes that lead to frozen configurations and to phase-ordered states in the system.

In Fig. (14.4d) for $\varepsilon > 1.526$, the maps become desynchronized and the corresponding probability distribution $\rho(x)$ is spread over a a subset of the interval $x \in [1, 1]$; its bimodal form reflects the underlying presence of the two attractors in the local chaotic dynamics. We refer to this collective state as turbulent. This corresponds to a desynchronized, disordered state for which $\langle\sigma\rangle > 0$, $p_\infty = 0$, and $\langle M\rangle = 0$.

If the initial conditions are modified in such a way that a fraction $N_1/N > 1/2$ of values of the maps is uniformly distributed on one attractor interval, either I^+ or I^-, while the remaining fraction $(1 - N_1/N)$ is similarly assigned to the other attractor, then the symmetry of the globally coupled system Eq. (14.1) is lost. We have found that the main features of the collective behavior of the system are maintained under such partition: the persistence probability p_t saturates after a few iterations for all values of the coupling parameter; there is a disordered state for low coupling values; and a synchronized phase-ordered state emerges for an intermediate range of the coupling strength.

In this situation, the mean field of the system initially acquires the sign of the attractor where the largest fraction N_1/N of maps lies. This attractor dominates the

dynamics of the globally coupled bistable system. However, for low enough intensity of the coupling, the maps tend to stay in their initial intervals and therefore they do not change the sign of their spin variable. Correspondingly, the asymptotic persistence probability has the value $p_\infty = 1$ and the average magnetization is $\langle M \rangle = 0$. As the coupling strength is increased, the maps in the smallest subset switch to the dominating attractor, eventually giving rise to a phase-ordered state. The initial fraction of maps N_1/N remain on that attractor and therefore do not change sign in their spin variables. Then, the saturation value of the persistence probability for ordered state in this case should be $p_\infty = N_1/N$. We have numerically verified these values for different partitions $(N_1, N - N_1)$ of initial conditions over the attracting intervals.

14.5 Conclusions

We have investigated the collective behavior of a system of globally coupled maps having bistable, chaotic local dynamics. The system possesses two types of synchronized dynamics: synchronized stationary states and synchronized chaotic states. We have analytically determined the stability boundaries of these states on the space of parameters (ε, μ) of the system. In addition, we have numerically measured the occurrence of synchronization by means of the statistical quantity $\langle \sigma \rangle$.

The presence of two symmetric attracting intervals in the local chaotic dynamics permits to assign a spin-like variable to each map and to define associated phases. The persistence probability p_t describes the evolution and competition of the phases. The absence of spatial relations in the system of globally coupled maps rules out the possibility of supporting spatial domains in either phase and a defined interface which would be necessary for a continuous phase growth. As a consequence, the phases always freeze in globally coupled maps, causing the saturation of the persistence probability in time for all values of the coupling parameter, in contrast to the transition observed in the temporal behavior of the persistence in coupled maps on regular lattices. We have found that the saturation value of the persistence probability p_∞ reaches different constant values in different intervals of the coupling parameter and shows discontinuous transitions at critical values $\varepsilon_1 = 0.43$ and $\varepsilon_2 = 1$.

We have introduced the magnetization-like order parameter $\langle M \rangle$ to characterize the phase-ordering behavior of the system. The phase-ordered state, corresponding to $\langle M \rangle = 1$, exhibits three distinct realizations as the coupling ε is varied and which can be discerned by employing the quantities $\langle \sigma \rangle$ and p_∞: (i) a desynchronized ordered state, with $\langle M \rangle = 1$, $\langle \sigma \rangle > 0$, and $p_\infty = 0.5$; (ii) a synchronized ordered state, characterized by $\langle M \rangle = 1$, $\langle \sigma \rangle = 0$, and $p_\infty = 0.5$; and (iii) a synchronized ordered state, distinguished by $\langle M \rangle = 1$, $\langle \sigma \rangle = 0$, and $p_\infty = 0$. Thus, the value of $\langle \sigma \rangle$ distinguishes between realizations (i) and (ii); while p_∞ differentiates realization (ii) from realization (iii).

There also exist two desynchronized, non-ordered collective states, both described by the values $\langle \sigma \rangle > 0$ and $\langle M \rangle = 0$. One of these states corresponds to the persistence of the initial symmetric distribution of spin variables, characterized by $p_\infty = 1$; and the other is a turbulent state, where $p_\infty = 0$. Our results reveal that the saturation value of the persistence probability can provide information about the transient behaviors that lead to the different phase configurations in the system.

In addition, we have studied the histograms and the time evolution of local map variables associated to the disordered and to the phase-ordered states in order to understand the appearance of these collective states in the globally coupled system.

The transitions between the disordered and the phase-order states occur discontinuously, as in a first-order phase transition, reflecting the global nature of the interaction in the system. In contrast, continuous transitions are typical in regular lattices.

In general, the investigation of dynamical processes in networks and the role of the topology in determining emerging collective behaviors is a topic of much interest in the current research on complex systems [8, 31].

Acknowledgement This work is supported by project No. C-1906-14-05-B from CDCHTA, Universidad de Los Andes, Venezuela. O. A. thanks Projet Prometeo, Secretaría de Educación Superior, Ciencia, Tecnología e Innovación, Senescyt, Ecuador. M. G. C. is grateful to the Senior Associates Program of the Abdus Salam International Centre for Theoretical Physics, Trieste, Italy.

References

1. Wiesenfeld, K., Hadley, P.: Attractor crowding in oscillator arrays. Phys. Rev. Lett. **62**, 1335–1338 (1989)
2. Wiesenfeld, K., Bracikowski, C., James, G., Roy, R.: Observation of antiphase states in a multimode laser. Phys. Rev. Lett. **65**, 1749–1752 (1990)
3. Kuramoto, Y.: Chemical Oscillations, Waves and Turbulence. Springer, Berlin (1984)
4. Nakagawa N., Kuramoto, Y.: From collective oscillations to collective chaos in a globally coupled oscillator system. Phys. D **75**, 74–80 (1994)
5. G. Grüner: The dynamics of charge-density waves. Rev. Mod. Phys. **60**, 1129–1181 (1988)
6. Kaneko K., Tsuda, I.: Complex Systems: Chaos and Beyond. Springer, Berlin (2001)
7. Yakovenko, V.M.: Encyclopedia of Complexity and System Science, edited by Meyers, R.A. Springer, New York (2009)
8. Newman, M., Barabási, A.L., Watts, D.J.: The Structure and Dynamics of Networks. Princeton University Press, Princeton (2006)
9. González-Avella, J.C., Eguiluz, V.M., Cosenza, M.G., Klemm, K., Herrera, J.L., San Miguel, M.: Local versus global interactions in nonequilibrium transitions: a model of social dynamics. Phys. Rev. E **73**, 046119 (2006)
10. González-Avella, J.C., Cosenza, M.G., San Miguel, M.: A model for cross-cultural reciprocal interactions through mass media. PLoS ONE **7**(12), e51035 (2012)
11. Manrubia, S.C., Mikhailov, A.S., Zanette, D.H.: Emergence of Dynamical Order: Synchronization Phenomena in Complex Systems. World Scientific, Singapore (2004)
12. Garcia-Ojalvo, J., Elowitz, M.B., Strogatz, S.H.: Modeling a synthetic multicellular clock: repressilators coupled by quorum sensing. Proc. Natl. Acad. Sci. USA **101**, 10955–10960 (2004)
13. Wang, W., Kiss, I.Z., Hudson, J.L.: Experiments on arrays of globally coupled chaotic electrochemical oscillators: synchronization and clustering. Chaos **10**, 248–256 (2000)

14. Miyakawa, K., Yamada, K.: Synchronization and clustering in globally coupled salt-water oscillators. Phys. D **151**, 217–227 (2001)
15. De Monte, S., dOvidio, F., Danø, S., Sørensen, P.G.: Dynamical quorum sensing. Proc. Natl. Acad. Sci. USA **104**, 18377–18381 (2007)
16. Taylor, A.F., Tinsley, M.R., Wang, F., Huang, Z., Showalter, K.: Dynamical quorum sensing and synchronization in large populations of chemical oscillators. Science **323**, 614–617 (2009)
17. Hagerstrom, A.M., Murphy, T.E., Roy, R., Hövel, P., Omelchenko, I., Schöll, E.: Experimental observation of chimeras in coupled-map lattices. Nat. Phys. **8**, 658–661 (2012)
18. Kaneko, K.: Clustering, coding, switching, hierarchical ordering, and control in networks of chaotic elements. Phys. D **41**, 137–172 (1990)
19. Miller, J., Huse, D.A.: Macroscopic equilibrium from microscopic irreversibility in a chaotic coupled map lattice. Phys. Rev. E **48**, 2528–2535 (1993)
20. O'Hern, C., Egolf, D., Greenside, H.S.: Lyapunov spectral analysis of a nonequilibrium Ising-like transition. Phys. Rev. E **53**, 3374–3386 (1996)
21. Lemaître, A., Chaté, H.: Phase ordering and onset of collective behavior in chaotic coupled map lattices. Phys. Rev. Lett. **82**, 1140–1143 (1999)
22. Kockelkoren, J., Lemaître, J., Chaté, H.: Phase-ordering and persistence: relative effects of space-discretization, chaos, and anisotropy. Physica A **288**, 326–337 (2000)
23. Wang, W., Liu, Z., Hu, B.: Phase order in chaotic maps and coupled map lattices. Phys. Rev. Lett. **84**, 2610–2613 (2000)
24. Schmüser, F., Just, M., Kantz, H.: On the relation between coupled map lattices and kinetic Ising models. Phys. Rev. E **61**, 675–3684 (2000)
25. Angelini, L., Pellicoro, M., Stramaglia, S.: Phase ordering in chaotic map lattices with additive noise. Phys. Lett. A **285**, 293–300 (2001)
26. Angelini, L.: Antiferromagnetic effects in chaotic map lattices with a conservation law. Phys. Lett. A **307**, 41–49 (2003)
27. Tucci, K., Cosenza, M.G., Alvarez-Llamoza, O.: Phase separation in coupled chaotic maps on fractal networks. Phys. Rev. E **68**, 027202 (2003)
28. Echeverria, C., Tucci, K., Cosenza, M.G.: Phase growth in bistable systems with impurities. Phys. Rev. E **77**, 016204 (2008)
29. Waller, I. Kapral, R: Spatial and temporal structure in systems of coupled nonlinear oscillators. Phys. Rev. A **30**, 2047–2055 (1984)
30. Derrida, B., Bray, A.J., Godrèche, C.: Non-trivial exponents in the zero temperature dynamics of the 1d Ising and Potts model. J. Phys. A **27**, L357–L361 (1994)
31. Herrera, J.L., Cosenza, M.G., Tucci, K., González-Avella, J.C.: General coevolution of topology and dynamics in networks. Europhys. Lett. **95**, 58006 (2011)

Chapter 15
Maximizing a Psychological Uplift in Love Dynamics

Malay Banerjee, Anirban Chakraborti and Jun-ichi Inoue

Abstract In this chapter, we investigate the dynamical properties of a psychological uplift in lovers. We first evaluate extensively the dynamical equations which were recently given by Rinaldi et al. (Physica A, 392: 3231–3239, 2013). Then, the dependences of the equations on several parameters are numerically examined. From the viewpoint of lasting partnership for lovers, especially, for married couples, one should optimize the parameters appearing in the dynamical equations to maintain the love for their respective partners. To achieve this optimization, we propose a new idea where the parameters are stochastic variables and the parameters in the next time step are given as expectations over a Boltzmann–Gibbs distribution at a finite temperature. This idea is very general and might be applicable to other models dealing with human relationships.

15.1 Introduction

> "Love is composed of a single soul inhabiting two bodies." – Aristotle
> "Love never dies a natural death. It dies because we don't know how to replenish its source. It dies of blindness and errors and betrayals. It dies of illness and wounds; it dies of weariness, of witherings, of tarnishings." – Anaïs Nin

Love—mysterious and unexplained—often forms the basis of a relationship between two persons; undoubtedly, a partnership between lovers is a time-dependent

A. Chakraborti (✉)
School of Computational and Integrative Sciences, Jawaharlal Nehru University, New Delhi 110067 India
e-mail: anirban@mail.jnu.ac.in

M. Banerjee
Department of Mathematics and Statistics, Indian Institute of Technology, Kanpur 208016, India
e-mail: malayscc@gmail.com

J.-I. Inoue
Graduate School of Information Science and Technology, Hokkaido University, N14-W9, Kita-ku, Sapporo 060-0814, Japan
e-mail: jinoue@cb4.so-net.ne.jp

R. López-Ruiz et al. (eds.), *Nonlinear Maps and their Applications,*
Springer Proceedings in Mathematics & Statistics 112, DOI 10.1007/978-3-319-12328-8_15

phenomenon. Even if a man and a woman were in deep love at some initial stages, the psychological uplift for one or both of them could eventually decay to very low-levels, and could even result in a breakup or divorce, in the worst scenario.

A simple mathematical model for the dynamics of love between a man and woman was introduced by Strogatz [2, 3]—the first attempt to model the love dynamics with the help of coupled ordinary differential equations. The idea of Strogatz was then extended by other researchers [4–6] to understand the influence of the factors like appeal, secure relation between the couple, and separation for a finite time period, which are important factors to maintain the relationship. Similar type of mathematical models have been proposed and analyzed up to certain extent for triangular love by Sprott [7, 8], but the uncertainty for the final outcome remains unclear. Recently, Rinaldi et al. [1] again proposed a simple dynamical model for lovers emotion to investigate a law of big hit film from the dynamical behavior of feeling in the partner for lovers. Their approach, based on a coupled differential equations, was applied to the movie "Gone With The Wind" (GWTW); they found that the resulting time series of lovers' feelings can mimic the story of the film to some extent. The differential equations contain several parameters and Rinaldi et al. chose them to mimic the lives of Scarlet and Rhett, with full of ups and downs. In the romantic film GWTW, the drastic ups and downs in the lovers' emotions indeed constituted a notable factor to attract the attention of audience, and the sequences of such psychological climaxes in the film might have been a key issue in making the film a big hit, as suggested by Rinaldi et al. [1].

In reality, for a married couple, such extreme ups and downs could however prove to be deterrent to the continuation of a peaceful married life. Hence, from the viewpoint of lasting partnership for lovers, especially for a married couple, one should optimize the parameters appearing in the dynamical equations to maintain the love for their partner. In other words, it would be interesting to obtain the optimum levels of the parameters in order to maintain the minimum level of love and happiness required to maintain a happy and prolonged marital life.

To this aim, we propose a simple new idea in this chapter. We assume that the parameters involved with the love dynamics are not constant over the entire time period, rather they are stochastic variables and the parameters in the next time step are given as expectations over a Boltzmann–Gibbs distribution at a finite temperature. By decreasing the temperature during the dynamics of coupled equations, one can accelerate the rate of increase of the sum of feelings (and decrease the difference of feelings) of lovers at each time step. The idea is quite general and might be applicable to other models dealing with human relationships.

15.2 Differential Equations of Gross and Gap for Lovers' Feelings

In the original model by Rinaldi et al. [1], the governing equations with respect to the feelings of lovers, denoted as x_1, x_2, are given by two coupled nonlinear ordinary differential equations:

$$\frac{dx_1}{dt} = -\alpha_1 x_1 + \rho_1 A_2 + k_1 x_2 \, \mathrm{e}^{-\eta_1 x_2}, \tag{15.1}$$

$$\frac{dx_2}{dt} = -\alpha_2 x_2 + \rho_2 A_1 + k_2 x_1 \, \mathrm{e}^{-\eta_2 x_1}, \tag{15.2}$$

subjected to the positive initial conditions, where the parameter α_i is *forgetting coefficient*, k_i and η_i are the parameters characterizing the measure of insecurity feelings, A_j is the measure of appeal toward x_i produced by x_j and ρ_i is a multiplicative factor representing the amount of recognition of the appeal A_j (see [1] for detailed interpretation). All the parameters involved with the model are positive. Interestingly, once we choose the initial values of x_1, x_2, these variables remain positive.

As one can see above, there are many parameters to be calibrated. From the engineering point of view, one could determine them by means of "optimization" of some appropriate cost functions. In the following, we consider several such cost functions.

First, we introduce the following new variables, namely, the "gross" S (sum) and "gap" D (difference):

$$S \equiv x_1 + x_2, \quad D \equiv (x_1 - x_2)^2 = x_1^2 + x_2^2 - 2x_1 x_2. \tag{15.3}$$

This allows us to write:

$$x_1 = \frac{1}{2}(S + \sqrt{D}), x_2 = \frac{1}{2}(S - \sqrt{D}), \tag{15.4}$$

where we should bear in mind that we have to consider the case $x_1 \geq x_2$ in order to have the well-defined expressions for x_1 and x_2 in terms of S and D. Of course, this condition may not always be satisfied. However, as we are focusing here on the gap D, the above choice might be indeed justified. It should be noted that the gross feelings S could be regarded as a cost function to be maximized. This is because the total degree of "passion" amongst the lovers might be one of the most important quantities to make the relationship strong and durable. On the other hand, the gap the two partners' love x_1, x_2 might determine the "stability" of the relationship—namely, even if the S is high, the mutual relation could be unstable when $x_1 \gg x_2$ or $x_1 \ll x_2$. In other words, it is very hard for the lovers to continue their good relationship if only one of them expresses too much love to his/her love partner and the other partner becomes indifferent about their relationship which was established due to their love affairs. Two hypothetical cases can be considered for illustrating this.

- For young lovers, the variable S takes high values temporally; however, one person (girl or boy) suddenly loses interest and becomes indifferent. As a result, the variable D increases rapidly and the love affair (marriage) breaks down prematurely.
- For senior lovers, the variable S normally does not take a high value; however, they know each other quite well, and as a result, the feelings x_1 and x_2 are quite similar. Hence, variable D increases and the love affair (marriage) becomes stable.

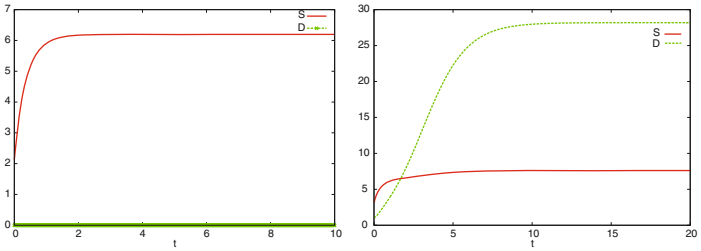

Fig. 15.1 The time-dependence of S and D calculated by Eqs. (15.5) and (15.6). We set the parameters as $\alpha_1 = \alpha_2 = \rho_1 = \rho_2 = \eta_1 = \eta_2 = 1$ and $k_1 = k_2 = 15, A_1 = A_2 = 1$. The initial condition are selected as $(x_1, x_2) = (1, 1)$ (*left*), this reads $D_0 = 0$, and $(x_1, x_2) = (2, 1)$ (*right*), this reads $D_0 \neq 0$

We do not have any real survey data to validate these idealized examples. Nevertheless, we consider an utility function S, which is to be maximized, and the energy function D, which is to be minimized, in order to determine the parameters appearing in the original model [1].

Then, the original equations are rewritten in terms of S and D. The equation for S is easy to obtain, and we have

$$\frac{dS}{dt} = -\alpha_1 \frac{S+\sqrt{D}}{2} + \rho_1 A_2 + k_1 \frac{S-\sqrt{D}}{2} \mathrm{e}^{-\eta_1 (S-\sqrt{D})/2} - \alpha_2 \frac{S-\sqrt{D}}{2} + \rho_2 A_1 + k_2 \frac{S+\sqrt{D}}{2} \mathrm{e}^{-\eta_2 (S+\sqrt{D})/2} \equiv f(\boldsymbol{\theta} : S, D) \tag{15.5}$$

$$\frac{dD}{dt} = 2(x_1 - x_2)\left(\frac{dx_1}{dt} - \frac{dx_2}{dt}\right) \equiv g(\boldsymbol{\theta} : S, D), \tag{15.6}$$

where $\boldsymbol{\theta} \equiv (\alpha_1, \alpha_2, \rho_1, \rho_2, A_2, A_2, k_1, k_2, \eta_1, \eta_2)$.

In the following sections, we discuss in detail the behavior of the nonlinear dynamics of Eqs. (15.5) and (15.6), within the framework of Rinaldi et al. [1] model, and consider the possible optimization of the parameters. Here, we have chosen the model by Rinaldi et al. just as a basic example, and in principle one could easily extend the study by taking into account much more complicated and appropriate lovers' interactions.

15.2.1 Some Specific Choices of Parameters

We first examine the behavior of the differential Eqs. (15.5) and (15.6) with respect to S and D for the case of a specific choice of parameters $\boldsymbol{\theta}$. Apparently, $D_t = 0$ is always a solution of the Eq. (15.6). In Fig. 15.1, we plot the S_t and D_t for two distinct initial conditions. In the left panel, we choose the initial condition so that $x_1(0) = x_2(0) = 1$, this reads $D_0 = 0$. From this panel we easily find that the gap D is time-independently zero. On the other hand, in the right panel, we choose

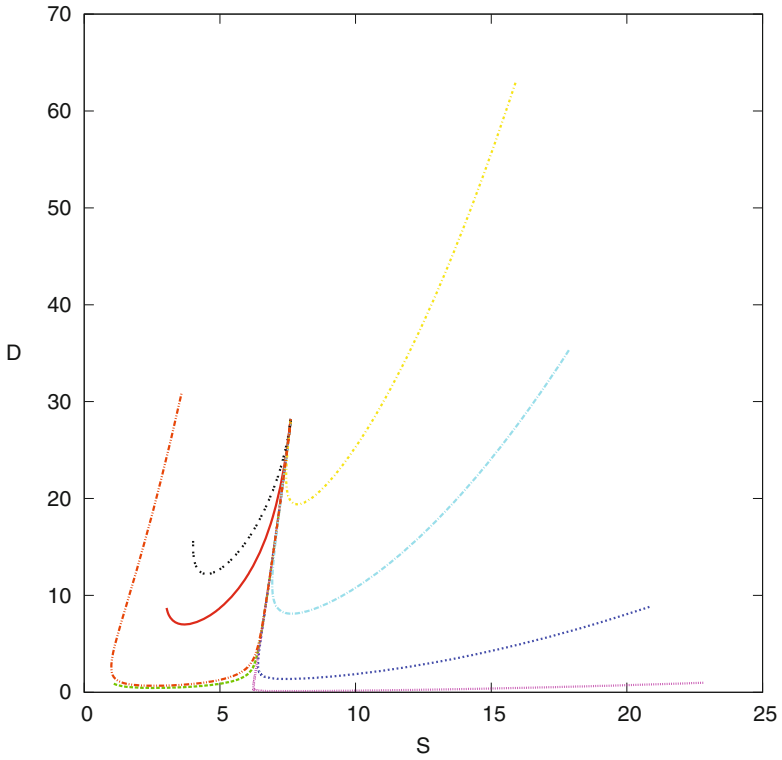

Fig. 15.2 The flows S-D calculated by Eqs. (15.5) and (15.6) for several distinct initial conditions. We find that for any initial conditions, the flows converge to $(7.61, 28.19)$. We set the parameters as $\alpha_1 = \alpha_2 = \rho_1 = \rho_2 = \eta_1 = \eta_2 = 1$ and $k_1 = k_2 = 15$, $A_1 = A_2 = 1$

as $x_1(0) \neq x_2(0)$, namely, $D_0 \neq 0$. For this case, the gap D evolves in time and converges to some finite value. In Fig. 15.2, we show the flows (trajectories) S-D for $D_0 \neq 0$. All flows converge to $(7.61, 28.19)$.

15.2.1.1 Symmetric Case

For symmetric case $D_t = 0$ ($x_1 = x_2$), the differential equation with respect to S is simply obtained by

$$\frac{dS}{dt} = -\alpha S + 2\rho A + kS\mathrm{e}^{-\eta S/2}. \tag{15.7}$$

The steady state is given by the following nonlinear equation.

$$\alpha S = 2\rho A + kS\mathrm{e}^{-\eta S/2} \tag{15.8}$$

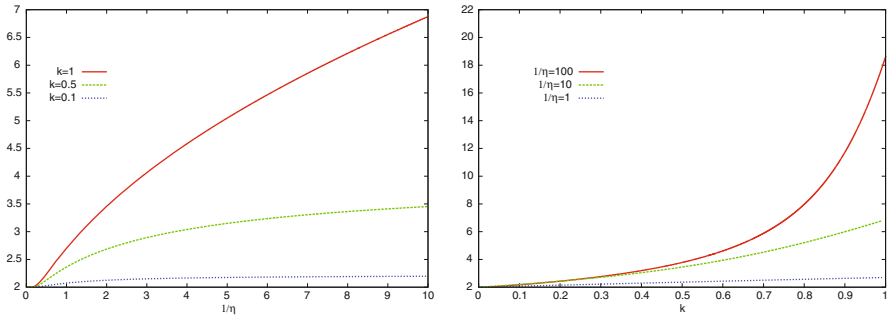

Fig. 15.3 The solution of the steady state which satisfies $\alpha S = 2\rho A + kSe^{-\eta S/2}$ as function of $1/\eta$ (*left*) and k (*right*). For simplicity, we set $\rho = A = 1$

In Fig. 15.3, we show the solution S of the steady state which satisfies Eq. (15.8) as function of $1/\eta$ (left) and k (right). From this figure, we find that the S in the steady state increases monotonically in $1/\eta$ and k. As we shall discuss in the next section, from the view point of maximization of the gross S, we should increase k and $1/\eta$ to infinity. Hence, one cannot choose these parameters as finite values as $k, 1/\eta < \infty$ in the limit of $t \to \infty$.

15.2.1.2 Breaking of Symmetric Phase by Noise

As we saw before, as long as we choose the parameters to satisfy $A_1 = A_2, \alpha_1 = \alpha_2, \cdots$, we have a symmetric solution $D_t = 0$. To break this symmetric phase, here we consider two types of additive noise, namely:

(a) Additive noise on A_1:

$$A_1 = A_2 + \delta n, \quad n \in [-1, 1] \text{ (uniform random number)}, \quad A_2 = 1$$

(b) Additive noise on $1/\eta_1$

$$1/\eta_1 = 1/\eta_2 + \delta|n|, \quad n \in [-1, 1] \text{ (uniform random number)}, \quad 1/\eta_2 = 1$$

and change the "amplitude," δ. The results are shown in Fig. 15.4. In this figure, we set the parameters as $\alpha_2 = \rho_1 = \rho_2 = 1/\eta_2 = 1$ and $k_1 = k_2 = 15, A_1 = A_2 = 1$. Then, we break the symmetry as $A_1 = A_2 + \delta n$ (left) and $1/\eta_1 = 1/\eta_2 + \delta|n|$ (right). The initial condition are selected symmetrically as $(x_1, x_2) = (1, 1)$.

From the left panel, we find that the symmetric phase specified by $D_t = 0$ remains up to t_c even if we add a noise on A_1. The t_c decreases as the amplitude δ increases. On the other hand, from the right panel, we find that the symmetric phase is easily broken when we add a small noise on $1/\eta_1$. In fact, even for $\delta = 0.1$, the critical time t_c is close to zero. Moreover, we find that D_t rapidly increases when δ increases and it takes a maximum at time t_p.

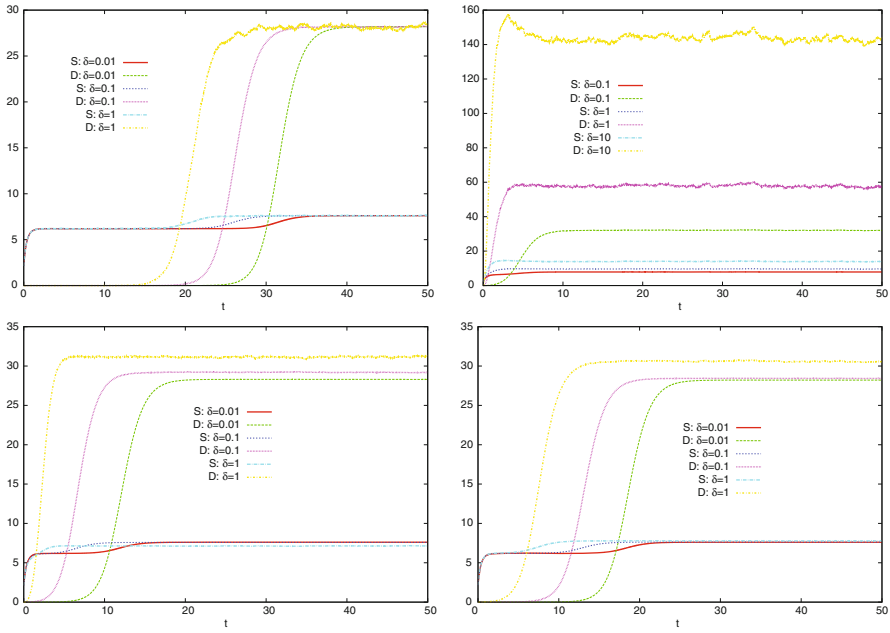

Fig. 15.4 The time-dependence of S and D calculated by Eqs. (15.5) and (15.6). We set the parameters as $\alpha_2 = \rho_1 = \rho_2 = 1/\eta_2 = 1$ and $k_1 = k_2 = 15$, $A_1 = A_2 = 1$. Then, we break the symmetry as $A_1 = A_2 + \delta n$ (*left*) and $1/\eta_1 = 1/\eta_2 + \delta|n|$ (*right*). The initial condition are selected symmetrically as $(x_1, x_2) = (1, 1)$

15.3 Optimization of Parameters

In the previous section, we examined the differential equations with respect to the gross S and the gap D of lovers' feelings for some specific choice of parameters $\boldsymbol{\theta}$.

In Rinaldi et al. [1], they chose those parameters to reproduce Scarlett O'Hara and Rhett Butler's feelings according to the fascinating plot of the movie GWTW. For this purpose, the parameters should be time-dependent because the fluctuating (up–down) behavior of main characters (Scarlett and Rhett) should be induced frequently. There is no doubt about this procedure of determining the parameters because the GWTH was historically a remarkable hit movie, and the scenario (plot) was the most important factor to make the movie success.

On the other hand, as explained earlier, in realistic situations of lovers or married couples, the persons do not have to make their feelings fluctuate (up–down) to disrupt their peaceful life and should instead enhance their psychological uplift so as to keep their affection for the partner strong. In this sense, we might treat the problem of psychology uplift for the lovers mathematically, by regarding it as an optimization or an optimal scheduling of parameters in the differential Eqs. (15.5) and (15.6), so as to maximize the gross S and minimize the gap D, as quickly as possible.

From this viewpoint, we should solve the optimization problem for each time step t because the optimal parameters are dependent on the time step through the gross and the gap. Hence, we might choose the variables $\boldsymbol{\theta}$, so as to satisfy:

$$\boldsymbol{\theta} = \arg\max_{\boldsymbol{\theta}} \phi(\boldsymbol{\theta}, \xi : S, D) \tag{15.9}$$

for each time step, where we defined the following utility function:

$$\phi(\boldsymbol{\theta}, \xi : S, D) \equiv f(\boldsymbol{\theta} : S, D) - \xi g(\boldsymbol{\theta} : S, D) \tag{15.10}$$

for $\xi \geq 0$. The maximization given by Eq. (15.9) means that we accelerate the speed of increase $dS/dt(= f)$ and $-dD/dt(= -g)$ as much as possible during the dynamics of S and D. Hence, when we choose the variable S for the case of $\xi = 0$ to be maximized for lovers, we should optimize the parameters appearing in the function f. For each time step, the landscape of f changes due to the dynamics of D and S, and one should choose the solution, say, $\boldsymbol{\theta} = (\alpha_1, \alpha_2, \cdots)$ so as to maximize the function f at each time step. As the result, we obtain the trajectory in the parameter space: $(\alpha_1(0), \alpha_2(0), \cdots) \to (\alpha_1(1), \alpha_2(1), \cdots) \to \cdots$.

15.3.1 *"Hard" and "Soft" Optimizations by Using a Concept of Physics*

In the following, for simplicity, we only consider the case of $\xi = 0$ and we also carry out the maximization of the speed of increase dS/dt (see Eq. (15.5) and do not take into account the maximization of $-dD/dt$ (see Eq (15.6)).

To achieve the parameter choice by means of physics, we start our argument from the following energy function:

$$E(\boldsymbol{\theta} : S_t, D_t) \equiv -f(\boldsymbol{\theta} : S_t, D_t). \tag{15.11}$$

Obviously, in terms of f, we should maximize f as a utility function. We should keep in mind that we use the definition of S_t, D_t instead of S, D to recall us that f is time dependent through those variables. We should bear in mind that the function f is defined at each time step t. In this sense, f is just a function of only parameters $\alpha_{1,2}$, etc., to be selected at each time step. Therefore, the function f is definitely conserved at each time t.

From the viewpoint of "hard optimization," we might utilize the following gradient descent learning for the parameters $\boldsymbol{\theta}$ as

$$\frac{d\boldsymbol{\theta}}{dt} = -\frac{\partial E}{\partial \boldsymbol{\theta}} = +\frac{\partial f}{\partial \boldsymbol{\theta}} \tag{15.12}$$

Obviously, the cost function for each time step is dependent on the state (S_t, D_t). As we mentioned in the previous section (see Fig. 15.4), S_t, D_t might contain some

noise and through the fluctuation in S_t, D_t, the parameters $\boldsymbol{\theta}$ fluctuate around the peak of the locally concave function f. To determine the parameters, we temporarily assume here that the parameters are all "stochastic" variables.

Namely, to adapt ourselves to such realistic cases, we consider ensemble of the parameters and we carry out the following maximization of Shannon's entropy under the usual two constraints of energy conservation and probability conservation:

$$H = -\int d\boldsymbol{\theta}\, P(\boldsymbol{\theta}) \log P(\boldsymbol{\theta}) + \beta \left(E - \int d\boldsymbol{\theta}\, E(\boldsymbol{\theta} : S_t, D_t) P(\boldsymbol{\theta}) \right) + \lambda \left(1 - \int d\boldsymbol{\theta}\, P(\boldsymbol{\theta}) \right) \tag{15.13}$$

where β, λ are Lagrange multipliers. By making use of derivative with respect to $P(\boldsymbol{\theta}), \lambda$, we have

$$P(\boldsymbol{\theta}) = \frac{\exp(\beta f(\boldsymbol{\theta} : S_t, D_t))}{\int d\boldsymbol{\theta} \exp(\beta f(\boldsymbol{\theta} : S_t, D_t))} \tag{15.14}$$

This is nothing but the Boltzmann–Gibbs distribution with temperature $T = \beta^{-1}$.

To obtain the appropriate parameters, we construct the following iterations:

$$\boldsymbol{\theta}^{(t+1)} = \int d\boldsymbol{\theta}\, P(\boldsymbol{\theta}) = \frac{\int d\boldsymbol{\theta}\, \boldsymbol{\theta} \exp(\beta f(\boldsymbol{\theta} : S_t, D_t))}{\int d\boldsymbol{\theta} \exp(\beta f(\boldsymbol{\theta} : S_t, D_t))} \tag{15.15}$$

We should keep in mind that the strict maximization of f is achieved by taking the limit of $\beta \to \infty$. Namely, the solution for "hard optimization" is recovered as

$$\boldsymbol{\theta}^{(t+1)}_{\text{hard}} = \lim_{\beta \to \infty} \frac{\int d\boldsymbol{\theta}\, \boldsymbol{\theta} \exp(\beta f(\boldsymbol{\theta} : S_t, D_t))}{\int d\boldsymbol{\theta} \exp(\beta f(\boldsymbol{\theta} : S_t, D_t))}. \tag{15.16}$$

These types of adaptive learning procedure have been well-known since the reference [9] in the literature of neural networks.

It is important for us to obtain the strict solution, of course. However, here we consider only the case of $\beta = 1$, since we are dealing with the situation in which the parameters $\boldsymbol{\theta}$ are not deterministic variables; rather, stochastic variables fluctuating around the peaks of f.

From the viewpoint of optimization, note that the function f is not locally "concave" for any choice of S_t, D_t. Hence, the parameters $\boldsymbol{\theta}$ which should be selected are trivially going to their "bounds." Nevertheless in the following, we derive the concrete update rule for each parameter. We first consider the parameter α_1. Here, we assume that $\alpha_{1,2}$ take any value in $[0, \infty)$. Hence, we obtain

$$\alpha_1^{(t+1)} = \frac{\int_0^\infty d\alpha_1 \alpha_1 \mathrm{e}^{-\alpha_1 (S_t + \sqrt{D_t})/2}}{\int_0^\infty d\alpha_1\, \mathrm{e}^{-\alpha_1 (S_t + \sqrt{D_t})/2}} = \frac{2}{S_t + \sqrt{D_t}}, \quad \alpha_2^{(t+1)} = \frac{2}{S_t - \sqrt{D_t}}. \tag{15.17}$$

Hence, we find that the parameters $\alpha_{1,2}$ decrease as inverse of the dynamics S_t to zero, when we consider the symmetric case $D_t = 0$. Therefore, as we expected, $\alpha_{1,2}$ go

to the bound $\alpha_{1,2} = 0$ but the optimal scheduling, namely, the speed of convergence to the bound $\alpha_{1,2} \sim 1/S_t$ is not trivial and would be worthwhile for us to investigate extensively.

We next consider $\rho_{1,2}$. For simplicity, we assume that these two parameters take values in $[0, 1]$. After simple algebra, we have

$$\rho_1^{(t+1)} = \frac{\int_0^1 d\rho_1 \rho_1 \mathrm{e}^{A_2\rho_1}}{\int_0^1 d\rho_1 \mathrm{e}^{A_2\rho_1}} = \frac{A_2^{(t)}\mathrm{e}^{A_2^{(t)}} - \mathrm{e}^{A_2^{(t)}} + 1}{A_2^{(t)}(\mathrm{e}^{A_2^{(t)}} - 1)}, \quad \rho_2^{(t+1)} = \frac{A_1^{(t)}\mathrm{e}^{A_1^{(t)}} - \mathrm{e}^{A_1^{(t)}} + 1}{A_1^{(t)}(\mathrm{e}^{A_1^{(t)}} - 1)}. \tag{15.18}$$

Since ρ and A are "conjugates" in the argument of the exponential, we immediately have

$$A_1^{(t+1)} = \frac{\rho_2^{(t)}\mathrm{e}^{\rho_2^{(t)}} - \mathrm{e}^{\rho_2^{(t)}} + 1}{\rho_2^{(t)}(\mathrm{e}^{\rho_2^{(t)}} - 1)}, \quad A_2^{(t+1)} = \frac{\rho_1^{(t)}\mathrm{e}^{\rho_1^{(t)}} - \mathrm{e}^{\rho_1^{(t)}} + 1}{\rho_1^{(t)}(\mathrm{e}^{\rho_1^{(t)}} - 1)}. \tag{15.19}$$

For $k_{1,2}$, the structures are exactly similar to those of A and ρ, when we assume that $k_{1,2} \in [0, 1]$. We easily obtain

$$k_1^{(t+1)} = \frac{Q_1^{(t)}\mathrm{e}^{Q_1^{(t)}} - \mathrm{e}^{Q_1^{(t)}} + 1}{Q_1^{(t)}(\mathrm{e}^{Q_1^{(t)}} - 1)}, \quad Q_1^{(t)} \equiv \frac{(S_t - \sqrt{D_t})}{2}\mathrm{e}^{-\eta_1^{(t)}(S_t - \sqrt{D_t})/2}, \tag{15.20}$$

$$k_2^{(t+1)} = \frac{Q_2^{(t)}\mathrm{e}^{Q_2^{(t)}} - \mathrm{e}^{Q_2^{(t)}} + 1}{Q_2^{(t)}(\mathrm{e}^{Q_2^{(t)}} - 1)}, \quad Q_2^{(t)} \equiv \frac{(S_t + \sqrt{D_t})}{2}\mathrm{e}^{-\eta_2^{(t)}(S_t + \sqrt{D_t})/2}. \tag{15.21}$$

Finally, we consider $\eta_{1,2}$. Here we also assume that $\eta_{1,2} \in [0, \infty)$. Then, we can write

$$\eta_1^{(t+1)} = \frac{\int_0^\infty d\eta_1 \eta_1 \exp[\frac{k^{(t)}(S_t - \sqrt{D_t})}{2}\mathrm{e}^{-\eta_1(S_t - \sqrt{D_t})/2}]}{\int_0^\infty d\eta_1 \exp[\frac{k^{(t)}(S_t - \sqrt{D_t})}{2}\mathrm{e}^{-\eta_1(S_t - \sqrt{D_t})/2}]} \tag{15.22}$$

$$\eta_2^{(t+1)} = \frac{\int_0^\infty d\eta_2 \eta_2 \exp[\frac{k^{(t)}(S_t + \sqrt{D_t})}{2}\mathrm{e}^{-\eta_2(S_t + \sqrt{D_t})/2}]}{\int_0^\infty d\eta_2 \exp[\frac{k^{(t)}(S_t - \sqrt{D_t})}{2}\mathrm{e}^{-\eta_1(S_t - \sqrt{D_t})/2}]} \tag{15.23}$$

Carrying out the above procedure, one could only "soft" (not "hard") optimize the quantity S. By substituting the results into the differential equation with respect to D (see Eq. (15.6)) at the same time, we may obtain the behavior of the gap.

15.4 Discussions and Remarks

In this chapter, we first introduced the Rinaldi model and the framework to discuss some kind of optimality of a person's behavior, in terms of optimization in the mathematical sense. For this, we have just formulated the acceleration rate of the gross

dS/dt, namely, the right-hand side of Eq. (15.5), the function f, at each time step. However, the function f is not locally concave and the value of optimal parameters go either to zero or to infinity, as $t \to \infty$. Nevertheless, we can still discuss the scheduling of parameters. For instance, the parameters $\alpha_{1,2}$ should decay as $\sim S_t^{-1}$ when we attempt to maximize the f from the viewpoint of "soft optimization." In near future, we would like to consider and discuss the result of optimization extensively, by considering the validity of the model itself.

Here, we have set $\beta = 1$ in the calculations. However, we can always regard β as a time dependent parameter—the "inverse-temperature," appearing in the context of "simulated annealing," and defined by

$$T_t = \beta_t^{-1} = \frac{c_1}{(t + c_2)^{\zeta}(\log(t + c_3))^{\varepsilon}} \tag{15.24}$$

where the coefficients $c_{1,2,3}, \zeta, \varepsilon$ determine the speed of convergence. As we already mentioned, the utility function f changes through the dynamical variables S_t, D_t. Hence, the utility surface also evolves in time. In the above scheduling, we have also assumed that the temperate is decreasing within the same time scale as dynamical variables S_t, D_t and parameters $\boldsymbol{\theta}$. However, we can also consider the case in which T is scheduled in much shorter time scale than S_t, D_t and in the same time scale as $\boldsymbol{\theta}$, namely, $T_\tau, \boldsymbol{\theta}_\tau$ with $\tau \ll t$. Then, the procedure defined by Eq. (15.16) is regarded as the "deterministic annealing" [10]. In such a general case, the optimal scheduling for the parameters $\boldsymbol{\theta}$ might be changed and extensive study along this direction will be reported in our forthcoming paper.

A few other specific remarks are mentioned below:

1. In the model considered here, the parameters values are the same as those of Rinaldi et al. [1], but this choice is neither unique nor true for all the "realistic" situations. A thorough study with other choices of parameters is very much necessary.
2. Identification of the most sensitive parameters responsible for the long-time survival of the relationship remains an interesting and open problem. Such identification and then introduction of stochastic fluctuations at the limiting situations could certainly provide more insight toward the modeling approach.
3. The present work is sort of a preliminary attempt of understanding the love dynamics—theory for the case of sustainability of the love relation between a couple. In reality, the dynamics of love affairs and related modeling approach need more careful and thorough investigations; the effects of several factors have not been considered so far, for example, how the presence of one or more competing person(s) along with the couple, who are in a love relation to each other, can influence the dynamics. Along the lines of the triangular love studies by Sprott [7, 8], it might be very interesting to investigate the role of S and D, in order to determine the steady-state relationship between a couple for the case of triangular love. Amongst many other interesting questions, one could also investigate how does a period of separation affect the system dynamics, within this modeling approach.

Acknowledgments One of the authors (JI) was financially supported by Grant-in-Aid for Scientific Research (C) of Japan Society for the Promotion of Science (JSPS) No. 2533027803, Grant-in-Aid for Scientific Research (B) No. 26282089, and Grant-in-Aid for Scientific Research on Innovative Area No. 2512001313.

References

1. Rinaldi, S., Della Rossa, F., Landi, P.: A mathematical model of “Gone with the Wind". Physica A **392**, 3231–3239 (2013).
2. Strogatz, S.H.: Love affairs and differential equations. Math. Mag. **61**, 35 (1998).
3. Strogatz, S.H.: Nonlinear Dynamics and Chaos: With Applications to Physics, Biology, Chemistry, and Engineering. Westview, Colorado 1994).
4. Gragnani, A., Rinaldi, S., Feichtinger, G.: Cyclic dynamics in romantic relationships. Int. J. Bifur. Chaos **7**, 2611–2699 (1997).
5. Rinaldi, S.: Love dynamics: the case of linear couples. Appl. Math. Comput. **95**, 181–192 (1998).
6. Rinaldi, S., Gragnani, A.: Love dynamics between secure individuals: a modeling approach. Nonlin. Dyn. Psych. Life Sci. **2**, 298–301 (1998).
7. Sprott, J.C.: Dynamical models of love. Nonlin. Dyn. Psych. Life Sci. **8**, 303–314 (2004).
8. Sprott, J.C.: Dynamical models of happiness. Nonlin. Dyn. Psych. Life Sci. **9**, 23–36 (2005).
9. Amari, S.: A Theory of Adaptive Pattern Classifiers IEEE Transactions on Electronic Computers **EC-16**(3), 299–307 (1967).
10. Levin, E., Tishby, N., Solla, S.: A statistical approach to learning and generalization in layered neural networks. Proc. IEEE **78**, 10, October, pp. 1568–1574 (1990).

Chapter 16
From Weak Allee Effect to No Allee Effect in Richards' Growth Models

J. Leonel Rocha, Abdel-Kaddous Taha and D. Fournier-Prunaret

Abstract Population dynamics have been attracting interest since many years. Among the considered models, the Richards' equations remain one of the most popular to describe biological growth processes. On the other hand, Allee effect is currently a major focus of ecological research, which occurs when positive density-dependence dominates at low densities. In this chapter, we propose the dynamical study of classes of functions based on Richards' models describing the existence or not of Allee effect. We investigate bifurcation structures in generalized Richards' functions and we look for the conditions in the (β, r) parameter plane for the existence of a weak Allee effect region. We show that the existence of this region is related with the existence of a dovetail structure. When the Allee limit varies, the weak Allee effect region disappears when the dovetail structure also disappears. Consequently, we deduce the transition from the weak Allee effect to no Allee effect to this family of functions. To support our analysis, we present fold and flip bifurcation curves and numerical simulations of several bifurcation diagrams.

16.1 Introduction and Motivation

The Richards' equation is one the most popular of the more flexible growth equations, since it was presented by Richards in 1959 (see [9]). It is used for diverse purposes, including modeling tree growth, growth of turkeys, growth of juvenile

J. L. Rocha (✉)
Instituto Superior de Engenharia de Lisboa - ISEL, ADM and CEAUL,
Rua Conselheiro Emídio Navarro 1, 1959-007 Lisboa, Portugal
e-mail: jrocha@adm.isel.pt

A.-K. Taha
INSA, University of Toulouse, 135 Avenue du Rangueil, 31077 Toulouse, France
e-mail: taha@insa-toulouse.fr

D. Fournier-Prunaret
LAAS-CNRS, INSA, University of Toulouse, 7 Avenue du Colonel Roche,
31077 Toulouse, France
e-mail: daniele.fournier@insa-toulouse.fr

R. López-Ruiz et al. (eds.), *Nonlinear Maps and their Applications,*
Springer Proceedings in Mathematics & Statistics 112, DOI 10.1007/978-3-319-12328-8_16

mammals and birds, and comparisons of treatment effects on plant growth, see for example references in [12]. The Richards growth dynamics is given by the following differential equation:

$$f(N(t)) = \frac{dN(t)}{dt} = r^* N(t)\left(1 - \left(\frac{N(t)}{K}\right)^{\beta}\right), \tag{16.1}$$

where t is a variable representing time; $N(t)$ is a value of a measure of size or density of an organism or population; $\beta > 0$ is an additional shape parameter, introduced as a power law so that it can define asymmetric curves (dimensionless scalar), considered as intraspecific competition factor; $r^* > 0$ is the maximum intrinsic rate of increase of $N(t)$ and K is the carrying capacity, for more details see for example [12] and [13].

The class of models given by Eq. (16.1), those with $\beta \in \ ]0, 1[$, do not exhibit Allee effect, because the *per capita* growth rates decrease at low densities. One of the main motivations of the present work are the results presented in [12], where we introduce correction factors in Richards' models with $\beta \in]0, 1[$, in such a way that the new generalized Richards' models have Allee effect.

The Allee effect is an important dynamic phenomenon first described by Allee in 1931. Stephens et al. in 1999 distinguished between component Allee effects and demographic Allee effects. All mechanisms giving rise to an Allee effect (for example, difficulty in finding mates or cooperative feeding) result in component Allee effects, i.e., a positive relationship between a component of individual fitness, e.g., survivorship or per capita reproduction, and population size or density. If these component Allee effects are not offset by negative density dependence in other components of fitness they may cause demographic Allee effects, i.e., positive density dependence manifested at the population level [5]. The population level consequences of demographic Allee effects are classified as either weak or strong, where a strong Allee effect results in a critical density below which per capita population growth rate is negative, while in the case of a weak Allee effects this critical density does not exist, see for example [5] and [12]. In this chapter, we use the concept of demographic Allee effect, which is manifested by a reduction in the per capita growth rate at low-population sizes. In this case, the per capita growth rates are higher than the population growth rate at the initial time. Such phenomenon can be observed in the evolution of biological species interacting with themselves and their environment. The definitions of strong and weak Allee effects that we will use are in the sense of [5], [12], and references therein.

The generalized population growth rate or generalized Richards' growth models are defined in [12] by the following differential equation:

$$f^*(N(t)) = \frac{dN(t)}{dt} = r^* N(t)\left(1 - \left(\frac{N(t)}{K}\right)^{\beta}\right)\frac{N(t) - E}{N(t) + C}, \tag{16.2}$$

with $r^* > 0$, $\beta \in \ ]0, 1[$, $C > 0$ and the Allee limit E satisfies $|E| < K$. The remaining quantities are defined as such in Eq. (16.1). The parameter C allows us to define and study more flexible models with variable extinction rates, see [12]. We

remark that the consideration of the parameter $-K < E < 0$ follows as a sufficient condition for *per capita* growth rates increasing at low densities (weak Allee effect) or decreasing for all densities (no Allee effect), as proven in Props. 2 and 3 of [12]. On the other hand, the consideration of the parameter $0 < E < K$ is a sufficient condition for the existence of strong Allee effect, i.e., there is a critical threshold below which populations experience rapid extinction, as proven in Prop. 1 of [12].

Motivated by the interest and relevance of the study of growth models and the extinction phenomenon, we propose to study in this chapter the transition from weak Allee effect to no Allee effect in Richards' growth models. The layout of this chapter is as follows. In Sect. 16.2, we present a new dynamical approach to Richards' growth equation: a new class of one-dimensional discrete dynamical systems, a family of unimodal maps which was first studied in [12], designated by generalized Richards' functions. For this family of functions, two classes of functions are established: weak Allee effect functions and functions with no Allee effect. Sect.16.3 is devoted to the study of bifurcation structure of this functions at the parameter plane (β, r). To support our results, we present fold and flip bifurcation curves and numerical simulations of the bifurcation diagrams. Generically, the dynamics of these functions are categorized in the following types: extinction, semistability, stability, period doubling, chaos and chaotic semistability. In Sect. 16.3.2 we study the evolution of bifurcation curves when the parameter E varies: the transition from the weak Allee effect to no Allee effect with respect to the parameter E is identified. This phenomenon is associated with the appearance and disappearance of a dovetail structure. Finally, we discuss our results and provide some relevant conclusions.

16.2 Generalized Richards' Functions

In this section, we present a dynamical approach to generalized Richards' growth models, new classes of functions describing the existence or nonexistence of Allee effect. Consider the families of functions $f_{r,\beta} : [0, 1] \to [0, 1]$, defined by

$$f_{r,\beta}(x) = rx\left(1 - x^{\beta}\right)\frac{Kx - E}{Kx + C}, \tag{16.3}$$

where $x = \frac{N(t)}{K}$ is the normalized population dimension, $r = r^*K > 0$ is an intrinsic growth rate of the number of individuals or organisms, $\beta \in]0, 1[$ is a shape parameter, with $|E| < K$ and $C > 0$. These families of functions will be designated by generalized Richards' functions, see some examples in Fig. 16.1. Generically, these functions are unimodal or bimodal maps and are proportional to the right-hand side of the generalized Richards' models, Eq. (16.2).

Let $A_r = f_{r,\beta}(A_r)$ be the first positive fixed point of $f_{r,\beta}$ and $A_r^* = max\{f_{r,\beta}^{-1}(A_r)\}$. The following conditions are satisfied:

(A1) $f_{r,\beta}$ is continuous on $[0, 1]$;
(A2) there exists $\left[A_r, A_r^*\right] \subset [0, 1] : f_{r,\beta}(x) \leq A_r, \forall x \in [0, 1] \setminus \left]A_r, A_r^*\right[$;

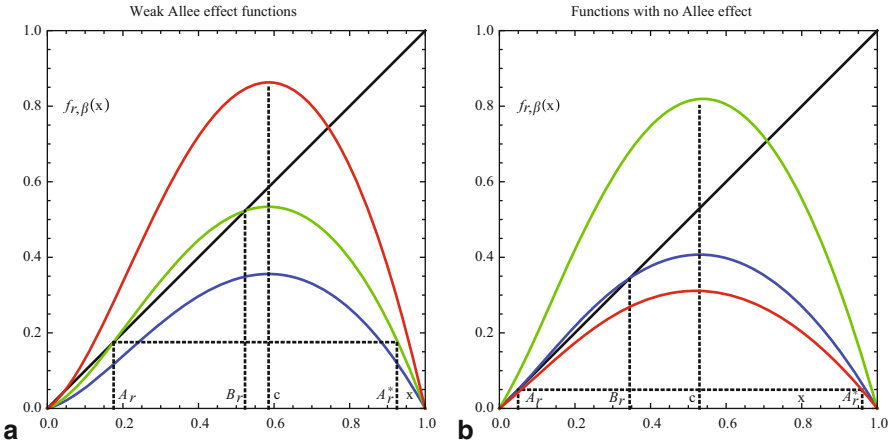

Fig. 16.1 Generalized Richards' functions $f_{r,\beta}(x)$: **a** weak Allee effect functions at $\beta = 7/9$, $r = 4,\ 6,\ 9.7$, $K = 10$, $C = 8.5$, and $E = -0.55$; (3 fixed points: 0, A_r and B_r); **b** functions with no Allee effect $f_{r,\beta}(x)$ at $K = 10, C = 7.5$, and $E = -1$: *red graphic* at $\beta = 0.2$ and $r = 10$ (2 fixed points: 0 and O_r; region R_4 in Fig.16.3); *blue graphic* at $\beta = 0.3$ and $r = 9$ (4 fixed points: 0, O_r, A_r and B_r; region R_3 in Fig.16.3); *green graphic* at $\beta = 0.4$ and $r = 14$ (2 fixed points; region R_4 in Fig.16.3)

(A3) $f_{r,\beta}$ has an unique critical point $c \in \left]A_r, A_r^*\right[$;
(A4) $f'_{r,\beta}(x) \neq 0, \forall x \in \left]A_r, A_r^*\right[\setminus \{c\}$, $f'_{r,\beta}(c) = 0$ and $f''_{r,\beta}(c) < 0$;
(A5) $f_{r,\beta} \in C^3\left(\left]A_r, A_r^*\right[\right)$;
(A6) the Schwarzian derivative of $f_{r,\beta}(x)$ given by

$$S\left(f_{r,\beta}(x)\right) = \frac{f'''_{r,\beta}(x)}{f'_{r,\beta}(x)} - \frac{3}{2}\left(\frac{f''_{r,\beta}(x)}{f'_{r,\beta}(x)}\right)^2$$

verifies $S\left(f_{r,\beta}(x)\right) < 0, \forall x \in \left]A_r, A_r^*\right[\setminus \{c\}$ and $S\left(f_{r,\beta}(c)\right) = -\infty$.

Conditions $(A1) - (A6)$ and more particularly the negative Schwarzian derivative ensures a "good" dynamic behavior of the models. In the case of unimodal maps there is at most one stable orbit, and in the case of bimodal maps there are at most two stable orbits. In general, the growth models studied have negative Schwarzian derivative and the use of unimodal maps is also frequent, see for example [10–12].

To generalized Richards' functions, Eq. (16.3), we define two classes of functions that describe the growth of a population with weak Allee effect and without Allee effect.

Definition 16.1 Consider $-K < E \leq 0$, $0 < \lim_{x \to 0^+} f'_{r,\beta}(x) < 1$, $C > 0$, $r > 0$, $\beta \in\ ]0, 1[$ and $f_{r,\beta}$ defined by Eq. (16.3). The generalized Richards' functions $f_{r,\beta} : [0, 1] \to [0, 1]$ attaining its maximum at c are a family of weak Allee effect functions, if there are numbers A_r and B_r such that:

Table 16.1 Summary of the most important properties for functions with no Allee effect, with weak Allee effect and with strong Allee effect, in the (β, r) parameter plane

	No Allee effect function	Weak Allee effect function	Strong Allee effect function, see [12]
Parameter values	$E < 0$, $C > 0$, $\|E\| < K$	$E < 0$, $C > 0$, $\|E\| < K$	$E > 0$, $C > 0$, $\|E\| < K$
Number of fixed points	Two $(0, B_r)$ or four $(0, O_r, A_r, B_r)$	One (0) or three $(0, A_r, B_r)$	One (0) or three $(0, A_r, B_r)$
Stability of origin	unstable	always stable	stable or unstable or negative values (E/K)
Extinction region	No $(\Lambda_1^* \equiv \Lambda_{NA})$	R_1 $(\Lambda_1^* \equiv \Lambda_{NA})$	r below $\Lambda_{(1)_0}$; essential ext. between Λ_1^* and Λ_{NA}
Weak Allee effect region	No	R_2	No
Strong Allee effect region	No	No	r above $\Lambda_{(1)_0}$ and r below Λ_1^*

(i) $0 < A_r < c < B_r < 1$;
(ii) $\forall x \in [0,1] \setminus [A_r, B_r] \Rightarrow f_{r,\beta}(x) < x$;
(iii) $\forall x \in]A_r, B_r[\Rightarrow f_{r,\beta}(x) > x$.

Note that, if $0 < E < K$ then $\lim_{x \to 0^+} f'_{r,\beta}(x) = -\infty$. This class of functions has been studied in [12] and is designated by strong Allee effect functions, see also Table 16.1. In the case of weak Allee effect functions, the fixed point $x = 0$ is always stable, see some examples in Fig. 16.1a. On the other hand, the generalized Richards' functions $f_{r,\beta}$ also includes another class of important functions.

Definition 16.2 Consider $-K < E \leq 0$, $C > 0$, $r > 0$, $\beta \in]0,1[$ and $f_{r,\beta}$ defined by Eq. (16.3). The generalized Richards' functions $f_{r,\beta} : [0,1] \to [0,1]$ attaining its maximum at c are a family of functions with no Allee effect, if there are numbers O_r, A_r, and B_r such that:

(i) $0 < O_r < A_r < c < B_r < 1$;
(ii) $\forall x \in [0,1] \setminus ([0, O_r] \cup [A_r, B_r]) \Rightarrow f_{r,\beta}(x) < x$;
(iii) $\forall x \in (]0, O_r[\cup]A_r, B_r[) \Rightarrow f_{r,\beta}(x) > x$.

The class of functions with no Allee effect verifies $\lim_{x \to 0^+} f'_{r,\beta}(x) > 1$, i.e., the fixed point $x = 0$ is always unstable. It is for this reason that this class of functions does not include extinction. From Definition 16.1 it follows that in the case of weak Allee effect functions, we will have at maximum three fixed points $0, A_r$,and B_r, see Fig. 16.1a. On the other hand, from Definition 16.2, in the case of functions with no Allee effect, we will have at least two fixed points 0 and O_r, and at most four fixed points $0, O_r, A_r$ and B_r, depending on the evolution of the parameter r, see some examples in Fig. 16.1b. In Table 16.1 we present a summary of the most important properties for this kind of functions.

16.3 Bifurcation Structure of Weak Allee Effect Functions and of Functions with No Allee effect

In this section we investigate the dynamical complexity of the proposed models at (β, r) parameter plane. The evolution of the bifurcation structure is studied by varying the third parameter E, parameters C and K being fixed. The analysis of their bifurcations structure is done based on the bifurcation diagrams, see Figs. 16.2, 16.3, 16.5, and 16.6. We will make use of the fold and flip bifurcations, related with some cycles of order $n \in \mathrm{IN}$ set of natural numbers. We recall that an order n cycle $(x_1, x_2, ..., x_n)$ is stable (or attractive) iff $\left|\frac{\partial f_r^n}{\partial x}(x_j)\right| < 1,\ \forall j = 1, 2, ..., n$. The fold bifurcation corresponds to the appearance of two order n cycles, one stable and the other unstable, when it is verified $\frac{\partial f_{r,\beta}^n}{\partial x}(x_j) = 1,\ \forall j = 1, 2, ..., n$. On the other hand, the flip bifurcation corresponds to the change of stability of an order n cycle and the appearance of an order $2n$ cycle. Before the bifurcation, the order n cycle is stable, after the bifurcation, the order n cycle is unstable and the $2n$ cycle is stable. At the bifurcation it is verified that $\frac{\partial f_{r,\beta}^n}{\partial x}(x_j) = -1,\ \forall j = 1, 2, ..., n$. For more details about bifurcation theory see for example [6] and [8].

Generically, to generalized Richards' functions $f_{r,\beta}(x)$, defined by Eq. (16.3), with $r > 0,\ \beta \in\ ]0, 1[,\ |E| < K$ and $C > 0$, the fold and the flip bifurcation curves relative to a cycle of order n are calculated as follows. In the (β, r) parameter plane, if $x \in [0, 1[$ is a point of an order n cycle that satisfies the equations

$$f_{r,\beta}^n(x, K, E, C) = x \ \text{ and } \frac{\partial f_{r,\beta}^n}{\partial x}(x, K, E, C) = 1 \tag{16.4}$$

then there exists a solution φ_n in implicit form, such that the fold bifurcation curves relative to a cycle of order $n \in \mathrm{IN}$ set of natural numbers are given by $r(\beta) = \varphi_n(x, \beta, K, E, C)$, and are denoted by $\Lambda_{(n)_0}^j$, where j differentiates cycles of same order. On the other hand, if $x \in [0, 1[$ and

$$f_{r,\beta}^n(x, K, E, C) = x \ \text{ and } \frac{\partial f_{r,\beta}^n}{\partial x}(x, K, E, C) = -1 \tag{16.5}$$

then there exists a solution ψ_n, in implicit form, such that the flip bifurcation curves relative to a cycle of order $n \in \mathrm{IN}$ set of natural numbers, in the parameter plane (β, r), are given by $\bar{r}(\beta) = \psi_n(x, \beta, K, E, C)$, and are denoted by Λ_n^j.

In [1] a necessary and sufficient condition is given for the existence of a cusp point on a fold bifurcation curve relative to a cycle of order n, in a parameter plane of a one-dimensional map, see also [2] and [4]. Generically, to the class of generalized Richards' functions with Allee effect $f_{r,\beta}(x)$, with $r > 0,\ \beta \in\ ]0, 1[,\ |E| < K$ and $C > 0$, that condition is given by the following expressions:

$$\begin{cases} f_{r,\beta}^n(x,K,E,C) = x, \ \frac{\partial f_{r,\beta}^n}{\partial x}(x,K,E,C) = 1 \\ \frac{\partial^2 f_{r,\beta}^n}{\partial x^2}(x,K,E,C) = 0, \ \frac{\partial^3 f_{r,\beta}^n}{\partial x^3}(x,K,E,C) \neq 0 \\ \frac{\partial f_{r,\beta}^n}{\partial \beta}(x,K,E,C) \ \frac{\partial^2 f_{r,\beta}^n}{\partial x \partial r}(x,K,E,C) - \frac{\partial f_{r,\beta}^n}{\partial r}(x,K,E,C) \ \frac{\partial^2 f_{r,\beta}^n}{\partial x \partial \beta}(x,K,E,C) \neq 0 \end{cases}. \tag{16.6}$$

16.3.1 Foliated Bifurcation Structure of Generalized Richards' Functions

In particular, to generalized Richards' functions $f_{r,\beta}(x)$, the Eqs. (16.4) and (16.5) for $n = 1$ are given by:

$$\begin{cases} f_{r,\beta}(x) = x \\ \varphi_1(x,\beta,K,E,C) = \frac{(Kx+C)^2}{(\beta E-(\beta+2)C)Kx^{\beta+1}+(\beta+1)x^\beta\left(EC-K^2x^2\right)+K^2x^2+2KxC-EC} \\ \psi_1(x,\beta,K,E,C) = -\varphi_1(x,\beta,K,E,C) \end{cases}. \tag{16.7}$$

For this family of functions, the condition (16.6) is equivalent to:

$$\begin{cases} x = 0 \\ r = -\frac{C}{E}, \ \forall\, C > 0, \ E \neq 0 \end{cases} \text{ or } \begin{cases} x = \frac{E(\beta-1)}{K(\beta+1)}, \ r = \frac{\beta-1}{x^\beta(\beta+1)+\beta-1} \\ C = \frac{E(1-\beta)\left(x^\beta(\beta+1)-2x^\beta+\beta+1\right)}{(\beta+1)\left(x^\beta(\beta+1)+\beta-1\right)} \end{cases}. \tag{16.8}$$

The first solution means that the fold bifurcation curve of the fixed point 0, $\Lambda_{(1)_0} := r = -\frac{C}{E}$, in the parameter plane (β, r), is a singular curve. Considering that $x \in [0,1]$, $r > 0$ and $\beta \in \,]0,1[$, by the above conditions for the existence of the cusp point (16.8), we have that $-K < E < 0$. Remark that if $0 < \lim_{x\to 0^+} f_{r,\beta}'(x) < 1$ and are satisfied the conditions of Definition 16.1, then the family $f_{r,\beta}(x)$ has weak Allee effect. Otherwise, if $\lim_{x\to 0^+} f_{r,\beta}'(x) > 1$, then this family has no Allee effect.

As stated in Lemma 4.1 of [12], the extinction region associated to weak Allee functions is characterized by the following propositions:

(i) If 0 is the unique fixed point of the weak Allee functions $f_{i;r_i,\beta}(x)$, then

$$\lim_{n\to\infty} f_{r,\beta}^n(x) = 0, \ \forall x \in [0,1];$$

(ii) If the weak Allee functions $f_{r,\beta}(x)$ have more than one fixed point, then

$$\lim_{n\to\infty} f_{r,\beta}^n(x) = 0, \ \forall x \in [0,1] \setminus \left[A_r, A_r^*\right].$$

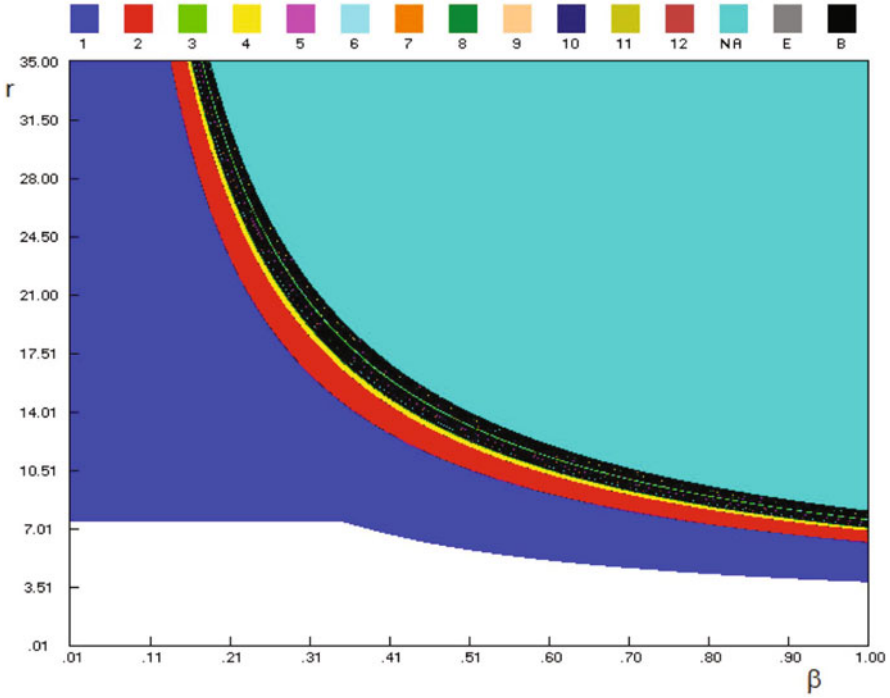

Fig. 16.2 Bifurcation diagram of generalized Richards' functions $f_{r,\beta}(x)$, in the (β, r) parameter plane at $K = 10$, $E = -1$, and $C = 7.5$. The *white region* is the extinction region. The *blue region* is the stability region. The region between the *blue* and the *turquoise* ones corresponds to period doubling region and chaotic region. The *turquoise* region is the no admissible region

Fig. 16.2 shows a bifurcation diagram of the family $f_{r,\beta}(x)$, at $K = 10, E = -1$ and $C = 7.5$. Each colored domain indicates existence of at least one stable cycle whose order corresponds to upper colored squares in figure. In the (β, r) parameter plane, for the parameter values considered, this family incorporates weak Allee effect functions and functions with no Allee effect. In this case, the extinction region is bounded below by $r(\beta) = 0$ and is upper bounded by the fold bifurcation curve $\Lambda^1_{(1)_0}$, of the fixed points 0 and O_r, and by the fold bifurcation curve ${}^a\Lambda^2_{(1)_0}$, of the fixed points A_r and B_r, see also Fig. 16.3. Remark that, the fold bifurcation curve $\Lambda^1_{(1)_0}$, of the fixed points 0 and O_r, and the fold bifurcation curve ${}^a\Lambda^2_{(1)_0}$, of the fixed points A_r and B_r, define the semistability curve associated to weak Allee functions, [12].

The blue region is the stability region, which is bounded below by the semistability curve and is upper bounded by the flip bifurcation curve Λ_1, of the stable fixed point nonzero B_r. The region between the blue and the turquoise ones corresponds to period doubling region and chaotic region. The period doubling region is bounded below by the flip bifurcation curve of the stable fixed point nonzero B_r, Λ_1. The upper limit of this region is defined by the accumulation value of the flip bifurcation curves of the cycle of order 2^n, of the stable fixed points nonzero, see [6]

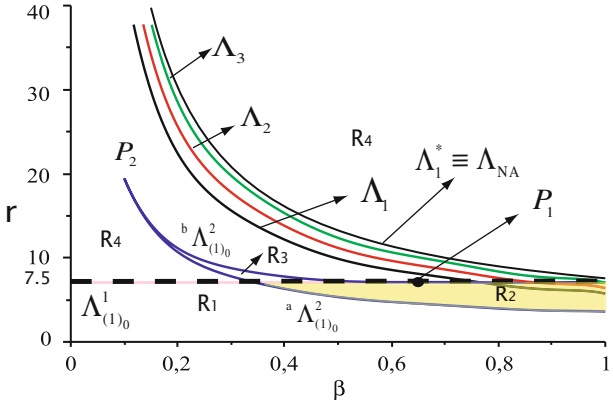

Fig. 16.3 Bifurcations curves of generalized Richards' functions $f^n_{r,\beta}(x)$, with $n = 1, 2, 3$, in the (β, r) parameter plane, at $K = 10, E = -1$ and $C = 7.5$. $\Lambda^1_{(1)_0}$, $^a\Lambda^2_{(1)_0}$ and $^b\Lambda^2_{(1)_0}$ are the fold bifurcation curves; Λ_1, Λ_2 and Λ_3 are the flip bifurcation curves of the cycles of order $n = 1, 2, 3$, respectively; Λ^*_1 is the chaotic semistability curve and Λ_{NA} is the bifurcation curve of non admissibility. In this case $\Lambda^*_1 \equiv \Lambda_{NA}$. The cusp points P_1 and P_2 correspond to solutions of Eq.(16.8). The *yellow* region is the weak Allee effect region R_2

and [8]. This bifurcation curve is denoted by Λ_∞ and from Eq. (16.5) we have,

$$\Lambda_\infty = \lim_{n\to\infty} \psi_{2^n}(x, \beta, K, E, C)$$

with $x \in [0, 1[$ a fixed point. In Fig. 16.2 the period doubling regions are well evidenced, highlighting in particular the cycles of order 2 and 4. Moreover, in Fig. 16.3 we can see some flip bifurcations curves corresponding to this region.

In Fig. 16.2, the chaotic region is bounded below by the accumulation value of the flip bifurcation curves of the cycle of order 2^n, Λ_∞, and is upper bounded by the chaotic semistability curve, when the maximum size of a growing population equals the critical density. In this region are observed all fold and flip bifurcation curves of the cycle of order different than 2^n, Λ_k, with $k \neq 2^n$, identified and ordered in the "box-within-a-box" bifurcation structure, [3], [6], [8] and [12]. In a general way, in this region, this bifurcation structure is limited by $\Lambda_\infty < r(\beta) < \bar{r}(\beta)$, where $\bar{r}(\beta)$ represents the chaotic semistability curve, in implicit form, defined by $f^2_{r,\beta}(c) = A_r$, with c the positive critical point and A_r the first positive fixed point, of each family of generalized Richards' functions.

The chaotic semistability is defined when it is verified $f^2_{r,\beta}(c) = A_r$, with A_r the first positive fixed point, i.e., the maximum size growth of the population is equal to the critical density, see [12]. This curve is a bifurcation curve that corresponds to the transition between chaotic region and essential extinction region, which is denoted by Λ^*_1, see Fig. 16.3. The essential extinction is defined by the condition $f^2_{r,\beta}(c) < A_r$, with A_r the first positive fixed point, i.e., when the maximum size growth of the population exceeds the critical density and the populations are almost surely doomed to extinction, see [12].

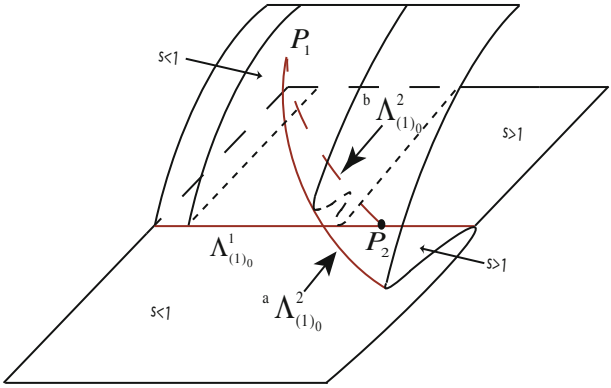

Fig. 16.4 Foliated bifurcation structure of generalized Richards' functions $f_{r,\beta}(x)$, at $K = 10$, $E = -1$ and $C = 7.5$ (*dovetail structure*). $\Lambda^1_{(1)_0}$, ${}^a\Lambda^2_{(1)_0}$ and ${}^b\Lambda^2_{(1)_0}$ are the fold bifurcation curves. The cusp points P_1 and P_2 correspond to solutions of Eq. (16.8)

Remark 16.1 In the cases where there is no Allee effect, the chaotic semistability curve is not defined. At this stage, the fixed point 0 is unstable and the chaotic region is upper bounded by the curve defined by $f_{r,\beta}(c) = 1$. Since, we are in the "fullshift" curve, which is denoted by Λ_{NA}. In these cases, there is no essential extinction region, after the chaotic region we have a no admissible region, it is verified that $\Lambda^*_1 \equiv \Lambda_{NA}$, see Fig. 16.3.

The no admissible region includes the values of the parameters for which the intrinsic growth rates $r(\beta) > \check{r}(\beta)$. The graphic of any family of functions, defined by Eq. (16.3), is no longer totally in the invariant set $[0, 1]$. The maps under these conditions do not already belong to the studied families of generalized Richards' functions and are not good models for populations dynamics, see [10–12].

In Fig. 16.3, we present some fold and flip bifurcation curves of $f^n_{r,\beta}(x)$ in the (β, r) parameter plane, for the same parameter values of Fig. 16.2. Figure 16.4 displays the three-dimensional representation of the sheets (foliated representation) associated with the same parameter plane of Fig. 16.3. The cusp point P_1 corresponds to the first solution of Eq. (16.8), associated to the fixed point $x = 0$. This cusp point is given by $P_1 = (\beta, r)$, where β is the intersection of the fold bifurcation curve $\Lambda^1_{(1)_0}$, of the fixed points 0 and O_r, and of the fold bifurcation curve ${}^b\Lambda^2_{(1)_0}$, of the fixed points A_r and B_r; and $r = -\frac{C}{E}$. The cusp point P_2 corresponds to the second solution of Eq. (16.8), intersection between the fold bifurcation curves ${}^a\Lambda^2_{(1)_0}$, of the fixed points A_r and B_r, and ${}^b\Lambda^2_{(1)_0}$, of the fixed points O_r and A_r. By fixing the parameters K, E, and C in the second solution of Eq. (16.8), the coordinates of the cusp point $P_2 = (\beta, r)$ are given by: β is a numerical solution of the expression of C, when we substitute the expression of x in the expression of C; and consequently, we obtain directly the expressions of the fixed point x and of r.

These threefold bifurcation curves, $\Lambda^1_{(1)_0}$, ${}^a\Lambda^2_{(1)_0}$, and ${}^b\Lambda^2_{(1)_0}$, define in the parameter plane $R = \{(\beta, r) \in R^2 : (\beta, r) \in]0, 1[\times]0, 40[\}$, the following regions:

(i) The extinction region, associated to weak Allee functions,

$$R_1 = \left\{(\beta, r) \in R : \ (\beta, r) < \Lambda^1_{(1)_0} \ \wedge \ (\beta, r) < {}^a\Lambda^2_{(1)_0}\right\},$$

with an unique fixed point 0, established in Lemma 4.1 of [12], see also Figs. 16.2, 16.3 and Fig. 16.1a (blue graphic);

(ii) The weak Allee effect region, with three fixed points 0, A_r and B_r,

$$R_2 = \left\{(\beta, r) \in R : \ {}^a\Lambda^2_{(1)_0} < (\beta, r) < \Lambda^1_{(1)_0}\right\},$$

see also Fig. 16.3 and Fig. 16.1a (green and red graphics). In this region, we verify that $0 < \lim\limits_{x \to 0^+} f'_{r,\beta}(x) < 1$ and the origin's basin of attraction is $\Omega_0 = [0, A_r[\cup]A^*_r, 1]$. Moreover, the basin of attraction of the second positive fixed point B_r is $\Omega_{B_r} =]A_r, A^*_r[$ and $\left|\lim\limits_{x \to B_r} f'_{r,\beta}(x)\right| < 1$. The fixed points 0 and B_r are stable, and the fixed point A_r is unstable;

(iii) The region of functions with no Allee effect, with four fixed points 0, O_r, A_r and B_r,

$$R_3 = \left\{(\beta, r) \in R : \ (\beta, r) > \Lambda^1_{(1)_0} \ \wedge \ {}^a\Lambda^2_{(1)_0} < (\beta, r) < {}^b\Lambda^2_{(1)_0}\right\},$$

see Fig. 16.3 and Fig. 16.1b (blue graphic);

(iv) The region,

$$R_4 = \left\{(\beta, r) \in R : \ (\beta, r) > \Lambda^1_{(1)_0} \ \wedge \ \left((\beta, r) < {}^a\Lambda^2_{(1)_0} \ \vee \ (\beta, r) > {}^b\Lambda^2_{(1)_0}\right)\right\},$$

which includes functions with no Allee effect, with two fixed points 0 and O_r, see Fig. 16.3 and Fig. 16.1b (red graphic); and functions with behavior like logistic functions, with two fixed points, see also Fig. 16.1b (green graphic).

In Fig. 16.5 we present the bifurcation diagram of a family of functions with no Allee effect $f_{r,\beta}(x)$, in the $(\beta, r) \in]0, 1[\times]0, 35[$ parameter plane at $K = 10$, $E = -2$ and $C = 3$. In this case, the extinction region is bounded by $0 < r(\beta) < 3/2$, where $\Lambda_{(1)_0} := r_1(\beta) = 3/2$ is a bifurcation curve that corresponds to the instability of the origin and the appearance of a stable fixed point, see also Fig. 16.6. The horizontal band (in white) corresponds to the positive region of stability of the fixed point 0. The blue region is the stability region. The region between the blue and the turquoise ones corresponds to period doubling region and chaotic region. The turquoise region is the no admissible region. The respective bifurcation curves are shown in Fig. 16.6.

16.3.2 Evolution of Bifurcation Curves When E Varies: Dovetail Structure

In this paragraph, the transition from the weak Allee effect to no Allee effect with respect to the third parameter E is investigated. Remark that the parameter E is

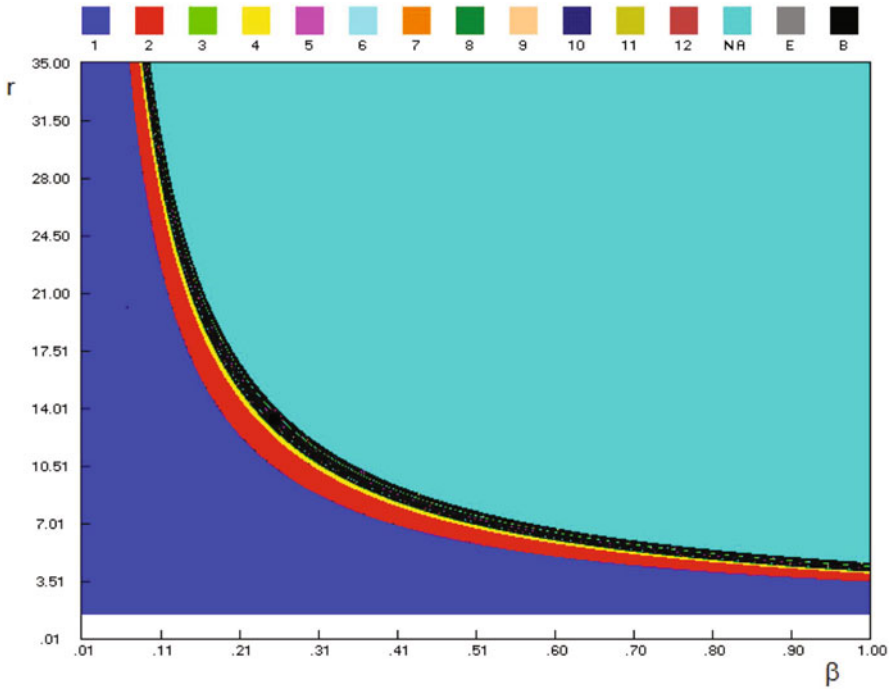

Fig. 16.5 Bifurcation diagram of generalized Richards' functions with no Allee effect $f_{r,\beta}(x)$, in the (β, r) parameter plane at $K = 10, E = -2$ and $C = 3$. The *white* horizontal band is the extinction region. The *blue* region is the stability region. The region between the *blue* and the *turquoise* ones corresponds to period doubling region and chaotic region (existence region of cycles as shown on top of figure). The *turquoise* region is the no admissible region

associated to the Allee limit. This phenomenon is described by the appearance and disappearance of a dovetail structure. We consider an initial situation, with weak Allee effect, illustrated in Fig. 16.3 ((β, r) parameter plane) and Fig. 16.4 (foliated representation) which provide a dovetail structure involving cycle of order 1 and made up of the two cusp points P_1 and P_2. See [7] for more details on dovetail bifurcation structure.

For the values of the parameters considered, we verify that when the parameter E tends toward -2, the cusp points P_1 and P_2 merge into the same point of the fold bifurcation curve $\Lambda^1_{(1)_0}$. Simultaneously the fold bifurcation curves ${}^a\Lambda^2_{(1)_0}$, of the fixed points A_r and B_r, and ${}^b\Lambda^2_{(1)_0}$, of the fixed points O_r and A_r, tend to merge with a fold bifurcation curve $\Lambda^1_{(1)_0}$, see Fig. 16.8. After the bifurcation, a dovetail structure disappears, because the two cusp points P_1 and P_2 disappear and the bifurcation curves ${}^a\Lambda^2_{(1)_0}$ and ${}^b\Lambda^2_{(1)_0}$ merge with a fold bifurcation curve $\Lambda^1_{(1)_0}$. The final situation is giving at Fig. 16.6 ((β, r) parameter plane) and Fig. 16.7 (foliated representation), where there is no Allee effect.

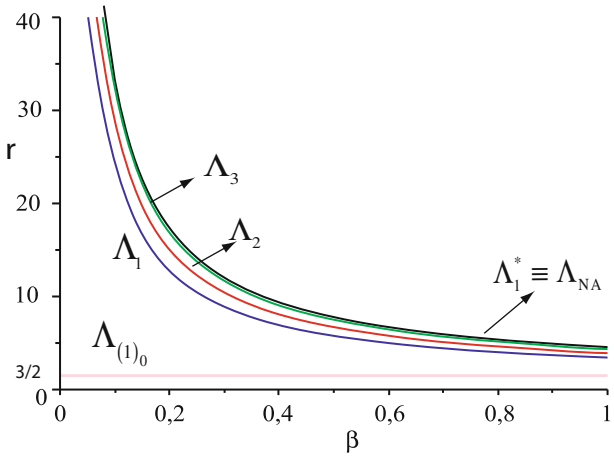

Fig. 16.6 Bifurcations curves of generalized Richards' functions with no Allee effect $f^n_{r,\beta}(x)$, with $n = 1, 2, 3$, in the (β, r) parameter plane at $K = 10$, $E = -2$ and $C = 3$. $\Lambda_{(1)_0}$ is the fold bifurcation curve; Λ_1, Λ_2 and Λ_3 are the flip bifurcation curves of the cycles of order $n = 1, 2, 3$, respectively; Λ_1^* is the chaotic semistability curve and Λ_{NA} is the bifurcation curve of non admissibility. In this case there is no Allee effect, hence $\Lambda_1^* \equiv \Lambda_{NA}$

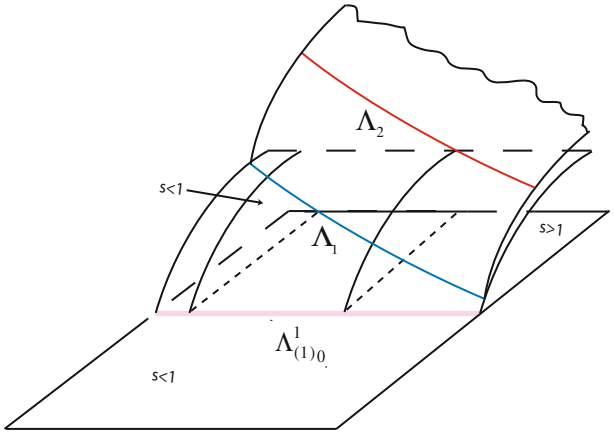

Fig. 16.7 Foliated bifurcation structure of generalized Richards' functions $f_{r,\beta}(x)$, at $K = 10$, $E = -2$ and $C = 3$. $\Lambda^1_{(1)_0}$ is the fold bifurcation curve and Λ_1 and Λ_2 are the flip bifurcation curves of the cycles of order $n = 1, 2$, respectively

16.4 Conclusion

The discussion and concern over the extinction of certain species of trees, plants, and mammals is one of the most current and worrying problems. In this chapter we studied the new classes of functions that contribute to understanding this ecological phenomenon: weak Allee effect functions and functions with no Allee effect, associated

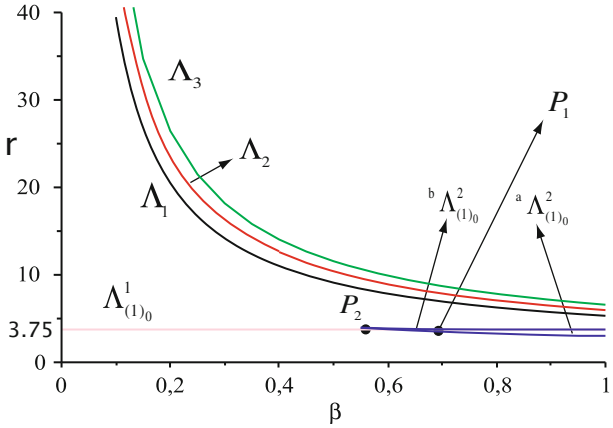

Fig. 16.8 Bifurcations curves of generalized Richards' functions with no Allee effect $f^n_{r,\beta}(x)$, with $n = 1, 2, 3$, in the (β, r) parameter plane at $K = 10, E = -1.85$ and $C = 7.5$. $\Lambda^1_{(1)_0}$, $^a\Lambda^2_{(1)_0}$ and $^b\Lambda^2_{(1)_0}$ are the fold bifurcation curves; Λ_1, Λ_2 and Λ_3 are the flip bifurcation curves of the cycles of order $n = 1, 2, 3$, respectively. The cusp points P_1 and P_2 correspond to solutions of Eq. (16.8)

to Richards' growth types. In Table 16.1 we present a summary of the most important properties for this kind of functions. The study of the foliated bifurcation structure of the generalized Richards' functions allows us to relate the classes of functions with Allee effect and those that have no Allee effect with the appearance and disappearance of a dovetail structure. Thus, the type of extinction studied, characterized by the existence of weak Allee effect, is associated with the emergence of cusp points of fold bifurcation curves of the fixed point.

Acknowledgment Research partially sponsored by national funds through the Fundação Nacional para a Ciência e Tecnologia, Portugal – FCT, under the project PEst-OE/MAT/UI0006/2014, CEAUL and ISEL.

References

1. Carcassès, J.P.: Determination of different configurations of fold and flip bifurcation curves of a one or two-dimensional map. Int. J. Bifurc. Chaos **3**, 869–902 (1993)
2. Carcassès, J.P.: A new kind of parametric singularities and their use for study of the bifurcation structure of an n-dimensional map. Int. J. Nonlinear Anal. Theory Methods Appl. **28**, 917–946 (1997)
3. Fournier-Prunaret, D.: The bifurcation structure of a family of degree one circle endomorphisms. Int. J. Bifurc. Chaos **1**, 823–838 (1991)
4. Kawakami, H.: Bifurcations of periodic responses in forced dynamic nonlinear circuits. Computation of bifurcation values of the systems parameters. IEEE Trans. Circuits Syst. **CAS-31**, 248–260 (1984)
5. Kramer, A.M., Dennis, B., Liebhold, A.M., Drake, J.M.: The evidence for Allee effects. Popul. Ecol. **51**, 341–354 (2009)

6. Mira, C.: Chaotic Dynamics. From the One-Dimensional Endomorphism to the Two-Dimensional Diffeomorphism. World Scientific, Singapore (1987)
7. Mira, C., Kawakami, H., Allam, R.: The dovetail bifurcation structure and its qualitative changes. Int. J. Bifurc. Chaos **3**, 903–919 (1993)
8. Mira, C., Gardini, L., Barugola, A., Cathala, J-C.: Chaotic Dynamics in Two-Dimensional Noninvertible Maps. World Scientific, Singapore (1996)
9. Richards, F.J.: A flexible growth function for empirical use. J. Exp. Botany **10**, 290–300 (1959)
10. Rocha, J.L., Aleixo, S.M.: An extension of Gompertzian growth dynamics: Weibull and Fréchet models. Math. Biosci. Eng. **10**, 379–398 (2013)
11. Rocha, J.L., Aleixo, S.M.: Dynamical analysis in growth models: Blumberg's equation. Discrete Contin. Dyn. Syst. Ser. B **18**, 783–795 (2013)
12. Rocha, J.L., Fournier-Prunaret, D., Taha, A-K.: Strong and weak Allee effects and chaotic dynamics in Richards' growths. Discrete Contin. Dyn. Syst. Ser. B **18**(3), 2397–2425 (2013)
13. Tsoularis, A.: Analysis of logistic growth models. Res. Lett. Inf. Math. Sci. **2**, 23–46 (2001)

Chapter 17
Systoles on Compact Riemann Surfaces with Symbolic Dynamics

Clara Grácio

Abstract In this chapter, systolic inequalities are established, precise values are computed, and their behavior is also examined with the variation of the Fenchel–Nielsen coordinates on a compact Riemann surface of genus 2.

17.1 Introduction

The metric and geometric structure of surfaces may be studied by using the closed geodesics spectrum and the Laplace–Beltrami operator spectrum. It is not easy to obtain these spectra and even more difficult is to describe their dependence on the parameters which determine the metric and geometric structure of a surface. The dependence of such spectra dependence is examined using a boundary map when a Riemann surface M of genus 2, thus with negative curvature, is considered.

From a classical point of view the hyperelliptic surfaces are the simplest Riemann surfaces [12]. They can be denned by an algebraic curve $y^2 = F(x)$ where $F(x)$ is a polynomial of degree $2\tau + 1$ or $2\tau + 2$ with distinct roots (τ is the genus of the surface). Hyperelliptic surfaces of genus τ are characterized by the fact that the number of different Weierstrass points is minimal, namely $2\tau + 2$ (the fixed points of the hyperelliptic involution), while the weight of each Weierstrass point is maximal, namely $\frac{1}{2}\tau(\tau - 1)$.

For our purposes, two results for surfaces (see [17]) are significant:

Theorem 17.1 *A closed surface M of genus $t = 2$ is hyperelliptic if and only if M contains $2t - 2$ different simple closed geodesics which all intersect at the same point and mutually intersect in no other point.*

Theorem 17.2 *All closed surfaces of genus 2 are hyperelliptic.*

The systole of a compact Riemann surface is defined as the minimum length of a noncontractile curve. In the 1990s, a number of studies developed this concept: in particular, the article published by Schmutz Schaller (see [17]) that spurred the

C. Grácio (✉)
CIMA-UE-DMAT, School of Science and Technology,
University of Évora, Rua Romao Ramalho 59, Évora, Portugal
e-mail: mgracio@uevora.pt

R. López-Ruiz et al. (eds.), *Nonlinear Maps and their Applications,*
Springer Proceedings in Mathematics & Statistics 112, DOI 10.1007/978-3-319-12328-8_17

search for maximum surfaces for the systole; also important is the contribution of Bavard (see [1]), which provides a good theoretical framework, modeled on network analysis.

The aim of the present chapter is to provide an understanding of the behavior of systolic quantities on a compact Riemann surface over the geodesic length spectrum of M, endowed with a metric of constant curvature -1. The use of symbolic dynamics, a powerful tool which allows the explicit calculation of the parameters considered, is an essential feature of this study.

The chapter is organized as follows: Sect. 17.2 introduces a geometric description of the surface and defines the Teichmuller space and the global coordinate system, coordinates of Fenchel–Nielsen. The method described in this section involve decomposing a Riemann surface into a set of "pairs of pants" using three simple closed geodesic. The Riemann surface is represented by a quotient space $M = H^2/G$ of the upper half-plane H^2 using a Fuchsian group G which is isomorphic to the fundamental group of M. In Sect. 17.3 a detailed construction of the fundamental domain is given, side-pairing transformations are determined, and the boundary map is obtained. These constructions are the main element of the computations which follow. In Sect. 17.4 the generators of the fundamental group are obtained, and the identification, enumeration, and codification of orbits is carried out. Finally, in Sect. 17.5, explicit values are calculated for the geodesic length spectrum and systolic inequalities are obtained, which is the main objective of this work, reflecting the behavior of the systoles spectrum with the variation of the parameters that characterize the Riemann surface. Applying the main theorems, in the final section, upper and lower limits are determined for the systoles length spectrum under deformation of the surface.

17.2 Geometric Description and Fenchel–Nielsen Coordinates

Let C be the Riemann sphere and $GL_2^+(\mathbb{R})$ the 2×2 matrices group with real entries and a positive determinant. Let us consider the action given by this group of Mobius transformations

$$(g, z) \to gz = \frac{az + b}{cz + d}, g = \begin{pmatrix} a & b \\ c & d \end{pmatrix}$$

where $g(-d/c)$ is interpreted as ∞, and $g(\infty)$ as a/c. It is observed that $\frac{(\lambda a)\, z + (\lambda b)}{(\lambda c)\, z + (\lambda d)} = \frac{az + b}{cz + d}$ for any matrices $\begin{pmatrix} a & b \\ c & d \end{pmatrix} \in GL_2^+(\mathbb{R})$ and $\lambda \in \mathbb{R}$, so any Mobius transformation can be realized by an element of $SL_2(\mathbb{R})$. Furthermore, a Mobius transformation

$$gz = \frac{az + b}{cz + d}, \quad a, b, c, d \in \mathbb{R}, ad - bc = 1$$

determines the matrix $\begin{pmatrix} a & b \\ c & d \end{pmatrix}$ less than signal, and $SL_2(\mathbb{R})$ contains the elements $1 = \begin{pmatrix} 1 & 0 \\ 0 & 1 \end{pmatrix}$ and $-1 = \begin{pmatrix} -1 & 0 \\ 0 & -1 \end{pmatrix}$ which act trivially. Then the quotient group is considered

$$PSL_2(\mathbb{R}) = SL_2(\mathbb{R})/\{\pm 1\}.$$

Given a surface $\mathcal{M}$ of negative curvature and genus $g = 2$, the universal covering surface of $\mathcal{M}$ is given by the hyperbolic plane which can be represented by the Poincaré disk, $D^2 = \{z \in \mathbb{C} : |z| < 1\}$, with metric $ds^2 = \frac{dz \cdot dz}{(1-|z|^2)^2}$ or upper half-plane, $H^2 = \{z = x + iy : y < 0\}$, with metric $ds^2 = \frac{dz \cdot dz}{y^2}$. In both realizations, the isometry group is made up of the linear fractional transformations $h(z) = \frac{az+b}{cz+d}$. In the half-plane H^2, the matrices $A = \begin{pmatrix} a & b \\ c & d \end{pmatrix}$, $a\,d - b\,c = 1$ belong to $SL_2(\mathbb{R})$, the *real unimodular group*. Schematically:

$$Aut(H^2) \cong PSL(2,\mathbb{R}) = SL(2,\mathbb{R})/\{\pm I\}$$
$$Aut(D^2) \cong PSU(1,1) = SU(1,1)/\{\pm I\}$$

The covering group G is a Fuchsian model of $\mathcal{M}$. In this case considering the half-plane H^2, then G is a subgroup of $Aut(H^2)$

The Fuchsian model of a closed Riemann surface of genus $g(\geq 2)$ may thus be characterized exactly. An element of a Fuchsian model of a closed Riemann surface of genus $g(\geq 2)$ is the identity map either a hyperbolic transformation (see [13]).

The pair $(\mathcal{M}, \delta)$ denotes a Riemann surface $\mathcal{M}$ equipped with a conformal structure δ (an equivalence class of metrics). When there is no risk of confusion, it is denoted only by $\mathcal{M}$.

Let $g_i : [0,1] \to \mathcal{M}$, $i = 1,2$ be curves, such that $g_1(0) = g_2(0) = p_0$ and $g_1(1) = g_2(1) = p_1$. It can be said that g_1 and g_2 are homotopic if there is a continuous map $g : [0,1] \times [0,1] \to \mathcal{M}$ such that $g : \{0\} \times [0,1] = p_0$, $g : \{1\} \times [0,1] = p_1$, $g : [0,1] \times \{0\} = g_1$ e $g : [0,1] \times \{1\} = g_2$.

For any $p_0 \in \mathcal{M}$, the *fundamental group* $\pi_1(\mathcal{M}, p_0)$ is the group of the homotopy classes $g : [0,1] \to \mathcal{M}$ such that $g(0) = g(1) = p_0$, i.e., the group of classes of closed paths with p_0 as a starting and terminal point. Often a system of generators $\Sigma_p = \left\{\left[A_j\right], \left[B_j\right]\right\}_{j=1}^{g}$ of a fundamental group $\pi_1(\mathcal{M}, p)$ of a genus 2 closed Riemann surface $\mathcal{M}$ is called a mark in $\mathcal{M}$. Since the choice of base point is irrelevant, the group $\pi_1(\mathcal{M})$ is called the fundamental group of $\mathcal{M}$.

Let us consider the triple$(\mathcal{M}, \delta, f)$, where δ is a conformal structure and $f : \mathcal{M} \to \mathcal{M}$ is a diffeomorphism.

Two triples $(\mathcal{M}, \delta_i, f_i)$, $i = 1, 2$ are considered equivalent if there is a conformal map $k : (\mathcal{M}, \delta_1) \to (\mathcal{M}, \delta_2)$ for which the diagram

$$\begin{array}{ccc} \mathcal{M} & \overset{f_1}{\to} & (\mathcal{M}, \delta_1) \\ & \overset{f_2}{\searrow} & \downarrow k \\ & & (\mathcal{M}, \delta_2) \end{array}$$

commutes by homotopy, i.e., $f_2 \circ f_1^{-1}$ and k are homotopic.

Definition 17.1 The space consisting of those equivalence classes, is called the Teichmüller space and is denoted by $\mathcal{T}_g$ (where g is the genus of $\mathcal{M}$).

In 1940, Teichmüller showed that $\mathcal{T}_g$ ($g \geq 2$) is homeomorphic to $\mathbb{R}^{6g-6}$. One way to realize this homeomorphism is through F-N coordinates. The Teichmüller space $\mathcal{T}_g$ of genus g is given by a system of generators of the fundamental group of closed Riemann surface $\mathcal{M}$ of genus g. The set of generators is denoted by $\left\{\left[\alpha_j\right], \left[\beta_j\right]\right\}_{j=1}^{g}$. As both an Fuchsian model G of $\mathcal{M}$ and $G' = h^{-1}Gh$, for any $h \in Aut(E)$, are Fuchsian models of $\mathcal{M}$, it is necessary to establish a normalization that allows to define what we call canonical system of generators. The conditions of normalization are:

(i) The generator β_g has the attractive fixed point at ∞ and the repulsive fixed point at 0.
(ii) The generator α_g has the attractive fixed point at 1.
(iii) The axes of these two generators are disjoint.

Such a system of generators satisfies a single fundamental relationship (obtaining the presentation of this discrete group), i.e.:

$$\alpha_1 \circ \beta_1 \circ \alpha_1^{-1} \circ \beta_1^{-1} \circ \ldots \circ \alpha_g \circ \beta_g \circ \alpha_g^{-1} \circ \beta_g^{-1} = id. \tag{17.1}$$

In order to obtain a geometric image of the correspondence between the Riemann surface $\mathcal{M}$ and its Fuchsian model G, let us use the concept of fundamental domain for G.

Definition 17.2 Let $E = D^2, H^2$ and F is an open subset of E. It is said that F is a fundamental domain for G if it satisfies the following conditions:

(i) $g(F) \cap F = \emptyset$ for any $g \in G$, with $g \neq id$.
(ii) If F is the closure of F in E, then $E = \bigcup g(\overline{F})$, $g \in G$.
(iii) The boundary ∂F of F in E is of measure zero (with respect to Lebesgue measure).

The family $\{g(F) : g \in G\}$ is called a pavimentation of E. This means that the Riemann surface $\mathcal{M} = E/G$ is considered to be $\overline{F}$, with points on ∂F identified by group G. In this chapter, H^2 is the universal covering space of $\mathcal{M}$ and the fundamental group G, is a subgroup of $SL_2(\mathbb{R})$.

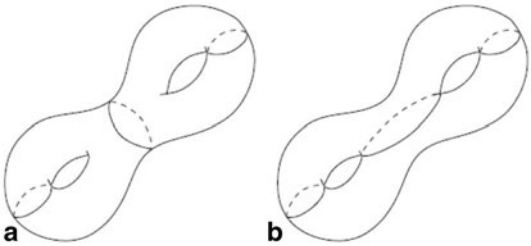

Fig. 17.1 Two pants decomposition

A domain of three circles is homeomorphic to the set

$$P = \left\{ z \in \mathbb{C} : |z| \leq 1, \left| z - \frac{1}{2} \right| \geq \frac{1}{4}, \left| z + \frac{1}{2} \right| \geq \frac{1}{4} \right\},$$

(a sphere with three holes in it), equipped with the hyperbolic metric, where the three components of boundary geodesics are simple. As explained above, P is usually called a "pair of pants." The complex structure of P is uniquely determined by the hyperbolic lengths of the ordered boundary components of P. $\mathcal{M}$ may be decomposed into a union of two "pairs of pants" (surfaces of genus zero with three boundary circles) (see Fig. 17.1).

Figure 17.2 represents an example of decomposition and gluing. This figure is considered $j = 1$, i.e., geodesic L_1.

In this figure c_i are the points of intersection between the geodesic L_1 and the geodesics $D_{1,i}$. The link between these geodesics is forged by means of another geodesic $D_{1,i}$, with minimum length. Denoted by T_1, the arc with the orientation of L_1 between the points c_1 and c_2 and the length of T_1 is denoted τ_1. Then the twist parameter for L_1 is defined by

$$\theta_1 = 2\pi \frac{\tau_1}{l_1}. \tag{17.2}$$

And, similarly, θ_j is well defined, module 2π

$$\theta_j = 2\pi \frac{\tau_j}{l_j}, \quad _{j=1,2,3}.$$

Definition 17.3 Let L_1, L_2, L_3 be the oriented decomposition curves. The functions l_j and θ_j, $j = 1, 2, 3$ denote the lengths and angles of torsion (twist) of L_1, L_2, L_3 used for gluing the pieces. This system of coordinates $\{l_j, \theta_j\}_{j=1,2,3}$ is called the Fenchel–Nielsen (F-N) coordinate system.

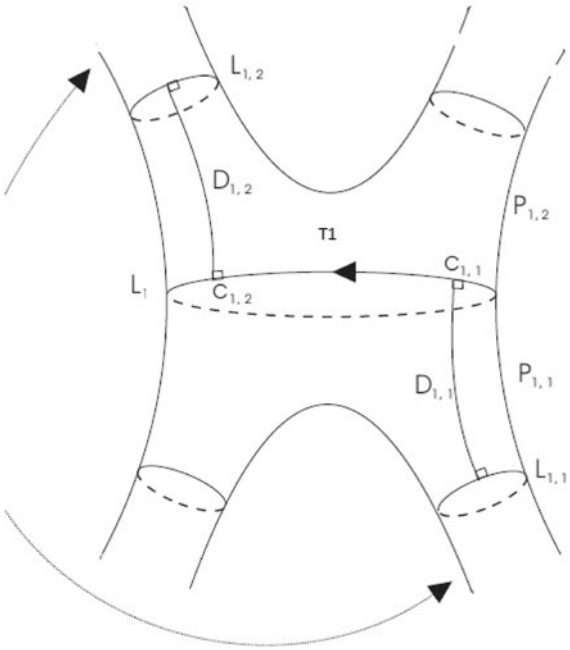

Fig. 17.2 Example of decomposition and gluing

17.3 Construction of Fundamental Domain and Definition of Boundary Map

A *chain* on a surface M is a set of four simple closed nondividing geodesics, labeled $\gamma_1, \gamma_2, \gamma_3, \gamma_4$, where γ_2 intersects γ_1 exactly once; γ_3 intersects γ_2 exactly once and is disjoint from γ_1; γ_4 intersects γ_3 exactly once and is disjoint from both γ_1 and γ_2. It is assumed throughout that these geodesics are directed so that, in terms of the homology intersection number, $\gamma_i \times \gamma_{i+1} = +1$.

Given the chain $\gamma_1, \gamma_2, \gamma_3, \gamma_4$, it can easily be seen that there are unique simple closed geodesics γ_5 and γ_6 so that γ_5 intersects γ_4 exactly once and is disjoint from γ_1, γ_2, and γ_3; and γ_6 intersects both γ_5 and γ_1 exactly once and is disjoint from the other γ_i. As above, it may be assumed that these geodesics are also directed so that, using cyclic ordering, $\gamma_i \times \gamma_{i+1} = +1$. This set of six geodesics is called a *geodesic necklace (*see[14] and Figure 17.3).

If the surface $\mathcal{M}_0$ is cut along the geodesics of a chain, a simply connected subsurface is obtained. It follows that elements A_0, B_0, C_0, D_0 may generate $\pi_1(\mathcal{M}_{00})$, and, conversely, the shortest geodesics in the free homotopy class of loops, corresponding to A_0, B_0, C_0, D_0, are, respectively, γ_1, γ_2, γ_3, γ_4. There are several possible choices for these elements; let us adopt Maskit's choice, which yields to defining relation: $A_0 B_0 D_0 A_0^{-1} C_0^{-1} D_0^{-1} C_0 B_0^{-1} = 1$ (see [13]).

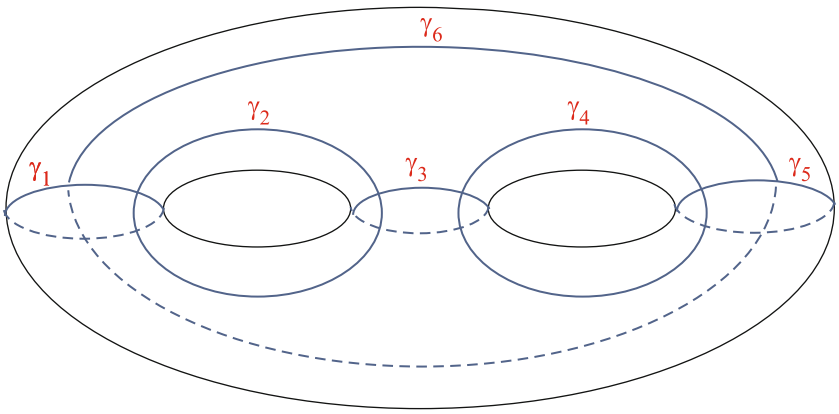

Fig. 17.3 Geodesic necklace

A particular system of generators of a Fuchsian group is obtained, (denoted by G_0) and our surface (nondeformed) $\mathcal{M}_0$ is given by $\mathcal{M}_0 = H^2/G_0$. It is possible to express explicitly the matrices $A_0, B_0, C_0, D_0, E_0, F_0 \in SL(2,\mathbb{R})$ (see [8], [14]).

A point in $\mathcal{T}$ can be regarded as being an equivalence class of orientation-preserving homeomorphisms h of H^2. Two such homeomorphisms are equivalent if the corresponding representations are equivalent; two such representations, A and B are equivalent if there is an element $S \in PSL(2,\mathbb{R})$ so that $SAS^{-1} = B$. When the rule of the decomposition (the way of gluing, see Fig. 17.2) and the lengths of closed geodesics are chosen, the decomposition is determined. The set of lengths of all geodesics used in the decomposition into pants, and the set of so-called twisting angles used to glue the pieces, provide a way of realizing this homeomorphism.

As this group G_0 is discrete, consisting only of hyperbolic elements, the surface, $\mathcal{M}_0$, represented by G_0, is our base surface. But our aim is to study the dependence of dynamic properties on the parameters which implies the variation of these parameters, forcing the consideration of the deformation spaces of the space base defined above. Deformation space $\mathcal{D}$ is defined as the space of representations $\varphi : G_0 \to PSL(2,\mathbb{R})$.

The image of the group $G = \varphi(G_0)$ is a discrete group with $\mathcal{M} = H^2/G$ a closed Riemann surface of genus 2.

Let us consider the chain $\gamma_1, \gamma_2, \gamma_3, \gamma_4$ in $\mathcal{M}$ which is decomposed along these geodesics in 4 hexagons triangles. These geodesics are the shortest length of the class of homotopy corresponding to some elements h_i $(i = 1, ..., 6)$ of $\pi_1(\mathcal{M})$, the fundamental group of $\mathcal{M}$. Building up hexagon H_1, as can be seen in Fig. 17.4, whose sides s_i are arcs γ_i, these arcs are contained in the axes of the hyperbolic transformations h_i $(i = 1, ..., 6)$. The translation distance of these axes (measured counterclockwise) along the axes is $2\,l_i$ where l_i denotes the length of $\gamma_i = l(\gamma_i)$.

From this initial hexagon H_1 the fundamental domain can be constructed by reflection and symmetry operations that reflect the decomposition of surface $\mathcal{M}$ along the geodesics (that form the chain γ_1 , γ_2, γ_3, γ_4 chosen). In this construction,

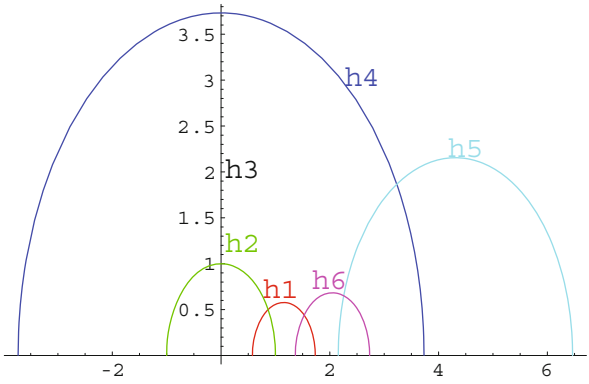

Fig. 17.4 Hexagons H_1

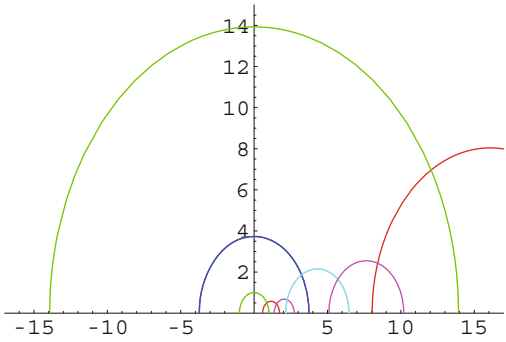

Fig. 17.5 Hexagons $H_1 \cup H_2$

a reflection on the axis of h_4 is considered, while hexagon H_1 is reflected in another hexagon H_2, see Fig. 17.5.

Finally, with the reflection in relation to the imaginary axis (symmetry) the other two hexagons H_3 and H_4 are obtained, building the dodecagon that is the fundamental domain: $F = H_1 \cup H_2 \cup H_3 \cup H_4$, see Fig. 17.6.

If this is not the case, it means that the glue is different and the fundamental domain is different as shown in Fig. 17.7.

This construction depends on the original choice of geodesic chain $\{\gamma_i\}$, and the form of gluing, i.e., the parameters considered.

Definition 17.4 Let us consider a geodesic necklace on a closed Riemann surface $\mathcal{M}$. When all the geodesics have the same length and there is no twist in the collage, it may be said that the regular case for the fundamental domain of a closed Riemann surface $\mathcal{M}$ in the F-N coordinates is being considered.

However, the form of the generators of the Fuchsian group G may be determined (for all cases) ([6], [14]).

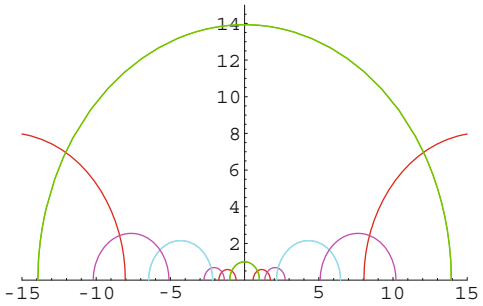

Fig. 17.6 Fundamental domain $F = H_1 \cup H_2 \cup H_3 \cup H_4$

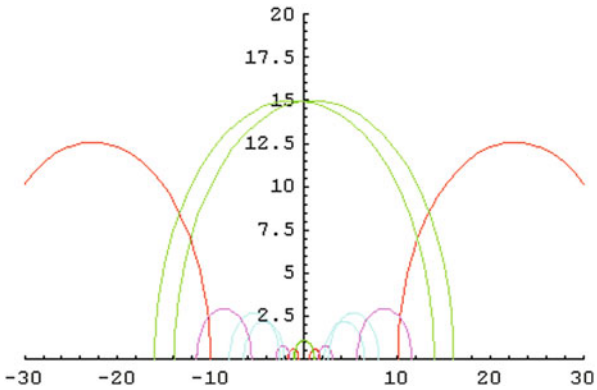

Fig. 17.7 Two dodecagons with twist angles zero ($\alpha_1 = \alpha_2 = \alpha_3 = 0$) and one with angles $\alpha_1, \alpha_2, \alpha_3 \neq 0$

Let us consider once more hexagon H_1. γ, the axis of h, which is also common among the orthogonal axes h_1 and h_3, and is chosen as a reference geodesic segment. Let $\mu' = |\gamma|$, and let us consider the ray joining the origin of the axes to the point of intersection between h and h_1, determining an angle μ between the axis of h_3 and this radius. Then, by using hyperbolic geometry, μ is defined by $\coth \mu = \cosh \mu$ (see [3]).

The point of intersection between h and h_3 is denoted by P and the point of intersection between h_2 and h_3 by P_2. The other parameters are given by the angles of gluing. Then σ is determined by the distance between the intersection of h with h_3 and the intersection of h_2 with h_3. Note that if $h_2 = h$ then σ is equal to zero. The other two parameters τ and ρ are determined by angle θ_2 and θ_3 between $h_2, h_3,$ and h_3, h_4, respectively, see Fig. 17.8. Schematically: $l_1 = l(\gamma_1)$, $l_2 = l(\gamma_2)$, $l_3 = l(\gamma_3)$, $l_4 = l(\gamma_4)$, $\mu = arc\coth(\cosh \mu')$, $\sigma = |P - P_2|$, $\tau = arc\tanh(\cos(\theta_2))$, and $\rho = arc\tanh(-\cos(\theta_3))$.

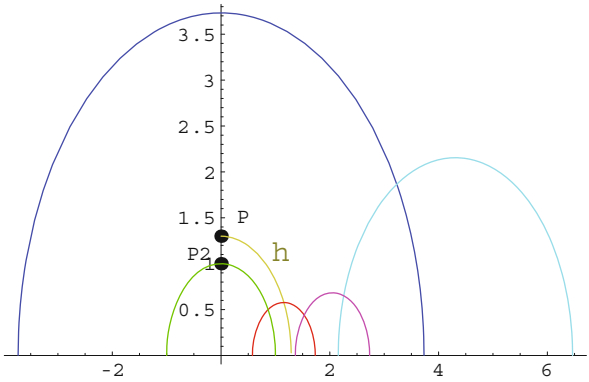

Fig. 17.8 Representation of the parameters in the hexagon

Through the operations of reflection and symmetry (as exemplified above) the following representations (see [9] and [14]) are obtained:

$$A = \frac{1}{\sinh \mu}\begin{pmatrix} \sinh(\mu-\alpha) & \sinh\alpha \\ -\sinh\alpha & \sinh(\mu+\alpha)\end{pmatrix}, C = \begin{pmatrix} e^{\gamma} & 0 \\ 0 & e^{-\gamma}\end{pmatrix},$$

$$B = \frac{1}{\cosh\tau}\begin{pmatrix} \cosh(\tau+\beta) & e^{\sigma}\sinh\beta \\ e^{-\sigma}\sinh\beta & \cosh(\tau-\beta)\end{pmatrix}, D = \frac{1}{\cosh\rho}\begin{pmatrix} \cosh(\rho-\delta) & -e^{\sigma+\gamma}\sinh\delta \\ -e^{-\sigma-\gamma}\sinh\delta & \cosh(\rho+\delta)\end{pmatrix}.$$

Teichmüller space $\mathcal{T}$ of genus 2 is given by a system of generators of a Fuchsian group, the fundamental group of the surface of the closed Riemann surface $\mathcal{M}$ of genus 2. A particular system of generators determined by following expressions may be considered: $h_1 = B$, $h_2 = A$, $h_3 = F$, $h_4 = E$, $h_5 = BD$, $h_6 = DF^{-1}$. $h_7 = h_1^{-1}, ..., h_{12} = h_6^{-1}$ (see Fig.17.9).

Proposition 17.1 *If the twist angles are zero, $\sigma_1 = \sigma_2 = \sigma_3 = 0$, then the fundamental domain is a right-angle polygon.*

Proof If $\tau = 0$, then $\theta_2 = \frac{\pi}{2}$ so the axes of B and C are orthogonal; if $\sigma = 0$ then $P = P_2$ so $h_2 \equiv h$. With this equality and the definition of h it may be concluded that the axis of h_2 is orthogonal to the axes of both h_3 and h_1; if $\rho = 0$, then $\theta_3 = \frac{\pi}{2}$, which implies that the axes of h_3 and h_4 are orthogonal. As we have a hyperbolic hexagon with three direct consecutive internal angles it may be concluded that the other three also are right angles and, thus, H_1 is a right-angled hexagon. As the hyperbolic reflection maintains the angles invariant, the resulting polygon F is a right-angled polygon.

This construction depends on the choice of original geodesics γ_i, $i = 1, ..., 4$. The chain is then dependent on the parameters $\ell_i = \ell(\gamma_i)$. The sides are obtained by the intersection of the axes, and are geodesic segments. The single point which is the intersection between two consecutive sides is called a vertex.The circular arc

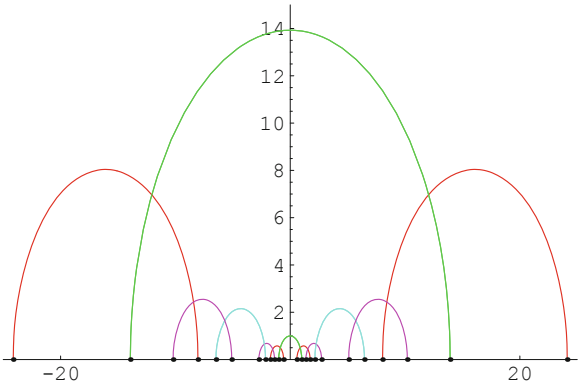

Fig. 17.9 Axes h_1,...,h_{12} and terminal points $\{p_i, q_i\}$, $i = 1, ..., 12$ on $\partial\mathcal{F}$

that contains a side s_i intersects the real axis at two points p_i and q_i (see Fig.17.9). The sides are labeled $s_1, ..., s_{12}$ reading counterclockwise from zero.

It is known (see [3]) that if $\mathcal{F}$ is any locally finite fundamental domain for a Fuchsian group G, then

$$\{g \in G : g(\overline{\mathcal{F}}) \cap \overline{\mathcal{F}} = \phi\}$$

generates G. The fundamental domain $\mathcal{F}$ is a bounded fundamental polygon whose boundary $\partial\mathcal{F}$ consists of the 12 geodesic segments $s_1, ..., s_{12}$. There is a bijection:

$$\Psi : \mathcal{L}_{\mathcal{F}} \to G_{\mathcal{F}}; \quad \Psi(g) = \overline{\mathcal{F}} \cap g(\overline{\mathcal{F}})$$

between the set of the sides of $\mathcal{F}$ and the set of elements g in G for which $\overline{\mathcal{F}} \cap g(\overline{\mathcal{F}})$ is a side of $\mathcal{F}$. These pairing transformations $g : s_i \to s_j$ identifying the sides (side-pairing), elements of $G_{\mathcal{F}}$, i.e., generate the group G.

The identification rule chosen is

$$\begin{aligned} &s_1 \lhd\rhd s_7\ ;\ \ s_2 \lhd\rhd s_{12};\ \ \ s_3 \lhd\ \rhd\ s_5; \\ &s_4 \lhd\rhd s_{10};\ \ s_6 \lhd\rhd s_8\ \ ;\ \ s_9 \lhd\rhd s_{11} \end{aligned} \tag{17.3}$$

Adopting this choice, formulas for the side pairing transformations $g_1, ..., g_{12}$ are calculated and the generators $g_i = g_i(\ell_1, \ell_2, \ell_3, \sigma_1, \sigma_2, \sigma_3)$, $i = 1, ..., 12$, where $\ell_1, \ell_2, \ell_3, \sigma_1, \sigma_2, \sigma_3$ are the F-N coordinates, are explicitly obtained. With the linear fractional transformations defined above the boundary map may be obtained: $f_\Gamma : \partial\mathcal{F} \to \partial\mathcal{F}$, defined by piecewise linear fractional transformations in the partition $P = \{I_i = [p_i, p_{i+1}),\ i = 1, ..., 11,\ [p_{12}, p_1)\}$, which is orbit equivalent to the action of the fundamental group G on $\partial\mathcal{F}$.

Adopting the identification rule, (17.3) formulas for the side pairing transformations $g_1, ..., g_6, g_7 = g_1^{-1}, ..., g_{12} = g_6^{-1}$ may be determined. This means that $s_7 = g_1(s_1)$, ..., $s_9 = g_6(s_{11})$, $s_1 = g_7(s_7)$, ..., $s_{11} = g_{12}(s_9)$.

Let $g_i(z) = (a_i z + b_i)/(c_i z + d_i)$ for $g_i(s_j) = s_k$, with

$$\begin{cases} r_i = (q_i - p_i)/2, \\ c_i = 1/(r_j r_k)^{1/2}, \\ b_i = (a_i d_i - 1)/c_i \end{cases}$$

then the following system of equations is solved

$$\begin{cases} (a_i p_j + b_i)/(c_i p_j + d_i) = q_k, \\ (a_i q_j + b_i)/(c_i q_j + d_i) = p_k \end{cases}$$

and $\{a_i, d_i\}$ is determined, $i = 1, ..., 12$. With $\{a_i, d_i\}$ the generators $g_i = g_i(\ell_1, \ell_2, \ell_3, \sigma_1, \sigma_2, \sigma_3)$, $i = 1, ..., 12$ are computed. The system of generators of G is denoted by G^0.

Let the partition be $\mathcal{Q} = \{I_i = [p_i, p_{i+1}), i = 1, ..., 11, [p_{12}, p_1)\}$. Although this is not a Markov partition it may be refined so as to obtain one that is. One way of doing this is to introduce the lateral limits $p_i^{\pm}$ of the discontinuity points p_i (see [9]).

By means of fractional linear transformations carried out on $\mathcal{Q}$, the boundary map $f_G : \partial\mathcal{F} \to \partial\mathcal{F}$ is defined, represented by:

$$f_G : \bigcup_{i=1,...,12} I_i \to \bigcup_{i=1,...,12} I_i; f_G(x)_{|I_i} = g_i(x), i = 1, .., 12.$$

17.4 Fundamental Group

The boundary map f_G determines the associated Markov matrix A. This matrix is given by (see [6])

$$a_{ij} = \begin{cases} 1 & \text{if } I_i \subset f_G(I_i) \\ 0 & \text{otherwise.} \end{cases}$$

The identification, enumeration, and codification of orbits use symbolic dynamics through constructions that involves the geometry of the surface and the algebraic structure of its fundamental group G. The action of this fundamental group on the Poincaré upper half plane boundary is shown to be orbit equivalent to the Markov map, f_G, which has been defined, and codification is obtained by the expansion of the boundary points.

Definition 17.5 *Let x_{i_0} be an element of the limit set of G . As it belongs to one of the intervals I_{i_0} of the Markov partition $\mathcal{W}$ the image under $f_G(x_{i_0}) = g_{i_0}(x_{i_0}) = x_{i_1}$, is* another boundary point x_{i_1}. *The point x_{i_1} belongs to the intervals I_{i_1} so $f_G(x_{i_1}) = g_{i_2}(x_{i_1}) = x_{i_2}$.*This process is repeated successively obtaining the (f_G-expansion) of boundary point x. This sequence is called the word associated with the point x.

Example 17.1

(1) Consider the regular dodecagon: $l_1 = l_2 = l_3 = \log(2+\sqrt{3})$ and $\sigma_1 = \sigma_2 = \sigma_3 = 0$.
$x = 1.5- >$ word $1- > 6, 12, 3, 8, 7, 3, 3, 7, 2, 3, 6, 12, 3, 8$
$x = 2.0- >$ word $2- > 11, 7, 11, 6, 10, 5, 11, 12, 3, 12, 3, 3, 10, 6$
(2) Consider the dodecagon: $l_1 = \log(2+\sqrt{3}) + 0.3$, $l_2 = l_3 = \log(2+\sqrt{3})$ and $\sigma_1 = \sigma_2 = \sigma_3 = 0$.
$x = 1.5- >$ word $1- > 6, 10, 7, 2, 10, 2, 7, 10, 12, 3, 4, 7, 7, 7$
$x = 2.0- >$ word $2- > 12, 6, 10, 7, 9, 12, 5, 4, 8, 7, 4, 1, 5, 4.$

Proposition 17.2 *Each point of the limit set is associated with a single word. This word is the $f_G-expansion$ boundary point. The admissibility of a given block or word is given by the Markov matrix A.*

Proof The Markov matrix A identifies the possible transitions between states and the associated subshift of finite type, (Σ_A, σ), is identified by the limit set. Thus the occurrences in the limit set are given by the admissibility in subshift of finite type, therefore by A.

The representation (codification) of a geodesic γ in H^2(or D^2) is the juxtaposition of f_G-expansions of its extreme points γ_- and γ_+ on the real axis (or the unit circle Σ).

$$\gamma \leftrightarrows \gamma_-.\gamma_+ \leftrightarrows \ldots g_{i_2} g_{i_1}.h_{i_1} h_{i_2} \ldots \text{ where } g_{i_2}, g_{i_1}, h_{i_1}, h_{i_2} \in G^0.$$

Definition 17.6 Given $g \in G$ (and $\gamma \in calM$) we define its word length $|g|$ to be the smallest number of elements from G needed in a presentation of g, i.e., $|g| = \inf\{n : g = g_1 \ldots g_n \text{ with } g_1, \ldots, g_n \in G^0\}$; for a closed geodesic γ and associated class $[h]$ in G, we denote $|\gamma| = \inf\{|g| : g \in G \text{ e } [g] = [h]\}$, that is the word length of γ; the geometric length of γ is given by $\ell(\gamma) = \int_\gamma m(z)\,|dz|$ and is dependent on the metric of the surface.

By convention, $|e| = 0$, where e is the identity element in G.

Theorem 17.3 *Admissible geodesics are conjugate underG if and only if the corresponding sequences are shift equivalent.*

Proof See [9].

Theorem 17.4 *On surfaces of negative curvature there is a bijection between closed geodesic, γ, in $\mathcal{M}$ and conjugacy classes of the fundamental group G associated with the fundamental domain F, i.e., each conjugacy class $[g_\gamma]$ to G represents a closed geodesic, γ, in $\mathcal{M}$.*

Proof See [15].

These results establish equivalence between concepts and different mathematical spaces.

Proposition 17.3 *With a finite number of exceptions there is a bijection between the closed geodesic, $\gamma \in \mathcal{M}$ (word length $|\gamma|$ and length $\ell(\gamma)$) and the primitive periodic orbits of period k, $\mathcal{O}(x) = \{x, f(x), f^2(x), ..., f^k(x)\}$.*

Proof See [16].

Schematically:

$$\begin{array}{ccc} \text{Periodic points for } f_G & \leftrightarrow & \text{Admissible sequences for the shift} \sigma \\ \updownarrow & & \updownarrow \\ \text{Primitive closed geodesics in } \mathcal{M} & \longleftrightarrow & \text{Conjugacy classes in} G \end{array}$$

If the elements of group G are viewed as matrices in $SL_2(\mathbb{R})$, then the identification of the matrices g and $-g$ in $PSL_2(\mathbb{R}) = SL_2(\mathbb{R})/\{\pm 1\}$ may be understood automatically. The following proposition allows for the identification of conjugacy classes, by algebraic methods, using the traces of these elements.

Proposition 17.4 *Consider two elements g and h of group G. Its conjugacy classes are equal, if and only if, the squares of its traces are also equal. That is,*

$$[g] = [h] \Leftrightarrow tr^2(g) = tr^2(h).$$

Proof See [3].

The identification of the conjugacy classes is dependent on traces of matrices that represent the elements of the group; but these matrices are, in turn, dependent on the choice of the parameters of F-N. Consequently, the following conclusion may be drawn:

Proposition 17.5 *The conjugacy classes of the fundamental group are dependent of the Fenchel–Nielsen coordinates.*

Example 17.2 If words of length 1 are considered for the case of regular domain ($l_1 = l_2 = l_3 = \log(2+\sqrt{3})$ and $\sigma_1 = \sigma_2 = \sigma_3 = 0$) there is only one conjugacy class (Table 17.4), while, for example, for $l_1 = l_2 = \log(2+\sqrt{3})$, $l_3 = 1.7$ and $\sigma_1 = \sigma_2 = \sigma_3 = 0$ 4 distinct classes of conjugation are obtained (Table 17.5).

$$\left[\begin{array}{cccccccccccc} tr(g_i) & 4 & 4 & -4 & -4 & 4 & 4 & 4 & 4 & 4 & 4 & -4 & -4 \\ tr^2(g_i) & 16 & 16 & 16 & 16 & 16 & 16 & 16 & 16 & 16 & 16 & 16 & 16 \end{array}\right]$$

$$\begin{cases} l_1 = l_2 = l_3 = \log(2+\sqrt{3}), \sigma_1 = \sigma_2 = \sigma_3 = 0 \\ 1 \text{ distinct class} \end{cases} \tag{17.4}$$

$$\left[\begin{array}{cccccccc} tr(g_i) & -4 & 5.65663 & -8.96989 & 2.89726 & -8.96989 & 5.65663 \\ tr^2(g_i) & 16 & 16 & 16 & 16 & 16 & 16 \end{array}\right]$$

$$\begin{bmatrix} ..... & 4 & 5.65663 & 8.96989 & 2.89726 & 8.96989 & 5.65663 \\ ..... & 16 & 16 & 16 & 16 & 16 & 16 \end{bmatrix}$$

$$\begin{cases} l_1 = l_2 = \log(2+\sqrt{3}), l_3 = 1.7, \sigma_1 = \sigma_2 = \sigma_3 = 0 \\ 4 \text{ distinct classes} \end{cases} \tag{17.5}$$

17.5 Systolic Inequalities

In order to examine systolic quantities, the spectrum length of the closed geodesics must be determined. This spectrum may be determined by means of the trace of the matrix associated with the boundary map. As g is an element of group G, its length is obtained by the expression (see [3]):

$$l(g) = 2\cosh^{-1}\left[\frac{tr(g)}{2}\right].$$

Consider two examples with the same word length, $|g| = 1$ (examples 17.6, 17.7), but different choices of F-N parameters:

Example 17.3

$$\begin{bmatrix} g_i & g_1 & g_2 & g_3 & \cdots & g_{10} & g_{11} & g_{12} \\ l(g_i) & 2.63392 & 2.63392 & 2.63392 & ... & 2.63392. & 2.63392 & 2.63392. \end{bmatrix}$$

$$\begin{cases} l_1 = l_2 = l_3 = \log(2+\sqrt{3}), \sigma_1 = \sigma_2 = \sigma_3 = 0 \\ 1 \text{ distinct class, word length, } |g| = 1. \end{cases} \tag{17.6}$$

Example 17.4

$$\begin{bmatrix} g_i & g_1 & g_2 & g_3 & g_4 & g_5 & g_6 \\ l(g_i) & 3.4 & 2.63392 & 3.85452 & 1.60608 & 3.85452 & 2.63392 \end{bmatrix}$$

$$\begin{bmatrix} \cdots & g_7 & g_8 & g_9 & g_{10} & g_{11} & g_{12} \\ ... & 3.4 & 2.63392 & 3.85452 & 1.60608 & 3.85452 & 2.63392 \end{bmatrix} \tag{17.7}$$

$$\begin{cases} l_1 = l_2 = \log(2+\sqrt{3}), l_3 = 1.7, \sigma_1 = \sigma_2 = \sigma_3 = 0 \\ 4 \text{ distinct classes, word length, } |g| = 1. \end{cases}$$

Consider two examples with the same Fenchel–Nielsen parameters but different word lengths, $|g| = 1$ and $|g| = 2$ (examples 17.8, 17.9). Let us choose the regular case, $\ell_1 = \ell_2 = \ell_3 = \log(2+\sqrt{3})$ and $\sigma_1 = \sigma_2 = \sigma_3 = 0$.

Example 17.5 If the word length, $|g| = 1$, then there is just one distinct element of the geodesic length spectrum that is, $\ell(g) \simeq 2.63392$.

$\mathbf{g}_i$	$\ell(\mathbf{g}_i) = l_i$
g_1	$l_1 = 2.63392...$
...	...
g_{12}	$l_{12} = 2.63392...$

(17.8)

Example 17.6 If the word length, $|g| = 2$, we have 9 distinct conjugacy classes, then there are 9 distinct values for the length spectrum. Some values:

$\mathbf{g}_1.\mathbf{g}_i$	$\simeq \ell(\mathbf{g}_1\mathbf{g}_i)$	$\mathbf{g}_2.\mathbf{g}_i$	$\simeq \ell(\mathbf{g}_2\mathbf{g}_i)$	$\mathbf{g}_3.\mathbf{g}_i$	$\simeq \ell(\mathbf{g}_3\mathbf{g}_i)$
$g_1.g_1$	5.26783	$g_2.g_1$	4.12687	$g_3.g_1$	5.98645
$g_1.g_2$	4.12687	$g_2.g_2$	5.26783	$g_3.g_2$	6.51323
$g_1.g_3$	5.98645	$g_2.g_3$	6.51323	$g_3.g_3$	5.26783
$g_1.g_4$	4.12687	$g_2.g_4$	5.98645	$g_3.g_4$	4.12687
$g_1.g_5$	2.63392	$g_2.g_5$	4.58486	$g_3.g_5$	0
$g_1.g_6$	4.12687	$g_2.g_6$	7.82325	$g_3.g_6$	4.58486
$g_1.g_7$	0	$g_2.g_7$	4.12687	$g_3.g_7$	2.63392
$g_1.g_8$	4.12687	$g_2.g_8$	7.05099	$g_3.g_8$	6.51323
$g_1.g_9$	2.63392	$g_2.g_9$	6.51323	$g_3.g_9$	7.05099
$g_1.g_{10}$	4.12687	$g_2.g_{10}$	2.63392	$g_3.g_{10}$	4.12687
$g_1.g_{11}$	5.98645	$g_2.g_{11}$	4.58486	$g_3.g_{11}$	7.82325
$g_1.g_{12}$	4.12687	$g_2.g_{12}$	0	$g_3.g_{12}$	4.58486

(17.9)

(...)

Every simple closed curve in the plane satisfies the inequality

$$\frac{A}{\pi} \leq \left(\frac{L}{2\pi}\right)^2$$

where L is the length of the curve and A is the area of the region it bounds. This is a classical *isoperimetric inequality*. In the 1950s, C. Loewer and P. Pu proved a classical *isosystolic inequality*(this result was not published, see [4]).

Let $\mathbb{RP}^2$ be the real projective plane endowed with an arbitrary metric, i.e., an embedding in some $\mathbb{R}^n$. Then

$$\left(\frac{L}{\pi}\right)^2 \leq \frac{A}{2\pi}$$

where A is its total area and L is the length of its shortest noncontractible loop. Similarly, every metric torus $\mathbb{T}^2$ satisfies the inequality

$$L^2 \leq \frac{2}{\sqrt{3}} A$$

In the 1970s, Marcel Berger began studying a new Riemannian invariant, which came to be know as the systole.

The systole of a compact Riemann surface is defined as the minimal length of a noncontractile curve, (by abuse language one employs the same word for the curves carrying out this length). The geometry of systoles was studied by Schmutz within the framework of hyperbolic geometry (see [17] and [18]) and Bavard (see [1]) in the context of abelian manifolds. The notion of systole, in particular, led to the characterization of arithmetic groups using the length spectrum. The study of systoles also provided geometrical answers to the Schottky problem on the Jacobian Riemann surface. This approach was developed by Buser and Sarnak in (to see [5]) Gromov in (to see [10]).

$sys\pi_1(\mathcal{M}, m)$ denoted as the shortest length of a noncontractible loop of M.

$$sys\pi_1(\mathcal{M}, m) = \min_{|\gamma| \neq 0, \gamma \in M} length(\gamma)$$

The systolic ratio SR of $(\mathcal{M}, m)$ is defined as

$$SR(\mathcal{M}, m) = \frac{sys\pi_1(\mathcal{M}, m)^2}{vol(\mathcal{M}, m)}, \tag{17.10}$$

and the optimal systolic ratio of $\mathcal{M}$ as

$$SR(\mathcal{M}) = \sup_m SR(\mathcal{M}, m), \tag{17.11}$$

where m runs over the space of all metrics, (see [11]).

The optimal systolic ratio of a genus 2 surface is unknown, but it satisfies the Loewner inequality $SR(\mathcal{M}) \leq 2/\sqrt{3}$, the best available upper bound for the optimal systolic ratio of an arbitrary genus 2 surface, (see [12]). However, the latter ratio is known for the Klein bottle, in addition to the torus, and also the real projective plane. It should be noted that averaging a conformal metric by hyperelliptic involution improves the systolic ratio of the metric. Systolic geometry has recently experienced a period of great development, (see [10], [11]). Thus, a surface is Loewner if $SR(\mathcal{M}) \leq 2/\sqrt{3}$, and in (see [12]) it has recently been shown that the genus 2 surface is Loewner.

In the case of hyperbolic surfaces, a compact surface, is entirely determined by a decomposition into a "pair of pants" and $6g - 6$ real parameters, the F-N coordinates. The regular domain choice corresponds, in geometric terms, to considing the non-deformed surface $\mathcal{M} = H^2/G$. With the explicit computation of geodesic length, explicit inequalities are obtained that show the dependence of systoles on F-N parameters. The variations of F-N coordinates modifies the metric structure of the surface and this implies the alteration of systole length.

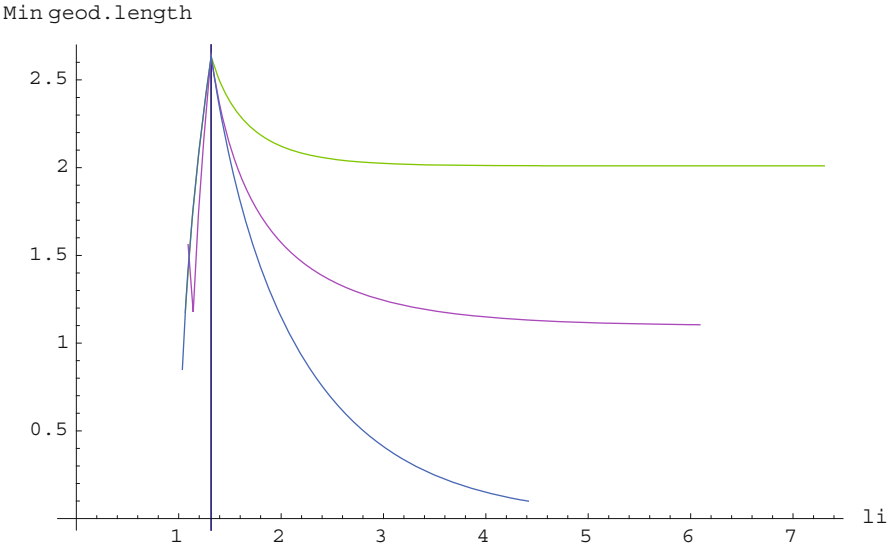

Fig. 17.10 Systoles with Fenchel–Nielsen coordinates variation

Let $\mathcal{M}_0$ be a closed, nondeformed, surface with genus $g = 2$ and $\ell_0 = \max\{\ell(\gamma(t))\}$ the maximum of the shortest closed geodesic lengths on$\mathcal{M}_0$The following result may be introduced:

Theorem 17.5 *Let M be a closed surface with genus $g = 2$. Thus the length $l(\gamma)$ of every systole, γ, verifies the inequality $l(\gamma) \leq \ell_0$.*

It is established that the regular case is a lower bound for systoles with F-N coordinates variation (see Fig. 17.10). Each line represents systole behavior for each F-N parameter: the blue line for ℓ_3; the magenta line for ℓ_3 and the green line for ℓ_1. The fundamental domain that was constructed in the previous section is a dodecagon. In order to maintain this structure in the present study, it was necessary to establish the possible intervals of variation for each of the F-N coordinates.

Computation of the values of systoles lengths was carried out considering these intervals.

Corollary L *et $\mathcal{M}$ be a closed, non-deformed, surface with genus $g = 2$. Then*

$$sys\pi_1(M, m) \leq \log(2 + \sqrt{3})$$

for every systole, $\gamma \in \mathcal{M}$.

However, our aim is a more global (not just two cases), study of this length spectrum with F-N coordinates, in order to provide an understanding of how the geodesic length spectrum behaves under deformation of the surface. Let us recall that these coordinates constitute a system of global coordinates in Teichmüller space $\mathcal{T}$. If considering the variation of the lengths, in function of the coordinates of F-N, also considering the maximum value as the minimum value of these lengths,

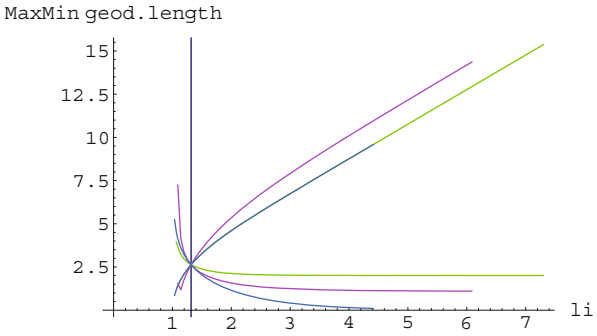

Fig. 17.11 Upper and lower limits of shortest closed geodesic length

the maximum and the minimum, respectively, are obtained, with the regular case. This regular case corresponds, in geometric terms, to surface $\mathcal{M}_0$ being a closed, non-deformed, surface with genus$g = 2$.

Definition 17.7 Let M_0be a closed, non-deformed, surface with genus$g = 2$ and $\ell_0 = \max\{\ell(\gamma(t))\}$ the maximum of the shortest closed geodesic length on$M$

It may be clearly observed (see Fig. 17.11), that it is in the regular case that the upper/lower limits of the shortest closed geodesic length are reached. In the figure, each of the F-N coordinates covers all the possible values (different limits for each ℓ_i) so that the basic domain remains a dodecagon. Thus the following is obtained:

Theorem 17.6 *Let$\mathcal{M}$ be a closed surface with genus$g = 2$. Thus the length $l(\gamma)$ of every systole,γ, verifies the inequality$\ell(\gamma) \leq \ell_0$.*

17.6 Final Considerations

In this chapter new insights have been provided into the study of the systoles length spectrum under deformation of a compact Riemann surface endowed with a metric of constant curvature -1. Rigorous detailed constructions have been achieved using the techniques of symbolic dynamics. Systolic inequalities that determine the upper limits of the systoles lengths spectrum have been established.

References

1. Bavard, C.: La systole des surfaces hyperelliptiques. Prépubl. no 71 ENS Lyon (1992)
2. Bavard, C.: Systole et invariant d'Hermite. J. Reine Angew. Math. **482** 93–120 (1997)
3. Beardon, A.: The Geometry of Discrete Groups. Springer, Berlin (1983)
4. Berger, M.: A l'ombre de Loewner. Ann. Sci. É cole Norm. Sup. **5**, 241–260 (1972)
5. Buser, P., Sarnak, P.: Markov maps associated with Fuchsian groups. Invent. Math. **117**, 27–56 (1994)

6. Grácio, C., Sousa Ramos, J.: Symbolic dynamics and hyperbolic groups. Grazer Math. Ber. **339**, 195–206 (1999)
7. Grácio, C., Sousa Ramos, J.: Boundary maps and Fenchel–Nielsen coordinates. Int. J. Bifurc. Chaos Appl. Sci. Eng. **13**(7), 1949–1958 (2003)
8. Grácio, C., Sousa Ramos, J.: Rigidity and flexibility for surface groups. Grazer Math. Ber. **346**, 1189-1195 (2006)
9. Grácio, C., Sousa Ramos, J.: Geodesic length spectrum on compact Riemann surfaces. J. Geom. Phys. **60**, 1643–1655 (2010)
10. Gromov, M., Systoles and intersystolicinequalities. In: Actes de la Table Ronde de Géométrie Diffé rentielle (Luminy 1992), 291–362. Séminaires et Congrès, 1 . Soc. Math. France, Institut Henri Poincaré, Paris (1996)
11. Katz, M., Sabourau, S.: Entropy of systolically extremal surfaces and asymptotic bounds. Ergon. Theory Dyn. Syst. **25**, 1209–1220 (2005)
12. Katz, M., Sabourau, S.: Hyperelliptic surfaces are Loewner. Proc. Am. Math. Soc. **134**, 1189–1195 (2006)
13. Ymayoshi, Y., Taniguchi, M.: An introduction to teichmuller space. Springer-Verlag 1992
14. Maskit, B.: New parameters for Fuchsian groups of genus 2. Proc. Am. Math. Soc. **127**(12), 643–3652 (1999)
15. McKean, H.: Selberg's trace formula as applied to a compact Riemann surface. Commun. Pure Appl. Math. **XXV**, 225–246 (1972)
16. Pollicott, M., Rocha, A.: A remarkable formula for the determinant of the laplacian. Invent. Math. **130,** 399–414 (1997)
17. Schmutz, P.: Riemann surfaces with shortest geodesic of maximal length. Geom. Funct. Anal. **3** , 564–631 (1993)
18. Schmutz, P.: Geometric characterization of hyperelliptic Riemann surfaces. Ann. Acad. Scien. Fenn. Math. **25**, 85–90 (2000)